SUBSEA PIPES UNDER HIGH-MASS LOW-VELOCITY IMPACTS

Shamsoon Fareed

Submitted for the degree of Doctor of Philosophy

Heriot Watt University

School of Energy, Geoscience, Infrastructure and Society

June 2017

ABSTRACT

Subsea steel pipes are often used to form networks for transporting oil and gas over large distances. Such pipes can potentially be subjected to actions characterised by high loading rates and intensities stemming from accidental loads caused by high-mass low-velocity impacts. In order to ensure that such networks can continue to operate after being subjected to such extreme loading conditions, it is essential that the behaviour of the pipes is characterised by a certain level of resilience. The short duration and high intensity that often characterises impact loads can potentially result in large strain-rates being exhibited within the pipes. To study the effects of the loading-rate on the material behaviour of steel and identify the causes that trigger the experimentally observed shift in specimen behaviour with increasing loading rates compared to that established under equivalent static testing, a review of the relevant experimental evidence is carried out. A review reveals that the specimen behaviour is significantly affected by the developing inertia forces and the interaction with the experimental setup. This suggests that the available test data describes structural rather than material behaviour, thus raising concerns regarding the validity of current practices to employ such data for the development of constitutive models capable of predicting material behaviour under high loading rates.

A numerical study is carried out investigating the behaviour exhibited by steel pipes under impact loading, accompanied by a limited number of drop-weight tests. The numerical predictions, which are validated against relevant test data reveal that number of parameters associated with the characteristics of the impacting object, the geometry and the support conditions of the pipes, the level of axial loading as well as the level of internal and external pressure imposed onto the walls of the pipes can significantly affect, often detrimentally, the exhibited behaviour under impact loading. Existing assessment methods employed in practice for predicting the level of damage sustained by pipes during impact do not accurately consider the effect of the above parameters. As a result questions rise concerning their ability to realistically predict the level of damage sustained by such pipes under impact. The numerical predictions are presented in the form of simple diagrams quantifying the individual and combined effect of the

above parameters on the level of damage sustained by the pipes when subjected to impact. The latter predictions can potentially form the basis for the development of more advanced analysis methods suitable for practice and leading to the development of more effective design solutions capable of safeguarding the intended level of resilience required to characterise the behaviour of subsea pipes. Finally, it is shown that the use of coatings, constructed from reinforced concrete or engineered cementitious composites, can potentially further reduce the level of damage sustained by pipes due to impact loading, however, further – more detailed – studies are required in order to accurately quantify these benefits.

LIST OF PUBLISHED AND PLANNED PUBLICATIONS

Publication submitted to conference proceedings

Fareed, S., (2013) Transverse Impact on Mild Steel Pipes, Infrastructure and Environment Scotland 1st Postgraduate Conference, Heriot Watt University, Edinburgh, 3rd June 2013.

Fareed, S., May, I. (2014) Response of mild steel pipes under high mass low velocity impacts, *Proceedings of the ASME 2014 33rd International Conference on Ocean, Offshore and Arctic Engineering*, Volume 6A: Pipeline and Riser Technology, San Francisco, California, USA, June 8–13, 2014.

Fareed, S., May, I. (2014) Impacted Subsea Pipes under Internal Pressure, Infrastructure and Environment Scotland 2nd Postgraduate Conference, The University of Edinburgh, Edinburgh, 2nd September 2014.

Fareed, S., Cotsovos, D.M. & Laghrouche, O. (2017) Assessing the behaviour of subsea pipes under impact, *Proceedings of the X International Conference on Structural Dynamics, EURODYN 2017*, September 10-13, 2017, Rome, Italy.

Publication submitted to peer-reviewed journals

Fareed, S., Cotsovos, D.M. & Laghrouche, O. (2017) Modelling the behaviour of structural steel under high loading rates, *Computers & structures.*

Fareed, S., Cotsovos, D.M. & Laghrouche, O. (2017) Behaviour of subsea pipes under impact, *International journal of impact engineering.*

Fareed, S., Cotsovos, D.M. & Laghrouche, O. (2017) Assessing the behaviour of steel pipe specimens under high rate loadings, *International journal of impact engineering.*

To my parents for their love,
support and continuous guidance.

ACKNOWLEDGEMENTS

I am greatly indebted to my supervisor Dr. Demitrios Cotsovos, for providing me guidance, his time and expertise, during my PhD studies without which, it would have been impossible to complete my PhD Thesis. I am extremely grateful to my second supervisor Professor Omar Laghrouche for his valuable help and for providing me with essential feedback, critical for the completion of my PhD Thesis. I would also like to thank Professor Ian May, under whose supervision initially I started my PhD studies.

I would like to express my gratitude to the NED University of Engineering & Technology and Higher Education Commission, Government of Pakistan, for providing a scholarship for the PhD studies.

I am thankful to Total E&P UK Limited and especially Mr. Sylvain Rabouille (lead engineer of Total E&P) for providing support for the pursuit of this research. I would like to thank lab technicians, especially Mr. Steve Ritch, for their continuous assistance in carrying out impact tests, and Ms. Gillian Rae and the EGIS Research and administration teams for providing support throughout my stay at the Heriot-Watt University.

Special thanks go to my mentors Professor S F A Rafeeqi, Professor Sarosh H Lodi, Professor S.M. Makhdumi and Professor Asad-ur-Rehman and my uncle Mr. Lala Gulsher for supporting and encouraging me to achieve my dreams. I would like to thank my friends and colleagues at Heriot Watt University for their friendship and support.

Finally, I would like to thank my sister Dr. Shameen Fareed. Although she is younger than me but she always inspires me by her courage.

Above all, I would like to express my utmost profound gratitude to my parents for their continuous support, teachings, prayers and love. My parents spend their whole life working hard for my education and living, for which words cannot adequately express the gratitude I feel for them.

ACADEMIC REGISTRY

Research Thesis Submission

Name*:*	**SHAMSOON FAREED**		
School/PGI:	**School of Energy, Geoscience, Infrastructure and Society**		
Version: *(i.e. First, Resubmission, Final)*	**Final**	Degree Sought (Award **and** Subject area)	**PhD in Civil Engineering**

Declaration

In accordance with the appropriate regulations I hereby submit my thesis and I declare that:

1) the thesis embodies the results of my own work and has been composed by myself
2) where appropriate, I have made acknowledgement of the work of others and have made reference to work carried out in collaboration with other persons
3) the thesis is the correct version of the thesis for submission and is the same version as any electronic versions submitted*.
4) my thesis for the award referred to, deposited in the Heriot-Watt University Library, should be made available for loan or photocopying and be available via the Institutional Repository, subject to such conditions as the Librarian may require
5) I understand that as a student of the University I am required to abide by the Regulations of the University and to conform to its discipline.

* *Please note that it is the responsibility of the candidate to ensure that the correct version of the thesis is submitted.*

Signature of Candidate*:*	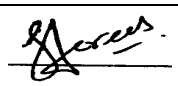	Date:	

Submission

Submitted By *(name in capitals):*	
Signature of Individual Submitting:	
Date Submitted:	

For Completion in the Student Service Centre (SSC)

Received in the SSC by (name in capitals):			
Method of Submission *(Handed in to SSC; posted through internal/external mail):*			
E-thesis Submitted ***(mandatory for final theses)***			
Signature:		Date:	

Please note this form should bound into the submitted thesis.
Updated February 2008, November 2008, February 2009, January 2011

TABLE OF CONTENTS

LIST OF TABLES

LIST OF FIGURES

SYMBOLS & ABBREVIATIONS

Chapter 1

ABS	:	American Bureau of Shipping
Mtoe	:	Million tonnes of oil equivalent
DNV	:	Det Norske Veritas
NLFEA	:	Non-Linear Finite Element Analyses
v	:	velocity
L/D	:	length to diameter ratio

Chapter 2

API	:	American Petroleum Institute
PSL	:	Product Specification Level
E_k	:	kinetic energy absorbed
x_0	:	penetration
b	:	breadth of the impacting object
h	:	depth of the impacting object
D	:	pipe diameter
Y	:	crushing strength of concrete
σ_h	:	hoop stress
SMYS	:	Specified Minimum Yield Strength of the material
k_T	:	temperature dependent material strength de-rating factor
η	:	usage factor
p_i	:	internal or external design pressure
p_o	:	external design pressure
t	:	nominal pipe wall thickness
σ_l	:	longitudinal stress
σ_e	:	equivalent stress
σ_{lh}	:	shear stress due to shear force and torsional moment
D/t	:	diameter to thickness ratio
ε	:	extreme fiber strain in the pipe

f_o : out-of-roundness

E : Young's modulus

k_{fab} : material resistance de-rating factor due to fabrication

P_t : hydrostatic test pressure in N/mm^2 (psi)

P_b : specified minimum burst pressure of pipe in N/mm^2 (psi)

P_d : pipeline design pressure in N/mm^2 (psi)

P_a : incidental overpressure in N/mm^2 (psi)

f_d : internal pressure (burst) design factor (0.9 for pipelines)

f_e : weld joint factor (longitudinal or spiral seam welds)

f_t : temperature de-rating factor, 1.0 for temperatures less than 121°C (250°F)

D_i : inside diameter of pipe in mm (in) (D_i =D-2t)

S : SMYS of pipe in N/mm^2 (psi)

t : nominal wall thickness of pipe in mm (in)

U : specified minimum ultimate tensile strength of pipe in N/mm^2 (psi)

T_{eff} : effective tension in the pipe in N (lb)

T_a : axial tension in pipe in N (lb)

T_y : yield tension of the pipe in N (lb)

A : cross-sectional area of pipe in mm^2 (in^2)

A_i : internal cross-sectional area of pipe in mm^2 (in^2)

A_o : external cross-sectional area of pipe in mm^2 (in^2)

P_i : internal pressure in the pipe in N/mm^2 (psi)

P_o : external hydrostatic pressure in N/mm^2 (psi)

σ_a : axial stress in the pipe wall in N/mm^2 (psi)

f_o : collapse factor

P_c : collapse pressure of the pipe in N/mm^2 (psi)

P_e : elastic collapse pressure of the pipe in N/mm^2 (psi)

P_y : yield pressure at collapse in N/mm^2 (psi)

υ : Poisson's ratio

ε : bending strain in the pipe

ε_b : buckling strain under pure bending

ε_1 : maximum installation bending strain

ε_2 : maximum in-place bending strain

f_1	:	bending safety factor for installation bending plus external pressure
f_2	:	bending safety factor for in-place bending plus external pressure
$g(\delta)$	:	collapse reduction factor
δ	:	ovality
D_{max}	:	maximum diameter at any given cross section in mm (in)
D_{min}	:	minimum diameter at any given cross section in mm (in)
p_{li}	:	local incidental pressure
p_b	:	pressure containment resistance
p_{lt}	:	local test pressure
p_h	:	mill test pressure
t_1	:	pipe wall thickness
γ_m	:	material resistance factor
γ_{SC}	:	safety class resistance factor
α_{spt}	:	system pressure test factor
α_{mpt}	:	mill pressure test factor
α_U	:	material strength factor
f_y	:	yield stress to be use in design
f_u	:	tensile strength to be use in design
p_{min}	:	minimum internal pressure that can be sustained
P_c	:	characteristic collapse pressure
M_{Sd}	:	design moment
S_{Sd}	:	design axial force
ϵ_{Sd}	:	design compressive strain
P_i	:	internal pressure
S_p	:	plastic capacity of pipe
M_p	:	plastic moment
α_c	:	flow stress parameter
α_p	:	pressure factor
β	:	factor used for combined loading
γ_c	:	condition load effect factor
$\gamma_f, \gamma_E, \gamma_A$	:	load effect factor for functional, environmental and accidental loads respectively

M_f, M_E, M_I, M_A	:	moment for functional, environmental, interface and accidental loads respectively
ϵ_f, ϵ_E, ϵ_I, ϵ_A	:	strain for functional, environmental, interface and accidental loads respectively
$\frac{R_{t\,0,5}}{R_m}$	:	depending on SMYS, ratio of yield to tensile strength
α_{gw}	:	Girth weld factor
E_s	:	impact energy associated with the steel mass of the trawl board
m_t	:	trawl board steel mass
R_{fs}	:	reduction factor depending on the outer diameter
C_h	:	span height correction factor for the effective pull over velocity
E_a	:	impact energy associated with the hydrodynamic added mass of the trawl board
F_b	:	impact force associated with the hydrodynamic added mass of the trawl board
k_b	:	lateral bending stiffness of the board
m_a	:	trawl board added mass
t	:	steel wall thickness
R_{fa}	:	reduction factor depending on the outer diameter
$f_{y,temp}$	:	temperature derating value of yield strength
α_U	:	material strength factor
F_{sh}	:	impact force of a bare steel pipe
H_t	:	dent depth of a bare steel pipe
C_b	:	factor taking into account the effective mass
m_a, m_t	:	hydrodynamic added mass and steel mass of the trawl gear
k_b, k_i	:	out of plane and in plane stiffness of the gear
k_{c1}	:	stiffness of the protective cover for heating cable attached to the pipeline
k_{c2}	:	stiffness of the coating
k_{c3}	:	possible effect it has on the steel shell stiffness by distributing the impact force over a large area by shear deformations in the coatings
k_s	:	local stiffness of the steel pipeline
m_p	:	effective mass of the pipe, including hydrodynamic added mass

k_{pb}	:	effective bending stiffness of the pipe
k_{pb}	:	effective soil stiffness of the pipe
k_s	:	local stiffness of the steel pipe
δ	:	deformation of the steel pipe
F	:	impact force between trawl board and steel pipe
σ_y	:	yield stress of steel pipe
LVDT	:	Linear Variable Differential Transformer
2L	:	span length
W_f	:	maximum permanent transverse displacement
E_k	:	initial kinetic energy
D/H	:	diameter to thickness ratio
DD	:	Ductile Deformation
λ_c	:	dimensionless threshold failure energy
H	:	wall thickness of the pipe
E_k^c	:	threshold failure energy
P_c	:	static plastic collapse load
$\overline{W_f}$	:	dimensionless maximum deformation
P_y	:	axial load
f	:	normalized force
x	:	normalized displacement
R	:	pipe radius
δ	:	local dent depth (without overall bending)
q	:	normalized pressure
φ'	:	soil friction angle
Em	:	Embedment depth
b/D	:	length of indentor to diameter of pipe ratio
δ_r	:	residual dent depth
r_o	:	radius of deformed cross-section of pipe
T_r	:	thickness of deformed cross-section of pipe
D_m	:	maximum width of deformed cross-section of pipe
W_1	:	local displacement of pipe
W_f	:	overall permanent displacement of pipe
W_g	:	global displacement of pipe

E	:	energy
m_p	:	plastic moment capacity of the wall
δ	:	dent depth

Chapter 3

ϵ_{total}	:	total strain
$\epsilon_{elastic}$	:	recoverable strain
$\epsilon_{plastic}$	:	Unrecoverable strain
A_o	:	initial cross-section area
L_o	:	initial length
A_f	:	final cross-section area
L_f	:	final length
f_c	:	concrete compressive strength
f_t	:	concrete tensile strength
SHPB	:	Split Hopkinson Pressure Bar
ε_i	:	tensile strain
ε_r	:	compressive strain
ε_t	:	output strain
σ_s	:	engineering stress
ε_s	:	engineering strain
$\dot{\varepsilon}_s$	:	strain rate
A	:	cross-sectional area of the bar
A_s	:	cross-sectional area of the specimen
L	:	gauge length of the specimen
C_o	:	speed of the stress wave in the bar
MP800HY	:	Multi-Phase 800 High Yield strength steel
CP800	:	Complex Phase steel
SPRC	:	Steel Plate Re-phosphorised Cold Rolled
TRIP	:	Transformation Induced Plasticity
DP	:	Dual Phase steel
DIF	:	Dynamic Increase Factor
F^{int}	:	internal force

U	:	element deformation
K	:	element stiffness
M	:	mass
$\ddot{U}$	:	acceleration
F_I	:	inertia forces
F_d	:	damping forces
C	:	damping constant
$\dot{U}$	:	velocity
Δt	:	time step
ΔU	:	change in displacement
K^*	:	effective stiffness matrix
ΔP^*	:	effective load vector
ΔP	:	loading vector
t	:	time
U_t , $U_{t+\Delta t}$	:	the value of displacement at t and $t + \Delta t$ respectively
$\dot{U}_t$, $\dot{U}_{t+\Delta t}$	:	the value of velocity at t and $t + \Delta t$ respectively
$\ddot{U}_t$, $\ddot{U}_{t+\Delta t}$	:	the value of acceleration at t and $t + \Delta t$ respectively
α, β, γ	:	numerical parameters associated with the Hilber-Hughes-Taylor operator
P	:	external forces
I	:	internal forces
K_o	:	structure's initial stiffness
C_a	:	displacement correction
R_a	:	force residual for the iteration
ε^{pl}	:	true plastic strain
ε^{t}	:	true total strain
ε^{el}	:	true elastic strain
$\tilde{\varepsilon}^{pl}{}_t$	:	tensile equivalent plastic strain
$\tilde{\varepsilon}^{pl}{}_c$	:	compressive equivalent plastic strain
d_t ,d_c	:	tensile and compressive damage variables respectively
E_o	:	initial (undamaged) elastic stiffness
ρ	:	density of the material

Chapter 4

FE	:	Finite Element

Chapter 5

g	:	acceleration due to gravity
h	:	height of the impactor
v	:	velocity
a	:	acceleration
s	:	spacing of springs
t	:	thickness of web
L	:	height of web
I	:	second moment of area

Chapter 6

C_V	:	coefficient for vertical soil stiffness
D	:	pipe diameter in meters
$\frac{\rho_s}{\rho}$	:	specific mass ratio between the pipe mass (excluding added mass) and the displaced water
υ	:	Poisson's ratio
K_V	:	vertical stiffness in kN/m/m
ECC	:	Engineered Cementitious Composite

CHAPTER 1

INTRODUCTION

1.1 BACKGROUND

Due to increasing energy demands across the globe (see Figure 1.1) subsea pipes are used to form an extensive network for transporting oil and gas over large distances. The smooth operation of these pipelines is essential as they play a vital role, not only for the oil and gas industry, but also for society and the global economy. Such pipelines can be subjected to a range of actions during their installation process and their operational life which can be broadly classified as (i) environmental, (ii) functional and (iii) accidental [ABS (2001)]. Loads induced due to the action of waves, ice and wind are considered as environmental actions. Functional loads include the self-weight of the pipe and its components (e.g. coatings, piggy-back electrical cables with protection structures etc.), the development of internal pressure due to the transportation of oil and gas and external pressure due to hydro-static loads [ABS (2001)]. Finally, accidental loads are usually generated due to the collision of objects (e.g. fishing trawl, rocks, icebergs, other pipes etc.) onto the pipes.

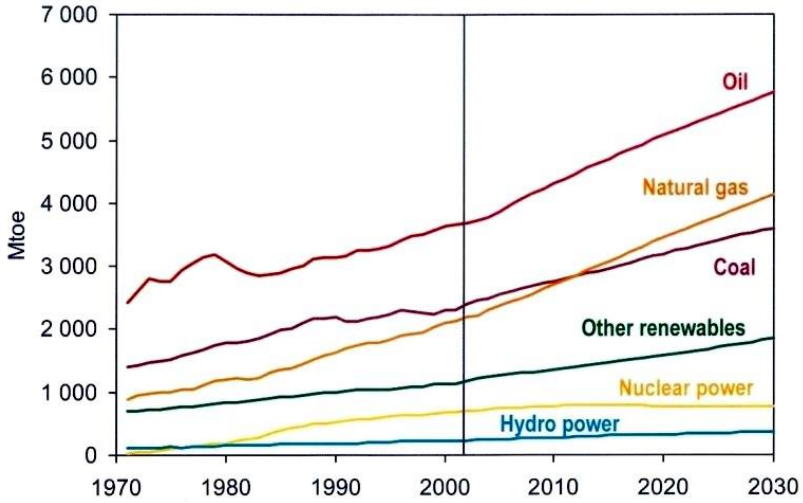

Figure 1.1: Increase of global energy consumption with time expressed in Million tonnes of oil equivalent (Mtoe) [Siciliano *et al.* (2008)].

Loads associated with the accidental collision of objects onto subsea pipelines are usually generated by high-mass low-velocity impacts and are generally characterised by high loading rates and intensities imposed over a small period of time (usually in the order of a few milliseconds). The level of damage sustained by the pipe during impact may pose a significant threat to human safety and the environment (due to the potential release of hydrocarbons) while at the same time causing disruptions in the supply of oil and gas to industry and society (due to the un-scheduled shutdown of the pipeline for repair). The repair of subsea pipes can be a time-consuming and costly process which can take up to three months to complete [DNV (2010b)] and can render the pipe, as well as the pipeline, non-operational for the duration of the works. Based on the above the development of effective design and analysis procedures for subsea pipes subjected to impact loading is of significant importance in order to safeguard an intended level of resilience that will allow it to continue to operate even when subjected to such extreme load conditions. The development of such a process will allow the realistic assessment of the level of damage sustained by the pipe that will in turn allow engineers to determine its post-damage operational capability. According to current practices the level of damage sustained by a pipe is usually assessed based on the reduction of its diameter exhibited during impact [DNV (2010b)].

It has been established that the dynamic response of pipes under impact loading exhibits significant departures from that, established under equivalent static loading as certain thresholds of the applied loading rates are surpassed [Jones *et al.* (1992)]. The available experimental data (discussed later in Chapter 2) reveals that this shift in structural response is predominantly owed to the inertia forces acting along the span of the pipe in combination with the localized response exhibited at the region close to the location where the impact load is imposed [Jones *et al.* (1992), Chen & Shen (1998), Ng & Shen (2006)]. Considering the nature of the problem at hand (a wave propagation problem within a nonlinear medium) it should be noted that a range of additional parameters can also considerably influence (potentially detrimentally) the *in-situ* behaviour (exhibited under operational conditions) of subsea pipes under impact loading. Such parameters are associated with the material properties of steel, the geometry of the pipe, the mass, shape and velocity of the impacting object, the boundary conditions imposed onto the pipe (i.e. the properties of the supporting soil, the end-conditions), the internal and

external pressures developing on the pipe walls as well as the level of imposed axial loading.

The accidental collision of trawl fishing gears/weights onto the subsea pipes is one of the main reasons that result in the generation of the impact loads. The amount of impact energy that these trawling gears impose onto the pipes depends largely on their mass (usually up to 9 tonnes) and the velocity of the trawl vessel. The latter speed is linked to a range of parameters associated with the fish movement patterns, the type of fish (swimming speed) targeted and the economic speed of the trawl vessels (e.g. trawling for prawns and fish is performed at speeds of 1 - 1.5m/s and 2.8m/s respectively) [DNV (2010a)]. Based on the above, the collision of the trawl gears/weights onto a pipeline is generally considered as a high-mass low-velocity impact problem.

The performance of the pipes under impact loading can be assessed (i) experimentally *via* drop-weight testing, (ii) numerically through the use of non-linear finite element analyses and (iii) by employing (usually in practice) simplified analytical methods. Most of the available analytical approaches [Wierzbicki & Suh (1988), Jones & Shen (1992)] consider the impact problem at hand as an equivalent static one by neglecting the developing inertia forces. Although these approaches can be used to form practical tools for quickly and easily assessing the level of damage sustained by pipes due to impact, they ignore that the problem at hand is a wave propagation problem within a nonlinear medium as well as the contribution of the parameters associated with the *in-situ* (subsea) conditions on the exhibited behaviour. As a result, such simplified approaches can only provide initial predictions/estimates of certain aspects of the response of the pipe as well as the level of damage sustained.

The experimental investigation of the dynamic response of pipes under impact loading is characterized by significant difficulties. These difficulties are linked to the short duration (only a few milliseconds) of the contact force generated during the collision of the impactor onto the pipe-specimen and the high intensity of the applied load which increases abruptly from zero to a maximum value. As a result, it is often difficult to obtain measurements describing in detail the dynamic response of full-scale specimens throughout the loading process. In addition, it is also difficult to account experimentally for the effect of the various parameters (associated with the sea-bed upon which the pipe is laid, the internal and external pressure imposed on the walls of the pipe as well

as the boundary conditions imposed at its two ends) on the behaviour of the pipe while in operation. Due to these restrictions test data is usually obtained from scaled pipe-specimens and does not provide a realistic representation of the actual problem at hand nor does it offer an accurate description of the actual *in-situ* behaviour exhibited by subsea pipes under operational conditions. The experimental setups used to date provide a simplified representation of the problem at hand that can potentially overestimate or underestimate certain aspects of the response of the pipe. However, the test data obtained can be used for: (i) investigating the effect of loading rate on the response of the pipes and (ii) validating the predictions obtained from Non-Linear Finite Element Analyses (*NLFEA*) allowing for the development of more complex numerical models based on the finite element method capable of representing more realistically the problem at hand.

1.2 OBJECTIVES

Based on the above, a detailed numerical study is presently conducted using ABAQUS [ABAQUS (2013)] investigating the behaviour of steel pipes under impact loading in order to study the effect of loading rate on the exhibited response. The numerical investigation is validated through the use of test data either obtained from the literature or from tests conducted on full scale pipe specimens in the present study. The validated models are then employed to investigate the effect of various parameters associated with the geometry of the pipes (thickness, diameter and length), the properties of the supporting soil, the internal and external pressures imposed onto the walls of the pipe as well as the development of axial loading. Finally, the numerical study is extended in order to investigate the benefits stemming from the use of coatings made from concrete or Engineered Cementitious Composites (ECC) on the level of damage sustained by pipes under impact.

More specifically the main objectives of the work conducted herein are to:

1. Assess the effect of the loading rate on the behaviour of steel and plain concrete specimens under uniaxial compression and tension in order to determine the underlying causes that trigger the experimentally observed shift in their behaviour

with increasing loading rates. This is achieved on the basis of the available published information.

2. Review and analyse the available experimental data in order to study the effect of impact loading on the local and global responses of steel pipes and determine the effect of various parameters (e.g. impact energy, pressure acting on the walls of the pipe, boundary conditions etc.) on the exhibited behaviour.

3. Investigate experimentally *via* drop weight testing the localised response exhibited by full scale pipes at the area of impact when subjected to impact loading.

4. Employ *NLFEA* (the predictions of which are validated against the available test data) to study in detail the global and local responses of pipes under impact. Emphasis will be focused on assessing the effect of various parameters (boundary conditions, impact energy, axial loading, pipe length, etc.) on the exhibited behaviour.

5. Develop finite element models in order to investigate in detail the *in-situ* behaviour of the subsea pipes under operational conditions. This study will focus on investigating the behaviour of pipes under impact loading while at the same time accounting for the combined effect of other parameters associated with the properties of the supporting soil, the internal and external pressure(s), the level of imposed axial loading and the cross-sectional properties of the pipes. This investigation also aims at assessing the reliability of the predictions provided by the available relevant codes or assessment methods concerning the level of damage sustained by steel pipes during collision.

6. Conduct a preliminary investigation on the ability of concrete and *ECC* coatings to reduce the level of damage sustained by pipes during impact.

1.3 CONTENTS OF THE THESIS

A comprehensive review of the available codes used by the oil and gas industry for the analyses and design of subsea pipes is presented in Chapter 2 in combination with other

recommendations and practices for assessing the level of damage sustained by pipes when subjected to impact loads. This is followed by a critical review of available published experimental, numerical and analytical studies investigating the response of pipes under impact loading. In the majority of experimental studies conducted to date emphasis is focused on investigating the behaviour of suspended pipes (usually supported with clamps at both ends) characterized by relatively small cross-sections and low impact energies which do not provide an accurate representation of the problem at hand. This is due to the fact that it is difficult to mimic the actual subsea conditions in the laboratory (e.g. subsea foundation, application of the internal and external pressures and axial loading). A review of the available published experimental studies is conducted which focuses on certain aspects (level of damage sustained, load time and displacement time histories etc.) of the response exhibited by the pipes under impact loading in combination with the effect of various parameters (impact energy, internal and external pressure acting on the wall of the pipe, support conditions etc.). It is important to note that a large part of the published *NLFEA* studies [Zeinoddini *et al.* (2013), Brooker (2004)] are carried out using quasi static analysis thus ignoring the inertia effects and the wave propagation problem at hand. An overview of available analytical approaches and empirical equations used for predicting certain aspects of the exhibited behaviour (e.g. the level of damages sustained) of steel pipes under impact loading is also presented.

Chapter 3 focuses on studying the behaviour of steel and concrete specimens under high rate loading conditions. An overview of the published experimental studies carried out to date investigating the behaviour of steel and plain concrete specimens under high rate loading is presented and the data gathered is critically analysed. On the basis of the available data it is shown that the behaviour exhibited by steel and plain concrete specimens under high loading rates differs from that established under equivalent static loading once certain limits of loading rate are surpassed. However, the available test data are characterized by considerable scatter and, as a result, cannot accurately quantify the observed differences nor can it provide the reasons that cause them.

In Chapter 4 a numerical investigation is carried out studying the response of steel subsea pipes under impact loading *via* nonlinear finite element analysis (NLFEA). The numerical predictions obtained are validated against the test results of Jones *et al.* (1992) who investigated the impact behaviour of scaled pipe-specimens via drop-weight

testing. Both static and impact tests are used to validate the *NLFEA* models. The aim of this investigation is to study the effect of the loading rate on the exhibited behaviour of the pipes in relation to the behaviour established under equivalent static loading. Emphasis is focused on certain important aspects of the exhibited behaviour (e.g. load carrying capacity, displacement profile of the pipes, damage sustained etc.). Following the validation of the *NLFEA* models employed, parametric studies are carried out and the predictions obtained are analysed and discussed in this Chapter. The influence of the velocity (v_i) of the impacting object, length to diameter ratio (*L/D*), the boundary conditions imposed onto the pipes, the development of axial loading as well as internal and external pressure(s) acting on the wall of the pipes under impact loading are considered in the parametric study.

The results of the impact tests carried out to study the behaviour of the full scale pipe specimens under high-mass low-velocity impacts are presented in Chapter 5. The tests are carried out to mainly study the localized behaviour exhibited by the pipes under impact loading. A high-speed high-resolution video camera is used to record the tests. The video recording obtained is used to track the movement of the impactor during and after impact. Based on the data acquired, the displacement, velocity and contact force time histories are obtained. These provided insight into the response of the subject specimens under impact loading and allowed for the validation of the *NLFEA* models developed for representing the subject problem.

In Chapter 6, the validated *NLFEA* models are employed to investigate the effect of various parameters associated with the geometry of the pipes (thickness, diameter and length), the properties of the supporting soil, the internal and external pressures as well as the development of axial loading on the local and global response of the pipes under impact loading. The investigation is then extended to study the influence of the use of concrete and *ECC* coatings on the impact behaviour of the subsea pipes and asses their effectiveness in reducing the level of damage sustained. The parametric study in this chapter provides a more realistic description of the dynamic behaviour of the pipes under impact compared to the majority of experimental and numerical studies carried out to date. The numerical predictions are presented in the form of simple diagrams quantifying the individual and combined effects of the above parameters on the level of damage sustained during impact. These diagrams will allow engineers to realistically

predict the level of damage sustained by the pipes and in turn assess the post-impact operation capability.

In Chapter 7, conclusions based on the studies presented in this thesis are presented followed by recommendations for future research.

CHAPTER 2

LITERATURE REVIEW

2.1 INTRODUCTION

Considering the importance of subsea pipeline networks for transporting oil and gas in order to supply fuel to societies and industries worldwide, it is essential that the operation of such systems is characterized by a certain level of resilience. More specifically it is vital that such networks continue to function even after being subjected to extreme loading conditions such as those encountered during accidental collisions of large objects onto subsea pipes.

Depending on the chemical composition and material properties of the steel used for manufacturing pipes employed for transporting oil and gas (see Table 2.1), the American Petroleum Institute [API (2004)] classifies such pipes into two main categories (Product Specification Levels): *PSL-1* and *PSL-2*. The main differences between these two categories are outlined in Table 2.1. The key factors considered for selecting the most suitable steel grade are associated with cost and performance requirements (e.g. resistance to corrosion, weldability, toughness, weight, etc.) of the pipe [Bai & Bai (2014)]. Based on this, *PSL-2* pipes are widely used for subsea transportation of oil and gas [Changjiang (2015)] and as a result the current study will mainly focus on studying the behaviour of such pipes under high-mass low-velocity impacts.

Subsea pipes are normally laid on the seabed, and as discussed in Chapter 1, can be subjected to a combination of environmental, functional and accidental actions. Environmental loads are generated due to the action of waves, currents, ice and wind [ABS (2001)]. For example wind forces are exerted on risers (i.e. pipes used to connect an offshore floating production structure or a drilling rig to a subsea system) that are located above the water surface [Tenaris (2015)]. Environment loads can be either static or dynamic in nature, whereas their intensity and directionality usually varies with time. Functional loads include dead loads (associated with loads applied permanently such as

self-weight) as well as live and deformational loads (occurring due to transportation, storage, installation, testing, operation and general use). Accidental loads are usually associated with blast, fire, impact and earthquakes and are usually characterised by a high level of uncertainty.

Table 2.1: Differences between PSL-1 and PSL-2 pipes [API (2004)].

Parameter	PSL-1	PSL-2
Grade range	A25 - X70	B - X80
Size range	10.3 – 2032mm	114.3 – 2032mm
Max. carbon content – Seamless pipe	0.28% for grades ≥ B	0.24%
Max. carbon content – Welded pipe	0.26% for grades ≥ B	0.22%
Phosphorus content	0.03% for grades ≥ A	0.025%
Sulphur content	0.03%	0.015%
Yield strength, maximum	None	Max. for each grade
Ultimate tensile strength, maximum	None	Max. for each grade
Fracture Toughness	None required	Required for all grades
Repair by welding- Pipe body	Permitted	Prohibited

Impact loads imposed onto subsea pipes are usually characterized by high loading rates and intensities as well as short durations (a few milliseconds). Such loads can be generated during the collision of objects (icebergs, rocks, fishing equipment) onto the pipes. The accidental collision of trawl fishing equipment (see Figure 2.1) onto the subsea pipes is one of the main reasons that result in the generation of the impact loads. Such equipment includes:

(i) Otter trawl boards [Figure 2.1(a)] which use hydrodynamic forces to keep open the trawl net which is dragged along the sea-bed and may accidentally collide with the pipe.

(ii) Transverse steel beams used to keep the fishing nets open (beam trawling, see Figure 2.1b). In the latter case steel shoes are mounted at each end of the beam (used to connect the fishing-nets) which may cause significant damage to pipelines due to their sharp edges.

(iii) Clump weights with a mass ranging between 2 and 9 tonnes used in the case of twin trawling [Figure 2.1(c)] which may result in collisions with pipelines characterised by higher impact energies compared to their counterparts associated with the case of trawl boards and beam trawls [DNV (2010a)].

The level of kinetic energy with which the trawling equipment can potentially impact onto the pipelines largely depends on the velocity of the trawl vessel which in turn is linked to a number of parameters such as (i) the fish movement pattern, (ii) the fish speed and (iii) the optimum economic speed of the vessels (speed of 1 - 1.5m/s and 2.8m/s are achieved when trawling for prawns and fish respectively) [DNV (2010a)].

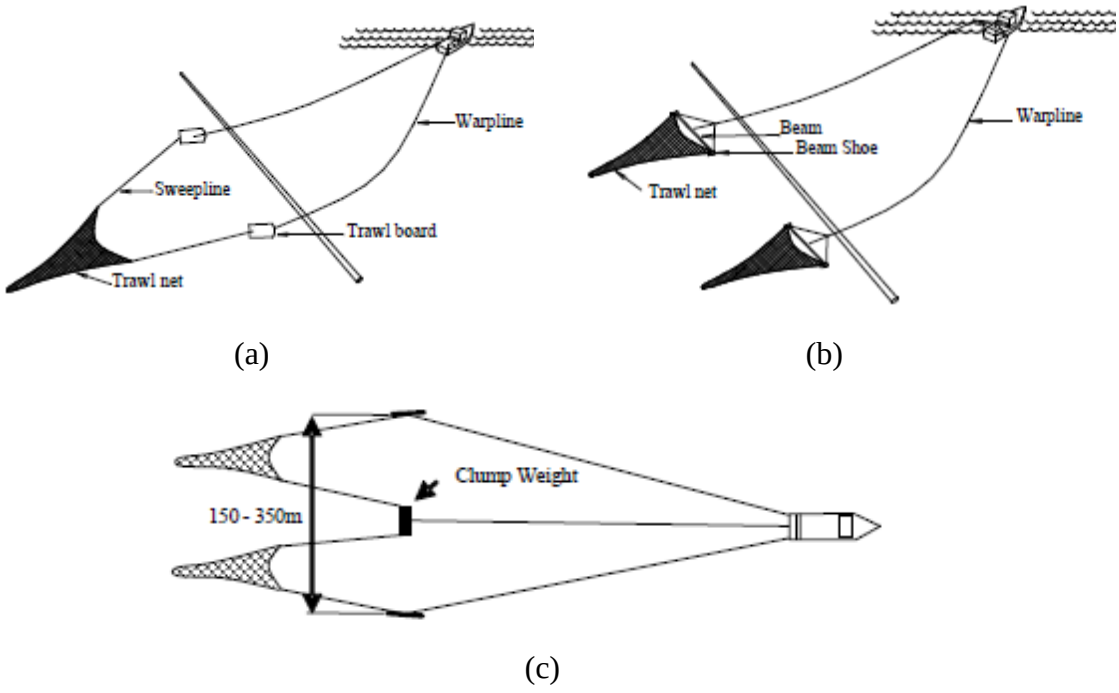

Figure 2.1: Typical components of trawl fishing equipment that can collide with subsea pipes (a) otter trawl gear (b) beam trawl gear (c) twin trawling with clump weight [DNV (2010a)].

Due to the short duration of the impact loads (a few milliseconds) generated during the collision of fishing equipment onto subsea pipes and its intensity, which increases rapidly from zero to its maximum value, such loads can potentially cause the rapid deformation of the pipe (especially in the region where the load is imposed) and as a result this may lead to large strain-rates being exhibited within the steel medium. Such elevated values of strain-rate are widely considered to affect the material properties of

steel (strain-rate sensitivity) and in turn the dynamic response of the pipes under impact loading [Jones & Birch (2010)]. Therefore, prior to investigating the behaviour of pipes under impact loading, it is important to study the effect of loading rate on the mechanical properties of the steel in order to determine the extent to which strain-rate sensitivity can affect its material properties and consequently the dynamic response of the pipe. A comprehensive review and analysis of the available published experimental studies carried out to date on the behaviour of the steel specimens (dog bone, reinforcing bars) under high-rates of tensile loading is presented in Chapter 3.

The dynamic response exhibited by steel pipes under impact loads is both local and global. This can be explained when viewing the problem at hand as a wave propagation problem within a non-linear medium. During collision waves are generated that travel away from the impact area. As a result, localised response is exhibited mainly in the form of damage observed locally at the contact area of the pipe and the impactor. The level of this localised damage can vary from a simple dent to localized failure (i.e. large deformation or even collapse of the pipe's cross-section which can potentially result in the formation of the ruptures/cracks). Global behaviour is exhibited due to the waves propagating away from the contact area resulting in the pipe deforming along its whole length.

The *in-situ* behaviour of subsea steel pipes under impact can be significantly influenced by a range of parameters associated with: (i) the geometry of the steel pipes, (ii) the characteristics of the impacting object (size, shape, speed and material properties), (iii) the boundary conditions imposed onto the pipe (end conditions, properties of the soil on which pipe is laid), (iv) the level of axial loading imposed and (v) the development of internal (due to the flow of oil and gas in the pipe) and external (hydro-static) pressure.

In addition to the above parameters, concrete coatings can be used for protecting the pipelines in order to reduce the level of damage sustained during impact [DNV (2010b)]. Figure 2.2 shows the schematic representation of the failure mechanism through which a portion of the impact energy is absorbed by the concrete coating. The amount of energy absorb is expressed as a function of penetrated volume ($= b \cdot h \cdot x_0$) and the crushing strength (Y), and it can be estimated by either Eq. (2.1) or Eq. (2.2) [DNV (2010b)]:

$$E_k = Y\, b\, h\, x_0 \qquad \text{Eq. (2.1)}$$

$$E_k = Y\, b \frac{4}{3} \sqrt{D x_0^{\,3}} \qquad \text{Eq. (2.2)}$$

where: E_k : kinetic energy absorbed
x_0 : penetration (see Figure 2.2)
b : breadth of the impacting object
h : depth of the impacting object
D : pipe diameter

The crushing strength (Y) is assumed to be 3 to 5 times the cube strength in compression for normal density concrete and 5 to 7 times for lightweight concrete. The typical concrete cube strength varies from 35 to 45MPa [DNV (2010b)]. In the absence of any relevant information, an energy absorption of 40kJ may be adopted for a 45mm thick normal density concrete coating subject to a 30mm wide indenting object.

Figure 2.2: Schematic representation of the failure mechanism through which a portion of the impact energy is absorbed by the concrete coating [DNV (2010b)].

In the present chapter a comprehensive review of the available design codes used for the analyses and assessment of subsea pipes is presented. The recommendations and assessment practices used by industry for the case of pipes subjected to impact loads are also discussed. A critical analysis of the available relevant published experimental *(via* drop-weight) and numerical (*via NLFEA*) investigations is conducted which focuses on certain aspects of the response exhibited by the pipes under impact loading considered in many cases in combination with the effect of other parameters (e.g. impact energy, support conditions, level of internal and external pressure, level of axial loading etc.) on behaviour of the pipe under operating conditions. An overview of the available

analytical approaches and empirical equations used in practice for predicting the behaviour of pipes under impact loadings are also presented.

2.2 DESIGN CODES FOR THE PIPELINES

A number of codes of practice are employed for the design and assessment of subsea pipelines. In this section, the design codes of the American Bureau of Shipping [ABS (2001)], the American Petroleum Institute [API (1999)] and Det Norske Veritas [DNV (2012)] for the design of subsea pipelines are reviewed. The aim is to determine the various parameters that can potentially affect the *in-situ* behaviour of subsea pipes as well as the various critical modes of failure considered by such codes.

2.2.1 American Bureau of Shipping (ABS)

The American Bureau of Shipping [ABS (2001)] strength criteria is based on the working stress design approach and considers the following failure modes: (i) yielding, (ii) local buckling, (iii) global buckling, (iv) fatigue and (v) cross sectional out-of-roundness.

2.2.1.1 Hoop stress

The selection of the pipe wall thickness is based on the internal pressure containment requirement which is given by the maximum allowable hoop stress (σ_h) specified by Eq. (2.3)

$$\sigma_h \leq \eta . \mathrm{SMYS} . k_T \qquad \text{Eq. (2.3)}$$

where: SMYS : Specified Minimum Yield Strength of the material

η : usage factor (see Table 2.2)

k_T : temperature dependent material strength de-rating factor (to be based on material tests or recognized codes such as ASME B31.8 for steel pipes [ASME (2003)] as given in Table 2.3)

The hoop stress developing due to the internal and external pressure imposed laterally on the walls of the pipe (see Figure 2.3) is given by Eq. (2.4):

$$\sigma_h = \frac{(p_i - p_o)(D - t)}{2\,t} \qquad \text{Eq. (2.4)}$$

where: p_i : internal or external design pressure

p_o : external design pressure

D : nominal outside diameter of the pipe

t : nominal pipe wall thickness

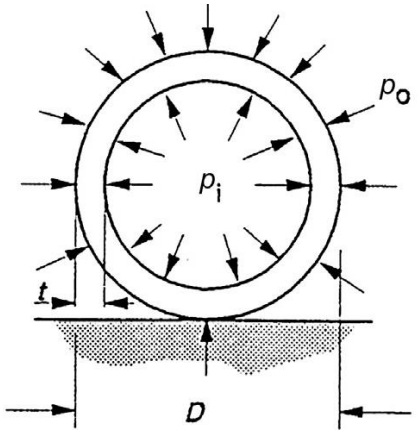

Figure 2.3: Internal and external pressure imposed on the walls of the pipe [Bai & Bai (2014)].

Table 2.2: Usage factors (**η**) for pipelines and risers [ABS (2001)].

	Hoop stress	**Longitudinal stress**	**Equivalent stress**
Oil pipelines & risers, gas pipelines	0.72	0.80	0.90
Gas risers connected unmanned platform	0.60	0.80	0.90
Gas risers connected manned platform	0.50	0.80	0.90

Table 2.3: Temperature de-rating factors (k_T) for steel pipelines [ASME (2003)].

Temperature (^{O}F)	**k_T**
250 or less	1.000
300	0.967
350	0.933
400	0.900
450	0.867

2.2.1.2 Longitudinal stress

The structural integrity against axial forces acting along the length of the pipe is safeguarded by longitudinal stress criteria given by Eq. (2.5)

$$\sigma_l \leq \eta . \text{SMYS}. \ k_T \qquad \text{Eq. (2.5)}$$

where: $\sigma_l = P/A$: longitudinal stress

2.2.1.3 Equivalent stress

The equivalent stress or stress intensity (see Figure 2.4) at any point of the pipe must satisfy the following condition given by Eq. (2.6):

$$\sigma_e = \sqrt{{\sigma_l}^2 + \ {\sigma_h}^2 - \ \sigma_l \, \sigma_h + \ 3 \, {\sigma_{lh}}^2} \ \leq \eta . \text{SMYS}. \ k_T \qquad \text{Eq. (2.6)}$$

where: σ_e : equivalent stress

σ_{lh} : shear stress due to shear force and torsional moment

2.2.1.4 Local buckling under external pressure and bending

When the pipe is subjected to external overpressure which may develop during the installation process or due to temporary conditions (e.g. transportation, system pressure test, shut-down and start up) the cross sectional instability in the form of local buckling may occur (see Figure 2.5). For pipes with diameter to thickness (*D/t*) ratios less than 50 and subjected to external overpressure combined with bending, the strain check is given by Eq. (2.7)

$$\left(\frac{\varepsilon}{\varepsilon_b}\right)^{0.8} + \frac{p_o - p_i}{p_c} \leq \eta \qquad \text{Eq. (2.7)}$$

where: ε : extreme fiber strain in the pipe

$\varepsilon_b = \left(\frac{t}{2D}\right)$

η : usage factor applied to bending strain

The usage factor (η) depends on uncertainties associated with in load effects, available means to detect and repair potential local buckles and the control of buckle propagation (see Figure 2.6) through use of buckle arrestors (design as devices attached to or welded to the pipe or buckle arrestors may also be used as joints of thicker pipe, see Figure 2.6) and are to be approved by the Bureau. If information on load effects is limited then η is to be set to 0.6.

The value of p_c is calculated from expression Eq. (2.8):

$$p_c^3 - p_{el}\, p_c^2 - \left[p_p^2 + p_{el}\, p_p f_o \left(\frac{D}{t}\right)\right] p_c + p_{el}\, p_p^2 = 0 \qquad \text{Eq. (2.8)}$$

where: $p_{el} = \dfrac{2E}{1-\upsilon^2}\left(\dfrac{t}{D}\right)^3$

$p_p = k_{fab} SMYS \left(\dfrac{2t}{D}\right)$

f_o : out-of-roundness, $\left(\frac{D_{max} - D_{min}}{D}\right)$, not to be taken less than 0.5%

E : Young's modulus

k_{fab} : material resistance de-rating factor due to fabrication (1.00 for seamless and annealed pipes, 0.93 for welded pipes not expanded and 0.85 for welded and expanded pipes)

The use of buckle arrestors is governed by Eq. (2.9)

$$(p_o - p_i) \geq 0.72\, P_{pr} \qquad \text{Eq. (2.9)}$$

where: P_{pr} : Buckling propagation pressure = $6 \cdot SMYS \cdot \left(\frac{2t}{D}\right)^{2.5}$

2.2.1.5 Global buckling

Internal pressure and increased operating temperatures may result in the development of compressive forces in a pipeline, which after start-up or after repeated start-up/shut down cycles may lead to global buckling of the pipelines. This phenomenon is to be dealt with either by predicting the position and amplification of buckles using advanced analysis or by demonstrating that the build-up of compressive force is less than the force needed to initiate the global buckling.

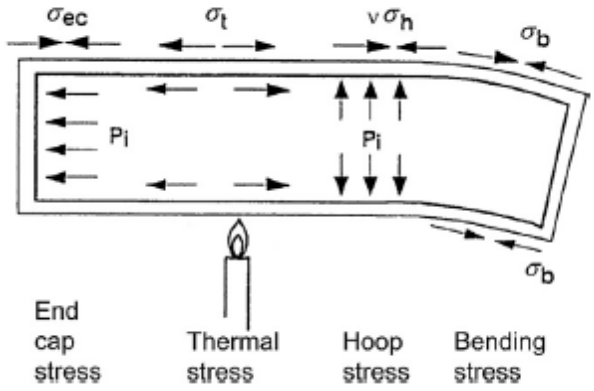

Figure 2.4: Stresses developing in the pipe [Bai & Bai (2014)].

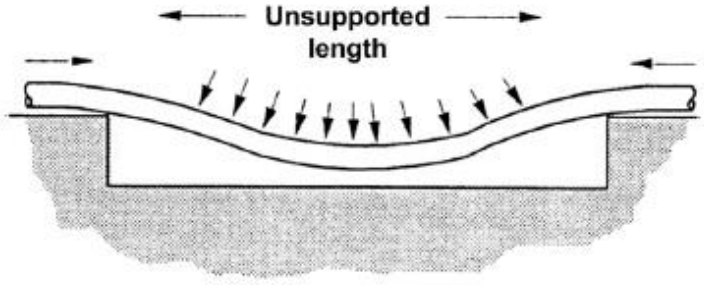

Figure 2.5: Local buckling in the pipeline [Bai & Bai (2014)].

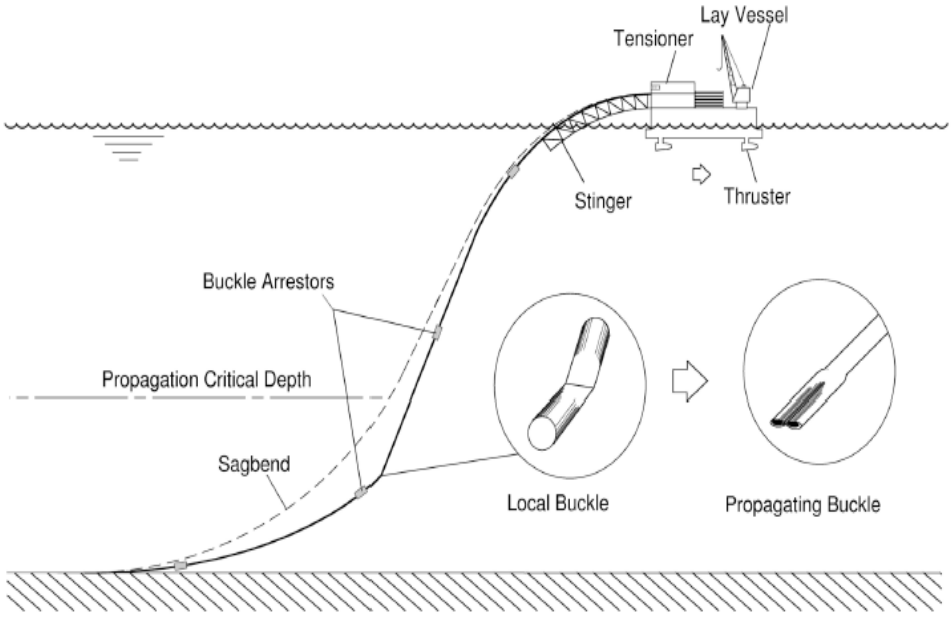

Figure 2.6: Schematic representation of the initiation of a propagating buckle in a pipeline [Lee (2007)].

2.2.2 American Petroleum Institute (API)

The American Petroleum Institute [API (1999)] design criteria for pipelines are based on the limit state design approach. The API (1999) criteria provide a more detailed design approach as compared to the ABS (2001) and consider the following modes of failure:

- Burst due to net internal pressure.
- Combined bending and tension during installation and operation.
- Collapse due to external pressure, with the pipe being either empty or filled.
- Buckling and collapse due to combined bending and external pressure.
- Pipeline stability against horizontal and vertical displacements during construction and operation.
- Effects of thermal expansion and contraction.
- In-place and in-service pipeline repair capabilities.
- Fatigue due to hydrodynamic and operational loading.

2.2.2.1 Internal pressure (Burst) Design

The hydrostatic test pressure (difference between internal and external pressure), or the pipeline design pressure, and the incidental overpressure (internal minus external pressure), including both internal and external pressures acting on the pipelines, should satisfy the formulae given by Eq. (2.10) to Eq. (2.12)

$$P_t \leq f_d f_e f_t P_b \qquad \text{Eq. (2.10)}$$

$$P_d \leq 0.8 P_t, \qquad \text{Eq. (2.11)}$$

$$P_a \leq 0.9 P_t \qquad \text{Eq. (2.12)}$$

where:
- P_t : hydrostatic test pressure in N/mm^2 (psi)
- P_b : specified minimum burst pressure of pipe in N/mm^2 (psi)
- P_d : pipeline design pressure in N/mm^2 (psi)
- P_a : incidental overpressure in N/mm^2 (psi)
- f_d : internal pressure (burst) design factor (0.9 for pipelines)
- f_e : weld joint factor (see Table 2.4)
- f_t : temperature de-rating factor (see Table 2.3)

The specified minimum burst pressure (P_b) is found by either Eq. (2.13) or Eq. (2.14)

$$P_b = 0.45\ (S+U)\ \ln\left(\frac{D}{D_i}\right) \qquad \text{Eq. (2.13)}$$

$$P_b = 0.90\ (S+U)\left(\frac{t}{D-t}\right) \qquad \text{Eq. (2.14)}$$

where: D : outside diameter of pipe in mm (in)

D_i : inside diameter of pipe in mm (in) (Di =D-2t)

S : *SMYS* of pipe in N/mm^2 (psi)

t : nominal wall thickness of pipe in mm (in)

U : specified minimum ultimate tensile strength of pipe in N/mm^2 (psi)

Table 2.4: Weld joint factors (f_e) [ASME (2003)].

Specification	**Pipe class**	**f_e**
ASTM A 53	Seamless	1.00
	Electric resistance welded	1.00
	Furnace butt welded	0.60
ASTM A 106	Seamless	1.00
ASTM A 134	Electric fusion arc welded	0.80
ASTM A 135	Electric resistance welded	1.00
ASTM A 139	Electric fusion welded	0.80
ASTM A 211	Spiral welded steel pipe	0.80
ASTM A 333	Seamless	1.00
	Electric resistance welded	1.00
ASTM A 381	Double submerged arc welded	1.00
ASTM A 671	Electric fusion welded (classes 13,23,33,43,53)	0.80
	Electric fusion welded (classes 12,22,32,42,52)	1.00
ASTM A 672	Electric fusion welded (classes 13,23,33,43,53)	0.80
	Electric fusion welded (classes 12,22,32,42,52)	1.00
API 5 L	Seamless	1.00
	Electric resistance welded	1.00
	Electric flash welded	1.00
	Submerged arc welded	1.00
	Furnace butt welded	0.60

2.2.2.2 Longitudinal load design

The static primary longitudinal loads that cause the effective tension should not exceed the value given by Eq. (2.15)

$$T_{eff} \leq 0.6\ T_y \qquad \text{Eq. (2.15)}$$

where: T_{eff} : effective tension in the pipe in N (lb) ($T_{eff} = T_a - P_iA_i + P_oA_o$)

T_a : axial tension in pipe in N (lb) ($T_a = \sigma_a A$)

T_y : yield tension of the pipe in N (lb) ($T_y = SA$)

A : cross-sectional area of pipe in mm^2 (in^2) [$A = A_o - A_i = \frac{\pi}{4}(D^2 - D^2{}_i)$]

A_i : internal cross-sectional area of pipe in mm^2 (in^2)

A_o : external cross-sectional area of pipe in mm^2 (in^2)

P_i : internal pressure in the pipe in N/mm^2 (psi)

P_o : external hydrostatic pressure in N/mm^2 (psi)

σ_a : axial stress in the pipe wall in N/mm^2 (psi)

2.2.2.3 Combined load design

The combination of primary longitudinal load (static and dynamic) and differential pressure load must satisfy Eq. (2.16):

$$\sqrt{\left(\frac{P_i - P_o}{P_b}\right)^2 + \left(\frac{T_{eff}}{T_y}\right)^2} \leq \begin{bmatrix} 0.90 \\ 0.96 \\ 0.96 \end{bmatrix} \begin{bmatrix} \text{For operational loads} \\ \text{For extreme loads} \\ \text{For hydrotest loads} \end{bmatrix} \qquad \text{Eq. (2.16)}$$

where : operational loads : loads that may occur during normal operation of the pipeline.

extreme loads : loads those are unlikely to be exceeded during the lifetime of the pipeline.

2.2.2.4 External pressure collapse

During the construction and operation of the subsea pipes, a situation may occur when the external pressure exceeds the internal pressure. The differential pressure acting on

the pipe wall due to hydrostatic head may cause collapse of the pipe. The relationship between the collapse pressure and the external pressure is given by Eq. (2.17)

$$P_o - P_i \leq f_o P_c \qquad \text{Eq. (2.17)}$$

where: f_o : collapse factor; 0.7 for seamless or Electric Resistance Welding (ERW) pipe, 0.6 for cold expanded pipe such as Double Submerged Arc Welded (DSAW) pipe

P_c : collapse pressure of the pipe in N/mm^2 (psi)

The collapse pressure can be calculated by Eq. (2.18)

$$P_c = \left(\frac{P_y . P_e}{\sqrt{P_y{}^2 + P_e{}^2}} \right) \qquad \text{Eq. (2.18)}$$

where: E : modulus of elasticity in N/mm^2 (psi)

P_e : elastic collapse pressure of the pipe in N/mm^2 (psi)

$$\left[P_e = 2 \cdot E \frac{\left(\frac{t}{D}\right)^3}{(1-\upsilon^2)} \right]$$

P_y : yield pressure at collapse in N/mm^2 (psi) $\left[P_y = 2 \cdot S \cdot \left(\frac{t}{D}\right) \right]$

Υ : Poisson's ratio (0.3 for steel)

The combined bending strain and external pressure load should satisfy Eq. (2.19)

$$\left(\frac{\varepsilon}{\varepsilon_b}\right) + \frac{p_o - p_i}{p_c} \leq g(\delta) \qquad \text{Eq. (2.19)}$$

The bending strains should be limited as per Eq. (2.20) and Eq. (2.21) to avoid buckling

$$\varepsilon \geq f_1 \varepsilon_1 \qquad \text{Eq. (2.20)}$$

$$\varepsilon \geq f_2 \varepsilon_2 \qquad \text{Eq. (2.21)}$$

where: ε : bending strain in the pipe

ε_b : buckling strain under pure bending $\left[\varepsilon_b = \left(\frac{t}{2D}\right) \right]$

ε_1 : maximum installation bending strain

ε_2 : maximum in-place bending strain

f_1 : bending safety factor for installation bending plus external pressure

f_2 : bending safety factor for in-place bending plus external pressure

$g(\delta)$: collapse reduction factor [$g(\delta) = (1+20\,\delta)-1$]

δ : ovality $\left[\delta = \left(\frac{D_{max} - D_{min}}{D_{max} + D_{min}}\right)\right]$

D_{max} : maximum diameter at any given cross section in mm (in)

D_{min} : minimum diameter at any given cross section in mm (in)

2.2.3 Det Norske Veritas (DNV)

According to the limit state design of Det Norske Veritas [DNV (2012)], the pipeline is checked for all relevant failure modes. The failure modes may vary in importance and can be divided into the following two categories:

- Serviceability limit state (associated with normal operation conditions for e.g. dent, ovalisation, ratcheting)
- Ultimate limit state (associated with extreme loading conditions that can cause failure such as bursting, fracture etc.)

The ultimate limit state is further divided into two sub-categories which account for accumulated cyclic loading effect and accidental loads respectively:

– Fatigue limit state

– Accidental limit state (The design against accidental loads may be performed by direct calculation of the effects imposed by the loads on the structure, or indirectly, by design of the structure as tolerable to accidents).

2.2.3.1 Pressure containment (bursting)

The pressure containment should satisfy the conditions analytically expressed by Eq. (2.22) and Eq. (2.23)

$$p_{li} - p_e \leq \text{Min}\left[\frac{p_b(t_1)}{\gamma_m \gamma_{SC}}, \frac{p_{lt}}{\alpha_{spt}} - p_e, \frac{p_h}{\alpha_{mpt}\alpha_U}\right] \qquad \text{Eq. (2.22)}$$

$$p_{li} - p_e \leq \text{Min}\left[\frac{p_b(t_1)}{\gamma_m \gamma_{SC}}, p_h\right] \quad \text{Eq. (2.23)}$$

where: p_{li} : local incidental pressure

p_b : pressure containment resistance

p_{lt} : local test pressure

p_h : mill test pressure

p_e : external pressure

t_1 : minimum wall thickness (where failure is likely to occur in connection with a low capacity)

γ_m : material resistance factor

γ_{SC} : safety class resistance factor

α_{spt} : system pressure test factor

α_{mpt} : mill pressure test factor

α_U : material strength factor

The pressure containment resistance [$p_b(t)$] is given by Eq. (2.24):

$$p_b(t) = \frac{2t}{D - t} f_{cb} \frac{2}{\sqrt{3}} \quad \text{Eq. (2.24)}$$

where: f_{cb} : $\min\left[f_y, \frac{f_u}{1.15}\right]$

f_y : yield stress to be use in design

f_u : tensile strength to be use in design

2.2.3.2 Local buckling

The external pressure at any point along the pipeline is satisfied using Eq. (2.25)

$$p_e - p_{min} \leq \left[\frac{p_c(t_1)}{\gamma_m \gamma_{SC}}\right] \quad \text{Eq. (2.25)}$$

where: p_{min} : minimum internal pressure that can be sustained. This is normally taken as zero for laid pipelines.

P_c : characteristic collapse pressure, Eq. (2.8)

2.2.3.3 Combined loading criteria

The combined loading criterion is divided into two different conditions:

- Load control: The structural response is governed by imposed loads.
- Displacement control: The structural response is governed by imposed geometric displacements.

Eq. (2.26) and Eq. (2.27) gives the load control design criteria for pipe members subjected to bending moment, effective axial force and internal overpressure, whereas Eq. (2.28) and Eq. (2.29) gives the displacement control design criteria for same conditions:

$$\left[\gamma_m\gamma_{SC}\frac{|M_{Sd}|}{\alpha_c M_p(t_2)}+\left[\frac{\gamma_m\gamma_{SC}S_{sd}(p_i)}{\alpha_c S_p(t_2)}\right]^2\right]^2+\left[\alpha_p\frac{p_i-p_e}{\alpha_c p_b(t_2)}\right]^2\le 1 \qquad \text{Eq. (2.26)}$$

$$\left[\gamma_m\gamma_{SC}\frac{|M_{Sd}|}{\alpha_c M_p(t_2)}+\left[\frac{\gamma_m\gamma_{SC}S_{sd}}{\alpha_c S_p(t_2)}\right]^2\right]^2+\left[\gamma_m\gamma_{SC}\frac{p_e-p_{min}}{p_c(t_2)}\right]^2\le 1 \qquad \text{Eq. (2.27)}$$

Eq. (2.26) is applicable for $15 \le D/t_2 \le 45$, $P_i > P_e$ and $|S_{sd}|/S_p < 0.4$ and Eq. (2.27) for $15 \le D/t_2 \le 45$, $P_i < P_e$ and $|S_{sd}|/S_p < 0.4$

$$\epsilon_{Sd} \le \epsilon_{Rd} = \frac{\epsilon_c(t_2, p_{min}-p_e)}{\gamma_\epsilon}$$

$$= \frac{0.78\left(\frac{t}{D}-.01\right)\left(1+5.75\frac{p_{min}-p_e}{p_b(t)}\right)\left[\left(\frac{R_{t\,0,5}}{R_m}\right)_{max}\right]^{-1.5}\alpha_{gw}}{\gamma_\epsilon} \qquad \text{Eq. (2.28)}$$

$$\left(\frac{\epsilon_{Sd}}{\frac{\epsilon_c(t_2,0)}{\gamma_\epsilon}}\right)^{0.8}+\frac{p_e-p_{min}}{\frac{p_c(t_2)}{\gamma_m\gamma_{SC}}}\le 1 \qquad \text{Eq. (2.29)}$$

Eq. (2.28) is applicable for $D/t_2 \leq 45$, $P_i \geq P_e$ and Eq. (2.29) is applicable for $D/t_2 < 45$, $P_{min} < P_e$.

where:

M_{Sd}	:	design moment ($M_{Sd} = M_f\gamma_f\gamma_c + M_E\gamma_E + M_I\gamma_f\gamma_c + M_A\gamma_A\gamma_c$)
S_{Sd}	:	design axial force ($S_{Sd} = S_f\gamma_f\gamma_c + S_E\gamma_E + S_I\gamma_f\gamma_c + S_A\gamma_A\gamma_c$)
ϵ_{Sd}	:	design compressive strain ($\epsilon_{Sd} = \epsilon_f\gamma_f\gamma_c + \epsilon_E\gamma_E + \epsilon_I\gamma_f\gamma_c + \epsilon_A\gamma_A\gamma_c$)
P_i	:	internal pressure
S_p	:	plastic capacity of pipe [$S_p(t) = f_y\pi\,(D - t)t$]
M_p	:	plastic moment [$M_p(t) = f_y\ (D - t)^2 t$]
α_c	:	flow stress parameter [$\alpha_c = (1 - \beta) + \beta(\frac{f_u}{f_y})$]
α_p	:	pressure factor $\left[\begin{matrix}\alpha_p = (1-\beta) & \text{for } \frac{p_i - p_e}{p_b} < \frac{2}{3}, \\ \alpha_p = 1 - 3\beta\left(1 - \frac{p_i - p_e}{p_b}\right) & \text{for } \frac{p_i - p_e}{p_b} \geq \frac{2}{3}\end{matrix}\right]$
B	:	factor used for combined loading $\left[\beta = \frac{60 - \frac{D}{t_2}}{90}\right]$
γ_c	:	condition load effect factor
$\gamma_f, \gamma_E, \gamma_A$	:	load effect factor for functional, environmental and accidental loads respectively
M_f, M_E, M_I, M_A	:	moment for functional, environmental, interface and accidental loads respectively
$\epsilon_f, \epsilon_E, \epsilon_I, \epsilon_A$	:	strain for functional, environmental, interface and accidental loads respectively
$\frac{R_{t\,0,5}}{R_m}$	:	depending on *SMYS*, ratio of yield to tensile strength
α_{gw}	:	Girth weld factor
t_2	:	Pipe wall thickness (where failure is likely to occur in connection with an extreme load effect at a location with average thickness)

2.2.4 Parameters associated with the design of pipes

Based on the review of the available design codes presented in the previous section it can be observed that various design criteria are associated with static loading. Thus it is important to investigate the effect of loading rate on the behaviour of the steel pipes in order to assess to what extent the dynamic nature of the problem at hand may affect the design process and the behaviour of the pipes. It is also important to note that the parameters such as (i) hoop stress (ii) axial stress (iii) development of the internal and external pressure can significantly influence the design criteria. As a result it is logical to assume that such parameters can affect the *in-situ* behaviour of the subsea pipes during operation when subjected to impact. Therefore it is important to assess in detail the effect of various parameters such as (i) material properties of steel, (ii) geometry of the considered pipe, (iii) mass, shape and velocity of the impacting object, (iv) boundary conditions imposed onto the pipe (i.e. the properties of the supporting soil, the end-conditions), (v) internal and external pressures developing on the walls of the pipe and (vi) the level of imposed axial loading on the *in-situ* behaviour of subsea pipes under impact loading.

2.3 ASSESSMENT OF SUBSEA PIPES SUBJECTED TO IMPACTS

In order to assess the level of damage sustained by pipes due to accidental collisions with fishing equipment (e.g. anchors and trawl gear) DNV-RP-F111 [DNV (2010a)] divides the subject impact problem into two main stages: (i) the initial impact stage and (ii) the pull over stage. A third special hooking stage may also be rarely considered.

The initial impact stage occurs when trawl-fishing equipment [e.g. trawl board, beam shoe or clump weight (see Figure 2.1)] collide with the pipeline. This stage is characterized by a very short duration (few milliseconds) and the generation of high intensity (impact) loads. The impact force at this stage is resisted mainly locally by the walls of the pipes in combination with additional stiffness provided by any protective coating surrounding the pipes or any attached electric cables (such cables may be attached externally to the pipes). This is followed by a stage during which the fishing equipment may be dragged over the pipeline. This stage is referred to as the pull-over stage. Depending on the water depth, span height (pipeline to sea-bed distance) and

other factors (e.g. effective axial force, axial restraints etc.) the latter stage may last from about 1 to 10 seconds usually resulting in the global response of the pipeline. In the rare case where the trawl equipment is tangled with or hooked on to the pipeline (hooking stage) the pipeline structural integrity has to be considered for hooking loads. During this third and final stage the most extreme condition can result in the vertical lifting of the pipeline until either the trawl gear is loose or the capacity of the lifting wire is reached which may result in the pipe sustaining further damage. From the latter 3 stages, described above, high rate (impact) loading is relevant only to the 1st stage (initial impact stage) whereas in the latter two stages (pull-over stage and hooking stage) the generated loads are characterised by considerably lower loading rates which should be considered essentially static in nature. Furthermore, the response in the latter two stages is dependent on the level of damage sustained during the initial stage.

According to DNV-RP-F111 [DNV (2010a)] the predictions of the behaviour of steel pipes under impact loading can be achieved in practice either by adopting simple conservative methods or by employing more advanced analysis methods which are discussed in the following sections.

2.3.1 Simplified assessment method adopted in practice

The simplified method [DNV (2010a)] adopted in practice for assessing the behaviour of steel pipes (i.e. bare pipes, pipes with concrete coating) under impact loading is based on the assumption that all impact energy is essentially absorbed locally by the pipe due to deformation of its cross-section at the area of impact. Global response is indirectly considered through the use of the correction factors shown in Figure 2.7 (a).

The impact energy associated with the steel mass of the trawl board is given by Eq. (2.30) [DNV (2010a)]:

$$E_s = R_{fs}\frac{1}{2} m_t (C_h V)^2 \qquad \text{Eq. (2.30)}$$

where: m_t : trawl board steel mass

R_{fs} : reduction factor depending on the outer diameter [see Figure 2.7 (b)].

C_h : span height correction factor for the effective pull over velocity [see

Figure 2.7 (b)]

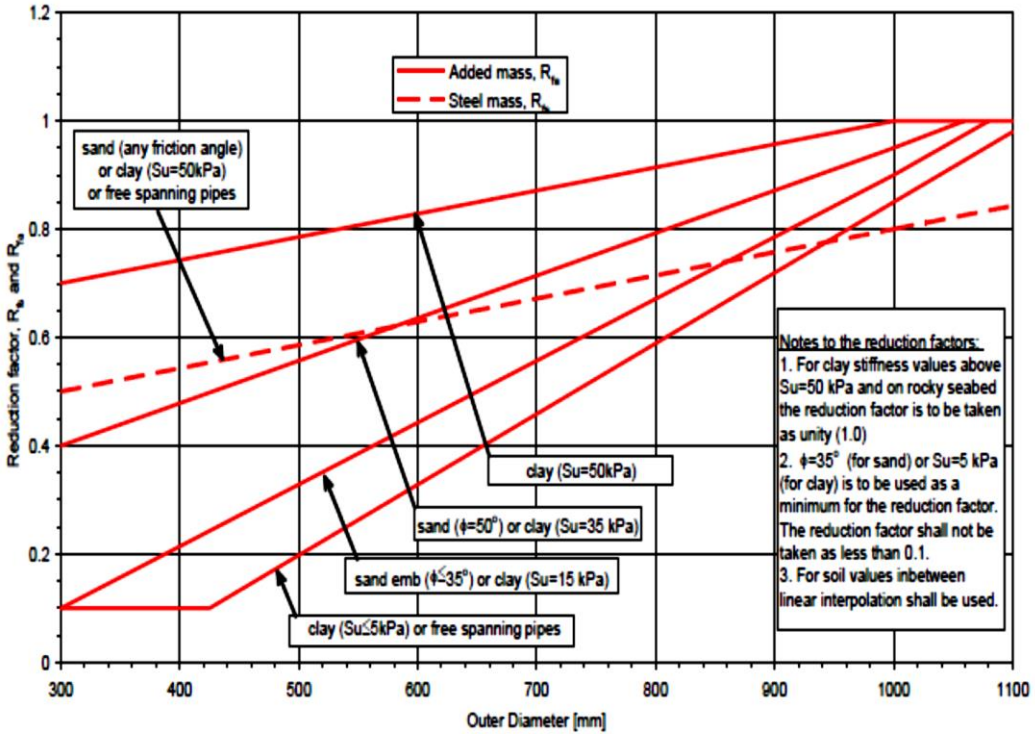

(a)

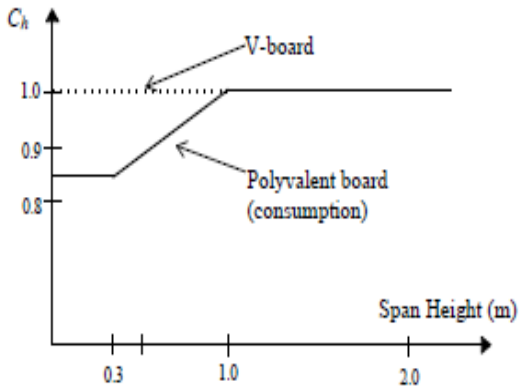

(b)

Figure 2.7: (a) Reduction factors employed for considering the global response (b) C_h coefficient for accounting effect of span height on impact velocity [DNV (2010a)].

The impact energy and impact force associated with the hydrodynamic added mass of the trawl board is given by Eq. (2.31) and Eq. (2.32) [DNV (2010a)] respectively.

$$E_a = R_{fa}\frac{2(F_b)^3}{75\,(f_y)^2(t)^3} \leq 0.5\, m_a(C_h V)^2 \qquad \text{Eq. (2.31)}$$

$$F_b = C_h V\sqrt{m_a k_b} \qquad \text{Eq. (2.32)}$$

where : k_b : lateral bending stiffness of the board

m_a : trawl board added mass

t : steel wall thickness

R_{fa} : reduction factor depending on the outer diameter [see Figure 2.7 (a)]

f_y = $(SMYS - f_{y,temp})\,\alpha_U$, [SMYS as defined in Eq. (2.3)]

$f_{y,temp}$: temperature derating value of yield strength

α_U : material strength factor [α_U = 0.96, except for pipeline material fulfilling supplementary requirements U [DNV (2012)] (α_U = 1.0)]

The impact force (F_{sh}) and associated dent depth (H_t) of a bare steel pipe is given by Eq. (2.33) [DNV (2010a)]:

$$F_{sh} = 5 f_y t^{\frac{3}{2}} H_t^{\frac{1}{2}} \qquad \text{Eq. (2.33)}$$

An estimate of the kinetic energy absorbed by local deformation of the coating and the pipe walls can be provided by taking maximum of E_s [Eq. (2.30)] and E_a [Eq. (2.31)].

The impact energy due to the beam trawls and clump weights absorbed by the pipe and its coatings can be estimated by Eq. (2.34) and Eq. (2.35) [DNV (2010a)] respectively.

$$E_{loc} = R_{fs}\frac{1}{2}\, C_b(m_t + m_a)V^2 \qquad \text{Eq. (2.34)}$$

$$E_{loc} = R_{fs}\frac{1}{2}\, (m_t + m_a)V^2 \qquad \text{Eq. (2.35)}$$

where C_b is a factor taking into account the effective mass (sum of mass of the clump weight and hydrodynamic added mass). C_b may be conservatively taken as 0.5 if a more precise estimation is not available.

In the absence of any relevant information concerning the impact problem, the relationship between the permanent local deformation and impact force of the pipe can be estimated from Eq. (2.36) and Eq. (2.37) [DNV (2010a)] respectively.

$$H_{p,c} = \left(\frac{F_{sh}}{5f_y t^{\frac{3}{2}}}\right)^2 - \left(\frac{F_{sh}\sqrt{0.005\,D}}{5f_y t^{\frac{3}{2}}}\right) \qquad \text{Eq. (2.36)}$$

$$F_{sh} = \left(\frac{75}{2} E_{loc} f_y{}^2\ t^3\right)^{\frac{1}{3}} \qquad \text{Eq. (2.37)}$$

2.3.2 Advanced impact method

More advanced analysis methods are employed for pipes with coatings or pipeline with piggy-back electrical cables (placed within protective structure) where a simplified approach (similar to that described in section 2.3.1) cannot be used in order to obtain the detailed and accurate representation of the dynamic problem at hand. A comprehensive representation of the analysis model employed in practice for the analysis of pipes under impact load due to collision with trawl boards is presented in Figure 2.8. The model comprises of a lumped mass-spring system. The latter model can also be used for assessing the response of pipes when colliding with beam trawls and clump weights by omitting the relevant stiffness and the associated mass of trawl boards. The abbreviations associated with each mass and spring stiffness's of the system presented in Figure 2.8 are defined in Table 2.5.

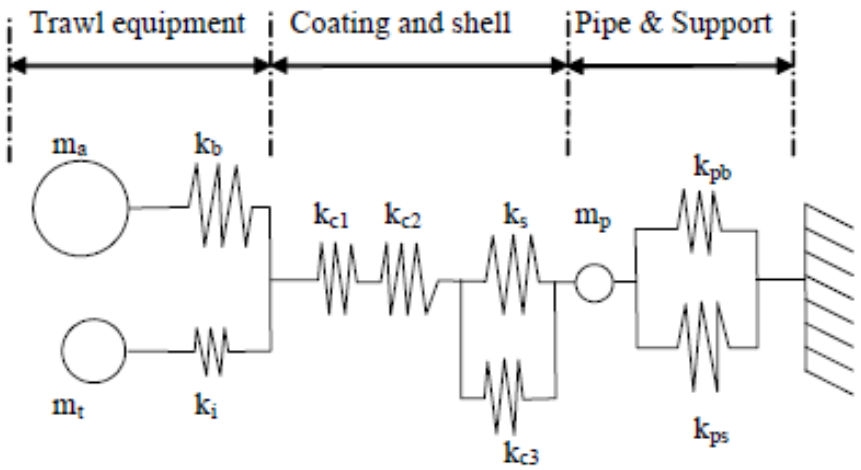

Figure 2.8: Analysis model assembly [DNV (2010a)].

Table 2.5: Symbols and abbreviations used in Figure 2.8.

Symbol	Description
m_a, m_t	Hydrodynamic added mass and steel mass of the trawl gear
k_b, k_i	Out of plane and in plane stiffness of the gear
k_{c1}	Stiffness of the protective cover for heating cable attached to the pipeline
k_{c2}	Stiffness of the coating
k_{c3}	Possible effect it has on the steel shell stiffness by distributing the impact force over a large area by shear deformations in the coatings
k_s	Local stiffness of the steel pipeline
m_p	Effective mass of the pipe, including hydrodynamic added mass
k_{pb}	Effective bending stiffness of the pipe
k_{pb}	Effective soil stiffness of the pipe

The local stiffness of the steel pipe (k_s) can be determined through the use of finite element static analysis (see step 1 & 2 in Figure 2.9). Alternatively, it can also be estimated using Eq. (2.36) [DNV (2010a)] or Eq. (2.38) [STATOIL (1996)]

$$\delta = \left(\frac{1}{25\sigma_y{}^2 t^3}\right) F^2 \qquad \text{Eq. (2.38)}$$

where: δ : deformation of the steel pipe

F : impact force between trawl board and steel pipe

σ_y : yield stress of steel pipe

Finite element analyses with non-linear beam elements employed to model the pipe can also be used for studying the behaviour of pipe under trawl board collision (see step 3 in Figure 2.9). The local stiffness of the steel pipe and its insulation coating are modelled using non-linear spring elements capable of resisting compressive forces only. The non-linear dynamic analysis is carried out based on the assumption that at the time of impact with the pipe the added mass of the trawl board has an initial velocity. It is important that sufficient length of the pipeline must be used so that the results are not influenced by the end effects. Based on the predictions of the finite element model, the displacement time histories for certain point in steel pipe and coating and the develop

impact force between the trawl board and the pipelines can be predicted (see step 4 in Figure 2.9).

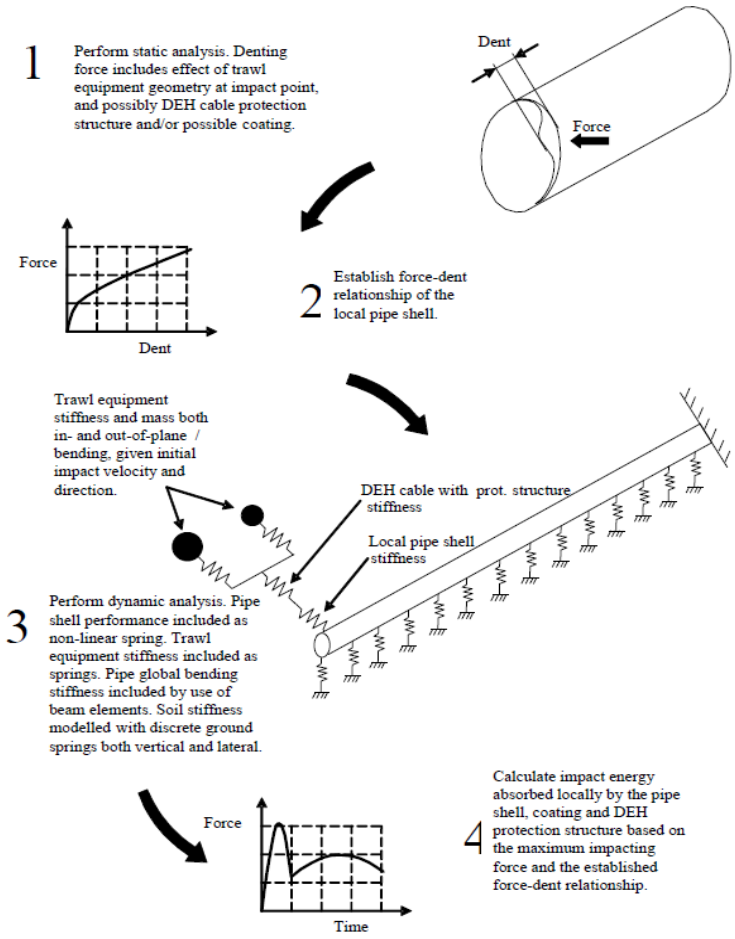

Figure 2.9: Scheme for simulating collision of trawl equipment onto the pipes with coating and Direct Electrical Heating (DEH) protection structure under impact load [DNV (2010a)].

2.3.3 Limitation of assessment approaches

Although both the simplified assessment methods and advanced analysis procedure can be used to form practical tools for predicting the damage sustained by the steel pipes under impact, however, such methods do not provide an accurate representation of the problem at hand. The simplified assessment method assumes that energy during impact is absorbed locally and the effect of global response and soil conditions may be considered through the use of correction factors. The advance analysis model, which comprised of the lumped mass spring systems, depends largely on the values of mass

and spring stiffness's which are used to create an approximate model of the system. Furthermore these models do not consider the combined action of other parameters such as the imposed axial load and the development of internal and external pressure on the impact behaviour of the pipe and therefore may provide conservative and un-conservative predictions. On the other hand the use of quasi-static *FE* models that do not account for the nature of the problem at hand (a wave propagation problem within a non-linear medium) can affect the accuracy of the predictions obtained as they essentially ignore the effect of the inertia forces developing both locally at the impact area and globally due to the deformation of the pipe.

2.4 IMPACT (DROP WEIGTH) TESTING

Drop weight hammer testing facilities are often used to study various important aspects of the dynamic behaviour exhibited by steel pipes under impact loading. These aspects include the time histories of the generated contact force and the displacement of certain points along the span of the pipe, the level of impact energy, the level of the damage sustained by the pipe, the deformation profile of the pipe (before and after impact) etc. Recommended practice for assessment of pipelines in DNV-RP-F107 [DNV (2010b)] gives the testing profile for establishing the impact performance [see Figure 2.10]. It is suggested [DNV (2010b)] that the impactors employed in such tests have a mass of 1tonne and its contact with the pipe can consist of a rectangular plate with a length of 300mm and width of 50mm with a conical shape and an edge radius of 7mm. For this purpose curved shape [Figure 2.11 (a)] and sharp shape [see Figure 2.11 (b)] impactors can be used or alternatively impactor(s) having shapes similar to the falling object if this is known. Although in practice (tests conducted for industry) no instrumentation is specified [DNV (2010b)] since only the measurement of permanent displacement (post-test) is required, however, in order to study in detail the response of the pipes under impact load, the load, displacement and velocity-time histories can be measured using dynamic load cells, high-speed high-resolution video recording, laser tracking, accelerometer, Linear Variable Differential Transformer (LVDTs) and strain gauges. The detailed response obtained from these test results can be used for validating the predictions obtained from *NLFEA* allowing for the development of more complex

numerical models based on the finite element method capable of representing more realistically the problem at hand.

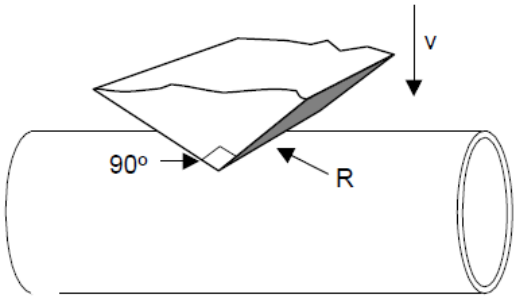

Figure 2.10: Test profile for estimating the impact capacity [DNV (2010b)].

(a) (b)

Figure 2.11: Impactor shapes (a) curved shape (b) sharp shape [DNV (2010a)].

DNV-RP-F107 [DNV (2010b)] classifies the level of damage sustained by pipelines into the following three categories:

- Minor damage (D1): A reduction of the pipes diameter by up to 5% which does not require repair and does not result in any release of hydrocarbons.
- Moderate damage (D2): A damage (dent in the steel pipe over 5% of the diameter) requiring repair but not resulting in any release of hydrocarbons.
- Major damage (D3): Damage which may result in release of hydrocarbons, which is further classified as:
  - No release of hydrocarbons (R0).

- Small release (R1): Release of hydrocarbons from small to medium holes (due to punctures) in the pipe wall (<80mm diameter).
- Major release (R2): Release of hydrocarbons from ruptured pipelines.

2.5 EXPERIMENTAL STUDIES

In order to measure in detail the various important aspects of the dynamic response of steel pipes drop weight tests are often conducted. These tests focus on studying certain important aspects of the behaviour exhibited by the pipe specimens which include: (i) imposed load (contact forces, reaction forces), (ii) velocity and (iii) displacement time histories. For this purpose a combination of conventional instrumentation (load cells, deflection transducers, accelerometers and strain gauges) and high-speed high-resolution video cameras are used. The experimental study of the dynamic response of pipe specimens under impact loading is usually characterized by significant difficulties associated with the short duration of these tests (a few milliseconds) and the high intensity of the generated loads (which are significantly higher than the loads recorded during static testing) which increases rapidly from zero to a maximum value. The experimental setups employed in the majority of tests conducted to date do not account for a range of parameters associated with the subsea conditions to which the pipe may be subjected to. Such conditions include: (i) the sea-bed properties, (ii) the development of internal and external pressure on the pipe walls and (iii) the application of axial loads. Usually scaled specimen, with smaller lengths and cross-sections compared to those of the pipes used by the industry in practice, are used in drop-weight tests. Although the majority of published tests conducted to date are not fully representative of the problem at hand, the obtained test data provide useful information concerning the response of such elements in relation to that established under equivalent static loading. Furthermore, the obtained test data can be used for validating the predictions acquired from *NLFEA*, allowing for the development of more intricate *NLFEA* models capable of representing more accurately the problem at hand by accounting for the effect of various parameters which are likely to affect the *in-situ* behaviour of subsea pipes under operational conditions.

Data describing the dynamic response of typical pipe-specimens subjected to drop-weight testing were reported by Jones *et al.* (1992). The latter study reported the data obtained from 130 impact tests on mild steel pipes-specimens with varying spans and

cross-sections. Seven different diameter (22mm, 42mm, 60mm, 80mm, 120mm and 324mm) pipes were used. Table 2.6 provides a summary of the main parameters associated with the geometry of the specimen used in the experimental investigation. Each pipe was supported at its ends through the use of clamps. A wedge-shape impactor was allowed to drop onto the pipe at three locations: (i) the mid-span (ii) the quarter-span, and (iii) near to the support of the pipe. The velocity of the impactor prior to impact varied from 6.2m/s to 14.0m/s. Figure 2.12 and Figure 2.13 show the time history of the (i) deflection, (ii) velocity and (iii) contact force-time recorded when testing 22mm and 42mm diameter pipes when subjected to loads with impact energies of 294J and 863J respectively at their mid-span region.

Table 2.6 : Details of the test specimens [Jones *et al.* (1992)].

Series code	**Span length (*2L*), mm**	**Diameter (*D*), mm**	**Thickness (*H*), mm**	***D/H***	***2L/D***
A	220	22	2	11	10
B	420	42	2	21	10
C	800	80	2	40	10
D	1200	120	2	60	10
E	600	60	2	30	10
F	1195	120	1.925	62.34	9.96
G	3194	324	9.40	34.47	9.86

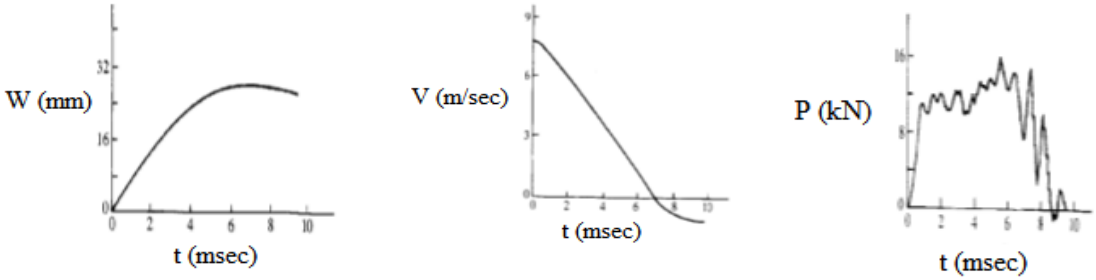

(a) (b) (c)

Figure 2.12: (a) Deflection (b) velocity (c) contact force time histories exhibited by pipe-specimen with a diameter of 22mm [Jones *et al.* (1992)].

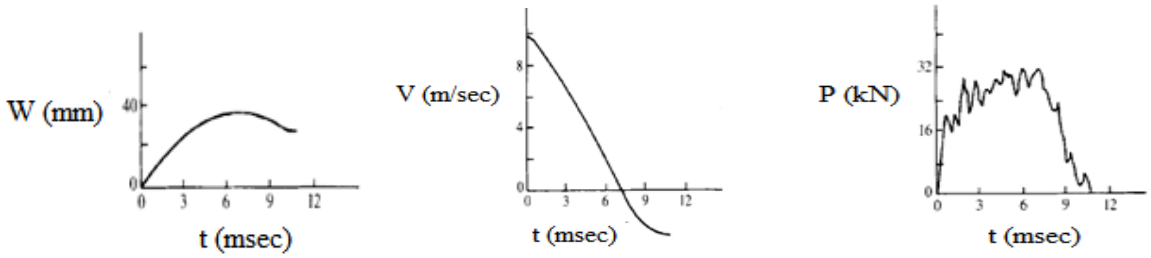

(a) (b) (c)

Figure 2.13: (a) Deflection (b) velocity (c) force-time histories exhibited by pipe specimen with diameter of 42mm [Jones *et al.* (1992)].

The variation of deformation profile exhibited by the specimen during testing is presented in Figure 2.14. This was recorded through the combined use of the high-speed video and laser traces on 120mm diameter pipe subjected to 79.5kg of mass and velocity of 10.84m/s at the mid-span. Based on these observations following three deformation processes were identified:

- Stage 1: This initiates immediately after the specimen and the drop-mass come into contact. During this stage local deformation is observed only in the impact region.
- Stage 2: The specimen begins to exhibit increasingly global deformation as the wave generated during the initial collision moves away from the impact region forcing an increasingly larger portion of the pipe span to respond to the imposed load.
- Stage 3: Elastic recovery is observed after the specimen reaches its maximum deformation and terminates when the impactor separates from the pipe.

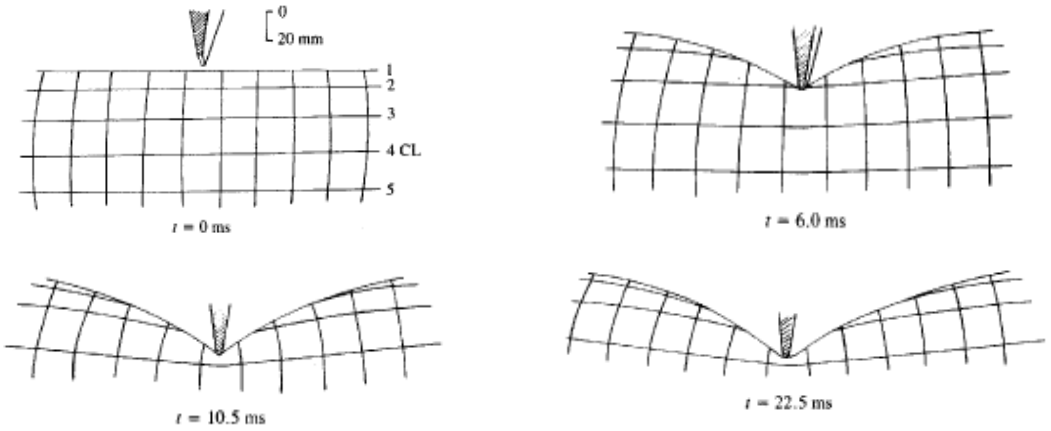

Figure 2.14: Deformation process of 120mm pipe-specimen [Jones *et al.* (1992)].

Figure 2.15 shows the different failure modes observed in the impact tests. These are: (i) Shear sliding on the inside surface of the pipe which is in contact with the edge of a support (Mode 1); (ii) Fracturing of a pipe surface at the support (Mode 2); (iii) Shear sliding at the impact point (Mode 3); (iv) Buckling on the bottom surface of a pipeline near a support (Mode 4).

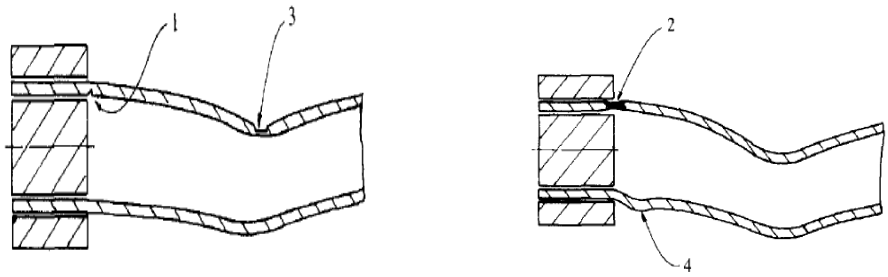

Figure 2.15: Failure modes exhibited by pipe-specimens [Jones *et al.* (1992)].

Figure 2.16 shows the variation between the maximum overall permanent transverse displacement (W_f) of the pipe and the initial kinetic energy (E_k) of the impactor. The results presented in Figure 2.16 are obtained from the tests conducted on pipe specimens with different diameter to thickness ratios (*D/H*) impacted at mid-span. It was observed that for a given pipe diameter, the maximum permanent transverse displacement (W_f) varied almost linearly with the initial kinetic energy (E_k) irrespective of the level of the sustained damage.

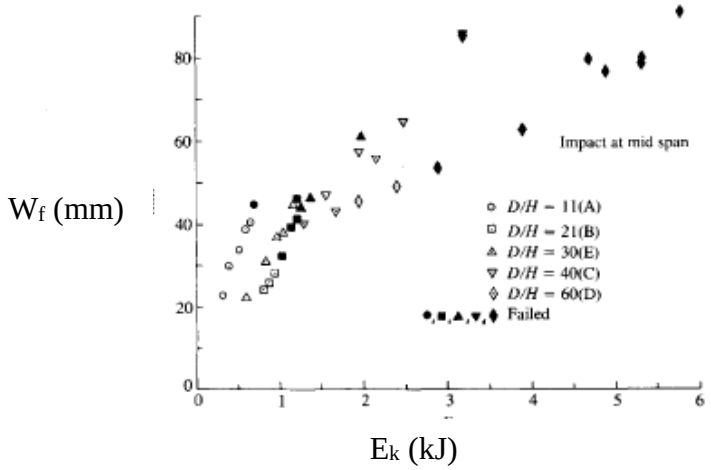

Figure 2.16: Maximum overall permanent transverse displacement (W_f) and initial kinetic energy (E_k) [Jones *et al.* (1992)].

Similar tests were conducted by Ishikawa & Hoshikawa (1994) investigating the behaviour of steel pipes under consecutive impacts. The pipe specimens were assumed fixed at both ends. The impactor was dropped three times onto the pipe at the same location in order to measure the damage sustained after each impact. The tested pipes had a diameter of 89.1mm, a thickness of 3.5mm and a length of 582mm. A spherical impactor, with a mass of 386kg and a diameter of 220mm was dropped onto the pipe with a velocity of 4.4m/s.

Figure 2.17 shows the response of pipes in the form of load-displacement curves. It was observed that for every consecutive impact the intensity of the contact force generated increased whereas the additional displacement (exhibited during each impact) decreased. The curves in Figure 2.18 (a) & (b) describe the relationship between the imposed contact force generated during each drop test and the associated local and global displacement exhibited at the impact region of the pipe specimens. A review of this data revealed that for every consecutive impact the displacement exhibited locally at the area of impact (expressed as the local reduction of diameter) decreased whereas the global displacement increased. This can be attributed to the fact that during the first impact the pipe exhibited localized response which resulted in localized damage being sustained which resulted in local deformation being exhibited. During the second and third impact because of the damage already sustained (from the first impact) locally in the contact region the pipe exhibited mainly global (instead of localized) response.

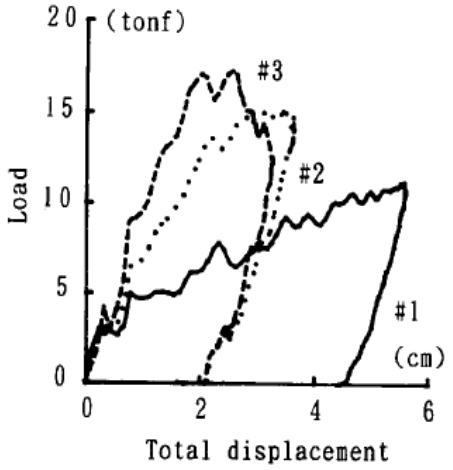

Figure 2.17: Load-displacement curves for consecutive (1st, 2nd and 3rd) impacts [Ishikawa & Hoshikawa (1994)].

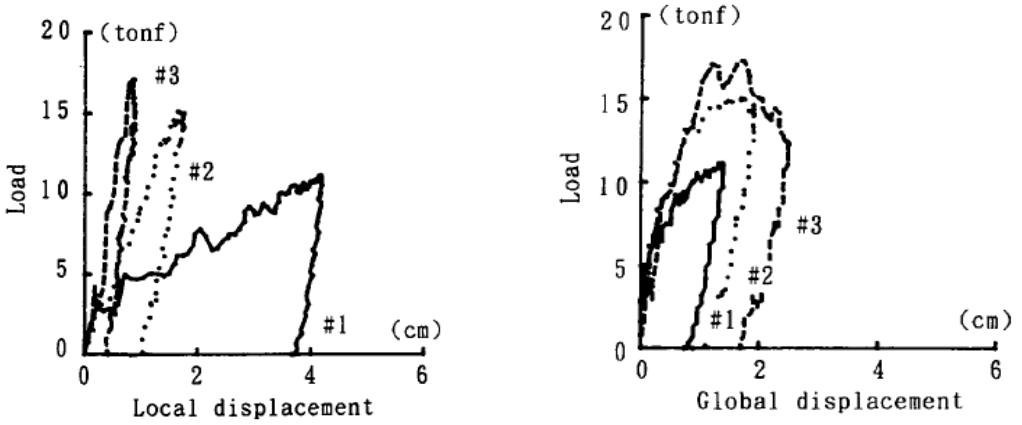

(a) (b)

Figure 2.18: (a) Load-local displacement (b) load-global displacement curves for consecutive (1st, 2nd and 3rd) impacts [Ishikawa & Hoshikawa (1994)].

Jones & Brich (2010) studied the behaviour of pressurized pipe specimens under low velocity impacts. For this purpose, mild steel pipes with a radius of 14.5mm and a thickness of 1mm were used. The pipes were fully clamped at both ends (see Figure 2.19) and pressurized (through the end clamps) with nitrogen gas. Each pipe had a span of 300mm and was struck transversely with a wedge-shape impactor with a mass of 10.75kg and 30mm wide impact face. The impactor was allowed to drop onto the pipe at two locations: (i) the mid-span and (ii) the quarter-span.

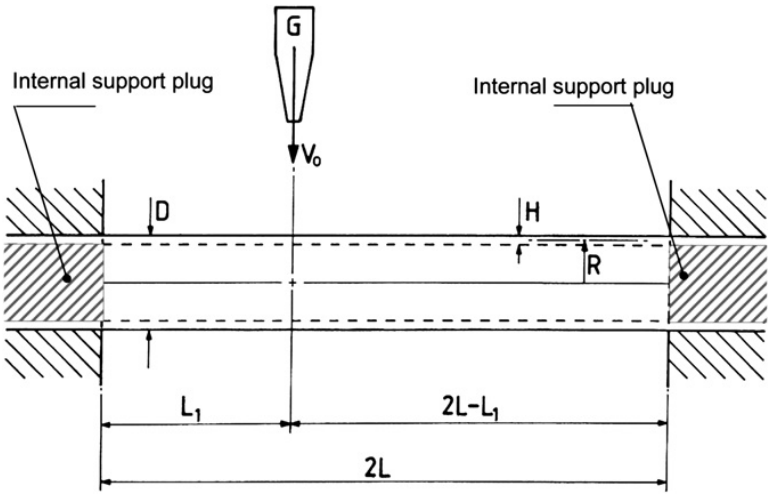

Figure 2.19: Pipe specimen fully clamped at the supports [Jones & Birch (2010)].

Figure 2.20 shows two major failure modes observed during the impact tests:

- Mode 1: Local failure due to the development of local cracking under the striking edge of the wedge-shape impactor.

- Mode 2: Failure occurs near the clamped supports in the pipeline wall which may be catastrophic as it causes sudden release of the internal pressure.

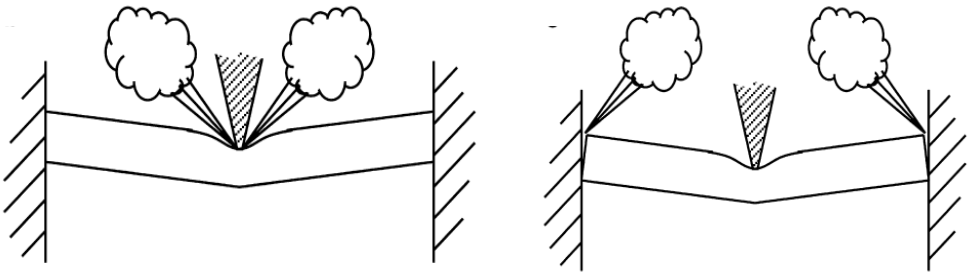

Mode 1 Mode 2

Figure 2.20: Failure modes observed for the case of pressurized pipes [Jones & Birch (2010)].

Table 2.7 and Table 2.8 provide the mode of failure observed under impact tests for the pipes impacted at mid-span and quarter-span respectively. It was found that the pipes tested without internal pressure and with relatively low impact energies (tests B5, B6, B7, B9 in Table 2.7 and Table 2.8) exhibited large Ductile Deformation (**DD**) as shown in Figure 2.21. A similar trend was also observed for pipes with internal pressure and tested with low impact energies (tests B19, B27 in Table 2.7) however the pipes subjected to higher impact energies resulted in failure being exhibited close to the clamped supports (Mode 2) which in turn resulted in the release of gas.

It is interesting to observe that for the case of a pipe impacted with the same velocities (tests B5, B23 in Table 2.7) the level of internal pressure affected the exhibited mode of failure. Pipes (test B5) without internal pressure exhibited large ductile deformations both locally and globally, however, in the case of pipes subjected to internal pressure (test B23) failure was observed near the clamped supports (Mode 2). Thus, it can be concluded that the presence of pressure inside the pipe affected the mode of failure exhibited resulting in failure being exhibited close to the supports and the release of gas.

Table 2.7: Impact test results for pipes impacted at mid span [Jones & Birch (2010)].

Test	Pressure (MPa)	Initial velocity (m/s)	Failure mode
B4	0	9.36	MODE 2
B5	0	8.10	DUCTILE DEFROMATION
B6	0	8.74	DUCTILE DEFROMATION
B7	0	9.04	DUCTILE DEFROMATION
B18	10	9.34	MODE 2 with both ends shearing off
B19	10	8.10	DUCTILE DEFROMATION
B20	10	8.74	MODE 2
B21	10	8.43	MODE 2
B23	15	8.10	MODE 2
B24	15	8.74	MODE 2
B26	15	8.43	MODE 2
B27	15	7.75	DUCTILE DEFROMATION

Table 2.8: Impact test results for pipes impacted at quarter span [Jones & Birch (2010)].

Test	Pressure (Mpa)	Initial velocity (m/s)	Failure mode
B8	0	9.34	MODE 2
B9	0	8.08	DUCTILE DEFROMATION
B10	0	10.43	MODE 1 & 2
B13	10	8.10	MODE 2 with both ends shearing off
B14	10	10.43	MODE 2 with both ends shearing off
B15	15	9.34	MODE 2 with both ends shearing off
B16	15	10.43	MODE 2 with both ends shearing off
B17	15	8.10	MODE 2 with both ends shearing off

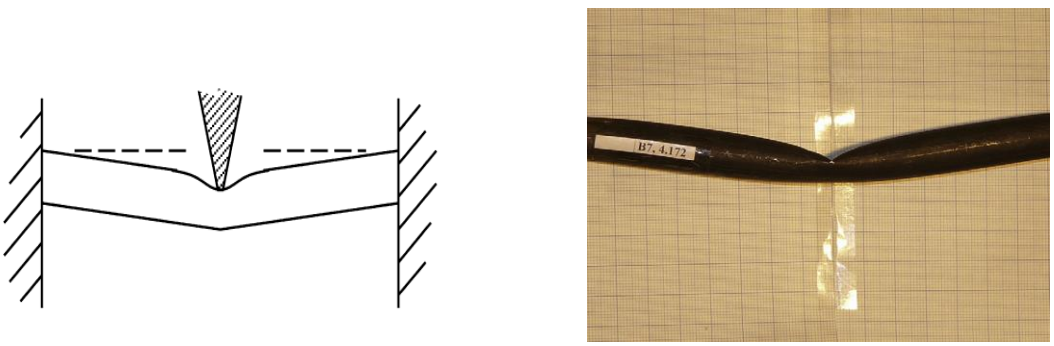

Figure 2.21: Large Ductile Deformation (DD) [Jones & Birch (2010)].

The failure mechanism of the pressurized and unpressurized pipes subjected to transverse impact load was also studied experimentally by Chen & Shen (1998). The pipes were suspended and considered fully clamped at both ends. They were subjected to impact *via* a rigid wedge-shaped impactor allowed to fall from a certain height onto the mid-span, quarter-span and adjacent to the supports (see Figure 2.22).

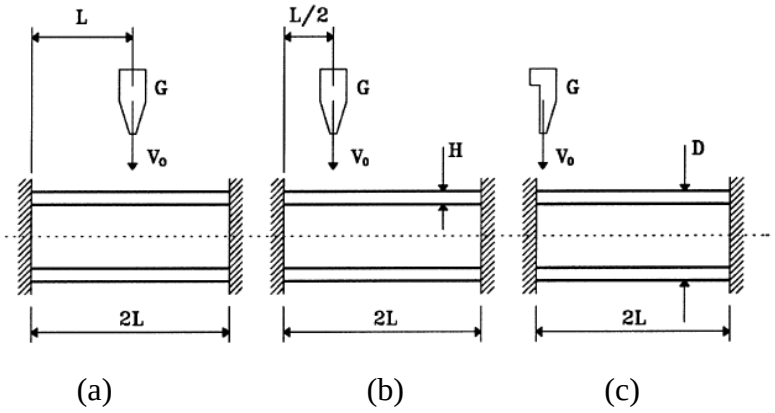

Figure 2.22: Drop weight tests conducted at (a) mid-span (b) quarter-span and (c) near the supports of the pipe specimens [Chen & Shen (1998)].

Figure 2.23 shows the impactors used in the experimental study which had cylindrical surface with a radius of 7mm. The mass of the impactors varied between 23kg and 48.7kg and the velocity with which they collided onto the pipes varied from 1.39m/s to 10.69m/s. A total of 226 impact tests were conducted on pipe specimens with different cross-sections and levels of internal pressure. The pipes used in the tests had an outer diameters of 19mm, 38mm, 57mm and 76mm, and a wall thicknesses of 0.9mm, 1.2mm and 1.6mm. The length (2L) to diameter (D) ratio (2L/D) of the pipes was 8.4, 9.5 and 10.6. Four different levels of internal pressure were used: 8.62MPa, 12.41MPa, 15.52MPa and 19.31MPa and were achieved using water.

Figure 2.24 shows the failure modes observed during the impact tests which were similar to those recorded by Jones *et al.* (1992). The three failure modes observed are:

- Mode I: Shear sliding at the impact point.
- Mode II: Buckling of the bottom surface of the pipe near the ends (supports).
- Mode III: Tensile tearing (fracturing) on the top surface of the pipe near the ends (supports).

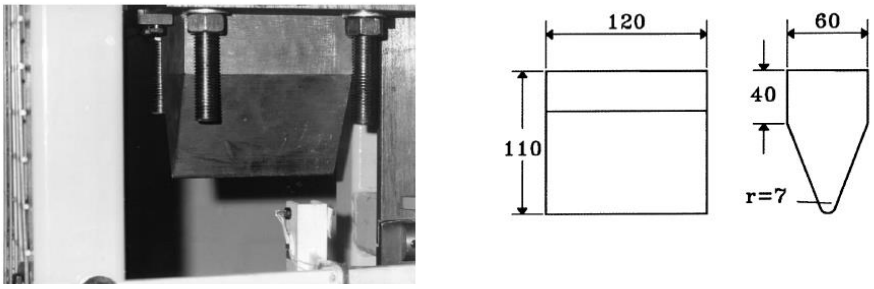

(a)

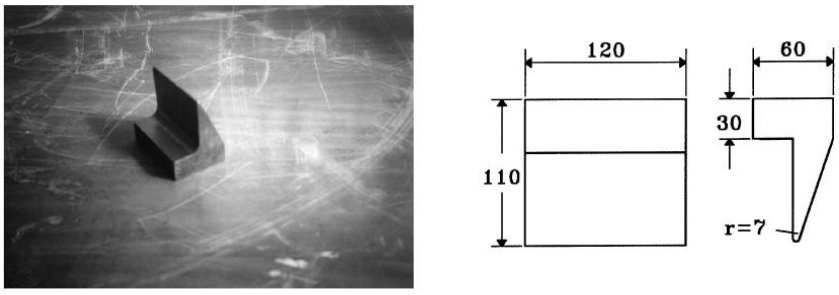

(b)

Figure 2.23: Impactors used for conducting drop weight tests at (a) mid-span and quarter-span (b) adjacent to a support [Chen & Shen (1998)].

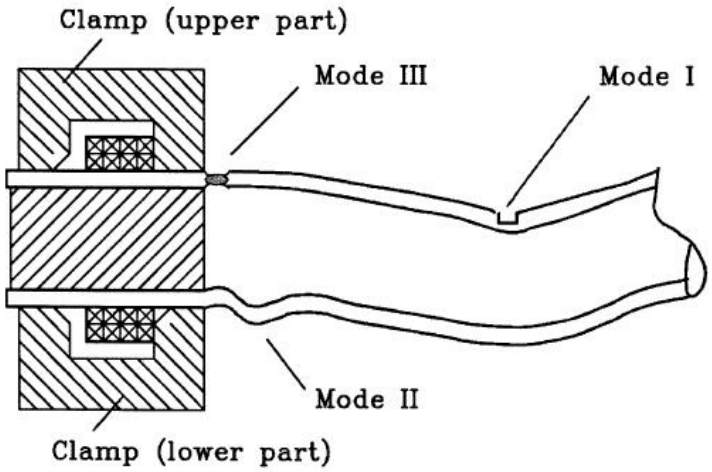

Figure 2.24: Failure modes exhibited by pipe specimens [Chen & Shen (1998)].

Figure 2.25 shows the impact force time history for the typical impact test. It was observed that the impact force increased quickly (within a period of 2-3ms) at the start of the impact and after attaining its peak value gradually decreased to zero when the impactor separates from the pipe after a period of 25ms.

Figure 2.26 shows the variation of the dimensionless parameter λ_c which expresses the threshold failure energy of the pipe based on Eq. (2.39) in relation to the *2L/D*.

$$\lambda_c = \frac{E_k^c}{P_c H} \qquad \text{Eq. (2.39)}$$

where: H : the wall thickness of the pipe

E_k^c : the threshold failure energy (the impact energy that results in small crack or which just initiates the onset of material rupture at the support was taken as E_k^c for the particular group of the specimen)

P_c : static plastic collapse load $\left(P_c = \frac{16R^2 H\sigma_y}{L}\right)$

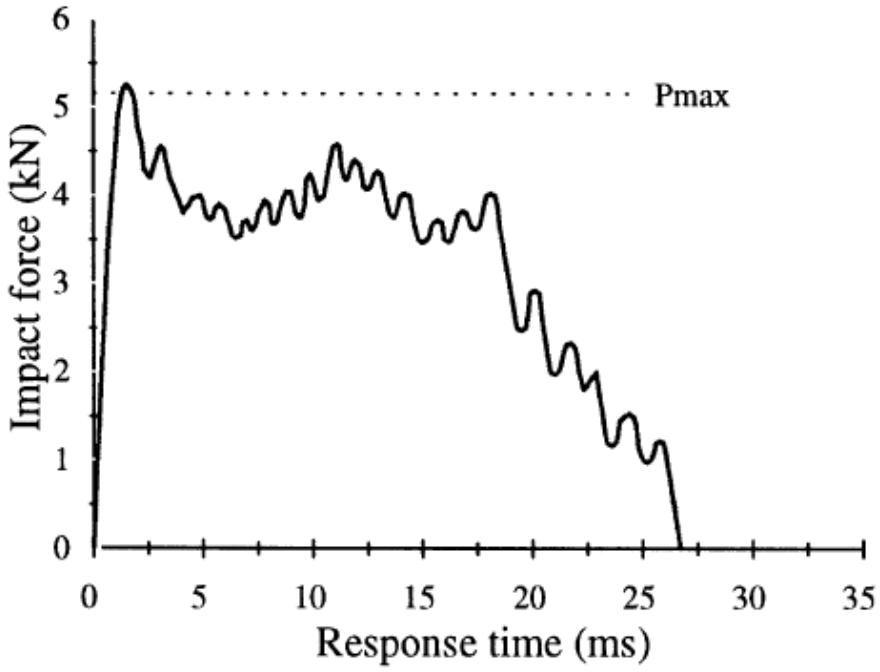

Figure 2.25: Impact load time history [Chen & Shen (1998)].

Reviewing the results obtained for pipes with particular geometric dimension which were impacted at mid-span and quarter-span, it was observed that the λ_c increases approximately linearly with increasing *2L/D* [see Figure 2.26 (a) & (b)]. It was also observed that the span length appeared to have little influence on λ_c for pipes impacted adjacent to the support [see Figure 2.26 (c)]. Furthermore, the permanent deformation exhibited at the impact zone (contact area of the pipe and the impactor) of the pressurized pipes was smaller than those of pipes with no internal pressure. This can be

attributed to the fact that the internal pressure counteracts to certain extent the impact load imposed resulting in the reduction of the localised deformation exhibited at the impact region. As a result it can be assumed that the imposed (impact) load will generate global deformation (along the full span of the pipe specimen).

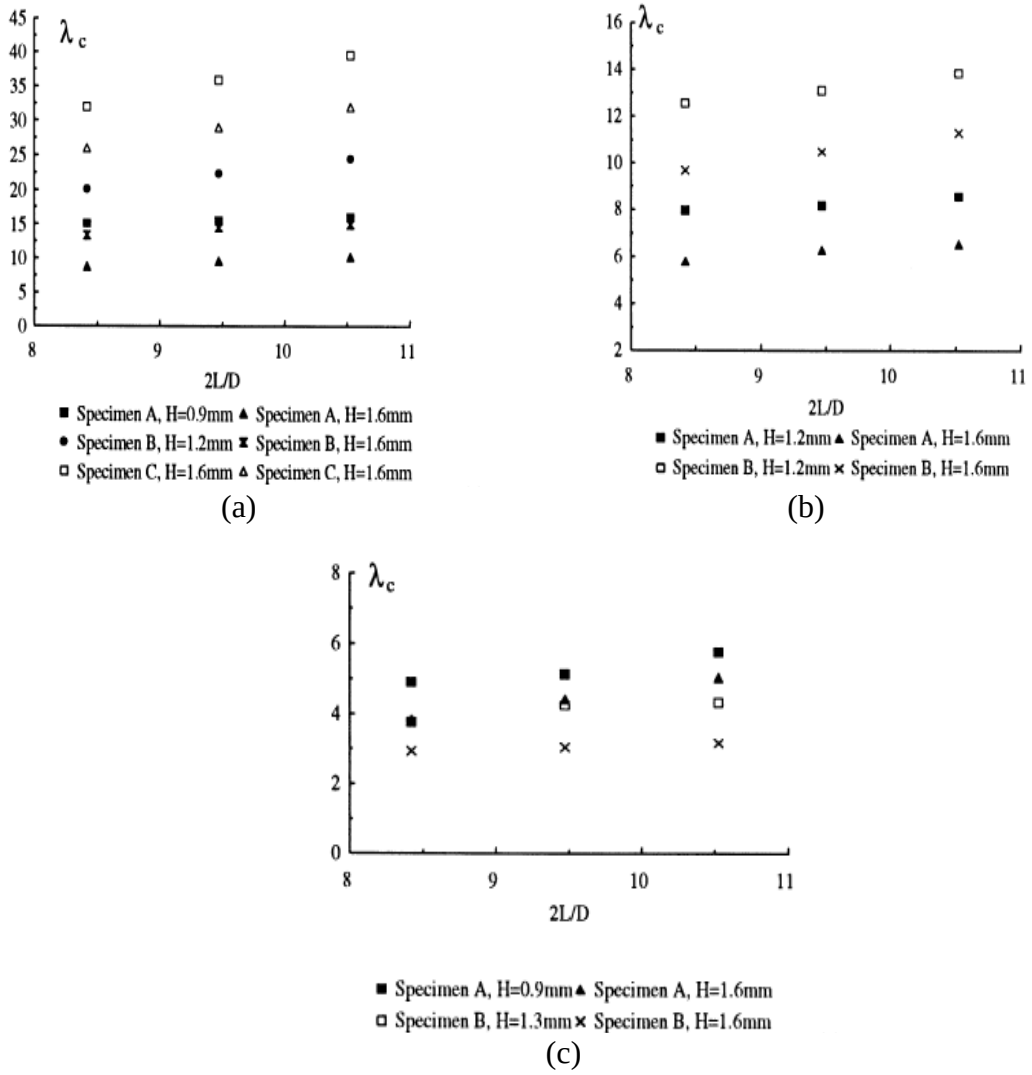

Figure 2.26: Test data describing the variation of λ_c with 2L/D for impact tests carried out at the (a) mid-span (b) one-quarter span and (c) adjacent to the support [Chen & Shen (1998)].

The non-linear dynamic response of the pipes with different levels of internal pressure and different support conditions (due to different material properties of the supporting soil) was studied by Ng & Shen (1996). For this purpose, a total of 52 impact tests were carried out on mild steel pipes, which were laterally impacted at their mid-span region. The pipes used in the impact tests had a diameter of 57mm, a thickness of 1.6mm, and a

span of 560mm. A circular surface wedge-shaped impactor with a radius of 2.65mm at its tip and a mass of 80kg was used to impact the pipes with an initial velocity which varied from 4.95m/s to 7.7m/s. The pipe specimens were fully clamped at both ends and were either laid on sand or kaolin soil layer [Figure 2.27 (a)] or were suspended [Figure 2.27 (b)]

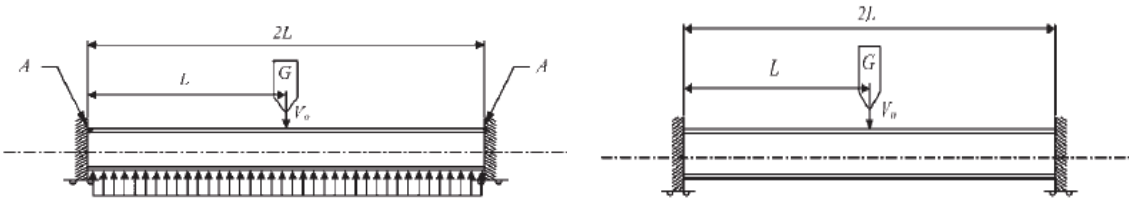

(a) (b)

Figure 2.27: Layout of pipe specimens (a) laid on sand or kaolin soil layer or (b) suspended [Ng & Shen (2006)].

Figure 2.28 shows how the pipes were supported on the soil. It was assumed that the soil provided a perfect line support for the pipe. The line support does not differ significantly from the support having about 30^o contact with the pipe. The specimens were divided into three groups (i) A, (ii) B and (iii) C. In Group A the pipe specimens were laid on sand, in Group B on kaolin and in Group C the pipes were suspended and supported only at their end. Three different levels of internal pressure were used: 6.3MPa, 9.5MPa and 12.5MPa which were achieved using nitrogen gas. Pipes with internal pressure were designated with LP, MP and HP. LP was used for the pipes with the internal pressure of 6.3MPa, MP for 9.5MPa and HP for 12.5MPa respectively.

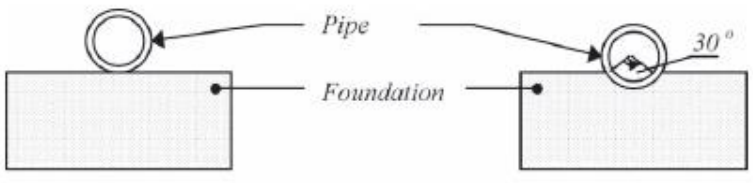

(a) (b)

Figure 2.28: Pipes supported on soil (a) perfect line support and (b) about 30^o contact with the pipe [Ng & Shen (2006)].

Figure 2.29 shows the failure modes observed in the impact test. The failure modes observed were similar to those observed by Jones *et al.* (1992) and Chen & Shen (1998). It was observed that the failure mode due to the tensile tearing (Mode III), resulted in the loss of integrity of the pipes and this type of failure occurs near the supports. Furthermore the failure modes due to shear sliding (Mode I) and buckling at the bottom surface of the pipe (Mode II) occurred in all pipe specimens tested under impact.

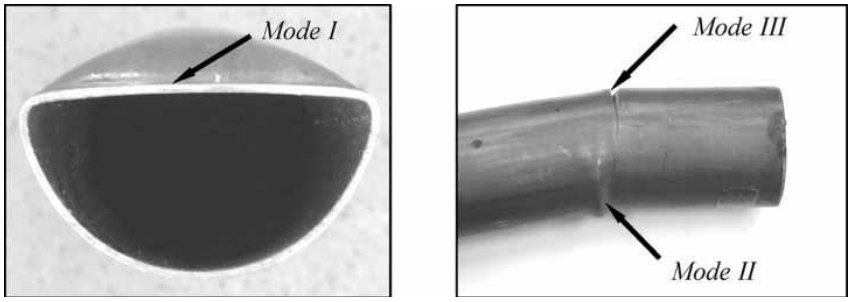

(a) (b)

Figure 2.29: Failure modes exhibited by the pipe specimens during impact: (a) shear sliding at the impact point (Mode I) (b) buckling on the bottom surface (Mode II) and tensile tearing on the top surface (Mode III) [Ng & Shen (2006)].

Figure 2.30 shows the variation of the dimensionless parameter $\overline{W_f}$ expressing maximum deformation given by Eq. (2.40) in relation to the dimensionless parameter λ expressing the initial impact energy provided by Eq. (2.39).

$$\overline{W_f} = \frac{W_f}{H} \qquad \text{Eq. (2.40)}$$

where: W_f : total maximum transverse plastic displacement

In the case of unpressurized specimens supported on sand layer (specimens A) or suspended (specimens C), the maximum permanent transverse deformation was found to be roughly proportional to the initial impact energy (kinetic energy of the impactor prior to coming in contact with the pipe) regardless of the different failure modes

[Figure 2.30(a) and (c)]. However the data is characterized by scatter for the case of pipe specimen's subjected to internal pressure.

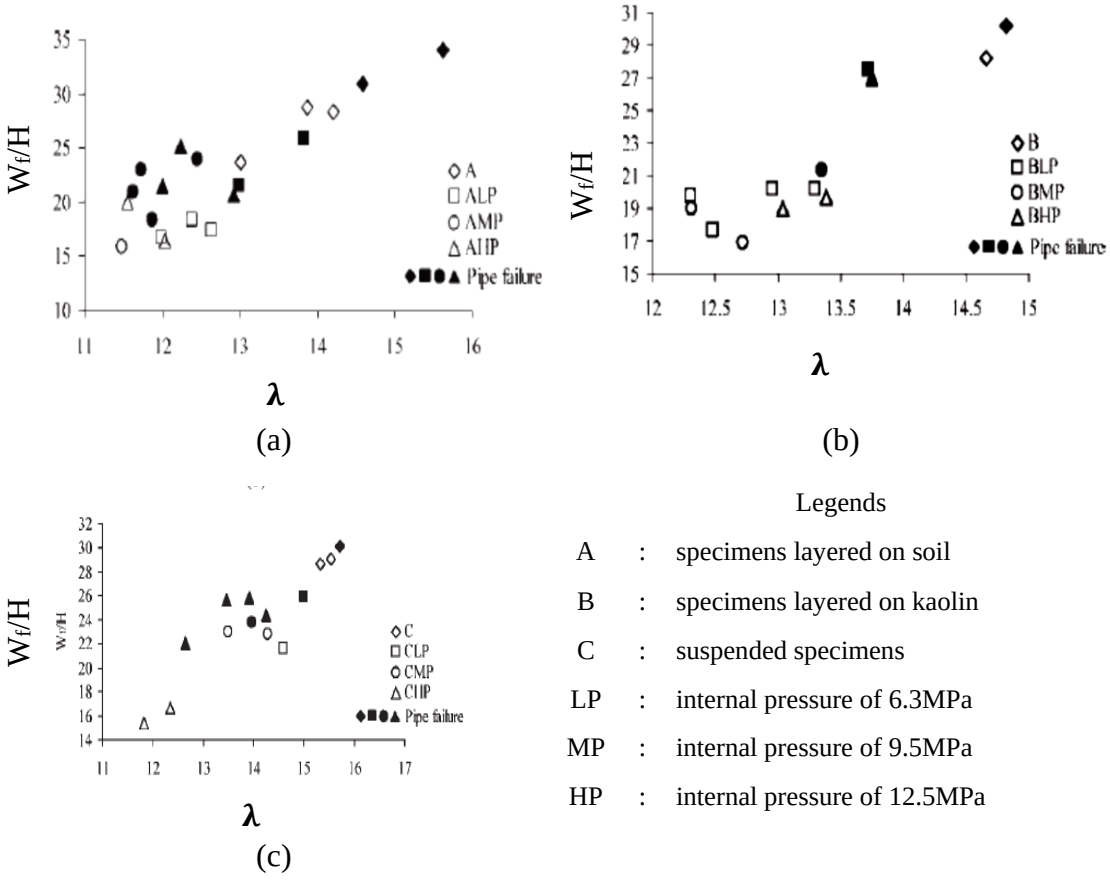

Figure 2.30: Test data describing the variation of W_f/H and λ for (a) specimens laid on sand layer (b) specimens laid on kaolin layer (c) suspended specimens [Ng & Shen (2006)].

The behaviour of axially pre-loaded tubes exhibited under lateral impact loads was studied by Zeinoddini *et al.* (2002). The tubes were impacted at the mid-span region with a 25.40kg impactor which had a velocity of 7m/s prior to contact. The impact tests were carried out for seven different levels of axial loading which were 0%, 25%, 50%, 60%, 65%, 70% and 75% of the cross-section axial load carrying capacity given by Eq. (2.41)

$$P_y = \pi D t \sigma_y \qquad \text{Eq. (2.41)}$$

where: P_y : axial load

Figure 2.31 (a) shows the variation of the impact load with time. It was observed that with the increase in the axial load, the maximum contact force generated decreases. This was more pronounced in the case of the tube with 0.7 P_y. This is due to the fact that the damage sustained by the tube was more concentrated (localised) in the area of impact as shown in Figure 2.31 (b).

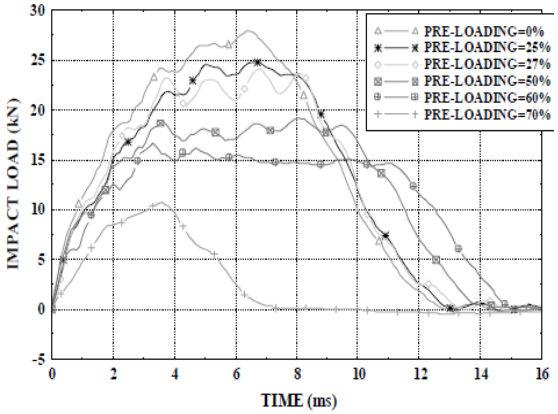

(a)

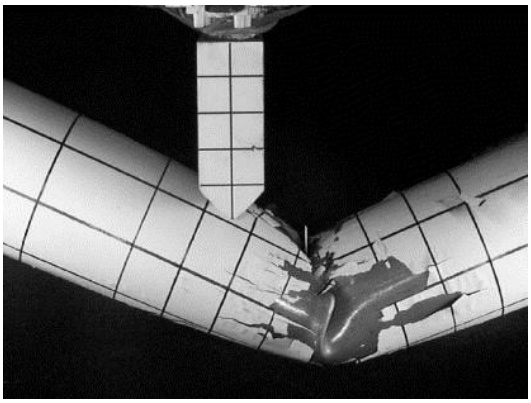

(b)

Figure 2.31: (a) Impact load time history for steel tubes with different level of axial loading (b) localised failure of tube preloaded with an axial force equal to 0.7$\boldsymbol{P_y}$ [Zeinoddini et al. (2002)].

2.5.1 Discussion of experimental results

The results of the experimental studies [Jones *et al.* (1992), Ishikawa & Hoshikawa (1994), Jones & Birch (2010), Chen & Shen (1998), Ng & Shen (2006)] carried out to investigate the behaviour of the pipes under impact have been used to compile a database, presented in Appendix A. The database consists of test results obtained from steel pipe specimens without any coating subjected to drop weight tests. 350 out of 427 impact tests were carried out without considering the effect of the internal pressure on the impact behaviour of the pipe. The effect of external pressure on the impact behaviour was not considered in the experimental studies reported in Appendix A.

The wedge-shape sharp impactor was generally used which was allowed to drop onto the mid-span (in the case of 222 tests), the quarter-span (in the case of 107 tests) and near to the support (in the case of 98 tests) of the pipe-specimens. Out of the 427 test considered, 390 were carried out on suspended pipes having clamped supports on both ends, and only 37 on clamped pipes which were supported on a soil bed.

Figure 2.32 (a) & (b) show the test data expressing relationship between impact energy and residual displacement for impact tests carried out on pipes with

- Suspended pipes (C) with clamped ends and
- Pipes laid on soil bed with clamped ends (C+SF).

Figure 2.32 (a) & (b) show the test data obtained from drop weight test characterised by impact energies less than 10kJ and greater than 10kJ respectively. It can be seen that in general the increase in impact energy results in an increase in residual displacement. It is observed that for tests carried out on suspended pipes (C) with impact energies of less than 10kJ, a parabolic relationship can be formed between the impact energy and the residual displacement. This parabolic relationship becomes linear as the impact energy increases. However, due to limited amount of relevant tests conducted and the scatter which characterises the available data, it is difficult to derive laws able to accurately quantify the effect of the soil bed on specific aspects of the behaviour exhibited by steel pipes under impact loading.

Figure 2.33 (a) & (b) show the available test data expressing relationship between impact energy and residual displacement as well impact energy and the peak value of the contact force generated for the case of specimens with (Pi > 0) and without internal pressure (Pi = 0). It is observed that for both the case of pipes, with (Pi > 0) and without internal pressure (Pi = 0), a parabolic relationship can be used to describe the relationship between the residual displacement and impact energy [see Figure 2.33 (a)]. An approximately parabolic relationship can be used to describe the relationship between the impact force and impact energy for pipes tested without internal pressure, however, due to the limited amount of data no relationship can be derived for the case of pipes tested with internal pressure [see Figure 2.33 (b)].

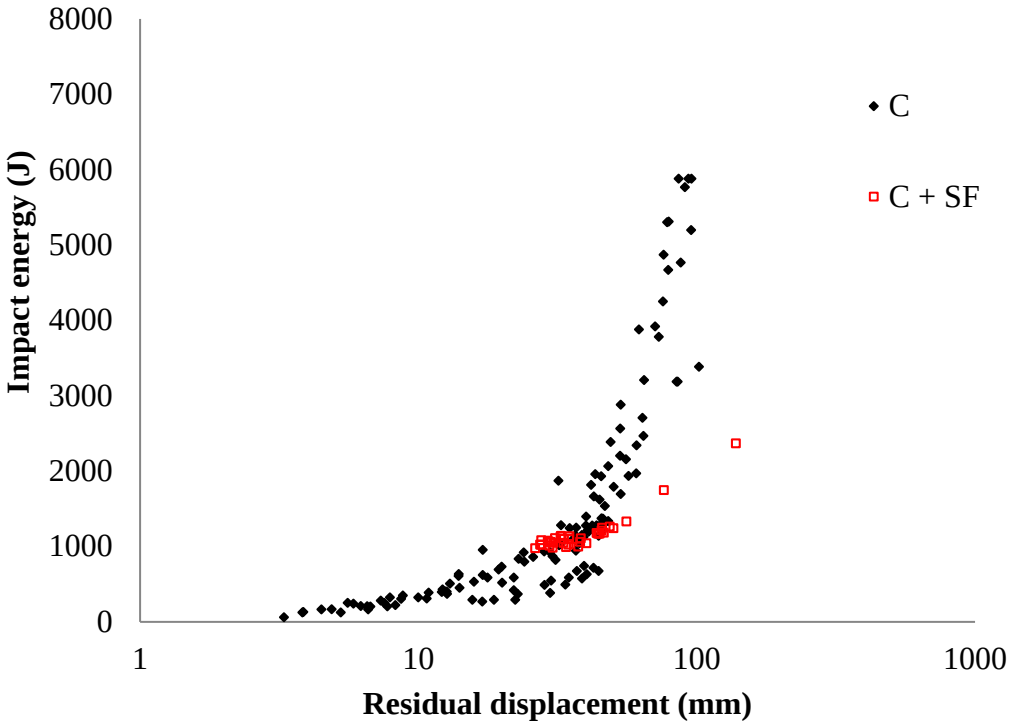

(a)

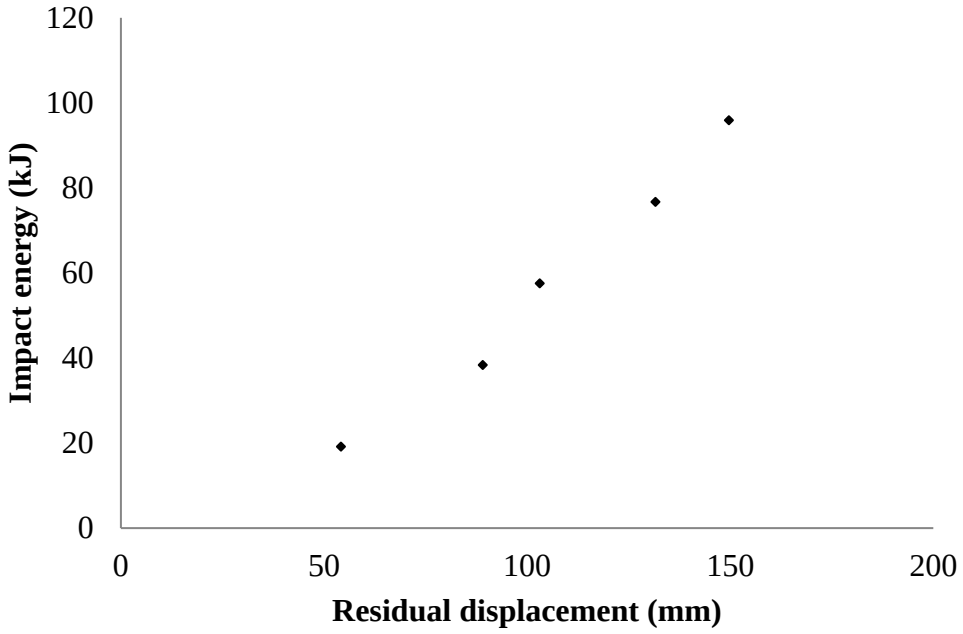

(b)

Figure 2.32: Test data describing the relationship between impact energy and residual displacement for tests on steel pipes subjected to impact energy (a) less than 10kJ and (b) greater than 10kJ.

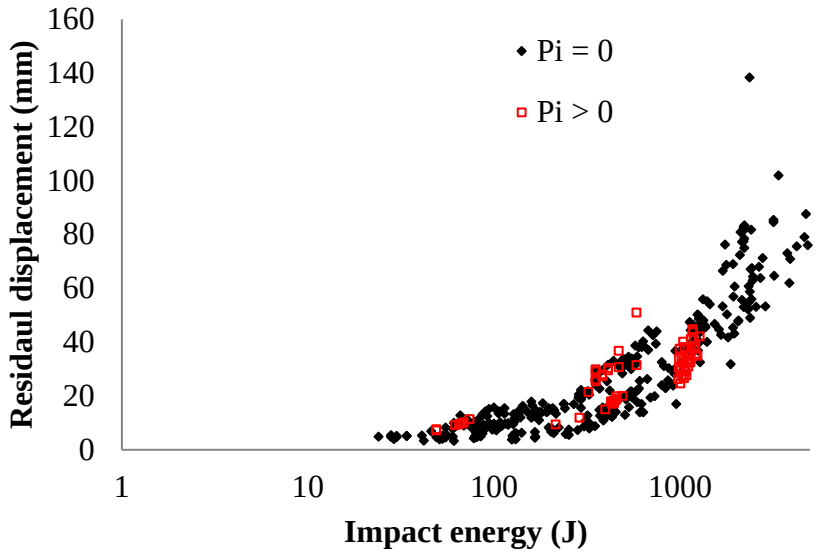

(a)

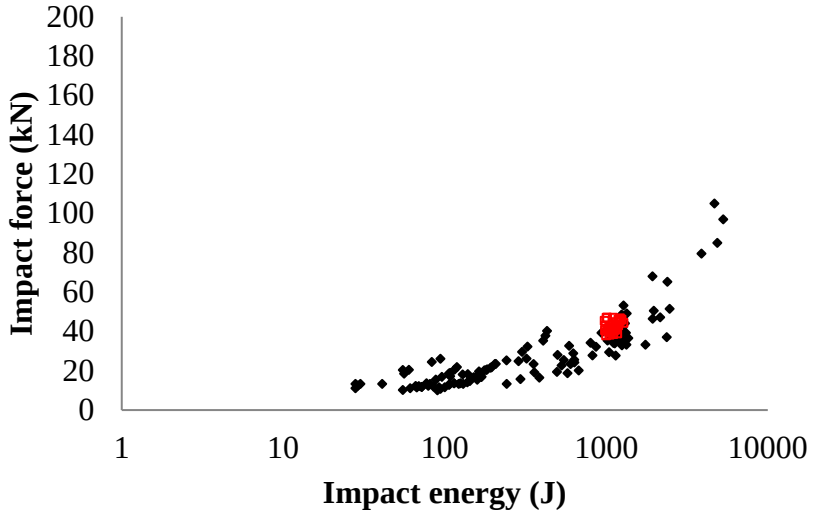

(b)

Figure 2.33: Test data describing the relationship between (a) residual displacement and impact energy and (b) peak value of generated impact force and impact energy for the case of steel pipes with (Pi > 0) and without internal pressure (Pi = 0).

Figure 2.34 (a) & (b) shows the data obtained from impact tests expressing the relationship between the impact energy and residual displacement [see Figure 2.34 (a)] as well as impact energy and the peak value of the impact force [see Figure 2.34 (b)] for the following cases:

- Without internal pressure (Pi = 0)
- With internal pressure (Pi > 0)
- Suspended pipes clamped on either side (C) and
- Pipes laid on soil and clamped on either side (C+SF)

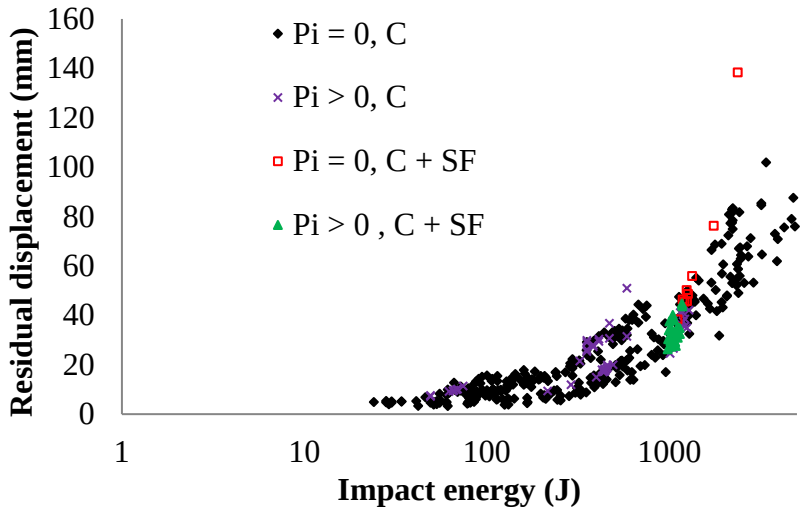

(a)

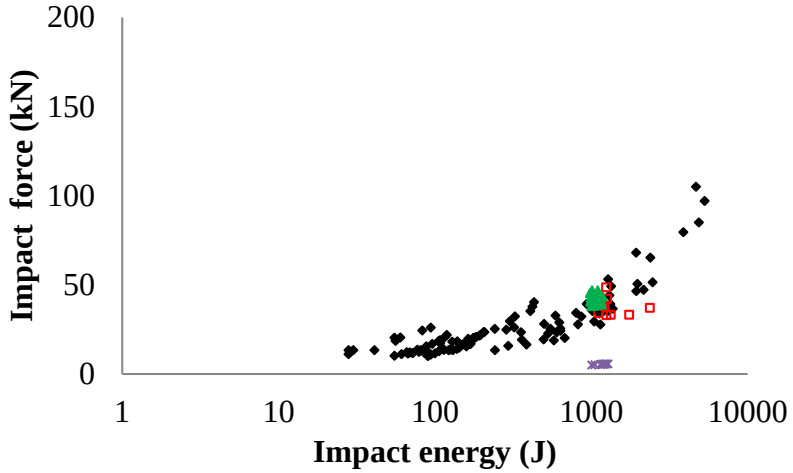

(b)

Figure 2.34: Test data describing the relationship between (a) residual displacement and impact energy and (b) peak value of generated impact force and impact energy for the case of steel pipes with (Pi > 0) and without internal pressure (Pi = 0) which are clamped at their end and their span is either suspended (C) or laid on soil foundation (C+SF).

It is found that approximately parabolic relationship is formed between the impact energy and residual displacement [see Figure 2.34 (a)] as well as the impact energy and

the peak value of the generated impact force [see Figure 2.34 (b)] for the case of suspended pipes without internal pressure. However latter relationships become not obvious for the other three cases due to the limited amount of scattered data.

Figure 2.35 and Figure 2.36(a, b) show the comparison of the impact energy and the residual displacement for the impact tests in which the impactor was dropped at mid-span and quarter-span & adjacent to the support of the pipe specimens. Based on these figures it can be observed that the relationship between the residual displacement and impact energy for the case of suspended pipes without internal pressure impacted at their mid-span [see Figure 2.35] quarter span and adjacent to the supports (see Figure 2.36) can be expressed by parabolic relation. However, it is quite difficult to derive an expression to accurately describe the relationship between the impact energy and the residual displacement of a pipe under the impact load for other cases.

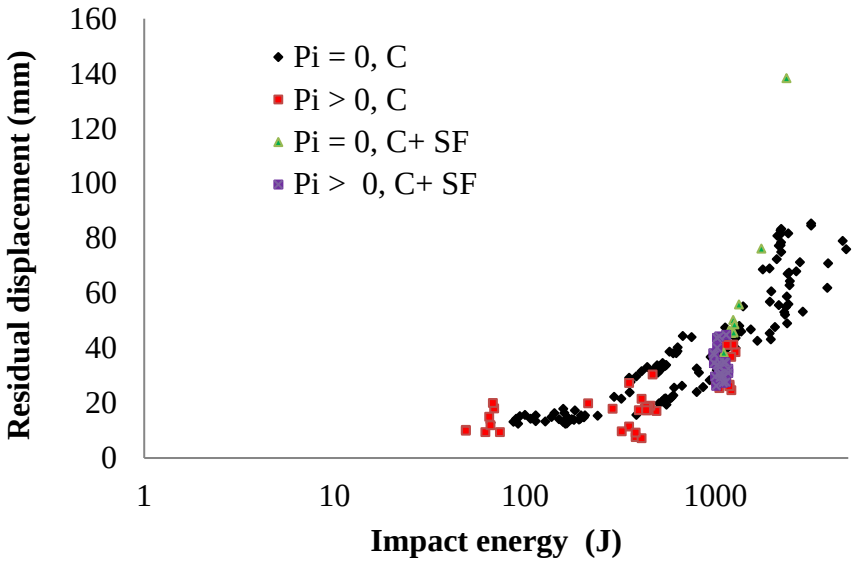

Figure 2.35: Test data describing the relationship between residual displacement and impact energy for pipes impacted at mid-span for following cases (i) with (Pi > 0) and without internal pressure (Pi = 0), (ii) suspended (C) and (iii) laid on soil and suspended on either side (C+SF).

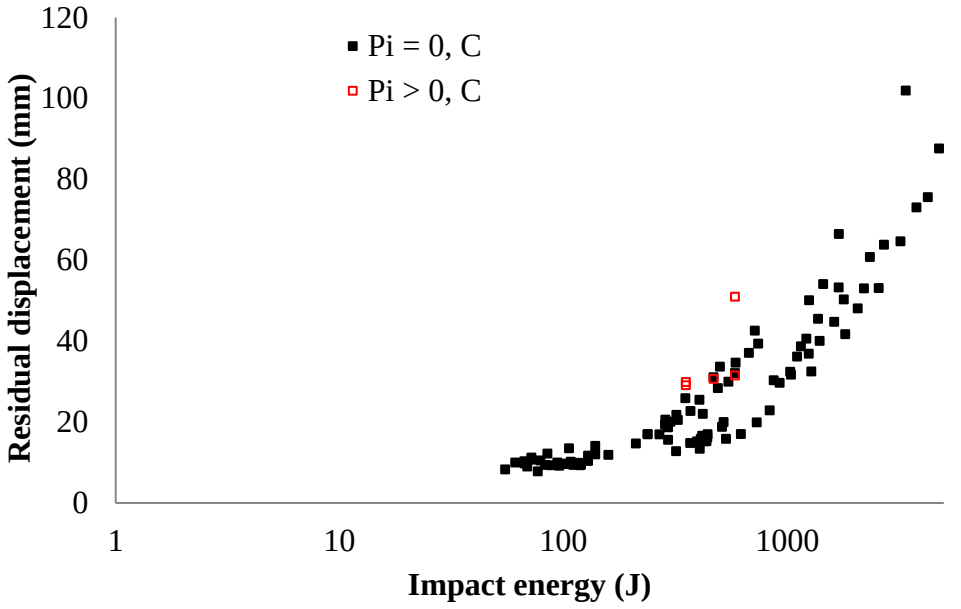

(a)

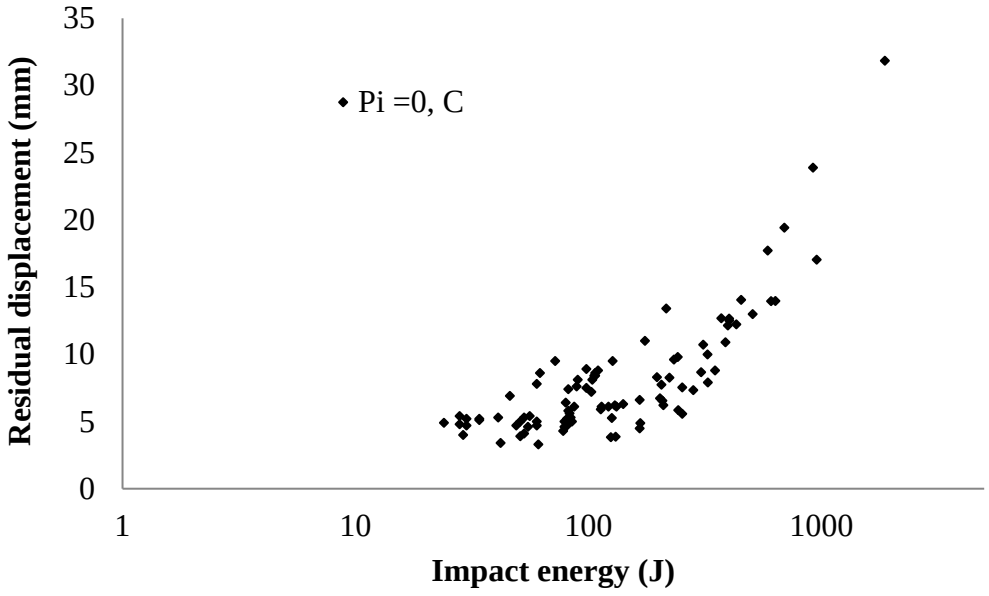

(b)

Figure 2.36: Test data describing the relationship between residual displacement and impact energy for steel pipes impacted at (a) quarter-span (b) adjacent to support for following cases (i) with (Pi > 0) and without internal pressure (Pi = 0) and (ii) suspended (C).

2.6 FINITE ELEMENT ANALYSES

The drop-weight tests conducted on steel pipe specimen do not provide a detailed description of the behaviour exhibited. Many focus on the residual damage caused to the pipe after the application of the impact loads, not providing a detail description of the exhibited behaviour throughout the loading process. Furthermore, the majority of the drop-weight tests are carried out on pipes with relatively small cross-sections which are subjected to low impact energies, not representative of actual problem at hand. At the same time it is difficult to mimic the actual subsea conditions in the laboratory (e.g. subsea foundation, application of the internal and external pressures and axial loading). Therefore *NLFEA* is used to develop complex numerical models which are more representative of the problem at hand.

The influence of the pipe-foundation interaction on the behaviour of offshore pipelines subjected to transverse loading was studied by Zeinoddini *et al.* (2013). ABAQUS, a well-established commercial finite element package, was used to model an internally pressurized pipe laid on a flexible bed (see Figure 2.37). Quasi-static analysis was used to study the behaviour of pipes for the case of three different end conditions: (i) free ends, (ii) caps ends and (iii) fixed ends. The effects of the pipe geometry, the level of internal pressure, the imposed boundary conditions, the indentor shape and its alignment with the pipe, the embedment depth (of the pipe into the soil bed) and the mechanical properties of the subsoil layer were studied.

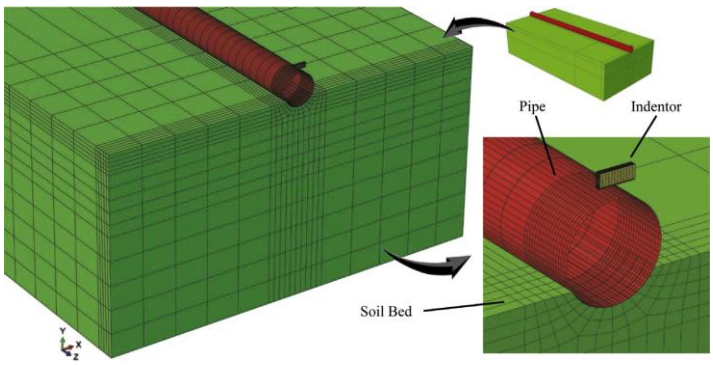

Figure 2.37: Finite element model [Zeinoddini *et al.* (2013)].

A pipe length of 50 times its diameter (50D) was used, which was found to be sufficient to ensure zero vertical displacement at the pipe ends. A soil bed with a depth of *6D* and a width of *12D* were used. The soil was assumed to have an elastic modulus of 5MPa, unsaturated density of 1923kg/m^3 and a Poison's ratio of 0.2. Isotropic material properties were considered in both the longitudinal and circumferential direction. Two types of indentors were used: (i) Type A and (ii) Type B (see Figure 2.38). The shapes of the indentors used were similar to those recommended by DNV [DNV (2010a)].

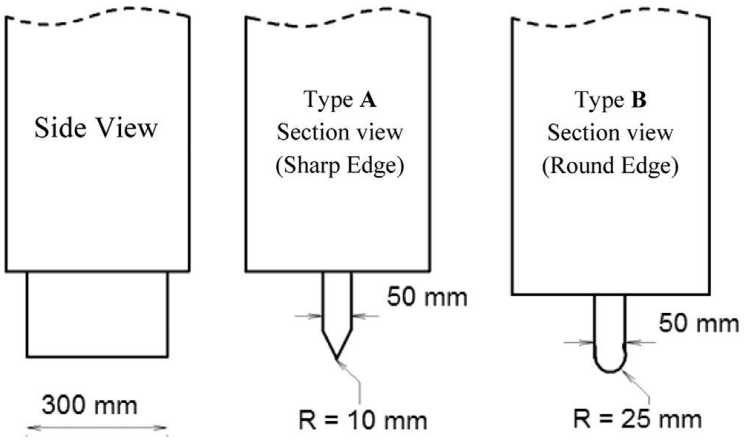

Figure 2.38: Indentors used in the study [Zeinoddini *et al.* (2013)].

Figure 2.39 (a) shows the relationship between the normalized force (f) [Eq. (2.42)] and the normalized displacement (x) of pipe [Eq. (2.43)] and Figure 2.39b shows the comparison of deformed cross-sectional shapes of pipes at the contact area (between the pipe and the indentor), for pipes without internal pressure when the load was applied through indentors which were aligned transversely and longitudinally to the axis of the pipe (see Figure 2.40) with a normalized displacement of $x = 1$.

$$f = \frac{F}{0.25\sigma_y t^2 \sqrt{\frac{D}{t}}} \qquad \text{Eq. (2.42)}$$

$$x = \frac{\delta}{R} \qquad \text{Eq. (2.43)}$$

where: F : load

σ_y : yield stress for steel material

R : pipe radius

δ : local dent depth

It was observed that the shape of indentors used in this study did not have significant influence on the normalized force and displacement curves. Furthermore, it was also observed that the normalized force and displacement curves were similar until a normalized displacement of $x < 0.6$, when the load was applied through both used indentors (Type A and Type B) irrespective with their alignment with the pipe. However, with further increase in the normalized displacement, the pipes exhibited stiffer response when the indentors (Type A and Type B) were aligned transversely. It was also observed that the indentor alignment had significant effect on the deformed cross-section of the pipe [see Figure 2.39 (b)].

Figure 2.41 (a) shows the variation of the normalized force (f) and normalized displacement (x) and Figure 2.41 (b) shows the deformed shapes of a pipe with different normalized internal pressures (q) for the pipes resting on the rigid bed. The normalized internal pressure (q) is given by Eq. (2.44)

$$q = \frac{P}{\frac{2\sigma_y t}{D}} \qquad \text{Eq. (2.44)}$$

where: P : internal pressure

It was observed that the increase in internal pressure resulted in the pipes exhibiting stiffer response [see Figure 2.41 (a)] whereas the level of damage sustained at the contact area of the pipe and the indentor decreases [see Figure 2.41 (b)].

Figure 2.42 shows the variation of the dent depth along the span of the pipes with different normalized internal pressures (q) for the pipes resting on the rigid bed. It was observed that for specific level of maximum dent depth, increasing levels of internal pressure will result in the reduction of the damage sustained along the whole span of the pipe as the response become more localized in the contact zone.

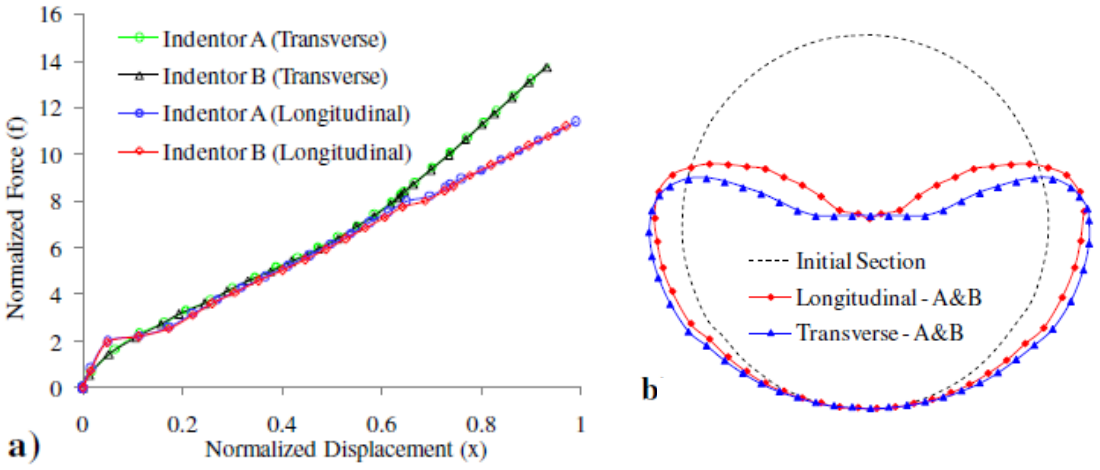

(a) (b)

Figure 2.39: (a) Normalized load displacement curve (b) comparison between deformed pipe cross-section for x = 1.0 for the case of pipes (D = 611mm, t = 8mm) with fixed ends and rested on a soil bed [Zeinoddini *et al. (2013)]*.

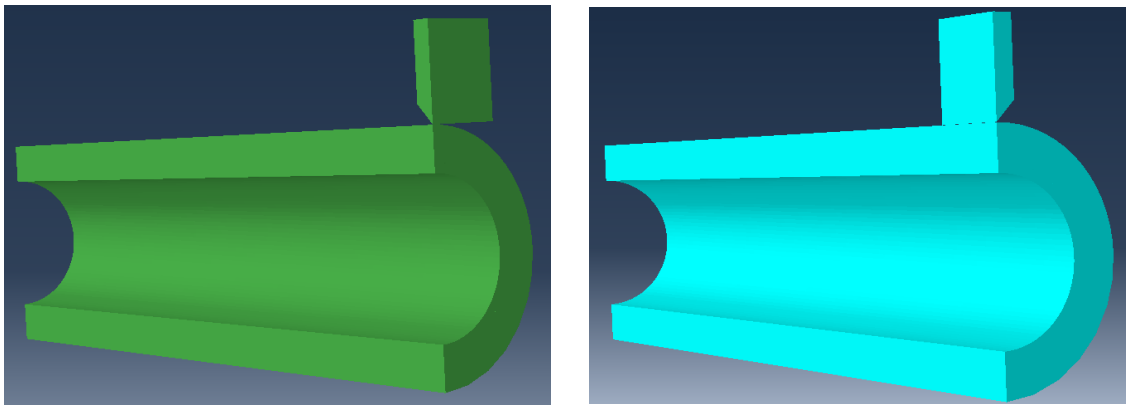

(a) (b)

Figure 2.40: Indentor aligned (a) transversely and (b) longitudinally to the axis of the pipe.

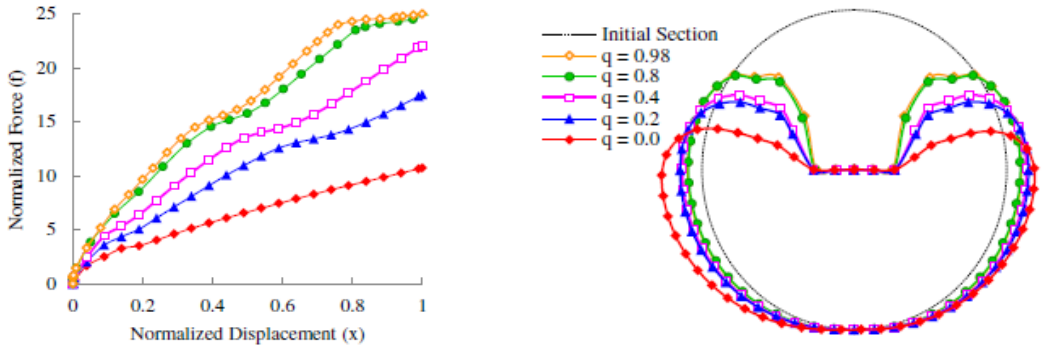

(a) (b)

Figure 2.41: Effect of internal pressure for the case of pipes with fixed ends and rested on a rigid base on the (a) normalized load displacement curves and (b) the deformation of cross-sections of the pipe at the area of contact (for D = 812mm, t = 19mm, σ_y = 530.9MPa) [Zeinoddini *et al.* (2013)].

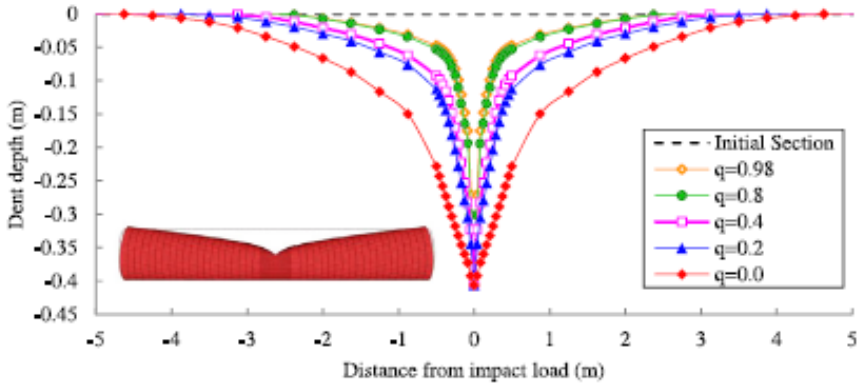

Figure 2.42: Comparison of longitudinal profile with varying normalized internal pressures (q) for the case of pipes with fixed ends and rested on a rigid base (for D = 812mm, t = 19mm, σ_y = 530.9MPa) [Zeinoddini *et al.* (2013)].

Figure 2.43 and Figure 2.44 show the relationship between the total input energy and the dent depth of the pipes when laid on rigid and soil beds respectively. The total energy was obtained by calculating the area under the load displacement curve. It was found that for the specific input energy, larger dent depth was produced in the case of

the rigid bed compared to that observed in the case of the soil bed. It was found that as the sand became denser i.e. the soil friction angle (φ') increases from 20° to 40°, a deeper dent is produced when subjected to a certain level of input energy.

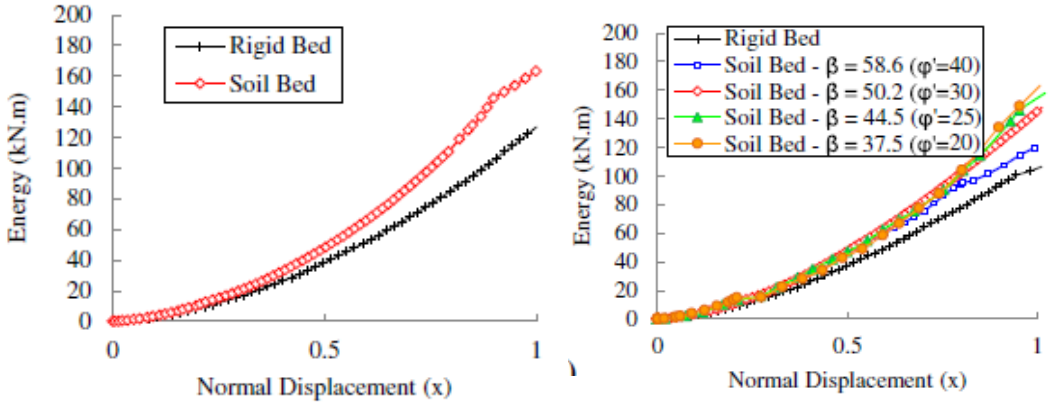

(a) (b)

Figure 2.43: Effect of bed stiffness on the behaviour of the pipe with (a) fixed ends and (b) free ends (D/t = 76, D = 611mm, t = 8mm, f_y = 517 MPa, embedment = 0) [Zeinoddini *et al.* (2013)].

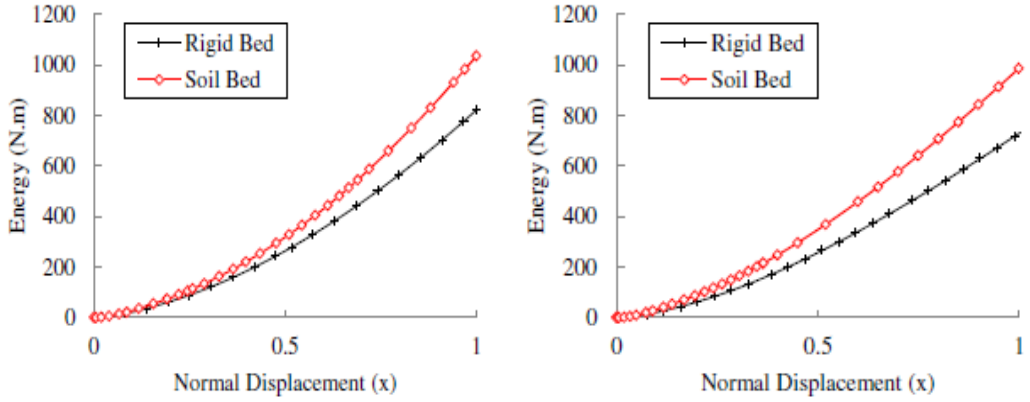

(a) (b)

Figure 2.44: Effect of bed type on the response exhibited by a steel pipe with (a) fixed ends and (b) free ends (for D/t = 42, D =812mm, t =19mm, f_y = 530.9MPa, embedment = 0) [Zeinoddini *et al.* (2013)].

Figure 2.45 shows the effect of end conditions on the behaviour of the pipes. Figure 2.45 (a) shows the relationship of the normalized force and normalized displacement for

the pipes laid on a rigid bed. The same relationship is presented in Figure 2.45 (b) for the case of pipes resting on soil bed ($\varphi' = 30^o$). It was observed that for the pipe with fixed ends a larger lateral load is required to produce a specific dent depth compared to the pipe with capped and free ends.

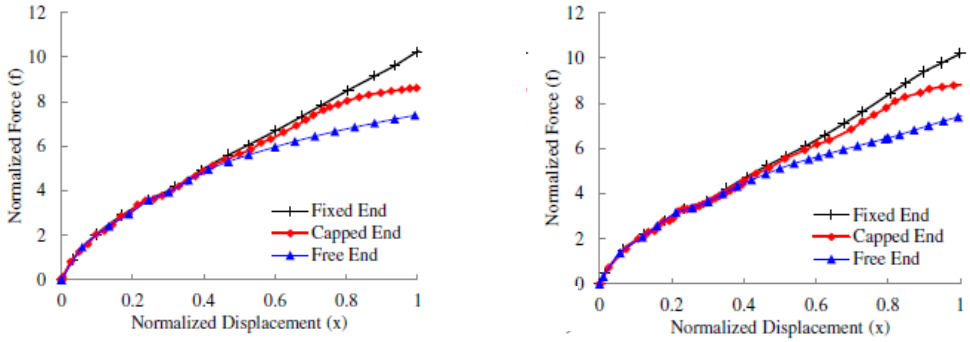

(a) (b)

Figure 2.45: Effect of end conditions on the response exhibited by steel pipes laid on (a) rigid and (b) a soil bed (for D/t = 74, D = 611mm, t = 8mm, f_y = 517MPa) [Zeinoddini *et al.* (2013)].

Figure 2.46 shows the influence of the embedment depth (Em) on the behaviour of the pipe. It was found that as the *Em* increases a larger lateral load is required to produce the same dent depth and at the same time however the level of damage sustained in the contact zone reduces.

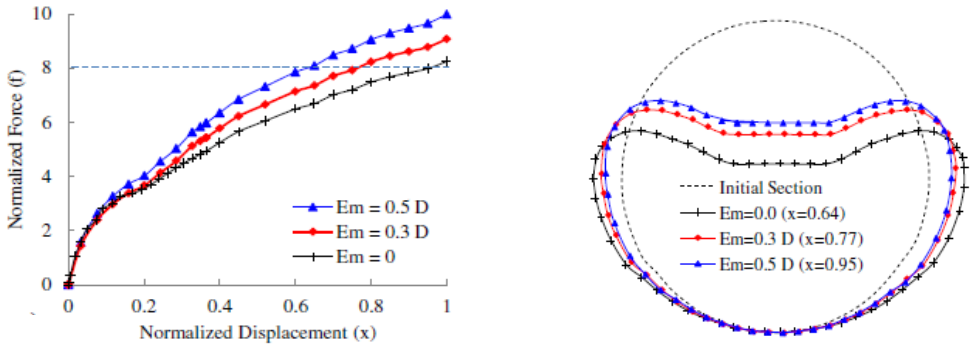

(a) (b)

Figure 2.46: Effect of Embedment depth (Em) on (a) normalized load displacement curves and the (b) deformed profile at the contact area (for D = 611mm, t = 8mm, *fy* = 517MPa, free ends) [Zeinoddini *et al.* (2013)].

Karamanos & Andreadakis (2006) investigated major parameters affecting the response of tubular members under quasi static lateral loads applied locally at the mid-span region [Figure 2.47(a)]. ABAQUS was used once again. Steel pipes with a diameter to thickness (D/t) ratio of 35 and 50 were used. A wedge-shape indentor [Figure 2.47(b)] with a round edge and a thickness of 15 mm were employed. The width (b) varied from 25% to 160% of the mean pipe diameter (D). The load was applied through the indentor at the mid-span of the pipe specimen. The latter indetntor was either transversely or longitudinally aligned with the axis of the pipe. The details of pipe specimens accompanied with loading conditions considered in the study are given in Table 2.9. Pipes with fully fixed, capped and free ends were considered.

Figure 2.48 (a) shows the relationship between normalized force (f) and the normalized displacement (x) for the short pipes (with above mentioned end conditions) with a length to diameter (L/D) ratio of 6, whereas, Figure 2.48 (b) shows results for the long pipes with *L/D* equal to 10. The normalized force (f) and normalized displacement (x) is given by Eq. (2.42) and Eq. (2.43) respectively. Figure 2.49 shows the deformed shapes of non-pressurized pipes (with above mentioned end conditions) having $D/t = 5$ and $L/D = 6$ accompanied by deformed and un-deformed cross-sections of the pipe with free ends at the contact area. It was found that for $L/D = 6$ the resistance force for free and capped ends are significantly different [see Figure 2.48(a)], as the pipes with free ends caused significant distortion of the end sections, which can be also seen in Figure 2.49. In case of the $L/D = 10$ almost identical resistance force was observed with that predicted in the case of free end and cap end conditions. However, for the fixed end condition increased resistance force was observed for both short and long pipes as the members with fixed ends are associated with membrane action in the longitudinal direction.

Figure 2.50 and Figure 2.51 show the relationship of the normalized force (f) and normalized displacement (x) of the capped and fixed end pipes respectively, with different normalized internal pressures (q) [see Eq. (2.44)]. The ratio between the length of the indentor and the diameter of pipe (b/D) was 1.6. A transverse load was applied through the indentor at the mid-span of the pipe specimen. It was observed that the force increased substantially with increasing values of internal pressure. The increase in the force was found to be more pronounced for pipes with fixed ends due to the

membrane action observed in the longitudinal direction, as compared to the pipe with capped ends.

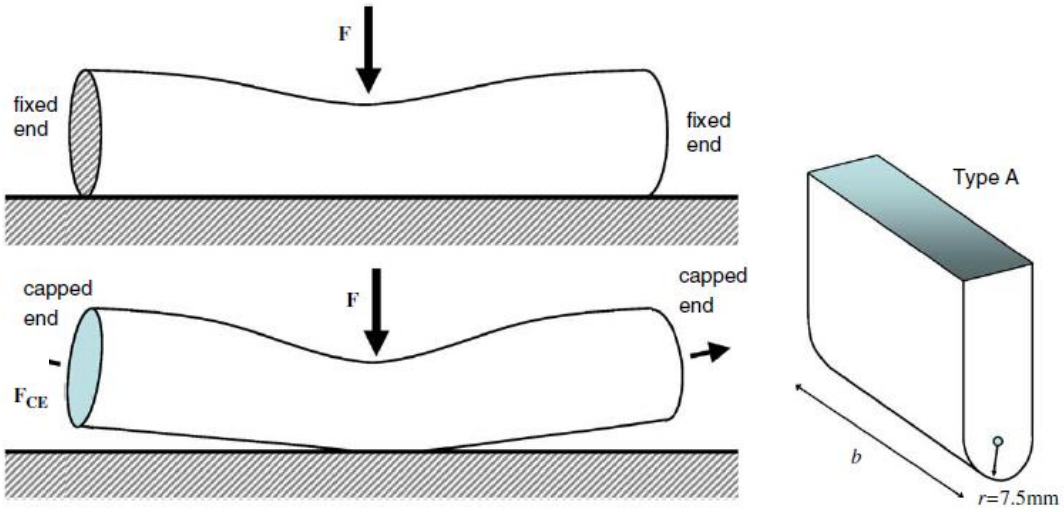

(a) (b)

Figure 2.47: (a) Pipe under quasi static load (b) wedge shape indentor [Karamanos & Andreadakis (2006)].

Table 2.9: Details of pipe specimens accompanied with loading conditions [Karamanos & Andreadakis (2006)].

Specimen	**Outer diameter (mm)**	**Thickness (mm)**	**Length (mm)**	**Pressure (bar)**	**Indentor orientation**
A1	165	4.82	2000	0	Longitudinal
A2	165	4.82	2000	0	Longitudinal
A3	165	4.82	2000	40	Longitudinal
B1	133	2.72	900	40	Transverse
B2	133	2.72	900	66.2	Transverse
B3	133	2.72	900	40	Longitudinal

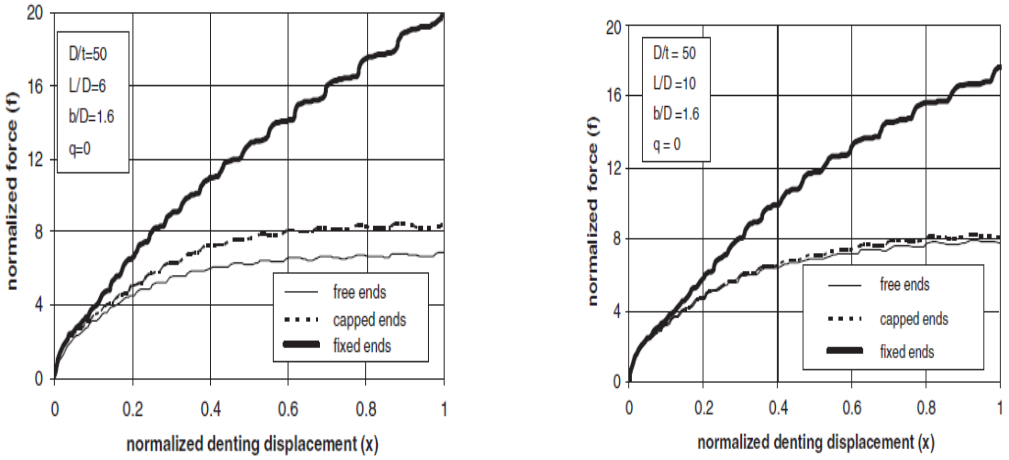

(a) (b)

Figure 2.48: Effects of end conditions on the response of pipes with (a) L/D = 6 and (b) L/D = 10 [Karamanos & Andreadakis (2006)].

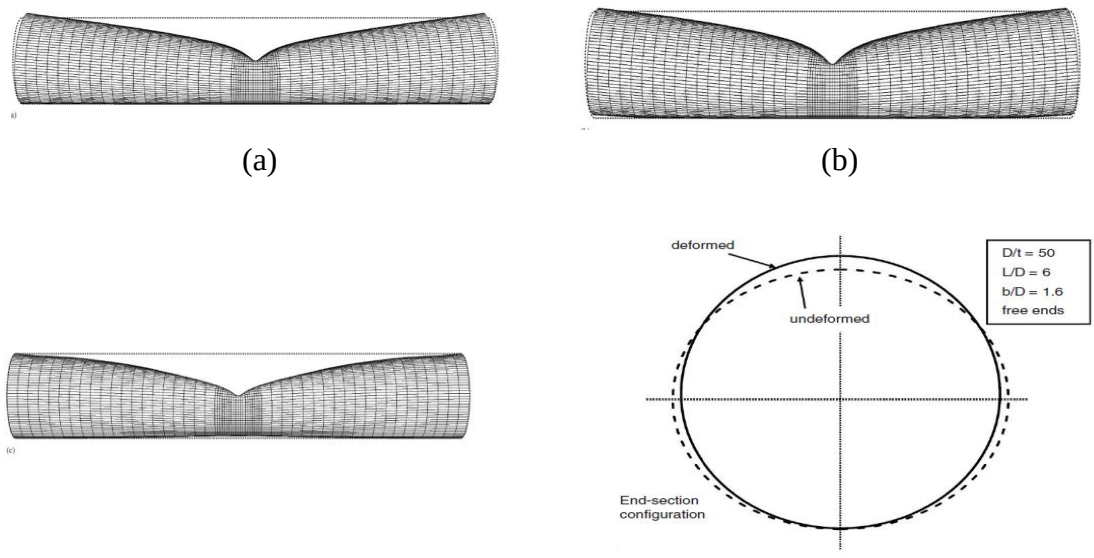

(a) (b)

(c) (d)

Figure 2.49: Deformed shapes of non-pressurized pipes (D/t = 50, L/D = 6) with (a) free ends, (b) capped ends and (c) fixed ends, accompanied by (d) deformed and un-deformed cross-sections of the pipe considered with free end [Karamanos & Andreadakis (2006)].

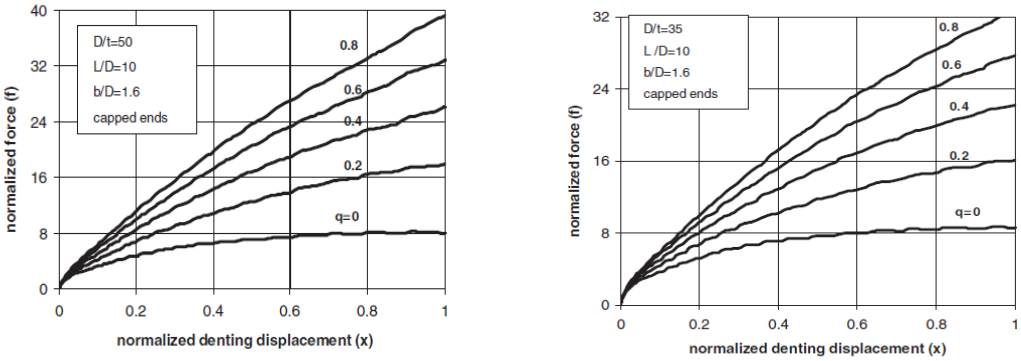

(a) (b)

Figure 2.50: Effects of internal pressure on the response for pipes with capped ends for (a) D/t = 50 and (b) D/t = 35 [Karamanos & Andreadakis (2006)].

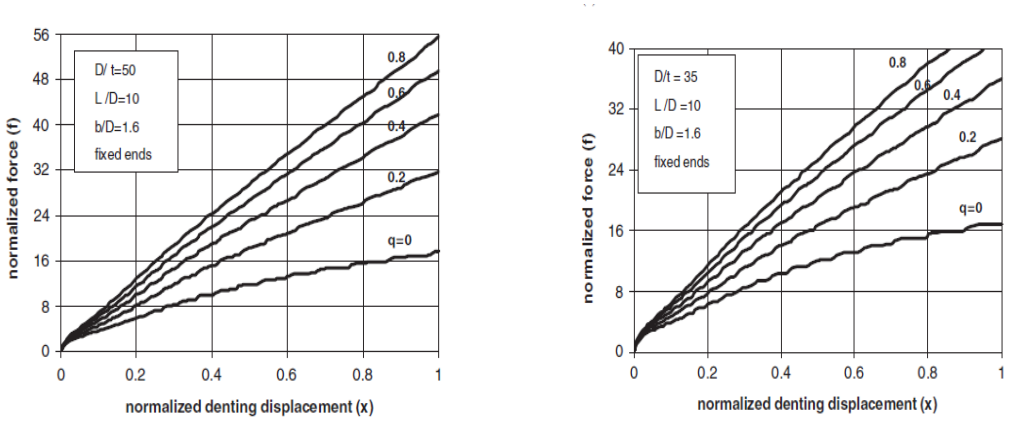

(a) (b)

Figure 2.51: Effects of internal pressure on the response for pipes with fixed ends for (a) D/t = 50 and (b) D/t = 35 [Karamanos & Andreadakis (2006)].

Figure 2.52 (a) & (b) shows the deformed shapes of capped-end pipes (with D/t = 50, L/D = 6) for different normalized internal pressures (q) under lateral loading. It was observed that the internal pressure resulted in more localized deformation. Figure 2.52 (c) and (d) shows the profile of the deformed cross-section at the mid-span of the pipes with normalized displacement (x) equals to 0.5 and 1 respectively. It was observed that the presence of the internal pressure did not cause significant variation in the profile of the deformed cross-section of the pipe.

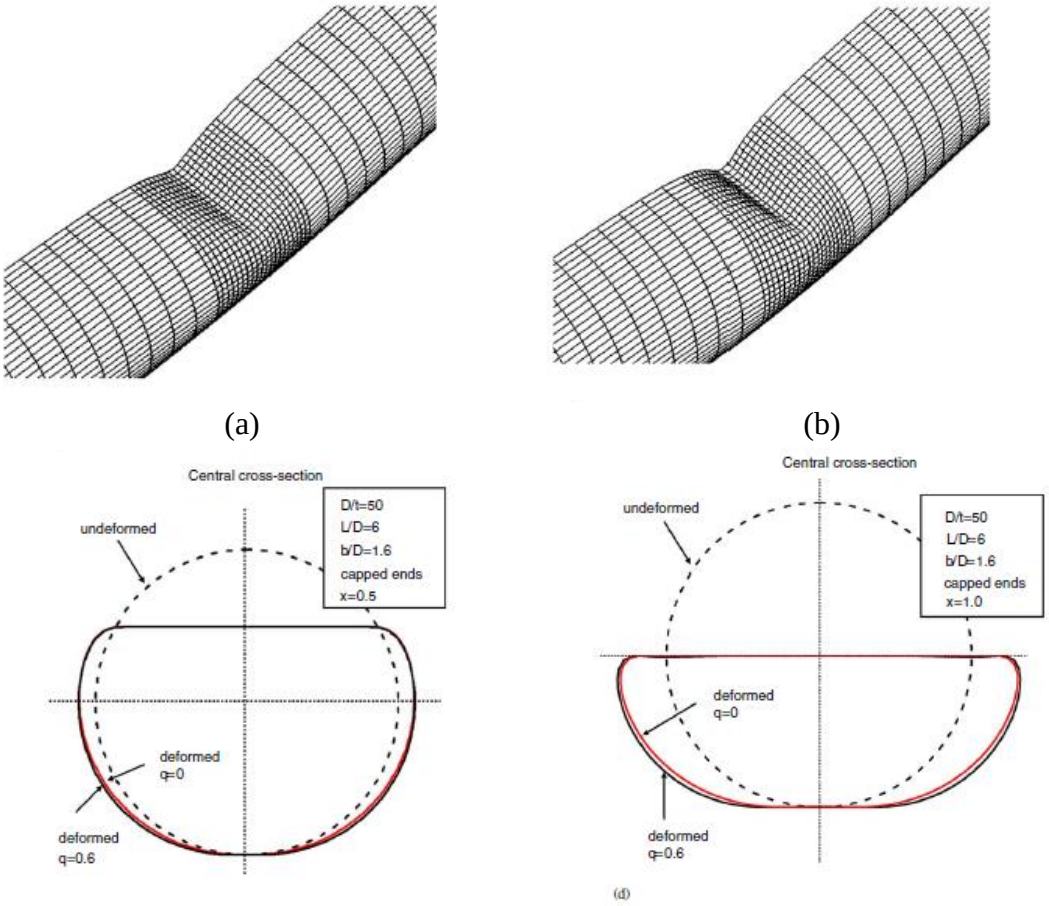

Figure 2.52: Deformed shapes of capped-end pipes (with D/t = 50, L/D = 6) for (a) q = 0 (b) q = 0.6, accompanied by the profile of the deformed cross section at (c) mid-span for x = 0.5 and (d) x = 1.0 [Karamanos & Andreadakis (2006)].

Figure 2.53 shows the effect of the ratio between the indentor length and the diameter of pipe (b/D) on normalized force-displacement curve of the capped pipe with and without internal pressure. It was observed that the response of the pipe is not significantly affected by the shape of the indentor. However, smaller values of *b/D* ratio resulted in lower forces.

Figure 2.54 shows the response of the pipe (with D/t = 50 and L/D = 10) when load was applied through an indentor which was aligned longitudinally to the pipe axis. On comparison of the response of pipe when subjected to a load through indentors which were aligned longitudinally and transversely it was observed that the shape of the normalized force displacement curve of the pipes is significantly different for both

cases (see Figure 2.53 and Figure 2.54). It was also observed that the force increased for the case when load was applied longitudinally.

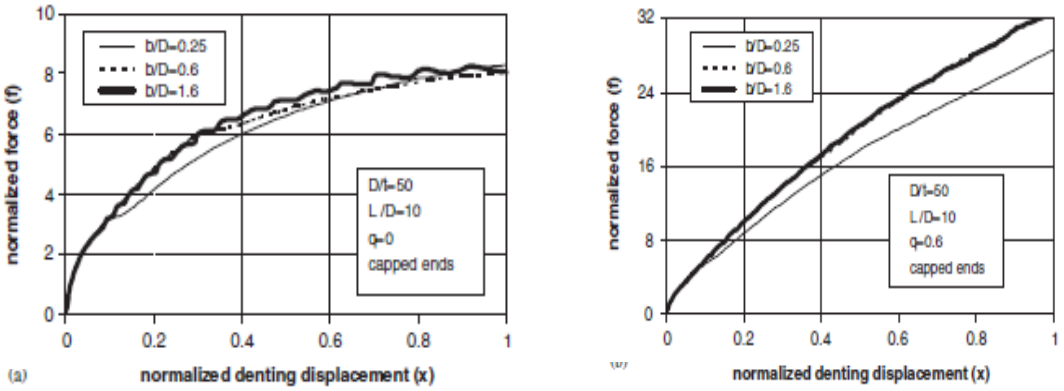

(a) (b)

Figure 2.53: Effect of indentor length to the diameter of pipe ratio (b/D) on the response of the capped end pipe for (a) q = 0 and (b) q = 0.6 [Karamanos & Andreadakis (2006)].

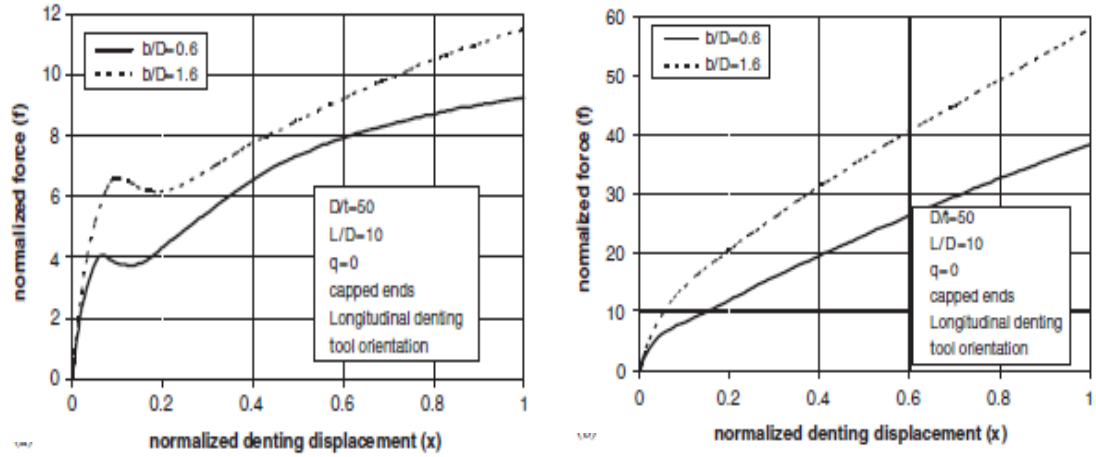

(a) (b)

Figure 2.54: Effect of indentor length to the diameter of pipe ratio (b/D) on the response of the pipe when load was applied longitudinally (a) q = 0 and (b) q = 0.6 [Karamanos & Andreadakis (2006)].

Brooker (2004) investigated the effect of various parameters on the impact behaviour of steel tubes. The parameters considered were: (i) the diameter, (ii) the wall thickness, and (iii) the material strength. For this purpose ABAQUS was used. The load was

applied with the knife-edge indentor which was aligned perpendicularly with the axis of the tube [see Figure 2.55]. The tube was fully restrained at each end and the load was applied quasi statically.

Figure 2.56 and Figure 2.57 show the load and residual dent depth relationship for various parameters considered. Based on the parametric studies a semi empirical equation [Eq. (2.45)] was proposed. The solid lines in Figure 2.56 and Figure 2.57 provide the predictions of Eq. (2.45) which are in reasonable agreement with the numerical counterparts.

$$Q = 2.841\ \sigma_y t^2 + 15.49\ \sigma_y\ \delta_r \frac{t^{1.4}}{D^{0.15} L^{0.25}} \qquad \text{Eq. (2.45)}$$

where: L : length of the pipe

σ_y : yield stress of steel

δ_r : residual dent depth

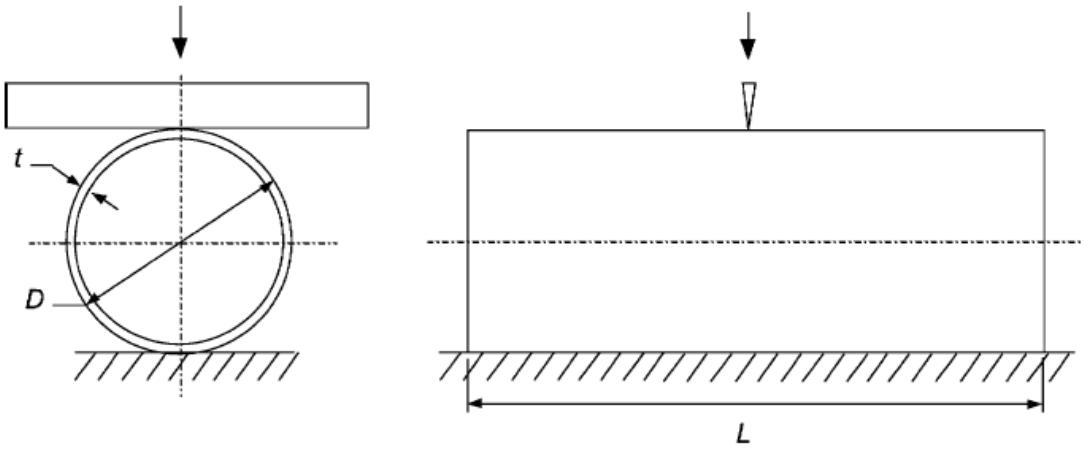

Figure 2.55: Steel tube subjected to lateral loading at mid-span through a knife-edge indentator [Brooker (2004)].

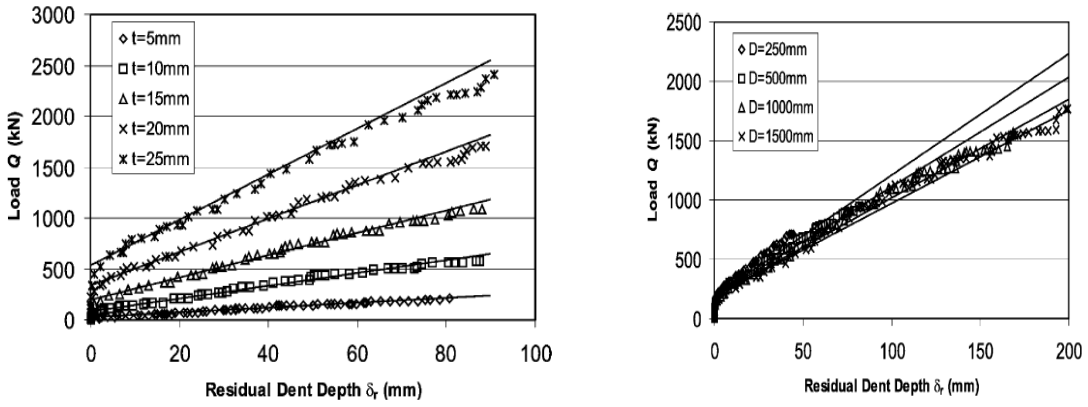

(a) (b)

Figure 2.56: FE results describing the relationship between the load and residual dent depth for different (a) wall thicknesses (D = 500mm, L = 3000mm, *f*y = 300MPa) and (b) diameters (t = 15mm, L = 6000mm, *f*y = 300MPa) [Brooker (2004)].

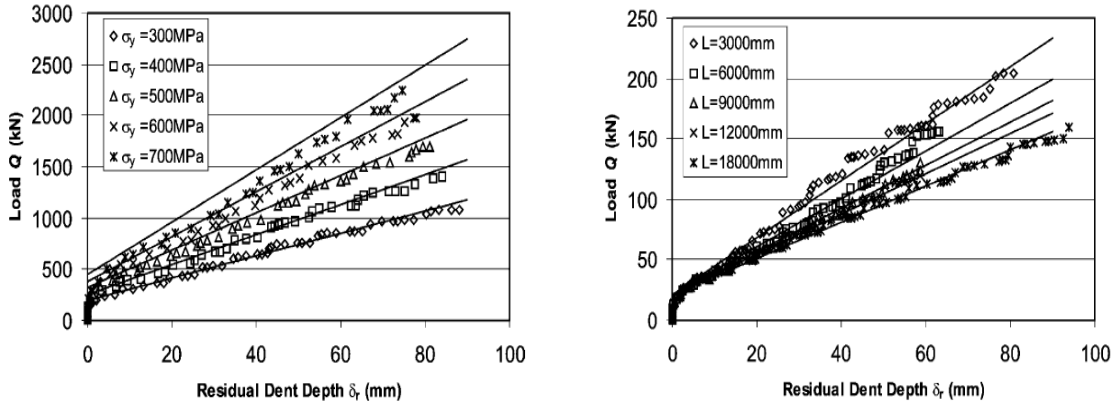

(a) (b)

Figure 2.57: FE results describing the relationship between the load and residual dent depth for different (a) yield stresses (D = 500mm, t = 15mm, L = 3000mm) and (b) tube lengths (D = 500mm, t = 5mm, σ_y = 300MPa) [Brooker (2004)].

2.7 ANALYTICAL APPROACHES

The full scale impact tests carried out to study the behaviour of the pipes under impact are characterized as expensive and significantly difficult (due to instrumentation). On the other hand nonlinear finite element analyses allow the development of complex model more representative of the problem at hand which may however require significant computational cost. In addition to these two approaches (experimental and numerical studies) analytical methods can be employed to form practical tools in order to study the behaviour of the steel pipes under impact load.

Jones & Brich (2010) idealized the behaviour of pipe under lateral impact load (Figure 2.58) and developed an analytical approach to calculate the local and global displacements exhibited by the pipe. It was assumed that the pipeline cross-section underneath the striker deformed in the circumferential sense and the centre of the undeformed circular cross-section is assumed to coincide with the deformed section of the pipe (see Figure 2.58).

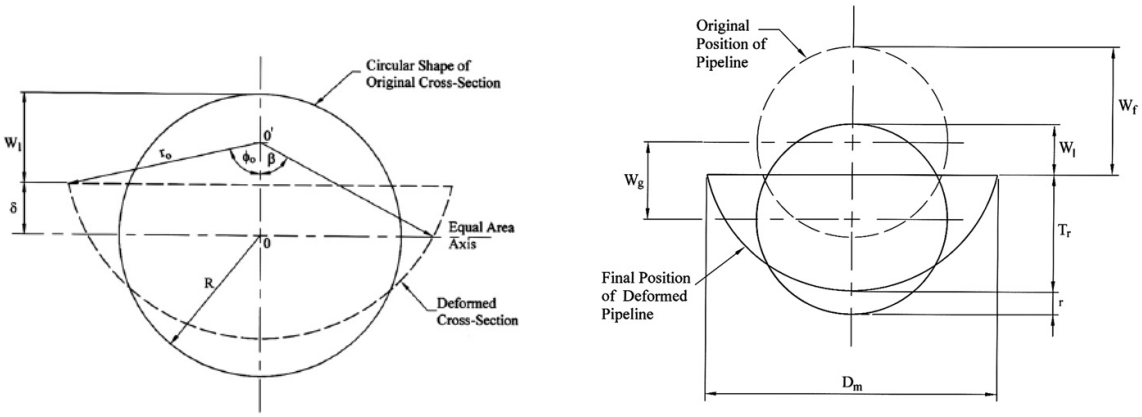

(a) (b)

Figure 2.58: (a) Idealized behaviour of pipe under impact (b) schematic representation of the local indentation (W_l), global displacement (W_g) and total displacement (W_f) of the idealised deformed cross-section of a pipe [Jones & Birch (2010)].

The properties of the deformed cross-section of the pipe are given by Eq. (2.46) to Eq. (2.49)

$$r_o = \frac{T_r[1 + \left(\frac{D_m}{2T_r}\right)]^2}{2} \quad \text{Eq. (2.46)}$$

$$\beta = \frac{\pi R}{2r_o} \quad \text{Eq. (2.47)}$$

$$\cos\emptyset_o = 1 - \frac{T_r}{r_o} \quad \text{Eq. (2.48)}$$

$$\delta = r_o(\cos\beta - \cos\emptyset_o) \quad \text{Eq. (2.49)}$$

The local and global deformation of the pipe is given by Eq. (2.50) and Eq. (2.51) respectively:

$$W_1 = R - \delta \quad \text{Eq. (2.50)}$$

$$W_g = W_f - W_1 \quad \text{Eq. (2.51)}$$

where:
- r_o : radius of deformed cross-section of pipe
- T_r : thickness of deformed cross-section of pipe
- D_m : maximum width of deformed cross-section of pipe
- R : mean radius of pipe
- W_1 : local displacement of pipe
- W_f : overall permanent displacement of pipe
- W_g : global displacement of pipe

An analytical solution [given by Eq. (2.52)] developed by Wierzbicki and Suh (1988), based on the following assumptions is suggested for use in risk assessment of denting of pipeline as per DNV-RP-F107 [DNV (2010b)].

1. The analytical model is based on the rigid-perfectly plastic material idealization.
2. The extent of the locally damaged zone is finite (see Figure 2.59).
3. The cross section at which the deformed part joins the undeformed part is assumed to be plane and circular i.e. no ovalization and warping of the tube exists beyond the dent affected zone.
4. It is assumed that, away from the deformed zone, all cross sections undergo rigid body translation and rotation.

$$E = 16\left(\frac{2\pi}{9}\right)^{\frac{1}{2}} m_p \left(\frac{D}{t}\right)^{\frac{1}{2}} D \left(\frac{\delta}{D}\right)^{\frac{3}{2}} \quad \text{Eq. (2.52)}$$

where: E : Energy

m_p : plastic moment capacity of the wall ($m_p = 0.25\sigma_y t^2$)

δ : pipe deformation, dent depth

D : steel outer diameter

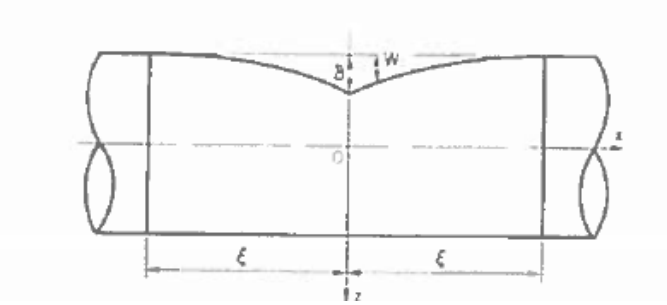

Figure 2.59: Idealized behaviour of pipe under impact [Wierzbicki & Suh (1988)].

Based on the predictions of the Eq. (2.52), DNV-RP-F107 [DNV (2010b)] proposed damage of the steel pipelines into different categories which is shown in Table 2.10. The conditional probabilities *D1, D2, D3, R0, R1,* and *R2* associated with the damage categories given in Table 2.10 are described in detail in section 2.4.

Table 2.10: Impact capacity and damage classification of steel pipelines [DNV (2010b)].

Dent / Diameter (%)	**Damage description**	**Conditional probability**					
		D1	**D2**	**D3**	**R0**	**R1**	**R2**
< 5	Minor damage	1.0	0	0	1.0	0	0
5 - 10	Minor damage, leakage anticipated	0.1	0.8	0.1	0.9	0.1	0
10 - 15	Major damage, leakage and rupture anticipated	0	0.75	0.25	0.75	0.2	0.05
15 - 20	Major damage, leakage and rupture anticipated	0	0.25	0.75	0.25	0.5	0.25
> 20	Rupture	0	0.1	0.9	0.1	0.2	0.7

Although analytical approaches can be used to assess the damage caused to the pipe due to impact, however they do not provide an accurate representation of the problem at hand as they ignore the dynamic aspects of the problem as well as the contributions of other parameters associated with the subsea conditions to which the pipe is subjected while in operation.

2.8 CONCLUSIONS

The behaviour of steel pipes under impact is influenced by a number of parameters which include (i) the material properties and geometry of the steel pipes, (ii) the characteristics of the impacting object (size, shape, and speed) and (iii) the imposed boundary conditions (end conditions, sea bed on which pipe is laid). The behaviour of pipes under impact can also be influenced by the development of internal (due to the oil and gas in the pipe) and external (hydro-static) pressure as well as axial loading.

The behaviour of pipes under impact is characterized by local and global response. The damage caused in the impact zone is associated with the localized behaviour and can vary from a simple dent to localized failure (collapse of the cross-section). The global behaviour results in pipe deformation along its whole length.

The design criteria of the relevant codes used for the analyses and assessment of subsea pipes are associated with static loading. Thus it is important to investigate the effect of loading rate on the behaviour of the steel pipelines in order to assess to what extent the dynamic nature of the problem at hand may affect the design process and the structural resistance of the pipes. It was observed that parameters such as (i) hoop stress (ii) axial stress (iii) development of the internal and external pressure can significantly influence the design criteria. As a result it is logical to assume that the combined effect of the above parameters can significantly affect the behaviour of the subsea pipes under the impact load while in operation.

Although both simplified assessment methods and advanced analysis procedures [DNV (2010a)] can be used to form practical tools for assessing the impact behaviour and the level of damage sustained by the pipes during collisions, they do not provide a detailed representation of the problem at hand. The simplified approach assumes that impact

energy is absorbed locally (in the impact region) and accounts for effect of global behaviour and soil conditions indirectly through the use of correction factors. On the other hand, advance analyses procedures depend largely on the values of the lumped masses and spring stiffness's which are used to create an approximate model of the subject system (pipe, supporting soil, impacting object). It should be mentioned that both of these methods do not consider the combined action of a range of parameters associated with the subsea and operational conditions which have been discussed above. The latter parameters can significantly affect the behaviour of the pipe exhibited during impact loading.

Most of the experimental studies have been carried out on pipe specimens with small cross-sections subjected to small impact energies. Therefore the test data obtained is not representative of the behaviour exhibited by subsea pipes under operational conditions. The available experimental studies mainly focus on measuring the damage sustained by the pipe (in the form of permanent deformation) after impact and do not provide a detailed description of the response exhibited throughout the loading process.

The finite element studies described in this chapter are usually carried out using quasi-static analysis thus ignoring the inertia effects and the wave propagation problem at hand. Considering that the duration of the generated impact load is very short (just a few milliseconds) the behaviour of these pipelines may also be influenced by the strain rates exhibited. Based on the above the use of quasi-static analysis is likely to ignore certain important aspects of the problem at hand.

Analytical approaches provide a practical tool for assessing the level of damage sustained by the pipe due to impact. However, these approaches are based on approximate models of the problem at hand and ignore the effect of certain parameters associated with subsea and operational conditions and the nature of the problem at hand (a wave propagation problem within a nonlinear medium). This can affect the accuracy of the predictions obtained. Furthermore the majority of these approaches consider only the local response of the pipe at the contact area essentially ignoring global behaviour.

CHAPTER 3

MATERIAL BEHAVIOUR UNDER INCREASING LOADING RATES

3.1 INTRODUCTION

Steel is widely used to construct a wide range of structural and non-structural components for offshore structures. As already discussed in the preceding chapter, steel is used to produce subsea pipes which form extensive networks enabling the transportation of oil and gas over large distances. Such pipelines may be subjected to a range of actions during their installation and operational life, including impact loads stemming from collisions. In order to improve their resilience and reduce the level of damage they sustain, a concrete layer (coating) can be used to provide additional protection against impact loading allowing the pipe to remain operational even after being subjected to extreme loading conditions such as those caused by accidental collisions [Palmer *et al.* (2006)].

Due to the short duration of the impact loads (a few milliseconds) generated during the collision of heavy objects (e.g. icebergs, rocks, fishing equipment) onto subsea pipes and their high intensity, which increases rapidly from zero to a maximum value, such loads can potentially cause rapid deformation of the pipe (especially in the region where the impact load is imposed). As a result, this may lead to large strain-rates being exhibited within the steel medium (or the concrete medium of the protective layer). Such elevated values of strain-rate are widely considered to affect the material properties of steel [Huh *et al.* (2002), Huh *et al.* (2008), Huh *et al.* (2009), Singh *et al.* (2011), Singh *et al.* (2013), Singh *et al.* (2014)] and concrete (strain-rate sensitivity) [Cotsovos & Pavlović (2008a), (2008b), (2008c), Lu & Li (2011), Cadoni *et al.* (2009), Zhang *et al.* (2009), Li *et al.* (2009), Zhou & Hao (2008b)] and as a consequence the dynamic response of the pipes under impact loading [Jones *et al.* (1992), Ishikawa & Hoshikawa (1994), Jones & Birch (2010), Chen & Shen (1998), Ng & Shen (2006)].

Thus prior to investigating the behaviour of subsea pipes under impact loading, it is worth studying the effect of increasing loading rates on the behaviour of specimens used for establishing the material properties of steel (and concrete) under static and high rate loading.

Steel is a ductile material and its behaviour under uniaxial compression or tension is described by stress-strain curves such as that presented in Figure 3.1. This is usually established through uniaxial tensile tests (coupon tests) conducted on dog-bone or bar specimens which are considered to represent material units from which average material properties can be determined. The behaviour of steel is characterized by the following four processes: (i) yielding, (ii) strain hardening, (iii) necking and (iv) rupture, which are associated with the different portions of the stress-strain curve in Figure 3.1. Steel initially exhibits elastic behaviour (during which deformation is recoverable after unloading) until the yield stress (f_y) is attained. The post-yielding behaviour of steel is usually characterized by strain hardening with the total strain ($\in_{total}$) exhibited beyond this limit not being fully recoverable thus consisting of a recoverable (elastic) and permanent (plastic) component [($\in_{total} = \in_{elastic} + \in_{plastic}$)]. Once the ultimate strength of steel is attained, necking initiates (reduction in cross-section of steel specimen). During this stage, an increase of the applied load results in further reduction of the specimen's cross-section, ultimately leading to rupture. Depending on the use of deformed or un-deformed (initial) geometry (i.e. cross-section area and length of the specimen) the behaviour of steel can be expressed by either true or engineering stress-strain curves. If the initial geometry [cross-section area (A_o) and length (L_o)] is used for calculating stresses and strains then engineering stress-strain curves are produced whereas the use of deformed geometry [cross-section area (A_f) and length (L_f)] results in the production of true stress-strain curves.

It has been experimentally established that the behaviour exhibited by steel (dog-bone or bar) specimens under high loading rates differs from that established under equivalent static loading once certain limits of applied loading rates are surpassed [Singh *et al.* (2013), Langseth *et al.* (1991), Huh *et al.* (2008)]. However, as it will be demonstrated later in this chapter, the available test data fails to accurately quantify the observed shift and provide the reasons that cause these differences as it is characterised by considerable scatter. The latter scatter is owed to a number of parameters which vary

from test to test such as the experimental technique employed, the shape and size of the specimens, the different types of steel used.

Concrete, unlike steel, is a brittle material with a high compressive strength (f_c) and significantly lower tensile strength ($f_t \approx 0.1 f_c$). Its behaviour is characterised by triaxiality and for the case of uniaxial compression and tension is described by the stress-strain curve shown in Figure 3.2. This is established experimentally by applying uniaxial compressive or tensile load on plain concrete prisms or cylinders under static loading conditions [Cotsovos & Pavlović (2008a), Kotsovos (2015)]. When subjected to external loading a complex tri-axial stress field develops within the concrete medium [Kotsovos (2015), Kotsovos & Pavlović (1995)] which is further accentuated by its cracking process [see Figure 3.3(a)] and the ensuing internal stress redistribution. The complexity of the stress field is due to the non-homogenous nature of the considered material characterized by the existence of micro-cracks [Kotsovos (2015), Kotsovos & Pavlović (1995)]. High concentrations develop at the tip of the micro-cracks and once the ultimate tensile strength of concrete is locally attained (at the tip of the cracks) the crack extends in the direction of principal maximum stress. Due to the extension of the crack, the tensile stresses at its tip decrease. The cracking process continues as the applied load increases until, at some stage, the edges of the micro-cracks meet and begin to form larger cracks (macro-cracks). Under uniaxial compression the final stage of macro-cracking is characterized by an increase in lateral strain which in the case of a plain concrete cylinders or prisms under uniaxial compression is exhibited at the mid height region of the subject specimen as shown in Figure 3.3 (b).

The application of the dynamic load at high rate causes the generation of stress waves which propagate through the concrete medium. This increases the complexity of the tri-axial stress field and potentially leads to the development of high stress concentration in certain regions of the specimen which can result in localized failure/cracking. The speed at which these waves propagate is dependent on the material properties of concrete and the level of damage (cracking) it has sustained. The magnitude of the developing stresses depends on the intensity of the imposed load and the rate at which it is applied. Based on the above, the behaviour of concrete specimen under high rate loading is a complicated wave propagation problem within a highly non-linear medium [Cotsovos & Pavlović (2008a), (2008b), (2008c)].

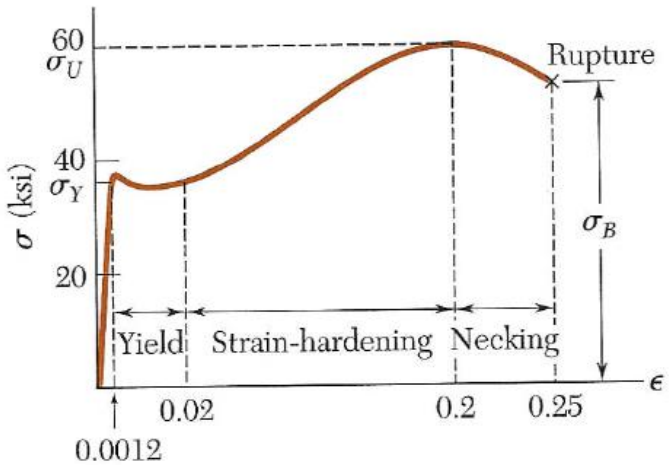

Figure 3.1: Typical stress-strain curve of steel under uniaxial static tensile load [OPTI (2015)].

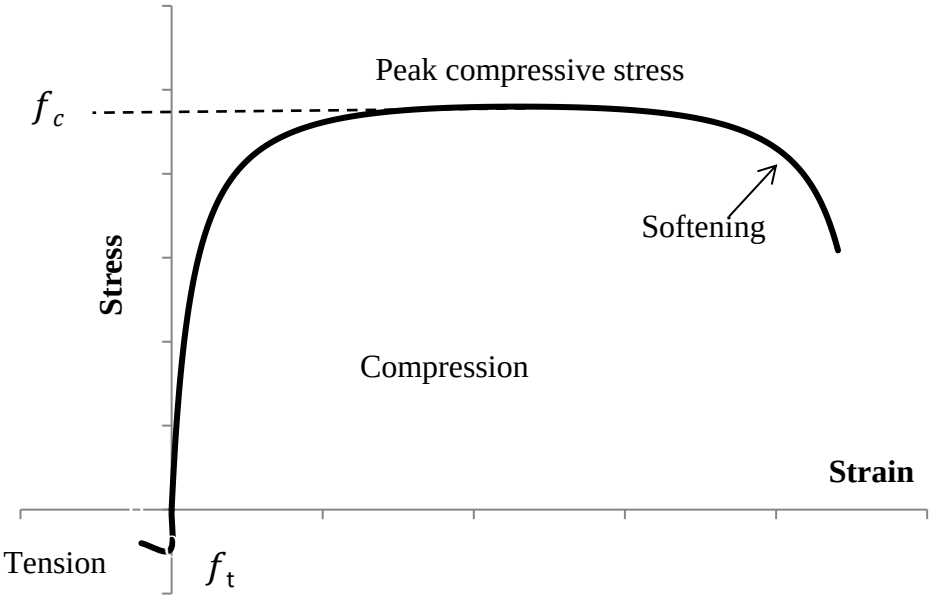

Figure 3.2: Typical stress-strain curve of concrete under uniaxial compression and tension.

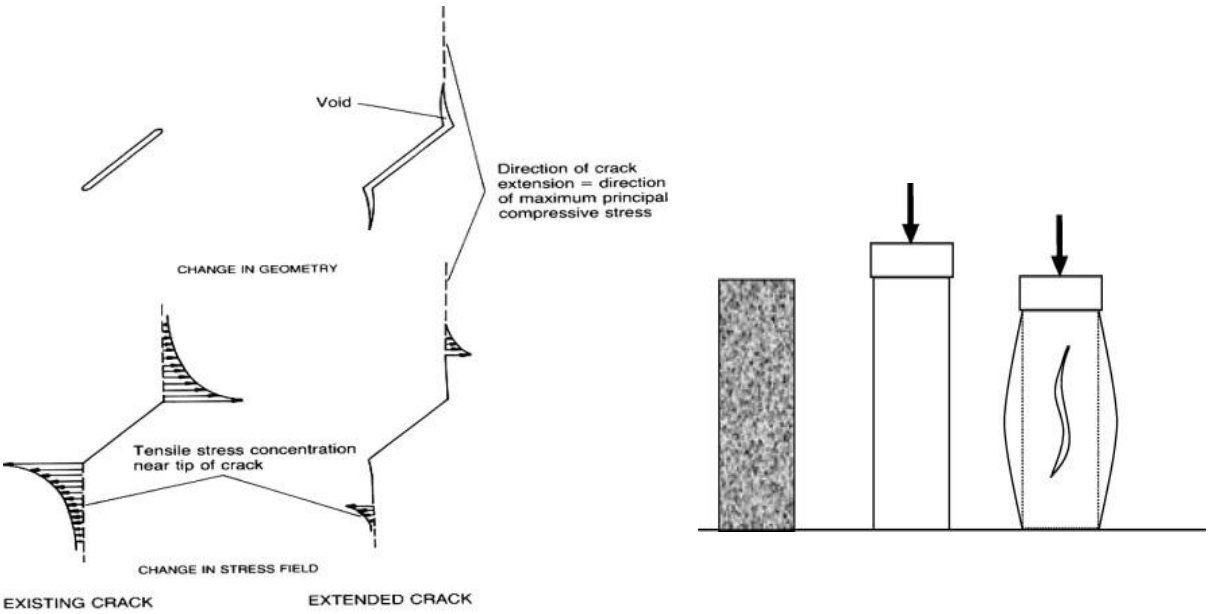

(a) (b)

Figure 3.3: (a) Micro cracking process in concrete (b) lateral deformation just prior to failure in a static test [Kotsovos & Pavlović (1995)].

In the present chapter emphasis is primarily focused on reviewing the available test data describing the behaviour of steel with increasing loading rates [Huh *et al.* (2008), Huh *et al.* (2009), Singh *et al.* (2013), Singh *et al.* (2011), Langseth *et al.* (1991), Cadoni *et al.* (2013), Cadoni *et al.* (2012), Boyce *et al.* (2007), Ozturk *et al.* (2013), Ogundare *et al.* (2013), Sun *et al.* (2012), Xu *et al.* (2013), Cotsovos & Pavlović (2008a), (2008b), (2008c), Cadoni *et al.* (2009), Lu & Li (2011), Zhang *et al.* (2009)]. This is then followed by a concise review of the experimental studies investigating the behaviour of concrete under high loading rates. The relevant test results are presented and critically analysed.

3.2 EXPERIMENTAL BACKGROUND

3.2.1 Experimental test setup

To date a range of different experimental setups have been employed for investigating the material behaviour of steel and plain concrete specimens under different loading rates. These include Split Hopkinson Pressure Bar (*SHPB*), hydro-pneumatic machine, drop-towers, and high speed servo-hydraulic testing machine.

Hydraulic testing machines are widely used for applying static loading characterised by a strain rates of up to $10^{-5}s^{-1}$. The use of fast pumps and valves can increase the flow of the oil achieving strain rates of up to $200s^{-1}$ [Huh *et al.* (2009)]. In the case of servo-hydraulic machines the specimen is gripped between two jaws and the load is applied through a moving cylinder as shown in Figure 3.4 (a). Electric motors [see Figure 3.4 (b)] are used to pressurise the operating hydraulic oil up to a certain level and in combination with accumulators achieve a faster response time. During testing, the applied load and displacement are acquired using load cells and Linear Variable Differential Transformers (*LVDTs*), respectively.

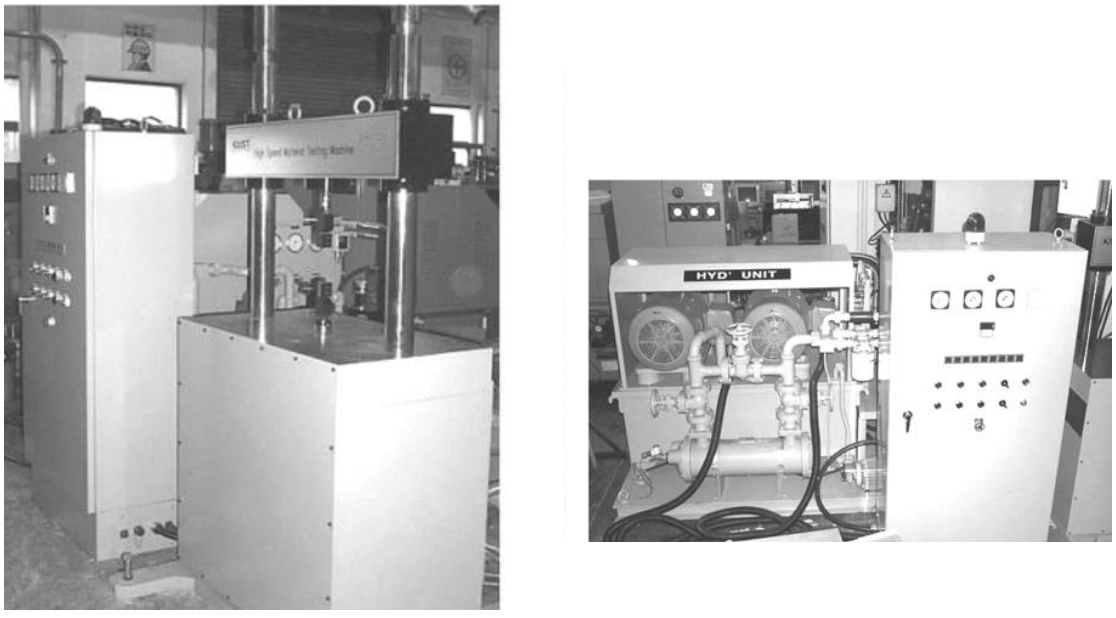

(a) (b)

Figure 3.4: Servo-hydraulic type high speed tensile testing machine (a) loading frame (b) servo-hydraulic unit [Huh *et al.* (2009)].

SHPB apparatus are the most commonly used loading technique capable of achieving strain rates of up to $5000s^{-1}$ [Othman *et al.* (2009)]. In this case the striker tube is fired from a gas gun and impacts an anvil as shown in Figure 3.5. As a result, a tensile pulse is generated which propagates along an incident bar towards the specimen. At the interface between the incident bar and the specimen, part of the pulse, passes into the specimen and then into the transmitted bar in the form of a tensile pulse whereas the rest of the pulse is reflected back into the incident bar as a compressive pulse. The strain gauges attached on two bars (at equal distances from each end of the bar) are used to measure the transmitted and reflected pulses.

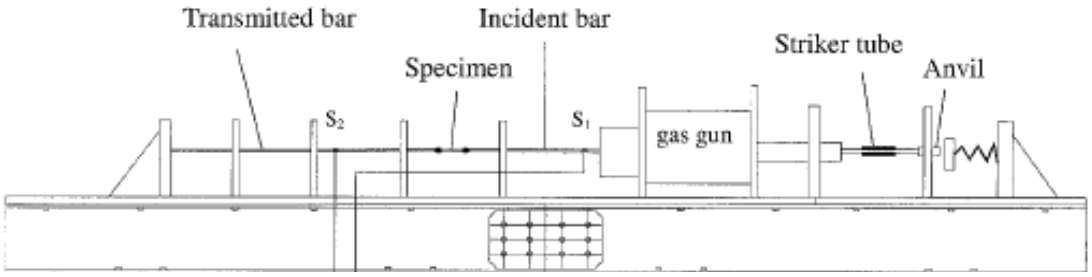

Figure 3.5: Schematic description of the *SHPB* [Huh *et al.* (2002)].

The modified Hopkinson bar setup has been used [Singh *et al.* (2013), Singh *et al.* (2011)] to investigate material behaviour at strain rates of $250\text{-}750s^{-1}$. In the modified Hopkinson bar setup the test specimen is fixed (screwed) between the input and output bars as shown in Figure 3.6. Mechanical energy is stored in the pre-stressed bar by means of a hydraulic actuator. With the release of the blocking device a tensile pulse (ε_i) is generated which propagates through the input bar towards the specimen. As in the case of *SHPB* at the interface between the input bar and the specimen, part of the pulse (ε_r) is reflected back into the input bar as a compressive pulse and the rest is transmitted (ε_t) through the output bar. Considering the bars are elastic: $\varepsilon_i + \varepsilon_r = \varepsilon_t$.

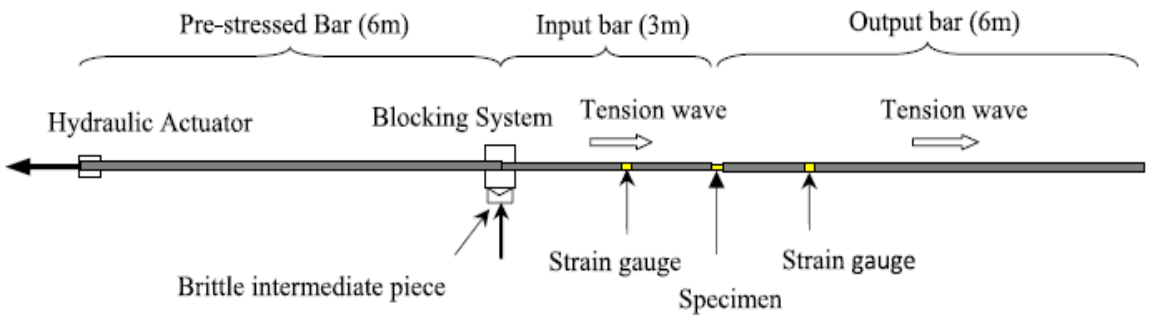

Figure 3.6: Modified Hopkinson bar apparatus [Singh *et al.* (2013)].

Hydro-pneumatic machines are used to study the material behaviour at strain rates up to 1-200s^{-1} [NTNU (2015)]. The stress wave is generated in a chamber with two compartments. One compartment is filled with pressurised air whereas the other is filled with water as shown in Figure 3.7. A tensile wave is generated due to a sudden release of the hydraulic pressure through a calibrated orifice using an electromagnetic valve. This wave is transmitted *via* a bar (piston shaft) to the specimen. The intensity of the generated stress wave is measured using strain gauges attached to the elastic bar which measures the specimen elongation with the help of non-contact displacement transducers.

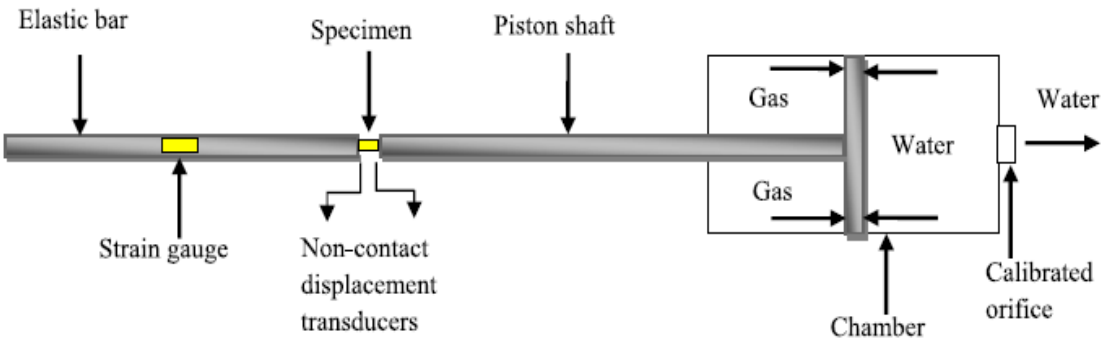

Figure 3.7: Hydro-pneumatic machine [Singh *et al.* (2013)].

The wave propagation in these apparatuses (*SHPB*, modified Hopkinson bar apparatus and hydro-pneumatic machine) can be described through the use of one dimensional elastic wave propagation theory. Neglecting wave dispersion effects, the engineering stress (σ_s), engineering strain (ε_s) and strain rate ($\dot{\varepsilon}_s$) exhibited by the specimen are given by Eq. (3.1) to Eq. (3.3)

$$\sigma_s = E \frac{A}{A_s} \varepsilon_t \qquad \text{Eq. (3.1)}$$

$$\varepsilon_s = \frac{2C_o}{L} \int_0^t \varepsilon_r dt \qquad \text{Eq. (3.2)}$$

$$\dot{\varepsilon}_s = \frac{2C_o}{L} \varepsilon_r \qquad \text{Eq. (3.3)}$$

The corresponding true stress (σ_T) and the true strain (ε_t) is given by Eq. (3.4) and Eq. (3.5) respectively:

$$\sigma_T = \sigma_s (1 + \varepsilon_s) \qquad \text{Eq. (3.4)}$$

$$\varepsilon_t = \ln (1 + \varepsilon_s) \qquad \text{Eq. (3.5)}$$

where: E : modulus of elasticity for the bar material
A : cross-sectional area of the bar
A_s : cross-sectional area of the specimen
L : gauge length of the specimen
C_o : speed of the stress wave in the bar

3.2.2 Test specimens

"Dog bone" and reinforcing bar steel specimens [see Figure 3.8 (a) & (b)] as well as plain concrete prismatic and cylindrical specimens [see Figure 3.8 (c) & (d)] are commonly used in order to experimentally study steel material behaviour under static loading. As a result these specimens are considered to constitute material units from which stress-strain curves are obtained describing material behaviour in tension or compression. Such curves are then used to establish certain material properties such as the values of stresses and corresponding strains at the yielding and at ultimate limit states as well as the modulus of elasticity (*E*).

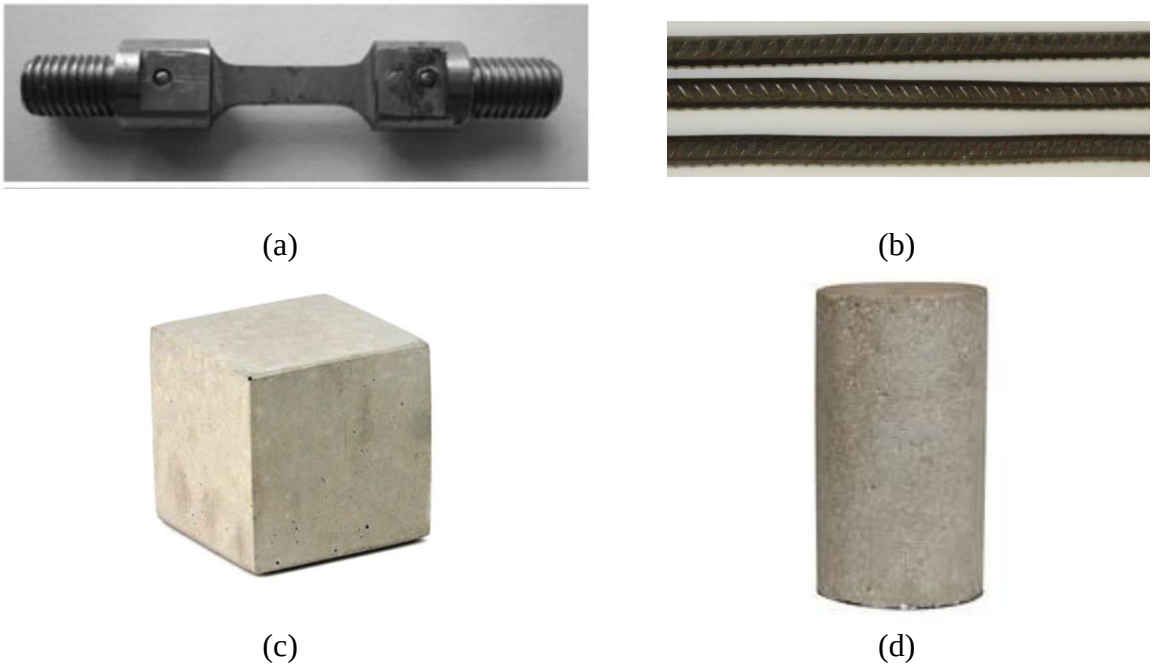

Figure 3.8: Typical specimens used for studying material behaviour (a) dog bone and (b) reinforcing bars (c) concrete cube and (d) concrete cylinder.

3.2.3 Tests results of steel specimens under increasing loading rate

Singh *et al.* (2013) investigated the behaviour of mild steel under increasing rates of tensile loading in relation to that established under static load. The study was carried out with strain rates of 0.001, 5, 25, 250, 500 and 750s^{-1}. The quasi static tests were carried out using a universal testing machine, whereas a hydro-pneumatic machine and a modified Hopkinson bar apparatus were used for testing under medium (5, 25s^{-1}) and high (250, 500 and 750s^{-1}) strain rates respectively. "Dog bone" specimens with a gauge length of 10mm, a width of 4mm and a thickness of 2mm were used. Figure 3.9 shows the engineering and true stress-strain curves obtained from the mild steel specimens tested under static (0.001s^{-1}) and dynamic (5, 25, 250, 500 and 750s^{-1}) strain rates. It is observed that the yield strength of the steel increased significantly with increasing strain rates. The increase in the ultimate strength was observed for strain rates of up to 250s^{-1} however the ultimate strength remained essentially constant for strain rates of 500 and 750s^{-1}. Therefore, the yield stress of the mild steel was found to be more strain-rate sensitive than its ultimate tensile strength.

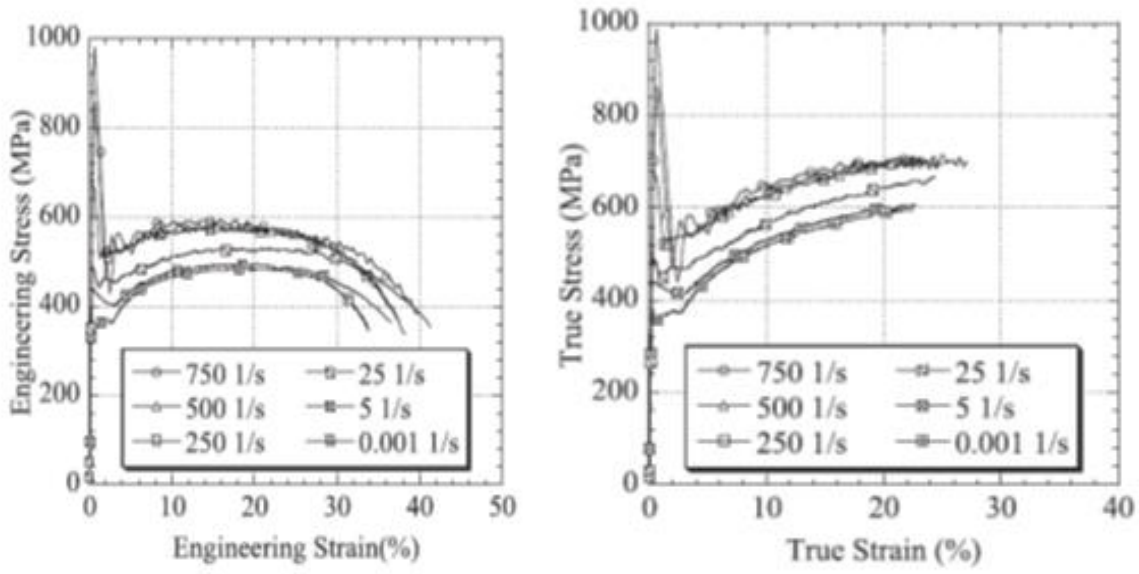

(a) (b)

Figure 3.9: Stress-strain curves (a) engineering (b) true [Singh *et al.* (2013)].

Langseth *et al.* (1991) investigated the effect of strain rate on the tensile behaviour of *ST 52-3N* grade mild steel. This grade of mild steel is commonly used in offshore platforms due to its good weldability and high ductility. A high rate biaxial testing machine was used for conducting tensile tests with strain rates of 0.0001 to $25s^{-1}$, whereas *SHPB* was employed for achieving strain rates of 100 to $1100s^{-1}$. "Dog bone" specimens with two different thicknesses of 8mm and 25mm were used.

Figure 3.10 shows the nominal stress-strain curves with increasing loading rates. It was observed that with the increase of the strain rate the yield strength also increased significantly. The increase in the yield stress was observed to be higher for the 8mm specimens compared to the 25mm specimens. Figure 3.11 shows the variation in stresses with varying strain rates at different levels of strain. It is observed that the yield stress of the mild steel is more sensitive than the stresses associated with specific values of strain in the hardening region under increasing strain rates.

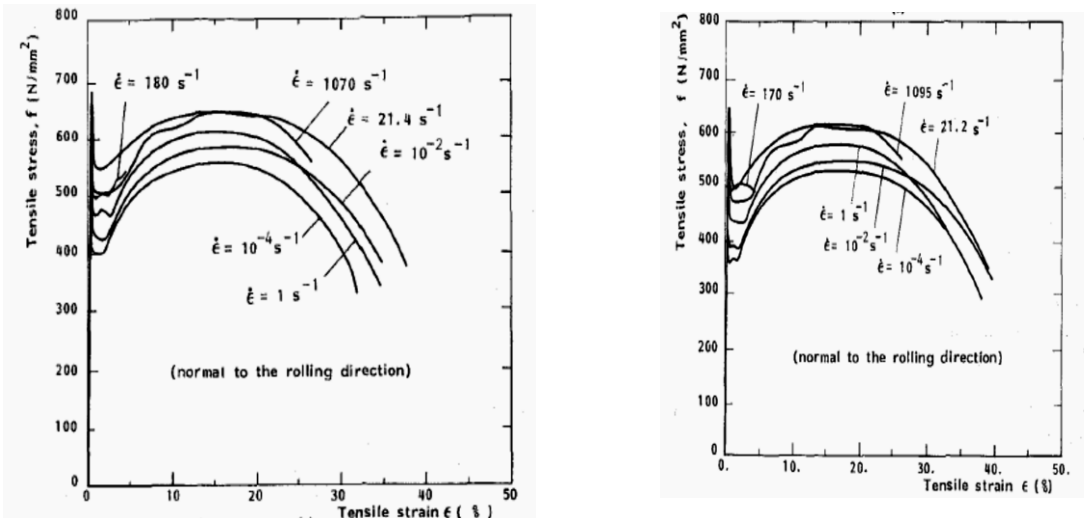

Figure 3.10: Stress-strain curves at various strain rates and with thicknesses of (a) 8mm (b) 25mm [Langseth *et al.* (1991)].

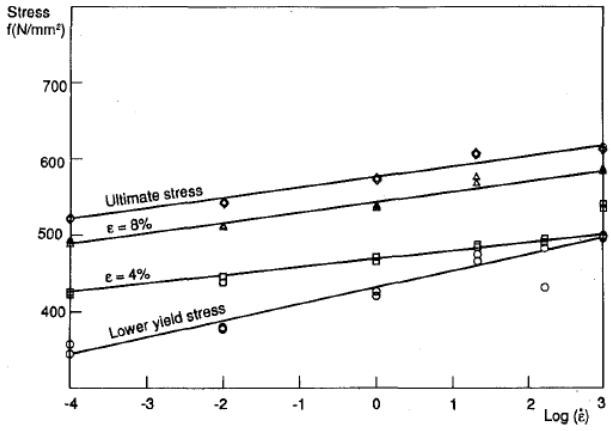

Figure 3.11: Variation of stresses with strain rate [Langseth *et al.* (1991)].

Singh *et al*. (2011) investigated the tensile behaviour of the Multi Phase 800 High Yield strength steel (MP800HY) under increasing strain rates. The tensile tests were carried out on dog-bone specimens with a gauge length of 10mm, a width of 4mm and a thickness of 2mm. An electromechanical universal testing machine was used to conduct the quasi static tests ($0.001s^{-1}$) whereas a hydro-pneumatic machine and a modified Hopkinson bar apparatus were used for conducting tests under intermediate (5, $25s^{-1}$) and high (250, 500, and $750s^{-1}$) strain rates respectively. By observing the engineering

and true stress-strain curves obtained with increasing strain rates presented in Figure 3.12 it can be observed that the values of stresses associated with specific values of strains beyond the yield point increased with increasing levels of strain rate. However this increase, especially in the case of the yield stress, was much smaller compared to that exhibited in previous studies investigating the behaviour of mild steel [Singh *et al.* (2013), Langseth *et al.* (1991)].

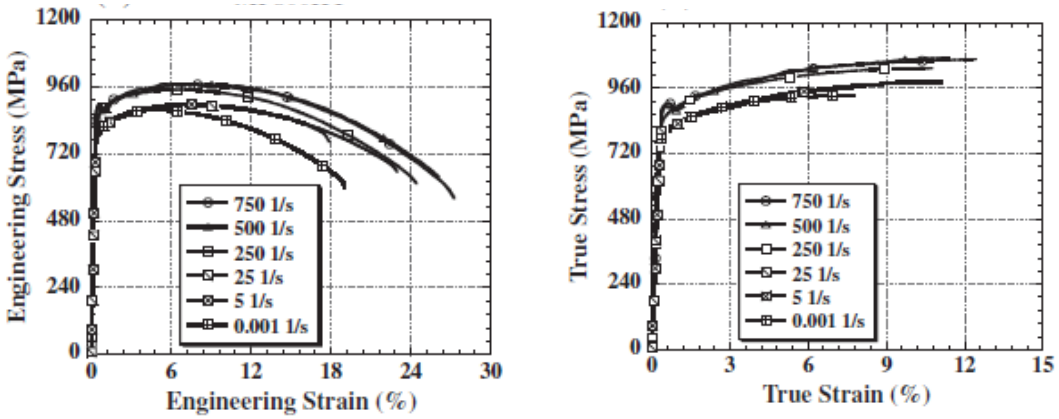

(a) (b)

Figure 3.12: Stress–strain curves (a) engineering (b) true [Singh *et al.* (2011)].

Singh *et al.* (2014) carried out an experimental investigation to study the tensile behaviour of the Complex Phase (CP800) steel at quasi static and high strain rates. "Dog bone" specimens with a gauge length of 10mm and a width of 4mm were used. A universal testing machine was used for conducting quasi static ($0.001s^{-1}$) tests, whereas hydro-pneumatic machine and modified Hopkinson bar apparatus were used for conducting tests under medium (5 and $25s^{-1}$) and high (250, 500, and $750s^{-1}$) strain rates respectively. Figure 3.13 shows the engineering and true stress-strain curves for specimens under increasing strain rates. It was observed that strain rates up to $25s^{-1}$ did not significantly affect the yield stress of *CP800* steel, however, the increase in the yield stress was more prominent for strain rates over $250s^{-1}$. A similar trend for the whole stress-strain curve beyond the yield point is observed. Stresses associated with certain values of strain in the above region increased significantly with values of strain-rate beyond $250s^{-1}$.

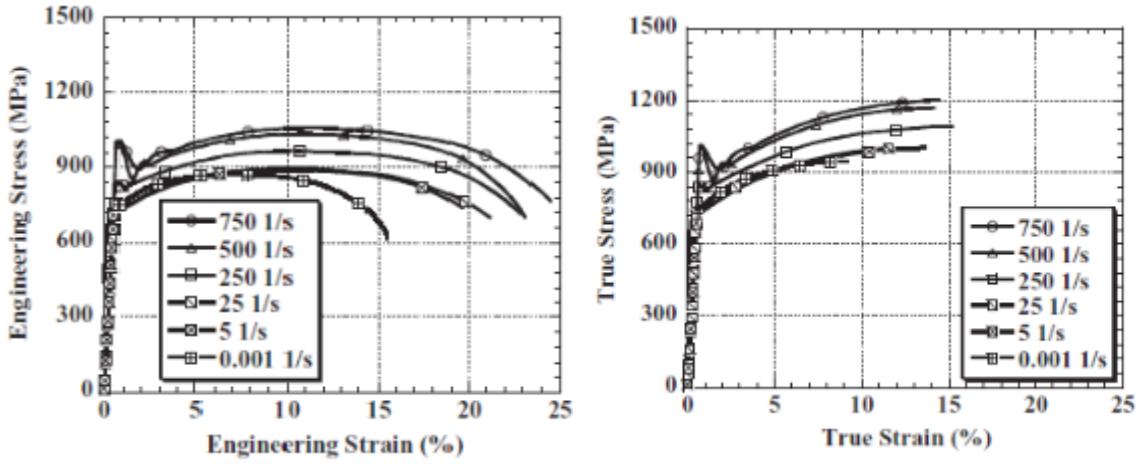

(a) (b)

Figure 3.13: Stress-strain curves (a) engineering (b) true [Singh *et al.* (2014)].

Huh *et al.* (2009) carried out tensile tests to investigate the effect of increasing strain rates on the behaviour of low and high strength steels. Steel Plate Re-phosphorised Cold rolled (SPRC), Transformation Induced Plasticity (TRIP) and Excel Zinc Nickel Cold-rolled Drawing quality (EZNCD) steel sheets were used in the investigation. Quasi static tests were carried out with strain rate of $0.003s^{-1}$ whereas for the dynamic tests strain rates of 1 to $200s^{-1}$ were achieved. Dog-bone specimens with a width of 6mm and gauge lengths of 15mm and 30mm were employed. The 15mm gauge length specimens were used in the tensile tests carried out with a strain rate of $200s^{-1}$, whereas 30mm specimens were used for tests with strain rates of 0.003 to $100s^{-1}$.

Figure 3.14 shows the true stress-strain curves recorded during testing under increasing strain rates. It was observed that with the increase in the strain rate, the yield stress of all specimens also increased. However, the effect was found to be more significant for *EZNCD* and *SPCC* steel specimens [see Figure 3.14 (a) and (b)] as compared to *SPRC390E-BH* and *TRIP60* steel specimens [see Figure 3.14 (c) and (d)]. Thus, the steel specimen with lower static yield strength (f_y) was affected more by the increase in strain rate compared to steel specimens with the higher static yield strength. This trend was also observed when comparing results of other experimental studies [Singh *et al.* (2011), (2014), Langseth *et al.* (1991)].

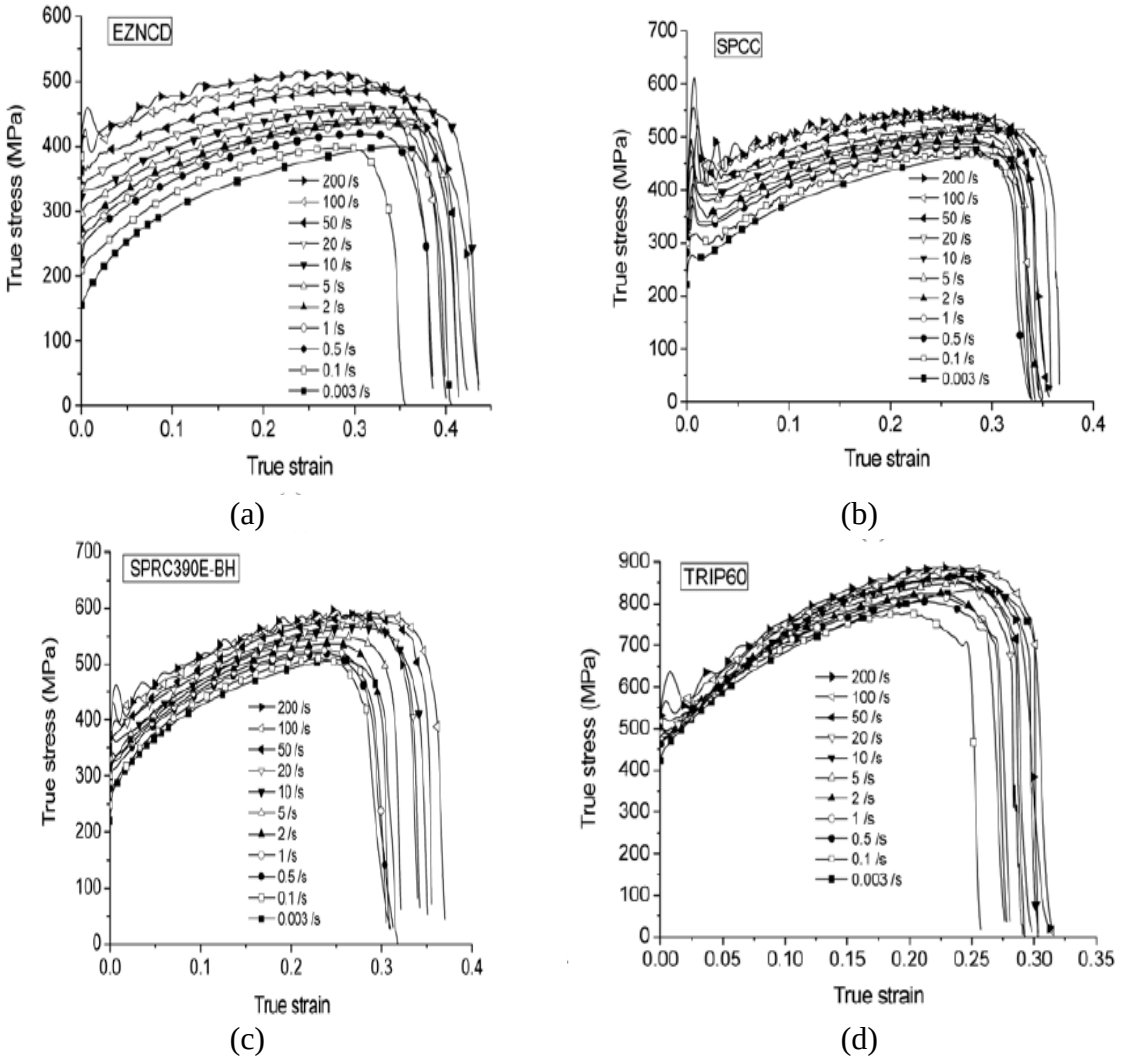

Figure 3.14: True stress-strain curves with different strain rates for (a) *EZNCD* (b) *SPRCC* (c) *SPRC390E-BH* (d) *TRIP60* [Huh *et al.* (2009)].

Figure 3.15 shows the relationship of flow stress associated with different values of strain with respect to the strain rate achieved during testing. In Figure 3.15, the experimental results are denoted by the hollow symbols whereas the solid lines indicate the fitted curves. The curves defined by the square symbols represent the variation of yield stress with increasing values of the strain-rate whereas the curves defined by other symbols show the variation of flow stress (associated with different values of strain) with the increasing strain-rate. The latter curves reveal that the yield and flow stresses increase as the values of strain rate become larger in the case of the *EZNCD* specimens

[see Figure 3.15 (a)]. The increase in the stress values remains essentially similar with increasing values of strain for the case of the *TRIP60* specimens [see Figure 3.15 (d)].

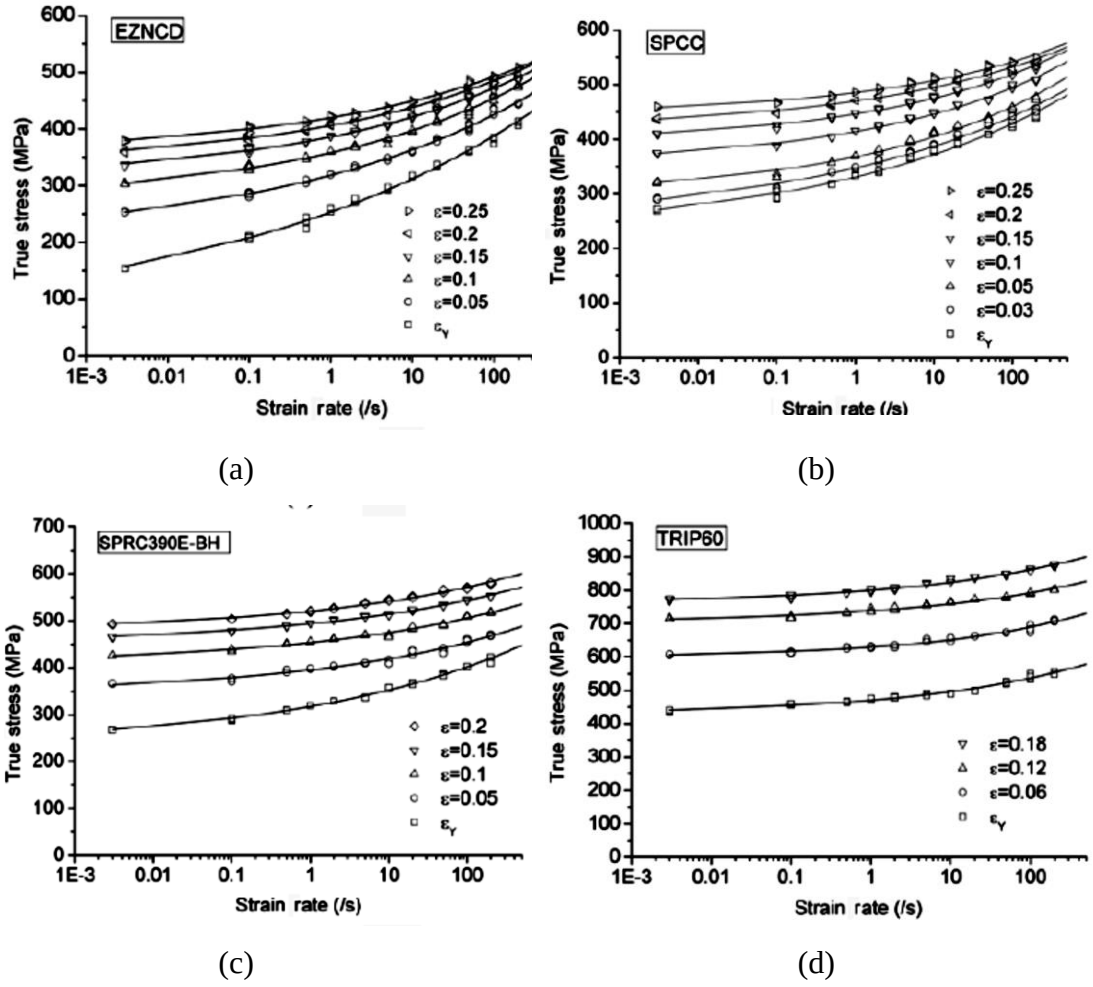

Figure 3.15: Relation of flow stress with respect to strain rate and with the variation of strain [Huh *et al.* (2009)].

Huh *et al.* (2008) investigated the dynamic tensile behaviour of the *TRIP* and Dual Phase (DP) type steel sheets. The static tensile machine was used to conduct tests under strain rates of $0.003s^{-1}$ whereas a high-speed hydraulic machine was used for achieving higher strain rates (e.g. 0.1, 1, 3, 10, 30, 100 and $200s^{-1}$). Figure 3.16 shows the yield stresses obtained from the steel specimens with increasing strain rates. When considering the specimens with the yield strength approximately equal to 400MPa the influence of the strain rate on the yield stress was found to be larger for the case of *DP* specimens as compared to *TRIP* specimens. However for the case of specimens

exhibiting higher values of static yield stress (DP800 & TRIP800) the increase observed in the yield stress with strain rate was similar.

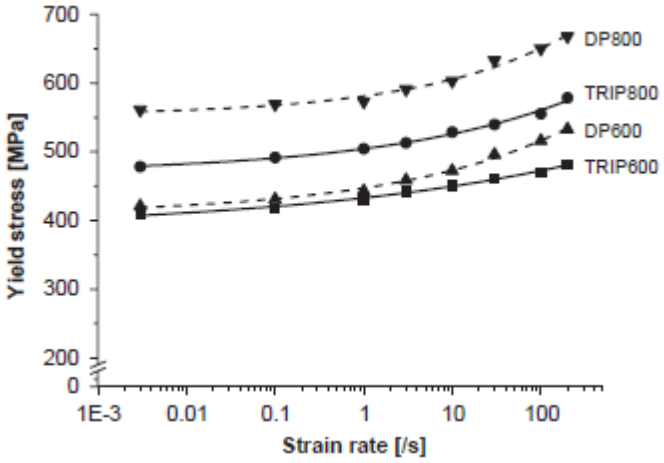

Figure 3.16: Yield stresses at different strain rates for *TRIP600*, *TRIP800*, *DP600* and *DP800* steel specimens [Huh *et al.* (2008)].

In addition to the tests carried out on dog-bone specimens, reinforcement bars specimens are also used for investigating the material behaviour of steel under static and increasing loading rates. Malvar and Crawford (1998) gathered and presented data obtained from experimental studies investigating the behaviour of reinforcement bars under high strain rates presented in Figure 3.17. The Dynamic Increase Factor (DIF), defined as the yield stress recorded under high rate (dynamic) loading normalised by the value of yield strength established under static loading, is used to present the influence of the strain rate on the yield stress of steel. It is observed that with the increase in the strain rate beyond a certain level the *DIF* also increases. The influence of strain rate on the *DIF* is observed to be more profound for the case of the reinforcing bars characterized by lower static yield strength values. This was also observed in the case of dog-bone specimens [Singh *et al.* (2011), (2014), Langseth *et al.* (1991)]. It can be seen from Figure 3.17 that most of the tests have been carried out with strain rates less than $1s^{-1}$ and very limited data is available for tests with strain rates greater than $10s^{-1}$. This is due to the fact that majority of these tests have been carried out using hydraulic type machines which is characterized by considerable scatter.

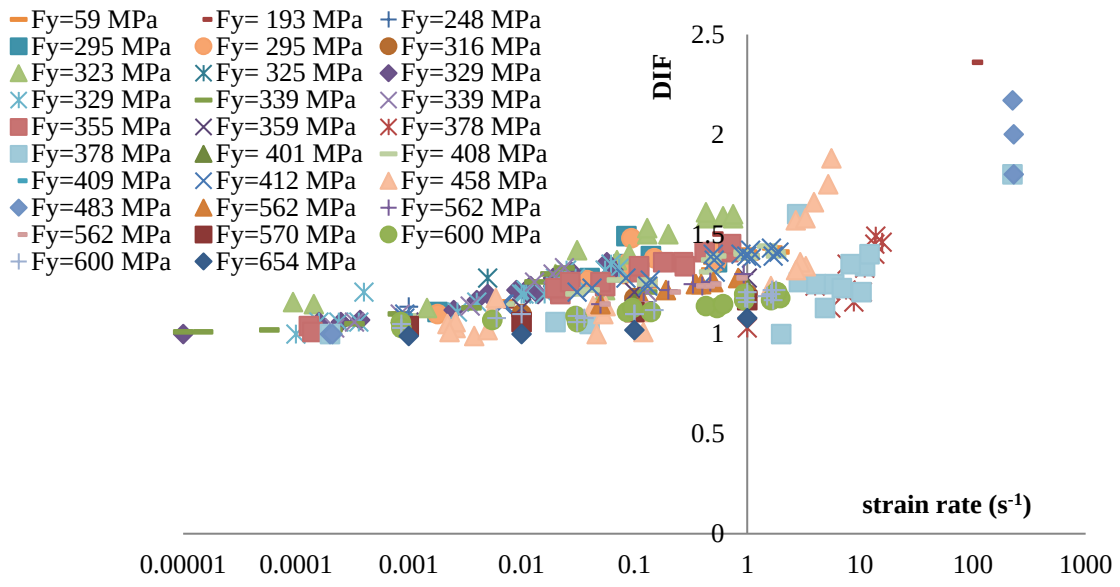

Figure 3.17: Reinforcing bars under different rates of loading [Malvar & Crawford (1998b)].

3.2.4 Discussion of experimental results

The test results obtained from the experimental studies conducted to date investigating the behaviour of steel specimens under high rate loading are used to compile a database, presented in detail in Appendix B. Figure 3.18 shows an overview of the relevant test data carried out on steel "dog bone" specimens under increasing rate of uniaxial tension [Huh *et al.* (2008), Huh *et al.* (2009), Singh *et al.* (2013), Singh *et al.* (2011), Langseth *et al.* (1991), Cadoni *et al.* (2013), Cadoni *et al.* (2012), Boyce *et al.* (2007), Ozturk *et al.* (2013), Ogundare *et al.* (2013), Sun *et al.* (2012), Xu *et al.* (2013)]. Although it is evident from Figure 3.18 that with increasing values of strain rates the *DIF* ($f_{y\text{-dynamic}}/f_{y\text{-static}}$) also increases, it should be pointed out that the experimental data is characterized by considerable scatter. This scatter is owed to a number of parameters (e.g. the experimental technique employed, the shape and size of the specimens, the different types of steel used, etc.) which vary from experiment to experiment. The available data is analysed in respect to the above parameters in an attempt to assess their contribution to the overall scatter that characterizes the relevant experimental data. Based on the analysis of the test data the effect of two parameters can be clearly identified; that (i) of the steel grade and (ii) of the loading apparatus employed during testing.

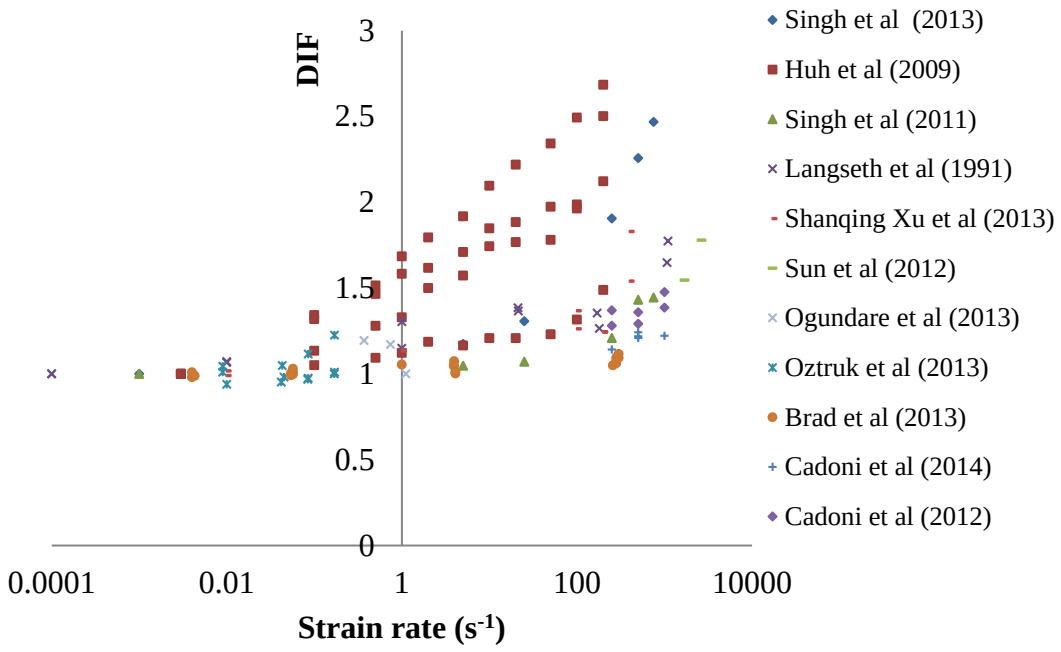

Figure 3.18: Test data describing the variation of the *DIF* ($f_{y\text{-dynamic}}/f_{y\text{-static}}$) with increasing strain rates.

Effect of steel grade: The effect of steel grade on *DIF* describing the variation (increase) of certain aspects of specimen behaviour (f_y, f_u) in relation to the exhibited strain rate $\dot{\varepsilon}$ is shown in Figure 3.19 to Figure 3.21. In general, it is observed that the increase of strain rate beyond a certain level resulted in an increase of *DIF* associated with yield strength. However, the effect is found to be more significant for low strength steel as compared to the high strength steel. It is also observed that the ultimate strength of the steel remains essentially constant with increasing strain rates [see Figure 3.19 to Figure 3.21]. Therefore, the yield stress of the steel was found to be more strain-rate sensitive than the ultimate tensile strength.

Effect of specimen size: The effect of specimen size on *DIF* describing the variation (increase) in relation to the exhibited strain rate $\dot{\varepsilon}$ is shown in Figure 3.22 to Figure 3.24. It can be seen that the data is characterized by considerable scatter, however, it is observed that for the case of steel having similar static yield strengths the increase of *DIF* associated with yield strength with increasing strain rates is higher for dog-bone specimens with smaller (thinner) cross-sections.

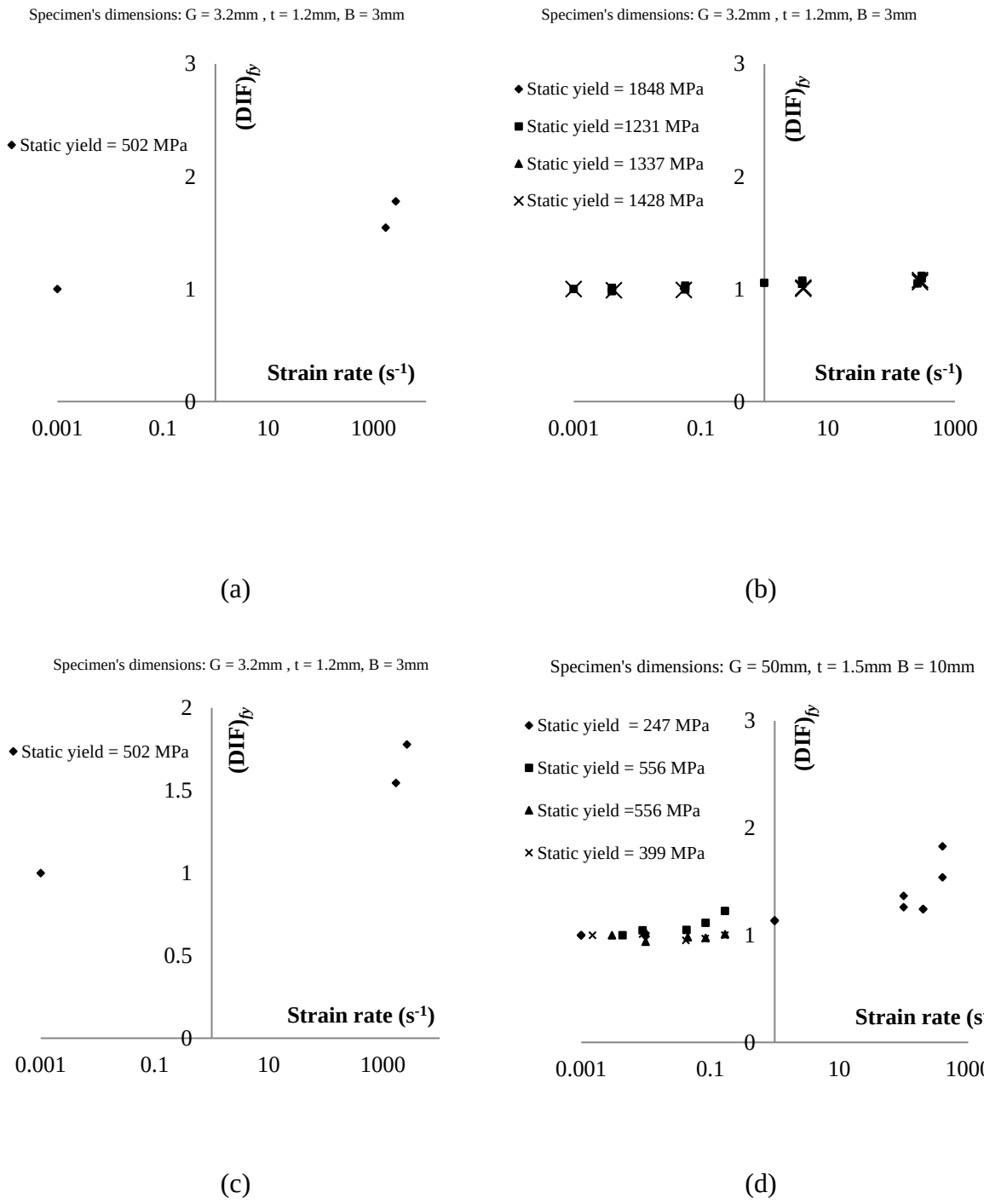

Figure 3.19: Variation of *DIFs* associated with the yield strength (f_y,) with increasing strain rate for different steel grades (where G: Gauge length, t = thickness, B = width).

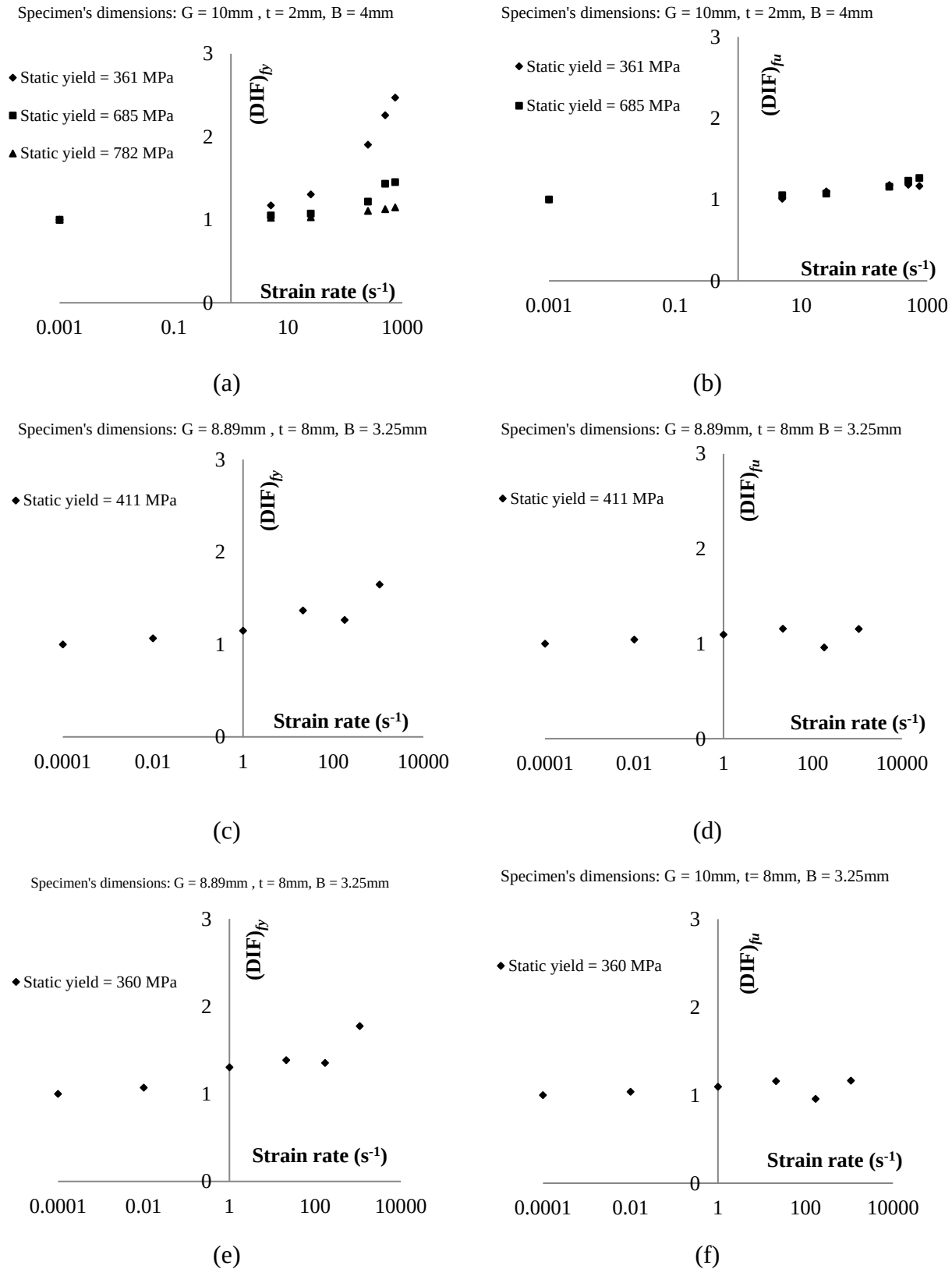

Figure 3.20: Variation of DIF associated with the yield (f_y,) and ultimate (f_u) stresses of the specimens with increasing strain rates for different steel grades.

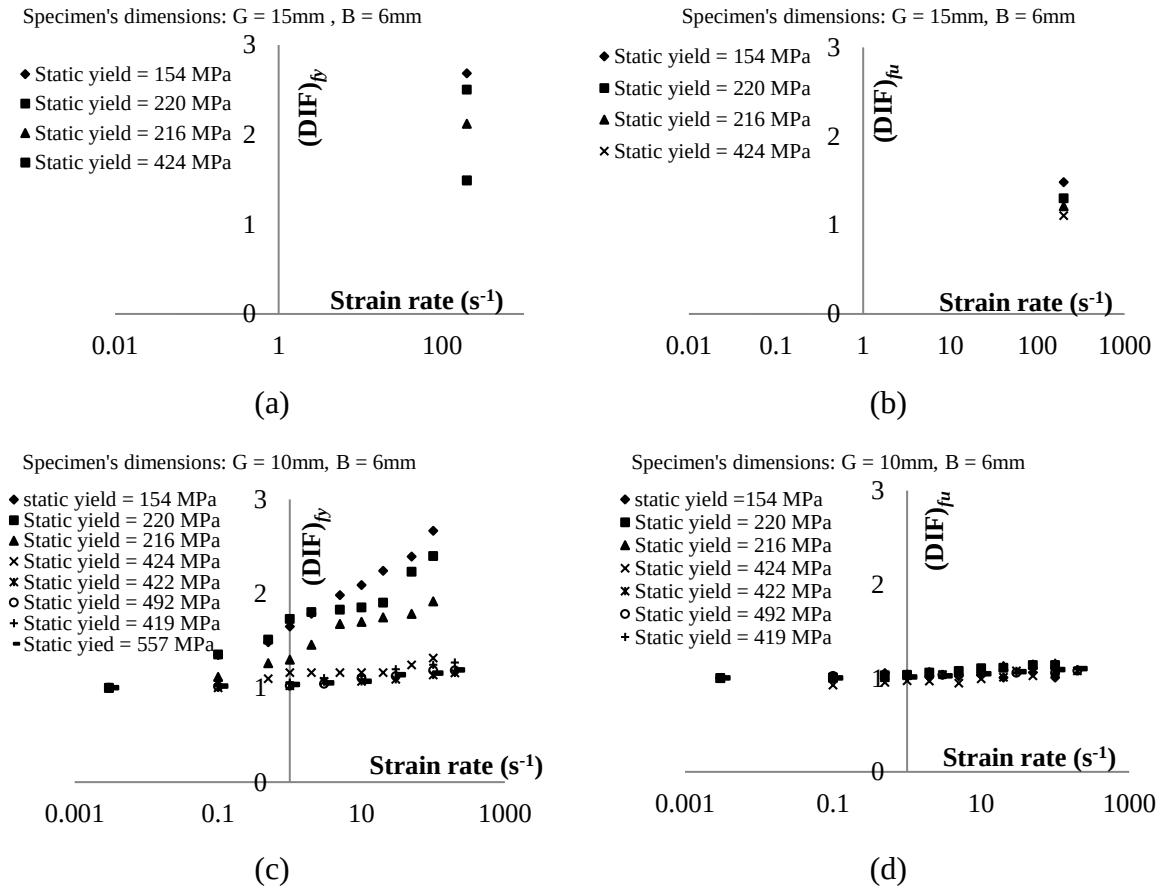

Figure 3.21: Variation of DIF associated with yield (f_y,) and ultimate (f_u) stresses with increasing strain rates for different steel grades.

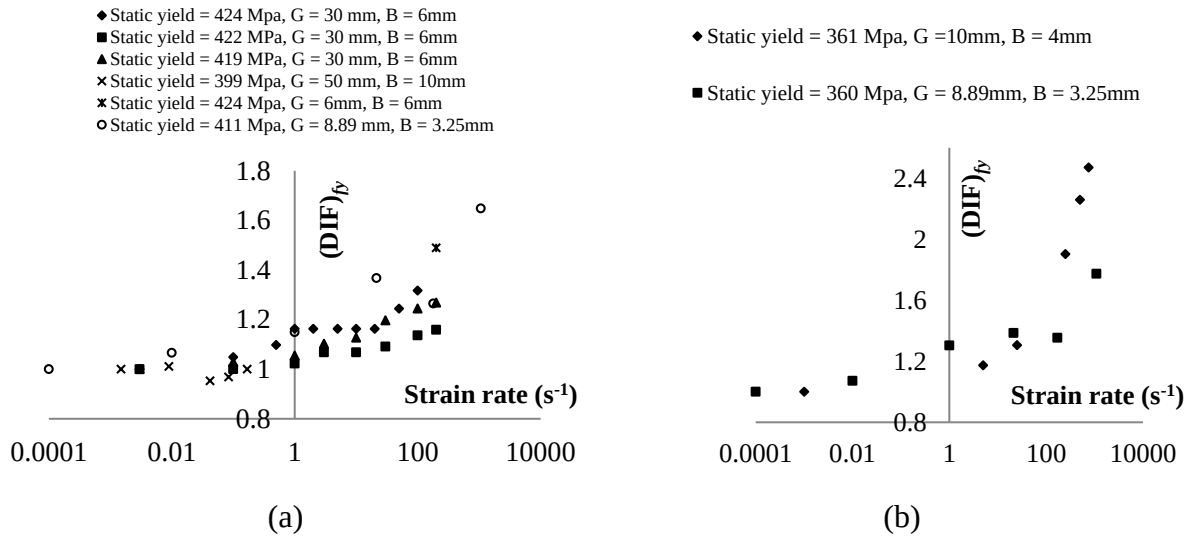

Figure 3.22: Variation of DIF associated with yield stresses (f_y,) with increasing strain rates for specimens with different cross-sections.

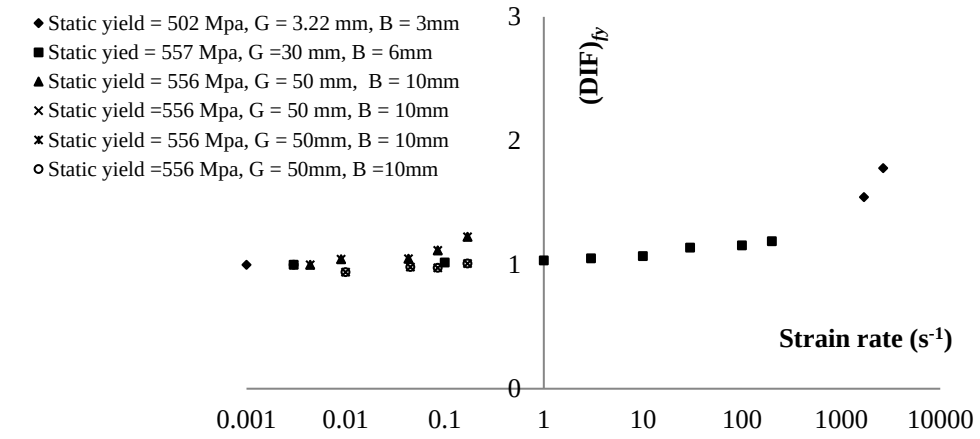

(a)

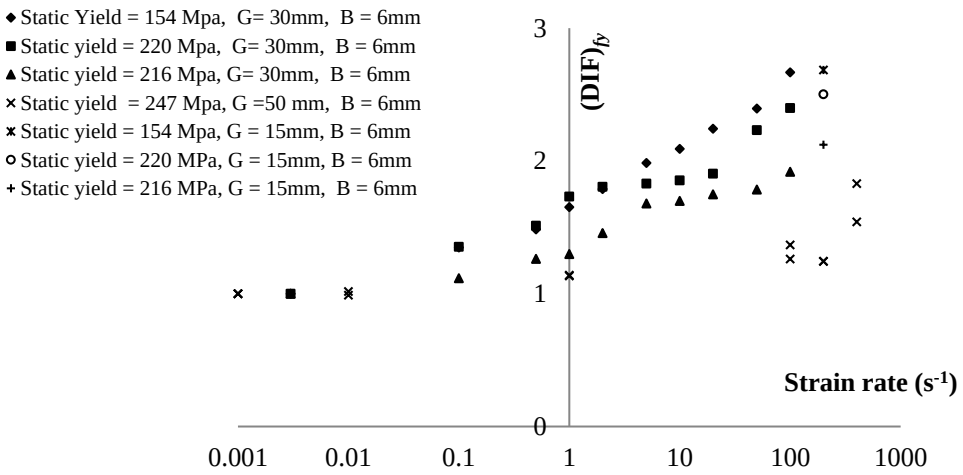

(b)

Figure 3.23: Variation of DIF associated with the yield stress (f_y,) with increasing values of strain rate for different specimen cross-sections.

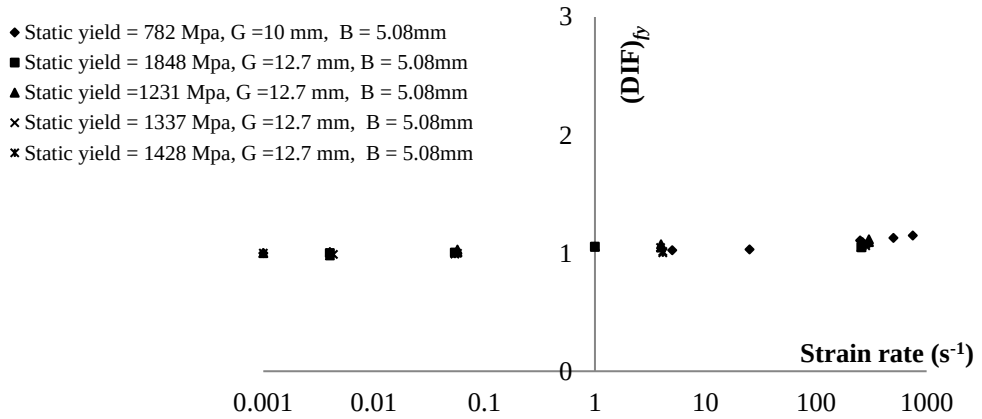

Figure 3.24: Variation of DIF associated with the yield stress (f_y,) with increasing values of strain rate for different specimen cross-sections.

Effect of loading technique: The effect of loading technique on the *DIF* expressing the ratio between the yield stress established under dynamic (high rate) loading and its counterpart established under static loading ($DIF = f_{y\text{-}dynamic}/f_{y\text{-}static}$) is shown in Figure 3.25. It can be seen that the data is characterized by considerable scatter and is very limited for some of the loading techniques considered, however, this scatter reduces when excluding the data obtained from hydraulic and biaxial machines as shown in Figure 3.26.

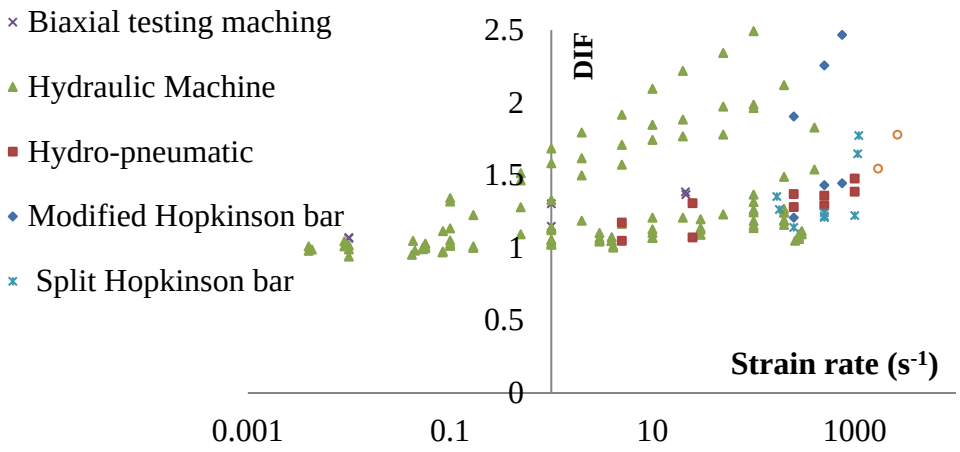

Figure 3.25: Data describing the variation of *DIF* ($f_{y\text{-}dynamic}/f_{y\text{-}static}$) under increasing values of strain rates obtained from different loading mechanisms.

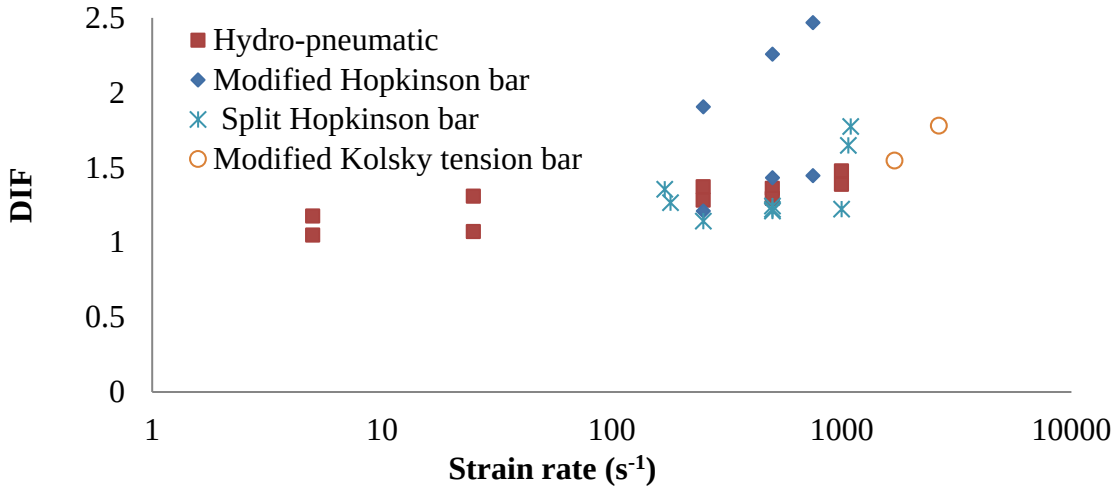

Figure 3.26: Data describing the variation of *DIF* associated with f_y under increasing values of strain rate obtained from the available loading mechanisms excluding hydraulic and biaxial loading machines.

3.2.5 Test results of concrete under increasing loading rates

An experimental investigation was carried out by Cadoni *et al*. (2009) to study the influence of high loading rates on the compressive and tensile behaviour of concrete. The study was carried out with three different levels of strain rate: quasi-static, intermediate and high. The quasi-static test was carried out with strain rates of $10^{-6}s^{-1}$, whereas, intermediate and high rate loading tests were carried with strain rates of $1s^{-1}$, $10s^{-1}$ and $15s^{-1}$. In order to study the influence of the aggregate and specimen size on the exhibited behaviour under increasing loading rates concrete cubes with length between 60 and 200mm and 5 to 25mm aggregates were used.

Table 3.1 provides the dynamic increase factors (DIF) for concrete cubes with 60mm length tested under increasing rates of tensile loading. A concrete mix designation of C40/C50 with aggregate sizes of 5 and 10mm was used. It was observed that with increasing loading rates the *DIF* also increased. This increase is more profound for the case of concrete specimens with smaller aggregate size (see Table 3.1).

Table 3.2 provides the dynamic increase factors (DIF) for concrete cubes with 200mm length tested under increasing rates of tensile loading. As in the case of the 60mm concrete cubes, C40/C50 concrete with aggregate size of 10 and 25mm was used. As observed for the case of concrete specimens with 60mm length, the *DIF* increases with the loading rate. It was also observed that for the case of concrete specimens with larger aggregate size, higher values of *DIF* was observed (see Table 3.2) which contradicts what was observed when testing the smaller specimens (see Table 3.1). Comparing the test results of 60 and 200mm length concrete specimens with 10mm aggregates exhibited values of *DIF* is higher for the case of smaller concrete specimens (see data in Table 3.2 in relations to that of Table 3.1).

Table 3.3 presents the values of *DIF* established for the case of 100mm concrete cubes tested under static and dynamic compressive loads. In general, it was observed that with the increasing values of loading rate the *DIF* also increases. It was also observed that for the low strength concrete (C25/30) the increase in *DIF* is higher (see Table 3.3) as compared to concrete cubes characterise by higher compressive strengths (C50/60 & C40/50). Furthermore, it was also observed that for a specific grade of concrete the increase in *DIF* was higher when using larger aggregate size.

Table 3.1: Dynamic increase factors (DIFs) established for the case of concrete cubes having 60mm length tested under increasing rates of tensile loading [Cadoni *et al.* (2009)].

Strain rate, $\dot{\epsilon}$ (s^{-1})	**Aggregate size, d_{max} (mm)**	**Strength (MPa)**	**Dynamic increase factor (DIF)**
10	5	11.8 ± 1.5	4.44
1	5	9.2 ± 0.8	3.45
10^{-6}	5	2.66 ± 0.7	1.00
10	10	10.5 ± 0.9	2.91
1	10	7.38 ± 3.2	2.04
10^{-6}	10	3.61 ± 0.6	1.00

Table 3.2: Dynamic increase factors for concrete cubes having 200mm length tested under static and dynamic tensile loading rates [Cadoni *et al.* (2009)].

Strain rate, $\dot{\epsilon}$ (s^{-1})	**Aggregate size, d_{max} (mm)**	**Strength (MPa)**	**Dynamic increase factor (DIF)**
10	10	8.68 ± 1.2	2.42
1	10	6.69 ± 2.5	1.87
10^{-6}	10	3.57 ± 0.4	1.00
10	25	7.99 ± 0.6	2.59
1	25	6.28 ± 0.3	2.03
10^{-6}	25	3.09 ± 0.4	1.00

Table 3.3: Dynamic increase factors for concrete cubes having 100mm length tested under static and dynamic compressive loading rates [Cadoni *et al.* (2009)].

Strain rate, $\dot{\epsilon}$ (s^{-1})	**Aggregate size, d_{max} (mm)**	**Concrete Grade -water cement ratio**	**Strength (MPa)**	**Dynamic increase factor (DIF)**
15	16	C25/30 - 0.65	71.8 ± 10.5	2.05
10^{-3}	16	C25/30 - 0.65	52.7 ± 2.8	1.51
10^{-6}	16	C25/30 - 0.65	34.9 ± 0.7	1.00
15	16	C50/60 - 0.38	119.8 ± 2.6	1.97
10^{-3}	16	C50/60 - 0.38	95.7 ± 4.9	1.57
10^{-6}	16	C50/60 - 0.38	61.0 ± 9.8	1.00
15	10	C40/50 – 0.50	97.2 ± 8.8	1.57
10^{-3}	10	C40/50 – 0.50	89.9	1.45
10^{-6}	10	C40/50 – 0.50	62.0	1.00
15	25	C40/50 – 0.50	99.6 ± 14.3	1.78
10^{-3}	25	C40/50 – 0.50	84.7	1.51
10^{-6}	25	C40/50 – 0.50	56.1	1.00

The data presented in Figure 3.37 shows the effect of strain rate on the DIF of concrete cubes. The DIF observed for uniaxial tension is higher compared to that observed for the case of uniaxial compression.

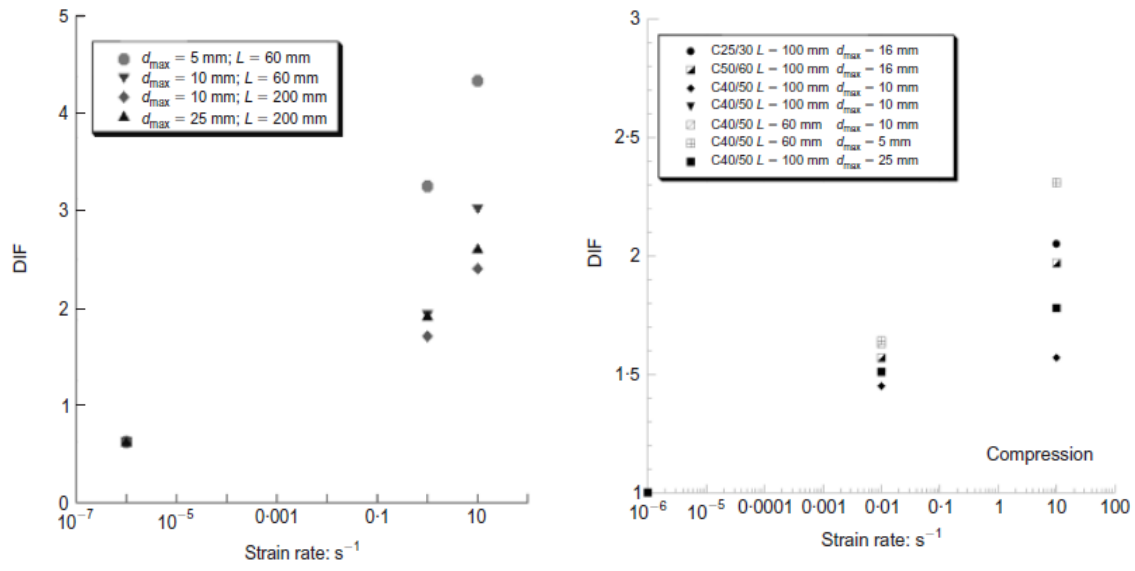

(a) (b)

Figure 3.27: Effect of strain rate on the dynamic increase factor (DIF) of concrete cubes under (a) tensile and (b) compressive loading [Cadoni *et al.* (2009)].

A numerical investigation was carried out by Lu & Li (2011) in order to study the uniaxial tensile strength of concrete under increasing loading rates. For this purpose, direct dynamic tests, dynamic splitting tests and spalling tests on concrete specimens were modelled numerically. Based on these numerical predictions it was observed that the enhancement in the tensile strength of concrete under increasing loading rates is due to the material property of concrete and it is largely attributed to the micro crack inertia [Lu & Li (2011)].

Zhang *et al.* (2009) investigated the variation of the compressive strength of concrete-like materials under increasing loading rates using a split Hopkinson pressure bar apparatus. Tubular and solid mortar specimens were investigated under increasing loading rates in order to correlate the axial strain rate and the axial strain acceleration on concrete-like materials. Figure 3.28 shows relationship between the axial strain acceleration and strain-rate in solid specimens (specimens AS37-18-00--, GS50-25-00--, MS74-21-00-- in Figure 3.28) and tubular specimens (specimens DH37-18-07--,

FH37-18-07--, IH50-25-25--, OH74-21-30-- in Figure 3.28) with different outer diameters. It is observed that axial strain acceleration increases with increase in the strain rate. As axial strain acceleration is associated with radial expansion in the material resulting in the radial confinement of the cylindrical specimens. Furthermore, it is also observed that axial strain acceleration is essentially independent of specimen geometry for a given diameter, however, the radial confinement in the tubular specimen is less due to its free inner surface compared to the same diameter solid specimen.

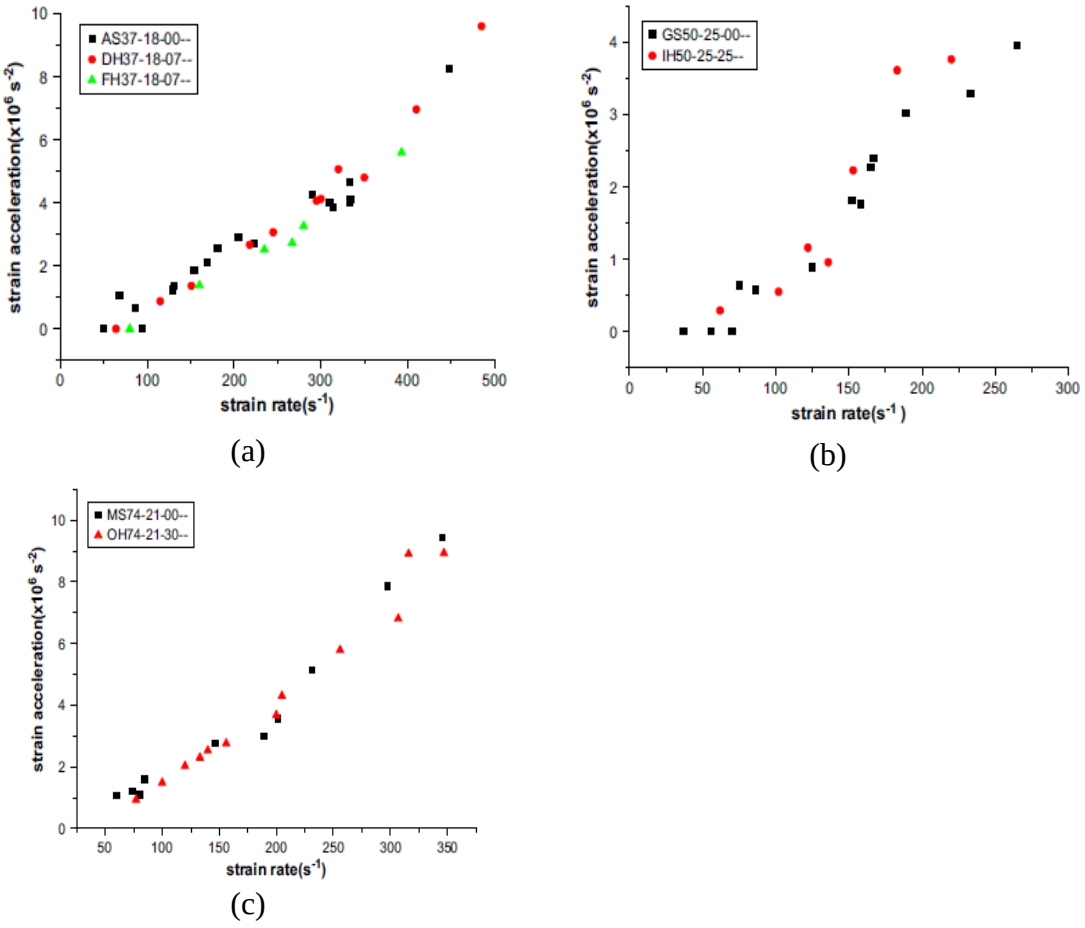

Figure 3.28: Correlations between the axial strain acceleration and strain-rate in solid (specimens AS37-18-00--, GS50-25-00--, MS74-21-00--) and tubular specimens (specimens DH37-18-07--, FH37-18-07--, IH50-25-25--, OH74-21-30--) with outer diameters of (a) 37mm (b) 50mm and (c) 74mm [Zhang *et al.* (2009)].

Figure 3.29 shows the correlation between the axial strain acceleration and strain-rate in solid specimens with outer diameters of 37mm (specimen AS37-18-00--) and 74mm

(specimen MS74-24-00--). It is observed that axial strain acceleration for a large diameter specimen is higher compared to specimens with smaller diameter. Therefore, from Figure 3.28 and Figure 3.29 it can be concluded that *DIF* observed from *SHPB* tests on concrete-like materials is less for tubular specimens compared to solid specimens and also the *DIF* of solid specimens is higher for larger diameter specimens compared to specimens with smaller diameters.

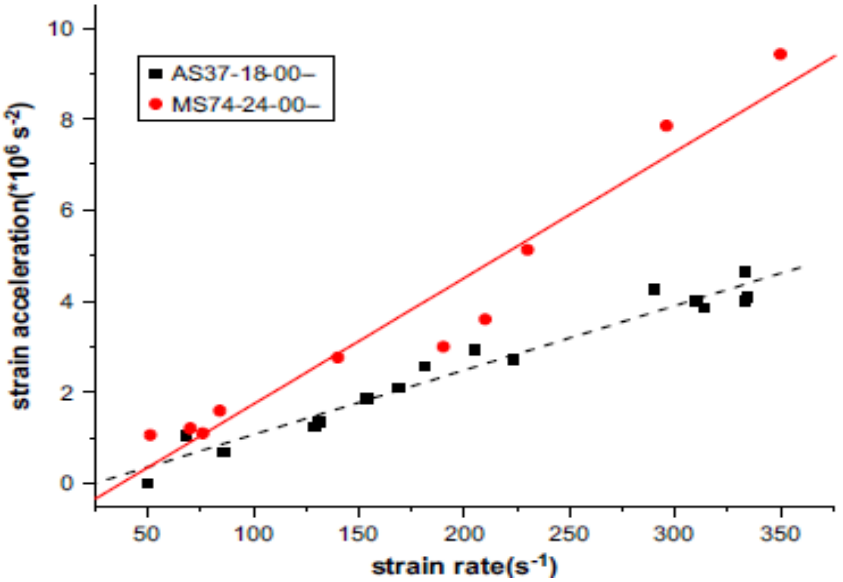

Figure 3.29: Correlations between the axial strain acceleration and strain-rate in solid specimens with outer diameters of 37mm (specimen AS37-18-00--) and 74mm (specimen MS74-24-00--) [Zhang *et al.* (2009)].

Figure 3.30 shows the variation of *DIF* with strain-rate for solid (specimens AS37-18-00--, GS50-25-00--, MS74-21-00-- in Figure 3.30) and tubular specimens (specimens DH37-18-07--, IH50-25-25--, OH74-21-30--, PH74-21-45-- in Figure 3.30) with different diameters. It is observed that for the same diameter the *DIF* of solid specimens is significantly higher as compared to tubular specimens under increasing loading rates. This increase in *DIF* for solid specimens is attributed due to the radial confinement.

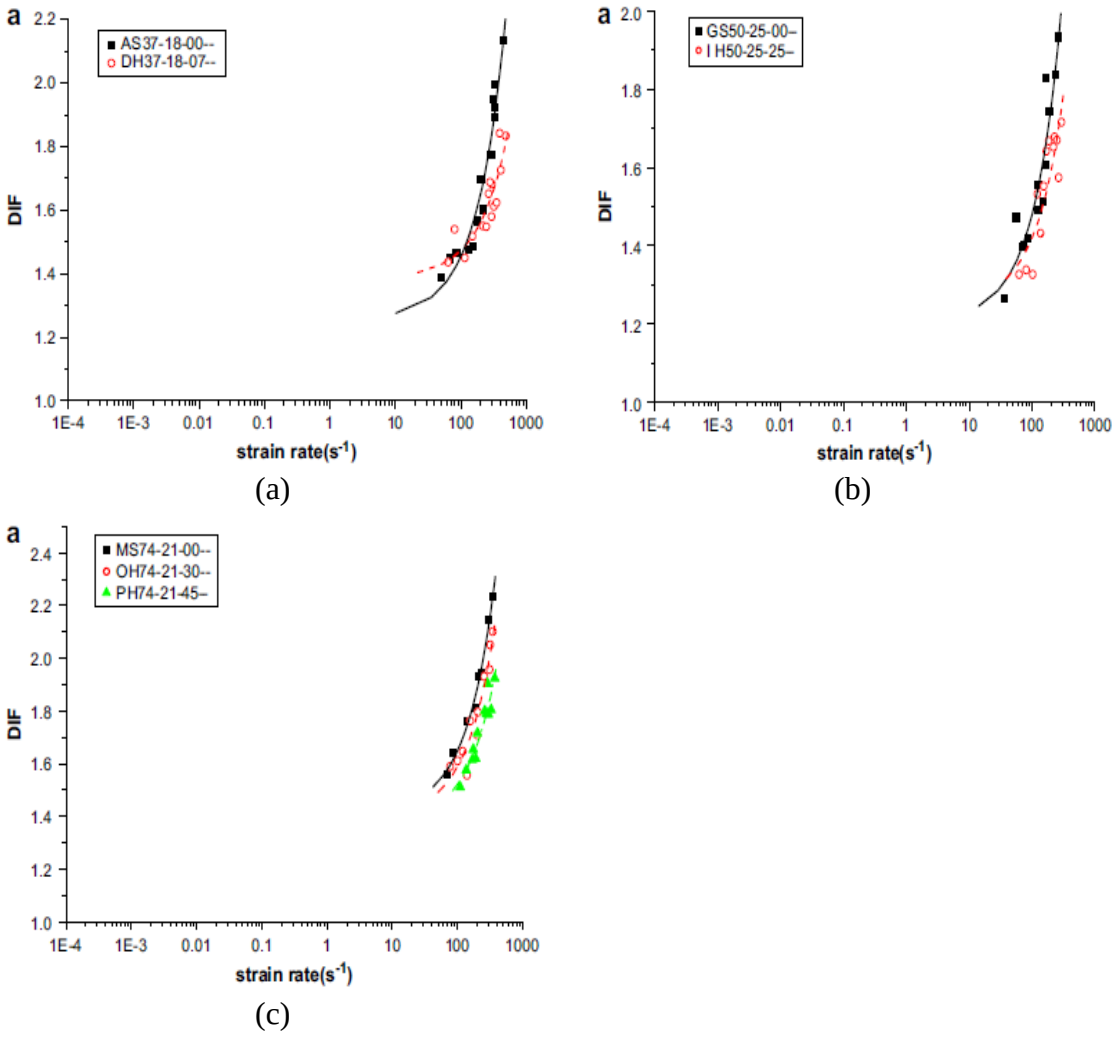

Figure 3.30: Variation of DIF with strain-rate for solid (specimens AS37-18-00--, GS50-25-00--, MS74-21-00--) and tubular specimens (specimens DH37-18-07--, IH50-25-25--, OH74-21-30--, PH74-21-45--) with outer diameters of (a) 37mm (b) 50mm and (c) 74mm [Zhang *et al.* (2009)].

The split Hopkinson pressure bar is the most widely used testing technique for studying the behaviour of concrete-like materials under increasing loading rates. The strain rate attained during these tests varies from 10 to 10000s^{-1}. However, it has been established that the increase in compressive strength of concrete under increasing loading rates in *SHPB* tests is mainly attributed due to the development of radial confinement

Davies and Hunter (1963), based on the *SHPB* studies of metals and polymers, proposed Eq. (3.6**)** for limiting specimens dimension in order to minimize the effect of

inertial radial and friction effect in SHPB test. However, it has been observed that the inertia effects cannot be avoided by adjusting the specimen geometry [through the use of Eq. (3.6)], therefore the effects induced due to inertia required to be checked carefully for brittle materials with large diameter specimens when studied under high strain rates especially when *SHPB* is used [Zhang *et al.* (2009)].

$$\frac{L}{D} = \frac{1}{2}\sqrt{3\nu_s} \qquad \text{Eq. (3.6)}$$

where : ν_s : Poisson's ratio

L : Length of the specimen

D : Diameter of the specimen

Figure 3.31 shows the variation of normalized quasi-static compressive strength with different length to diameter ratios (λ = L/D). Specimens used in *SHBP* tests, are usually characterised by values of λ ranging from 0.3 to 1.0. Therefore, as can be seen in Figure 3.31, the reduction of λ can result in an increase in the radial confinement of the specimen.

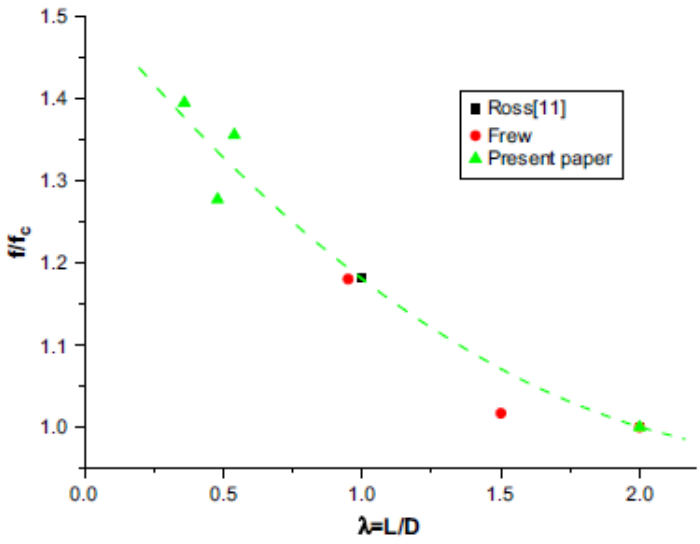

Figure 3.31: Variation of normalized quasi-static compressive strength different values of length to diameter ratio (L/D) [Zhang *et al.* (2009)].

Based on Figure 3.28 to Figure 3.31, it can be concluded that the factors such as specimen geometry (diameter & length to diameter ratio) can significantly influence the behaviour exhibited by concrete-like material specimens under increasing compressive loading rates. As a results it could be suggested that the observed increase of load-carrying capacity (expressed in the form of DIFs) represents the effect of loading rate on the structural response of the specimen rather than on the actual material properties.

In order to investigate the behaviour of the concrete-like specimens under increasing loading rates Li *et al.* [Li *et al.* (2009)] carried out numerical investigation on *SHBP* tests. When considering different stress-strain relationship of unconfined mortar under uniaxial compression (characterised by different levels of residual strength) (see Figure 3.32 a) it is observed that the post-failure (residual) strength has negligible influence on *DIF* under increasing loading rates [see Figure 3.32 (b)].

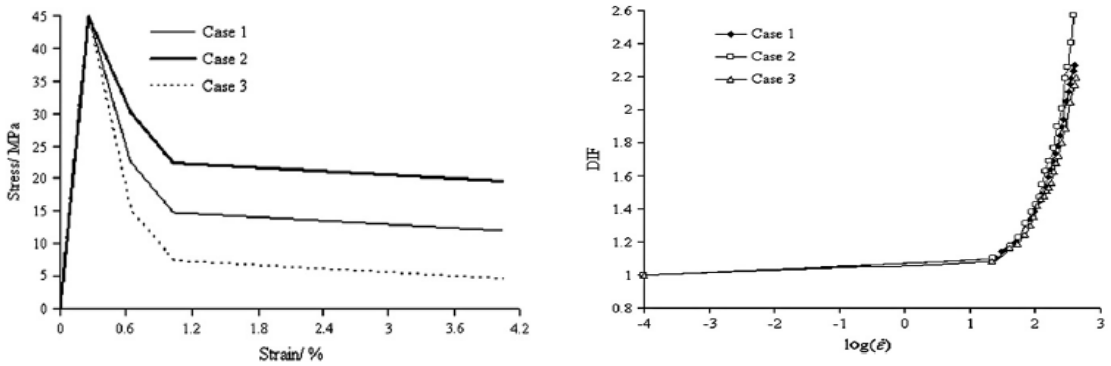

(a) (b)

Figure 3.32: (a) Stress-*strain* relationship of unconfined mortar under uniaxial compression with various residual strengths (b) variation of *DIF* with strain rate for mortar with various residual strengths.

Li and Meng [Li & Meng (2003)] investigated the use of *SHPB* technique for measuring the dynamic strength enhancement of concrete under high rate loading. The *SHPB* test results obtained for the case of concrete specimens tested under high loading rates reveal that the compressive strength increases once a certain threshold value of strain rate is exceeded, however, the finite element analyses carried out to examine the *SHPB* loading technique shows that the enhancement in concrete strength is caused due to the lateral inertia confinement rather than the actual strain rate effect of the concrete material. Figure 3.33 shows the stress-strain curves introduced into the finite element

package to describe material behaviour and the predicted behaviour obtained from the numerical predictions. It can be seen that for strain rates of $27s^{-1}$ no strain rate effect was observed as the input and output curves were found to be very similar. The hydrostatic stress was found to be about 1/3 of the compressive stress thus the uniaxial compressive stress state was observed in the finite element *SHPB* test [see Figure 3.33 (a)]. However, for the finite element analysis with strain rate of $390s^{-1}$ the measured compressive strength was found to be twice of the corresponding quasi static value, which in real *SHPB* test would be attributed to the strain rate effect [see Figure 3.33 (b)]. The increase in concrete strength is due to the lateral inertia effect rather than the strain rate effect as the hydrostatic stress was found to be more than half of the compressive stress which means the two other principal stresses are not zero hence the lateral inertia restricts the radial expansion of the specimen and caused lateral confinement.

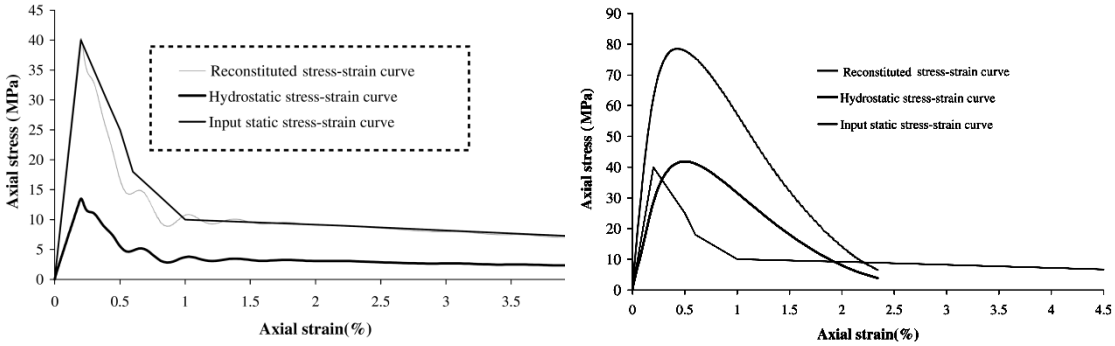

Figure 3.33: Stress strain curves at strain rates of (a) $27s^{-1}$ (b) $390s^{-1}$ [Li & Meng (2003)]

A numerical investigation carried out by Cotsovos & Pavlović (2008a, 2008b, 2008c) to study the behaviour of concrete under high rate uniaxial compressive and tensile loading suggested that the specimen behaviour observed in the high rate loading tests do not represent the material behaviour of concrete but rather it represents the structural behaviour. It was also found that inertia of mass both in axial and lateral direction under dynamic compressive loading [Cotsovos & Pavlović (2008a), (2008b)] has a significant effect on the concrete strength, however, for concrete specimen under high rate tensile loading [Cotsovos & Pavlović (2008c)] the inertia of the mass in the lateral direction is

insignificant but the inertia along the length of the specimen significantly effects the specimen behaviour.

3.2.6 Discussion of experimental results

To date a significant number of experimental studies have been conducted by many researchers (a thorough review of all relevant data is provided by [Bischoff & Perry (1991), Bischoff & Perry (1995), Cotsovos & Pavlović (2008a), (2008b), (2008c), Li & Meng (2003), Lu & Li (2011), Zhang *et al.* (2009)]) to investigate the behaviour of concrete prismatic or cylindrical specimens under high rates of uniaxial compressive and tensile loading. Figure 3.34 shows an overview of the results obtained from the experimental studies investigating the behaviour of concrete under increasing strain rates. Although it is suggested that the increase of strain rates beyond certain levels results in a substantial increase of the maximum load ($maxP_d$) sustained by the specimen (compared to that recorded under equivalent static loading, $maxP_s$) the available test data is characterised by considerable scatter and therefore it cannot quantify this effect accurately nor can it provide the reasons that trigger this shift in specimen behaviour. This scatter is owed to a number of parameters (e.g. the experimental technique employed, the shape and size of the specimens, the different types of concrete used, etc.) which vary from experiment to experiment [Cotsovos & Pavlović (2008a), (2008b), (2008c)]. The available data is analysed in respect to the above parameters in an attempt to assess their contribution to the overall scatter that characterizes the relevant experimental data. Based on the analysis of the test data the effect of two parameters can be clearly identified; that (i) of the concrete strength and (ii) of the loading apparatus employed during testing.

Effects of concrete strength: Based on the relevant test data the concrete compressive strength (f_c) appears to influence the behaviour of concrete under increasing loading rates [Cotsovos & Pavlović (2008b)]. In particular, it suggests that the influence of the strain rate is more significant in the case of low strength concrete (see Figure 3.35).

Effects of loading technique: Different experimental techniques have been used to investigate the behaviour of concrete under high rate loading, which include the use of screw and lever to apply the loading, hydraulic machine, gas gun, drop hammer and

SHPB. Figure 3.36 shows the experimental data obtained from hydraulic apparatus, drop hammer and *SHPB* experiments [Cotsovos & Pavlović (2008b)]. In general, it is found that with the increase in the strain rate beyond a certain level the specimen strength also increased. It can be also seen that the use of different loading techniques is an important factor contributing to the scatter that characterizes the data. When considering only test data obtained from *SHPB* apparatus the scatter reduces significantly showing sudden increase in specimen strength once the level of the strain rate exceeds the value of 10-100s^{-1}.

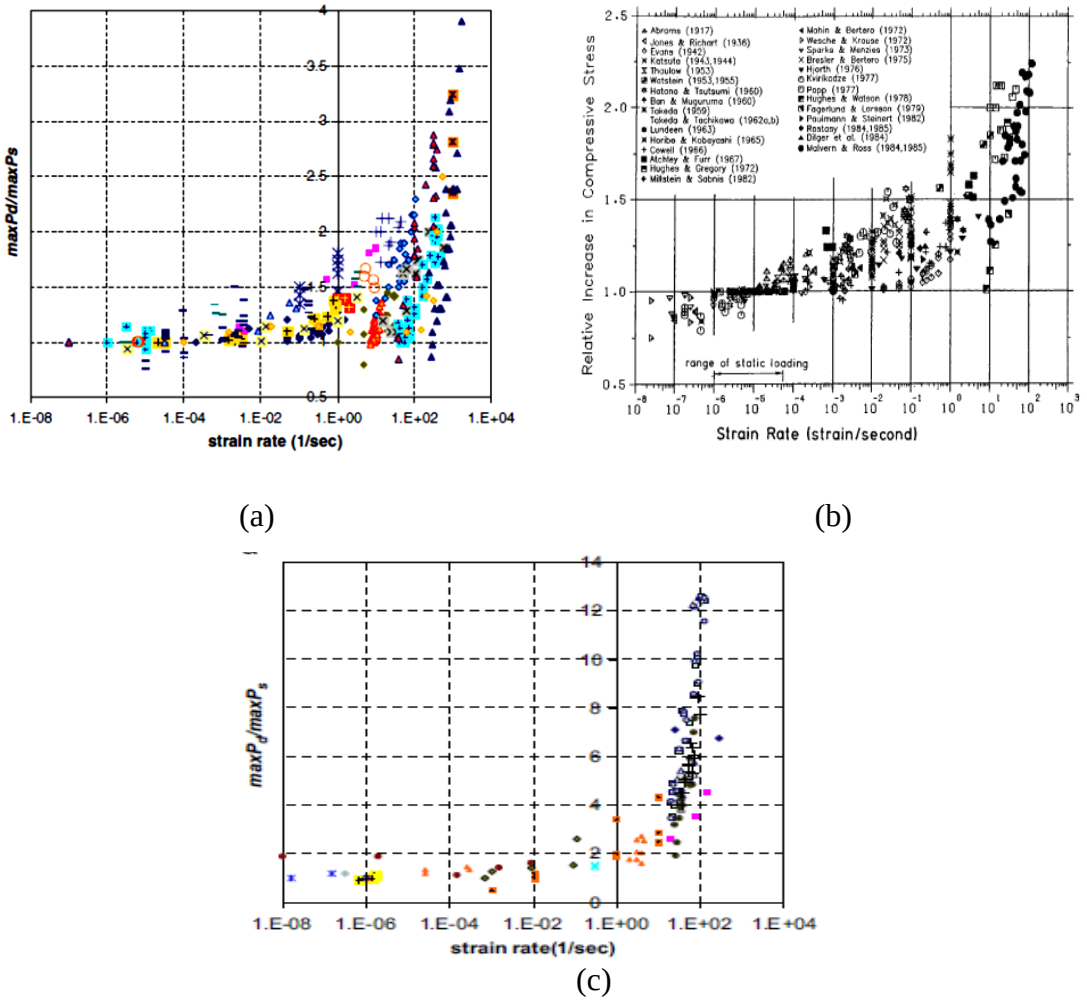

Figure 3.34: Summary of test data expressing the variation of the load-carrying capacity with the strain rate exhibited by prismatic concrete specimens under uniaxial (a) & (b) compression [Cotsovos & Pavlović (2008a), Bischoff & Perry (1991)] and (c) tension [Cotsovos & Pavlović (2008c)].

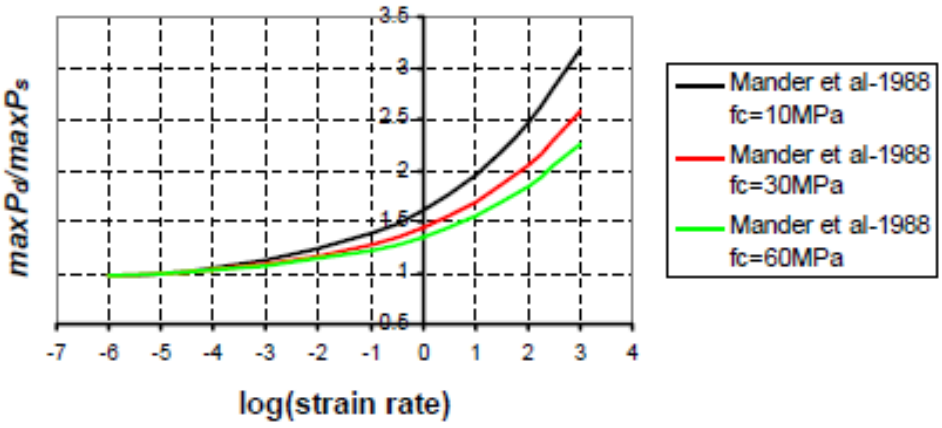

Figure 3.35: Curves proposed by Mander *et al.* (1988) describing the effect of strain rate on the strength of concrete in compression [Cotsovos (2004)].

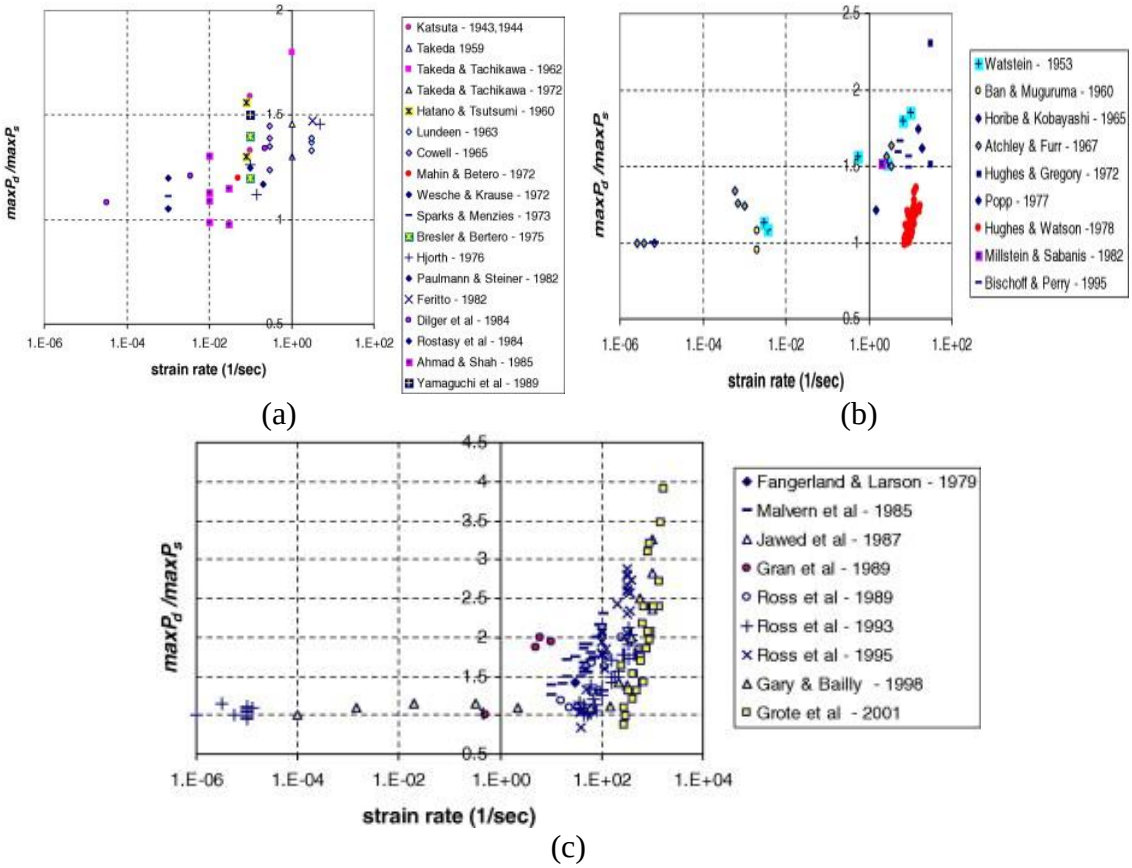

Figure 3.36: Experimental data obtained from (a) hydraulic loading (b) drop hammer (c) *SHPB* experiments [Cotsovos & Pavlović (2008b)].

3.2.7 Review of design formulae describing the variation of DIF with srain-rate

Based on the above review it has been established that the behaviour exhibited by steel and plain concrete specimens under high-rate loading differs significantly from that established under equivalent static loading. In an attempt, to quantify the effect of loading rate on material behaviour a number of analytical expressions have been provided [Army TM 5-855-1 Air Force AFPAM 32-1147(I) (1998), Malvar & Crawford (1998b), CEB-FIP (1990), Zhou & Hao (2008a), Tedesco & Ross (1998), Katayama *et al.* (2007), Grote *et al.* (2001)]. These expressions are usually obtained by performing regression analyses on the available test data.

Eq. (3.7) gives the *DIF* formula recommended by CEB [CEB-FIP (1990)] for concrete in tension. This formula can be used to calculate the *DIF* for concrete subjected to strain rates up to $300s^{-1}$.

$$DIF = \frac{\sigma_{td}}{\sigma_{ts}} = \begin{cases} 1 & \dot{\epsilon}_z \leq \dot{\epsilon}_s \\ \left(\frac{\dot{\epsilon}_z}{\dot{\epsilon}_s}\right)^{1.016\alpha_s} & \dot{\epsilon}_s < \dot{\epsilon}_z \leq 30s^{-1} \\ \gamma_s \left(\frac{\dot{\epsilon}_z}{\dot{\epsilon}_s}\right)^{0.33} & \dot{\epsilon}_z > 30s^{-1} \end{cases} \qquad \text{Eq. (3.7)}$$

where : σ_{ts} : Unconfined uniaxial tensile strength under quasi-static loading

σ_{td} : Unconfined uniaxial tensile strength under dynamic loading

$\gamma_s = 10^{(7.11\alpha_s - 2.33)}$

$\alpha_s = \frac{1}{\left(10 + 6\frac{\sigma_{cs}}{\sigma_{co}}\right)}$

$\dot{\epsilon}_s = 3 \times 10^{-6}\ s^{-1}$

$\sigma_{co} = 10$ MPa

σ_{cs} : Unconfined uniaxial quasi-static compressive strength in MPa

Eq. (3.8) gives the *DIF* formula recommended by CEB [CEB-FIP (1990)] for concrete in compression.

$$DIF = \frac{f_{cd}}{f_{cs}} = \begin{cases} \left(\frac{\dot{\epsilon}}{\dot{\epsilon}_s}\right)^{1.026\alpha_s} & \dot{\epsilon} \leq 30s^{-1} \\ \gamma_s \left(\frac{\dot{\epsilon}}{\dot{\epsilon}_s}\right)^{0.33} & \dot{\epsilon} > 30s^{-1} \end{cases} \qquad \text{Eq. (3.8)}$$

where : f_{cs} : Unconfined uniaxial compressive strength under quasi-static loading

f_{cd} : Unconfined uniaxial compressive strength under dynamic loading

$\gamma_s = 10^{(6.156\alpha_s - 2)}$

$\alpha_s = \frac{1}{\left(5 + 9\frac{f_{cs}}{f_{co}}\right)}$

$\dot{\epsilon}_s = 3 \times 10^{-6}\ s^{-1}$

$f_{co} = 10$ MPa

σ_{cs} : Unconfined uniaxial quasi-static compressive strength in MPa

Malvar & Crawford [(1998b)] modified the CEB formula [see Eq. (3.7)] for concrete in tension which takes the form as given in Eq. (3.9)

$$DIF = \frac{\sigma_{td}}{\sigma_{ts}} = \begin{cases} 1 & \dot{\epsilon}_z \leq \dot{\epsilon}_s \\ \left(\frac{\dot{\epsilon}_z}{\dot{\epsilon}_s}\right)^{\alpha_s} & \dot{\epsilon}_s < \dot{\epsilon}_z \leq 1s^{-1} \\ \gamma_s \left(\frac{\dot{\epsilon}_z}{\dot{\epsilon}_s}\right)^{0.33} & \dot{\epsilon}_z > 1s^{-1} \end{cases} \qquad \text{Eq. (3.9)}$$

where : $\gamma_s = 10^{(6\alpha_s - 2)}$

$\alpha_s = \frac{1}{\left(1 + 8\frac{\sigma_{cs}}{\sigma_{co}}\right)}$

$\dot{\epsilon}_s = 1 \times 10^{-6}\ s^{-1}$

Zhou & Hoa [(2008b)] recommended tensile *DIF* formula for concrete like material as given in Eq. (3.10)

$$DIF = \frac{\sigma_{td}}{\sigma_{ts}} = \begin{Bmatrix} 1 & \dot{\epsilon}_z \leq 10^{-4}s^{-1} \\ 1 + 0.26\,[\lg \dot{\epsilon}_z + 4.0769] & 10^{-4}s^{-1} < \dot{\epsilon}_z \leq 1s^{-1} \\ 1 + 2\,[\lg \dot{\epsilon}_z + 0.53] & \dot{\epsilon}_z > 1s^{-1} \end{Bmatrix} \quad \text{Eq. (3.10)}$$

Tedesco & Ross [(1998)] conducted a series of dynamic splitting tests on concrete specimens and based on these test results a bilinear tensile *DIF* regression formula as given in Eq. (3.11) is suggested

$$DIF = \frac{\sigma_{td}}{\sigma_{ts}} = \begin{Bmatrix} 1 + 0.1425\,[\lg \dot{\epsilon}_z + 5.8456] \geq 1.0 & \dot{\epsilon}_z \leq 2.32s^{-1} \\ 1 + 2.929\,[\lg \dot{\epsilon}_z - 0.0635] \leq 6.0 & \dot{\epsilon}_z > 2.32s^{-1} \end{Bmatrix} \quad \text{Eq. (3.11)}$$

Tedesco & Ross [(1998)] based on the experimental results of *SHBP* tests developed a *DIF* regression formula for concrete in compression as given in Eq. (3.12)

$$DIF = \begin{Bmatrix} 1 + 0.00965\,[\lg \dot{\epsilon} + 6] \geq 1.0 & \dot{\epsilon} \leq 63.1s^{-1} \\ 1 + 0.758\,[\lg \dot{\epsilon} - 0.938] \leq 2.5 & \dot{\epsilon}_z > 63.1s^{-1} \end{Bmatrix} \quad \text{Eq. (3.12)}$$

Katayama *et al.* [Katayama *et al.* (2007)] suggested a parabolic tensile *DIF* expression for concrete as given in Eq. (3.13)

$$DIF = \frac{\sigma_{td}}{\sigma_{ts}} = 0.4379\left[\lg(\dot{\epsilon}_z)\right]^2 - 0.02987\lg(\dot{\epsilon_z}) + 0.8267 \quad \text{Eq. (3.13)}$$

Grote *et al.* [Grote *et al.* (2001)] recommended equations to measure the compressive *DIF* of mortar in the strain-rate range of 250–1700 s^{-1} as given in Eq. (3.14) and Eq. (3.15)

$$DIF = \begin{cases} 1 + 0.0235\ [\log\dot{\varepsilon} + 2.979] & \dot{\varepsilon} \leq\ 266s^{-1} \\ 0.882(log\dot{\varepsilon})^3 - 4.4(log\dot{\varepsilon})^2 + 7.22log\dot{\varepsilon} - 2.64 & \dot{\varepsilon}\ > 266s^{-1} \end{cases} \quad \text{Eq. (3.14)}$$

$$DIF = \begin{cases} 1 + 0.0157\ [\log\dot{\varepsilon} + 3] & \dot{\varepsilon} \leq\ 266s^{-1} \\ 0.383(log\dot{\varepsilon})^2 + 0.266log\dot{\varepsilon} - 1.765 & \dot{\varepsilon}\ > 266s^{-1} \end{cases} \quad \text{Eq. (3.15)}$$

Based on the experimental results of reinforcing bars having static yield strength in the range of 290 to 710MPa, Malvar & Crawford (1998) recommended equations to measure both yield and ultimate strength of steel as given in Eq. (3.16) under increasing strain rates. This equation can be used to calculate *DIF* of steel for the strain rate in the range 10^{-4} and $225s^{-1}$ [Malvar & Crawford (1998a)].

$$DIF = \left(\frac{\dot{\epsilon}}{10^{-4}}\right)^{\alpha} \quad \text{Eq. (3.16)}$$

where : α : function of f_y

$$\alpha_{fy} = 0.074 - .040\frac{fy}{60}$$

$$\alpha_{fu} = 0.019 - .009\frac{fy}{60}$$

The graphical representation of the analytical expressions provided earlier in the form of curves describing the effect of strain rate on the DIF of compressive and tensile concrete strength are shown in Figure 3.37 to Figure 3.40. Similar curves are provided for the case of steel in Figure 3.41 and Figure 3.42.

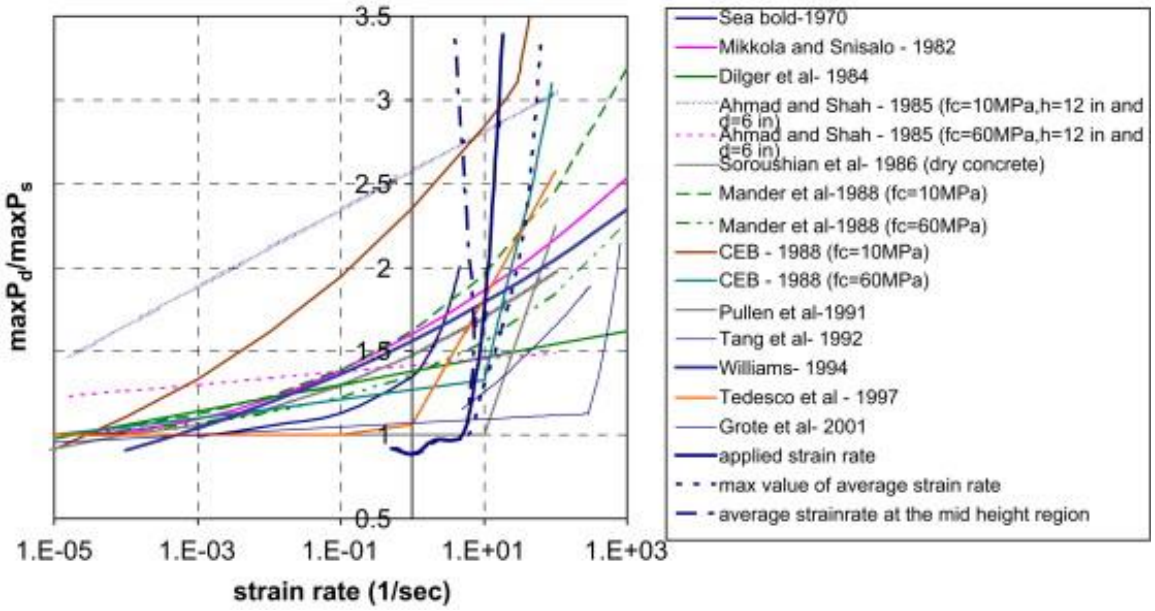

Figure 3.37: Best- fit curves describing the effect of strain rate on the strength of concrete in compression [Cotsovos & Pavlović (2008a)].

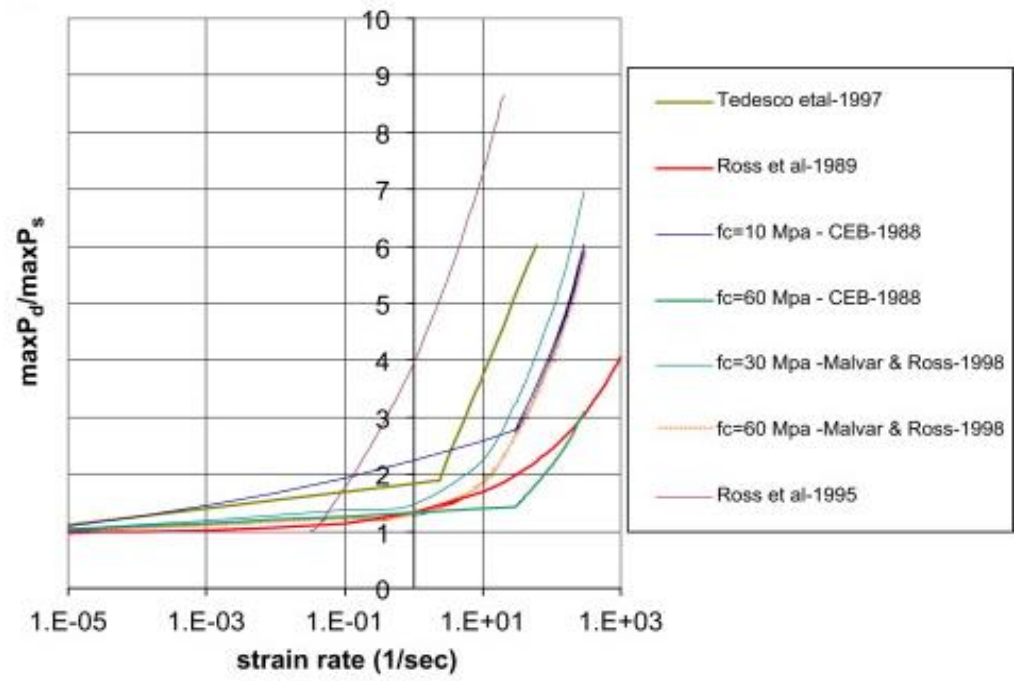

Figure 3.38: Best- fit curves describing the effect of strain rate on the strength of concrete in tension [Cotsovos & Pavlović (2008c)].

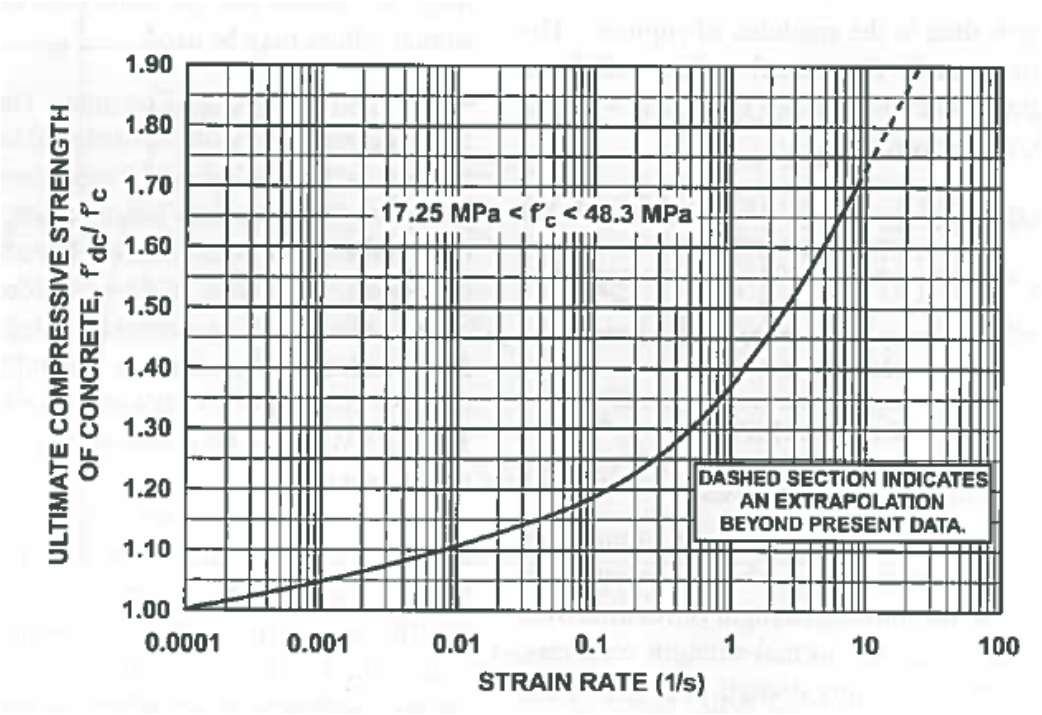

Figure 3.39: Design curve describing the effect of strain rate on the ultimate strength of concrete in compression [Army TM 5-855-1 Air Force AFPAM 32-1147(I) (1998)].

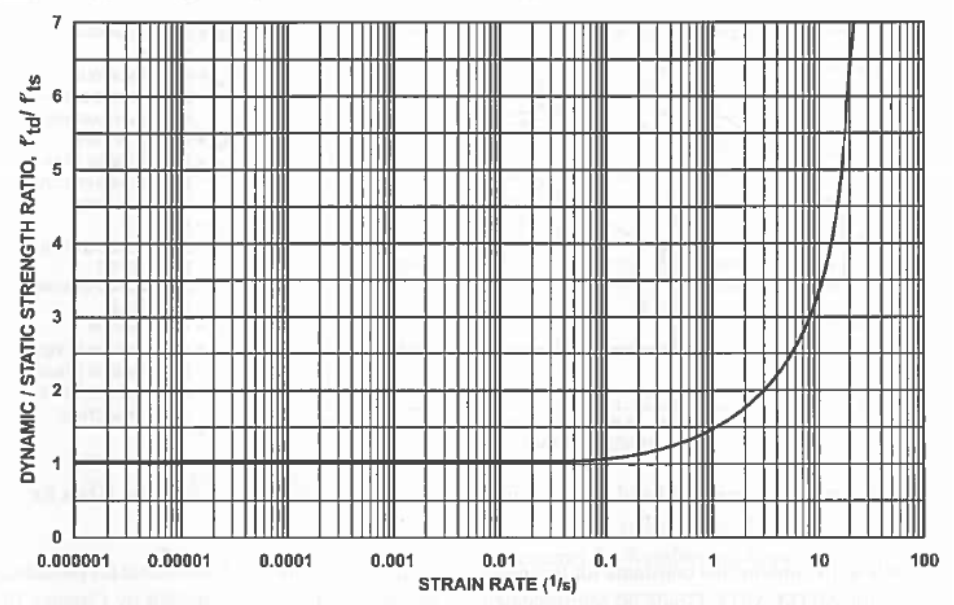

Figure 3.40: Design curve describing the effect of strain rate on the tensile strength of concrete [Army TM 5-855-1 Air Force AFPAM 32-1147(I) (1998)].

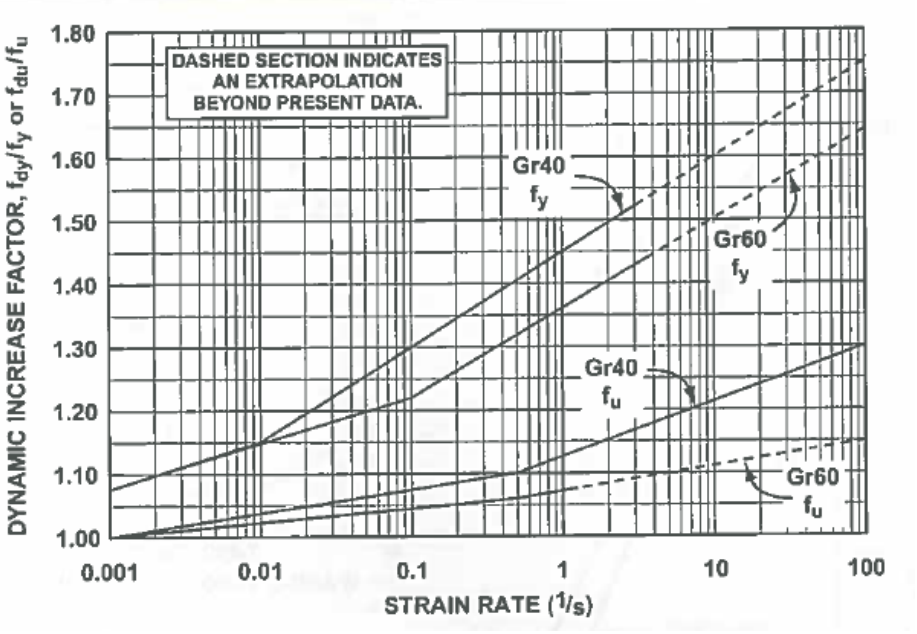

Figure 3.41: Design curve describing the effect of strain rate on the yield and ultimate strength of *ASTM A615* Grades 40 and 60 reinforcing steel [Army TM 5-855-1 Air Force AFPAM 32-1147(I) (1998)].

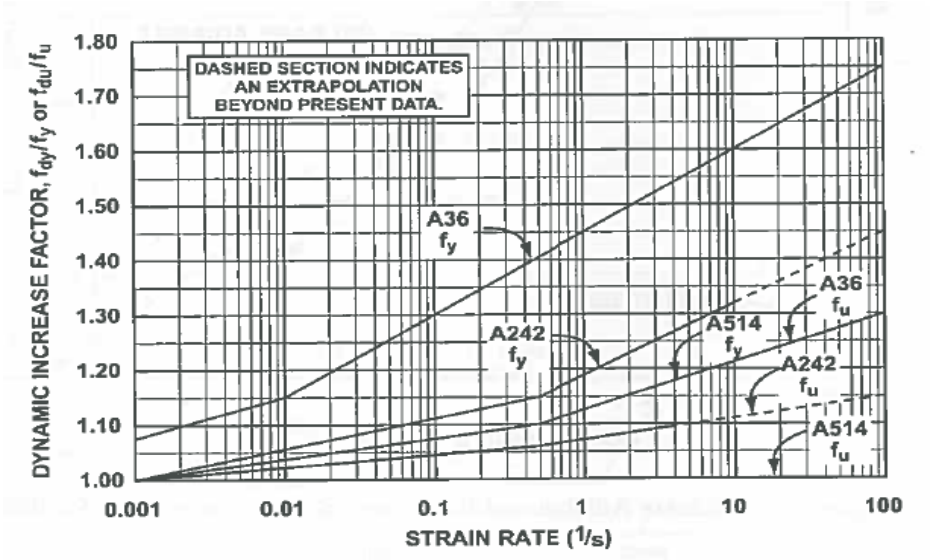

Figure 3.42: Design curve describing the effect of strain rate on the yield and ultimate strength of *ASTM A615* Grades *A36*, *A242* and *A514* steel [Army TM 5-855-1 Air Force AFPAM 32-1147(I) (1998)].

3.2.8 Limitations & findings of experimental data

The behaviour exhibited by steel specimens under high-rate loading differs significantly from that established under equivalent static loading. However, the experimental data is characterised by considerable scatter owed to a number of parameters (e.g. the experimental technique employed, the shape and size of the specimens, the different types of steel or concrete used, etc.) which vary from experiment to experiment. Furthermore, the available test data cannot provide a detailed description (for e.g. stress-strain distribution, effect of interaction of specimen and apparatus etc.). It is important to note that the available test data fails to accurately quantify the effect of strain rate on the material behaviour and cannot provide the reasons that trigger this shift in specimen behaviour. As a result, it is difficult to derive laws capable of realistically quantifying the change in the specimen behaviour under increasing loading rates.

More specifically based on the test results of steel specimens it is observed that:

- The strain rate effect is more significant for low strength steel as compared to high strength steel [see **Figure 3.19** to **Figure 3.21**]. It is also observed that the ultimate strength of steel remains essentially constant with increasing strain rates. Therefore, the yield stress of steel was found to be more strain-rate sensitive than its ultimate tensile strength [see **Figure 3.19** to **Figure 3.21**]. It is important to point out at this point that the steel used to construct the pipes as described in the subsequent chapters of this thesis has a static yield strength (f_y = 468MPa) which is not significantly influenced by the strain rate effects as observed in section 3.2.4.

- For the case of steel having similar static yield strengths an increase of $DIF_{(fy\text{-dynamic}/fy\text{-static})}$ with increasing strain rates is higher for dog bone specimens with smaller cross-sections areas.

- The test data is characterized by considerable scatter and very limited for some loading techniques, however, this scatter reduces when excluding the data obtained from hydraulic and biaxial machines (see Figure 3.26).

Similar to the behaviour of steel, it was found that the concrete strength increases with increasing loading rates. However, for the case of concrete compressive strength this enhancement is attributed to the structural property of the specimen rather than the actual strain rate material property of concrete. Some consensus is found among researchers [Lu & Li (2011), Zhang *et al.* (2009), Li & Meng (2003), Cotsovos & Pavlović (2008a), (2008b)] that the increase in compressive strength of concrete under increasing loading rates is largely attributed due to the development of radial confinement in high loading rate tests which cannot be considered as the material property of the concrete.

In the case of the dynamic tensile strength of concrete numerical work carried out by Cotsovos & Pavlović (2008c) consider that the strength enhancement is largely attributed to the inertia acting along the length of the specimen which is the structural property of concrete. This argument is supported by the findings of Cadoni *et al.* [Cadoni *et al.* (2009)] as it was observed in the high rate loading tests that the tensile strength of concrete under increasing loading rates is influenced by the specimen size. However, Lu & Li (2011) consider this enhancement in the concrete tensile strength due to the material property of concrete and it is largely attributed to the micro crack inertia.

3.3 CONCLUSIONS

Based on the critical analysis of the experimental studies carried out on steel specimens under increasing loading rates the following conclusions are drawn:

- The behaviour exhibited by steel specimens under high loading rates differs from that established under equivalent static loading once certain limits of loading rate are surpassed.

- Increasing loading rates have a more significant effect on steel specimen characterised with a lower static yield strength.

- The experimental data are characterised by considerable scatter owed to a number of parameters (e.g. the experimental technique employed, the shape and size of the specimens, the different types of steel used, etc.) which vary from

experiment to experiment. As a result, it is extremely difficult to derive laws able to realistically quantify the experimentally observed change in the specimen behaviour with increasing loading rates.

Based on the critical analysis of the experimental studies carried out on plain concrete specimens under increasing loading rate the following conclusions are drawn:

- It is observed that beyond certain levels of strain rate a substantial increase of the maximum load sustained by the plain concrete specimen is exhibited compared to that recorded under equivalent static loading.

- The increase in compressive strength of concrete under increasing loading rates is mainly attributed due to the development of radial confinement in high loading rate tests which cannot be considered as the material property of the concrete.

- There exists a difference of opinion regarding the dynamic tensile strength of concrete. Cotsovos & Pavlović (2008c), Cadoni *et al.* [Cadoni *et al.* (2009)] consider this strength enhancement in concrete due to the inertia acting along the length of the specimen which is the structural property of concrete. However, Lu & Li (2011) consider this enhancement in the concrete tensile strength due to the material property of concrete and it is largely attributed to the micro crack inertia.

CHAPTER 4

RESPONSE OF SCALED PIPE-SPECIMENS UNDER DROP WEIGHT TESTS

4.1 INTRODUCTION

The dynamic response exhibited by steel pipes under impact loads (which, as discussed in Chapter 2, are characterised by short durations and high intensities) is both local (i.e. when part of the span of the pipe reacts to the applied load) and global i.e. when the full span of the pipe reacts to the applied load. This can be explained when considering the problem at hand as a wave propagation problem within a non-linear medium. Since due to the collision of heavy objects (icebergs, rocks, fishing equipment etc.) onto the walls of the pipes, waves are generated which propagate away from the impact area. As a result a localized response is often exhibited which is often observed in the form of damage concentrated in the area where the impact load is exerted due to the development of high stress concentrations in that region. The level of the localized damage sustained by the pipe may range from a simple dent (i.e. small reduction in the diameter of the pipe) to larger permanent deformations that can potentially result in the collapse of the pipe's cross-section and/or the development of fractures. Global response is exhibited due to the waves propagating away from the contact area which results in the pipe deforming along its whole length.

As already discussed in previous chapters, the *in-situ* behaviour of subsea steel pipes under impact can be significantly influenced by a range of parameters associated with: (i) the characteristics of the impacting object (size, shape, speed and material properties), (ii) the boundary conditions imposed onto the pipe (end conditions, properties of the soil on which the pipe is laid), (iii) the level of axial loading imposed and (iv) the development of internal (due to the oil and gas transportation through the pipe) and external (due to hydro-static load) pressure. Such parameters can potentially

affect, often detrimentally, the dynamic response exhibited by the steel pipes when subjected to impact.

Drop-weight testing facilities are often used to study various important aspects of the dynamic behaviour exhibited by steel pipes under impact loading. These aspects include the time histories of the generated contact and reaction forces, the variation of the displacement of certain points along the pipe's span throughout the loading process, the level of the damage sustained by the pipe (both locally at the area of impact or in other regions such as the supports) and its deformation profile (before and after impact) exhibited during different stages of the loading process. The experimental study of the dynamic response of pipe specimens under impact loading is usually characterized by significant difficulties associated with the duration of these tests and the intensity of the loads generated which increases rapidly from zero to a maximum value within an few milli-seconds. The experimental setups employed in the majority of tests conducted to date (discussed in Chapter 2) do not account for a range of parameters associated with the subsea conditions. Furthermore it is common practice in drop-weight tests to employ scaled specimens, with smaller lengths and cross-sections compared to those of the actual pipes used by industry. Although the majority of relevant experimental studies published to date are not fully representative of the problem at hand (i.e. the behaviour of subsea pipes under impact loading), the test data obtained provides useful information concerning the response of such elements in relation to that established under equivalent static loading. Furthermore, the obtained tests data can also be used for validating the predictions acquired from *NLFEA*, allowing for the development of more intricate numerical models capable of predicting more accurately the behaviour exhibited by subsea pipes used in practice by accounting for the effect of various parameters mentioned earlier which are likely to affect the *in-situ* behaviour of subsea pipes under operational conditions.

In this chapter a numerical investigation is carried out to study the response of scaled pipe-specimens under drop weight tests. For this purpose the *FE* models adopted for representing the subject problem (steel pipe subjected to drop-weight testing) and its predictions are initially validated against published tests data [Jones *et al.* (1992)] describing the behaviour of the scaled pipe-specimens under drop-weight testing. Following the validation of the model and its numerical predictions, a parametric investigation is carried out to study the influence of a number of parameters on the

response of the subject pipe specimens under impact loading. These parameters include: the velocity with which the impactor collides onto the specimen (v), the length to diameter ratio (L/D) and the support conditions of the pipe as well as the level of axial loading and pressure developing on the walls of the pipes.

Due to the short duration and high intensities characterising the impact loads generated during the collision of objects onto subsea pipes, such loads can potentially cause the rapid deformation of the pipe (especially in the region where the load is imposed) which can in turn result in high strain-rates being exhibited within the steel medium. Such elevated values of strain-rates are widely considered to affect the material properties of steel (strain-rate sensitivity) and in turn the dynamic response of the pipes under impact loading [Jones *et al.* (1992)]. Based on the comprehensive review of published experimental and numerical studies (presented in Chapter 3) concerning the behaviour of steel and concrete specimens under high rate loading it was observed that the behaviour exhibited by steel and concrete specimens under high-rate loading differs significantly from that established under equivalent static loading. However, the experimental data is characterised by considerable scatter owed to a number of parameters (e.g. the experimental technique employed, the shape and size of the specimens, the different types of steel or concrete used, etc.) which vary from experiment to experiment. Furthermore, the available test data fails to accurately quantify the effect of strain rate on the material behaviour and cannot provide the reasons that trigger this shift in specimen behaviour. As a result, it is difficult to derive laws capable of realistically quantifying the change in the specimen behaviour under increasing loading rates. Therefore in this Chapter static material properties are employed for describing steel behaviour under high loading rates in order to investigate the response of scaled pipe-specimens under drop weight testing and to elucidate to what extent can strain rate sensitivity effect the exhibited response.

4.2 NUMERICAL INVESTIGATION

The numerical investigation is carried out using a well-established commercial finite element software ABAQUS [ABAQUS (2013)] capable of solving complex non-linear static and dynamic problems. The aim is to study the response of scaled pipe-specimens under drop weight tests. In this section a brief description of the non-linear strategy and material models adopted are provided.

4.2.1 The equation of motion in non-linear dynamic analyses

The application of an external force onto a structural form will set it into motion. As a result the structural form deforms and internal forces (F^{int}) will develop to resist the element deformation (U). F^{int} is the product of the element stiffness and stresses (K) and the deformation (U) i.e. $F^{int} = KU$. In addition inertia and damping forces also develop due to the motion of the object. The inertia forces (F_I) are defined as the product of mass (M) and acceleration ($\ddot{U}$) i.e. $F_I = M\ddot{U}$ whereas the damping forces (F_d) are provided by the product of the damping matrix (C) and velocity ($\dot{U}$) i.e. $F_d = C\dot{U}$. Depending on the rate of loading static or dynamic analysis can be used. Static analysis is used when the accelerations and velocities exhibited by the structural form are not significant and hence can be ignored. Therefore, the inertia and damping forces can be overlooked.

Dynamic analysis is used when the external force is applied at such loading rates that the acceleration and the velocity of the structural form can no longer be ignored. As a result the inertia forces (F_I) and the damping forces (F_d) become significant and cannot be ignored either. The equation of motion governing the problem at hand is no longer a simple algebraic equation but a second order differential equation of motion given by Eq. (4.1):

$$M\,\Delta\ddot{U}(t) + C\,\Delta\dot{U}(t) + K(t)\,\Delta U(t) = \Delta F^{ext}{}_t \qquad \text{Eq. (4.1)}$$

Because of the complexity of the problem considered herein (a wave propagation problem within a nonlinear medium), the equation of motion [Eq. (4.1)] is solved numerically through the use of the finite element method. For each time step (Δt) the second-order differential equation of motion is transformed into an equivalent static problem which can be solved easily. This is achieved by expressing the acceleration ($\ddot{U}$) and velocity ($\dot{U}$) as a function of the change in displacement (ΔU) usually through the use of the Newmark family approximation methods, the Wilson method and the Hilber-Hughes-Taylor method [Steven (2000)].

As a result the equation of motion for a given time step can be transformed into an equivalent static algebraic problem expressed by Eq. (4.2)

$K^* \Delta U = \Delta P^*$ Eq. (4.2)

where: K^* : effective stiffness matrix

ΔP^* : effective load vector

The effective stiffness matrix and the effective loading vector are functions of the structure stiffness matrix (K) and loading vector (ΔP) respectively, as well as the structure's mass (M) and damping (C) matrices. It also depends on the time step used to solve the equation of motion numerically.

The solution of the equation of motion can be achieve through the use of explicit or implicit methods. When employing the explicit method the evaluation of the acceleration and velocity is carried out once for each time step. This is followed by the construction of the effective stiffness matrix and the load vectors. Eq. (4.2) is then solved in order to evaluate the displacement increment. In order to achieve high level of accuracy in our predictions the time step must be chosen appropriately. The advantage of this method is that the effective stiffness matrix and loading vector are formed only once during each time step. As a result, the computational cost of the numerical procedure for each time step is low. However, the overall computational cost of the whole problem may increase especially if it is a long duration problem. Furthermore, the error at each time step is accumulated and is added to the next time step, therefore resulting in a continuous increase of the divergence between the numerical predictions and the actual behaviour of the structure analysed.

The implicit scheme calculates the velocity and displacement at $t+\Delta t$ based not only on the values at time t, but also at $t+\Delta t$ obtained from previous iterations. After computing the values of velocity and acceleration, the effective stiffness matrix and loading vector are constructed, Eq. (4.2) is solved in order to evaluate the displacement increment. If the difference between internal and external forces (residual force) is too high, then the residual force is re-applied onto the system as an external load and the whole procedure is repeated. If the difference is smaller than a predefined value (convergence criteria) the solution procedure moves on to the next time step.

4.2.2 The Hilber-Hughes-Taylor method

The numerical solution of the equation of motion [Eq. (4.2)] depends on the particular method used. In ABAQUS, the Hilber-Hughes-Taylor method is used for implicit scheme. The Hilber-Hughes-Taylor operator is an extension of the Newmark β-method.

During each iteration the displacement and velocity are given by Eq. (4.3) and Eq. (4.4) respectively:

$$U_{t+\Delta t} = U_t + \Delta t\dot{U}_t + [(0.5-\beta)\Delta t^2]\ddot{U}_t + [\beta\Delta t^2]\ddot{U}_{t+\Delta t} \quad \text{Eq. (4.3)}$$

$$\dot{U}_{t+\Delta t} = \dot{U}_t + [(1-\gamma)\Delta t]\ddot{U}_T + [\gamma\Delta t]\ddot{U}_{t+\Delta t} \quad \text{Eq. (4.4)}$$

where: $\beta = \frac{1}{4}(\alpha-1)^2$

$\gamma = \frac{1}{2} - \alpha$

α : $-\frac{1}{3} \leq \alpha \leq 0$

$U_t , U_{t+\Delta t}$: the value of displacement at t and $t+\Delta t$ respectively

$\dot{U}_t, \dot{U}_{t+\Delta t}$: the value of velocity at t and $t+\Delta t$ respectively

$\ddot{U}_t, \ddot{U}_{t+\Delta t}$: the value of acceleration at t and $t+\Delta t$ respectively

The equation of motion is given by Eq. (4.5)

$$R_{t+\alpha\Delta t} = F^{ext}{}_{t+\Delta t} - M\ddot{U}_{t+\Delta t} - C\dot{U}_{t+\alpha\Delta t} - F^{int}(U_{t+\alpha\Delta t}) \quad \text{Eq. (4.5)}$$

where the displacements ($U_{t+\alpha\Delta t}$) and velocities ($\dot{U}_{t+\alpha\Delta t}$) at the intermediate points are given by Eq. (4.6) and Eq. (4.7)respectively:

$$U_{t+\alpha\Delta t} = (1-\alpha)U_t + \alpha U_{t+\Delta t} \quad \text{Eq. (4.6)}$$

$$\dot{U}_{t+\alpha\Delta t} = (1-\alpha)\dot{U}_t + \alpha\dot{U}_{t+\Delta t} \quad \text{Eq. (4.7)}$$

The ABAQUS default values of the parameters associated with the Hilber-Hughes-Taylor operator are provided in Table 4.1. The values of the parameters depend on the selection of the application type. The transient fidelity application is used for the analysis which requires small time increments to accurately resolve the vibrational

response of the structure and the numerical energy dissipation is kept to a minimum. The moderate dissipation application capable of carrying out the impact analysis uses energy dissipation (*via* plasticity, viscous damping, or numerical effects) to reduce the solution noise and improve the convergence behaviour without significantly degrading the solution accuracy. The program is allowed to select the most suitable procedure depending on the type of problem considered. Analyses involving contact problem are treated as moderate dissipation applications, whereas analyses without contact are treated as transient fidelity applications.

Table 4.1: Default Hilber-Hughes-Taylor parameters used in ABAQUS (2013).

Parameter	**Application**	
	Transient Fidelity	**Moderate Dissipation**
α	-0.05	-0.41421
β	0.275625	0.5
γ	0.55	0.91421

4.2.3 Equilibrium, iterations and convergence in ABAQUS

For a body to be in static equilibrium the residual force acting at each node must be zero, therefore

$$P - I = 0 \qquad \text{Eq. (4.8)}$$

where: P : external forces
I : internal forces

The Newton-Raphson method is used in ABAQUS to solve non-linear problems. This process is shown in Figure 4.1 for a given load increment. ABAQUS uses the structure's initial stiffness (K_o) based on its configuration at u_o and ΔP to calculate a displacement correction (C_a) for the structure. Using C_a, the structure's configuration is updated to u_a and a new stiffness (K_a) is formed for the structure.

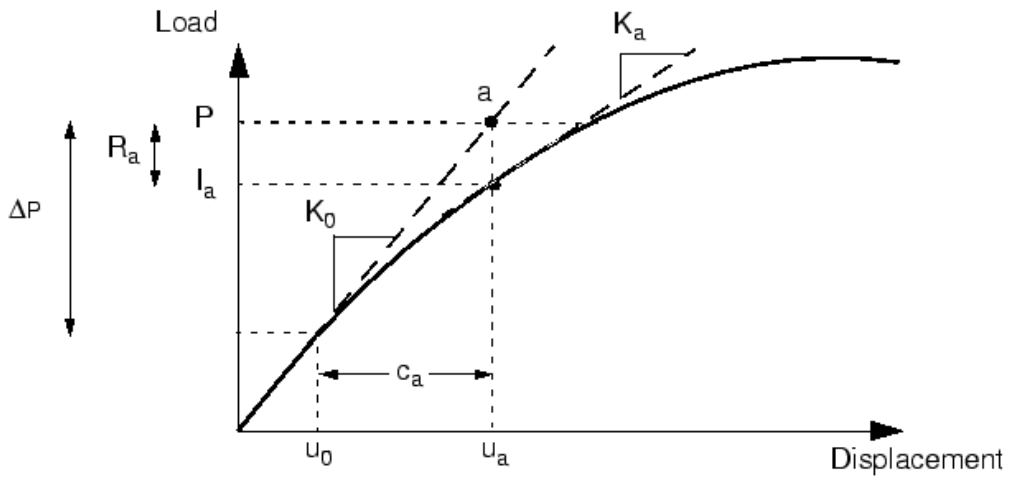

Figure 4.1: First iteration in an increment [ABAQUS (2013)].

The difference between the total applied load (P) and internal load (I_a) is given by Eq. (4.9)

$$R_a = P - I_a \qquad \text{Eq. (4.9)}$$

where: R_a : residual force for the iteration

If R_a is zero at every degree of freedom, point "*a*" in Figure 4.2 would lie on the load-deflection curve, and the structure would be in equilibrium. In a nonlinear problem it is difficult to have R_a equal zero, therefore ABAQUS uses a tolerance value to ensure the solution procedure converges. The default tolerance value is 0.5% of an average force in the structure, averaged over time. If R_a is less than this force residual tolerance, then the structure's updated configuration is considered in equilibrium. However, a displacement correction (C_a) is also checked to ensure it is small relative to the total incremental displacement ($\Delta u_a = u_a - u_o$). If C_a is greater than 1% of the incremental displacement then another iteration is performed. The solution is considered when both R_a and C_a convergence criteria are satisfied.

If the solution does not converge, then another iteration is performed until the convergence is accomplished. The second iteration uses the stiffness (K_a) calculated at the end of the previous iteration together with R_a to determine another displacement correction (C_b) so that the solution converges (see point *b* in Figure 4.2).

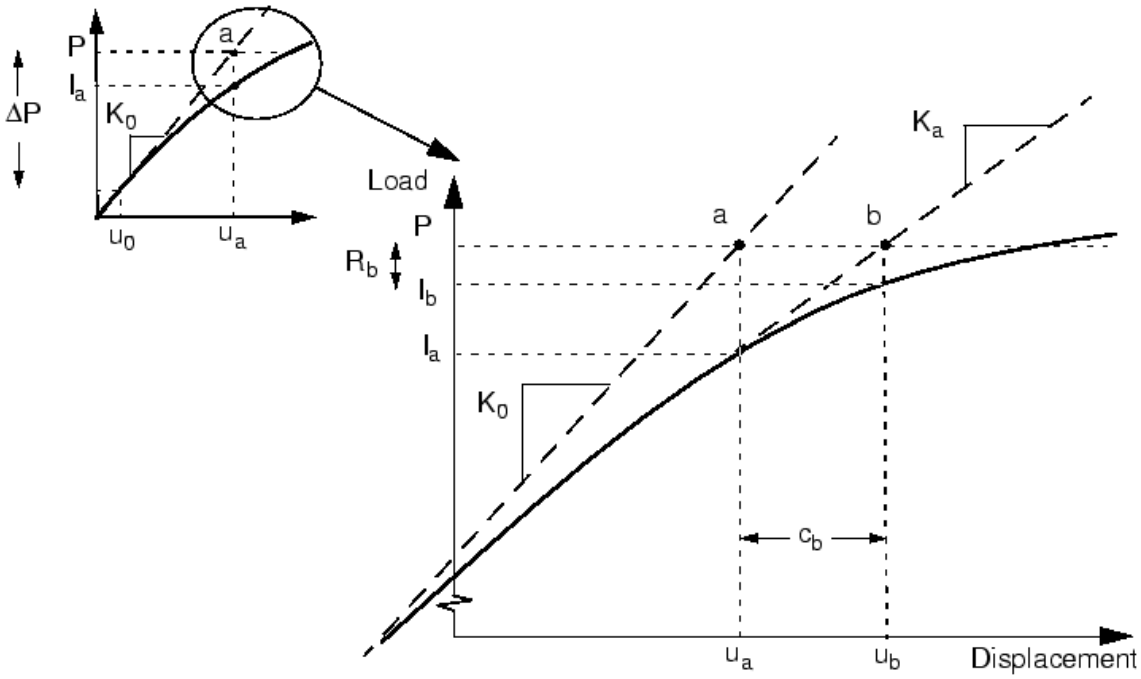

Figure 4.2: Second iteration in an increment [ABAQUS (2013)].

4.2.4 Modelling material behaviour

In order to describe the behaviour of steel and concrete two constitutive models are incorporated into the non-linear finite element analysis (*NLFEA*) package employed. The formulation of these models is based on static material properties. A concise description of the concrete and steel constitutive models used in this numerical study to investigate the behaviour of steel and plain concrete specimens under increasing loading rate are concisely described.

4.2.4.1 Steel

The classical metal plasticity model in ABAQUS (2013) is used to describe the behaviour of steel. This model uses Mises or Hill Yield surfaces with associated plastic flow, which allow for isotropic and anisotropic yield and can be used as a perfect plastic or isotropic hardening model.

The Mises yield surface is used to describe isotropic yielding. It is defined by giving the value of the uniaxial yield stress as a function of uniaxial equivalent plastic strain as shown in Figure 4.3. The plastic strain is given by Eq. (4.10)

$$\varepsilon^{pl} = \varepsilon^{t} - \varepsilon^{el} = \varepsilon^{t} - \frac{\sigma}{E} \qquad \text{Eq. (4.10)}$$

where: ε^{pl} : true plastic strain

ε^{t} : true total strain

ε^{el} : true elastic strain

σ : true stress

E : Young's modulus

The classical metal plasticity model used for numerical investigation for defining material properties of steel is assumed to be strain rate independent. As discussed in section 3.2.8, the ultimate strength essentially remains constant under increasing loading rates, therefore, the study focuses mainly on investigating the increase in yield strength of steel under high rate loading, and hence, failure of steel is not modelled explicitly.

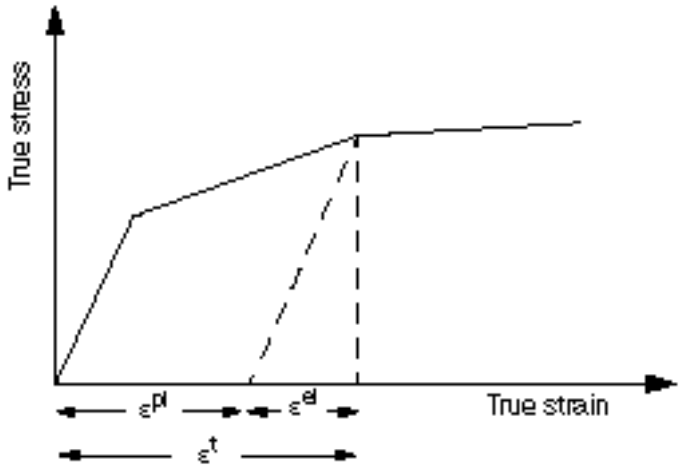

Figure 4.3: Stress-strain relationship of steel used in ABAQUS [ABAQUS (2013)].

It should be noted that the material behaviour of steel is presently assumed to be independent of the loading rate and therefore only static material properties are considered when investigating numerically the behaviour of steel pipes under impact. However, for each case study carried out the distribution of the strains and strain-rates developing along each specimen throughout the loading process are considered and

assessed in order to determine the region of the specimen likely to be affected by high values of strain-rate.

4.3 DESCRIPTION OF THE PROBLEM AT HAND

Jones *et al.* (1992) investigated the behaviour of mild steel pipes subjected to drop-weight testing. A total of 130 impact tests were carried out on mild steel pipes with a length to diameter ratio (L/D) of 10. The emphasis of the numerical investigation presented in this chapter mainly focuses on predicting the response of a pipe specimen with a diameter (D) of 42mm, a thickness (t) of 2mm and a span length (L) of 420mm. The reason for choosing this specimen is mainly associated with the fact that the test data describing certain important aspects of the response exhibited by the subject specimens under static and high rate loading (i.e. contact force, displacement and velocity-time histories) were provided and hence used to validate the predictions of *NLFEA*.

During static testing the load was applied through a rigid wedge-shape indentor on the top of the pipe at its mid-span. Impact (drop-weight) test was carried by allowing a 17.5kg impactor to drop onto the top surface of the pipe's cross-section at mid-span with an initial velocity of 9.93m/s and an impact energy of 863J. Figure 4.4 shows the geometry of the impactor and the test setups used in the experimental study. In both (static and drop weight) tests the pipe was considered fully clamped at both its ends.

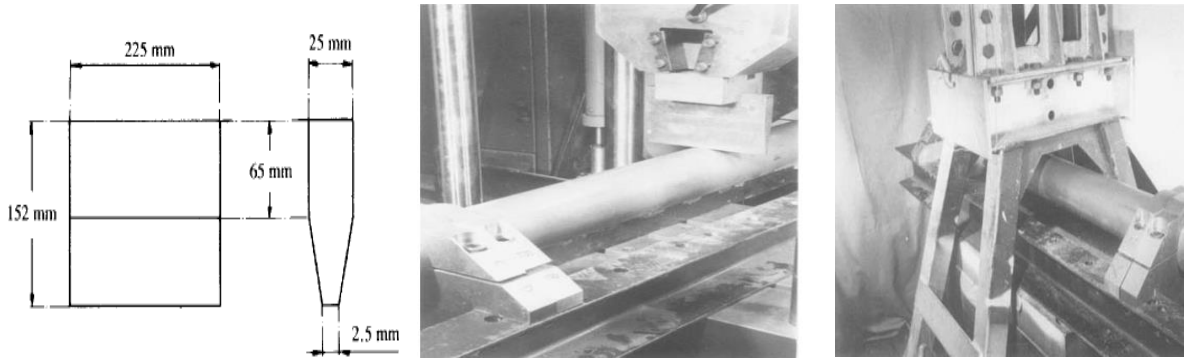

(a) (b) (c)

Figure 4.4: (a) Cross-sectional dimensions of the impactor (b) static test setup (c) impact test set up [Jones *et al.* (1992)].

4.4 DEVELOPMENT OF THE FINITE ELEMENT MODEL

Static and dynamic *NLFEA* are carried out using ABAQUS [ABAQUS (2013)]. The iterative solution strategy adopted for conducting static and dynamic *NLFEA* and a detailed description of the relevant material model adopted by ABAQUS are presented in detail in Chapter 3. Figure 4.5 (a) presents the *FE* model used in the numerical investigation. Due to the double symmetry characterising the problem at hand only a quarter-model is developed which allows a reduction in the computational cost required for solving the problem at hand. A contact surface between the pipe and the impactor is defined with a coefficient of friction of 0.3 [MAE (2016)]. When considering the equivalent static problem, the load is imposed in the form of displacement increments (displacement control) at the top of the indentor, whereas in the case of the dynamic problem the impactor is assumed to have an initial velocity prior to coming into contact with the steel pipe. It should be mentioned that large displacement analysis is conducted when solving both static and dynamic problems in order to account for the geometrical non-linearities (i.e. buckling) which can have a significant effect on the response of the specimens.

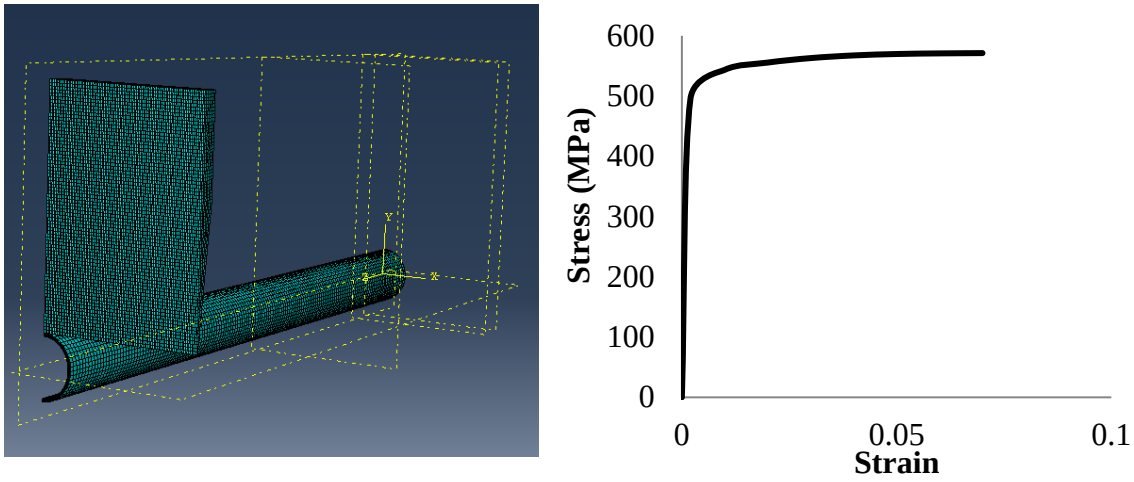

(a) (b)

Figure 4.5: (a) Finite element model (b) stress-strain curve describing material behaviour of steel.

The stress-strain curve describing the behaviour of the mild steel used for constructing the subject pipes was not reported [Jones *et al.* (1992)], therefore the true stress-strain

curve [see Figure 4.5 (b)] obtained from coupon tests conducted on mild steel specimens with similar characteristics (e.g. yield and ultimate stress) to the steel used in the actual tests is employed. In the experimental study [Jones *et al.* (1992)] the pipes were considered fully fixed at both ends. These supports were achieved through the use of clamps, however, it is possible that the subject end conditions may not have been fully achieved during testing due to the deformation/distortion exhibited in the area of the supports which may have in turn resulted in some slippage being exhibited at the clamps during testing. Therefore, two different case studies are considered. In the first the pipe is assumed fully fixed at its supports (axial restraint) whereas in the second the pipe is allowed to slide along at the supports (no axial restraint). Based on a mesh sensitivity conducted, a uniform mesh size of 3.1 x 2.7 is selected and 8-node brick elements are used to mesh the pipe. Table 4.2 gives the number of elements used in the pipe.

Table 4.2: Number of element used for the pipe.

Section	Number of elements
Thickness	4
Circumference	24
Length	85

4.5 DISCUSSION OF RESULTS

4.5.1 Static case studies

The comparison of the test data and the corresponding numerical predictions is shown in Figure 4.6 in the form of load-deflections curves associated with the specimen's mid-span. The latter curves reveal a reasonably good agreement between the numerical predictions and their experimental counterparts. More specifically, the numerical predictions concerning the load-carrying capacity (peak load) obtained when considering the pipe supports fully fixed is in good agreement with that established experimentally, however the response predicted by the *NLFEA* is characterised by higher stiffness and lower deflection than those recorded during testing [see Figure 4.6].

When assuming that the pipe is allowed to move axially (slide) at the supports (no axial restraint) the form of the numerically predicted load-deflection curve provides a closer fit to that recorder during testing for applied loads up to 20kN. Divergence is observed in the load-deflection curves for applied loads over 20kN with the experimentally established behaviour being characterised by higher stiffness and load-bearing capacity compared to that predicted numerically. However both numerically and experimentally predicted values of established maximum deflection exhibited prior to failure at mid-span are in agreement.

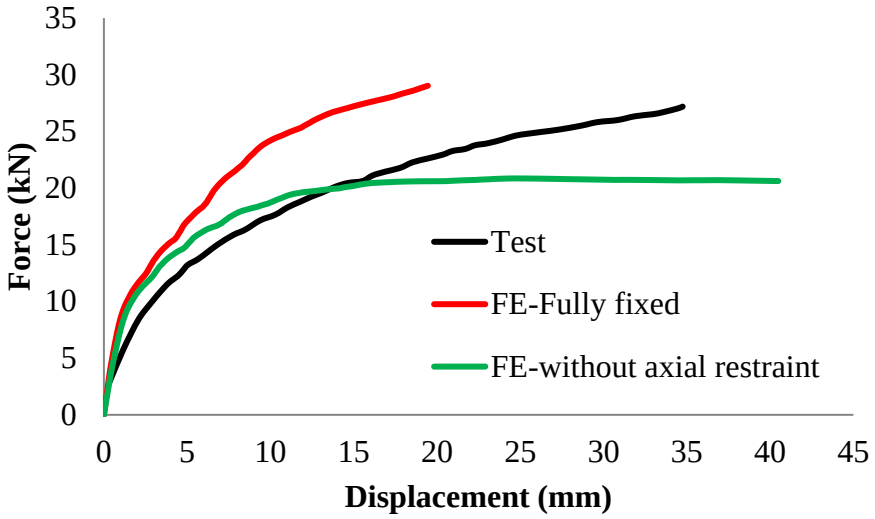

Figure 4.6: Comparison of the force-mid-span deflection curves established experimentally and numerically.

This divergence between the experimental and numerical data can be partly attributed to the fact that the supports in the experimental study are neither fully fixed nor do they allow the pipe to freely slide axially. In reality the supports are likely to allow some sliding of the pipe at high levels of applied loading due to the deformation/distortion of the pipe's cross-section observed at those regions. Thus the end conditions achieved at the supports during testing may be intermediate to the supports adopted by the two case studies considered numerically and therefore it is not easy to accurately define in the numerical model. This conclusion is supported by the overall comparison of the experimental and numerical load-deflection curves which reveals that the experimentally established curve appears to be in between its counterparts predicted

numerically by the two case studies considered. Another reason for the differences observed between the experimental and numerical data can be associated with the fact that the stress-strain introduced into the numerical model is an approximation of the behaviour of the steel used to construct the pipes since the actual stress-strain curves are not available.

Figure 4.7 and Figure 4.8 show the predicted post loading deformation profile of the pipe established numerically when assuming that the pipe supports are fully fixed ends (including axial restraint) and without axial restraint. As discussed above it is observed that the pipe with fully fixed ends is associated with higher stiffness and lower deflection as compared to the pipe without axial restraint.

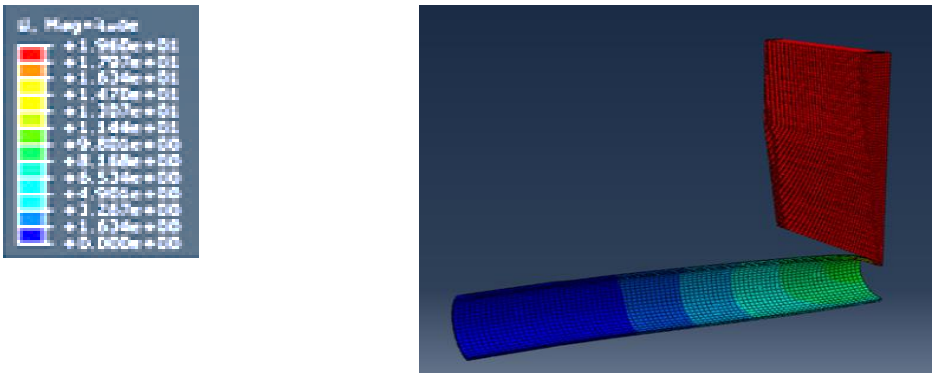

Figure 4.7: Predicted post loading deformation profile of the pipe established numerically when assuming that the pipe supports are fully fixed ends (including axial restraint).

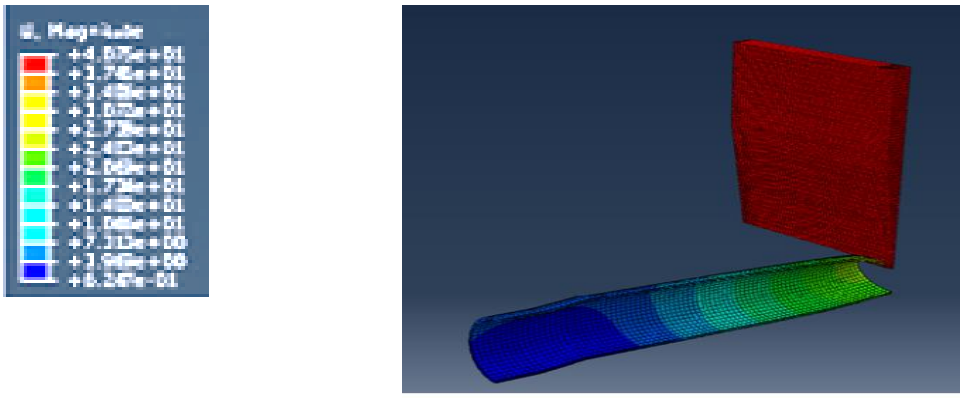

Figure 4.8: Predicted post loading deformation profile of the pipe established numerically when assuming that the pipe supports are without axial restraint.

4.5.2 Dynamic case studies

The comparison of the test data obtained from the drop-weight tests and the numerical predictions obtained from ABAQUS concerning the time history of the contact force (developing at the interface between the impactor and the steel pipe) and the vertical displacement at mid-span (at the top of pipe cross section) are shown in Figure 4.9 (a) and (b) respectively. The contact force-displacement curves predicted from *NLFEA* and recorded during testing are shown in Figure 4.9 (c). The comparison of the numerical predictions and the test results reveals agreement until 3ms after initial contact is observed between the pipe and the impactor. Beyond this point divergence is observed between the test results and the *NLFEA* predictions. *NLFEA* predicted larger global deformation compared to that recorded experimentally [see Figure 4.9(b)]. As in the static case study, the pipe with fully fixed ends is found to exhibit a stiffer response compared to that established experimentally [Figure 4.9 (c)]. As a result the intensity of the contact force developing during impact was higher than that recorded experimentally. In spite of the higher stiffness the maximum deflections [see Figure 4.9 b)] and the duration of the impact [see Figure 4.9 (a)] predicted from the subject case study (fully fixed supports) are in good agreement to that recorded experimentally. On the other hand when assuming that the pipes at the supports are able to move axially (no axial restraint), the predicted response is characterised by considerably less stiffness resulting in an increase of the duration of impact and the displacement (both maximum and residual) compared to its counterparts established in the previous case study (fully fixed ends) and the test. It should be noted however that the maximum contact force is in good agreement with its experimental counterpart [Figure 4.9 (a) & (c)]

As in the static case study, the divergence observed between the numerical and experimental data are probably due to the end conditions attained in the impact tests as well as the difference in the material behaviour described by the constitutive model adopted for the analysis and the true steel behaviour of the pipe.

Figure 4.10 shows the vertical displacement exhibited along the top and bottom profile of the pipe throughout the loading process when assuming that the pipe supports are fully fixed ends (including axial restraint) and without axial restraint. As expected it is observed that the pipe with fully fixed ends is associated with higher stiffness and lower deflection as compared to pipe without axial restraint.

The maximum reduction in the diameter (25.74mm) is exhibited at mid-span (where the applied load is exerted) of the pipe recorded during drop-weight testing. The *NLFEA* predictions for the reduction in diameter along the length of the pipe are shown in Figure 4.11. Good agreement is observed between the *NLFEA* predictions (24.27 mm and 19.786 mm for pipe without axial restraint and with fully fixed ends respectively) and the relevant test data (25.74mm). It can be observed in Figure 4.11 that the damage (permanent deformation) due to impact is localized in the contact zone where a significant reduction in the diameter of the pipe is observed, however, this reduction quickly becomes very small away from the impact zone.

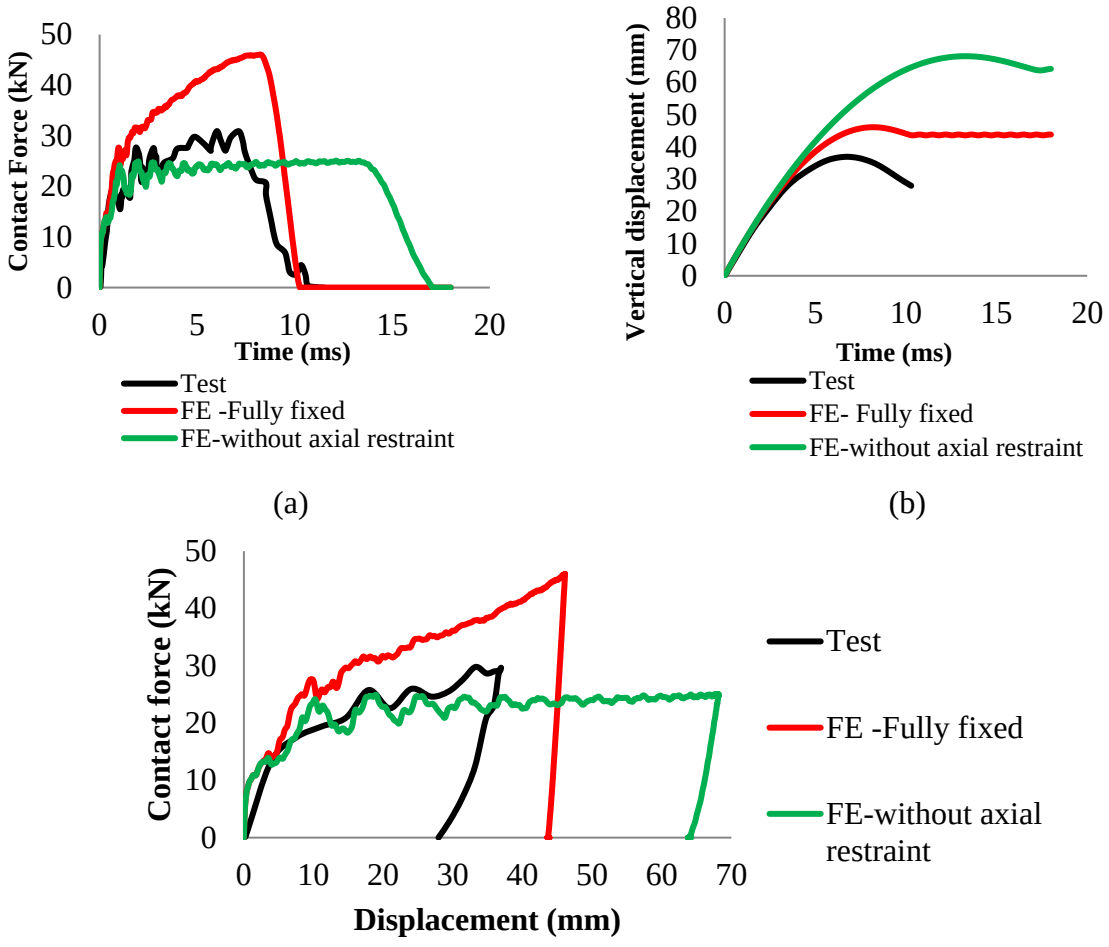

Figure 4.9: Comparison of experimental and numerical result expresses (a) the contact force time histories (b) the mid-span displacement time histories and (c) the relation between contact force and mid-span displacement.

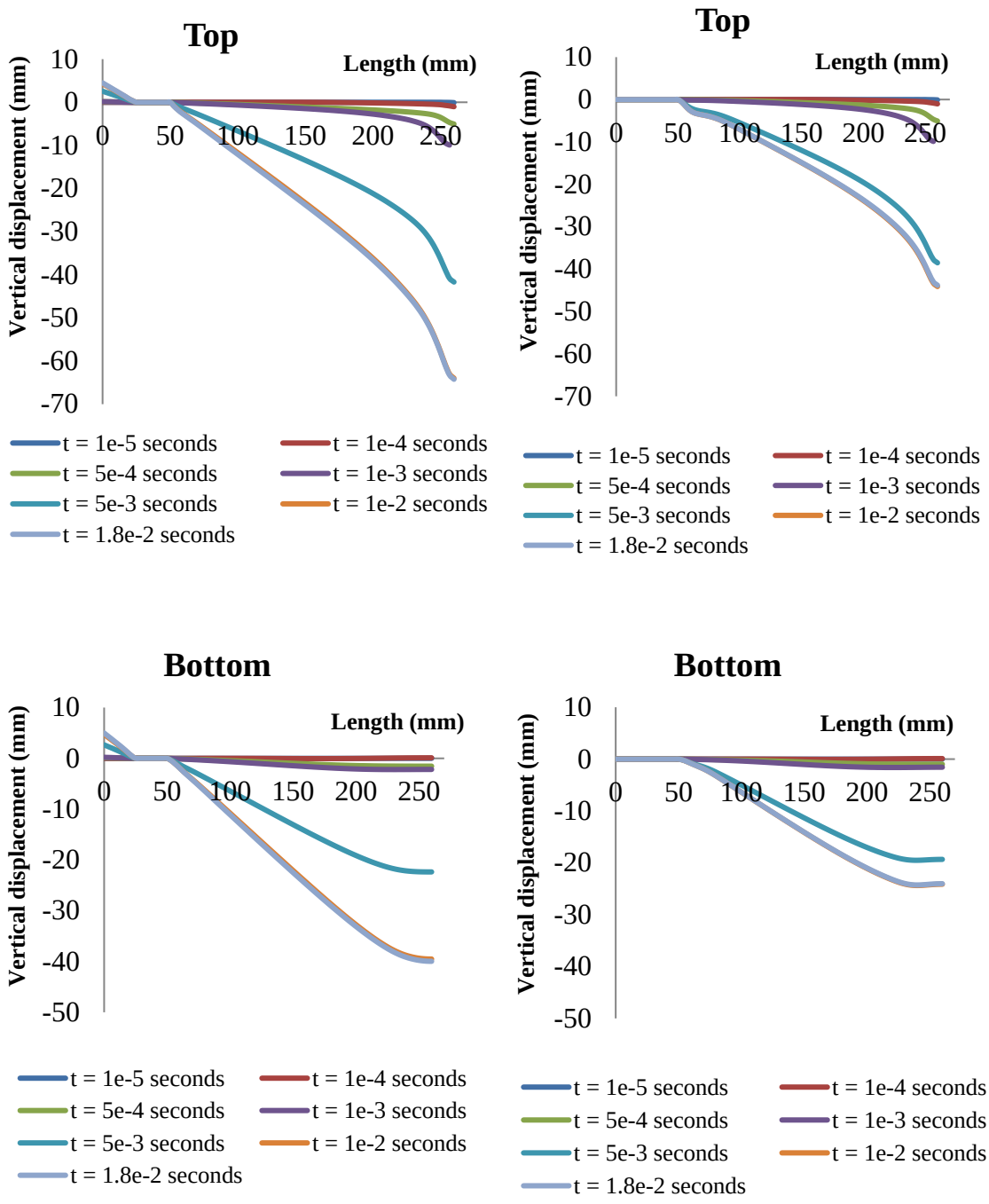

(a) (b)

Figure 4.10: Numerically predicted top and bottom profile of the pipe (a) without axial restraints (b) with axial restraints (fully fixed ends).

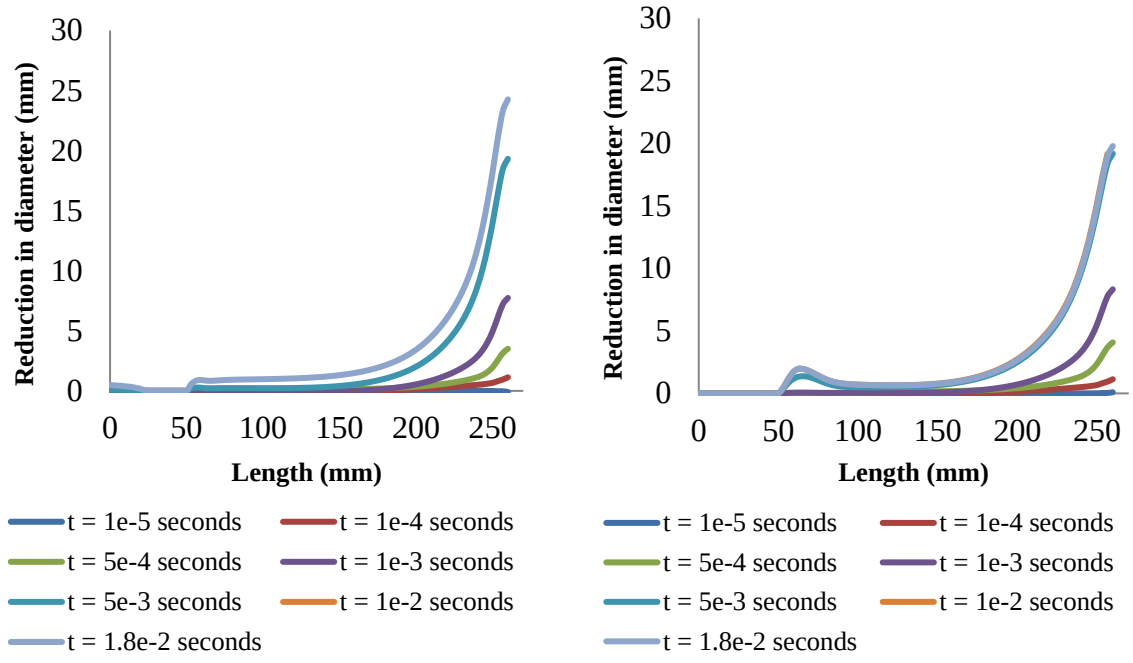

(a) (b)

Figure 4.11: Predicted reduction in pipe diameter assuming that end supports are (a) without axial restraint and (b) with axial restraint (fully fixed ends).

Figure 4.12 shows the post-impact cross-sections and longitudinal profiles of the pipe. As mentioned previously, the pipe with fully fixed ends is found to be stiffer; as a result a reduction in the diameter and global deformation are lower compared to its counterparts predicted in the case of the pipe without axial restraint at its supports. As can be seen in Figure 4.12, the predicted failure modes are in agreement with the four different failure modes observed experimentally (see section 2.5) and shown in Figure 4.13 which included:

- Shear sliding on the inside surface which is in contact with the edge of a support (Mode 1).
- Ductile fracture of a pipe surface at a support (Mode 2).
- Shear sliding at the impact point (Mode 3).
- Buckling on the bottom surface of a pipe near a support (Mode 4).

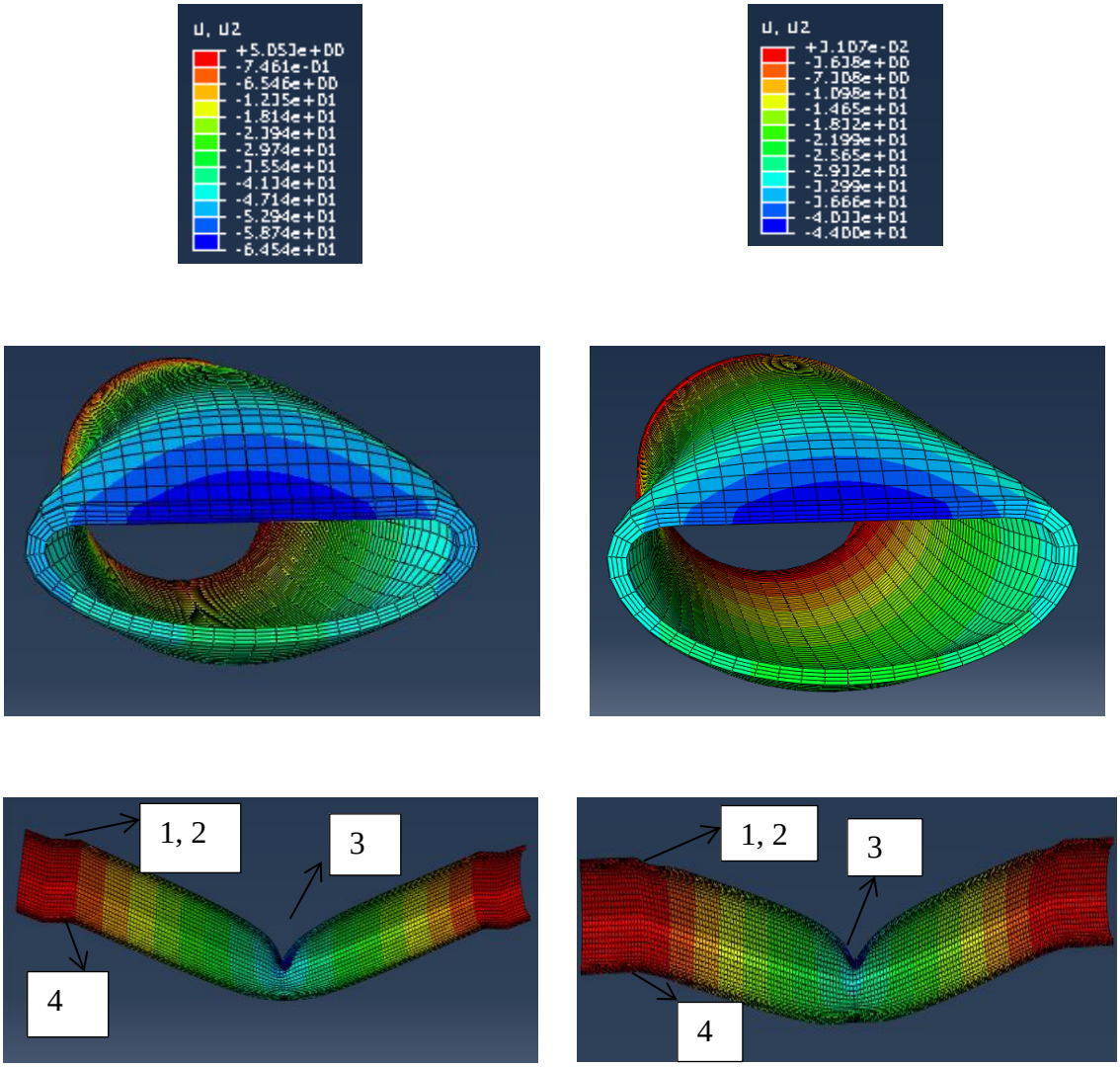

(a) (b)

Figure 4.12: Predicted deformed cross-sections and profiles of the pipes with modes of failure assuming pipe (a) without axial restraint and (b) with axial restraint (fully fixed ends).

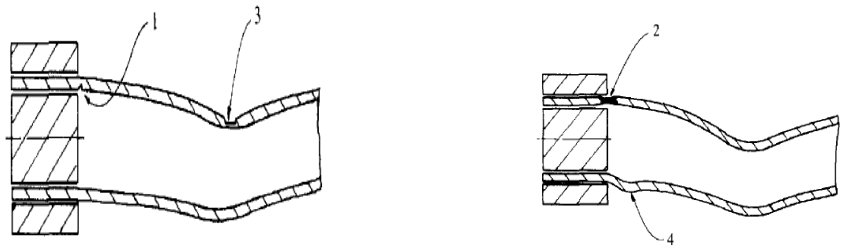

Figure 4.13: Failure modes exhibited by pipe-specimens observed in tests [Jones *et al.* (1992)].

Based on the comparison of the test data and the corresponding numerical predictions a reasonably good agreement is observed. The *NLFEA* capture main aspects of the pipe behaviour (the predicted failure modes, the load-displacement curves) which are in reasonable agreement with their experimental counterparts.

4.6 PARAMETRIC STUDY

As discussed in Chapter 2, a range of parameters can potentially influence the behaviour of subsea steel pipes under impact. Following the validation of the *NLFEA*, a parametric investigation is carried out to study the influence of these parameters on the behaviour of the scaled steel pipe specimens exhibited under impact loading. The parameters considered in this study are the velocity with which the impactor collides with the pipe (v), the length to diameter ratio (L/D), the support conditions of the pipe, the development of strain rates ($\dot{\epsilon}$) as well as the level of axial loading and internal and/or external pressure acting on the walls of the pipes.

4.6.1 Influence of velocity

In order to investigate the influence of the impact velocity, *v*, (with which the impactor comes into contact with the specimen) on the behaviour of the pipe, two case studies are carried out. In the first case study, the pipe is impacted with half the velocity ($0.5v_{exp}$ = 4.965m/s) used in the impact test described in section 4.3 [Jones *et al.* (1992)], whereas in the second case study twice the velocity used during testing ($2v_{exp}$ = 19.86 m/s) is considered. Each case study is carried out with the two end conditions described in section 4.4. The pipe cross-section at the supports is either considered fully fixed or is allowed to move axially.

The curves in Figure 4.14 shows the variation of the contact force generated during impact with time and the reduction in the diameter along the length of the pipe exhibited after impact for the case in which the pipe is considered to be fixed at the supports [see Figure 4.14 (a)] and for the case in which the pipe is allowed to slide horizontally at the supports [see Figure 4.14 (b)]. It is observed that with increasing values of impact velocity, the magnitude of the maximum contact force and the reduction in diameter (expressing the level of damage sustained along the length of

specimen) also increase. The pipe with fully fixed ends is found to exhibit a stiffer response, resulting in higher values of contact forces being generated, the shorter duration of impact and smaller reduction in diameter with maximum damage being mainly concentrated at mid-span and the supports [see Figure 4.14(a)].

For the case of pipes without axial restraint the magnitude of the contact force is significantly lower (as the duration of the contact was higher), the level of damage sustained is higher and extended over the full span of the pipe. In both cases the maximum reduction in diameter is observed at mid-span. For velocity equal to $2v_{exp}$, the impactor did not rebound (plastic impact) after initial contact as shown in Figure 4.14(b) as the pipe cross-section appeared to have collapsed at mid-span.

Figure 4.15 and Figure 4.16 show the deformed profile exhibited along the length of the pipe (at the top and bottom of the pipe cross sections) at different stages of the loading process for the case in which the pipe is allowed to slide horizontally at the supports and for the case in which the pipe is considered to be fixed at the support respectively. It is found that irrespective of the velocity of the impactor, the behaviour of the pipe is localized during the initial phase of loading as the deformation due to the applied load is initially limited to the contact area. This can also be seen in Figure 4.17 which shows the reduction of the pipe diameter at different stages of loading process. The behaviour becomes more global with time as the generated waves gradually move away from the contact area.

Figure 4.18 and Figure 4.19 show the post-impact cross-section of the pipes and deformed shapes along the length of the pipes, respectively. Figure 4.19 also shows the modes of failure predicted by *NLFEA* for different case studies considered. It is found that for an impact velocity equal to $0.5v_{exp}$ the damage is limited to the impact zone. However, as the velocity considered increased the damaged is distributed over a larger portion of the pipe. It is also observed that for the low impact velocity ($0.5v_{exp}$) the shear sliding at the impact zone (failure mode 3) is observed, however with the velocity of $2v$, the pipe cross-section completely collapsed locally.

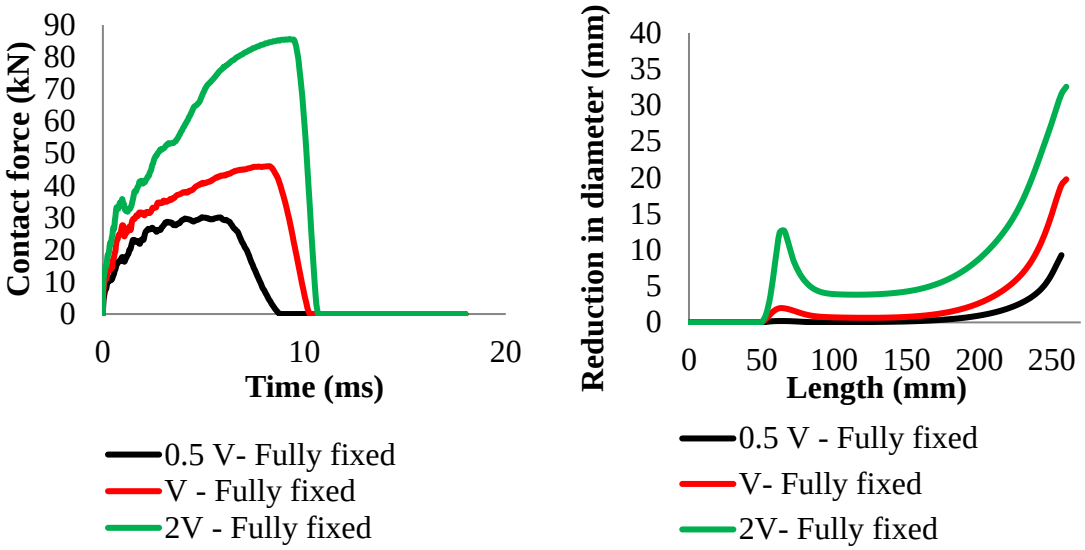

(a)

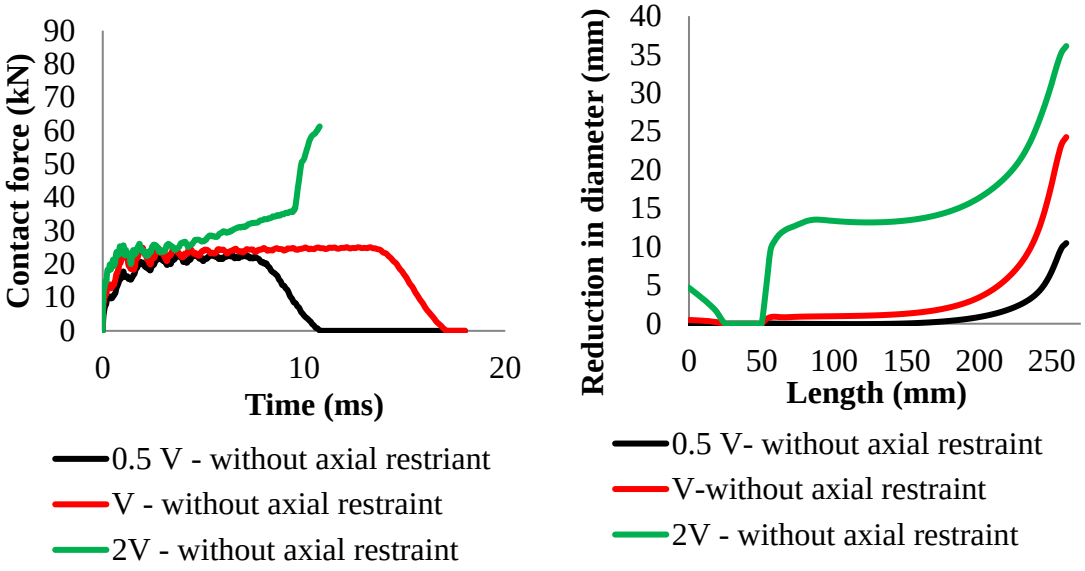

(b)

Figure 4.14: Contact force time-histories and reduction in the diameter along the length of the pipe (a) with axial restraint (fully fixed ends) (b) without axial restraint.

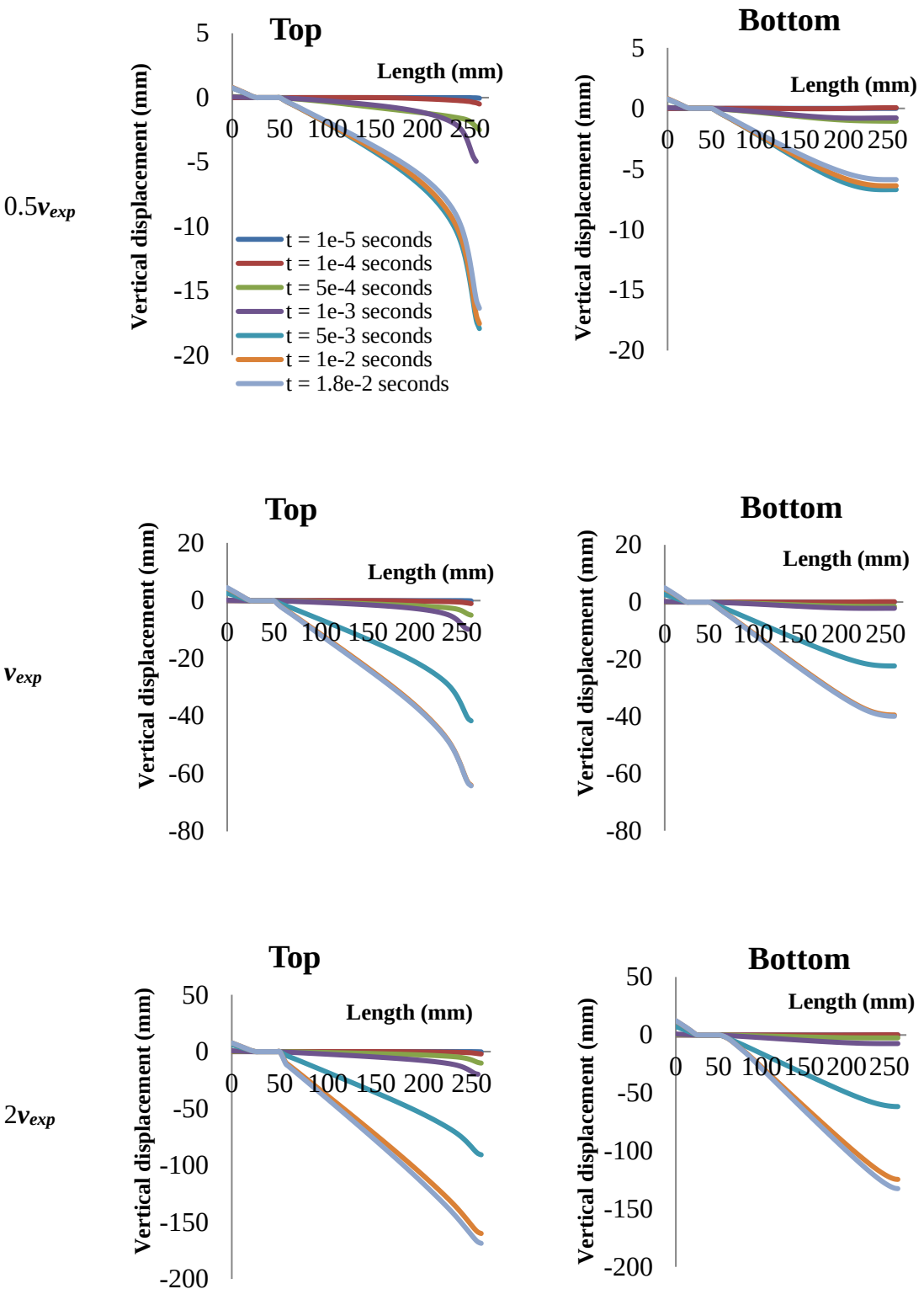

Figure 4.15: Predicted vertical displacement along the length of the pipe at the top and bottom of its cross section for different impact velocities (i) 0.5v_{exp} (ii) v_{exp} *and (iii)* $2v_{exp}$ when no axial restraint at its end supports was considered.

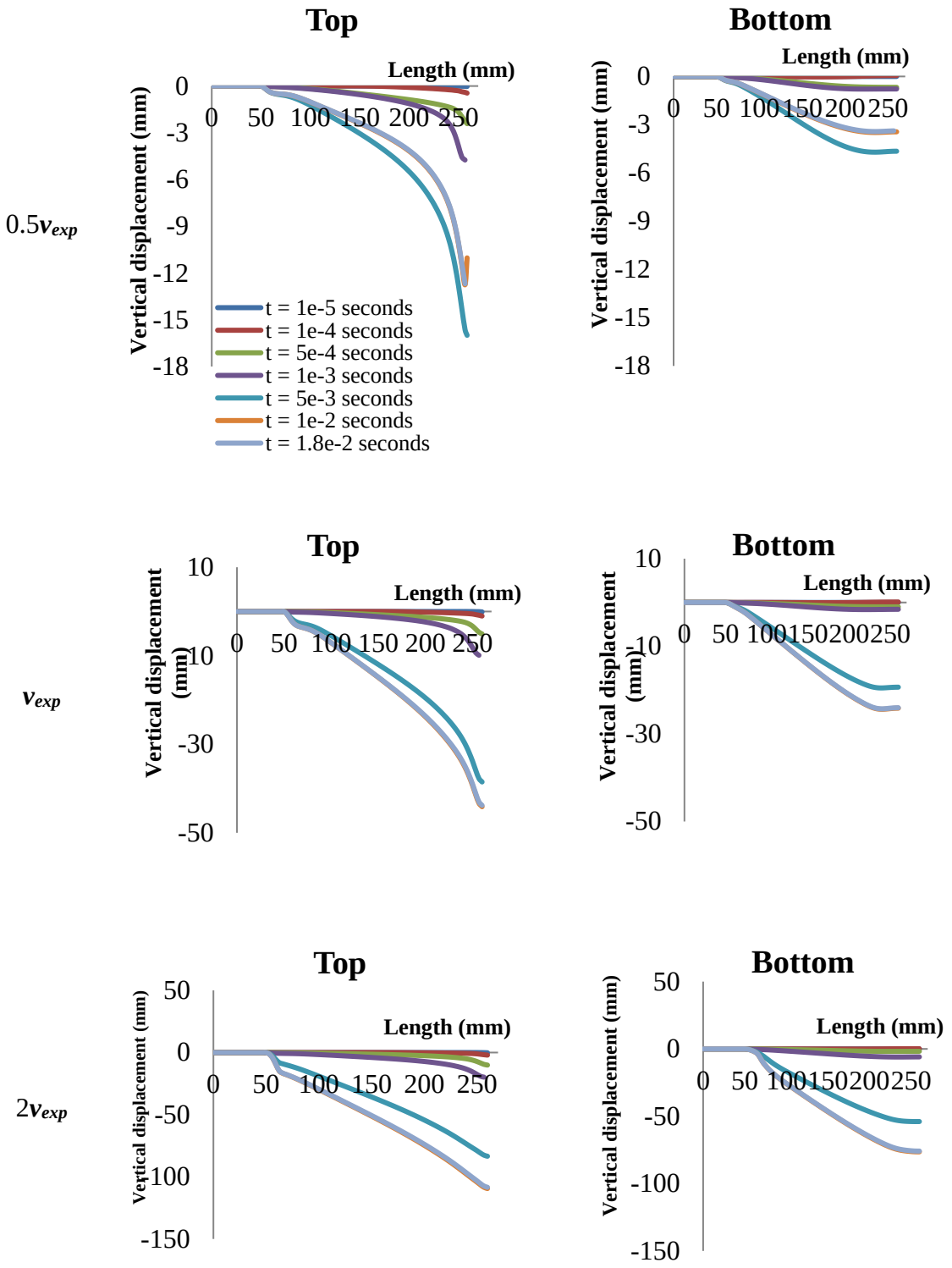

Figure 4.16: Predicted vertical displacement along the length of the pipe at the top and bottom profile of its cross section for different impact velocities (i) $0.5v_{exp}$ (ii) v_{exp} and (iii) $2v_{exp}$ when axial restraint (fully fixed ends) at its end supports was considered.

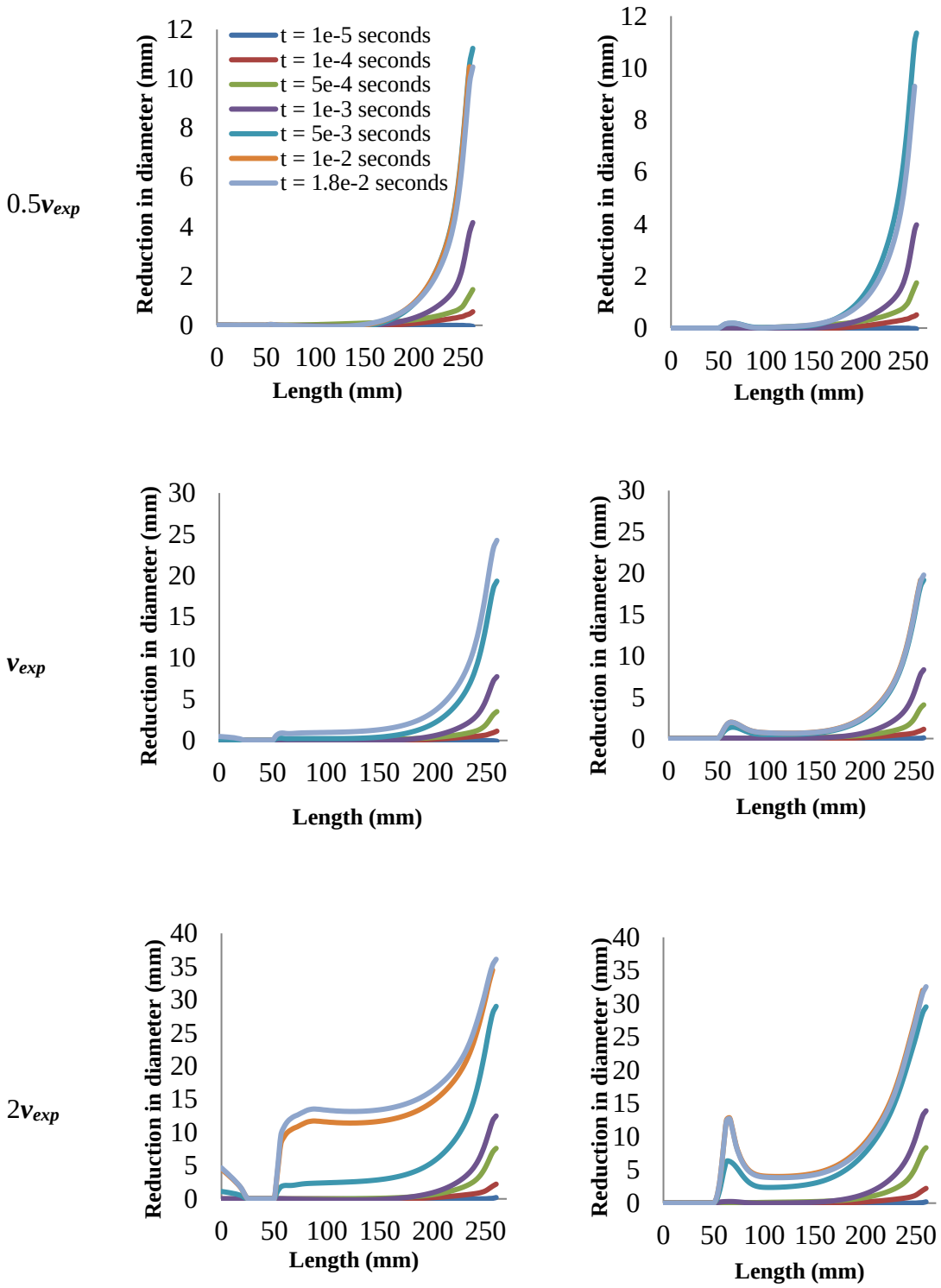

Figure 4.17: Predicted reduction in diameter along the length of the pipe (a) without and (b) with axial restraint at its end supports for different impact velocities (i) 0.5 v_{exp} (ii) v_{exp} *and (iii)* $2v_{exp}$.

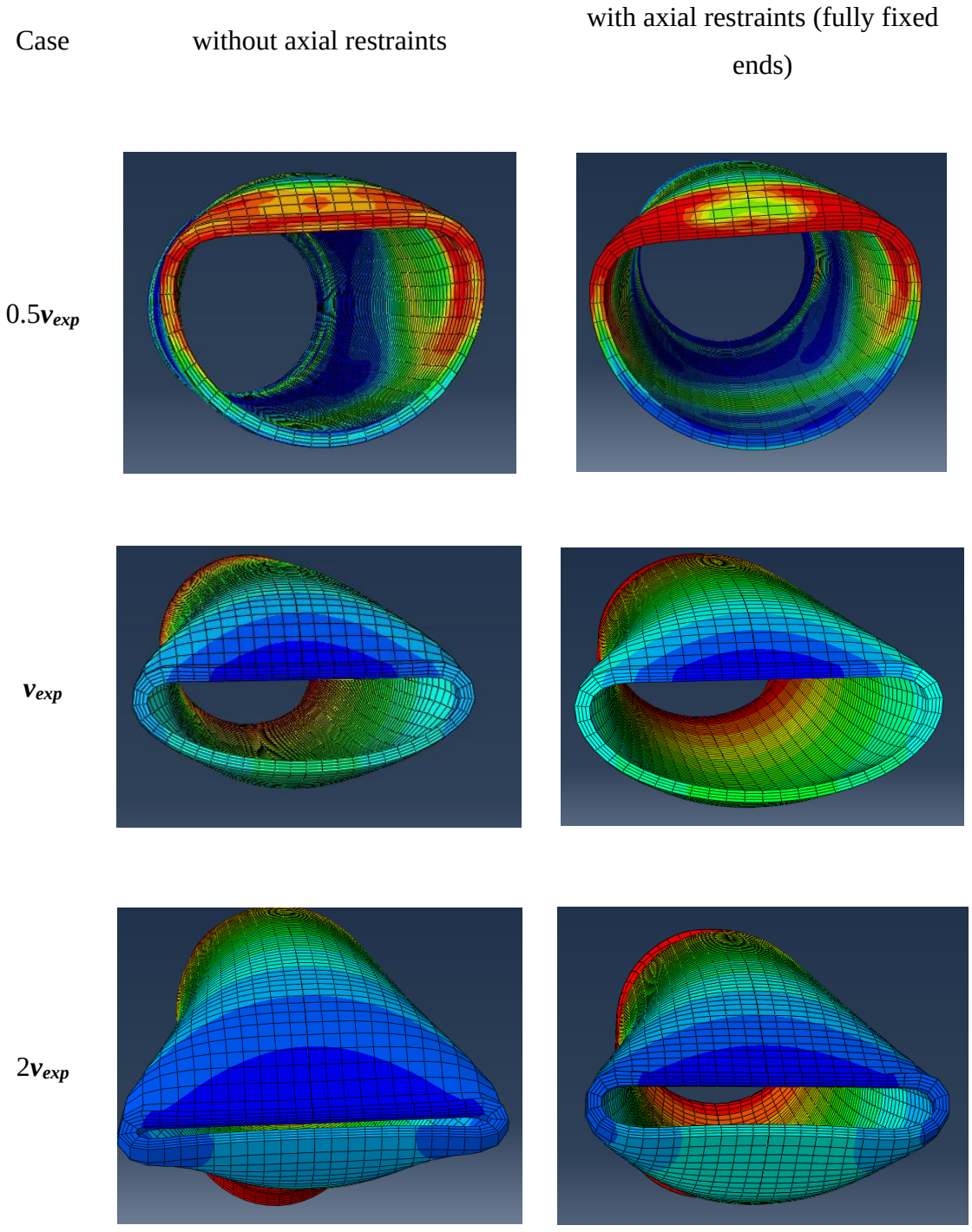

Figure 4.18: Predicted deformed shapes of the pipe cross-sections with and without axial restraints for different impact velocities (i) $0.5v_{exp}$ (ii) v_{exp} *and (iii)* $2v_{exp.}$

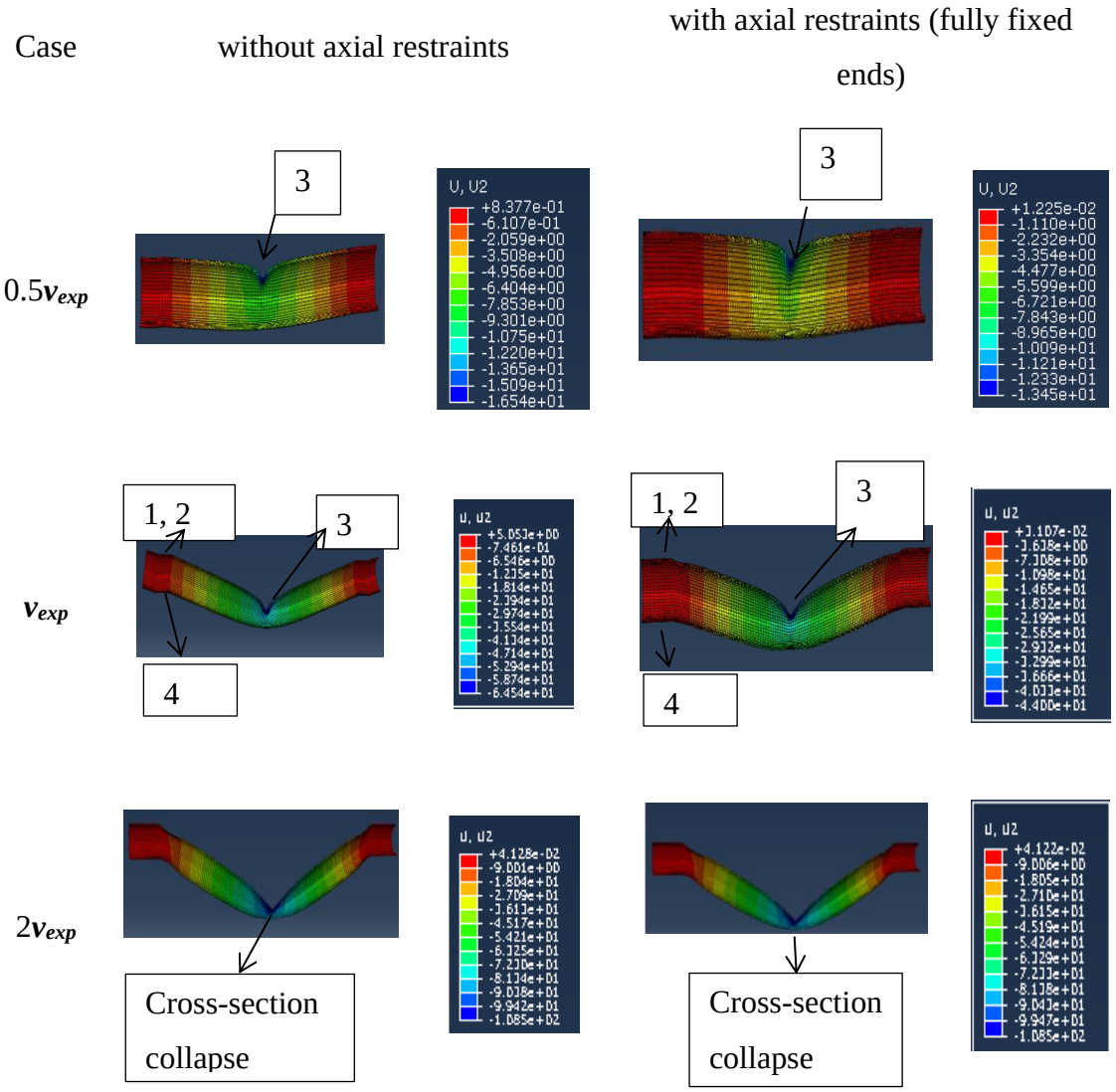

Figure 4.19: Predicted deformed shape and modes of failure along the length of the pipe with and without axial restraints for different impact velocities.

4.6.2 Influence of length to diameter ratio

In order to investigate the influence of the length to diameter ratio (L/D) on the impact behaviour of the pipe, two case studies are carried out. In the first case study a value of *L/D* equal to 25 is adopted whereas in the second case study *L/D* is considered equal to 60. In both case studies the pipe had the same cross-section and end conditions as described in section 4.6.1.

Figure 4.20 shows the reduction in the diameter of the pipe and contact force-time histories for different *L/D* ratios. It is found that as *L/D* increased the magnitude of the

maximum contact force developing during impact decreased. It is also found that for the case of pipes with *L/D* equal to 25 and 60 which had no axial restraint at their support the impactor did not rebound after the first impact (see Figure 4.20) due to collapse of the cross-section (plastic impact). A similar observation is also made for the pipe with *L/D* of 60 which had fully fixed ends.

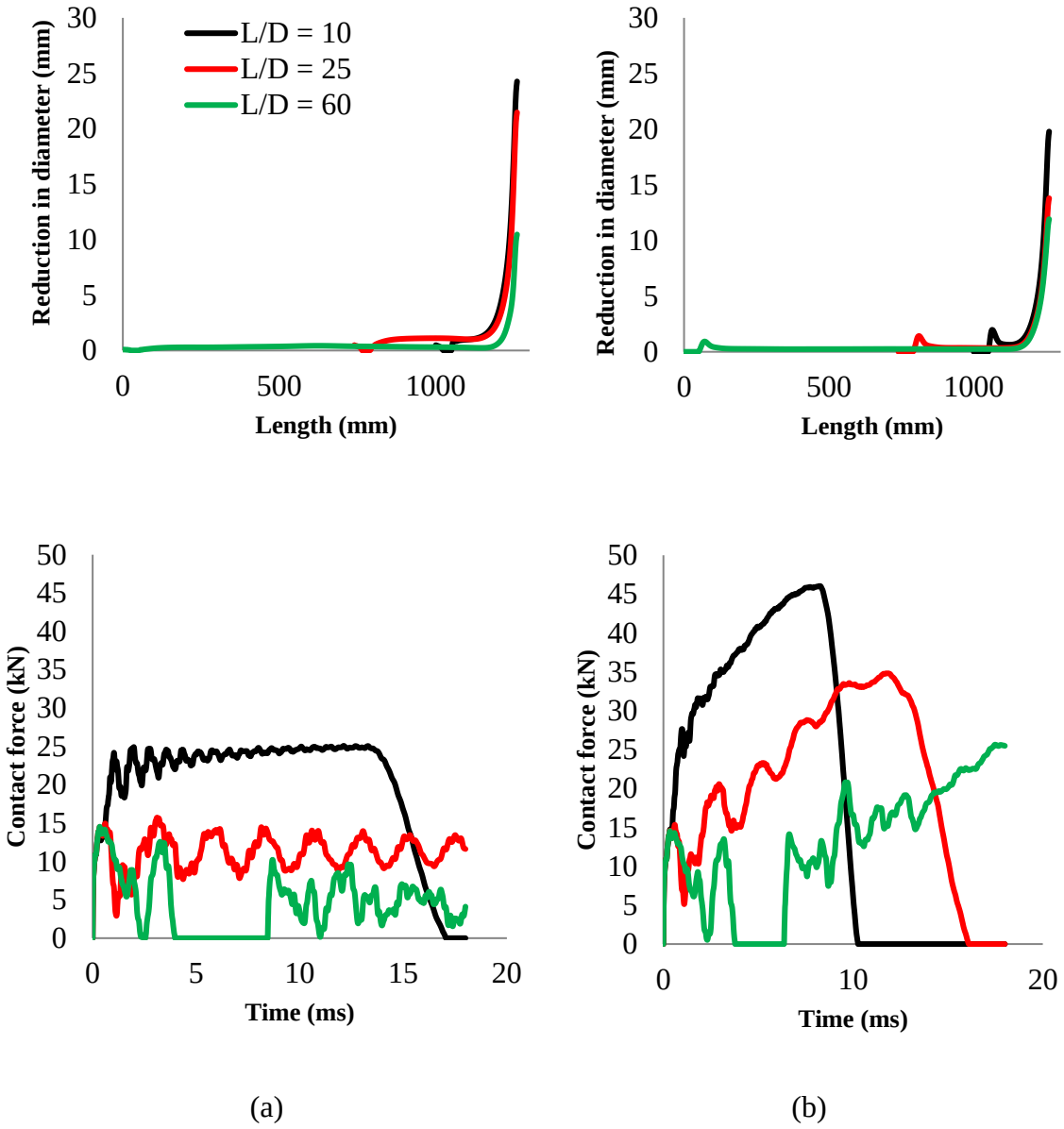

Figure 4.20: Predicted reduction in the diameter along the length of the pipe and contact force time-histories for pipe with different *L/D* ratios assuming its end supports (a) without and (b) with axial restraints.

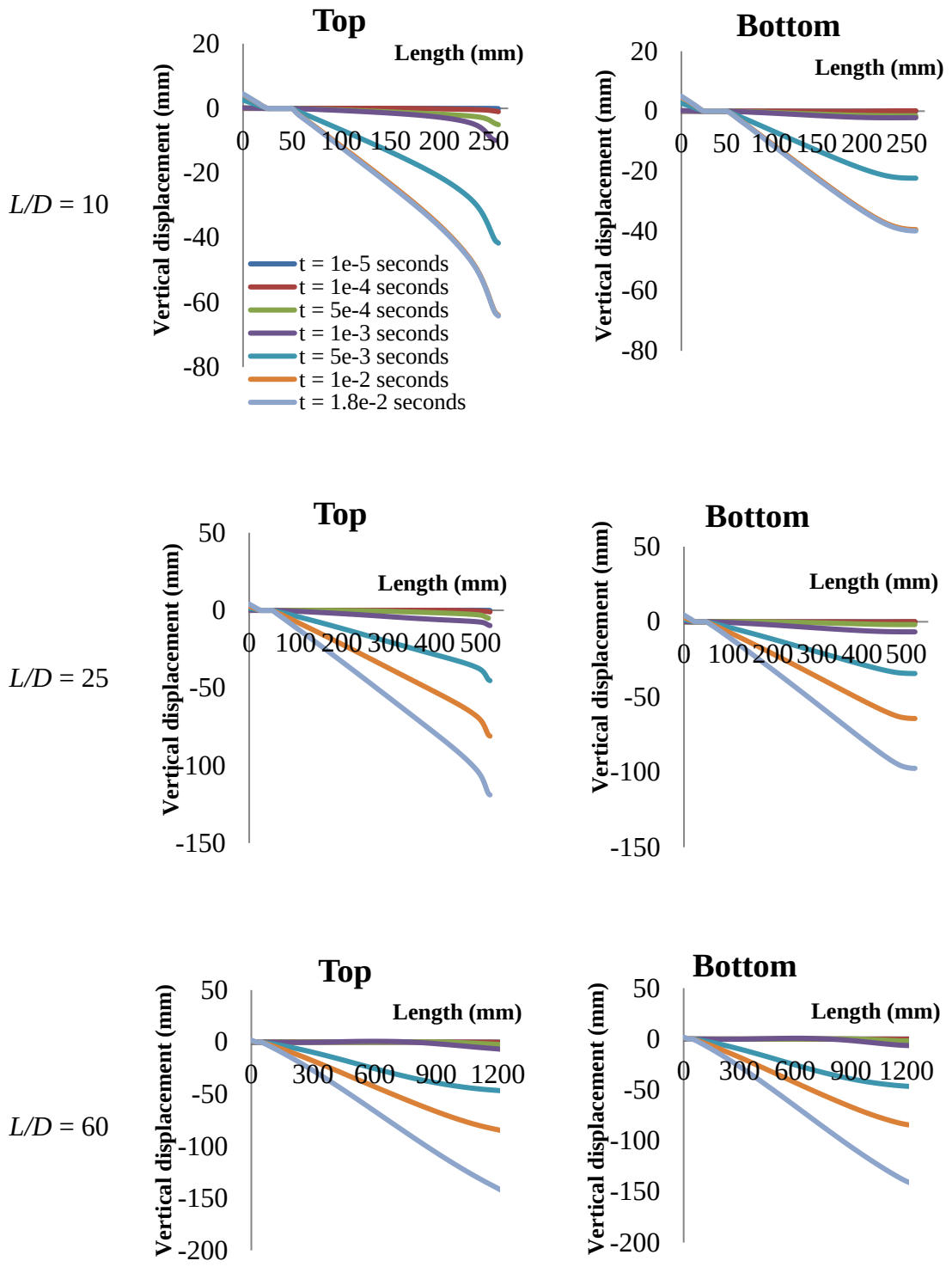

Figure 4.21: Predicted vertical displacement along the length of the pipe without axial restraint at the top and bottom profile of its cross section for different *L/D* ratios considered.

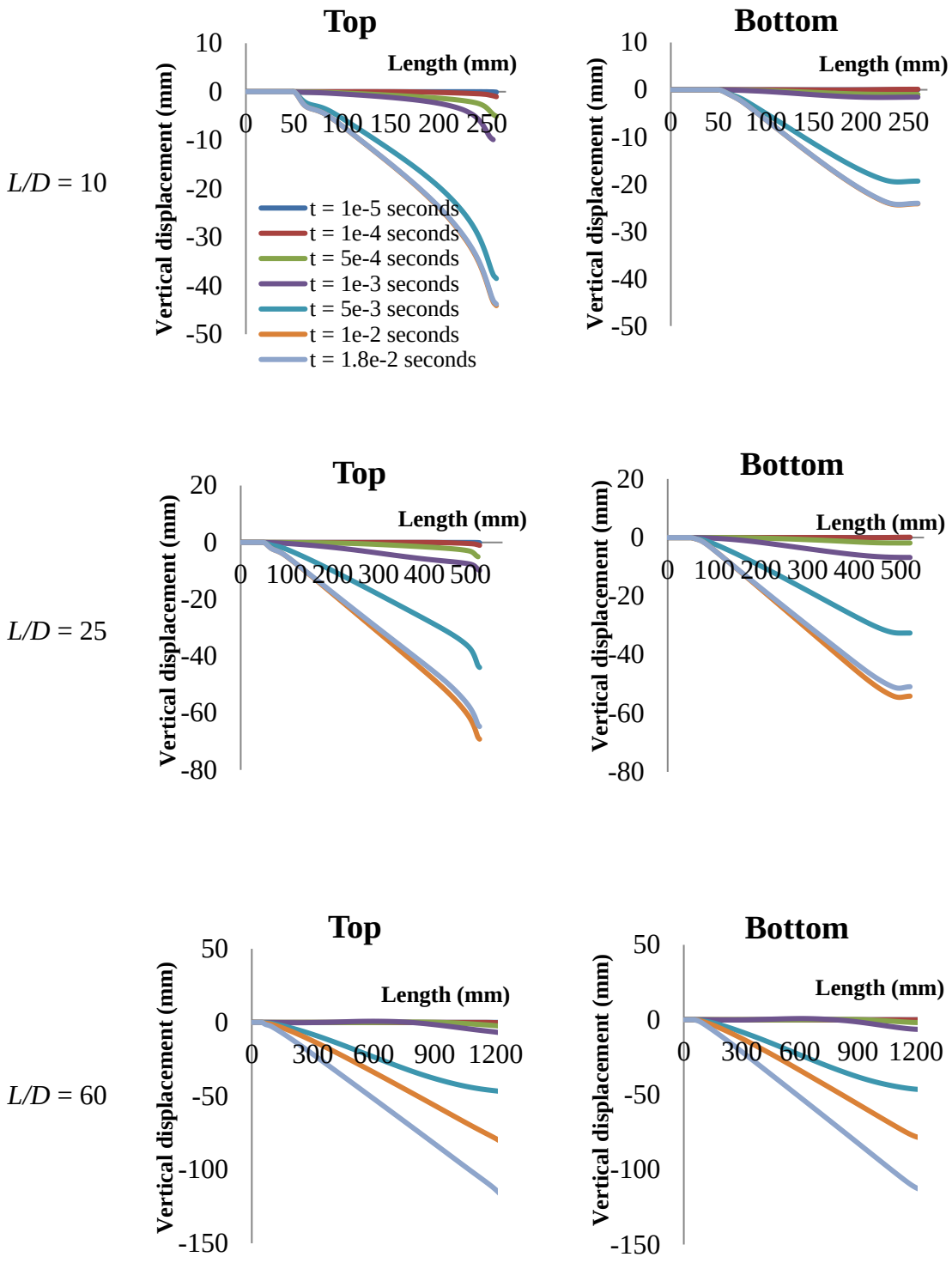

Figure 4.22: Predicted vertical displacement along the length of the pipe with axial restraint at the top and bottom profile of its cross section for different *L/D* ratios considered.

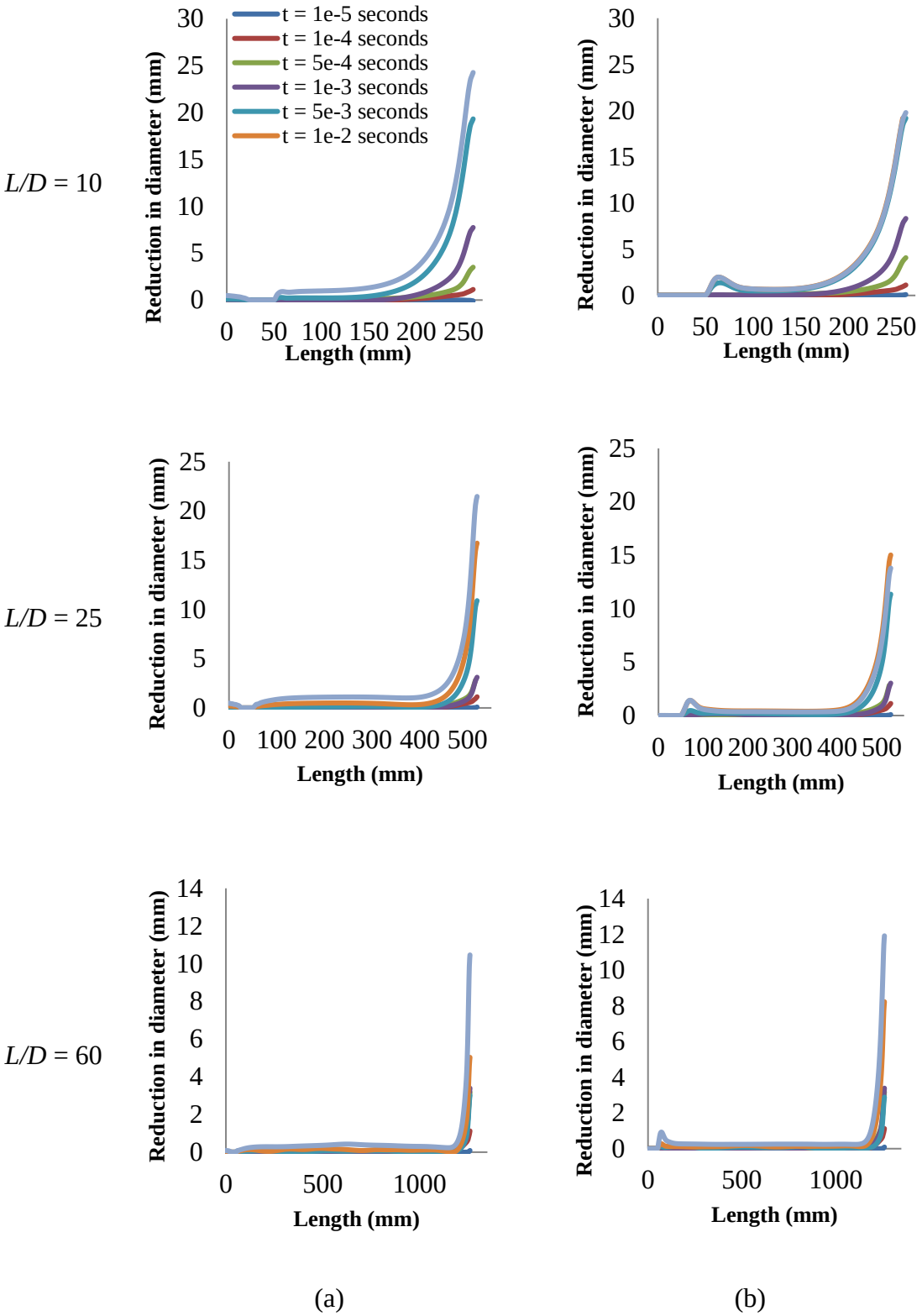

Figure 4.23: Predicted reduction in diameter along the length of the pipe (a) without and (b) with axial restraint at its end supports for different *L/D* ratios considered.

Figure 4.21 and Figure 4.22 show the deformed profile (at the top and bottom of the pipe cross-section) along the length of the pipe for the case in which the pipe is allowed to slide horizontally at the supports and for the case in which the pipe is considered to be fixed at the support respectively. Figure 4.23 shows the reduction of the diameter of the pipe with different *L/D* ratios at different times during the loading process. It is found that as *L/D* increases the response exhibited is more global as a larger span of the pipe appears to react to the impact load. It is also found that for the ratio *L/D* of 60, the end conditions do not influence the behaviour of the pipes as a very similar reduction in the diameter of the pipe and global deformation are observed [see Figure 4.23].

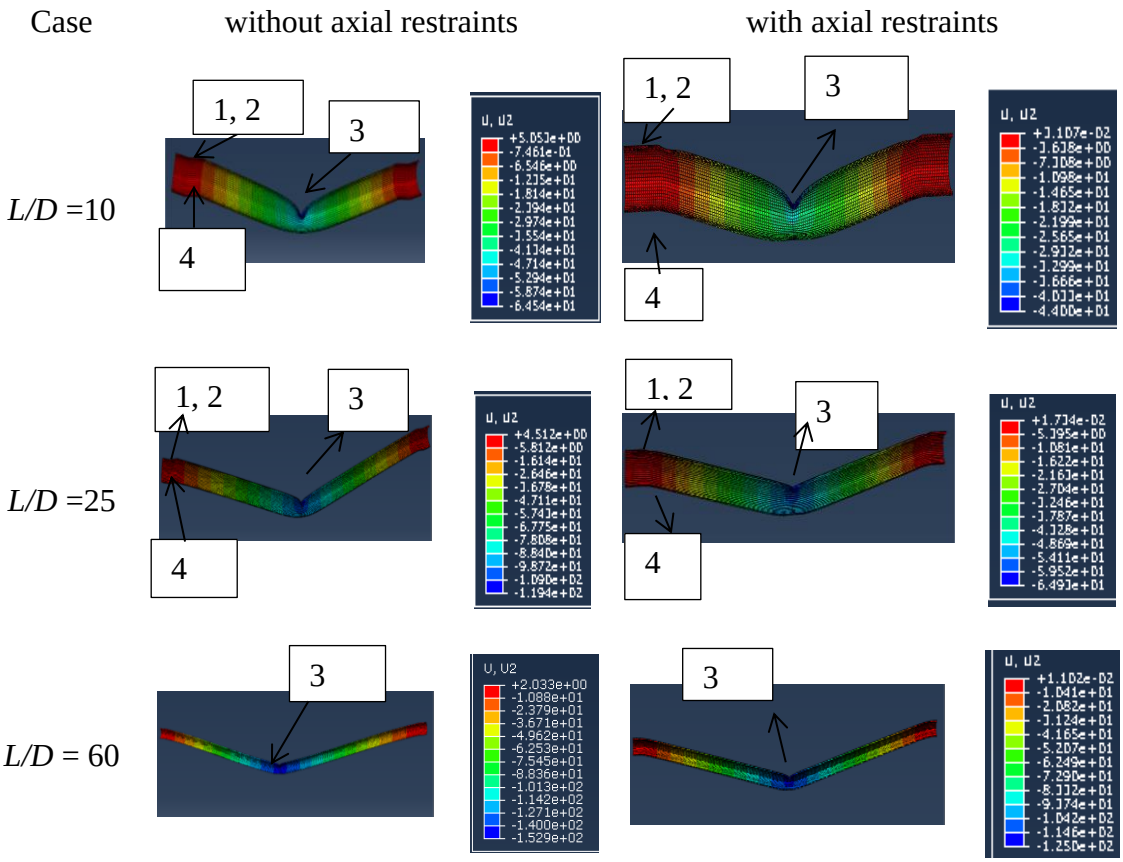

Figure 4.24: Predicted deformed shape and modes of failure along the length of the pipe with and without axial restraints for different *L/D* considered.

Figure 4.24 and Figure 4.25 show the deformed shapes along the length of the pipes and post-impact cross-section of the pipes respectively. It is observed that with the increase in the ratio *L/D*, the reduction in the diameter decreases, however, the global vertical displacement increases. It is also observed that for the ratio *L/D* of 10 and 25, all four failure modes ae observed, however, for the ratio *L/D* of 60 only shear sliding at the impact point (Mode 3, see Figure 4.13) is observed. It is also observed that with the increase of *L/D* the buckling becomes more prominent.

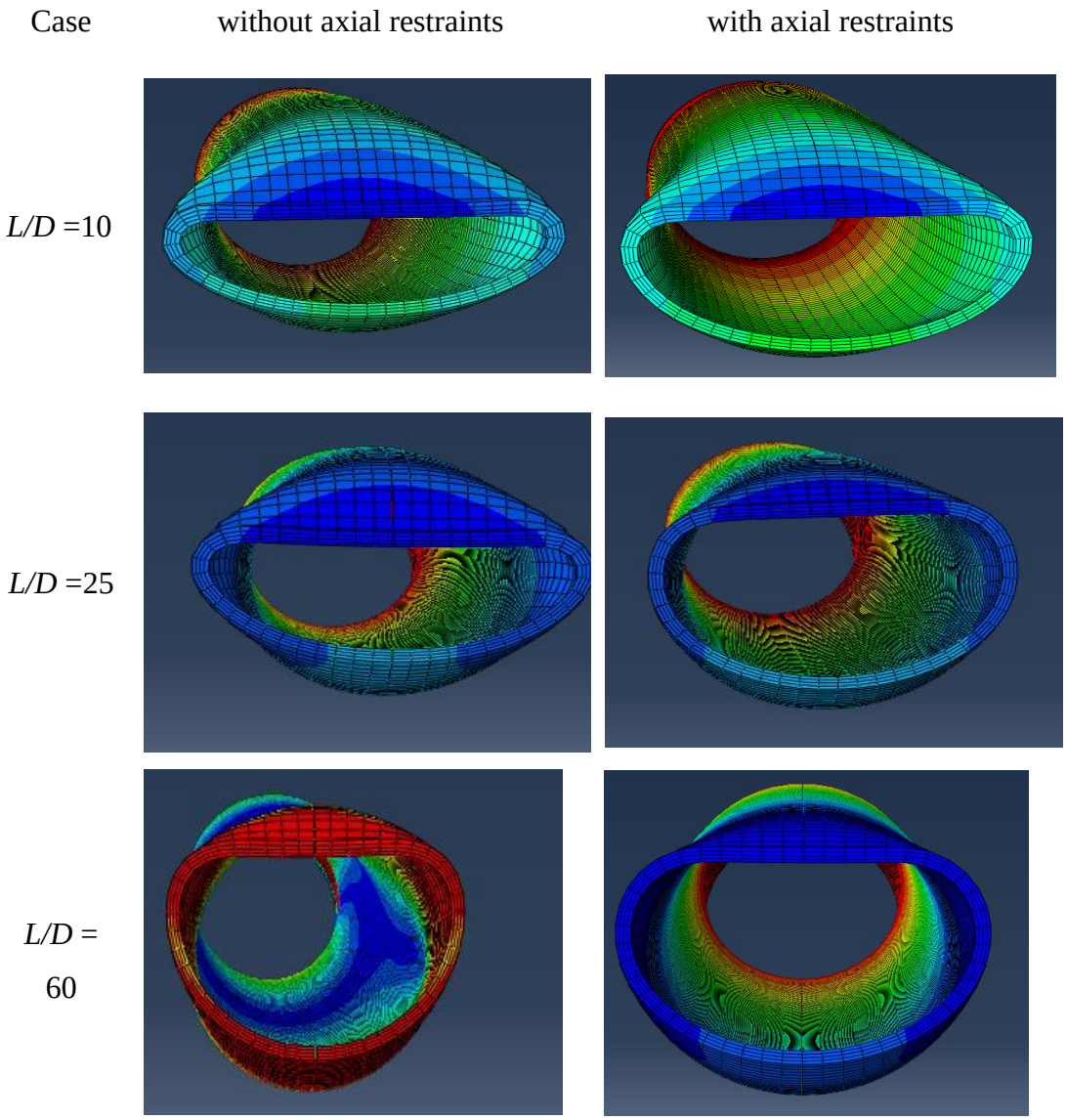

Figure 4.25: Predicted deformed shapes of the pipe cross sections with and without axial restraints for different *L/D* considered.

4.6.3 Influence of strain rate

In order to investigate the influence of the strain rate ($\dot{\epsilon}$) for the case of different impact velocities (with which the impactor comes into contact with the specimen) on the behaviour of the pipe, two case studies are considered. In the first case study, the pipe is impacted with the velocity (v_{exp} = 9.93m/s) as used in the impact test [Jones *et al.* (1992)], whereas in the second case study twice the velocity ($2v_{exp}$ = 19.86m/s) is considered. The pipe cross-section at the supports is allowed to move axially.

The variation of lateral (vertical) and longitudinal (axial) strain rate with time for the case of pipe impacted with velocity of (i) v_{exp} = 9.93m/s and (ii) $2v_{exp}$ = 19.86m/s is shown in Figure 4.26. The maximum value of exhibited strain rate (both vertically and axially) is observed in the impact zone (localized response) and quickly became negligible away from the impact zone. It is also observed that the strain rate reaches its maximum value during the initial contact period, however, its value significantly reduces as the contact between the pipe and the impactor is over. As expected, it is observed that with the increase in the velocity, the magnitude of the strain rate also increased.

Although for the case of pipes impacted with different velocities the observed strain rate is significantly higher [see Figure 4.26] at the contact region (locally) but it is important to note that the affect is limited to very short duration and its effect become almost negligible 20mm away from the impact zone. Therefore even if the strain rate sensitivity exists, it does not appear to significantly affect the behaviour of the pipe. Thus the static material properties of steel used to investigate the response of scaled pipe-specimens under drop weight tests are justified.

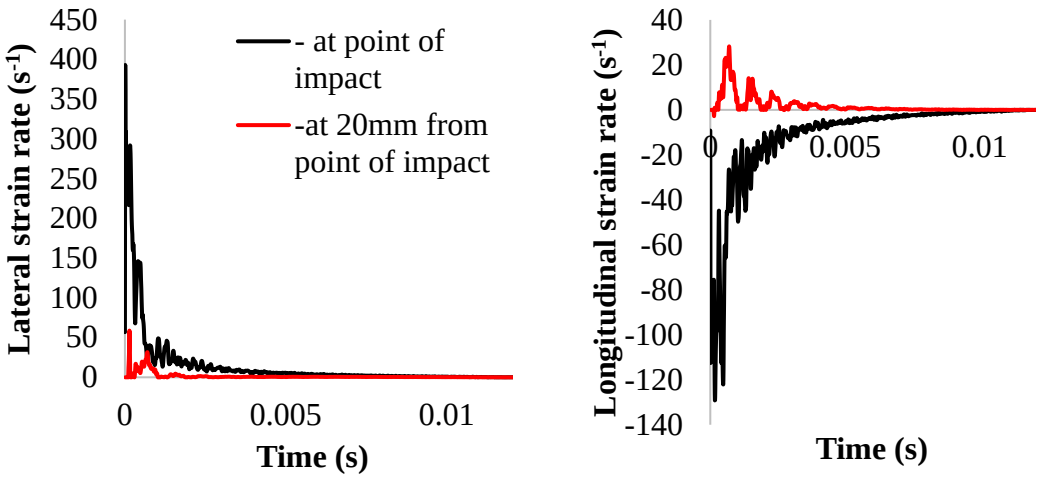

(a)

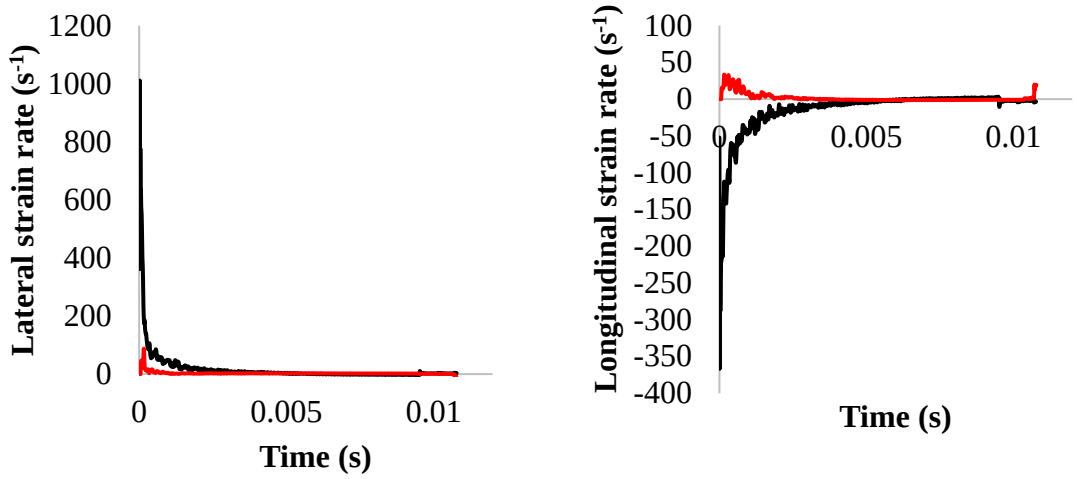

(b)

Figure 4.26: Variation of lateral (vertical) and longitudinal (axial) strain rate with time for the case of pipe impacted with velocity of (a) v_{exp} = 9.93m/s and (b) $2v_{exp}$ = 19.86m/s.

4.6.4 Influence of axial loading

In order to study the influence of the development of axial loading on the impact behaviour of the subsea pipes an investigation is carried out considering three different levels of axial compressive loading equal to 10%, 30% and 50% of the yield stress of

steel (f_y) from which pipes are constructed. These pipes are subjected to impact energy of 863J which is similar to the impact energy used in the tests [Jones *et al.* (1992)] for the purpose of comparison. The pipe is assumed fully fixed at both ends and the impactor is allowed to drop at the mid-span region. The displacement control is used to apply the axial loading.

The comparison of the contact force-time histories and the reduction of the diameter along the length of the pipe with different levels of axial loading are shown in Figure 4.27 and Figure 4.28, respectively. It is observed that the development of the axial loading does not seem to affect the generated contact force time histories. However, the reduction in the pipe diameter increases with the development of higher values of axial loading.

Figure 4.29 shows the deformed profile (at the top and bottom of the pipe cross-section) along the length of the pipe with different levels of axial loadings. It is found that as the level of the axial loading increases, the vertical displacement also increases. Thus with the increase of the axial loading the pipe behaves globally i.e. the pipe deforms along its whole length. It is observed that with the increasing level of axial compressive loading the reduction in the diameter of the pipe (in the impact zone) also increases (see in Figure 4.30 to Figure 4.32).

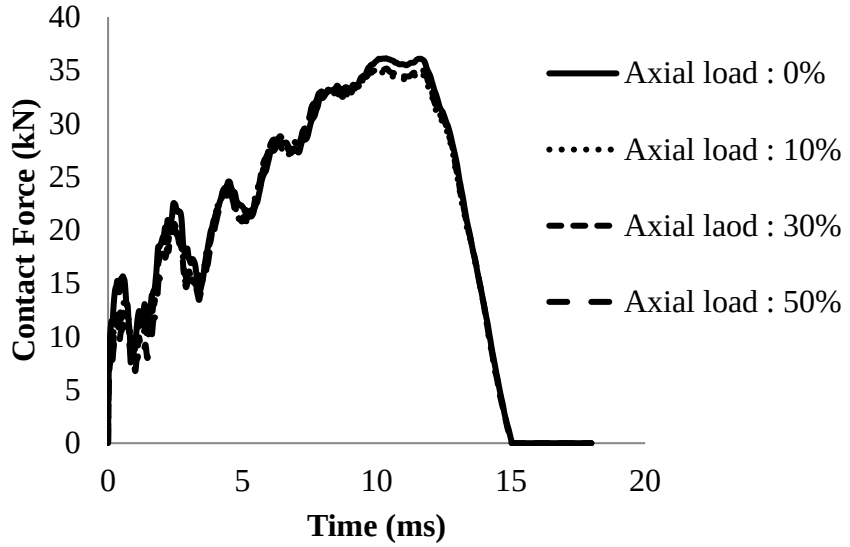

Figure 4.27: Comparison of contact force time histories with different levels of axial loadings.

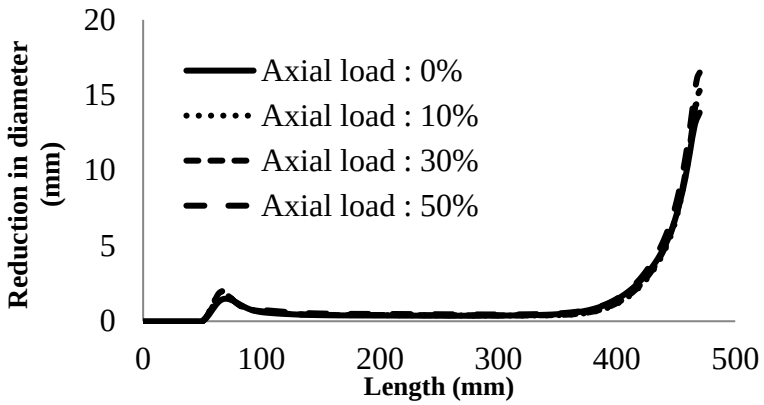

Figure 4.28: Comparison of reduction in diameter along the length of the pipe with different levels of axial loadings.

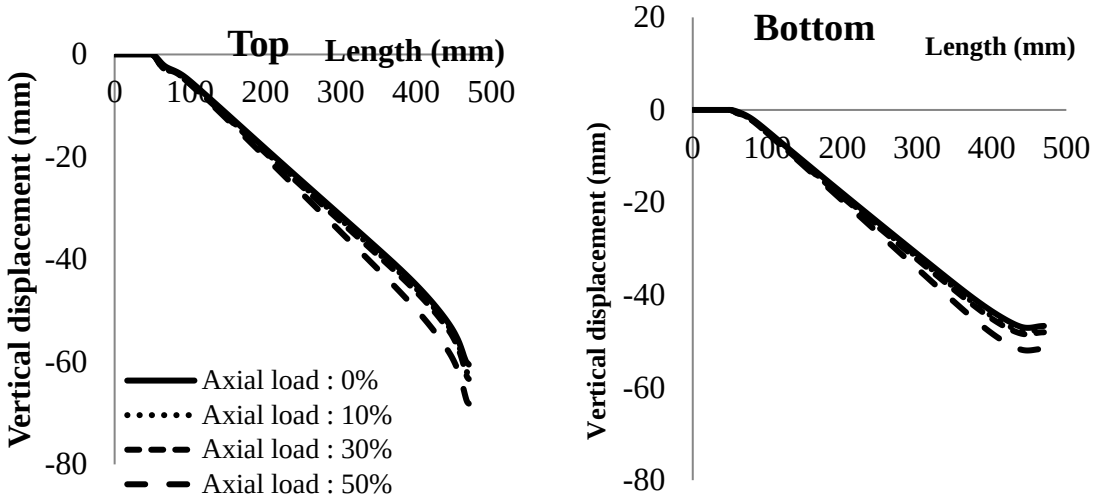

(a) (b)

Figure 4.29: Vertical displacement along the length of the pipe with different levels of axial loadings (a) top profile (b) bottom profile.

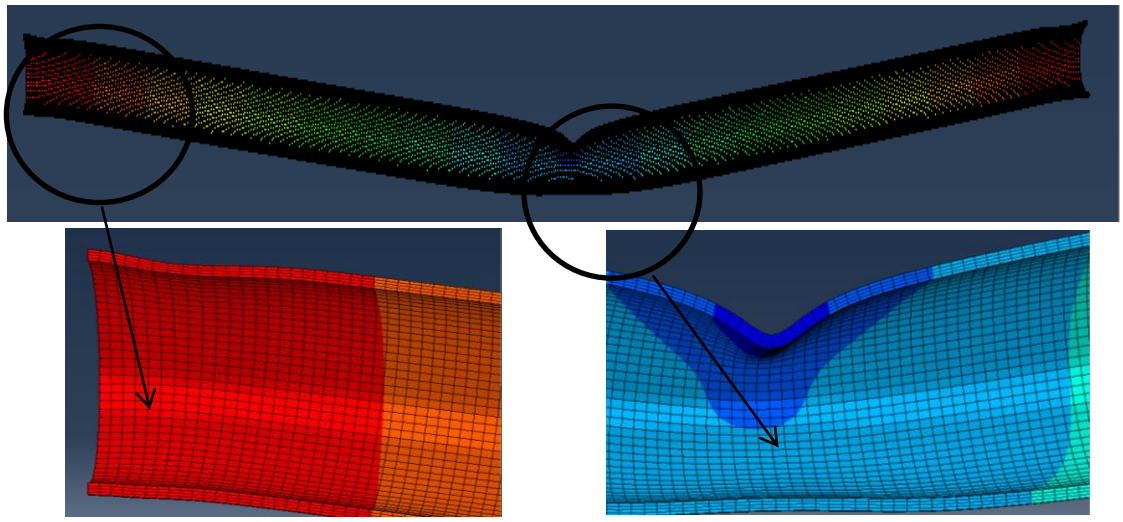

Figure 4.30: Deformed shape of pipe with axial load of 10% f_y.

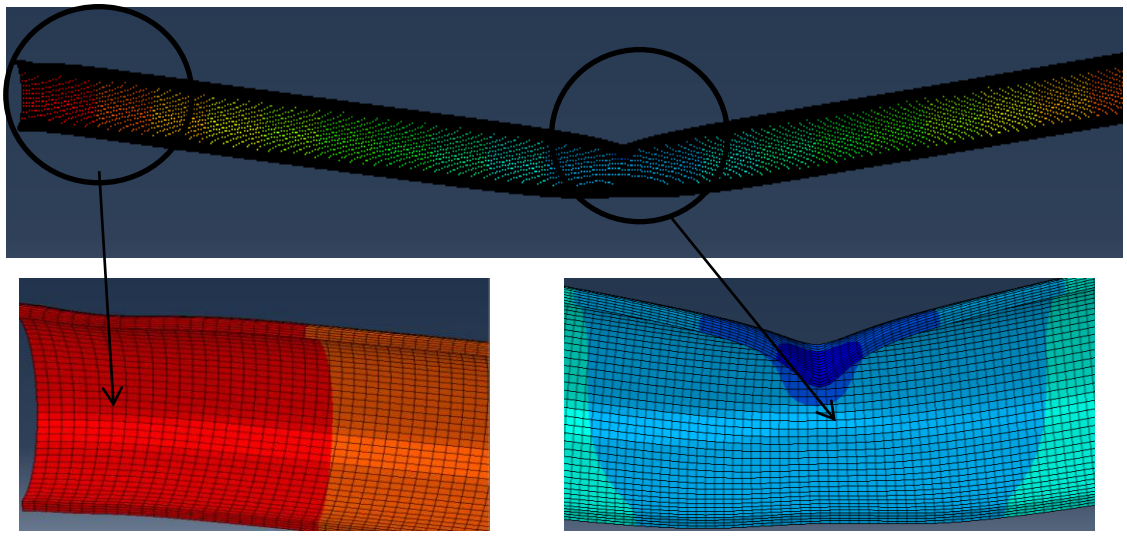

Figure 4.31: Deformed shape of pipe with axial load of 30% f_y.

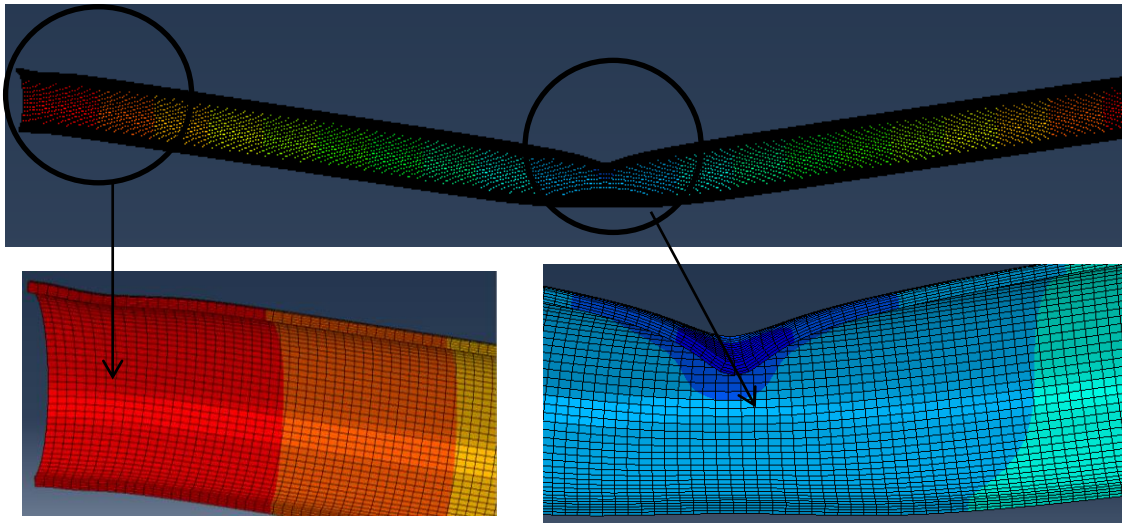

Figure 4.32: Deformed shape of pipe with axial load of 50% f_y.

Figure 4.33 shows the *R/D* ratios predicted by *NLFEA* and Eq. (2.52) (DNV [4] assessment method used in practice) for pipes along with the damage classifications [4]. Based on the *NLFEA* predictions it is observed that when considering pipes subjected purely to impact unsafe predictions are obtained compared to the pipes subjected to the combined action of impact and axial load. The impact test setup and assessment methods [DNV (2010b)] used by the industry do not consider the combined action of the axial load and pressure on the impact behaviour of the pipes. It is also observed that

the damages caused to the pipe with different end conditions lie in the rupture category [DNV (2010b)] as R/D is greater than 20%. Furthermore, based on the predictions of DNV [4] it is observed that irrespective of level of axial loading, the *R/D* ratio remains same and are found to be unsafe. This can be attributed to the fact that Eq. (2.52) (DNV [4] assessment method used in practice) only consider the localized response of the pipe without considering the effect of axial loading.

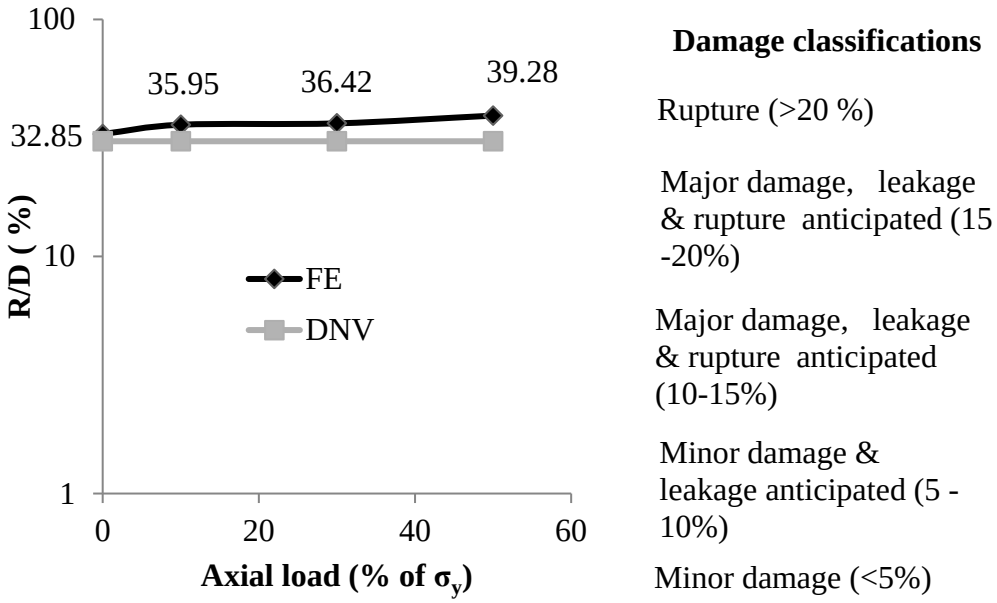

Figure 4.33: Reduction in diameter to diameter (R/D) ratios for the case of pipes with different levels of axial loadings.

4.6.5 Influence of pressure

In order to study the influence of the pressure on the impact behaviour of the pipes an investigation is carried out. As discussed in Chapter 2, the internal pressure containment requirement in design codes is governed by the maximum allowable hoop stress (σ_h) criteria. Therefore in this parametric study three differential pressures (difference of internal and external pressure) acting on the pipe wall are considered:

(i) $\sigma_h = 5\%\ \sigma_y$ (Pressure = 2.5 MPa)

(ii) $\sigma_h = -5\%\ \sigma_y$ (Pressure = - 2.5 MPa)

(iii) $\sigma_h = 10\%\ \sigma_y$ (Pressure = 5 MPa)

The positive pressure is considered as an internal pressure whereas negative pressure is considered as an external pressure. In order to study the combined effect of pressure with the impact load, the pipe is impacted with similar impact energy as used in the tests of Jones *et al*. (1992). The pipe is fully fixed at both ends and the impactor is allowed to drop at the mid-span region.

The comparison of the contact force time-histories and the reduction in the diameter along the length of the pipe with different levels of pressure is shown in Figure 4.34 and Figure 4.35, respectively. In general it is observed that the development of the pressure significantly affects the behaviour of the pipe under impact loading. It is found that for the case of pipe with a positive pressure (internal) of 2.5MPa the magnitude of the maximum contact force decreases and the impact duration increases compared to the case of pipe without pressure (see Figure 4.34). It is also found that for the case of pipes with pressures of -2.5MPa and 5MPa the impactor did not rebound after the first impact (see Figure 4.34) due to collapse of the cross-section (plastic impact).

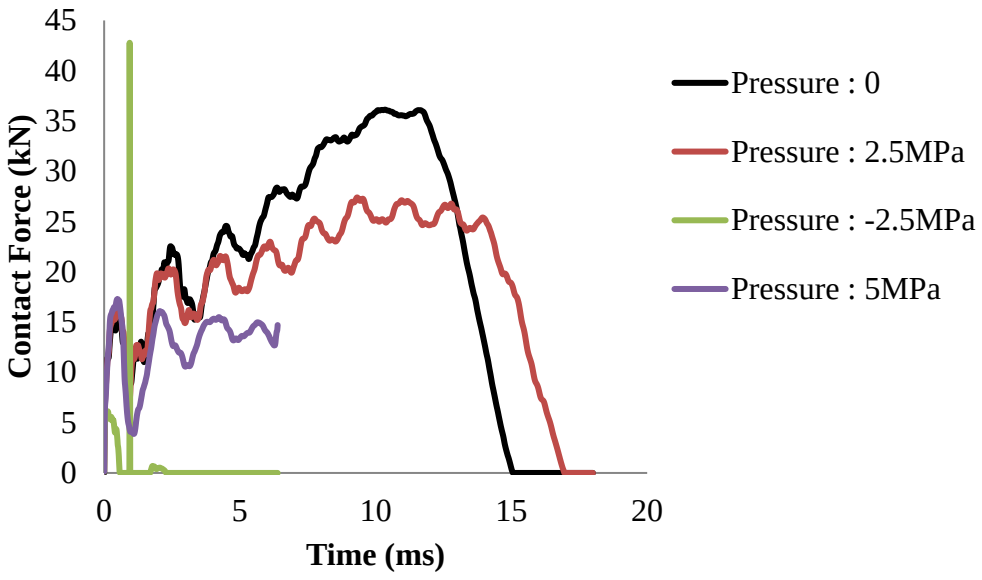

Figure 4.34: Comparison of contact force-time histories with different level of pressure.

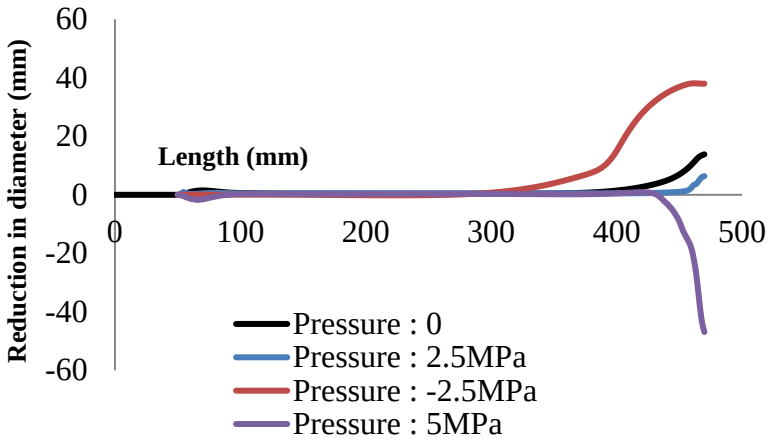

Figure 4.35: Reduction in the diameter along the length of the pipe with different level of pressure.

The comparison of the behaviour of the pipe without pressure and with a pressure of 2.5MPa is shown in Figure 4.36. It can be seen that due to the development of the pressure, the damage caused to the pipe (reduction in the diameter) in the impact zone reduces, however, the global displacement increases. This observation is similar to the findings of other researchers [Jones & Birch (2010), Chen & Shen (1998)] as discussed in Chapter 2.

The behaviour of the pipe with pressure levels of -2.5MPa and 5MPa is shown in Figure 4.37. It is observed that the pipe cross-section in the impact zone completely collapsed. Therefore additional analyses with further increase in pressure level are not carried out, as it will also eventually result in collapse of the pipe cross section.

It is also interesting to observe that when the pipe is subjected to a positive pressure of 2.5MPa, the cross-section did not collapse (see Figure 4.36) however, the behaviour is affected significantly when a pressure of -2.5MPa is applied. As discussed in Chapter 2, design codes provide provisions to check, cross sectional instability in the form of local buckling/collapse when the pipe is subjected to external overpressure due to installation process and temporary conditions (e.g. transportation, system pressure test, shut-down and start up). It is important to note that these design provision do not consider the effect of the external pressure combined with the impact load acting on the pipe which can significantly influence the design criteria as shown in Figure 4.37.

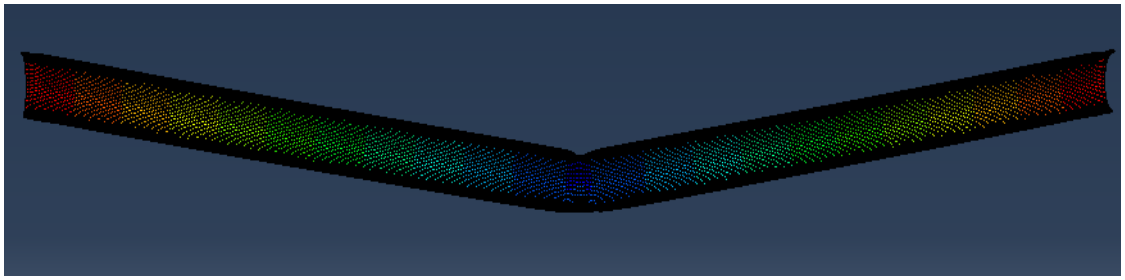

(a)

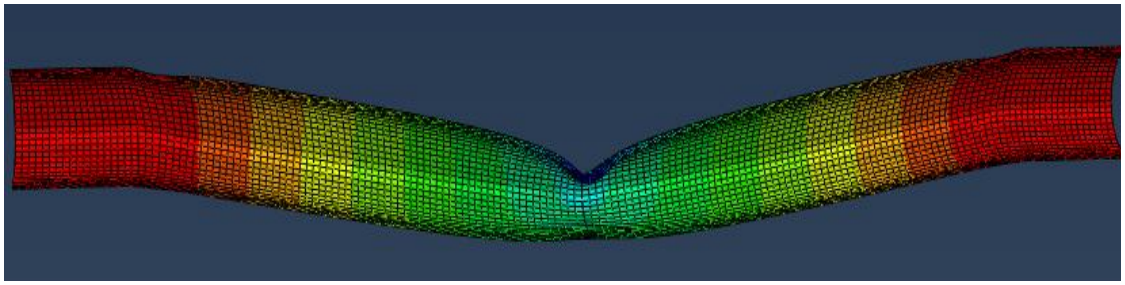

(b)

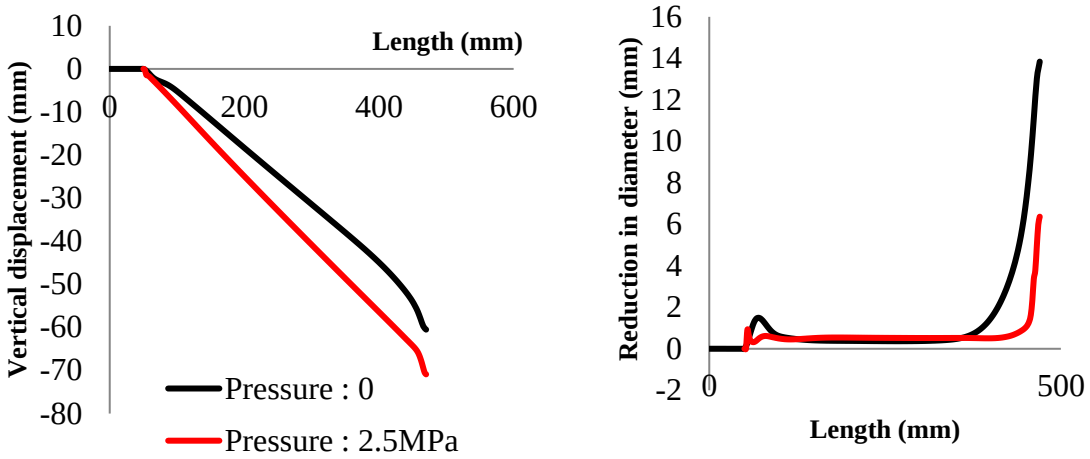

(c) (d)

Figure 4.36: (a) Post-impact length of the pipe with pressure of 2.5MPa (b) Post-impact length of the pipe without pressure (c) comparison of vertical displacement (d) comparison of reduction in diameter along the length of the pipe

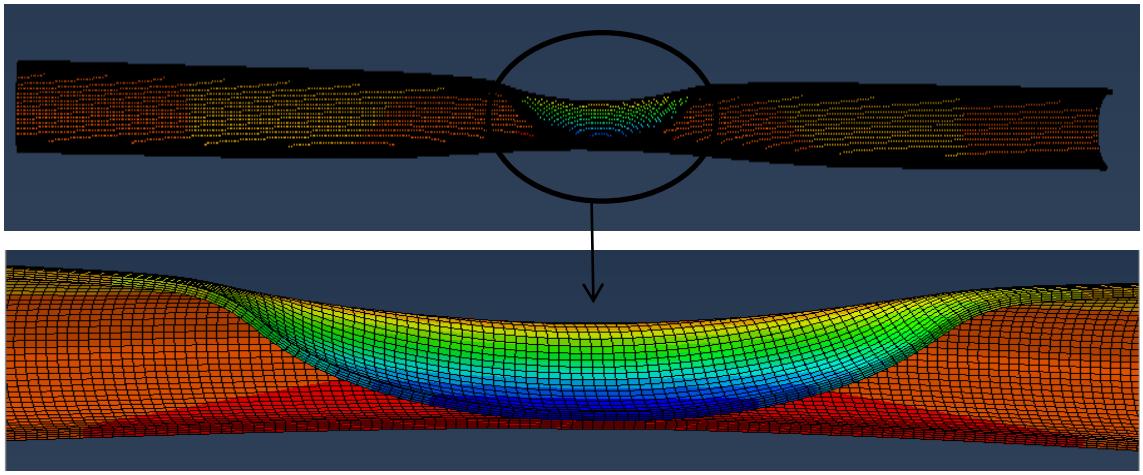

(a)

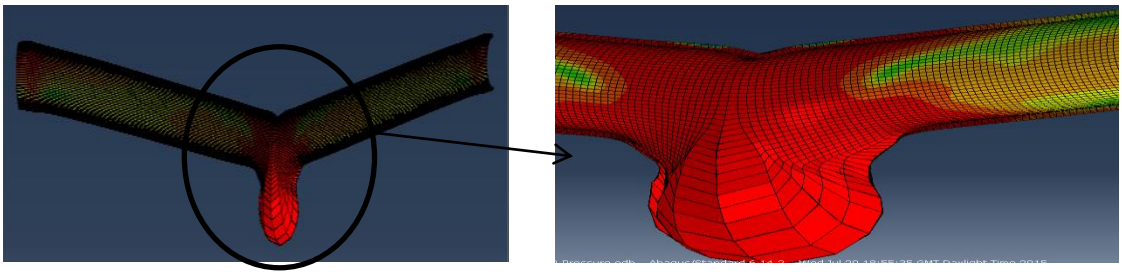

(b)

Figure 4.37: Deformed shape of the pipe with pressure of (a) - 2.5MPa (b) 5MPa.

Figure 4.38 shows the *R/D* ratios predicted by *NLFEA* and Eq. (2.52) (DNV [4] assessment method used in practice) for pipes along with the damage classifications [4]. Based on the *NLFEA* predictions it is observed that when considering pipes subjected purely to impact unsafe predictions are obtained compared to the pipes subjected to the combined action of impact and pressure. It can be seen that the damages caused to the pipe with different end conditions lie in the rupture category [DNV (2010b)] as *R/D* is greater than 20%. Furthermore, based on the predictions of DNV [4] it is observed that irrespective of level of pressure acting on the pipe, the *R/D* ratio remains same and is found to be unsafe. This can be attributed to the fact that Eq. (2.52) (DNV [4] assessment method used in practice) only consider the localized response of the pipe without considering the effect of pressure.

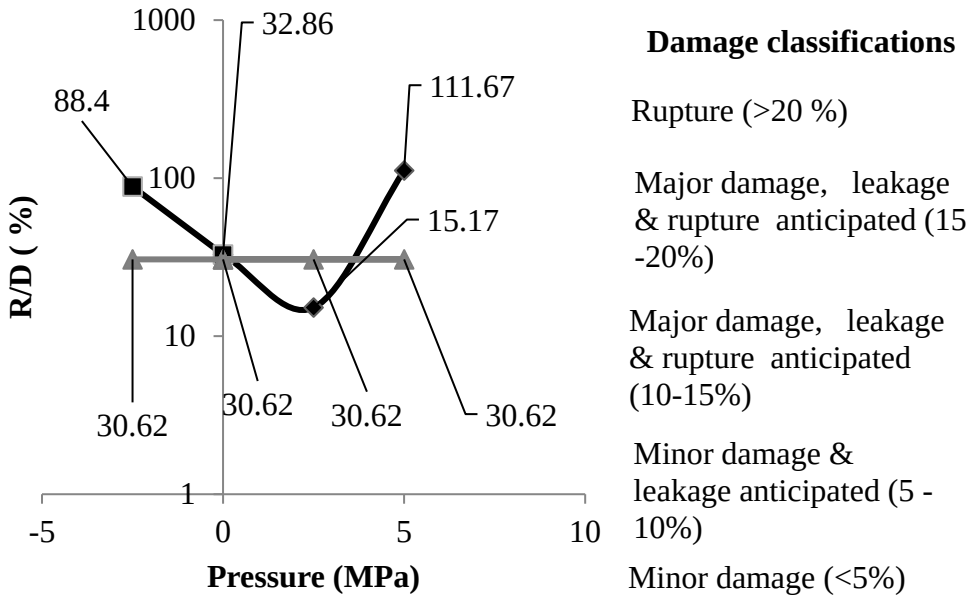

Figure 4.38: Reduction in diameter to diameter (R/D) ratios for the case of pipes with different levels of pressures.

4.7 CONCLUSIONS

Based on the investigation carried out in this chapter in order to study the response of scaled pipe-specimens under impact loading the following conclusions are drawn:

- The behaviour of the steel pipe-specimens considered under impact is significantly influenced by parameters associated with: (i) the characteristics of the impacting object (speed), (ii) the boundary conditions imposed onto the pipe (end conditions) (iii) the level of axial loading imposed and (iv) the development of internal (due to the oil and gas transportation through the pipe) and external (hydro-static) pressure. Such parameters can potentially affect, sometimes detrimentally, the dynamic response exhibited by the steel pipes when subjected to impact.

- Increasing values of *L/D* of the pipe results in global behaviour dominating the structural response and less damage (expressed as the reduction in the diameter of the cross-section of the pipe) being observed in the impact area.

- For the case of pipes impacted with different velocities, the observed strain rate is significantly higher at the contact (impact) region. However, its affect is limited to

very short duration and becomes almost negligible 20mm away from the impact zone. Therefore the use of static material properties for describing the behaviour of steel in the *FE* models developed for investigating the response of pipe-specimens under drop weight tests is justified.

- The development of axial loading resulting in compressive stresses of up to 50% of the yield stress of steel does not appear to have a significant influence on the level of damage exhibited by the pipe in the impact zone.

- The application of the internal (positive) pressure reduces the level damage caused to the pipe (expressed by the reduction in the diameter of the pipes cross-section) in the impact zone and increase the global deformation along the length of the pipe. The application of an external (negative) pressure of 2.5MPa results in collapse of pipe cross-section in the impact region.

CHAPTER 5

FE MODELLING OF LOCALIZED BEHAVIOUR OF PIPES UNDER IMPACT

5.1 INTRODUCTION

The experimental studies presented in Chapter 2 investigating the behaviour of steel pipes under impact loading have been mainly conducted on scaled specimens, which have small cross-sections and lengths compared to the actual pipes used by offshore industry for transporting of oil and gas. Furthermore during these tests the specimens were subjected to significantly less impact energies compared to those encountered during accidental collisions of large objects (e.g. icebergs, rocks, fishing equipment etc.) onto subsea pipes. It is also important to notice that a large part of the published *NLFEA* studies investigating the behaviour of pipes under impact loading presented in Chapter 2 were carried out using quasi static analysis thus ignoring the effects of inertia and the wave propagation problem at hand. Based on the numerical investigation carried out in Chapter 3, studying the behaviour of steel and concrete specimens under increasing rate of uniaxial compressive and tensile loading, it was observed that the behaviour exhibited by subject specimens (considered by many to represent material units from which average material properties are obtained) differs from that established under equivalent static loading once certain limits of loading rate are surpassed. The comparison of the numerical predictions obtained with their experimental counterparts revealed that the observed shift in specimen behaviour is primarily attributed to parameters associated with structural response, the interaction with the experimental setup employed and the nature of the problem at hand; a wave propagation problem within a nonlinear medium.

Based on the numerical investigation carried out in Chapter 4 studying the behaviour of the scaled pipe-specimens under impact, it was observed that pipe specimens exhibit both local and global behaviours under impact loading. A localised response is exhibited in the form of damage observed at the contact area of the pipe and the

impactor, whereas a global behaviour results in the pipe deforming along its whole length. In order to study the behaviour of full scale pipes under impact, drop-weight tests and numerical studies are carried out in the present chapter. For this purpose, two full scale impact tests are initially conducted focusing on the local response of the subject specimens under impact loading. As discussed in Chapter 2, clump weights (used in trawl fishing) with masses ranging between 2 to 9 tonnes may accidentally collide with subsea pipelines. Such collision can be characterised by high impact energies. However due to constraints in test facilities available at Heriot Watt University [strength of strong floor, accuracy of equipment to measure dynamic load and displacements during impact (a few milliseconds)] the pipes are impacted by a dropped mass of only 2 tonnes resulting in impact energy of 16kJ. The same problem is also modelled in *FE* using ABAQUS [ABAQUS (2013)] in order to study in detail the impact problem which is often not provided when conducting drop-weight tests due to the constraint discussed above. The aim is also to use the validated *FE* model in a detailed parametric investigation to study the effect of various parameters associated with the geometry of the pipes (thickness, diameter, length), the properties of the supporting soil, the internal and external pressure acting on the walls of the pipe, as well as the development of axial loading on the local and global response of subsea pipes under impact loading. The results of the later detailed parametric studies are presented and discussed in Chapter 6.

In order to assess the prediction of the analytical solution [given by Eq. (2.52)] suggested by DNV (2010b) used by offshore industry to predict the damage casused to the pipe under impact loading, the results of the impact tests and *NLFEA* are also compared with the analytical solution [DNV (2010b)].

5.2 IMPACT TEST SET UP

5.2.1 Specimens

The pipes specimens used in the experimental investigation had a diameter of 457mm, a thickness of 25.4mm and a length of 2000mm as shown in Figure 5.1. The pipes are impacted at the mid-span region with an “impacting mass” comprising of 2 parts (see Figure 5.2), the impactor and a large section of steel having a width of 324mm, a depth

of 1270mm and a length of 610mm, which provides most of the mass. The total mass of the impacting system is 2.2 tonnes. Two different shape impactors: (i) sharp impactor and (ii) curved impactor are used. The shape of the impactors is similar to that specified by the relevant code of practice [DNV (2010a)] used by the offshore industries to investigate the behaviour of the pipes under impact. The impactors had a width of 50mm, a depth of 125mm and a length of 200mm. The dimensions of the impactors are shown in Figure 5.3.

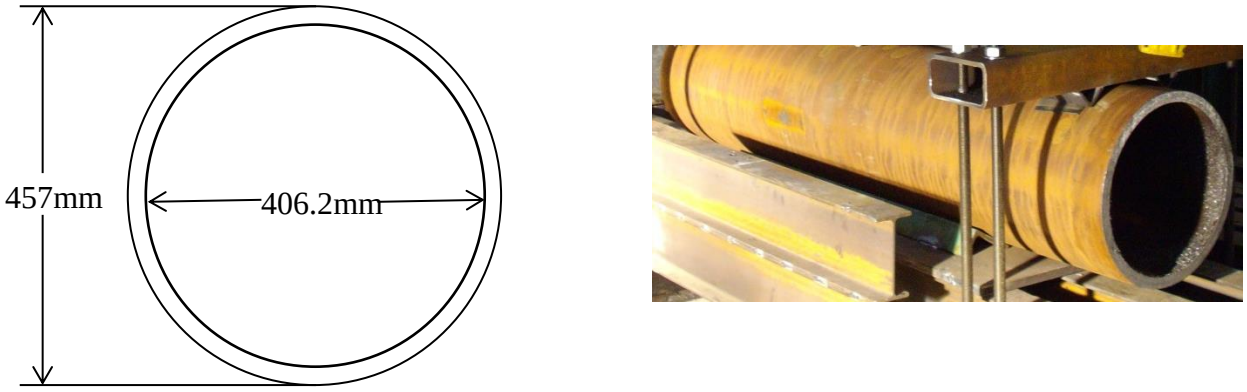

(a) (b)

Figure 5.1: (a) Pipe cross-sectional dimensions (b) length of the pipe used.

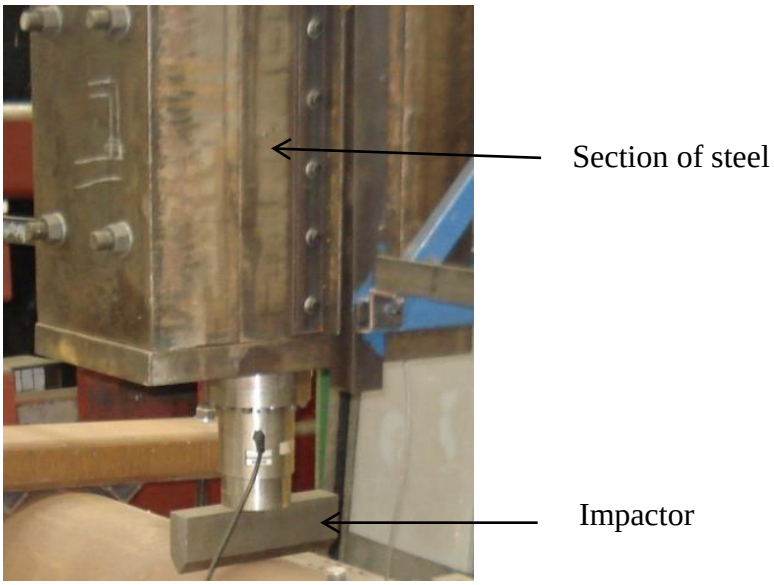

Figure 5.2: Impacting mass used in the impact test.

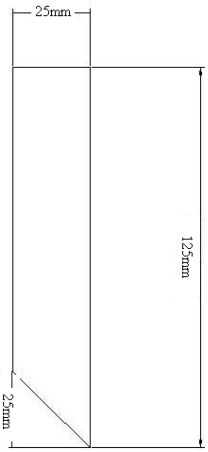

(a)

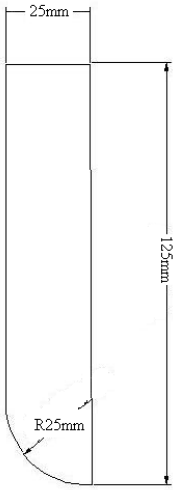

(b)

Figure 5.3: (a) Sharp impactor (b) curved impactor.

It is estimated that about 8 million tonnes of pipes are produced every year, however a major part consists of pipes which are produced from standard material grades of up to *X65* [Hillenbrand *et al.* (2001)]. As a result pipes made from *X65* mild steel grade having nominal yield strength of 448MPa are used in this study. The engineering stress-strain curve describing the material behaviour of the mild steel pipe is shown in Figure 5.4, which is obtained by conducting uniaxial tensile test on dog bone specimen and provided by TOTAL [TOTAL (2016)] . The description of the dog bone specimen used is also shown in Figure 5.4. The true stress-strain curve describing the material behaviour of the mild steel pipe is shown in Figure 5.5. Four uniaxial tensile tests are carried out on dog bone specimens (see Figure 5.5) by EXOVA [EXOVA (2016)].

Table 5.1 provides the yield strength and modulus of elasticity of the pipes obtained from these tests.

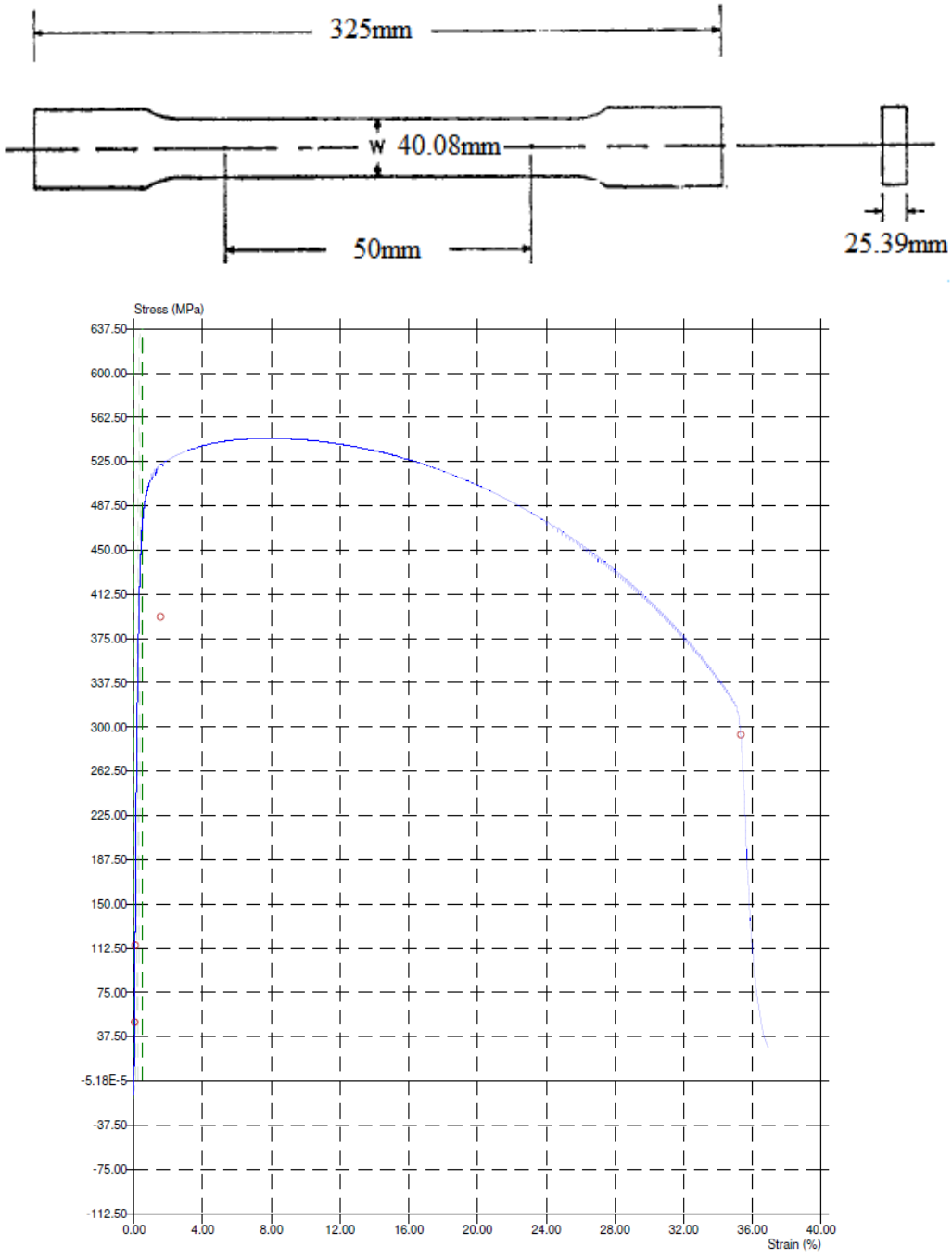

Figure 5.4: Engineering stress-strain curve of pipe made from *X65* mild steel.

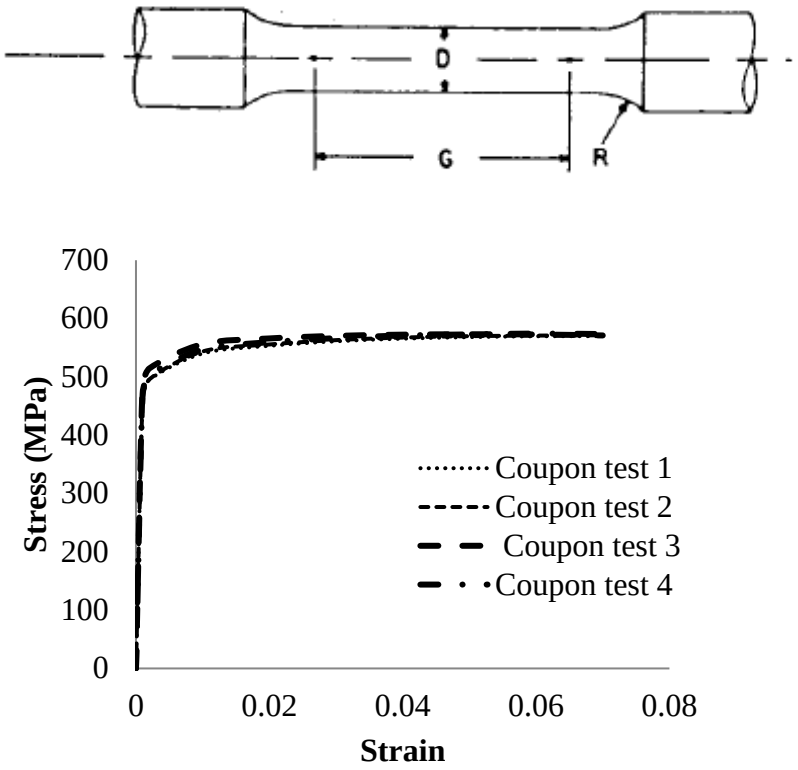

Figure 5.5: True stress-strain curves of the pipe made from *X65* mild steel.

Table 5.1: Yield strength and modulus of elasticity obtained from the coupon tests.

Coupon test	**Yield Strength (MPa)**	**Young's modulus of elasticity (MPa)**
1	462.21	170300
2	458.00	205000
3	483.55	189300
4	471.18	198800

5.2.2 Boundary conditions

The pipes are placed on a steel plate which rests on steel girders (having thickness of 5mm and height of 145mm) supported by a strong floor [see Figure 5.6 (a)]. The welded angles and clamps are used at both ends of the pipe in an attempt to prevent lateral movement and uplift as shown in Figure 5.6 (a) & (b).

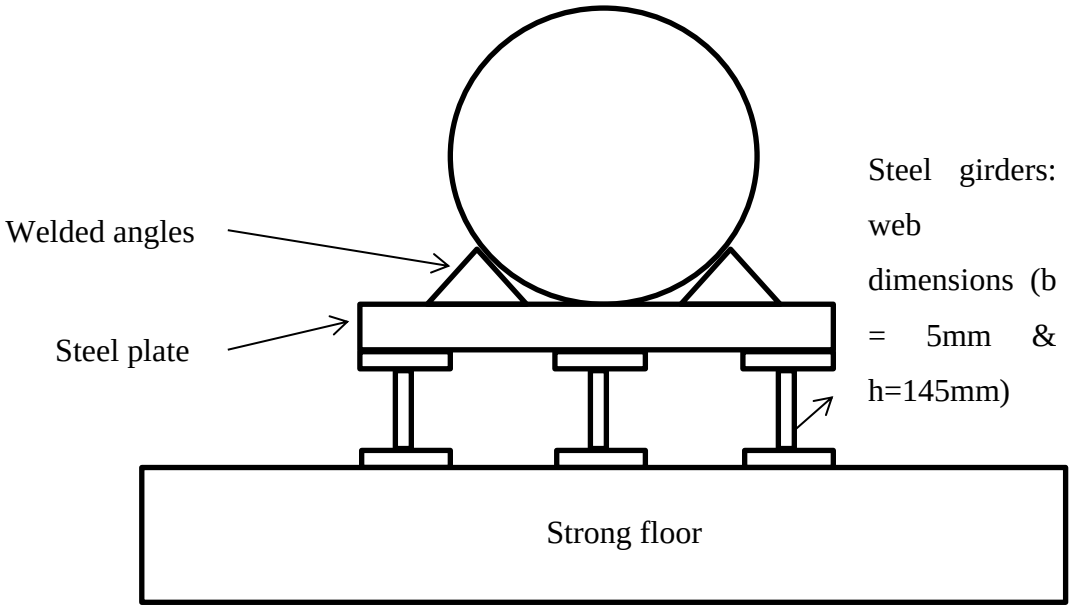

(a)

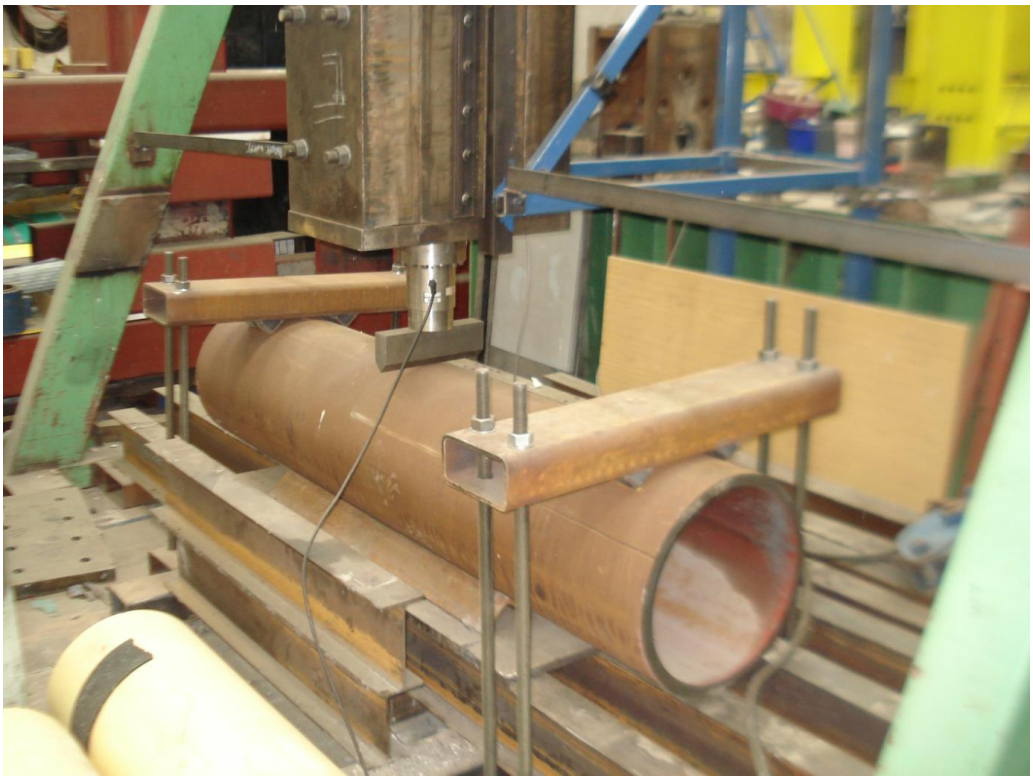

(b)

Figure 5.6: (a) Schematic representation of the boundary conditions used in the impact test (b) impact test set up.

5.2.3 Experimental drop weight test set up

The impact tests on the steel pipes are carried out at the Structures Laboratory of the Heriot Watt University. The impact test rig consists of two steel angle legs which function as a guide for the “impacting mass” as shown in Figure 5.7. The impact test rig is supported by a rigid frame to prevent side-sway out-lift.

Figure 5.7: Impact test rig.

For each impact test, the impacting mass was raised using the overhead crane to the required height of 750mm in order to achieve an impact energy of 16kJ. The impacting mass was then dropped on the pipe at the mid-span region with the help of an automatic releasing system which is attached to the overhead crane as shown in Figure 5.8. The

impacting mass usually bounced a few times before ultimately resting on the pipe. After the impact test was conducted, it was lifted again with the overhead crane so that the impact zone could be observed.

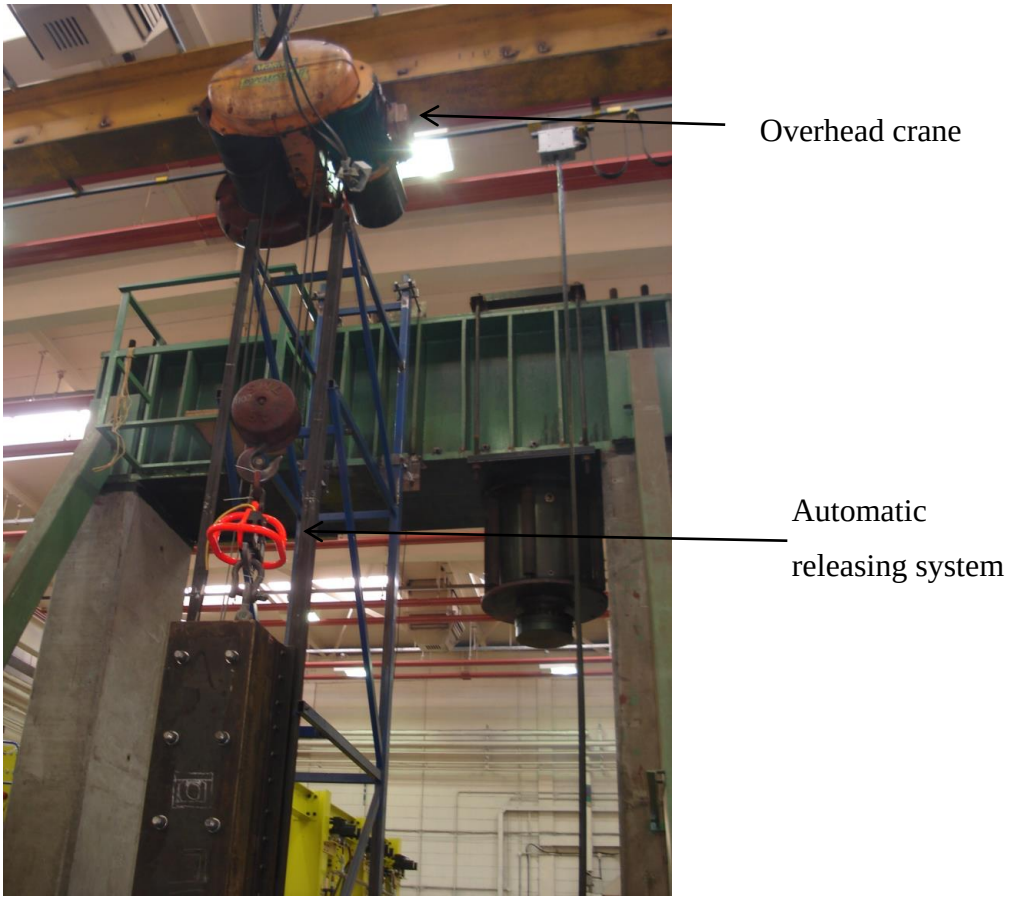

Figure 5.8: Crane and automatic release system.

5.2.4 Instrumentation and data digitilization

An Olympus *ispeed* series high speed high resolution video camera (see Figure 5.9) was used to record the behaviour of the pipe during the tests. The use of video recording has been proven to be a valuable source of data to give insight into transient features of the impact test for e.g. deformation process during impact event, velocity-time history of the impacting object etc. [Jones *et al.* (1992), Abbas *et al.* (2010)]. In the current study a high speed video camera with 2000 frames per second (fps) is used to record the behaviour of the pipe under impact loading. The frames from the high speed video are initially digitized using the open source software TRACKER [Brown (2009)]. The data

obtained is used to describe certain aspects (the time histories of deflection - contact force and velocity of the impactor) of the behaviour of the pipe under impact.

(a)

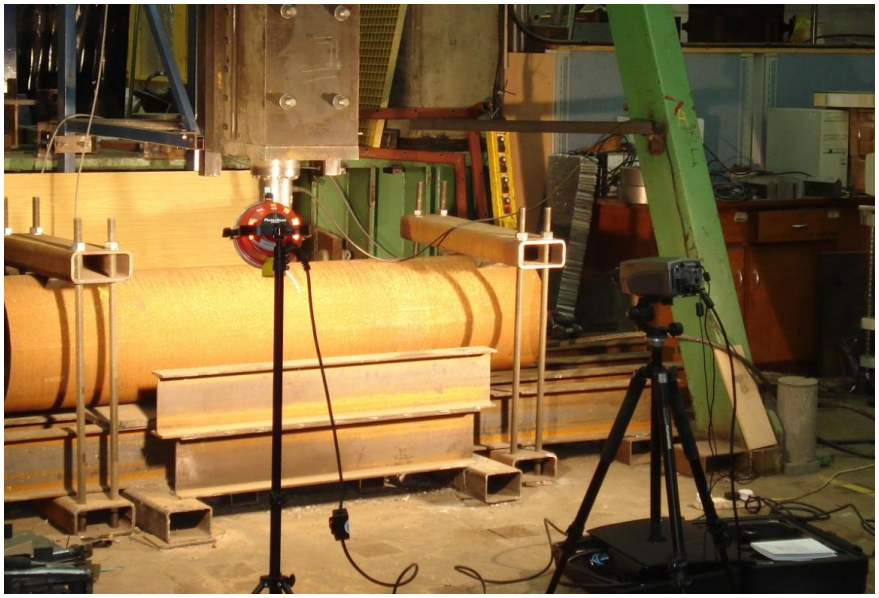

(b)

Figure 5.9: (a) Olympus high speed high resolution camera [Engineering (2015)] (b) high speed video recording setup during impact tests.

5.3 IMPACT TEST RESULTS

Two impact tests were carried out in which pipes were impacted at its mid-span length with impact energy of 16kJ. In first test the pipe was impacted with a curved shape impactor whereas sharp shape impactor was used in second test. The behaviour of the pipes in both tests is found to be similar. Before contact occurred between the pipe and the impactor, the energy is stored in the impactor in the form of kinetic energy. During the contact, the energy is transferred from the impactor into the pipe. At some stage during impact the velocity of the impactor reduces to zero and the pipe reached the maximum displacement. This is followed by the reduction in the pipe displacement and as a result the impactor started to move upwards with a residual kinetic energy which is less than that of just prior to the initial impact. The loss of kinetic energy exhibited during the contact period largely resulted in the permanent plastic deformation in the contact area of the pipe and the impactor. It is also observed that during the impact period and after the separation of the impactor from the pipe, the pipe also deformed along its whole length, however, the resulting deformation is not permanent (i.e. elastic deformation).

It is found that the pipe responded to the impact load locally. The damage caused to the pipe is localized in the contact region shown in Figure 5.10. The indentation is produced due to the initial impact and this is followed by smaller indentations, produced due to the rebounds of the impactor.

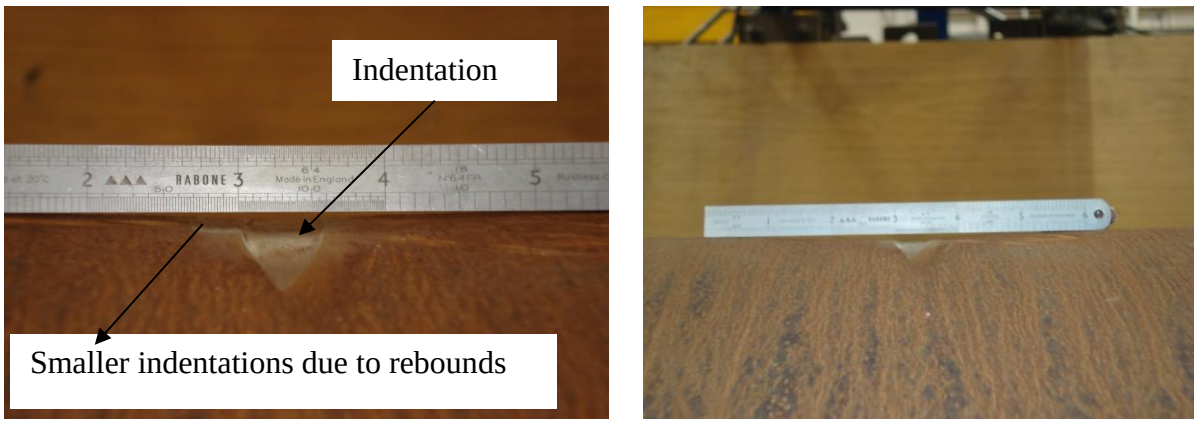

Figure 5.10: Damage caused to the pipe in the impact region.

The frames from the high speed video were used to describe certain aspects of the behaviour of the pipe under impact. The location at the top of the impactor as shown in Figure 5.11 is used to trace the vertical displacement of the impactor.

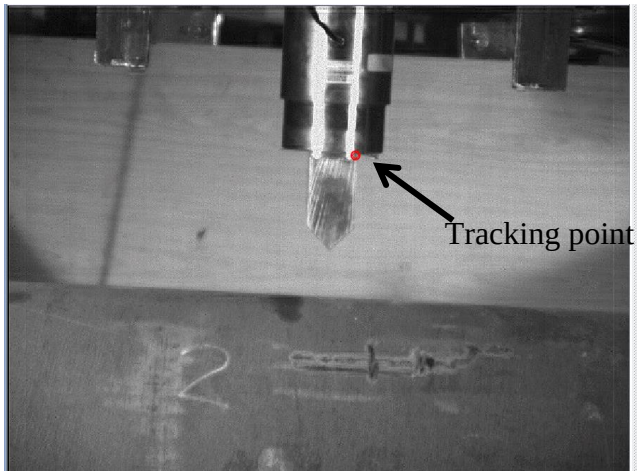

Figure 5.11: Tracking point for the vertical displacement of the impactor using the high speed video.

Figure 5.12 and Figure 5.13 show the time histories for vertical displacement and vertical velocity of the impactor for the case of pipe impacted with curved and sharp impactors. The data obtained is characterized by significant noise associated with the accuracy of the high speed high resolution video camera and the tracker software. In order to reduce the solution noise, the velocity time history curves are smoothed as shown in Figure 5.13.

The vertical velocity obtained is then differentiated to get the acceleration of the impactor as given by Eq. (5.1). The acceleration is then used to calculate the contact force time history as shown in Figure 5.14.

$$a = \frac{dv}{dt} \qquad \text{Eq. (5.1)}$$

where: v : velocity
a : acceleration

It is observed that the contact duration is shorter for the case of curved impactor as compared with the case of sharp impactor (see Figure 5.14). The divergence is also observed for the vertical velocity time history of the curved and sharp impactors [see Figure 5.13]. It is found that the slope of the vertical velocity of the curved impactor is steeper as compared to the sharp impactor; as a result larger contact duration is recorded for the sharp impactor compared to the curved impactor. In spite of the above differences the rebound velocities are found to be similar. Furthermore, although both tests are carried out with the same impact energy the magnitude of the maximum contact force for the case of curved impactor is higher as compared to that observed in the case of sharp impactor (see Figure 5.14). This difference can be attributed to the fact that the contact surface of the curved impactor with the pipe is relatively larger as compared to its sharp counterpart. As a result the curved impactor resulted in the generation of a higher contact force. The difference in the magnitude of the contact force may also be due to the fact that for the case of the curved impactor no permanent plastic deformation is observed in the impactor itself, however damage is observed in the contact area of the sharp impactor (see Figure 5.15). Thus the sharp impactor is observed to be less stiffer compared to that of the curved impactor and as a result a lower contact force is observed.

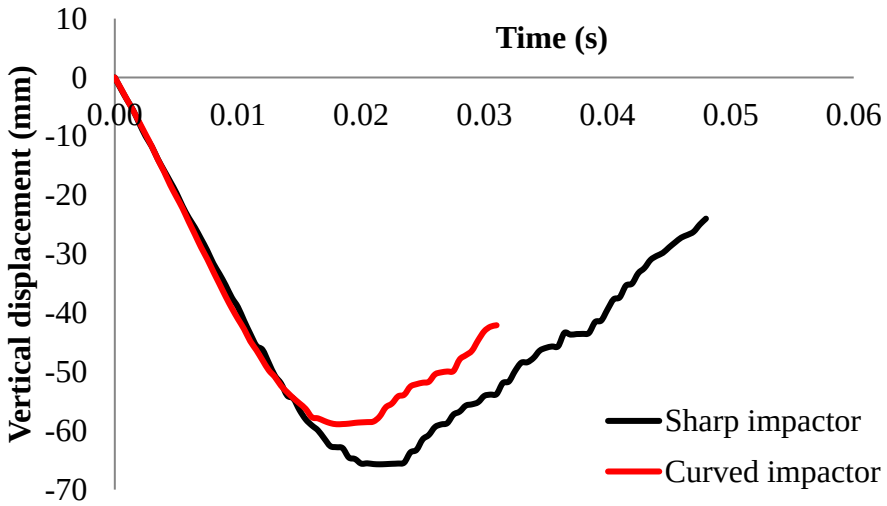

Figure 5.12: Comparison of the vertical displacement time histories for the case of pipe impacted with curved and sharp impactor.

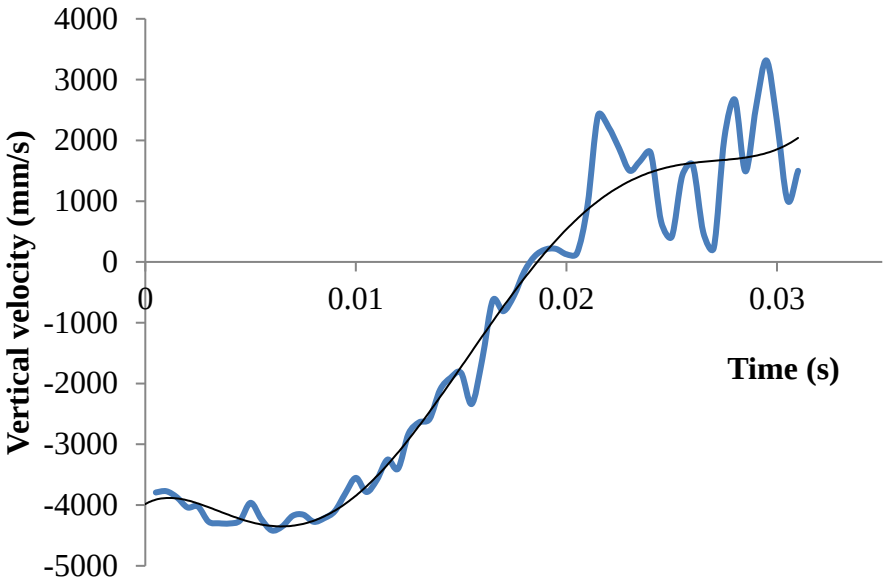

(a)

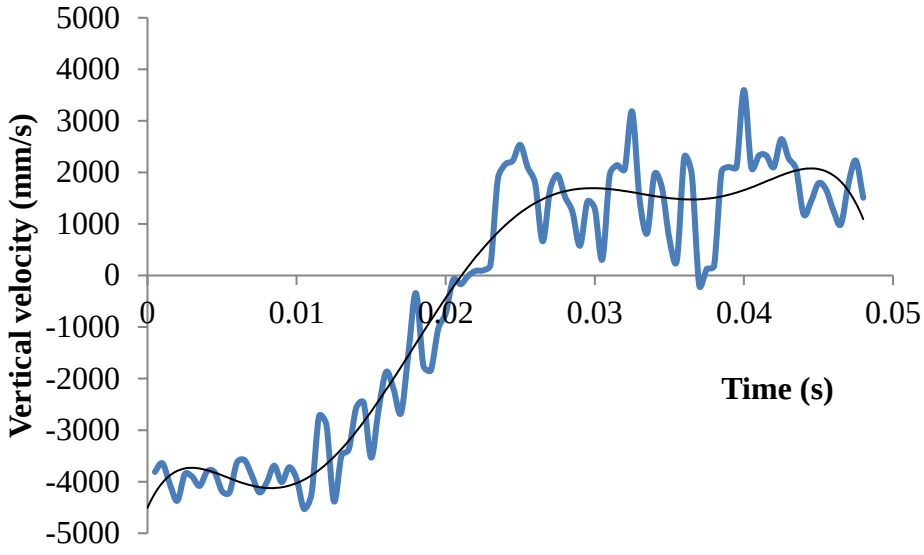

(b)

Figure 5.13: Vertical velocity time histories for the case of pipe impacted with (a) curved and (b) sharp impactor.

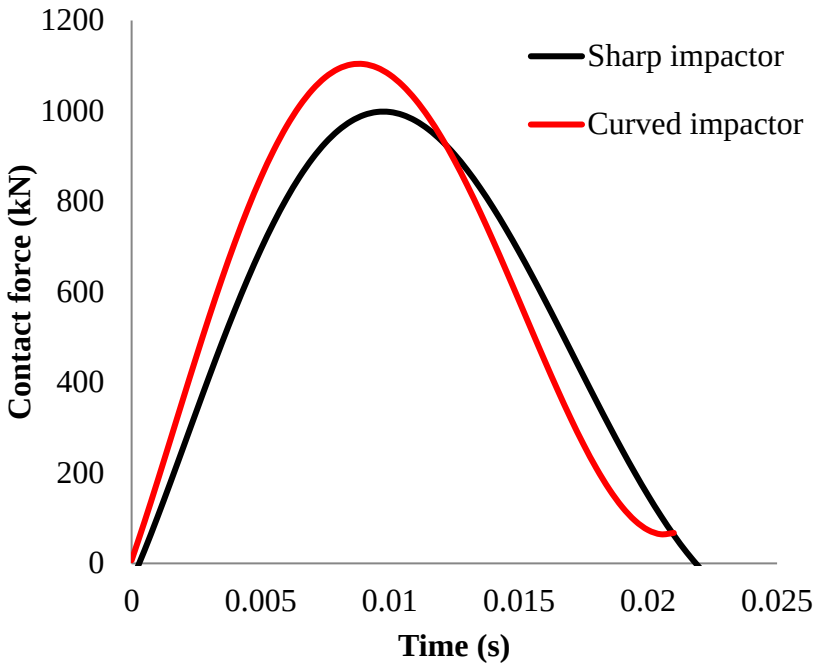

Figure 5.14: Contact force time histories for the case of pipe impacted with sharp and curved impactor.

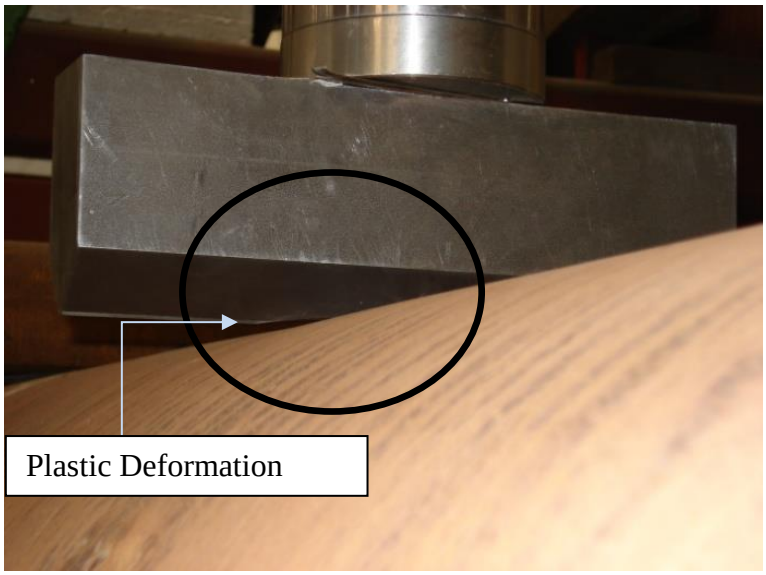

Figure 5.15: Permanent damage caused to the sharp impactor due to its collision with the pipe.

Figure 5.16 shows different stages of the impact event. From the high speed video recording the following four stages are identified:

- Stage I: The impactor initially comes into contact with the pipe (t= 0s).

- Stage II: The contact between both the pipe and the impactor occurred and both moves vertically downwards until at some point deformation of the pipe is maximum and velocity of the impactor is zero.

- Stage III: During this stage the pipe displacement decreases and as a result the impactor started to move upwards with a residual kinetic energy.

- Stage IV: The separation of the pipe and the impactor occurred and the impactor moved up with a residual velocity and the pipe oscillated.

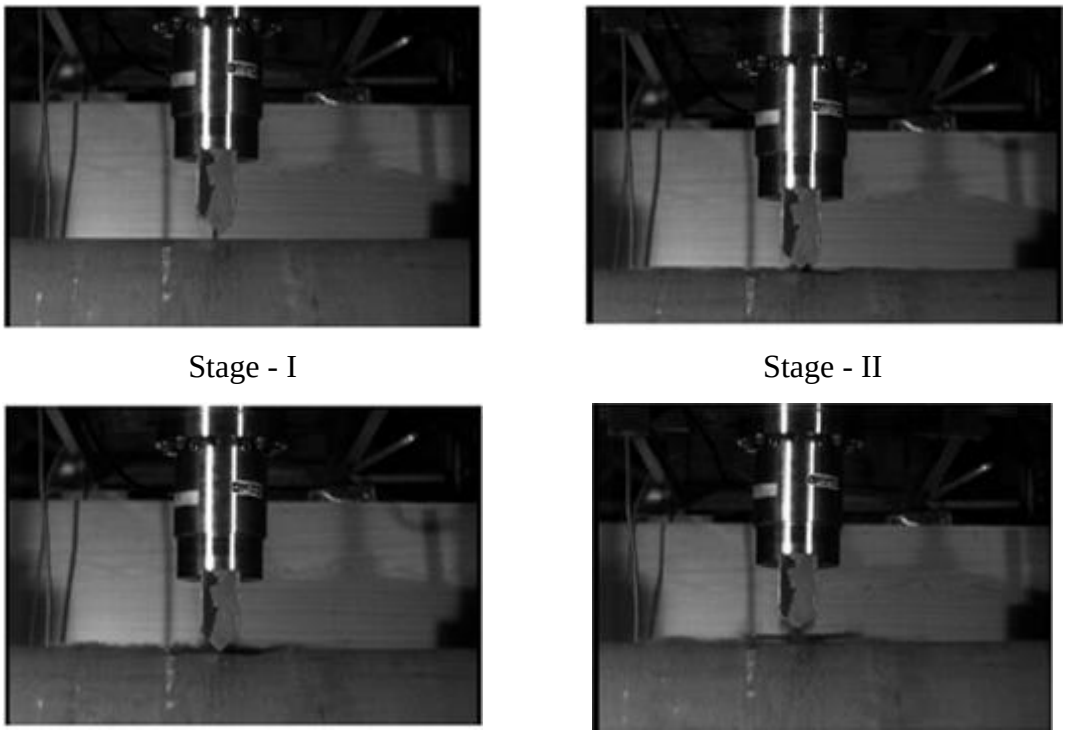

Stage - I Stage - II

Stage - III Stage - IV

Figure 5.16: Different stages observed in the impact tests from high speed video recording.

Table 5.2 gives the reduction in the diameter of the pipe for the case of the pipe impacted with sharp and curved shape impactors. It is observed that both impactors lead to similar reductions in the pipe diameter in the impact region.

Table 5.2: Impact test results for reduction in diameter of pipes.

Impact test	Reduction in diameter (mm)
– with sharp impactor	4.48
– with curved impactor	4.47

5.4 FINITE ELEMENT MODELLING

In order to investigate in detail certain important aspects of the response exhibited by pipes such as stress-strain distribution, deformation profile throughout impact event, time histories of contact force, velocity etc. (which is not provided by the experimental studies) *NLFEA* is employed. In order to reduce the computational cost and due to the symmetry of the impact test (see Figure 5.17), only a quarter-model is considered. In the quarter model, the pipe has a diameter of 457mm, a thickness of 25.4mm and a length of 1000mm. The modelled impactor has a width of 25mm and depth of 125mm. Figure 5.18 shows the support conditions used in the finite element model. Initially the pipe is supported vertically along the base (see Figure 5.19) for the full length. In the tests the pipe was not laid on rigid supports but rather it was placed on steel plate which was supported by steel girders along its whole length. In order to investigate the latter effect the *FE* model will be discussed later in section 5.8.

In the *FE* analyses, the impactor and drop mass are modelled as a single mass which have the dimensions of the impactor. A higher density is used so that the mass of the impactor modelled in *FE* is equal to the whole mass used in the experiment. In order to reduce the duration of the analyses, in the initial phase of the problem the mass is considered to be in contact with the pipe and is given an initial velocity of 3.87m/s. In impact test, the impacting mass was dropped from the height of 750mm in order to achieve an impact energy of 16kJ. Based on this height, the initial velocity is calculated using Eq. (5.2)

$$v = \sqrt{2gh} \qquad \text{Eq. (5.2)}$$

where : g : acceleration due to gravity

h : height of the impactor

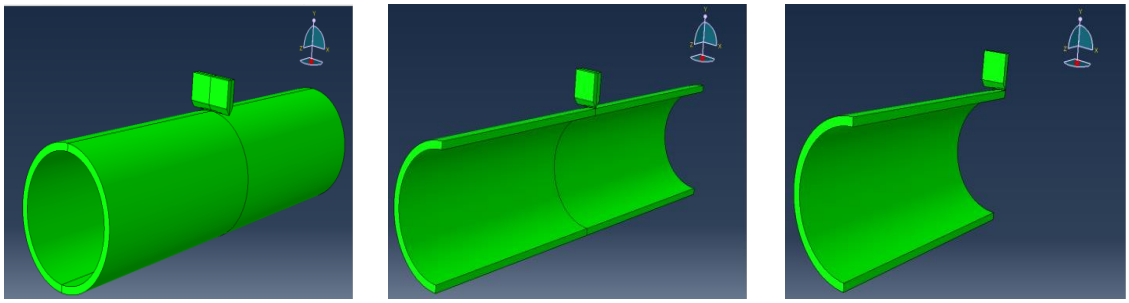

Figure 5.17: Symmetry of the impact test set up.

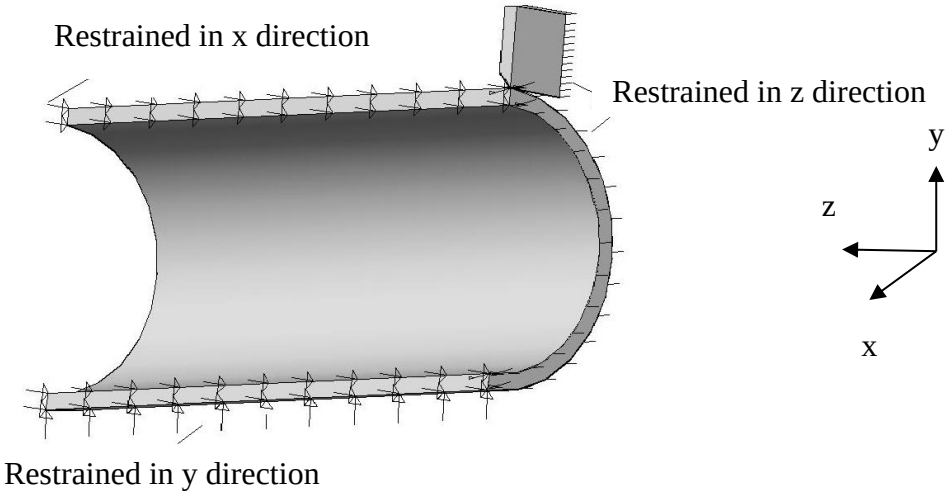

Figure 5.18: Support conditions in the finite element model.

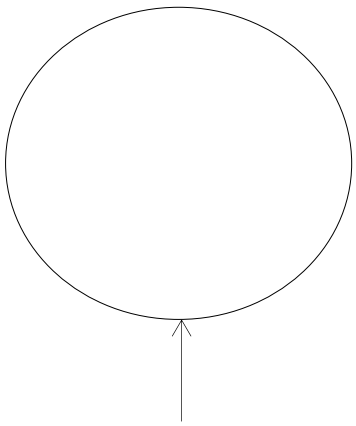

Figure 5.19: Pipe vertically restrained along the base.

Acceleration due to gravity is applied in the vertical downward direction with a magnitude of 9.81m/s^2. Figure 5.20 shows the true stress-strain curve describing the material behaviour of steel in tension and compression used in the *FE* analysis, obtained by averaging the static uniaxial tensile test data of coupon tests as described in section 5.2.1. The impactor is assumed as elastic. Table 5.3 gives a summary of the density and Poisson's ratio used for pipe and impactor. The classical metal plasticity model (described in detail in Chapter 4) in ABAQUS [ABAQUS (2013)] is used to describe the material properties of steel. A non-linear dynamic implicit analysis is used in order to solve the problem. The non-linear iterative solution strategy adopted by ABAQUS (2013) is presented in detail in Chapter4. A contact surface is defined between the pipe and the impactor with a coefficient of friction of 0.3 [MAE (2016)].

Table 5.3: Material properties used in the *FE* analyses.

	Pipe	**Impactor**
Density (kg/m^3)	7850	1770000
Poisson's ratio	0.29	0.29

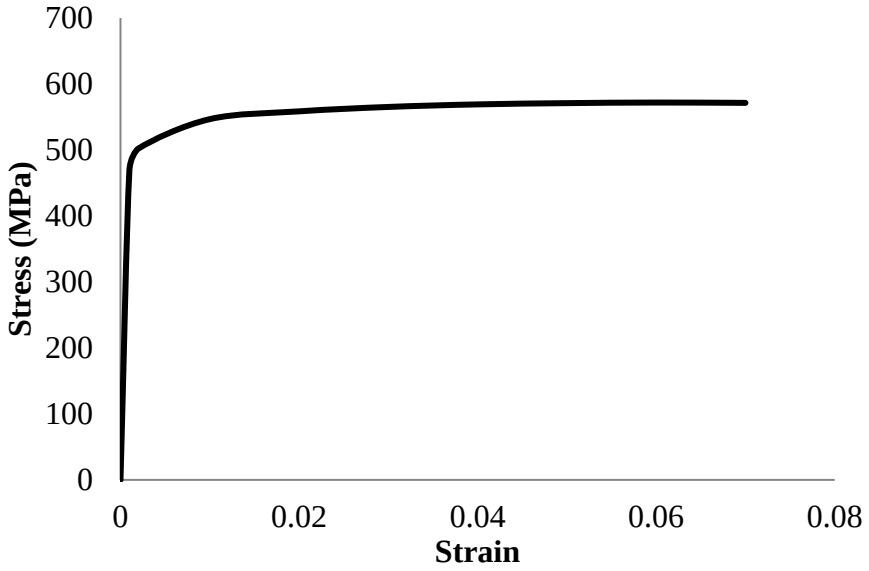

Figure 5.20: True stress-strain curve used in the *FE* analyses.

5.5 MESH SENSITIVITY

In order to check the accuracy of the *FE* solution, a mesh sensitivity analysis is carried out. For this purpose three different meshes as shown in Figure 5.21 (a), (b) and (c) are used. For all three *FE* models, 8-node bricks elements are used for both the pipe and the impactor. A finer mesh is used in the contact area between the pipe and the impactor in order to better capture the stress-strain distributions which are high in the contact region. A coarser mesh is used away from the contact area considering the stress-strain distributions are low.

Figure 5.22 shows the vertical displacement-time histories obtained for all three meshes. It is observed that in spite of the differences in the mesh density the solutions obtained are not different. As a result the denser mesh [see Figure 5.22 (c)] is used.

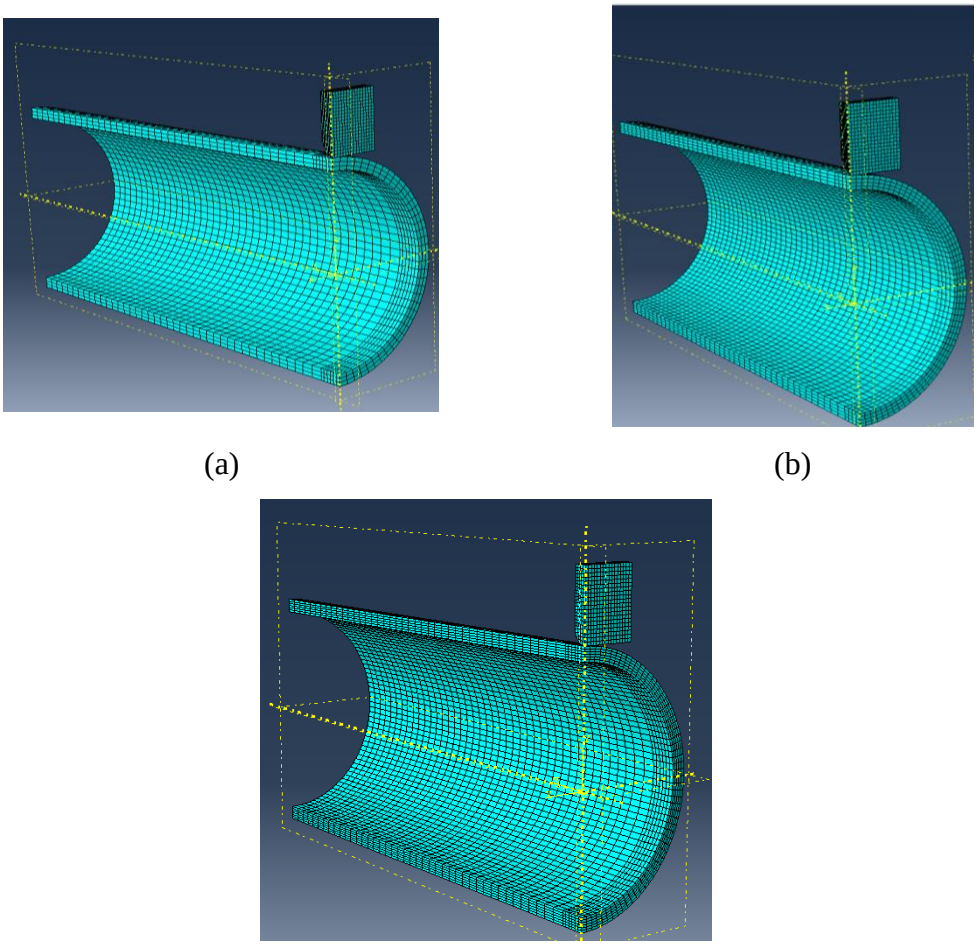

(a) (b)

(c)

Figure 5.21: Mesh sensitivity (a) mesh 1 (b) mesh 2 (c) mesh 3.

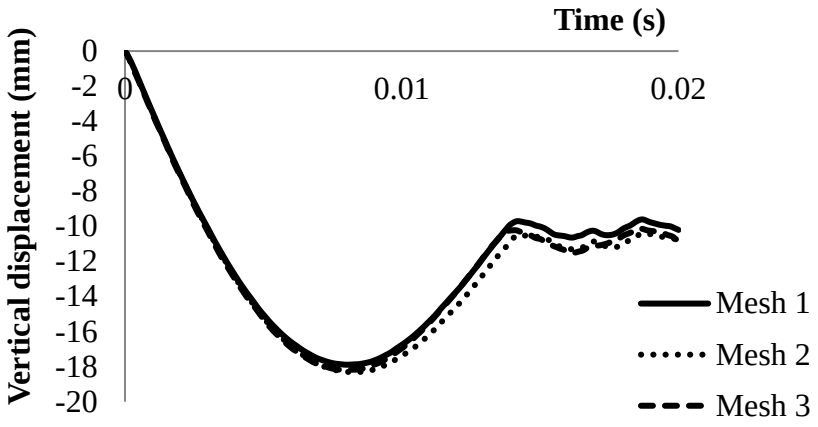

Figure 5.22: Vertical displacement time history with different meshes.

5.6 DISCUSSION OF IMPACT ANALYSES

A comparison of the predictions of the vertical velocity and contact force time histories obtained from the *FE* models when employing a sharp or curved impactor are shown in Figure 5.23. It is observed that the predicted velocity time histories for both cases are similar [see Figure 5.23 (a)]. It is also observed that after initial contact the velocity reduces rapidly until the velocity of the impactor reaches zero. It then starts to increase until it reaches a maximum value when the separation of the pipe and impactor occurred after which it reduces due to gravity. In both cases it is observed that the predicted contact force appears to increase until it reaches its peak value [see Figure 5.23 (b)]. After attaining its peak value it started to decrease until the impactor separates from the pipe and the force becomes zero. It is observed that although both analyses are carried out with the same impact energy however the magnitude of the maximum contact force for curved impactor is larger as compared to the sharp impactor as observed in the impact tests.

Figure 5.24 shows the comparison of the reduction in diameter along the length of the pipe impacted with curved or sharp impactor.

Table 5.4 shows the comparison of the reduction in the diameter of the pipe in the impact area for the case of pipe impacted with sharp or curved impactor. It is found that the reduction in the diameter is very similar for both cases in the impact area (see

Figure 5.24 & Table 5.4). However it is observed that the curved impactor resulted in slightly higher global deformation (pipe deformed along the length of the pipe as a whole unit) compared to the sharp impactor case.

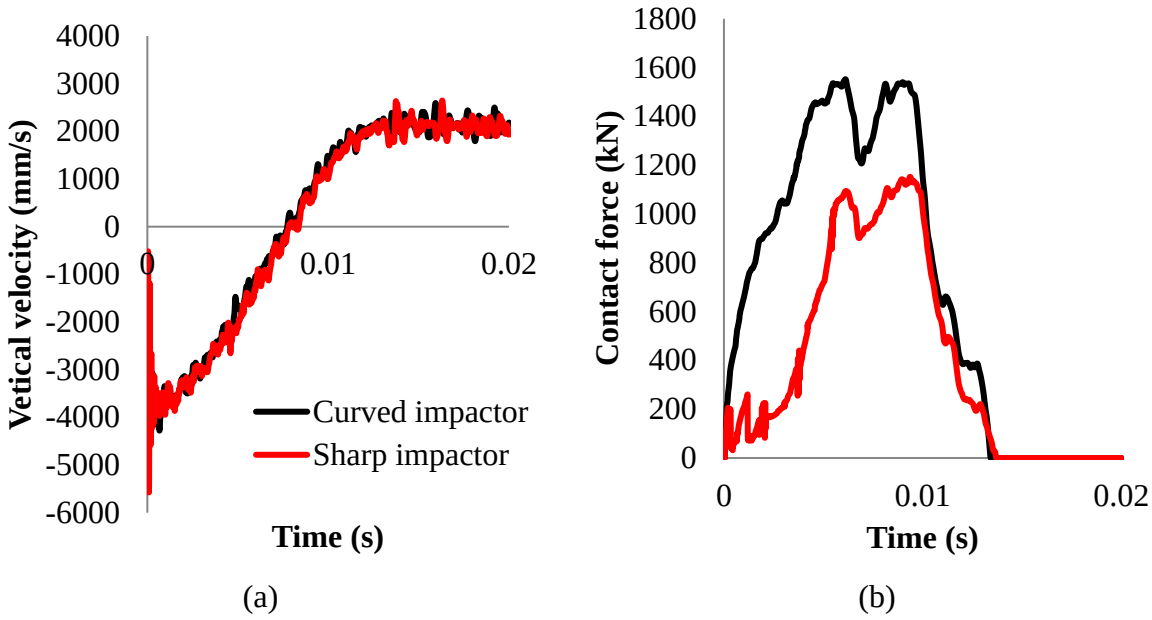

Figure 5.23: (a) Vertical velocity time history (b) contact force time history for the case of pipes impacted with curved and sharp impactor.

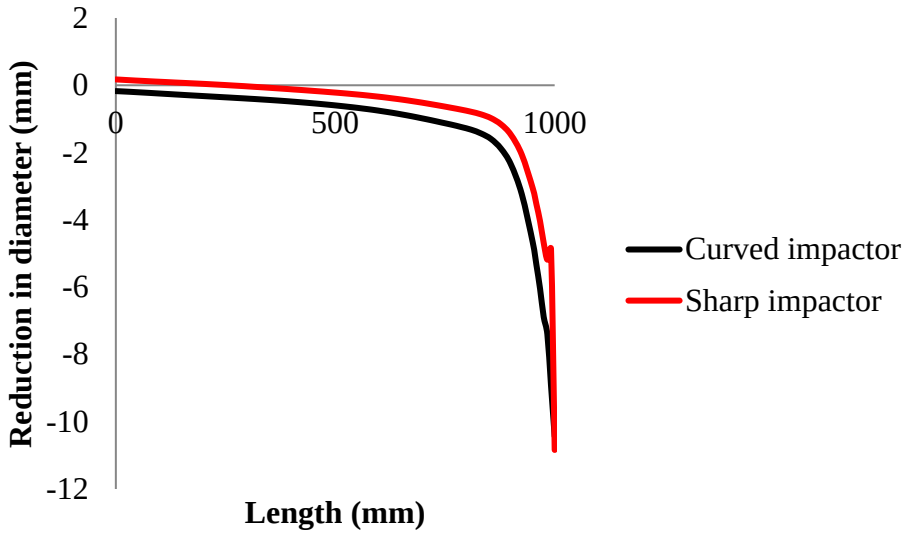

Figure 5.24: Comparison of the reduction in diameter along the length of the pipe impacted with curved and sharp impactor.

Table 5.4: Comparison of the reduction in the pipe diameter in the impact region.

Impactor shape	**Reduction in diameter (mm)**
Sharp	10.84
Curved	10.43

Figure 5.25 shows the variation of the plastic strains along the length of the pipe for the case of the pipe impacted with curved or sharp impactor. It is observed that the plastic strains are similar for both cases considered and the affect is limited to the impact zone.

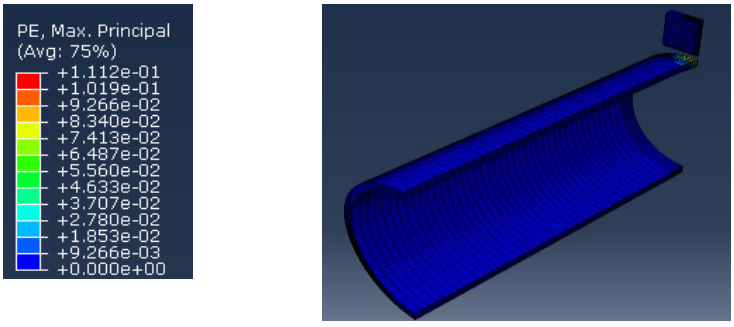

(a)

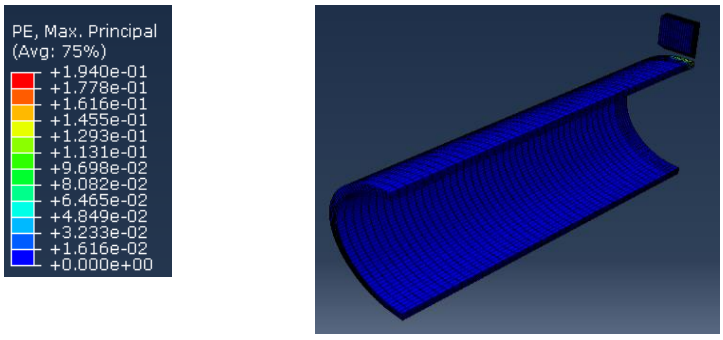

(b)

Figure 5.25: Plastic strains along the length of the pipe impacted with (a) curved impactor (b) sharp impactor.

Figure 5.26 shows the variation of the strain rate (in the vertical direction) with time along the length of the pipe for the case of the pipe impacted with sharp or curved

impactor. It is found that the effect of the strain rate is localized in the impact zone and is limited to very short duration and relatively low magnitude of the strain rate is observed away from the impact zone.

Based on the experimental and numerical studies described in Chapter 3 to study the behaviour of steel under increasing loading rates it was found that steel having static yield strength similar to yield strength of the steel from which pipe (used herein) is constructed has very little influence of strain rate on its behaviour till the strain rate of $100s^{-1}$. It can be seen in Figure 5.26 that the strain rate for both cases considered are found to be well below the level of $100s^{-1}$, therefore the use of the static material properties in the *FE* analyses is justified.

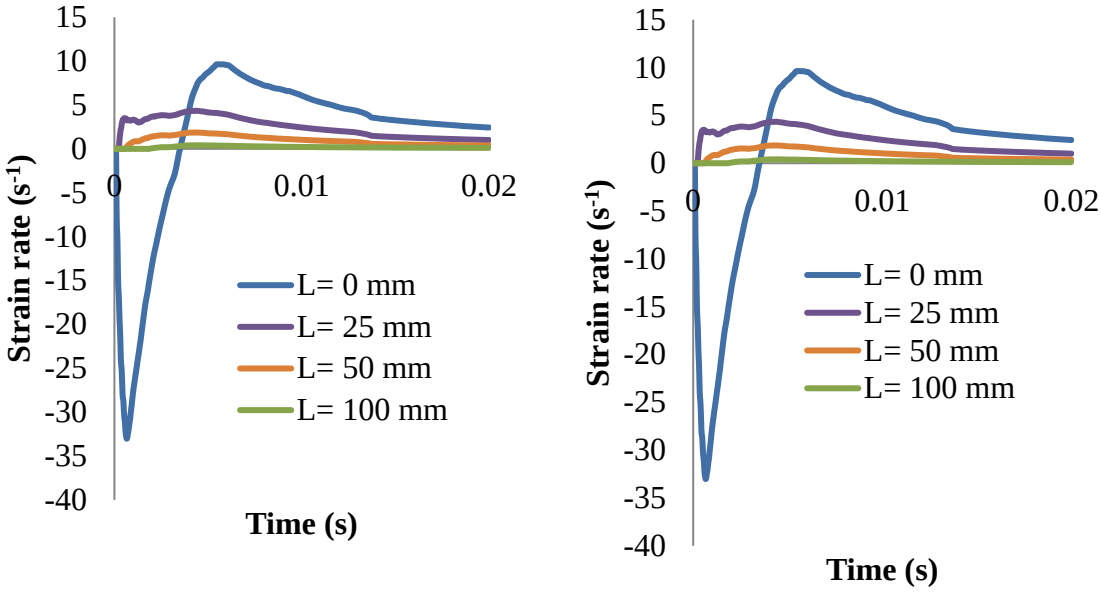

Figure 5.26: Variation of the strain rate with time when pipe is impacted with (a) sharp impactor (b) curved impactor.

5.7 COMPARISON OF THE EXPERIMENTAL AND FE RESULTS

The comparisons of the contact force and vertical velocity time histories are shown in Figure 5.27. For the case of sharp impactor good agreement is found for the magnitude of maximum contact force between the *NLFEA* predictions and the impact test results, however, divergence is observed for the impact duration [see Figure 5.27 (a)]. This can

be explained due to the fact that for the impact tests, a permanent plastic deformation in the impactor is observed (see Figure 5.15) whereas for the case of *NLFEA*, the impactor is assumed to be elastic. As a result, the stiffness of the impactor in *NLFEA* is higher than the impactor in the test. Therefore *NLFEA* predicted lower impact duration for the case of pipe impacted with sharp impactor.

Discrepancies are also observed for the contact force time history between the impact tests results and the *NLFEA* predictions for the case of curved impactor [see Figure 5.27 (b)]. It is observed that *NLFEA* predicted higher contact force and lower impact duration compared to the impact test results. The overall differences in the *NLFEA* predictions and the impact test results for the case of contact force time histories may also be due to the fact that the experimental contact force time histories are obtained by differentiating the vertical velocity of the impactor which is obtained by digitizing data from the high speed video. Thus any error in the vertical velocity may result in the error in the contact force time history. In spite of the above differences the velocity time histories observed from the impact tests and predicted from the *NLFEA* analyses are similar [see Figure 5.27 (a) & (b)].

The comparison of the reduction in the pipe diameter in the impact region for the predictions of the *NLFEA* analyses and impact test results is shown in Table 5.5. It is found that the *NLFEA* analyses predicted larger reduction in the diameter of the pipe compared to the impact tests. This can be explained by the fact that during the impact tests pipes were placed on a steel plate which rests on steel girders supported by a strong floor (see Figure 5.6), as a result pipes are not fully fixed (as modelled in *FE* study) along its base. Therefore the stiffness of the supporting system considered in the *NLFEA* is higher than the actual support conditions attained during impact tests, thus it is logical that the *NLFEA* predicted higher reduction in the diameter due to the higher stiffness of the system. In order to investigate the effect of the boundary condition on the impact behaviour of the pipe a numerical study is carried out which is discussed later in section 5.8.

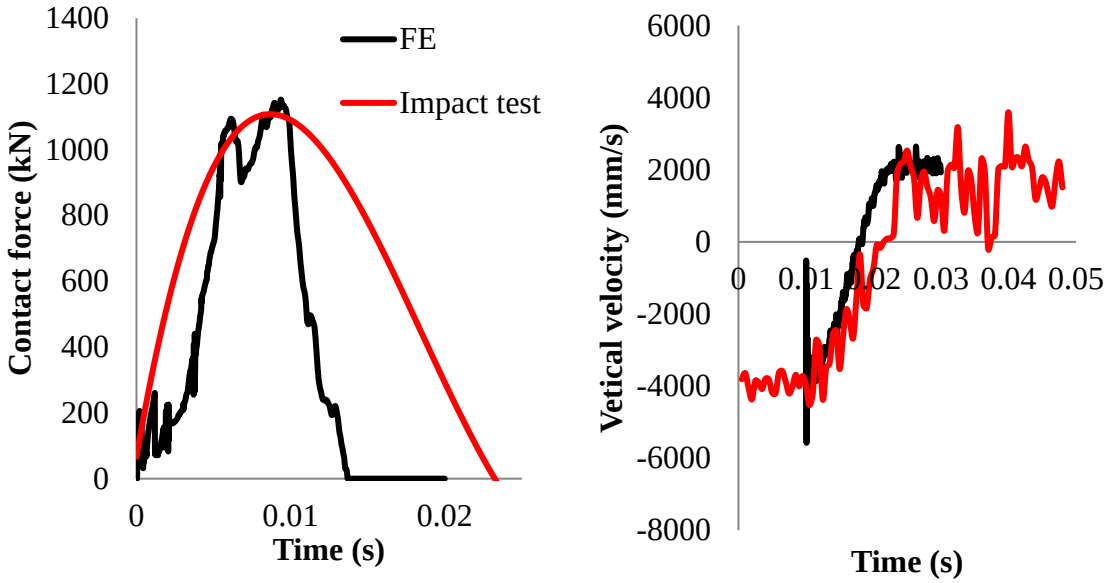

(a)

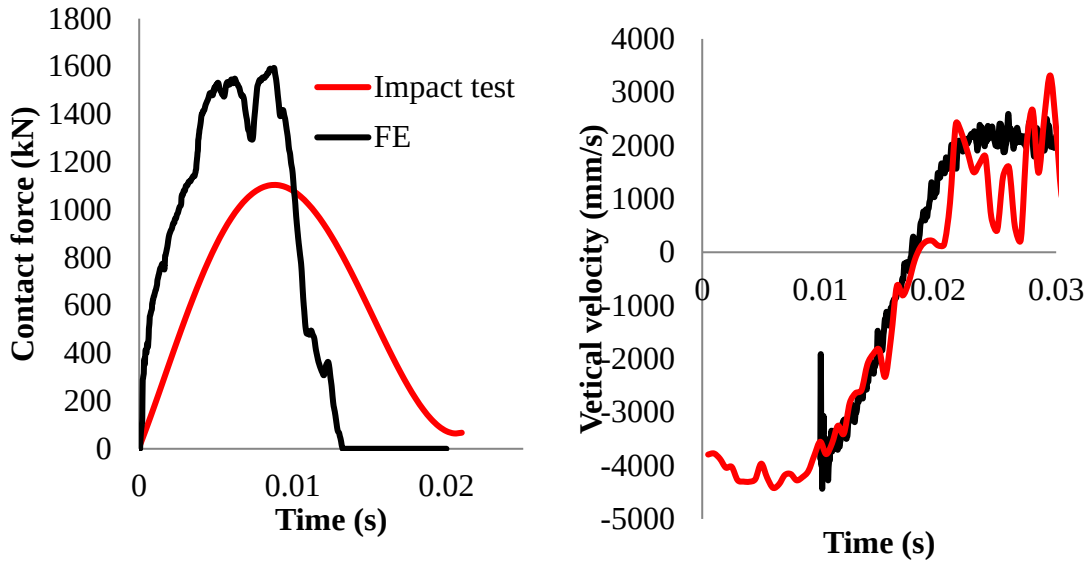

(b)

Figure 5.27: Comparison of the finite element analysis and impact test results for contact force and vertical velocity time histories for the case of pipe impacted with (a) sharp impactor (b) curved impactor.

Table 5.5: Comparison of *NLFEA* predictions and impact test results for the reduction in the pipe diameter in the impact zone.

Results	Reduction in the diameter (mm)
FE- sharp impactor	10.84
FE- curved impactor	10.43
Impact test - sharp impactor	4.48
Impact test - curved impactor	4.47

5.8 EFFECT OF BOUNDARY CONDITIONS

In order to investigate the influence of the boundary conditions on the impact behaviour of the pipe, the following case studies are carried out:

- Pipe supported by springs at the base (SB) – [see Figure 5.28 (a)]
- Pipe supported by springs at the base and along the circumference (SBC) – [see Figure 5.28 (b)]

The pipe with a span length of 2000mm [see Figure 5.28 (c)] is impacted at its mid-span with a curved impactor. The same material properties of pipe and impactor are used as described in section 5.4. The springs *K-1* are used to model the stiffness provided by the steel girders whereas *K-2* and *K-3* are used for steel girders and welded angles respectively as used in the impact tests [see Figure 5.6(a)]. The springs are placed at 110mm spacing.

The stiffness *K-1* and *K-2* are calculated based on Eq. (5.3), whereas Eq. (5.4) was used to calculate the stiffness of *K-3*. Due to the symmetry of the *FE* model, half of the stiffness is used for *K-1*. The values of stiffness used in the *FE* model are given in Table 5.6. The pipes are also axially restrained along the base for the whole length.

$$\mathrm{K}-1, \mathrm{K}-2 = \frac{\mathrm{EA}}{\mathrm{L}} \qquad \text{Eq. (5.3)}$$

$$K-3=\frac{3EI}{L^3}$$ Eq. (5.4)

where: A = s x t

s : spacing of springs = 110mm

t : thickness of web = 5mm

L : height of web = 145mm

I : second moment of area

E : Young's modulus of elasticity = 210e3MPa

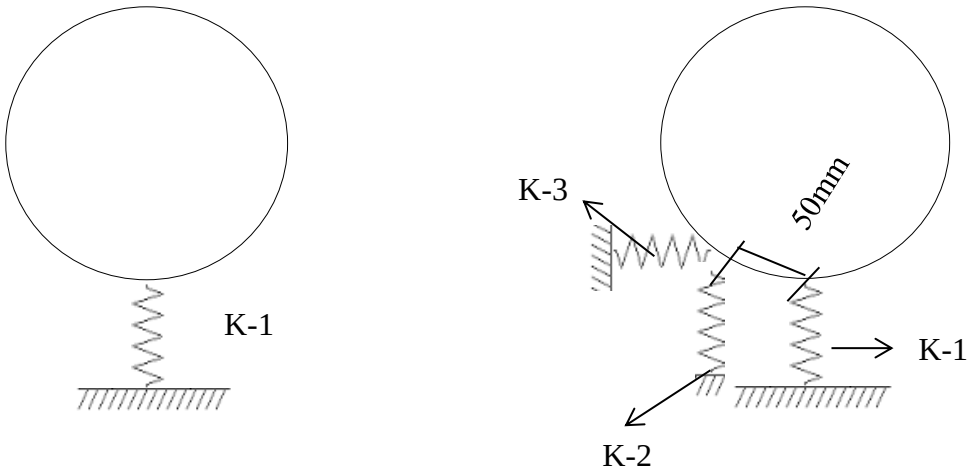

(a) (b)

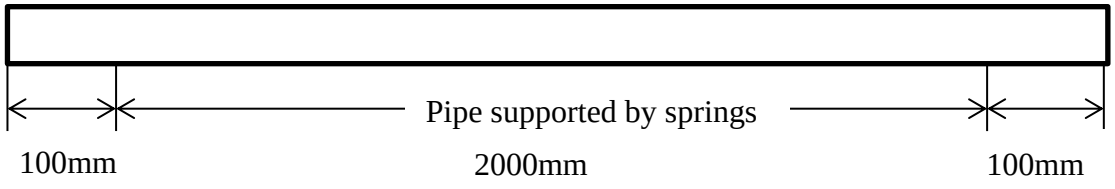

(c)

Figure 5.28: Pipe supported by springs (a) at the base (SB) (b) at the base and along the circumference (SBC) (c) support conditions along the length of the pipe.

Table 5.6: Stiffness of springs used in the *NLFEA* model.

Spring	Stiffness (kN/m)
K-1	398276
K-2	796552
K-3	2841

Figure 5.29 shows the comparison of the vertical velocity and contact force time histories and the reduction in the diameter along the length of the pipe with different boundary conditions for the case of pipe impacted with a curved impactor. Table 5.7 shows the comparison of the reduction in the diameter of the pipe in the impact region. The results of the *FE* analyses are also compared with pipe supported vertically along the length of the pipe (RS) as described in section 5.6. It is observed that the boundary conditions do not appear to significantly influence the vertical velocity and contact force time histories [see Figure 5.29 (a) & (b)]. However, it is observed that the deformed profile of the pipe after impact is different for each case study [see Figure 5.29 (c)]. A higher reduction in diameter in the pipe in the impact zone is observed for the case of pipe with rigid supports (RS) and pipe with springs at the base and circumference (SBS) compared to the pipe supported by springs at the base (SB). This is due to the fact that the stiffness of the supporting system is higher and as a result a more localized response is observed. A detailed parametric study investigating the influence of different stiffnesses of subsea soil on the impact behaviour of the pipe is presented in Chapter 6.

Table 5.7: Comparison of the reduction in diameter of the pipe in the impact region with different boundary conditions.

Boundary condition	Reduction diameter (mm)
RS	10.43
SB	9.88
SBC	11.17

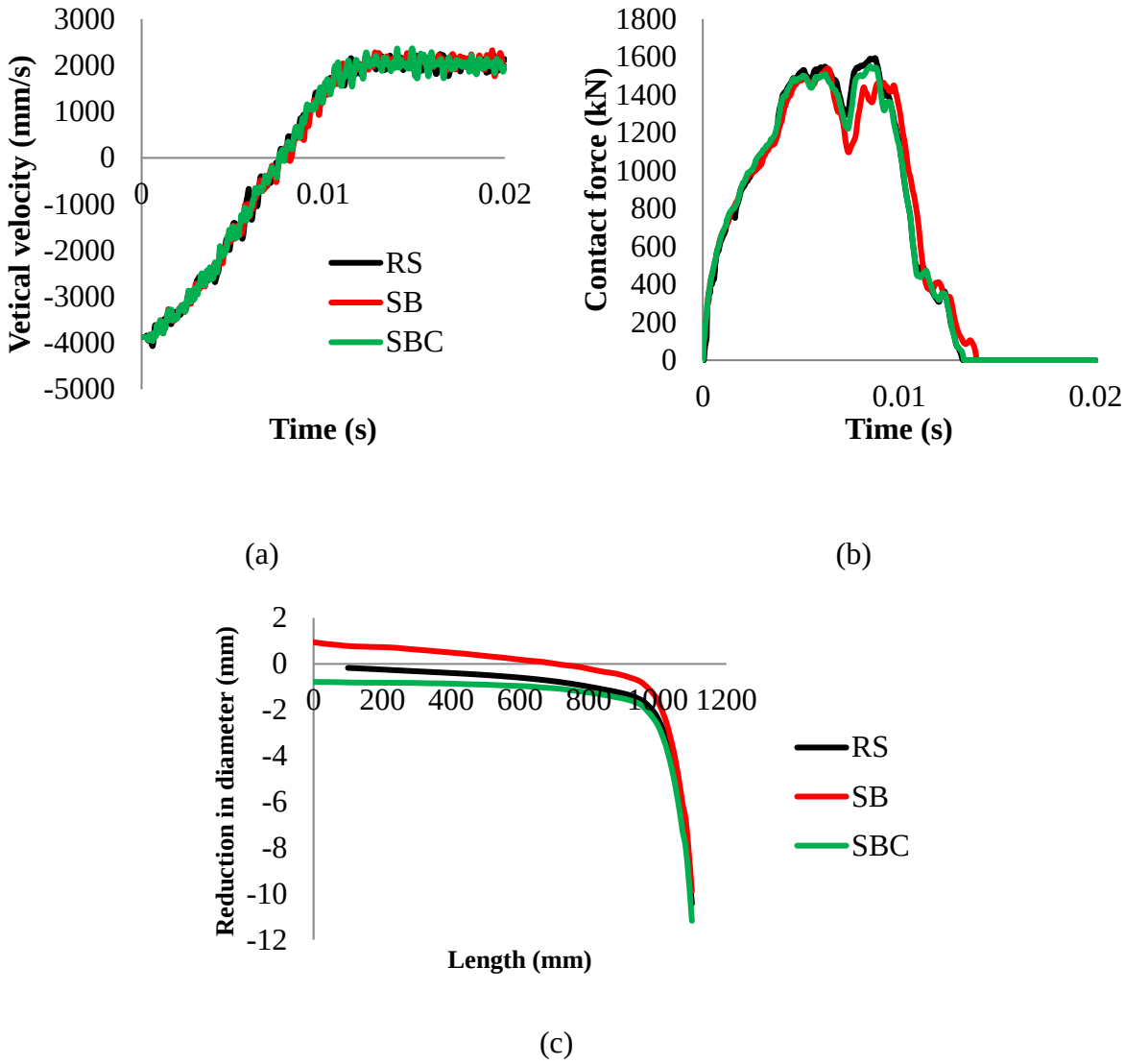

Figure 5.29: Comparison of (a) contact force (b) vertical velocity time histories (c) reduction in the diameter along the length of the pipe for the pipe with different boundary conditions.

5.9 ANALYTICAL SOLUTION

An analytical solution [Wierzbicki & Suh (1988)] given by Eq. (5.5), suggested for use in risk assessment of denting of pipeline [DNV (2010b)] is compared with the impact test and predictions of the *FE* results. The analytical solution is explained in detail in Chapter 2.

$$\mathrm{E} = 16\left(\frac{2\pi}{9}\right)^{\frac{1}{2}} m_p \left(\frac{D}{t}\right)^{\frac{1}{2}} \mathrm{D}\left(\frac{\delta}{D}\right)^{\frac{3}{2}} \qquad \text{Eq. (5.5)}$$

Table 5.8 shows the comparison of the results for the impact tests, *FE* analyses and Eq. (5.5). The analytical solution is found to be conservative compared to the *FE* analyses and impact test results. The divergence is found between results which may be due to the fact that the analytical solution is based on quasi-static solution ignoring the inertia effects and the wave propagation problem at hand.

Table 5.8 also gives reduction in diameter to diameter ratio (*R/D*) which is used for describing the damage description [DNV (2010b)]. It is found that the *R/D* obtained from the impacts tests, *FE* analyses and Eq. (5.5) is less than 5%. The *R/D* less than 5% represents a minor damage which is defined as the "Damage neither requiring repair, nor resulting in any release of hydrocarbons" [DNV (2010b)]. Further details for the damage classification are given in Chapter 2. Therefore it is found that the damage caused to the pipe due to an impact load of 16kJ predicted by all three solutions i.e. Eq. (5.5), impact tests and FE analyses resulted in minor damage description.

Table 5.8: Comparison of the reduction in diameter for impact tests, *FE* analyses and Eq. (5.4).

Results	**Reduction in diameter (mm)**	***R / D* (%)**
Eq. (5.5)	18.55	4.05
FE- Sharp	10.84	2.37
FE- Curved (*RS*)	10.43	2.28
FE- Curved (*SB*)	9.88	2.16
FE- Curved (*SBC*)	11.17	2.44
Impact test – Curved impactor	4.47	0.94
Impact test – Sharp impactor	4.48	0.98

5.10 CONCLUSIONS

In order to study the behaviour of full scale pipes under impact, drop-weight tests and numerical studies are carried out in the present chapter. For this purpose, two full scale impact tests are initially conducted focusing on the local response of the subject specimens under impact loading. Based on the experimental investigation the following conclusions are drawn:

- The pipe responded to the impact load locally. The local behaviour of the pipe is considered as the indentation which is produced in the contact area of the pipe and the impactor.

- A higher magnitude of the maximum contact force is measured when using the curved impactor compared to that recorded for the case of the sharp impactor. The difference in the magnitude of the contact force can be attributed to the fact that after impact the curved impactor exhibited no permanent deformation. However, damage is observed in the contact area of the sharp impactor after impact.

- The shape of the impactor did not influence the permanent damage sustained locally (deformation in the contact area of the pipe and the impactor) by the pipe.

Based on the *NLFEA* investigations the following conclusions are drawn:

- For the case of a sharp impactor good agreement is observed between the experimentally and numerically established values concerning the magnitude of maximum contact force.

- The velocity time histories measured during drop-weight testing and their numerically established counterparts are found to be in reasonable agreement.

- The reduction in the diameter in the impact zone predicted numerically is similar for both cases of curved and sharp impactors. However, it is observed that the curved impactor resulted in slightly higher global deformation.

- The effect of the strain rate is localized in the impact zone and a relatively low magnitude of strain rate is observed. Therefore the use of the static material properties in the *NLFEA* analyses is justified for the subject case study.

Based on the comparison of the predictions of the assessment method used by the industry and the *FE* analysis with their experimentally established counterparts the following conclusions are drawn:

- The predictions of the simplified assesment method employed in this chapter for assessing the level of damage sustained by the pipe due to impact are found to be conservative compared to their counterparts estabished numerically (*via* NLFEA) and experimentally (*via* drop-weight testing). The divergence found between the results can be explained by considering the limitations characterising such methods discussed in Chapter 2.

- It is observed that the reduction in the diameter expressed by R/D established experimentally, numerically (*via* NLFEA) and analytically (from the simplified assessment method) is less than 5%. Thus the predictions of all three of the latter methods suggest that the level of damage sustained by the pipe due to impact (characterised by an impact energy of 16kJ) is minor and therefore does not require any repair according to the recommended practice [DNV (2010b)] used by industry.

CHAPTER 6

PARAMETRIC STUDIES

6.1 INTRODUCTION

It has been established, both experimentally and numerically, that the dynamic response of steel pipes under impact loading exhibits significant departures from that established under equivalent static loading when certain thresholds of the applied loading rates are surpassed (see discussion in section 2.5.1). Furthermore, based on the predictions obtained from the numerical investigation presented in Chapter 4, which focuses on studying the dynamic response exhibited by scaled steel pipe-specimens during drop-weight testing, it was observed that a number of parameters associated with: (i) the characteristics of the impacting object (impact speed), (ii) boundary conditions imposed onto the pipe specimen (iii) the level of axial loading applied as well as (iv) internal (due to the oil and gas in the pipe) and external (hydro-static) pressures imposed onto the walls of the pipes can potentially have a significant effect on the exhibited behaviour under impact loading. In addition it is important to note that the available assessment methods [DNV (2010a)] adopted by industry for predicting the level of damage sustained by pipes due to impact do not consider the effect of the above parameters. As a result questions rise concerning the ability of the available assessment methods employed in practice to provide (i) accurate predictions concerning the exhibited behaviour of the pipe specimens under impact loading while in operation and (ii) effective design solutions (in terms of safety and economy) capable of safeguarding an intended level of resilience. The latter level of resilience is vital for subsea pipes in order to continue to operate even after being subjected to extreme loading conditions, such as those stemming from accidental collisions of large objects onto the walls of the subject pipes.

In this Chapter, the *NLFEA* models validated in Chapters 4 and 5 are employed to investigate in detail the *in-situ* behaviour of subsea steel pipes under impact. A comprehensive parametric study is carried out on full-scale steel pipe specimens used

by the oil and gas industry (refer to [Tenaris (2015)]) in order to assess the individual and combined effect of various parameters on the exhibited behaviour. The parameters considered are:

(i) The level of impact energy with which the object collides onto the pipe (associated with the mass of the object impacting onto the pipe and its speed).
(ii) The boundary conditions (e.g. end support conditions, the properties of the soil on which the pipe is laid) imposed onto the steel pipe.
(iii) The level of axial loading imposed (i.e. due to temperature changes and the boundary conditions) onto the pipe.
(iv) The level of internal (due to the oil and gas transported within the pipe) and external (hydro-static) pressures imposed on the walls of the pipes.

In order to further protect the integrity of the subsea pipes and reduce the level of damage sustained during impact, various types of coating are often employed [see Figure 6.1]. Thick coatings are often used to protect the external surface of pipes against corrosion, to resist the damage caused during transportation and installation [Bai & Bai (2014)] and to add weight to the pipe. Several types of coatings are used depending on the design temperature and the cost [Bai & Bai (2014)]. These include:

- Tape wrap
- Asphalt
- Coal tar enamel
- Fusion-bonded epoxy (FBE)
- Cigarette wrap polyethylene (PE)
- Extruded thermoplastic *PE* and polypropylene (PP) and
- Concrete and other cement based materials

Concrete coatings can be used for protecting pipelines and for reducing the level of damage sustained due to impact [Palmer *et al.* (2006)]. The typical compressive cube strength of concrete used for this purpose varies from 35 to 45MPa [DNV (2010b)]. The recommended practice adopted by industry [DNV (2010b)] suggests that in the absence of relevant information normal density concrete coating with a thickness of 45mm may be used for achieving energy absorption of 40kJ when impacted by a 30mm wide indenting object.

In the present Chapter two different coatings of concrete are considered: (i) Plain or reinforced concrete and (ii) Engineered Cementitious Composite (*ECC*). This study sets out to assess the ability of these coatings with different thicknesses to absorb part of the energy transmitted during impact (impact energy), thus protecting the pipe and reducing the level of damage sustained.

Figure 6.1: Pipe with concrete coating [lincoln (2015)].

6.2 EFFECT OF END CONDITIONS

Different types of end conditions may be imposed to the ends of the subsea pipes. For example the ends of the pipes may be considered (i) fixed when using anchor blocks (see Figure 6.2), (ii) free when the pipes are attached with bends or dead ends for future extensions and (iii) pinned if the pipe is allow to rotate at the end of the span considered. It was established numerically in Chapter 4 that support conditions imposed onto the pipe ends can significantly affect the exhibited response under impact loading. As a result, in order to investigate the effect of the end conditions on the behaviour of pipes under impact loading the following case studies are considered:

- Case study 1: Pipe ends assumed to be restrained vertically.
- Case study 2: Pipe ends assumed to be fully fixed (clamped).
- Case study 3: Pipe with ends allowed to move freely.

The schematic representation of the end conditions used in this investigation is shown in Figure 6.3. In the case studies 1 to 3, the pipe is considered to be laid on a soil bed (see Figure 6.4). In case study 4, the free end pipe is vertically restrained along its whole length to mimic boundary conditions imposed onto the specimens when conducting the impact tests (see Figure 5.18) described in Chapter 5 which is used as a benchmark test in this investigation.

Figure 6.2: Pipe anchored at ends [Gbenga Sueiman (2015)].

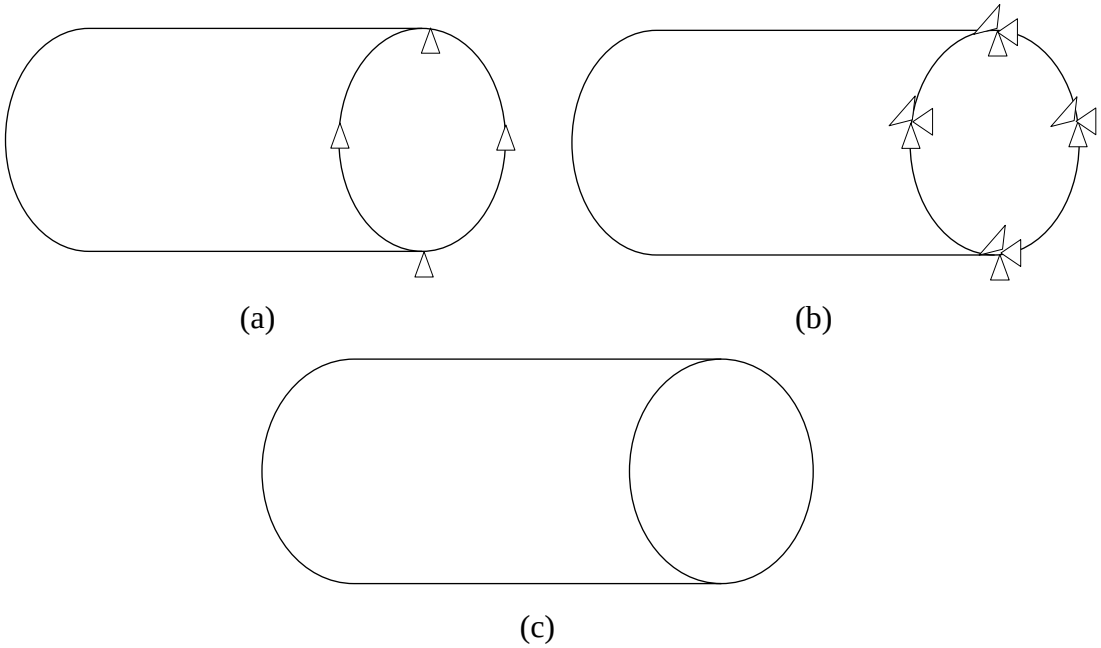

Figure 6.3: Schematic representations of pipes with different end conditions for (a) case study 1 (b) case study 2 (c) case study 3.

As already discussed impact loads are often generated during the collision of equipment used in trawl fishing onto subsea pipes. The weights of these objects may vary from 2

and 9 tonnes [DNV (2010a)]. Therefore in this parametric study, a mass of 2.2 tonnes is used in order to produce an impact energy of 16kJ, similar to the impact energy used in the full scale impact tests described in Chapter 5. A sharp impactor is allowed to drop with an initial vertical velocity of 3.87m/s onto the mid-span region of the pipe. Due to the double symmetry characterizing the problem at hand and in an attempt to reduce the computational cost of the analyses, a quarter model is employed. The geometry of the pipe, the material properties of the steel (used to construct the pipes) and of the impactor are the same as those used in Chapter 5 (see Figure 5.20 & Table 5.3 in section 5.4).

In order to reduce the computation cost, the soil layers upon which the pipe is laid are modelled as an elastic foundation. The pipe is assumed to have an embankment depth of *D/8* (see Figure 6.4). The value of the subsoil stiffness is calculated through the use of Eq. (6.1), which is considered valid when the seabed topographical profiles are not complex and the soil is not stratified, and hence can be considered homogeneous [DNV (2006)].

$$K_V = \frac{C_V}{1-\upsilon}\left(\frac{2}{3}\frac{\rho_s}{\rho}+\frac{1}{3}\right)\sqrt{D} \qquad \text{Eq. (6.1)}$$

where :
- C_V : coefficient for vertical soil stiffness
- D : pipe diameter in meters
- $\frac{\rho_s}{\rho}$: specific mass ratio between the pipe mass (excluding added mass) and the displaced water ($1.2 < \frac{\rho_s}{\rho} < 2.0$)
- υ : Poisson's ratio of the soil
- K_V : vertical stiffness in kN/m/m

The values for the coefficient of vertical soil stiffness (C_v) and Poisson's ratio (υ) are determined based on the classification of soil provided in the available assessment method [DNV (2006)] considered and are given in Table 6.1. The analyses in this section are carried out on pipes assumed to be laid on an elastic foundation with vertical stiffness (K_v) of 9990kN/m/m. This stiffness is associated with stiff and very stiff clay

(see Table 6.1). A detailed parametric study investigating the influence of different stiffnesses of subsea soil on the impact behaviour of the pipe is presented in section 6.4.

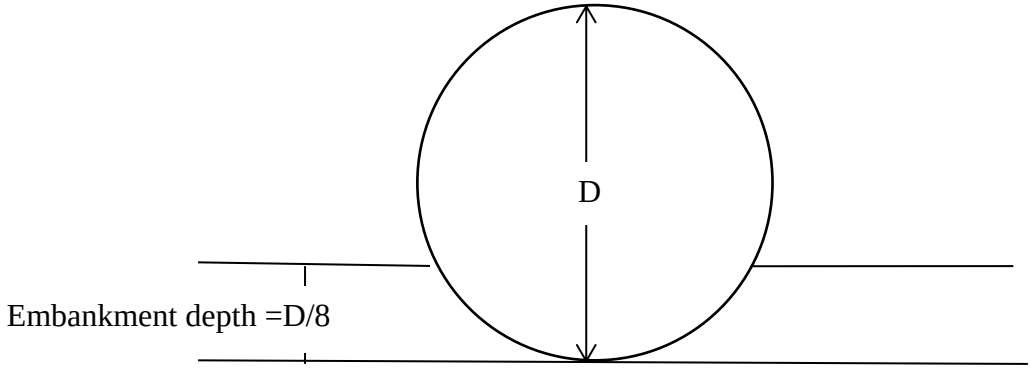

Figure 6.4: Pipe-soil interaction profile.

Table 6.1: Stiffness factors and Poisson's ratio for pipe soil interaction [DNV (2006)].

Sand type	**C_v (kN/m$^{5/2}$)**	**υ**	**K_v (kN/m/m)**
Loose	10500	0.35	18200.48
Medium	14500	0.35	25133.99
Dense	21000	0.35	36400.96
Clay type	-	-	
Very soft	600	0.45	835.80
Soft	1400	0.45	2867.95
Firm	3000	0.45	6145.61
Stiff	4500	0.45	9218.42
Very stiff	11000	0.45	22533.93
Hard	12000	0.45	24582.46

The present investigation focuses on studying certain important aspects of the dynamic response of the pipe under impact loading. These aspects include the contact force time histories and the level of damage sustained by the pipe due to impact load.

Impact force: The comparison of the contact force time-histories generated during the collision/impact in case studies 1 to 4 is shown in Figure 6.5. The magnitude of the maximum contact force obtained in case study 4 (pipe vertically restrained along its whole length) is significantly higher than that predicted for the other case studies

considered [see Figure 6.5 (a)]. This can be explained by the fact that the magnitude of the generated contact force depends on the stiffness of the pipe. Considering that the pipe is vertically restrained (at the base of its cross-section) along its span it is logical to expect that its stiffness will be higher than that of the other case studies thus resulting in a higher contact force being generated. However the magnitude of the contact force significantly reduces when the pipe is assumed to rest on a soil bed (modelled as elastic foundation). When considering the pipe ends to be restrained vertically (case study 1), fully fixed (case study 2) and free (case study 3), it is observed that the pipe with free end exhibited a lower magnitude of the maximum contact force as its stiffness is lower than that of the other case studies considered [see Figure 6.5 (b)].

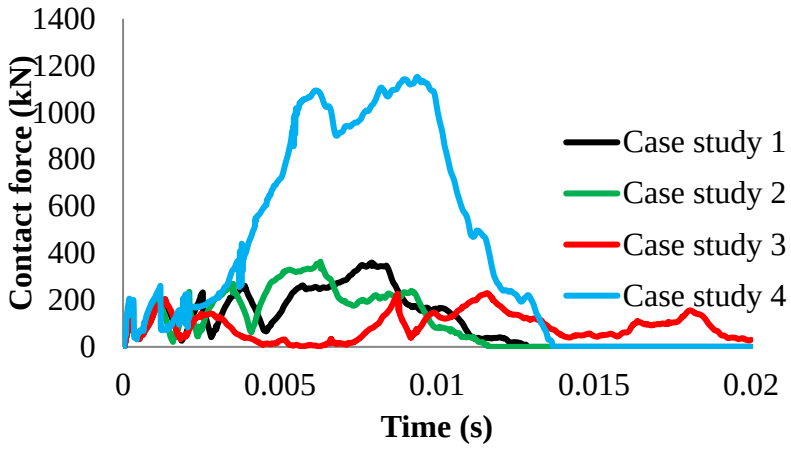

(a)

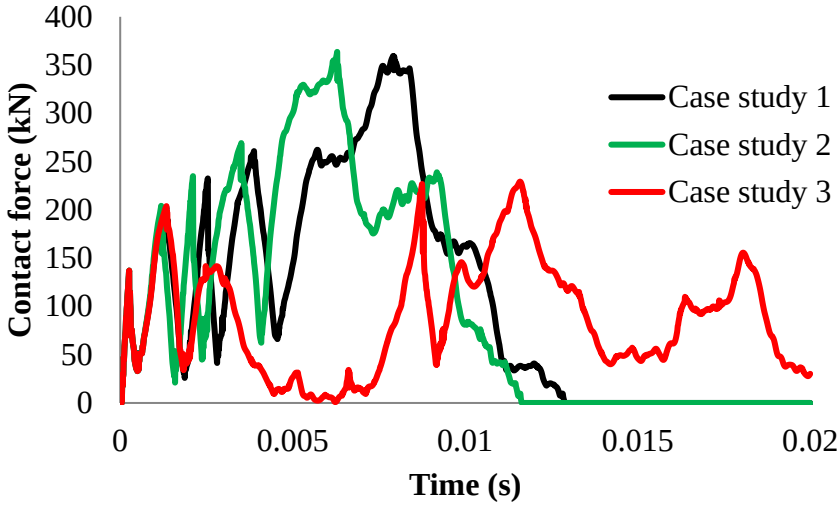

(b)

Figure 6.5: Comparison of the contact force time histories with different end conditions for case studies (a) 1 to 4 and (b) 1 to 3.

Damage sustained: The reduction in the diameter along the length of the pipes after impact (permanent deformation) for case studies 1 to 4 is shown in Figure 6.6. In general it is observed that irrespective of the end conditions used, the maximum reduction in the diameter of the pipe is observed at the impact area. This reduction in diameter decreases rapidly as one moves away from the impact zone. It is also observed that the pipe with its end being vertically restrained (case study 1) and free (case study 3) exhibit more global deformation compared to the pipes with fixed ends (case study 2) the latter exhibiting however higher levels of local damage in the impact region. This can be also seen in Figure 6.7 to Figure 6.9 which shows the deformed profile of the pipes after impact. When considering the pipes with free ends (case studies 3 & 4), it is observed that the pipe in case study 4 (restrained vertically along its length) exhibits a larger reduction in the diameter and less global deformation along its length (see Figure 6.6, Figure 6.9 and Figure 6.10). This can be explained by the fact that the pipe vertically restrained (at the base of its cross-section) has higher stiffness thus resulting in a more localized response.

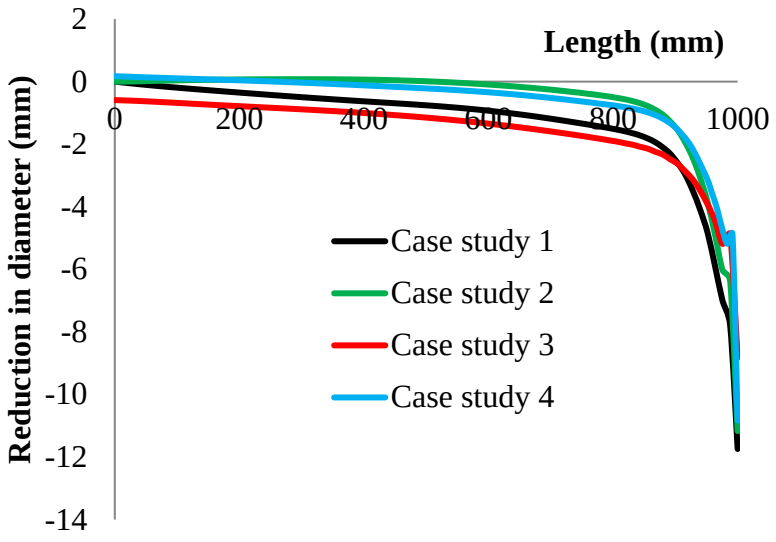

Figure 6.6: Comparison of the reduction in the diameter along the length of the pipe for different end conditions.

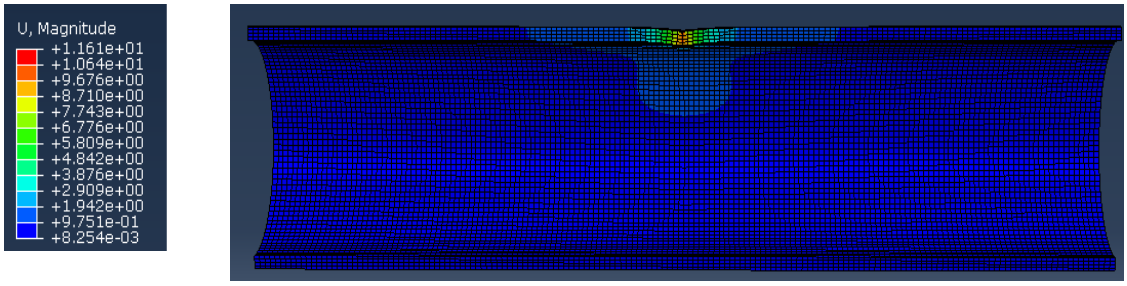

Figure 6.7: Permanent deformation (values expressed in mm) exhibited along the length of the pipe for case study 1.

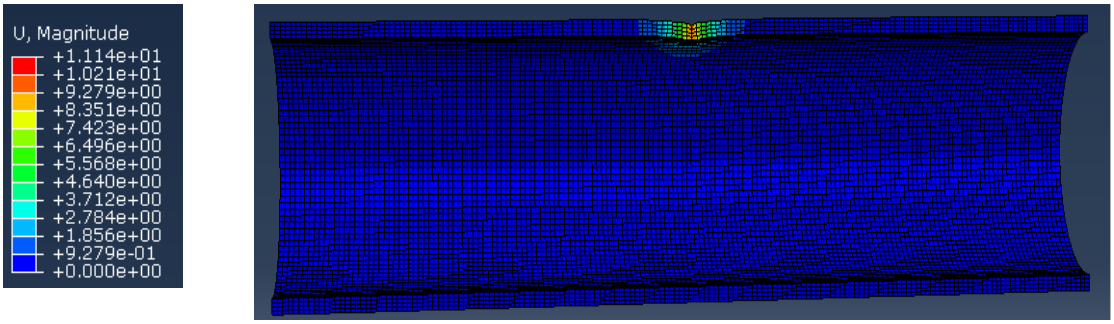

Figure 6.8: Permanent deformation (values expressed in mm) exhibited along the length of the pipe for case study 2.

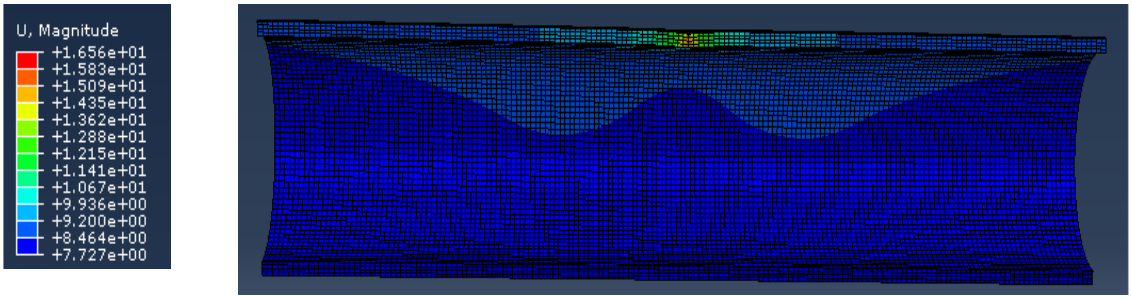

Figure 6.9: Permanent deformation (values expressed in mm) exhibited along the length of the pipe for case study 3.

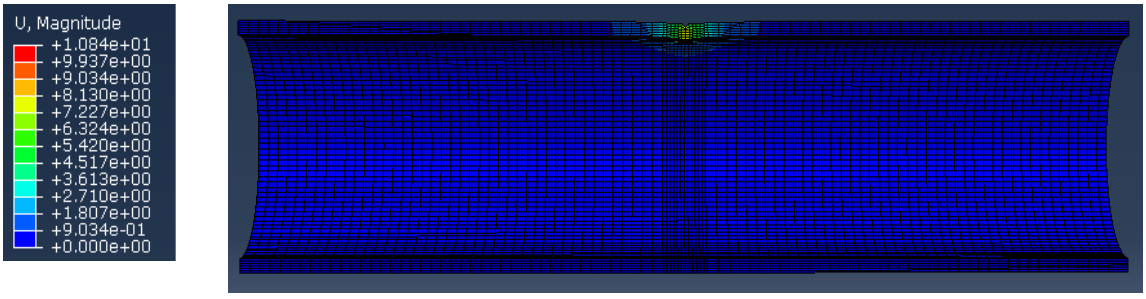

Figure 6.10: Permanent deformation (values expressed in mm) exhibited along the length of the pipe for case study 4.

The reduction in the diameter (R) of the pipes exhibited in the region at which impact occurs is shown in Figure 6.11. The maximum reduction in the diameter of the pipe is observed for the case of pipes with its ends vertically (without axial) restrained (case study 1) and fully fixed (case studies 1& 2 respectively). This can be explained by the fact that they exhibited higher stiffness thus resulting in a more localized response and resulting in larger reduction in the diameter. It appears that end conditions used in case study 1 and case study 2 does not appear to influence the damage caused to the pipe locally as similar reduction in the diameter is observed in the region where impact occurs. It is also observed that the pipe with free ends (case study 3) exhibited the lowest reduction in diameter (due to its lower stiffness) compared to other case studies considered.

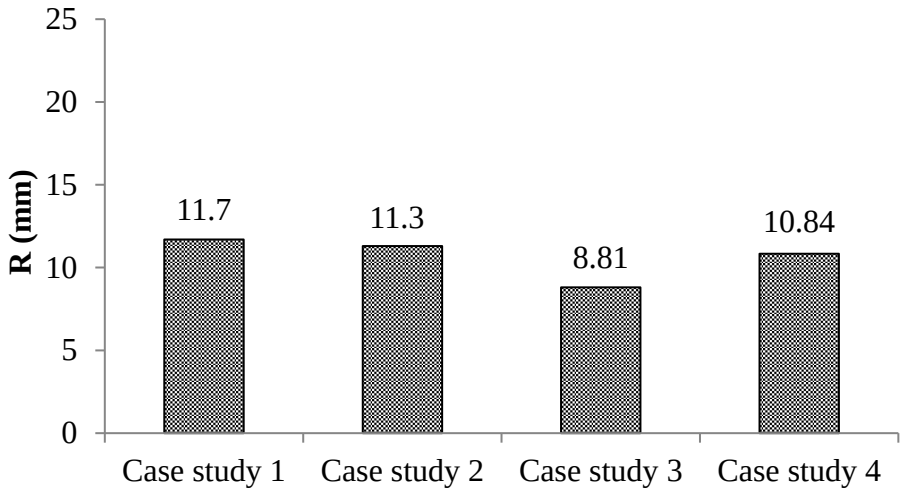

Figure 6.11: Comparison of the reduction in diameter (R) of the pipes in the impact zone for different case studies.

As discussed in Chapter 2 the level of damage sustained by the pipe is usually assessed in practice on the basis of the diameter reduction [DNV (2010b)] exhibited due to impact. DNV-RP-F107 [DNV (2010b)] classifies the level of damage sustained by pipelines into five different categories based on the reduction in diameter to diameter ratio (*R/D*) presented in Table 2.10. Figure 6.12 shows the *R/D* ratios predicted by

NLFEA for pipes with different end conditions along with the damage classifications [DNV (2010b)]. It can be seen that the damages caused to the pipe with different end conditions lie in the minor damage category [DNV (2010b)] as *R/D* is less than 5% (for detailed description of damage categories see Table 2.10).

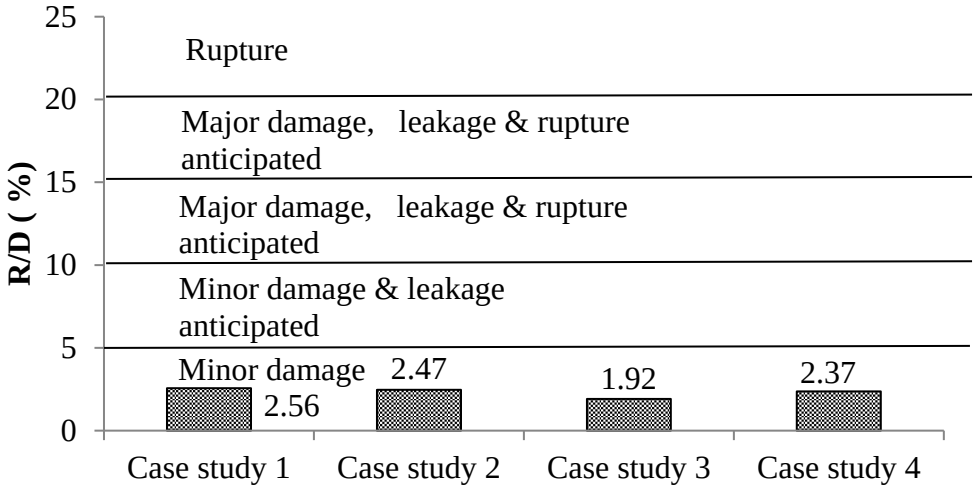

Figure 6.12: Reduction in diameter to diameter (R/D) ratios for pipes with different end conditions.

6.3 EFFECT OF LENGTH

In order to determine the sufficient length (L) of pipe for which the response to impact remains unaffected by the support conditions imposed at its end, the following case studies are investigated numerically:

- Case study L-1 : L = 2000mm, impact energy = 16kJ
- Case study L-2 : L = 4000mm, impact energy = 16kJ
- Case study L-3 : L = 6000mm, impact energy = 16kJ
- Case study L-1a : L = 2000mm, impact energy = 67kJ
- Case study L-2a : L = 4000mm, impact energy = 67kJ
- Case study L-3a : L = 6000mm, impact energy = 67kJ

The pipe is considered to be laid on an elastic foundation (see Figure 6.4) with vertical stiffness (K_v) of 9990kN/m/m. This stiffness of elastic foundation is associated with stiff and very stiff clay (see Table 6.1). As discussed in Chapter 2, the impact loads generated during the collision of equipment used in trawl fishing onto subsea pipes results in high mass low velocity impacts. The masses used for the similar cases vary between 2 and 9 tonnes. Therefore in this parametric study masses of 2.2 and 9 tonnes are used producing impact energies of 16kJ and 67kJ respectively. A sharp impactor is allowed to drop on the mid-span region of the pipe and a quarter model is used with the same cross-section and material properties of the pipe and the impactor as described in Chapter 5 (see Figure 5.20 & Table 5.3 in section 5.4). In all cases considered herein the pipe is assumed to be fixed (clamped) at both ends.

Figure 6.13 shows the comparison of the reduction in the diameter exhibited along the length of the pipes. It is observed that the length of 4000mm for the pipe considered herein is sufficient to ensure that the behaviour of the pipe is not influenced by the end conditions as a similar reduction in the diameter is observed in the impact zone for case studies *L-2* & *L-3* and case studies *L-2a* & *L-3a* respectively.

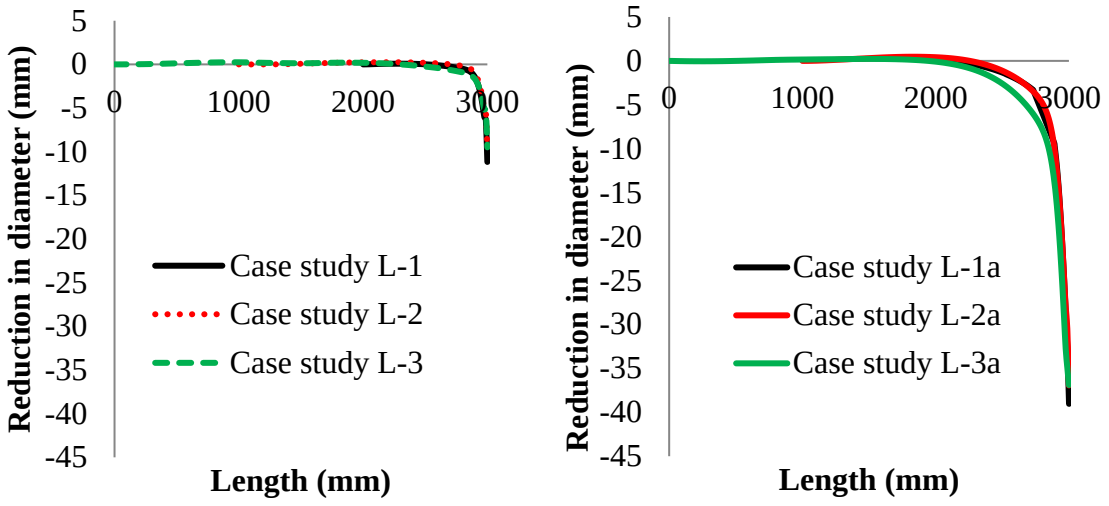

(a) (b)

Figure 6.13: Comparison of the reduction in diameter along the length of the pipe for the case of the pipes impacted with impact energies of (a) 16kJ (b) 67kJ.

Figure 6.14 (a) shows the variation of the reduction in the diameter (R) in the region at which impact occurs, whereas, Figure 6.14 (b) shows the variation of reduction in diameter to diameter ratio (R/D) with increasing lengths of the pipes along with the damage classifications [DNV (2010b)] respectively. It is observed that, irrespective of the length of the pipe used in this investigation, the damage caused to the pipe due to impact energies of 16kJ and 67kJ is minor [DNV (2010b)]. However, the damage caused to the pipe due to impact energies of 67kJ may result in release of hydrocarbons [see Figure 6.14 (b)] and will require repair. The result in Figure 6.14 also reveals that beyond 4000mm in the length of the specimen, the reduction in the pipe diameter may not be significantly affected. It is also observed that smaller length is associated with localized damage resulting in higher reduction in the diameter of the pipe as it exhibits a higher stiffness.

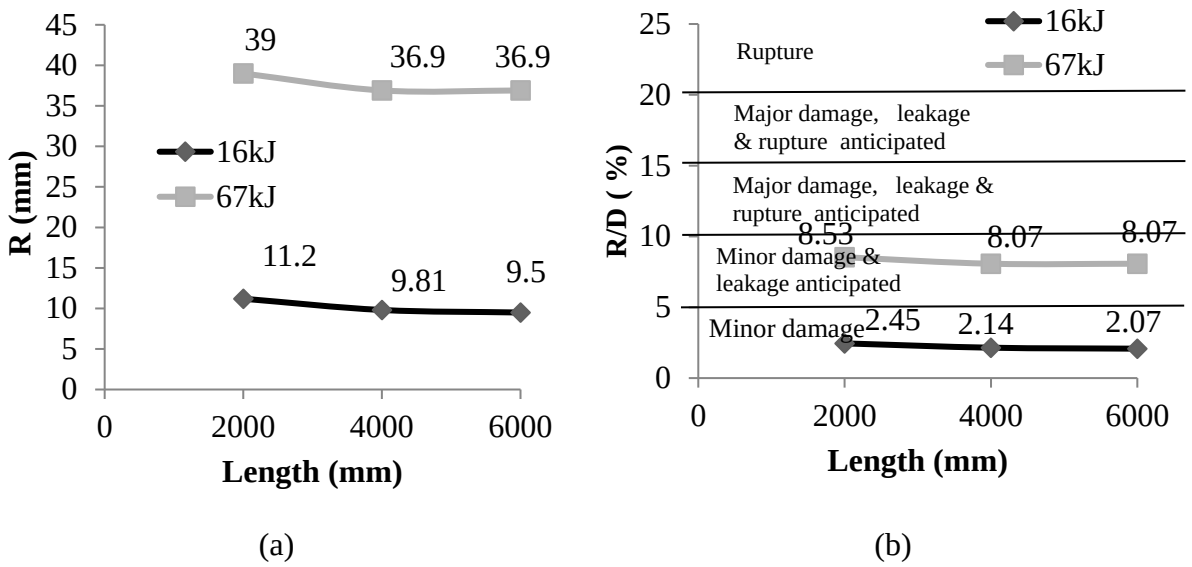

(a) (b)

Figure 6.14: (a) Variation of reduction in diameter (*R*) and (b) reduction in diameter to diameter (*R/D*) ratios with different lengths of the pipes.

6.4 EFFECT OF SOIL BED

Subsea pipes are usually laid on the seabed. Its stiffness depends on the subsea soil conditions where the pipeline is laid. In order to investigate the effect of the latter on the impact behaviour of the pipes, the following five case studies are investigated:

- Case study SB-1: Pipe laid on a rigid base (e.g. rock).

- Case study SB-2: Suspended pipe (e.g. part of the pipe length may be suspended due to soil erosion).
- Case study SB-3: Pipe laid on low stiffness soil.
- Case study SB-4: Pipe laid on medium stiffness soil.
- Case study SB-5: Pipe laid on high stiffness soil.

In this parametric study a sharp impactor is allowed to drop on the mid-span region of the pipe with impact energy of 16kJ as used in drop weight testing discussed in Chapter 5. A quarter model is employed which adopts same cross-sectional and material properties of the pipe and the impactor as used in the *NLFEA* in section 6.3. It was observed in section 6.3 that the 6000mm length of pipe is sufficient to ensure that the behaviour of the pipe is not influenced by the end conditions during impact. Therefore in this investigation, pipes fully fixed at both ends with a length of 6000mm are used. The same *FE* model discussed in section 6.2 is adopted. For the case of the pipe laid on a rigid (e.g. rock) surface (case study SB-1), the base of the pipe is assumed to be fully restrained along the vertical axis.

Due to erosion (resulting from underwater currents) of the supporting soil on which pipe is laid, the pipe for that particular length becomes essentially suspended and as a result the pipe will be partly unsupported (see Figure 6.15). Therefore case study *SB-2* is carried out for the case of a suspended pipe.

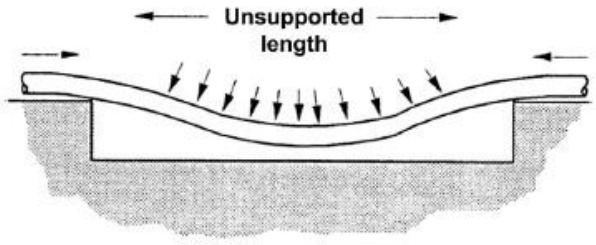

Figure 6.15: Unsupported length of the pipe [Bai & Bai (2014)].

Table 6.2 gives the values of the soil stiffness calculated based on Eq. (6.1) [DNV (2006)]. Based on the soil classification adopted by the latter code the values of soil

stiffness of 450kN/m/m, 13140kN/m/m and 21600kN/m/m are used which are associated with low (case study SB-3), medium (case study SB-4) and high (case study SB-5) stiffness soils respectively.

Figure 6.16 shows the reduction of the diameter exhibited after impact along the length of the pipe, for the different soil conditions considered. Figure 6.17 shows the comparison of the deformation profile (local and global displacement) of top and bottom surface along the length of the pipe for the above conditions. It is observed that as the stiffness of the subsea soil (and therefore the stiffness of the system) decreases, the maximum reduction in the diameter close to the impact region also decreases. This can also be explained from Figure 6.17, which shows that the global behaviour exhibited by the pipes laid on rigid base (case study SB-1) and high stiffness soil (case study SB-5) is significantly less [see Figure 6.16 (a) & Figure 6.17 (a)] compared to pipes laid on low stiffness soils. However, higher levels of localized damage are sustained by the pipes for the cases of rigid base (case study SB-1) and high stiffness soil (case study SB-5). Thus with the increase in the soil stiffness the impact energy is absorbed more locally through the permanent deformation (level of damage) sustained by the pipes cross-section at the area of the impact. It is also observed that as the stiffness of the supporting soil decreases, the level of damage sustained along the length of the pipe increases thus allowing impact energy to be absorbed along a larger length of the pipe.

Table 6.2: Stiffness of different types of soils.

Soil Type	**C_v (kN/m$^{5/2}$)**	**υ**	**ρ_s/ρ**	**D (m)**	**K_v (kN/m/m)**
Sand					
Loose	10500	0.35	2	0.457	18200.48
Medium	14500	0.35	2	0.457	25133.99
Dense	21000	0.35	2	0.457	36400.96
Clay					
Very soft	600	0.45	1.2	0.457	835.80
Soft	1400	0.45	2	0.457	2867.95
Firm	3000	0.45	2	0.457	6145.61
Stiff	4500	0.45	2	0.457	9218.42
Very Stiff	11000	0.45	2	0.457	22533.93
Hard	12000	0.45	2	0.457	24582.46

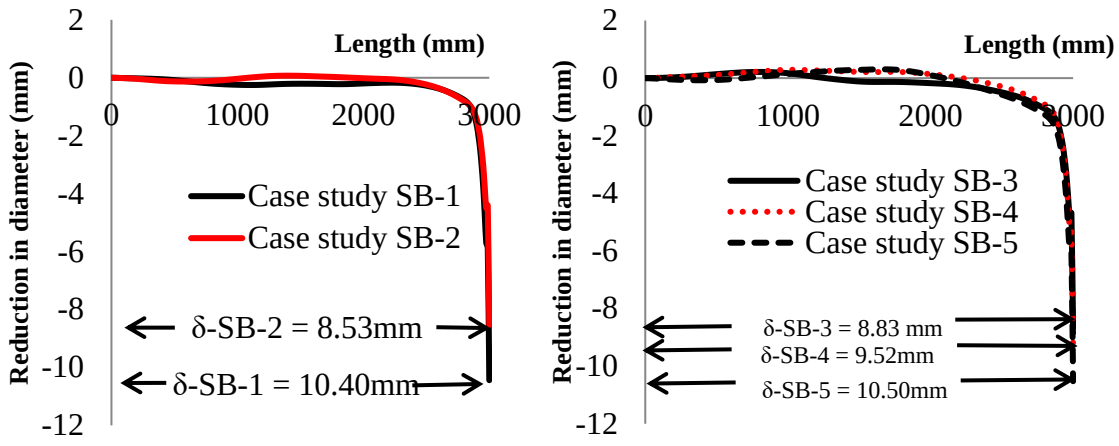

(a) (b)

Figure 6.16: Comparison of reduction in pipe diameter exhibited along the length of the pipe for case studies (a) *SB-1* & *SB-2* (b) *SB-3*, *SB-4* & *SB-5*.

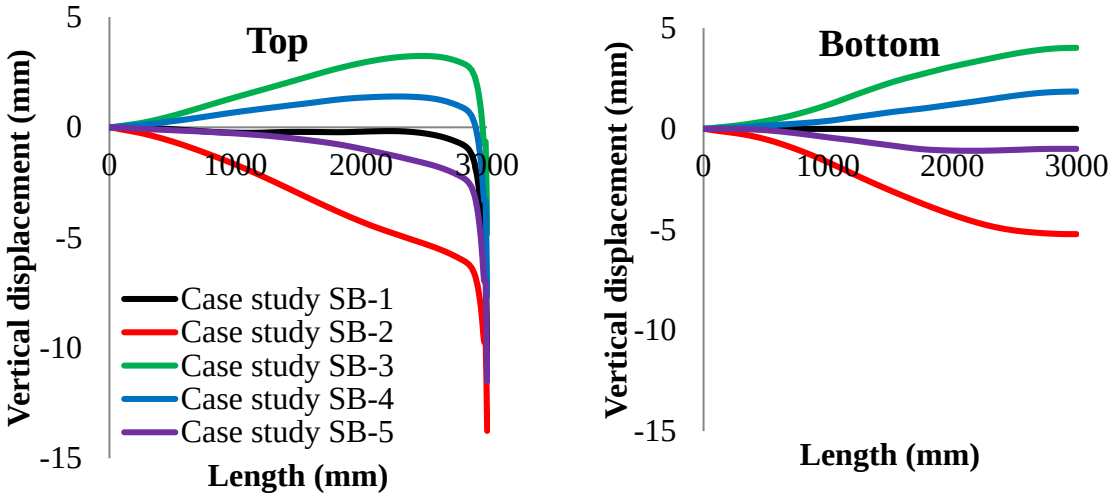

(a) (b)

Figure 6.17: Comparison of deformation profile exhibited (a) on the top profile and (b) bottom of the pipe cross-section for the different case studies considered.

Figure 6.18 shows the comparison of the contact force time-histories exhibited when the pipes are laid on soil with different stiffnesses. It is observed that as the stiffness of the soil increases, the maximum value of the contact force also increases. It is also observed that with the decreasing values of the soil stiffness, the duration of the impact increases. This can also be observed in Figure 6.19 (a) and (b), which shows the total vertical displacement time-histories of the pipe measured at mid-length of the pipe

(centre of impact region), and vertical velocity time-histories of the impactor measured at the centre of the impactor respectively. The latter figures revealed that the total vertical displacement (local and global displacement) and vertical velocity time-histories are very similar up to time t = 0.004s. However, during impact, the suspended pipe (case study SB-2) and the pipe laid on low stiffness soil (case study SB-3) deform more globally, compared to those supported on stiffer soils. This results in an increase of the duration of impact [see Figure 6.19 (a)] and in a reduction of the rate at which the velocity of the impactor reduces [see Figure 6.19 (b)].

Figure 6.20, (a) and (b), shows the reduction of diameter (R) in the impact region and reduction in diameter to diameter ratios (R/D*)* for the case of the suspended pipe (case study SB-2) and the pipe laid on rigid stiffness soil (case study SB-1). Figure 6.21, (a) and (b), shows the *R* and *R/D* ratios for pipes laid on soil with different stiffnesses. It can be seen that the damage caused to the pipe laid on different soil conditions lie in the minor damage category [DNV (2010b)] as the ratio *R/D* is less than 5%. Therefore the damage caused to the pipes laid on different types of soil beds considered in this investigation and impacted with 16kJ is not severe and therefore would not require immediate action for repair. However, a trend in the reduction of the diameter is observed [see Figure 6.20 (a) and Figure 6.21(a)] which show that as the stiffness of the subsea soil increases, the maximum reduction in the diameter also increases.

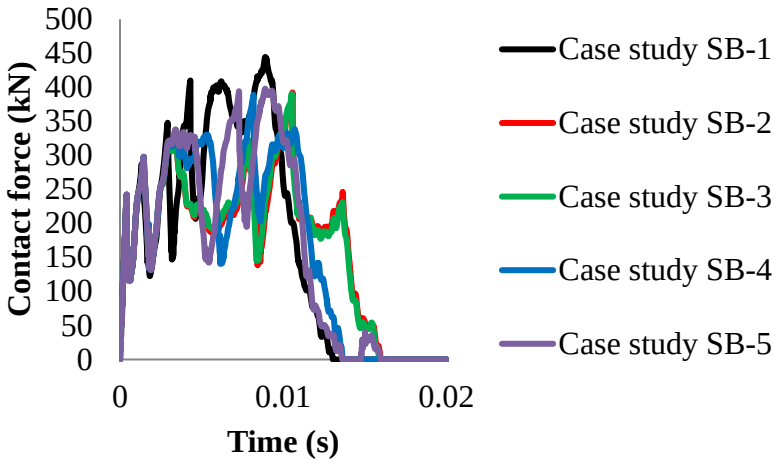

Figure 6.18: Comparison of contact force time-histories for pipes laid on different subsea soil conditions.

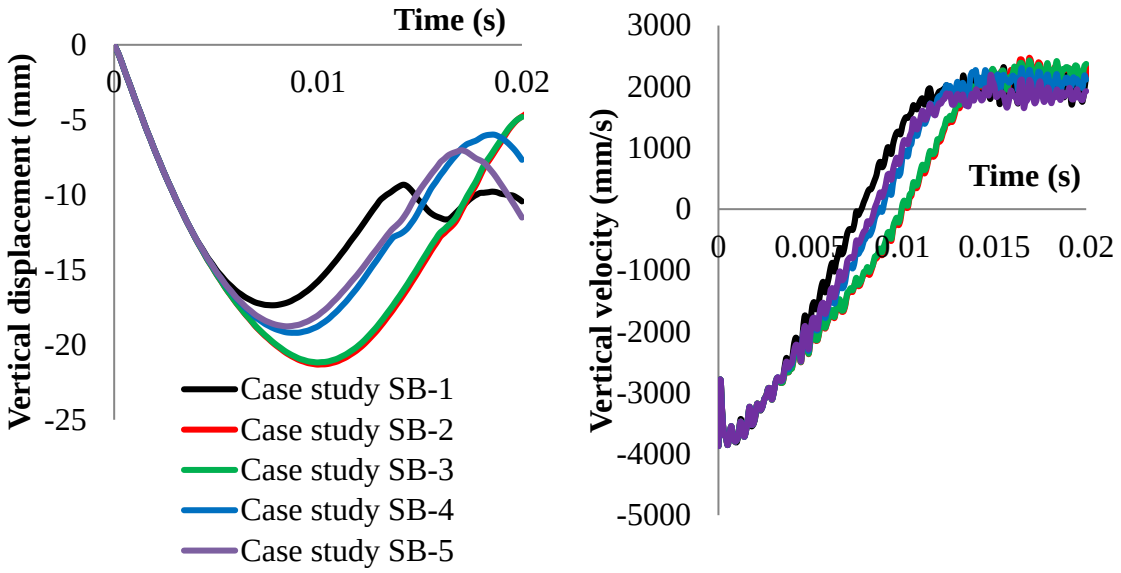

(a) (b)

Figure 6.19: (a) Vertical displacement (b) vertical velocity time-histories for the different case studies considered.

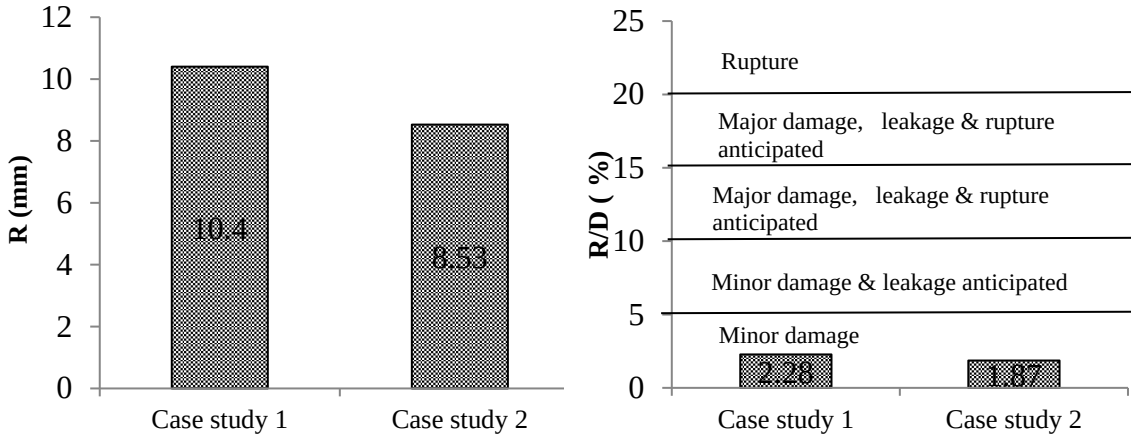

(a) (b)

Figure 6.20: (a) Reduction in diameter (R) and (b) reduction in diameter to diameter (R/D) ratios for pipe laid on rigid stiffness (case study SB-1) and suspended pipe (case study SB-2).

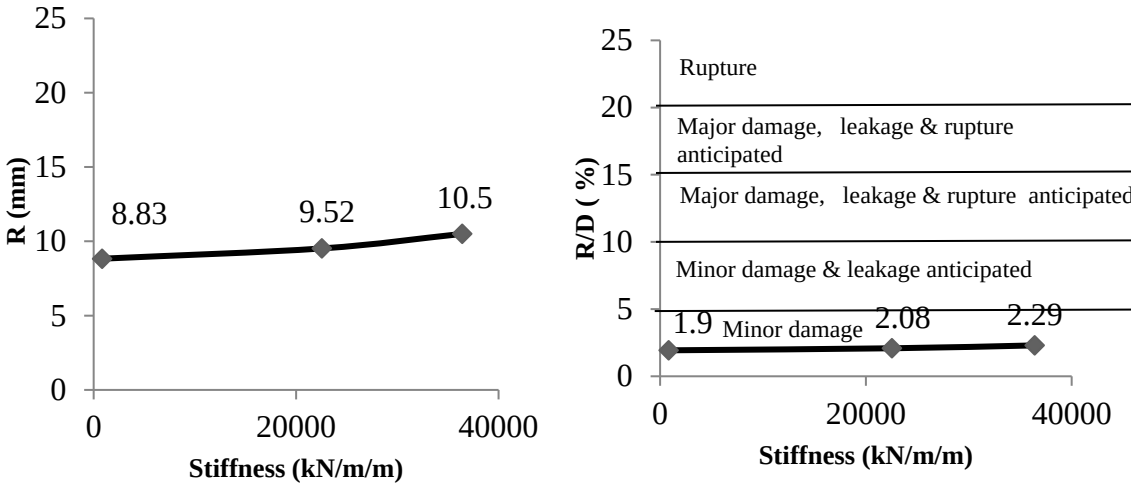

(a) (b)

Figure 6.21: (a) Reduction in diameter (R) and (b) reduction in diameter to diameter (R/D) ratios for pipe with different stiffness of soils.

6.5 EFFECT OF AXIAL LOAD

The American Bureau of Shipping [ABS (2001)] provides guidance for safeguarding the structural integrity against axial forces acting along the span of the pipe given by Eq. (2.5). A similar approach is used by the American Petroleum Institute [API (1999)] expressed by a design criteria given by Eq. (2.15).

Based on the review of the above design codes it can be observed that the development of the axial stresses can influence significantly the design criteria. Therefore it is logical to assume that the axial stress can affect the *in-situ* behaviour of the subsea pipes under impact. In order to investigate this effect the following five case studies are investigated considering the effect of different levels of axial loadings (N) expressed as percentage (%) of the yield stress of steel (from which pipes are constructed) on the behaviour of steel pipes under impact:

- Case study A-1: No axial load
- Case study A-2: Axial loading resulting in the development of axial compressive stresses equal to 10% of yield stress (σ_y)
- Case study A-3: Axial loading resulting in the development of axial compressive stresses equal to 30% of σ_y

- Case study A-4: Axial loading resulting in the development of axial compressive stresses equal to 50% of σ_y
- Case study A-5: Axial loading resulting in the development of axial tensile stresses equal to 30% of σ_y

Pipes with a length of 6000mm are used in this investigation, which are fully fixed at both ends. In this parametric study a sharp impactor is allowed to drop on the mid-span region of the pipe with impact energy of 16kJ as used in drop weight testing discussed in Chapter 5. A quarter model is again employed which adopts same cross-sectional and material properties of the pipe and the impactor used in the *NLFEA* in section 6.3. The pipes are laid on a subsea bed with a stiffness of 13140kN/m/m which is associated with medium stiffness soil.

Figure 6.22 (a) shows the comparison of the contact force time-histories exhibited by pipes subjected to different levels of axial loading. It is observed that increasing the values of the compressive axial loading results in a reduction of the values of the magnitude of the maximum contact force generated during impact. It is observed that the contact force time histories of the pipe with axial compressive loading of up to 30% are similar to that of the pipe without axial loading. This observation is similar to the findings of the numerical predictions obtained in Chapter 4 when investigating the behaviour of the scaled pipe specimens under impact loading. However, this is not the case when axial loading results in the development of axial compressive stresses equal to 50% of σ_y (case study A-4), as the magnitude of the maximum contact force is significantly lower and the impact duration is significantly higher. The trend observed in the *NLFEA* is similar to the one observed in the experimental study of axially pre-loaded scaled tubular specimens under the lateral impact loads [Zeinoddini *et al.* (2002)] as described in Chapter 2. This can be also explained by Figure 6.23, (a) & (b), which shows the comparison of the total vertical displacement (due to local and global response) and vertical velocity time-histories of the pipe for different levels of axial loading respectively. As can be seen in Figure 6.23 (a), during impact for case study A-4 (pipe subjected to axial compressive stresses equal to 50% of σ_y), the pipe deforms more. As a result, the duration of the impact becomes longer and the rate at which the velocity of the impactor reduces during impact is lower.

Figure 6.22 (b) shows the comparison of the contact force time-histories exhibited by pipes when axial loading results in the development of axial compressive and tensile stresses equal to 30% of σ_y (case study A-3 and case study A-5 respectively). Figure 6.23, (c) & (d), shows the comparison of the total vertical displacement time history (due to local and global response) measured at the top of the pipe at its mid-span and vertical velocity time-history of the impactor for case study *A-3* and case study *A-5* respectively. It is observed that the pipe with axial tensile loading (case study A-5) result in the generation of higher peak values of the contact force, a reduced total deformation and high rebound velocity.

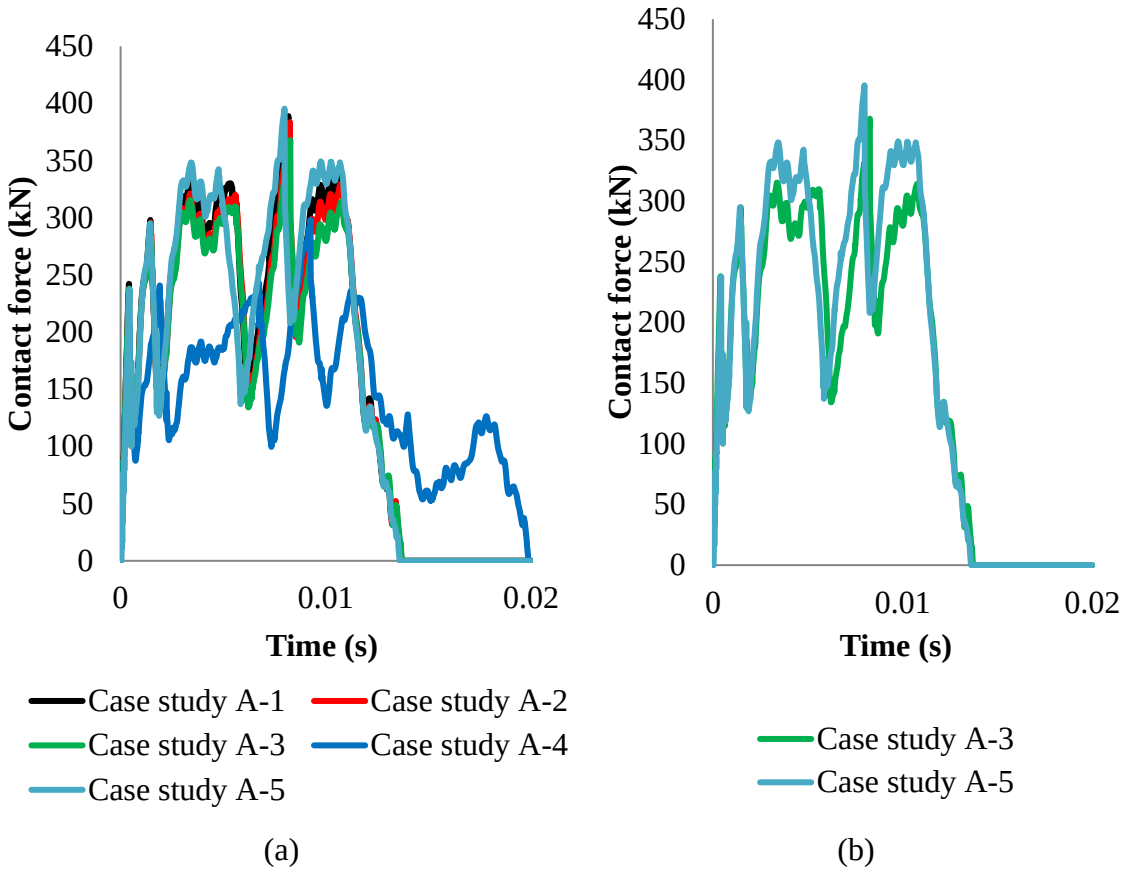

Figure 6.22: Comparison of the contact force time histories for case studies (a) A-1 to A-5 (b) A-3 & A-5.

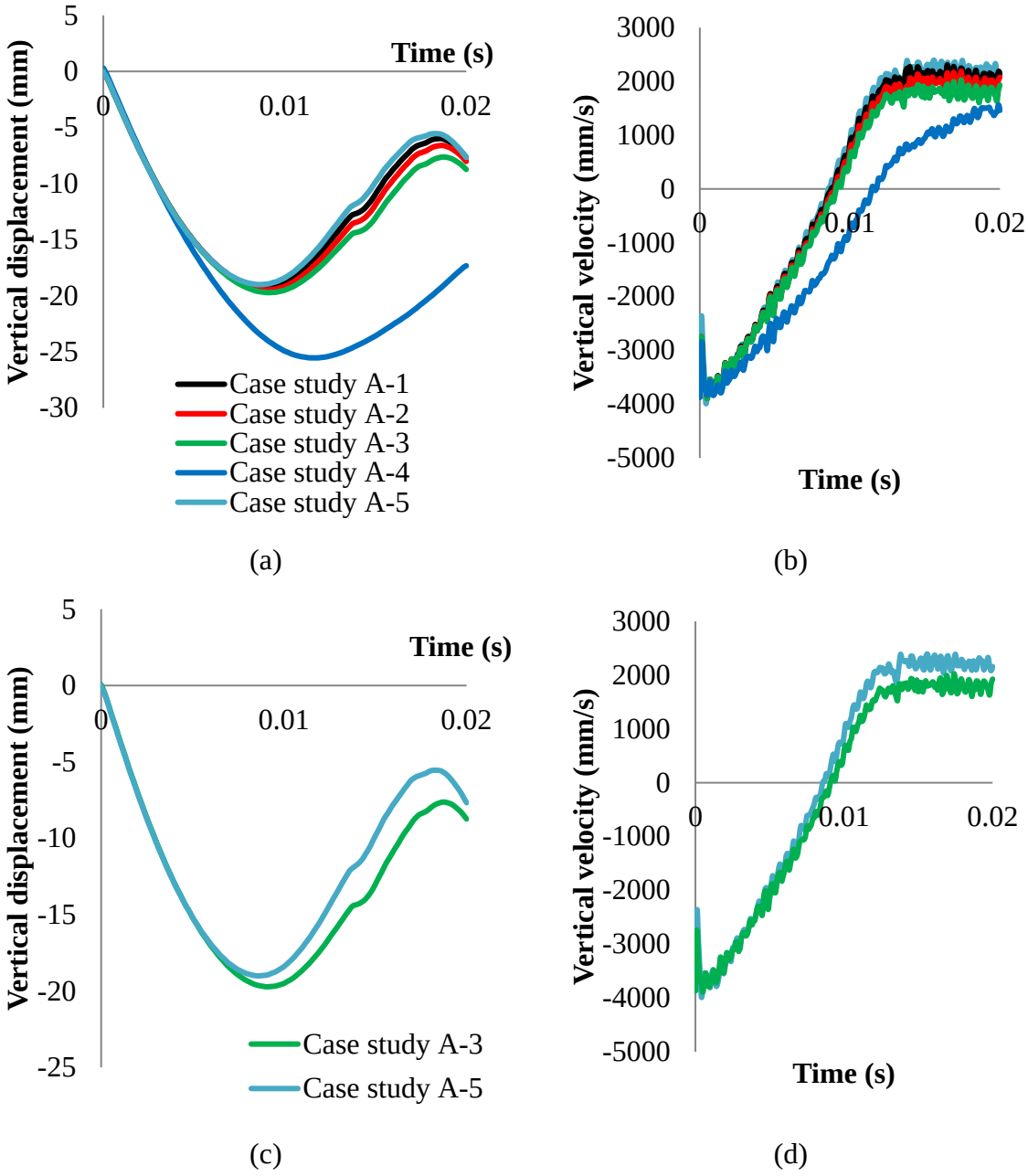

Figure 6.23: Comparison of vertical displacement and vertical velocity time-histories for case studies (a) & (b) A-1 to A-5 and (c) & (d) A-3 & A-5.

Figure 6.24 (a) shows the comparison of the reduction in the diameter along the length of the pipes subjected to different levels of axial loading. It is observed that increasing values of the axial loading results in an increase in the reduction of the diameter. It is also observed that the length of the pipe which exhibits localized damage increases with higher levels of the axial compressive loading. Figure 6.24 (b) shows the comparison of the reduction in the diameter along the length of the pipe when axial loading results in

the development of axial compressive and tensile stresses equal to 30% of σ_y (case study A-3 and case study A-5 respectively). It is observed that the pipe with axial tensile loading (case study A-5) exhibited less localized reduction of the diameter at the area of impact and whereas for the pipe subjected to axial compressive load the behaviour is influenced by the end conditions as pipe exhibits a higher global deformation along its whole length. Based on the observations of the *NLFEA* predictions it can be concluded that axial loading can have a significant effect on the *in-situ* behaviour of the subsea pipes during impact.

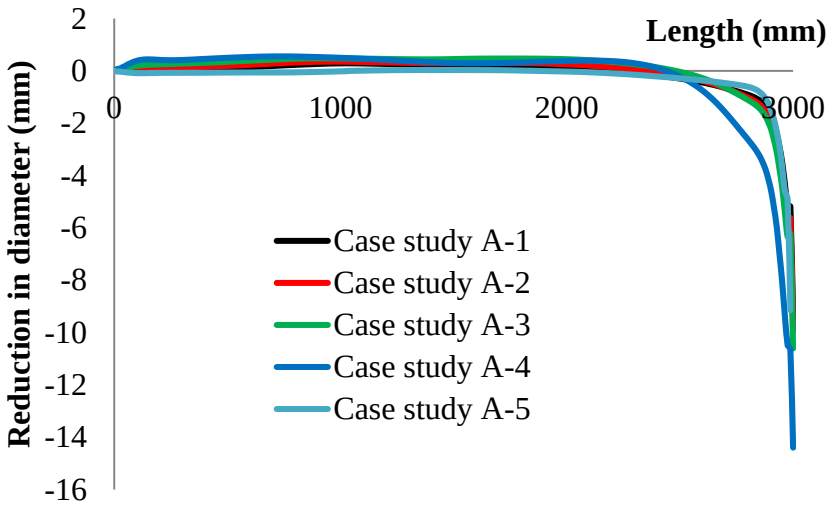

(a)

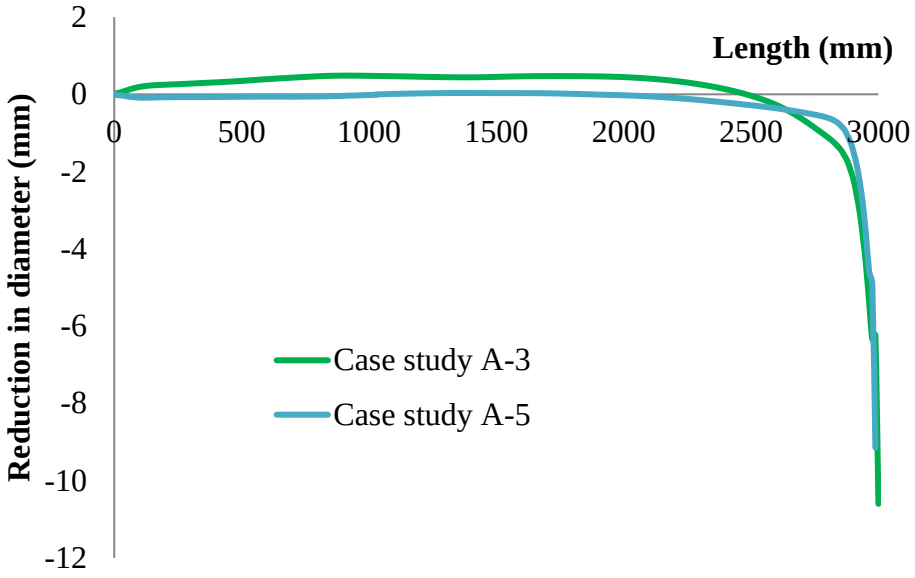

(b)

Figure 6.24: Comparison of the reduction in the diameter along the length of the pipe for case studies (a) A-1 to A-5 (b) A-3 & A-5.

Figure 6.25, (a) and (b), shows the reduction of diameter (R) in the impact zone and reduction in diameter to diameter ratios (R/D) for pipes subjected to different levels of axial loading. It can be seen that the damage caused to the pipes lie in the minor damage category [DNV (2010b)] as *R/D* is less than 5%. Therefore, the damage caused to the pipes subjected to different levels of axial loading although not severe in the present case studies, increases with increasing level of compressive axial loading and decreases with increasing level of tensile axial loading.

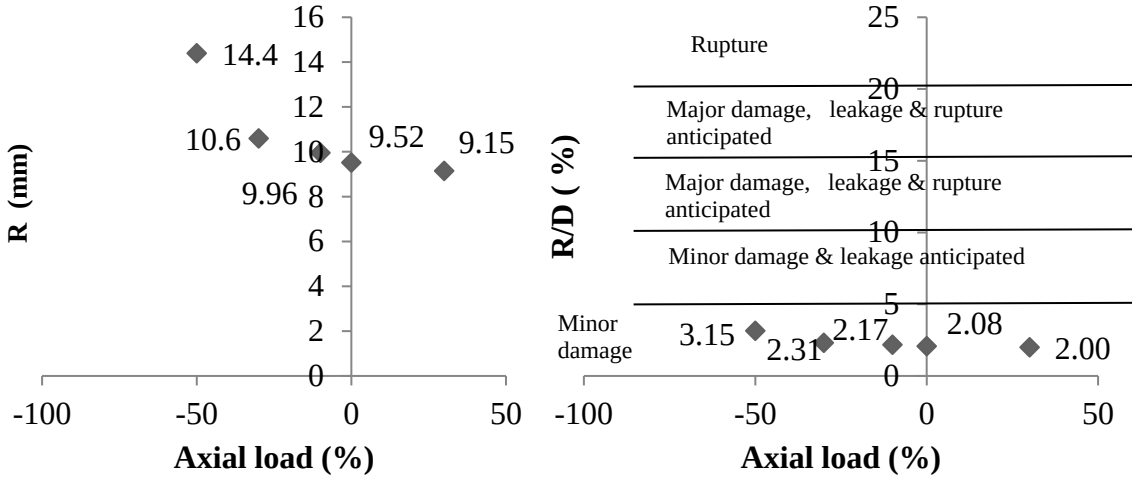

(a) (b)

Figure 6.25: (a) Reduction in diameter (R) and (b) reduction in diameter to diameter ratios (*R/D*) for pipe with increasing axial loads.

6.6 EFFECT OF PRESSURE

Subsea pipes during their operational life are subjected to internal pressure due to the oil and gas in the pipes and external (hydro-static) pressure. ABS (2001) provides provisions to design the wall thickness based on the pressure acting on the walls of the pipe and is given by Eq. (2.3). The design criterion is based on limiting the value of the hoop stress (σ_h) acting on the wall of the pipe beyond a certain level.

As discussed in Chapter 2 and presented in Appendix A, the level of internal pressure used in drop weight tests to study the behaviour of pipe specimens under impact loading varies between 6.3 and 19.31MPa. It is important to note that the typical operating pressure of offshore gas pipelines varies between 10 and 18MPa [DANS *et al.* (2001)]. Otter trawl boards [see Figure 2.1(a)] which may accidentally collide with the pipe

occurs at depth of more than 400m. Based on the latter an external pressure of 4MPa may act externally on the walls of the pipe. As a result, in order to study the effect of the differential pressure (i.e. the difference between the internal and external pressures acting on the pipe wall) on the impact behaviour of the subsea pipes, the following case studies are investigated:

- Case study P-1: Zero pressure ($\sigma_h = 0$)
- Case study P-2: σ_h = 5% of yield stress (σ_y)
- Case study P-3: σ_h = 10% σ_y
- Case study P-4: σ_h = 15% σ_y
- Case study P-5: σ_h = -5% σ_y
- Case study P-6: σ_h = -10% σ_y

Table 6.3 gives the values of the hoop stress and the pressure (internal or external) acting on the walls of the pipe. The positive pressure refers to the case when the internal pressure is higher than the external pressure and *vice versa*.

Table 6.3: Values of hoop stress and pressure acting on the walls of the pipe for the various case studies considered.

Case study	Hoop stress (MPa)	Internal or external pressure (MPa)
P-1	0	0
P-2	22.85	2.68
P-3	45.70	5.37
P-4	68.55	8.10
P-5	-22.85	-2.68
P-6	-45.70	-5.37

Pipes with a length of 6000mm are used in this investigation and are fully fixed at both ends. In this parametric study a sharp impactor is allowed to drop on the mid-span region of the pipe with impact energy of 16kJ as used in drop weight testing discussed in Chapter 5. The quarter model is employed with the same cross-sectional and material properties of the pipe and the impactor as used in the *NLFEA* in section 6.3. Pipes are

laid on a subsea bed with a stiffness of 13140kN/m/m which is associated with medium stiffness soil.

The comparison of the contact force-time histories of pipes subjected to different levels of pressures is shown in Figure 6.26. In general it is observed that for the positive pressures (case studies P-2, P-3 & P-4), the contact force time-histories are not significantly affected. However, for the case of negative pressures (case studies P-5 & P-6), the magnitude of the contact force significantly decreases compared to that generated for the case of the pipe without pressure (case study P-1).

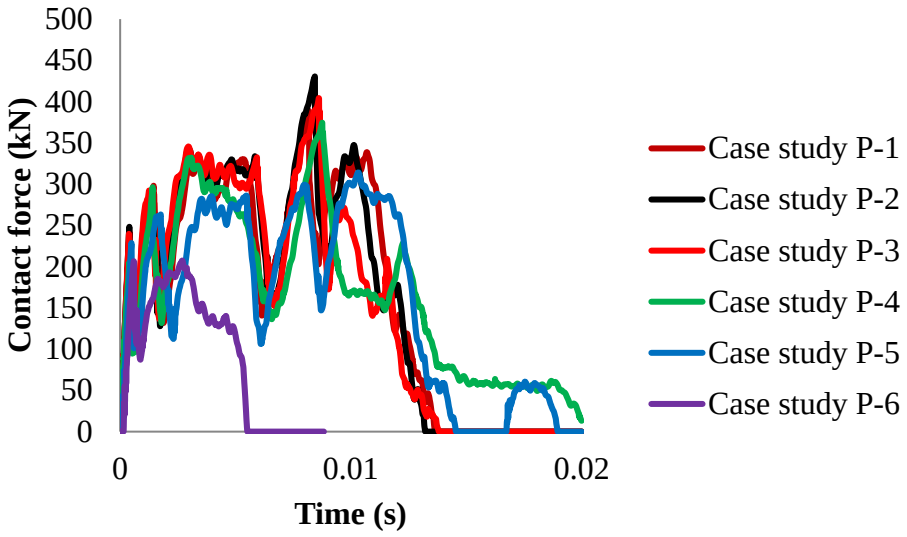

Figure 6.26: Comparison of the contact force time histories predicted for different case studies.

Figure 6.27 shows the comparison of the reduction in the diameter along the length of the pipes. It is observed that with increasing positive pressure, the localized damage exhibited in the pipe decreases and global deformation increases. This observation is confirmed experimentally [Jones & Birch (2010), Chen & Shen (1998)] (see Chapter 2) and numerically by the predictions obtained in Chapter 4 when investigating the behaviour of the scaled pipe specimens under impact loading.

The deformed profile of the pipe after impact for the case study P-6 (σ_h = -10% σ_y) is shown in Figure 6.28. It is observed that the pipe cross-section in the impact zone completely collapses. It is interesting to observe that when the pipe is subjected to positive pressure of same magnitude (case study P-3, σ_h = 10% σ_y), the cross-section does not collapse (see Figure 6.27).

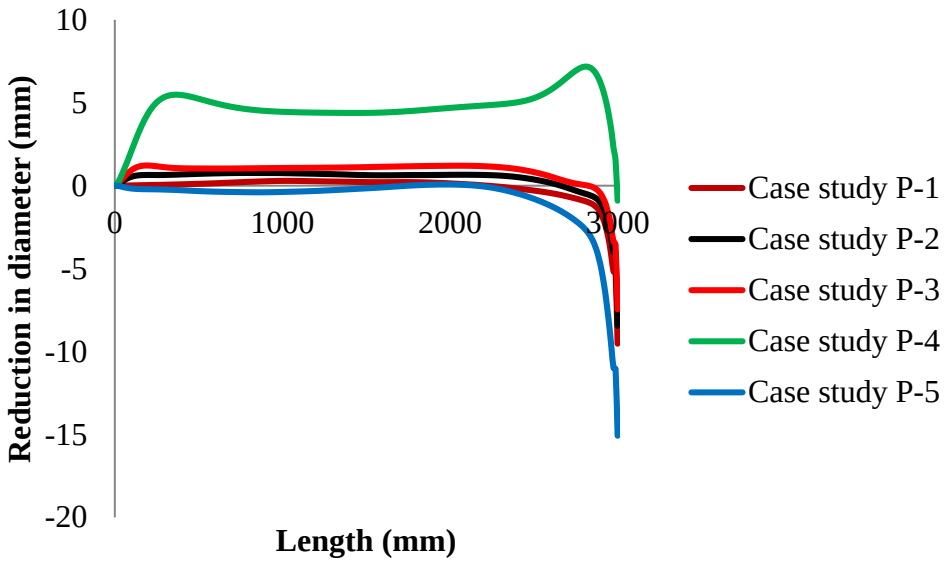

Figure 6.27: Comparison of the reduction in the diameter along the length of the pipe predicted for different case studies.

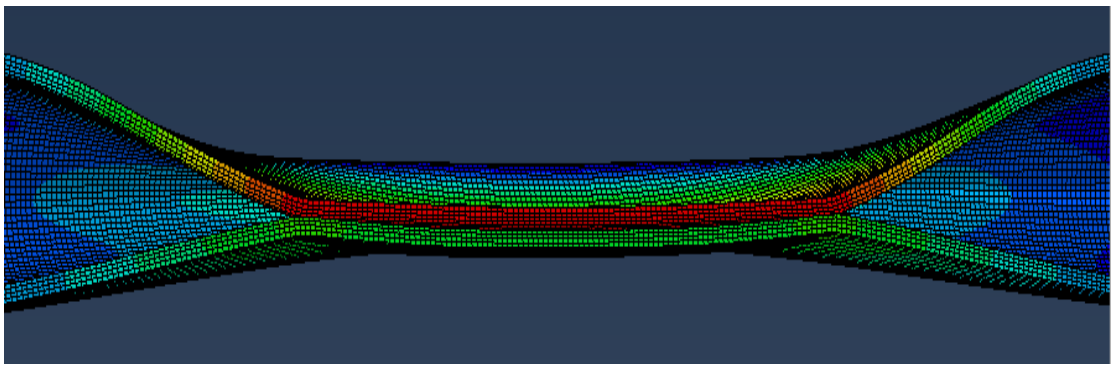

Figure 6.28: Post-impact length of the pipe for case study *P-6*.

Figure 6.29, (a) and (b), shows the reduction of pipes diameter (R) at the area of impact and the reduction in diameter to diameter ratios (R/D) for pipes subjected to increasing positive pressures, whereas, Figure 6.30, (a) and (b), shows the same quantities for increasing negative pressures. It is observed that with the increase in the positive pressure, the damage caused to the pipe locally at the impact region decreases. However, for the case of the negative pressure, the increase in the value of applied pressure results in an increase of the damage sustained locally in the impact region during impact. It can be seen that the damage caused to the pipes lie in the minor damage category when considering pipes with positive pressures. It is also observed that for the case of pipe subjected to the increasing external (negative) pressure the damage caused to the pipe locally in the impact region increases compared to its counterpart for the case of pipe subjected to same magnitude of internal (positive) pressure. It is observed that for the case of pipe subjected to a negative pressure of σ_h = -10% σ_y (case study P-6) the pipe cross-section completely collapse (rupture).

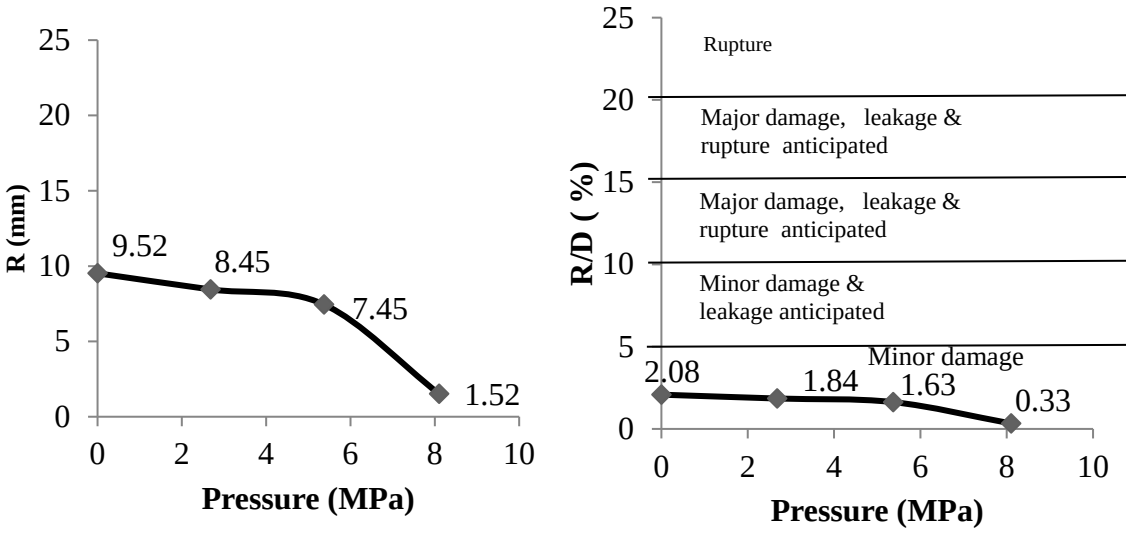

(a) (b)

Figure 6.29: (a) Reduction in diameter (R) and (b) reduction in diameter to diameter ratios (R/D) for pipe with increasing positive pressure.

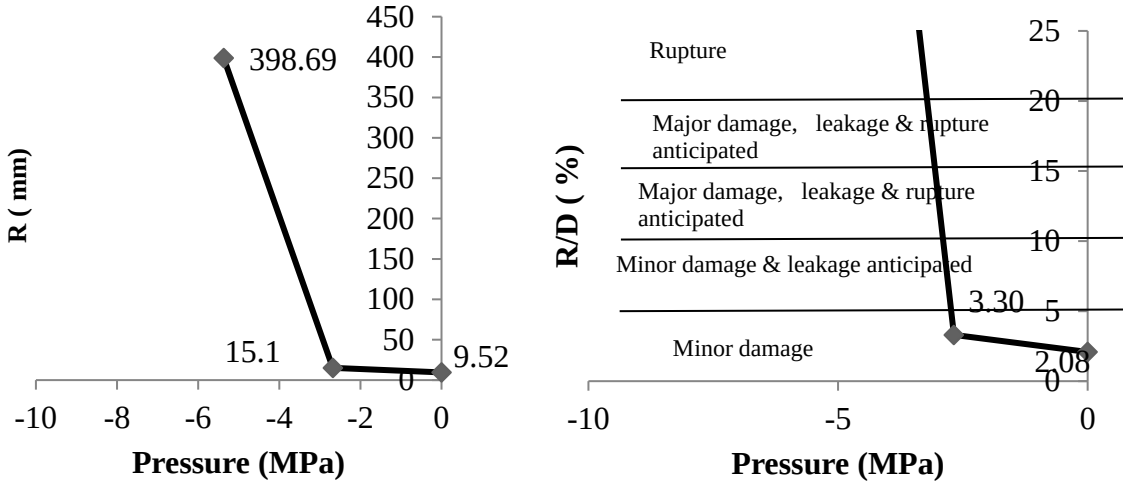

(a) (b)

Figure 6.30: (a) Reduction in diameter and (b) reduction in diameter to diameter ratios (*R/D*) for pipe with increasing negative pressure.

6.7 EFFECT OF IMPACT ENERGY

As discussed in Chapter 2, impact loads are generated during the collision of equipment used in trawl fishing onto subsea pipes. Such equipment [see Figure 2.1] often includes (i) otter trawl boards, (ii) transverse steel beams (used in beam trawling) and (iii) clump weights (detailed discussion is given in Chapter 2). Among the latter three objects the clump weights used in the case of twin trawling with a mass ranging between 2 and 9 tonnes may result in collisions with pipelines characterised by higher impact energies compared to those associated with the case of trawl boards and beam trawls [DNV (2010a)].

In order to study the influence of the level of impact energy on the behaviour of the subsea pipes under impact loads, case studies with masses of the object colliding onto the pipe ranging between 2.2 and 9 tonnes producing impact energies of 16 to 67kJ are investigated. The details of these case studies are shown in Table 6.4.

Pipes with a length of 6000mm are used in this investigation and are fully fixed at both ends. In this parametric study a sharp impactor is allowed to drop on the mid-span region of the pipe with impact energy of 16kJ as used in drop weight testing discussed in Chapter 5. A quarter model is employed which adopts same cross-sectional and material properties of the pipe and the impactor as used in the *NLFEA* in section 6.3.

Pipes are laid on a subsea bed with a stiffness of 13140kN/m/m which is associated with medium stiffness soil.

Table 6.4: Data describing the details of mass, velocities and impact energies used in the investigation.

Case study	Mass (tonnes)	Velocity (m/s)	Impact energy (kJ)
I-1	2.2	3.87	16
I-2	4.0	3.87	30
I-3	6.0	3.87	45
I-4	9.0	3.87	67

Figure 6.31 shows the comparison of the contact force time histories generated during collisions characterises by increasing impact energies. In general it is observed that with the increase in the impact energy, the magnitude of the maximum contact force generated and the impact duration also increases. This can be also observed in the case of Figure 6.32, which shows the velocity time histories of the impactors when colliding with the pipe with increasing impact energies. It is observed that with the increase in the impact energy the rate at which the value of velocity reduces become smaller. Furthermore, the rebound velocity of the impactor after the initial contact also decreases. As a result for increasing levels of impact energy (achieved due to use of heavier drop weights) a larger level of energy is absorbed by the pipe (through plastic deformation of cross-section).

Figure 6.33 (a) shows the comparison of the maximum contact force with increasing impact energies as described for the test data presented in Appendix A and Figure 6.33 (b) shows same relationship for the case studies (I-1, I-2, I-3 & I-4) currently considered. As already discussed in Chapter 2, the test data in Appendix A is obtained from scaled pipe specimens subjected to smaller impact energies, therefore it is difficult to draw relationship between both sets of data. However, it is observed that with the increase in the impact energy the magnitude of the maximum impact force also increases.

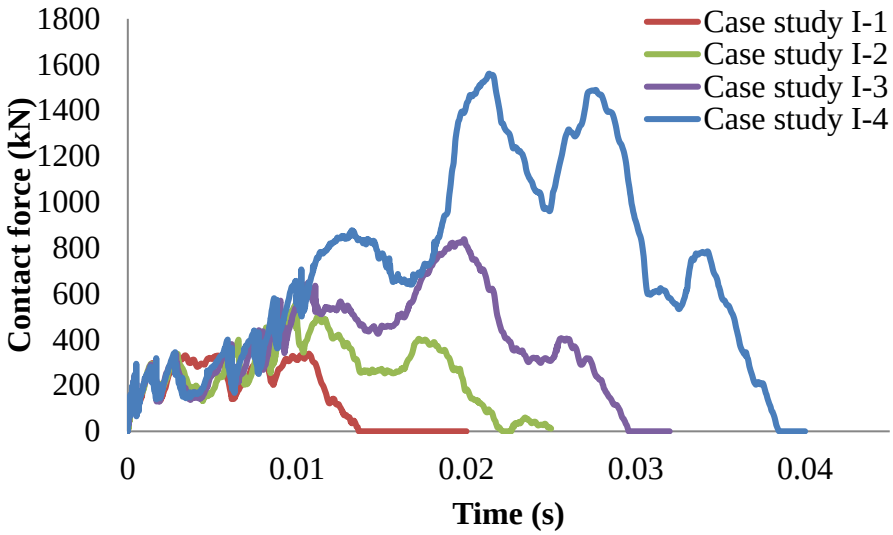

Figure 6.31: Comparison of the impact force time histories with different impact energies.

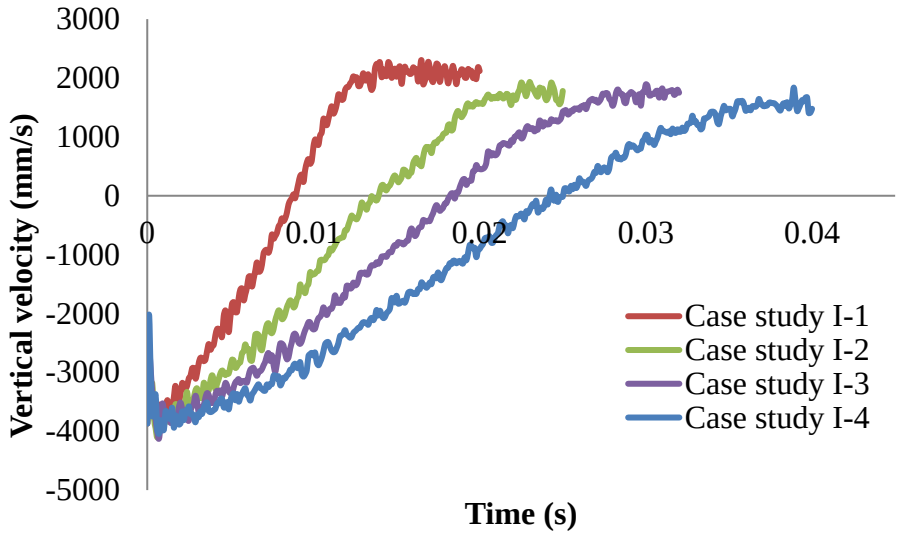

Figure 6.32: Comparison of the velocity time histories with different impact energies.

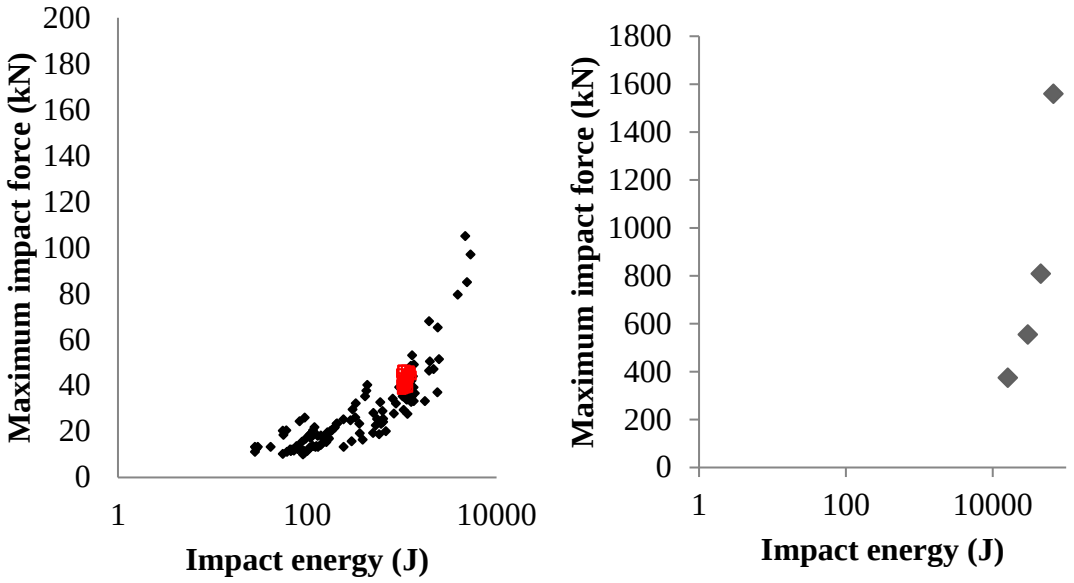

(a) (b)

Figure 6.33: Variation of maximum impact force with increasing impact energies (a) database (Appendix-A) (b) current case studies.

Figure 6.34 shows the comparison of the reduction in the diameter exhibited along the length of the pipe when subjected to increasing impact energies. In general, it is observed that with the increase in the impact energy the reduction in the diameter of the pipe also increases. It is also observed that as the impact energy increases, the length of the pipe which exhibits damage close to the impact region also increases.

Figure 6.35, (a) and (b), shows the reduction of diameter (R) in the impact zone and reduction in diameter to diameter ratios (R/D*)* for pipes subjected to increasing impact energies. An approximately linear relationship is observed between *R* and impact energy and *R/D* and impact energy for the case of pipes impacted with impact energies of 16 to 67kJ. It is observed that the damage caused to the pipes for the case studies *I-1* and *I-2* lie in the minor damage category [DNV (2010b)] as the *R/D* ratio is less than 5%. Thus the level of damage sustained is considered to have no significant impact on the operation of the pipes for the case of impact energies equal to 16kJ and 30kJ. However, the level of damage sustained by the pipes impacted with impact energy of 45kJ and 67kJ (case studies I-3 & I-4) lies in the second category (minor damage with

R/D is greater than 5%). Therefore the damage sustained may result in release of hydrocarbons and will require repair.

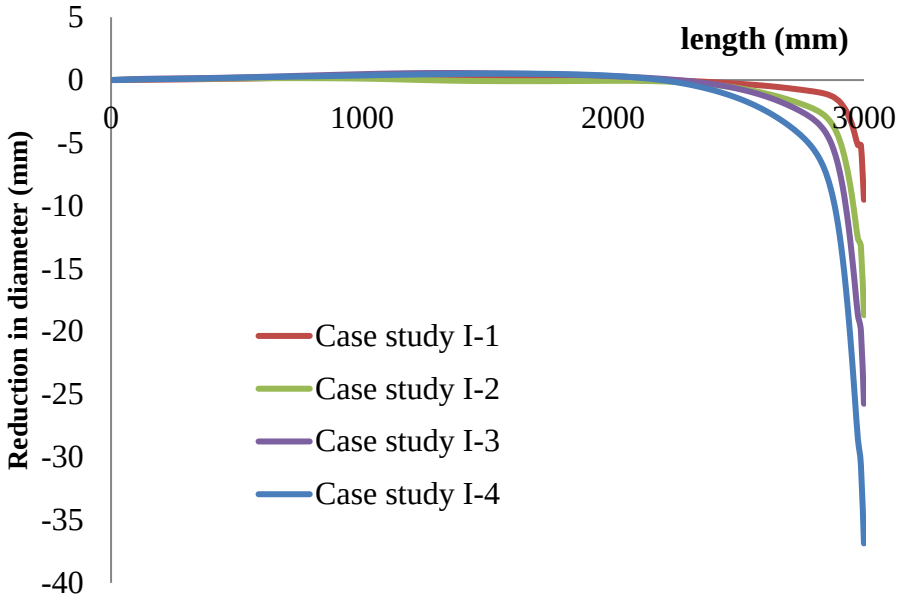

Figure 6.34: Comparison of the reduction in the diameter along the length of the pipe for different impact energies.

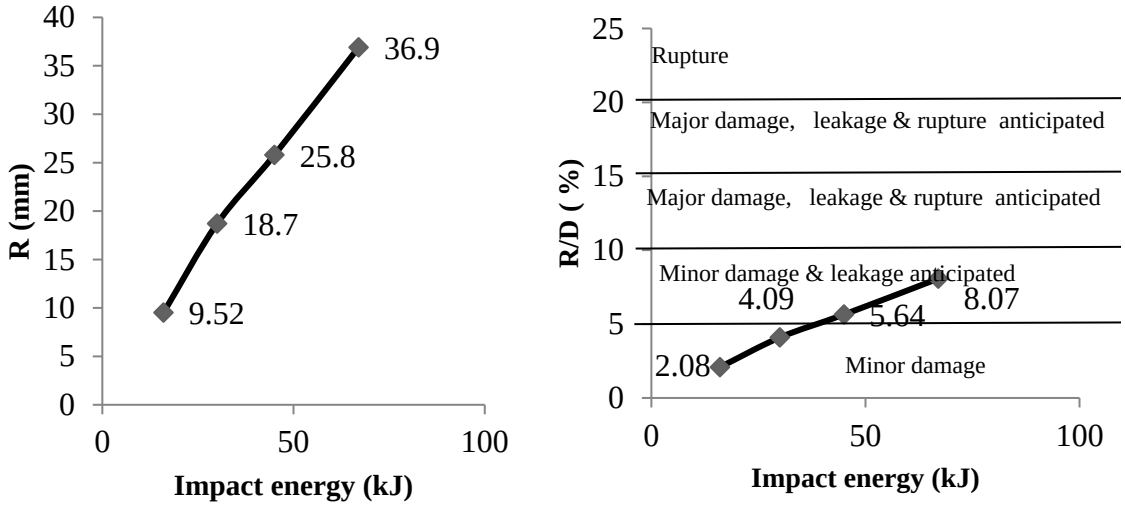

(a) (b)

Figure 6.35: (a) Reduction in diameter (R) and (b) reduction in diameter to diameter ratios (R/D) for pipe with increasing impact energies.

6.8 EFFECT OF THE GEOMETRY OF THE PIPE

In order to study the influence of the geometry of the pipe on the impact behaviour, an investigation is carried out. The details of the geometry of pipes (diameter and thickness) used in this investigation is presented in Table 6.5.

Table 6.5: Data describing the details of geometry of pipes used in the investigation.

Case study	Diameter (mm)	Thickness (mm)
G-1	457	25.4
G-2	457	17.5
G-3	228.5	12.7
G-4	228.5	25.4

Pipes considered in this investigation are used in practice by the offshore industry for transportation of oil and gas (for thorough catalogue of pipes used for the transportation of oil and gas refer to [Tenaris (2015)]). Pipes with a length of 6000mm are used in this investigation and are fully fixed at both ends. In this parametric study a sharp impactor is allowed to drop on the mid-span region of the pipe with impact energy of 16kJ as used in drop weight testing discussed in Chapter 5. Pipes are laid on a subsea bed with a stiffness of 13140kN/m/m (for case studies G-1 & G-2) and 4900kN/m/m (for case studies G-3 & G-4) which are associated with medium stiffness soil.

Figure 6.36 shows the comparison of the contact force time histories exhibited by the pipes due to impact. It is observed that for the particular diameter of the pipe, as the thickness of the wall decreases, the magnitude of the maximum contact force also decreases (case studies G-1 & G-2 and G-3 & G-4). This can be explained by the fact that as the local stiffness of the pipe reduces, the contact duration increases and as a result the maximum value of the contact force generated decreases. In the case of pipes with same thicknesses but different diameters (case studies G-1 & G-4) it is observed that the pipe with smaller diameter (case study G-4) exhibit higher values of contact force. This can be explain by the fact that the localized stiffness of the pipe in the

impact region is higher for the case of pipe with smaller diameter (case study G-4) as a result the magnitude of maximum contact force generated is also higher.

Figure 6.37 shows the reduction in the diameter exhibited along the length of the pipe due to impact load. It is observed that for particular diameter of pipe, as the thickness of the wall decreases, the reduction in diameter increases (case studies G-1 & G-2 and G-3 & G-4). On comparison of pipes with same thicknesses but different diameters (case studies G-1 & G-4) it is observed that the pipe with smaller diameter (case study G-4) exhibits lesser level of damage (reduction in the diameter) at the impact area. It is also observed that the global deformation exhibited by the pipe with smaller diameter (case study G-4) is significantly high compared to the pipe with larger diameter (case study G-1).

Figure 6.38, (a) and (b), shows the reduction of diameter (R) in the impact zone and reduction in diameter to diameter ratios (*R/D)* for pipes with different thicknesses. It is observed that the damage caused to the pipes used in case studies G-1 & G-2, lie in the minor damage category [DNV (2010b)] as the *R/D* ratio is less than 5%. Thus the level of damage sustained is considered to have no significant impact on the operation of the pipes. However, for the case of the pipes used in case studies G-3 & G-4 the damage lies in second category (minor damage with *R/D* is greater than 5%). The latter level of damage requires repair as it may result in the release of hydrocarbons.

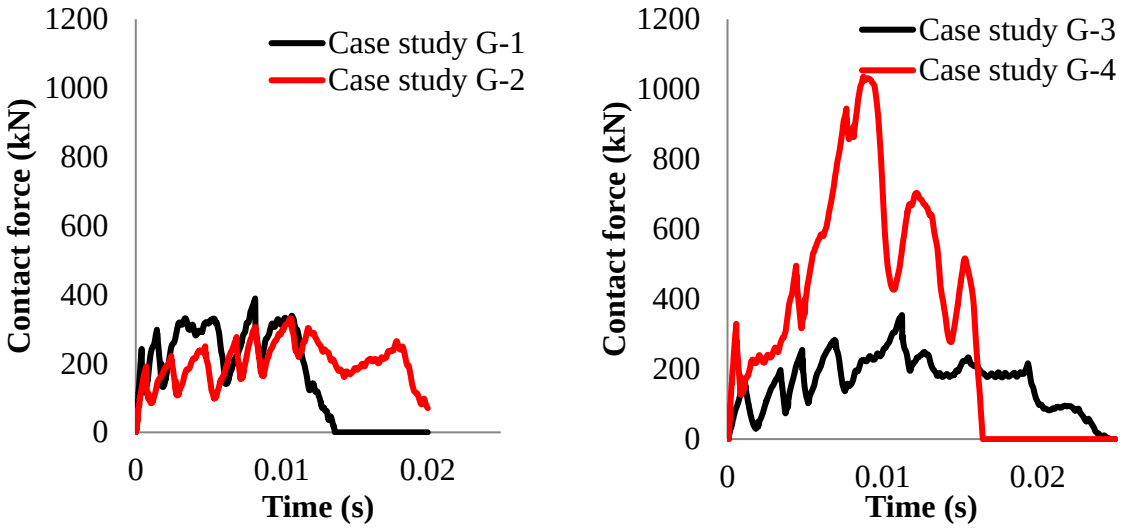

Figure 6.36: Comparison of the contact force time histories for the case studies (a) G-1 & G-2 (b) G-3 & G-4.

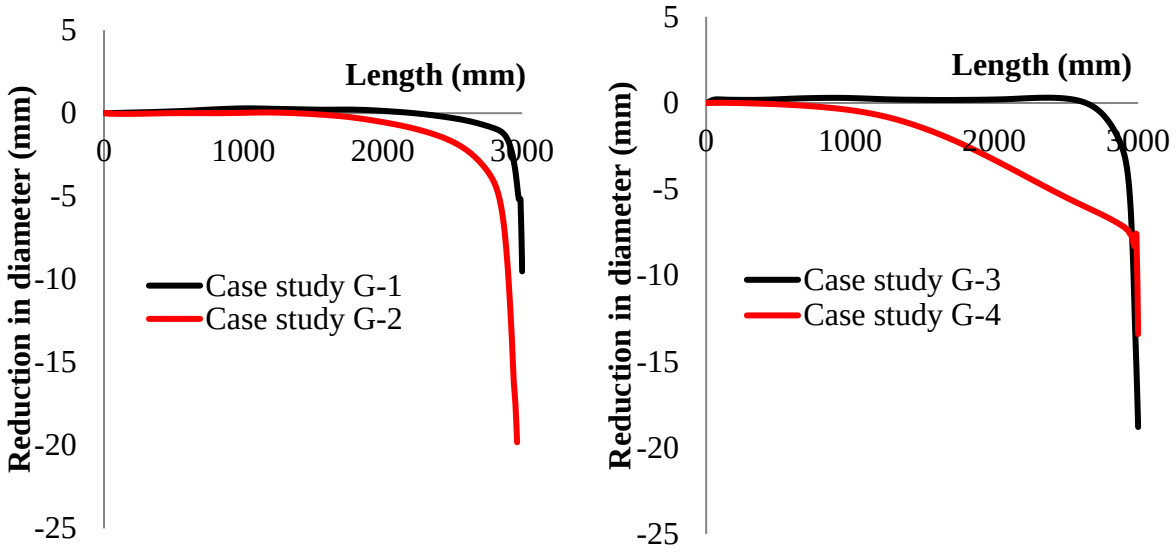

(a) (b)

Figure 6.37: Comparison of the reduction in the diameter along the length of the pipes for the case studies (a) G-1 & G-2 (b) G-3 & G-4.

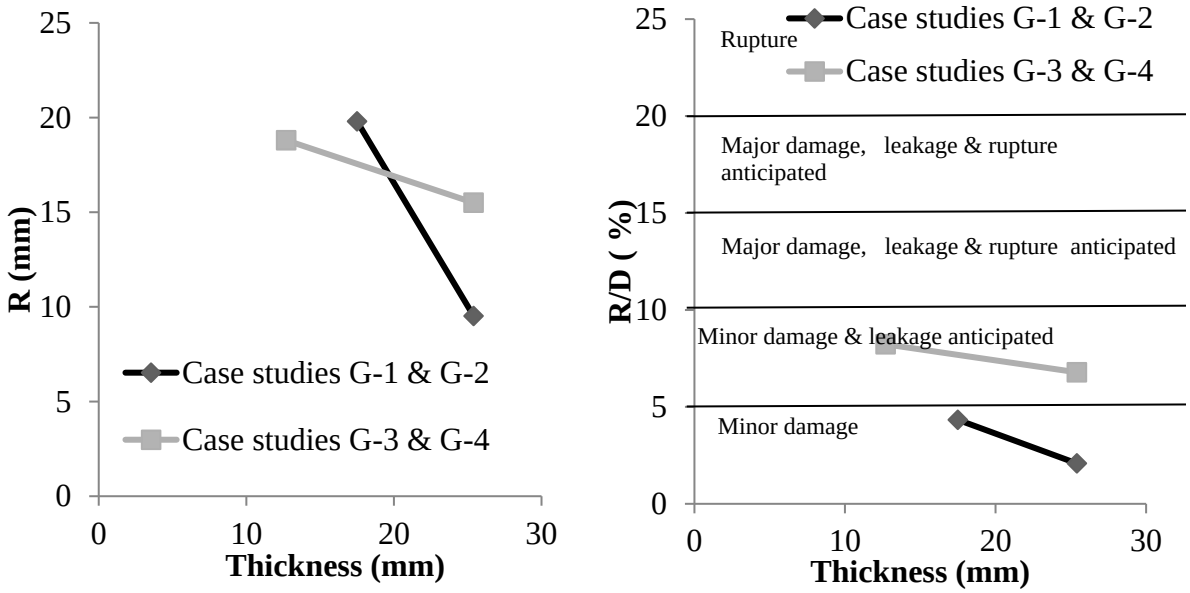

(a) (b)

Figure 6.38: (a) Reduction in diameter (R) and (b) reduction in diameter to diameter ratios (*R/D)* for pipe with different thicknesses.

6.9 IMPACT BEHAVIOUR OF PIPE UNDER COMBINED ACTION

As observed in sections 6.5 and 6.6, the impact behaviour of the pipe is significantly influenced by the level of imposed axial loading and the development of internal (due to the oil and gas in the pipe) and external (due to hydro-static load) pressures. Subsea steel pipes can be subjected to a combination of axial loading and the differential pressure acting on the wall of the pipe. Therefore in order to investigate the impact behaviour of the pipe under combined action of pressure and level of axial loading (expressed as percentage (%) of yield stress of steel from which pipes are constructed) case studies as described in Table 6.6 are carried out.

Table 6.6: Data describing the details of parameters used in the investigation.

Case study	**Mass (tonnes)**	**Impact energy (kJ)**	**Axial compressive load (% of σ_y)**	**Pressure (% of σ_y)**
O-1	2.2	16	10	5
O-2	4.0	30	10	5
O-3	6.0	45	10	5
O-4	9.0	67	10	5
O-5	2.2	16	10	-5
O-6	9.0	67	10	-5

Pipes with a length of 6000mm are used in this investigation and are fully fixed at both ends. In this parametric study a sharp impactor is allowed to drop on the mid-span region of the pipe with impact energy of 16kJ as used in drop weight testing discussed in Chapter 5. A quarter model is employed which adopts same cross-sectional and material properties of the pipe and the impactor as used in the *NLFEA* in section 6.3. Pipes are laid on a subsea bed with a stiffness of 13140kN/m/m which is associated with medium stiffness soil.

Figure 6.39 shows the comparison of the contact force time histories for the case of pipes subjected purely to impact (case studies I-1, I-2, I-3 & I-4 as presented in section 6.7) and combined impact, axial load & pressure (case studies O-1, O-2, O-3, O-4, O-5 & O-6). Figure 6.40 shows the comparison for the reduction in diameter exhibited along

the length of the pipe for the above case studies. Comparing the predictions obtained from case studies associated with pipes with identical level of internal (positive) pressure, axial load and increasing levels of impact energy it is observed that pipes in case studies *O-1, O-2, O-3* & *O-4* exhibit higher values of contact force and less reduction in diameter at the impact area [see Figure 6.39 & Figure 6.40 (a) to (d)] compared to the pipes subjected to purely impact (case studies I-1, I-2, I-3 & I-4). However for the case of pipes with identical level of external (negative) pressure, axial load and with increasing levels of impact energy it is observed that pipes in case studies *O-5* & *O-6* exhibit lower magnitude of the contact force [see Figure 6.39 & Figure 6.40 (e) & (d)] compared to the pipes subjected to purely impact (case studies *I-1& I-4*).

Figure 6.41 shows the reduction in diameter to diameter ratios (R/D) for the case of pipes with and without combined effects (axial load & pressure acting on the walls of the pipes). In general it is found the when considering pipes subjected purely to impact conservative predictions are obtained compared to the pipes subjected to the combined action of impact, axial load and pressure. However, it is important to note that for the case study *I-6* (pipe subjected to purely impact) the predictions are unsafe compared to their counterparts obtained for the case of the pipe subjected to combined action (case study O-6). As discussed in Chapter 2, the impact test setup and assessment methods used by the industry do not consider the combined action of the axial load and pressure on the impact behaviour of the pipes. As a result they may not always provide conservative (safe) predictions as it is observed from Figure 6.39 to Figure 6.41.

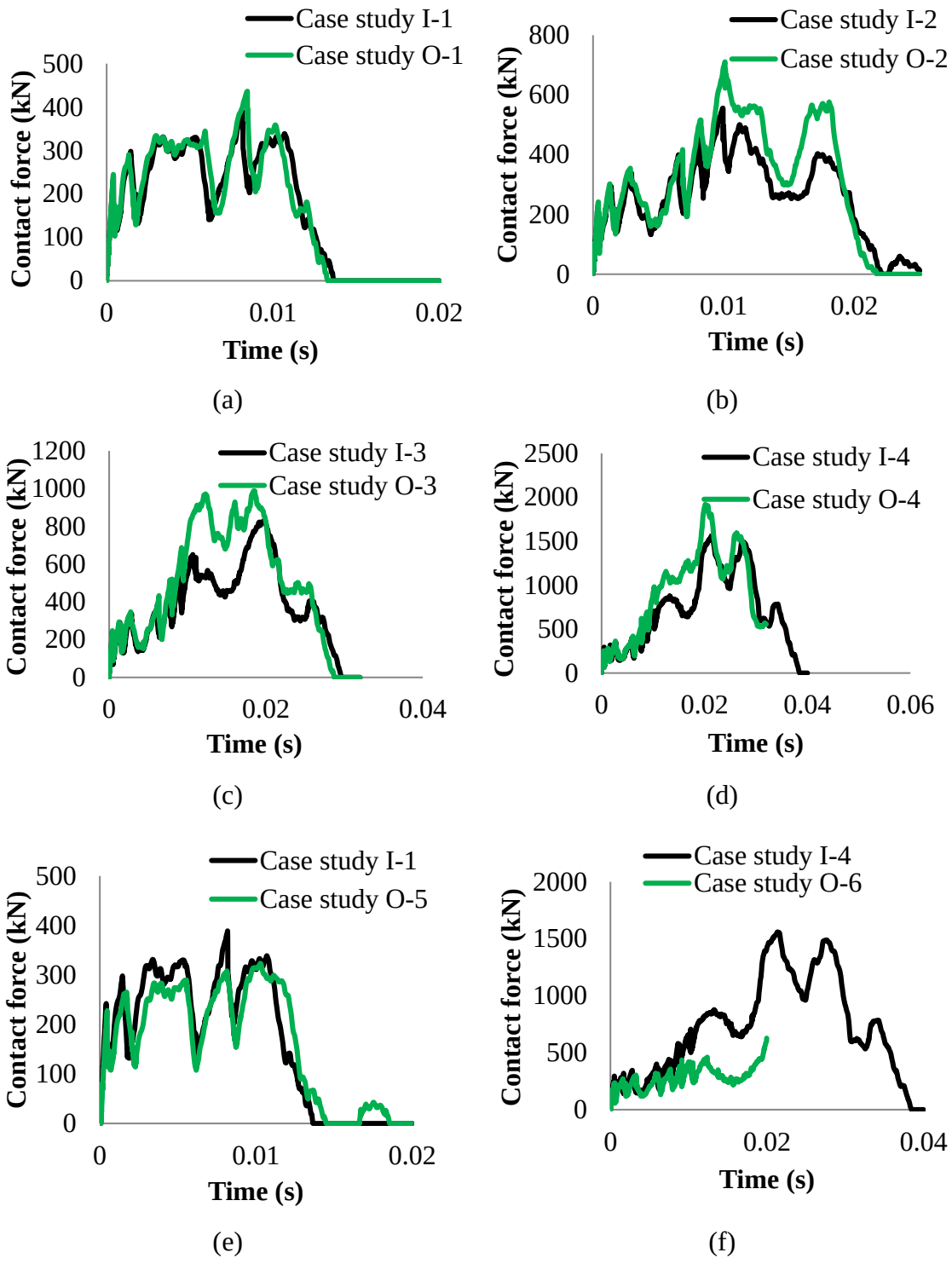

Figure 6.39: Comparison of the contact force time histories for the case of pipes with and without combined effects (axial load & pressure acting on the walls of the pipes).

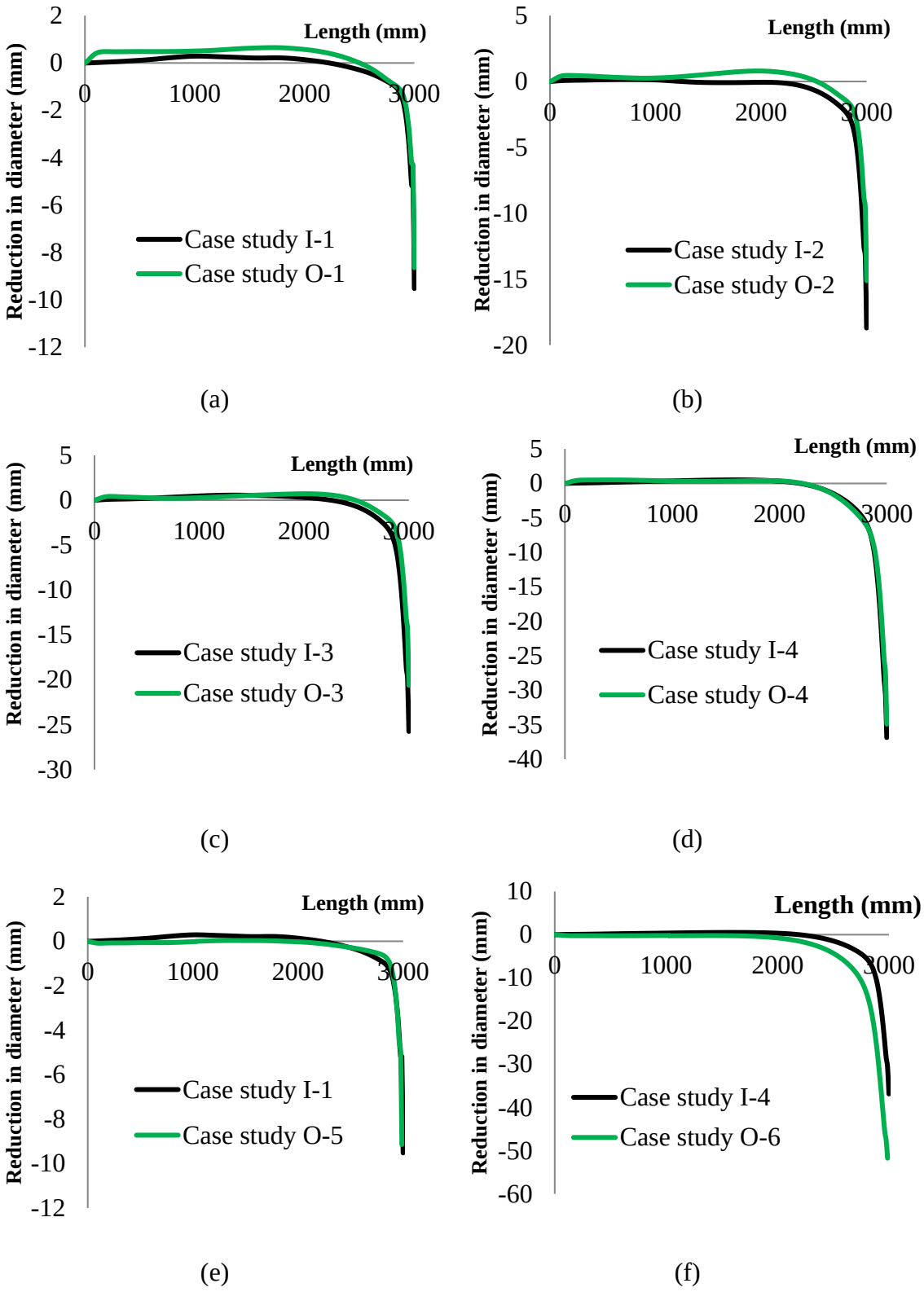

Figure 6.40: Comparison of the reduction in the diameter along the length of the pipes for the case of pipes with and without combined effects (axial load & pressure acting on the walls of the pipes).

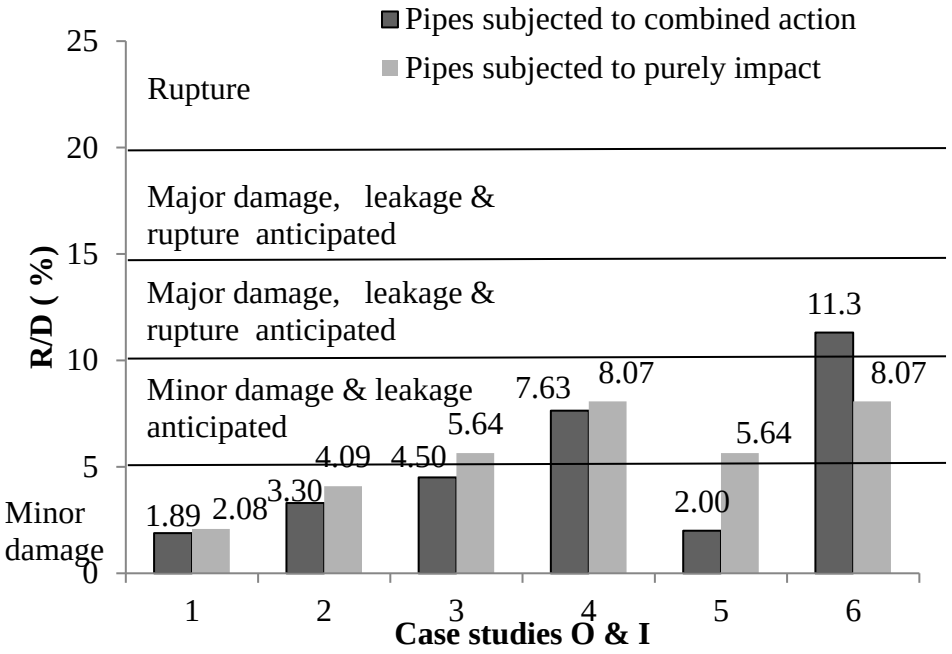

Figure 6.41: Reduction in diameter to diameter ratios (R/D) for pipe with and without combined effects (axial load & pressure acting on the walls of the pipes).

6.10 EFFECT OF COATING

Different types of coating, as discussed in section 6.1, are often used for protecting pipelines and reducing the level of damage they sustain when subjected to impact loading. In this study two types of concrete coating are considered:

- Plain and reinforced concrete
- Engineered cementitious composite (ECC)

In section 6.8 the *NLFEA* predicted that a pipe with a diameter of 228.5mm and a thickness of 12.7mm subjected to impact energy of 16kJ sustained damage which may result in release of hydrocarbons. This level of damage is characterized by a ratio *R/D* greater than 5% thus requiring repair. This pipe is used presently to investigate the ability of the protective coatings (i) to reduce the level of damage sustained by the pipe due to impact loading and (ii) to safeguard a certain level of resilience. The pipe is considered fully restrained at its base (see Figure 5.19) in the vertical axis along its full

length and is considered as fixed at its both ends. The pipe is impacted at the mid-span region with a sharp impactor with impact energy of 16kJ which was used in the experimental study as presented in Chapter 5.

6.10.1 Plain and reinforced concrete coating

As discussed in Chapter 2, the code of practice used in industry [DNV (2010b)] suggests that in the absence of more detail information additional protection may be offered by a 45mm thick concrete coating which is considered capable of absorbing energy of up to 40kJ when subjected to a 30mm wide indenting object. In order to investigate the potential benefits stemming from the use of the concrete coating, following case studies are considered:

- Case study CC-1: No coating
- Case study CC-2: Coating having thickness of 25.4mm
- Case study CC-3: Coating having thickness of 45mm
- Case study CC-4: Lightly reinforced concrete coating having thickness of 45mm

Perfect bond is assumed between the concrete coatings and the pipes. The *FE* model employed to study the influence of the plain concrete coating on the impact behaviour of the pipe is shown in Figure 6.42. Figure 6.43 (a) shows the *FE* model employed for the pipe with reinforced concrete coating. A 8mm diameter steel bars are used and placed at 50mm spacing (similar to thickness of concrete coating). A cover equal to half a thickness of the coating is adopted for bars as shown in Figure 6.43 (b).

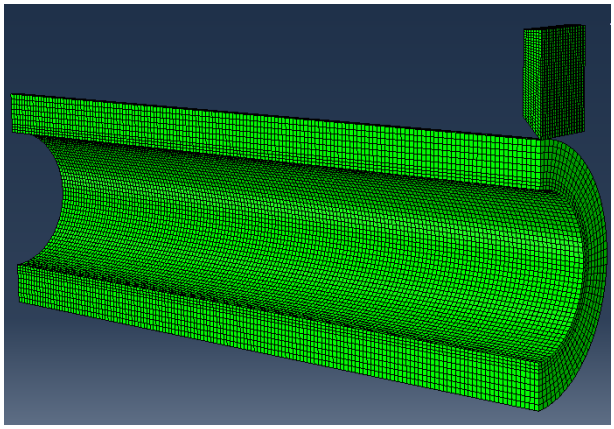

Figure 6.42: *FE* model for pipe with concrete coating.

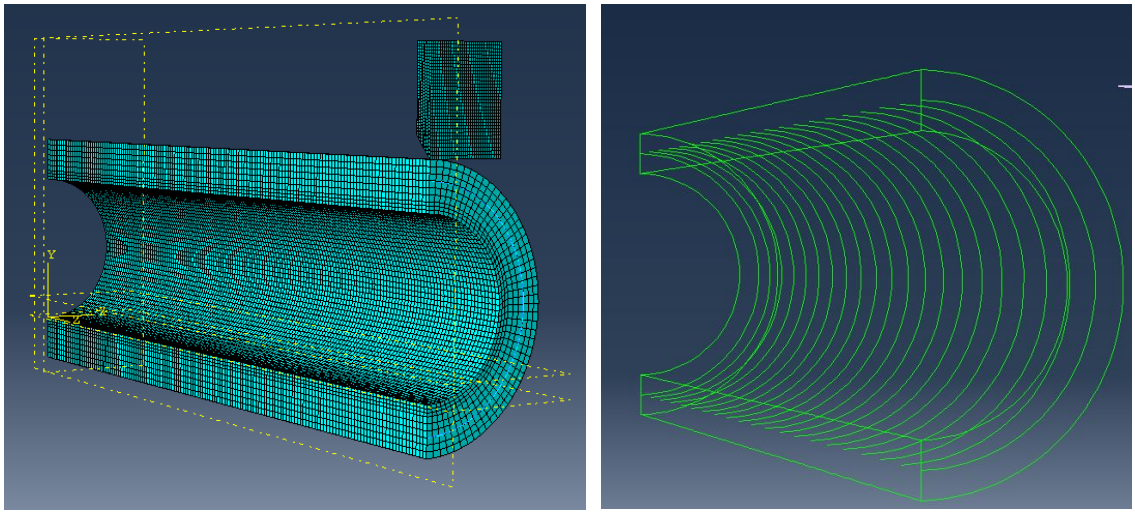

(a) (b)

Figure 6.43: (a) *FE* model of reinforced concrete coating pipe under impact (b) layout of reinforcement in concrete coating.

The concrete damage plasticity model in ABAQUS (2013) is used to define the material properties of concrete. The model uses the concepts of isotropic damaged elasticity in combination with isotropic tensile and compressive plasticity to represent the inelastic behaviour of the concrete. Two main failure mechanisms assumed in concrete damaged plasticity model are:

- Tensile cracking
- Compressive crushing

Figure 6.44 and Figure 6.45 show the response of concrete under the uniaxial tensile and compressive loading respectively. The tensile behaviour is assumed to be linear elastic until the peak stress is reached which is followed by a softening stress-strain response. Under uniaxial compression concrete behaviour is described by a stress-strain curve which consists of an ascending and a descending branch. The ascending branch consist of a linear portion until the initial yield point which is followed in the non-linear plastic region until the peak stress is attained (stress hardening). After peak stress is attained the behaviour of concrete is describe by a strain softening branch.

The yield (or failure) surface is controlled by two hardening variables: tensile equivalent plastic strain ($\tilde{\varepsilon}^{pl}{}_{t}$) and compressive equivalent plastic strain ($\tilde{\varepsilon}^{pl}{}_{c}$), linked to the failure mechanisms under tension and compression loading, respectively. As the concrete specimen is unloaded from any point on the strain softening branch, the

unloading response becomes weakened and as a result the elastic stiffness of the material becomes damaged or degraded. The degradation is defined by two damage variables, d_t and d_c. These damage variables can take values from zero (the undamaged material) to one (total loss of strength). The stress-strain relationship under uniaxial tension and compression are given by Eq. (6.2) and Eq. (6.3), respectively:

$$\sigma_t = (1 - d_t)E_o(\varepsilon_t - \tilde{\varepsilon}^{pl}{}_t) \qquad \text{Eq. (6.2)}$$

$$\sigma_c = (1 - d_c)E_o(\varepsilon_c - \tilde{\varepsilon}^{pl}{}_c) \qquad \text{Eq. (6.3)}$$

where: E_o : initial (undamaged) elastic stiffness

The parameters associated with the concrete damage plasticity model are described in Table 6.7. Similar to the classical steel model, the material properties of concrete is assumed to be strain rate independent in finite element investigation. Therefore, the apparent increase in the tensile strength of concrete under increasing loading rates represent the structural effects rather the material property of concrete.

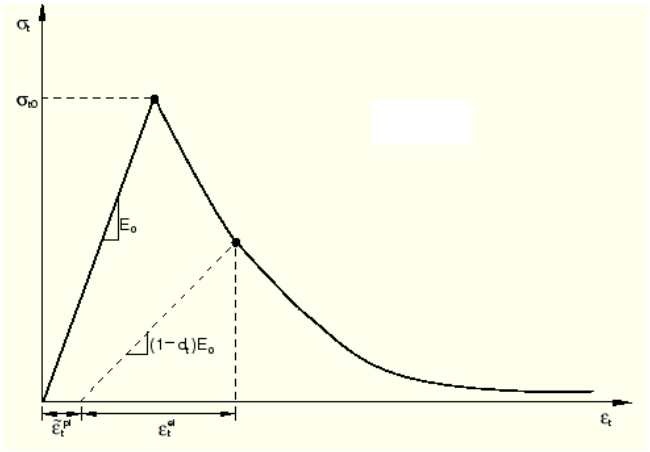

Figure 6.44: Response of concrete in uniaxial tension [ABAQUS (2013)].

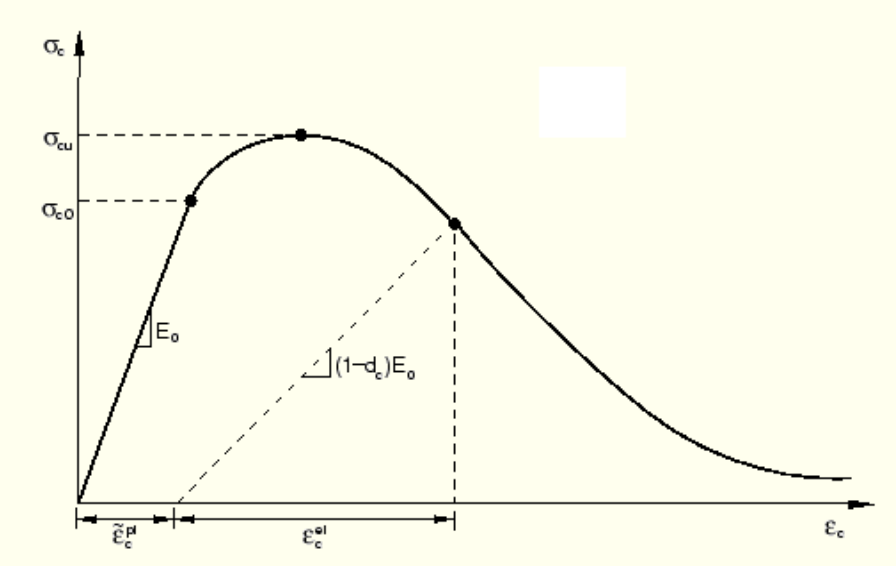

Figure 6.45: Response of concrete in uniaxial compression [ABAQUS (2013)].

Table 6.7: Parameters associated with the concrete damage plasticity model.

Parameters	Description
ψ	Dilation angle
ϵ	Flow potential eccentricity
f_{bo}/f_{co}	Initial equibiaxial compressive yield stress to initial uniaxial compressive yield stress
K	Ratio of the second stress invariant on the tensile meridian to that on compressive meridian at initial yield for any given value of pressure invariant such that the maximum principal stress is maximum
μ	Viscosity parameter

In this investigation the uniaxial compressive strength of concrete (fc) is assumed to be 40MPa, a typical value used in offshore practice [Abdou & Abuseda (2014)]. Figure 6.46 shows the stress-strain curves used for defining the material properties of concrete in compression and tension. The stress-strain curve describing the behaviour of concrete in compression (until maximum compressive strength) is established based on the equation of Eurocode [Eurocode-EC2 (2004)]. The values of the parameters associated with concrete damage plasticity model are given in Table 6.8. The stress-strain curve describing the material behaviour of the reinforcing bars under uniaxial compression

and tension is shown in Figure 6.47. This represent typical S500 bars derived from test conducted at Heriot Watt University.

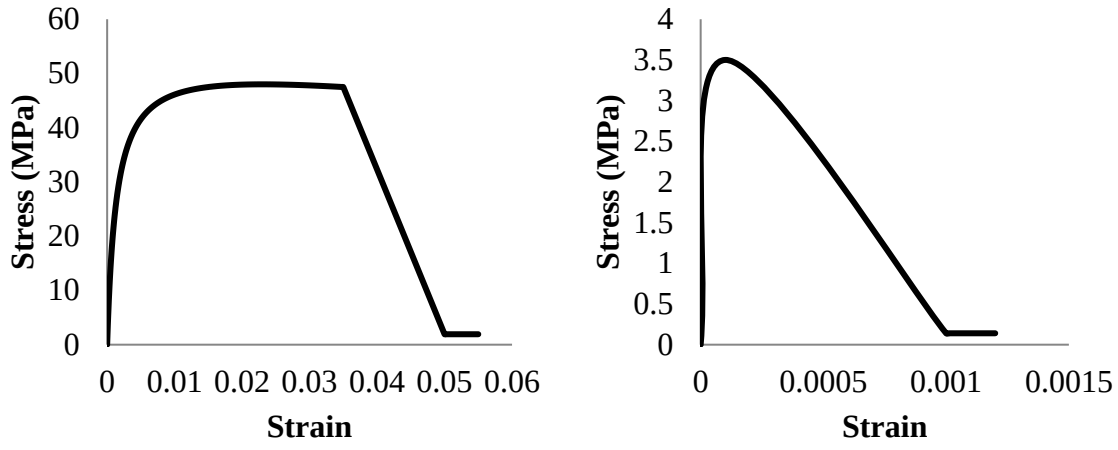

(a) (b)

Figure 6.46: Stress-strain curve for concrete in (a) compression (b) tension used in finite element analyses.

Table 6.8: Parameters used in concrete damage plasticity model.

Parameters		Reference
ψ	38°	[Jankowiak & Lodygowski (2005)]
ϵ	0.1	[Birtel & Mark (2006), Kmiecik & Kamiński (2011)]
f_{bo}/f_{co}	1.16	
K	0.66	
μ	0	[Kmiecik & Kamiński (2011)]

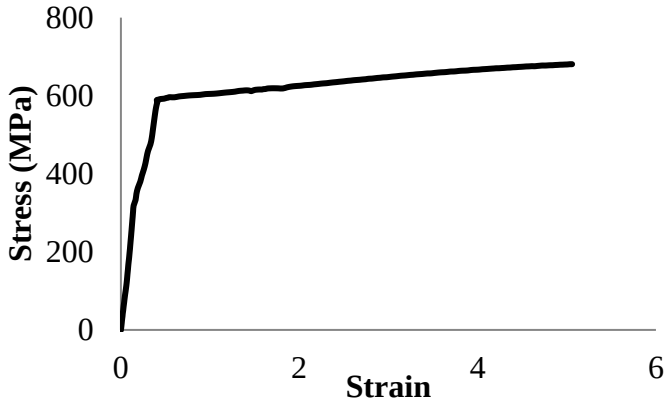

Figure 6.47: Stress-strain curve describing material behaviour of the reinforcing bar.

Table 6.9 gives the computational cost of the analyses. It is observed that the analysis carried out with concrete coating results in significant increase in the computational cost. The latter cost increases significantly when considering concrete coating with larger thicknesses. It is also observed that the analysis carried out with the reinforced concrete coating resulted in a significant increase in the computational cost compared to the pipe with and without concrete coatings. This is due to the fact that tensile stresses are taken by reinforcement allowing for the analysis to continue further.

Table 6.9: Computational cost of concrete coating analyses.

Case study	Time (hours)
CC-1	24
CC-2	61
CC-3	166.5
CC-4	623.5

Figure 6.48 shows the comparison of the contact force time histories predicted numerically for case studies considered herein. It is observed that the magnitude of the maximum contact force is higher for the pipes with the concrete coating. This can be explained due to the fact that the stiffness of the composite member (steel pipe + concrete coating) is higher compared to that of plain pipes. It is also observed that the further increase in the thickness of the concrete coating does not appear to influence the magnitude of the maximum contact force. Comparing the results for the case of pipes coated with concrete (CC-3) and lightly reinforced concrete (CC-4) it is observed that a higher values of contact force are exhibited when using reinforced concrete (RC) coating. This is due to the increased stiffness which results in shorter impact duration and higher values of contact force being generated.

Figure 6.49 shows the reduction in the diameter exhibited during impact along the length of the pipe. It is observed that the concrete coating significantly reduced the level of damage caused to the pipe due to impact. It is also observed that the increase in the thickness of the concrete coating resulted in a decrease in the reduction in the pipe diameter in the impact area and in the length in which reduction was observed.

Furthermore it is also observed that the behaviour of the pipe with plain and reinforced concrete coating (case studies CC-3 and CC-4) appear to be very similar.

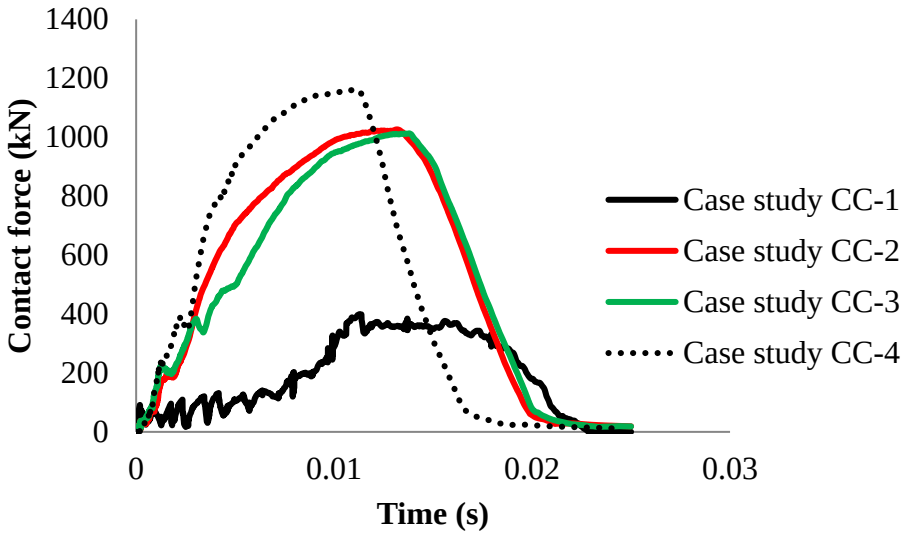

Figure 6.48: Comparison of the contact force time histories for pipe with different thicknesses of concrete.

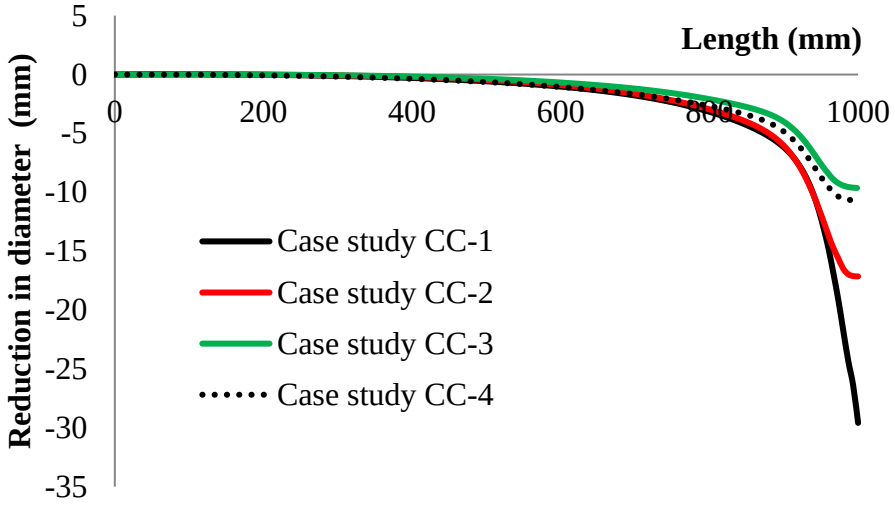

Figure 6.49: Reduction in the diameter along the length of the pipe with different thicknesses of concrete.

Figure 6.50 shows the top profile of the concrete layer along the length of the pipe. It is observed that the damage caused to the thickness of the concrete coating is maximum at the area of impact. It is also observed that as the thickness of the concrete coating increases the damage caused to the coating along the length of the pipe decreases.

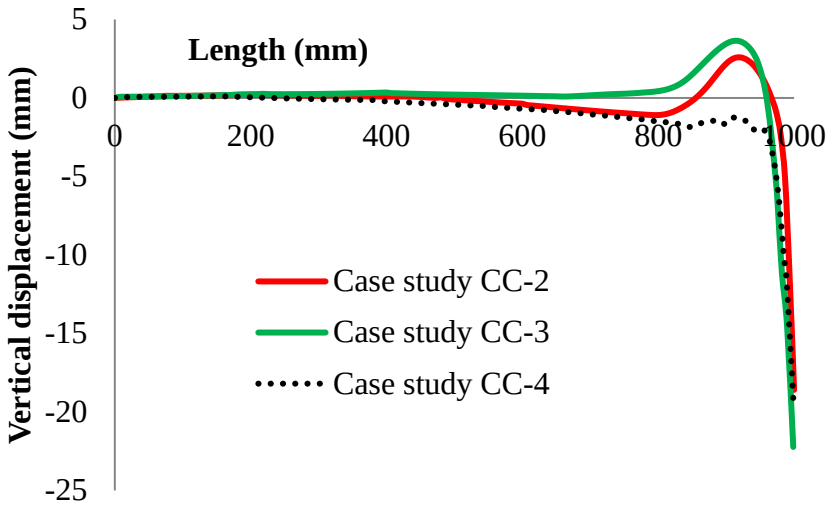

Figure 6.50: Top profile of the concrete layer along the length of the pipe for different case studies.

Figure 6.51 shows the maximum principal plastic strains in the thicknesses of the concrete coating along the length of the pipe. In general it is observed that irrespective of the thickness of the concrete coating the maximum plastic strains are observed in the impact area. It is also observed that the magnitude of the plastic strain is lower for the case study *CC-4* (pipes with reinforced concrete coating having thickness of 45mm) as compared to case studies *CC-2* and *CC-3* (pipe with plain concrete coating having thickness of 25.4mm and 45mm respectively). It is important to observe that for different thicknesses of the concrete coating, the plastic strains extend more than half the length of the pipes circumference in the impact region and the effect is more pronounced for the lesser thickness of the concrete coating (case study CC-2).

Figure 6.52 shows the maximum principal plastic strains in the pipe (within steel) along its length. It is observed that the concrete coating significantly reduces the magnitude of the plastic strains irrespective its thickness used. It is also observed that as the thickness of the concrete coating increases the plastic strains in the pipe section along the length of the pipe decrease significantly.

Figure 6.53, (a) and (b), shows the reduction of diameter (R) in the impact area and reduction in diameter to diameter ratios (R/D*)* for pipes with different thicknesses of concrete coating. It is observed that the use of concrete coating significantly decreases the damage caused to the pipe due to impact loading and reduces the severity of the damage from major to minor [DNV (2010b)]. In general it is observed that with the increase in the thickness of concrete coating, the damage caused to the pipe decreases. It is important to note that the suggested 45mm thickness of concrete coating [DNV (2010b)] is observed to be sufficient to reduce the level of damage sustained by the pipe considered herein.

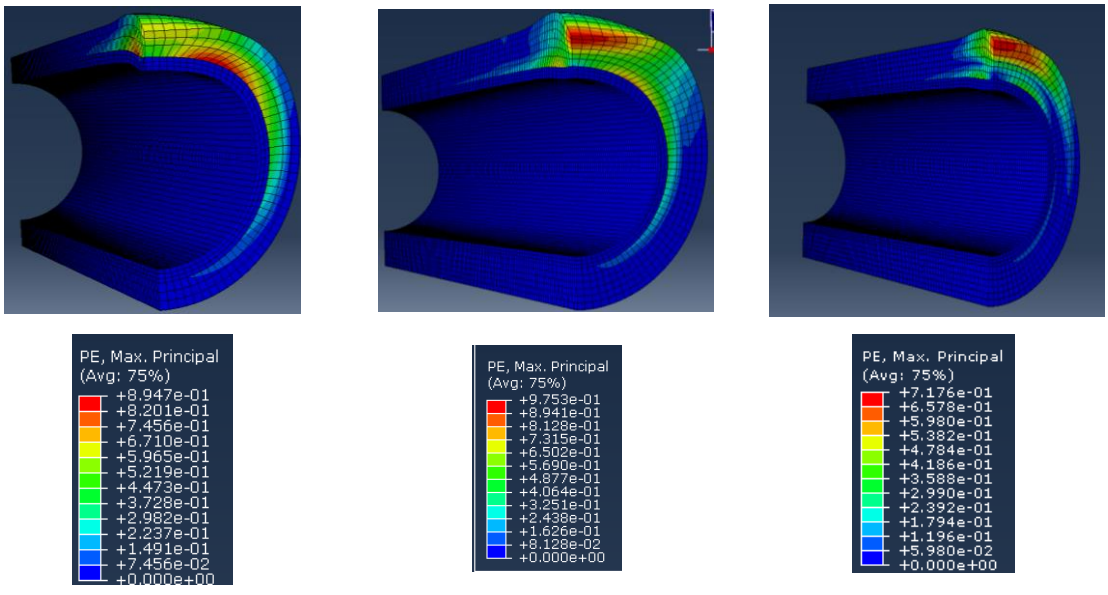

(a) (b) (c)

Figure 6.51: Maximum principal plastic strains in the thicknesses of the concrete coatings for case studies (a) CC-2 (b) CC-3 (c) CC-4.

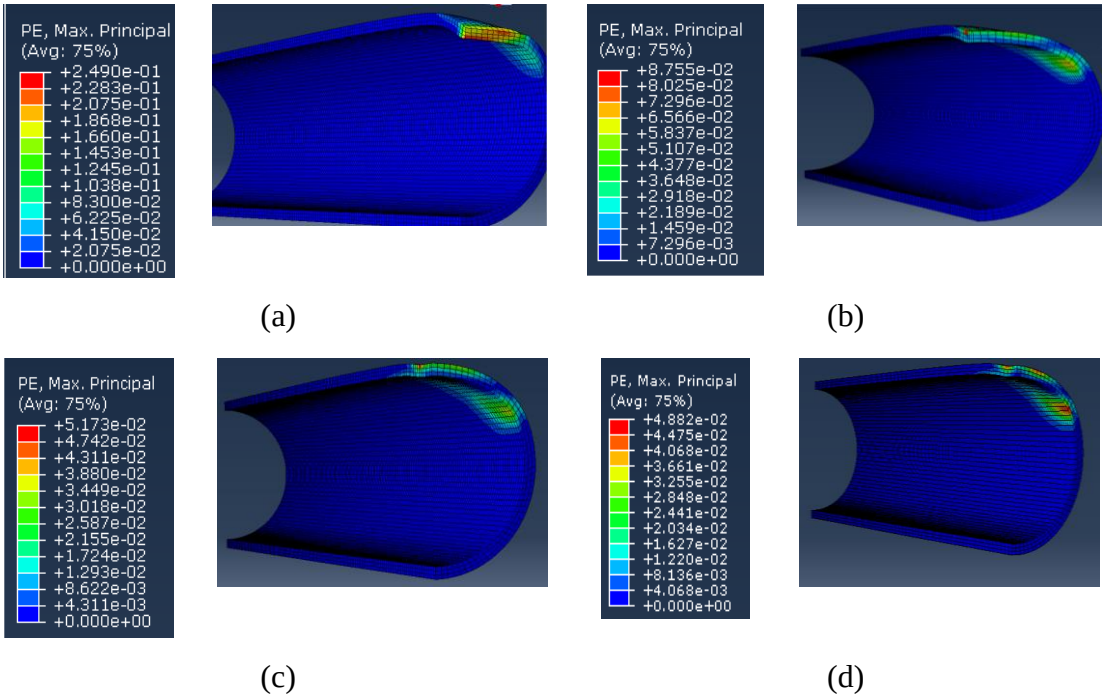

Figure 6.52: Maximum principal plastic strains along the length of the pipe for the case studies (a) CC-1 (b) CC-2 (c) CC-3 (d) CC-4.

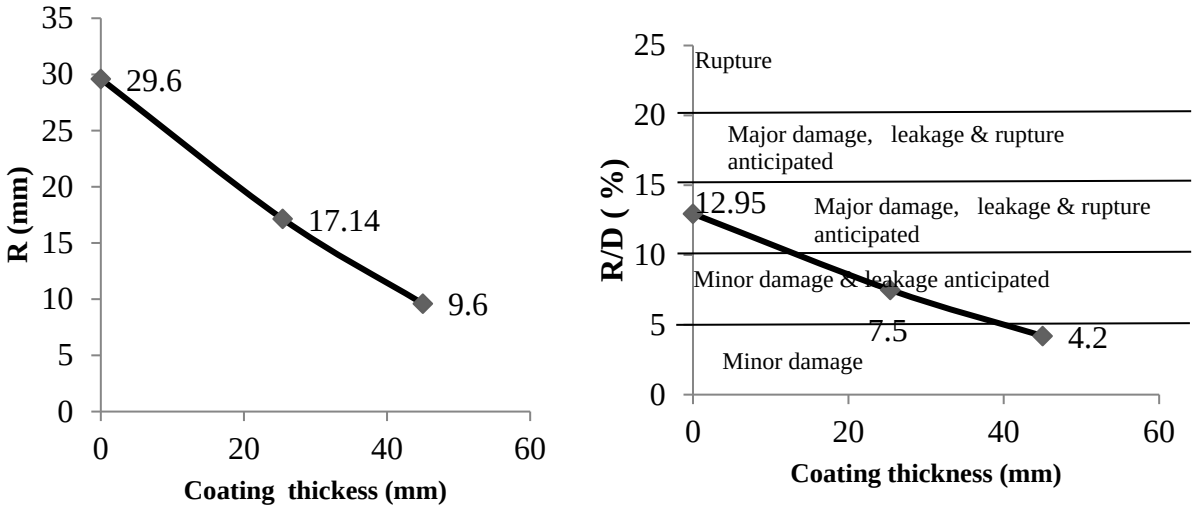

Figure 6.53: (a) Reduction in diameter (R) and (b) reduction in diameter to diameter ratios (R/D) for pipe with different thicknesses of concrete coating.

6.10.2 Engineered cementitious composite (ECC) coating

Engineered Cementitious Composite (ECC) consists of cement paste or mortar matrix with a low volume fraction of fibres [for e.g. Ultra High Molecular Weight Polyethylene (UHMWPE) or PolyVinyl Alcohol (PVA)]. The development of the *ECC* material is based on tailoring the micro-mechanical properties of the material to produce steady-state cracking (cracks propagating without an increase in applied load) when the material is subjected to tensile loading. As a result it exhibits strain hardening behaviour (the increase in stress with increasing strain after the initial crack formation) when multiple cracks are able to form in the material [Kesner & Billington (2004)].

The comparison of the stress-strain curves describing the material behaviour of *ECC*, concrete and fibre reinforced concrete (FRC) is shown in Figure 6.54 (a). When subjected to tension, in contrast to the brittle behaviour of plain concrete, *ECC* material exhibits multiple cracking in tension [see Figure 6.54 (b)], which provides significant tensile strain capacity ranging from 0.5 to 6% and tensile strengths from 2 to 8MPa [Kesner & Billington (2004)]. The response of *ECC* material in compression is similar to the behaviour of mortar. Due to the absence of aggregate, the modulus of Elasticity of *ECC* is lower than that of the traditional concrete. However, the ultimate compressive strength (f_c) is similar to plain and fibre reinforced concretes.

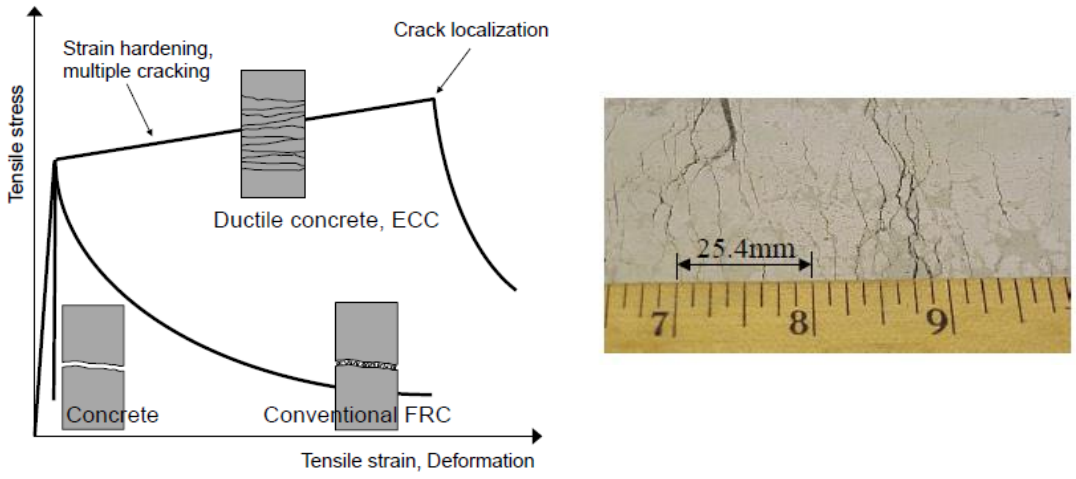

(a) (b)

Figure 6.54: (a) Comparison of the stress-strain curves describing the behaviour of *ECC* concrete and *FRC* [Polymers (2010)] (b) multiple cracking exhibited by *ECC* materials [Kesner & Billington (2004)].

ECC has been used in several civil engineering projects such as in seismic resistant structures, surface repairs and for infrastructure rehabilitation as shown in Figure 6.55. This investigation explains the possibility of using *ECC* coating on subsea pipes to reduce the level of damage sustained during impact, as *ECC* is found effective in absorbing the energy of dynamic loads (impacts). For this purpose the following case studies are investigated:

- Case study EC-1: No coating
- Case study EC-2: Coating with a thickness of 31.75mm
- Case study EC-3: Coating with a thickness of 45mm
- Case study EC-4: Coating with a thickness of 63.5mm

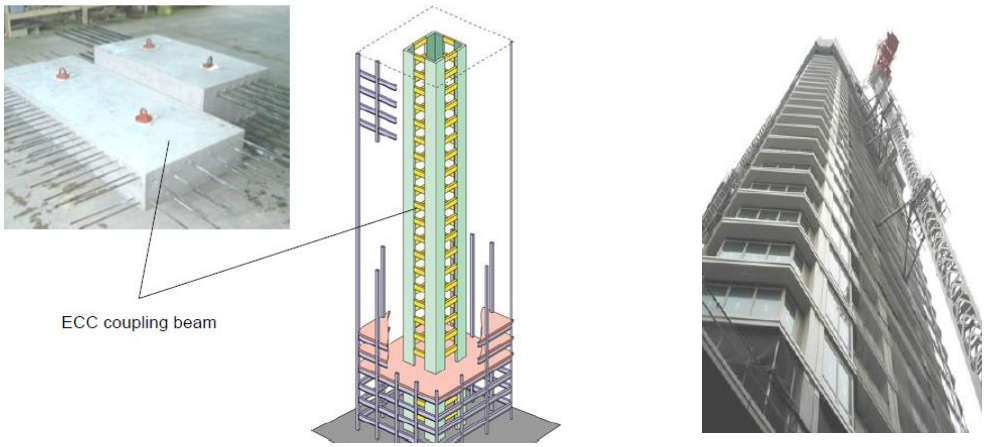

(a)

(b)

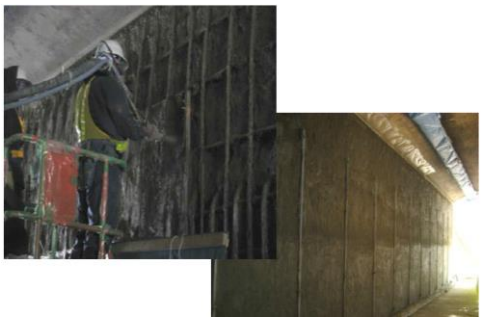

(c)

Figure 6.55: Application of *ECC* in civil engineering projects (a) *ECC* coupling beam in Nabeaure Yokohama Tower (b) resurfacing of an ASR (alkali silica reaction) damaged retaining wall in Japan (c) Replacement of chloride-contaminated concrete on a motorway bridge [Polymers (2010)].

In this investigation, the *NLFEA* model used for studying the influence of the concrete coating on the impact behaviour of the pipe is employed. The stress-strain curves describing the material behaviour of 35MPa *ECC* in uniaxial compression and tension is shown in Figure 6.56. Perfect bond is assumed between the *ECC* coatings and the pipes. A effect of bond on the behaviour of pipe is discussed in section 6.10.2.1.

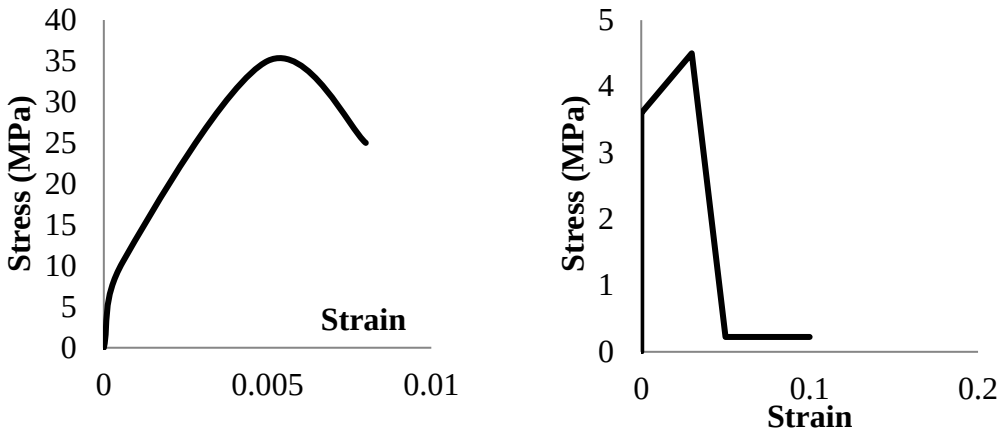

(a) (b)

Figure 6.56: Stress-strain curves describing the material behaviour of ECC under (a) compression (b) tension.

The computational cost of the analyses is given in Table 6.10. It is observed that with the increase in the thickness of *ECC*, unlike in the analysis with concrete coating, the computational cost of the analysis slightly decreases. It is due to the fact that *ECC* material unlike concrete exhibits multiple cracking in tension which provides significant tensile strain capacity. This help with distribution of stresses enhancing the numerical stability of a solution of *NLFEA* method.

Table 6.10: Computational cost of *ECC* analyses.

Case study	Time (hours)
EC-1	24
EC-2	68
ECC-3	61
ECC-4	54

Figure 6.57 shows the comparison of contact force time histories generated during impact for different thicknesses of *ECC* coating. It is observed that the magnitude of the maximum contact force is higher for the pipes with the *ECC* coatings. It is also observed that the increase in the thickness of the *ECC* coating influences the magnitude of the maximum contact force and contact duration.

Figure 6.58 shows the top profile of the *ECC* coating along the length of the pipe. It is observed that with the increase in the thickness of the *ECC* coating, the damage caused to the coating along the length of the pipe decreases.

Figure 6.59 shows the reduction in the diameter along the length of the pipe. It is observed that the *ECC* coating significantly reduced the level of damage caused to the pipe due to impact. It is also observed that with the increase in the thickness of the *ECC* coating the reduction in the pipe diameter and length of the pipe in which level of damage (expressed as reduction in pipe diameter) is observed decreases. Therefore the use of *ECC* coating not only reduces the damage caused to the pipe locally (impact area) but also along its whole length.

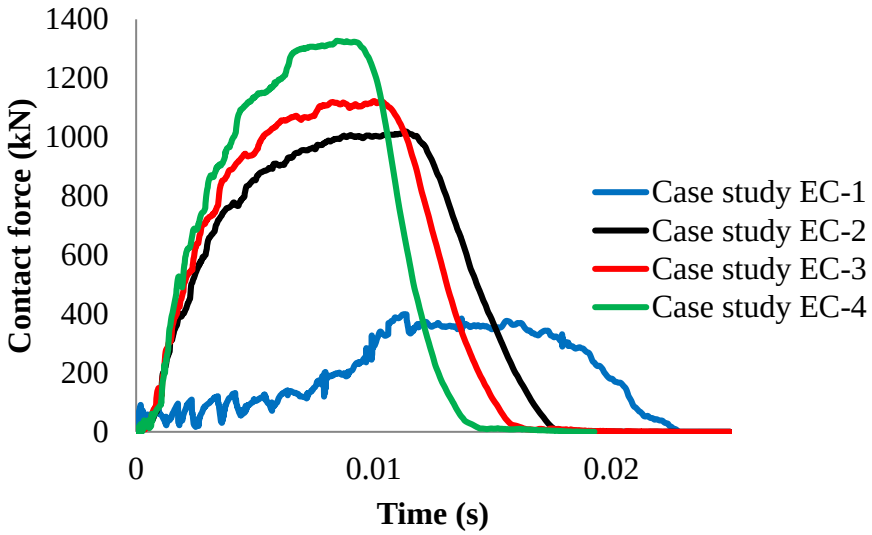

Figure 6.57: Comparison of contact force time histories with different thicknesses of *ECC*.

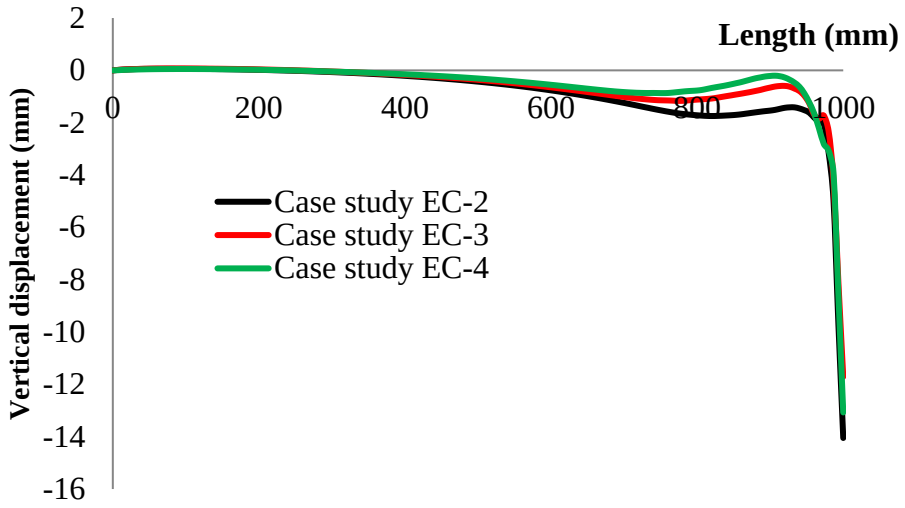

Figure 6.58: Top profile of *ECC* coatings along the length of the pipe.

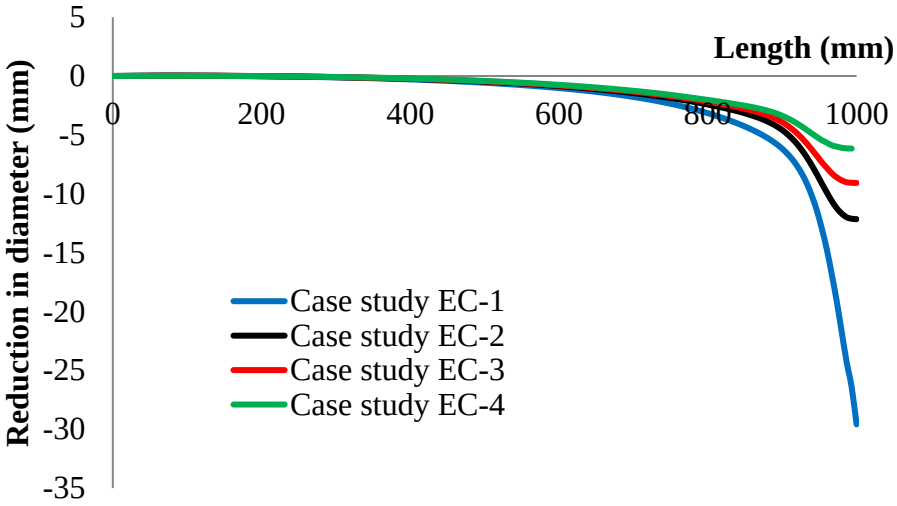

Figure 6.59: Reduction in the diameter along the length of the pipe with different thicknesses of *ECC*.

Figure 6.60 shows the maximum principal plastic strains in the thicknesses of the *ECC* coating along the length of the pipe. In general it is observed that irrespective of the thickness of the *ECC* coating the maximum plastic strains are observed in the impact

zone. It is also observed that the magnitude of the plastic strain is higher for the case study *EC-2* (pipes with *ECC* coating having thickness of 31.75mm) as compared to case studies *EC-3* and *EC-4* (pipes with *ECC* coating having thickness of 45mm & 63.5mm respectively). This was not observed for the case of concrete coatings (discussed in section 6.10.1) and it is due to the fact that *ECC* exhibits multiple cracking in tension and absorbs the impact energy more effectively.

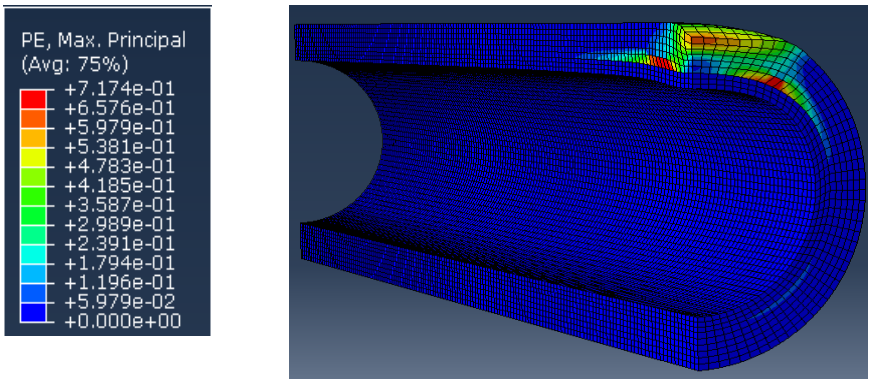

(a)

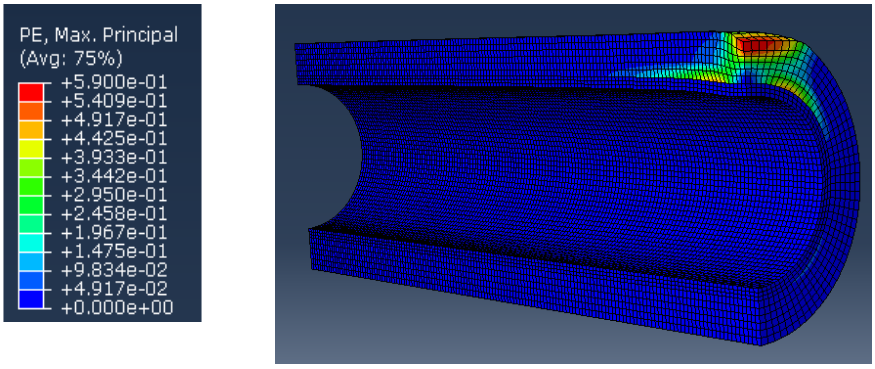

(b)

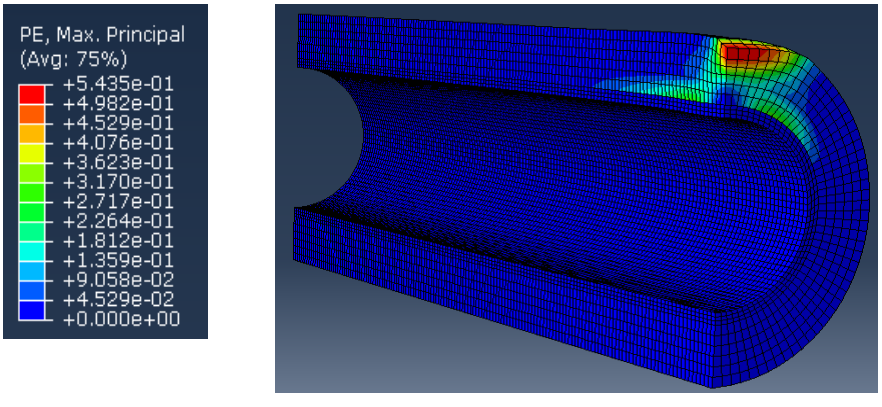

(c)

Figure 6.60: Maximum principal plastic strains in the *ECC* coating along the length of the pipe for case studies (a) EC-2 (b) EC-3 (c) EC-4.

Figure 6.61 shows the maximum principal plastic strains in the pipe section along the length of the pipe. It is observed that the *ECC* coating significantly reduces the magnitude of the plastic strains irrespective of the thickness of the coating used in the pipe section. It is also observed that as the thickness of the *ECC* coating increases the plastic strains in the pipe section along the length of the pipe decrease significantly.

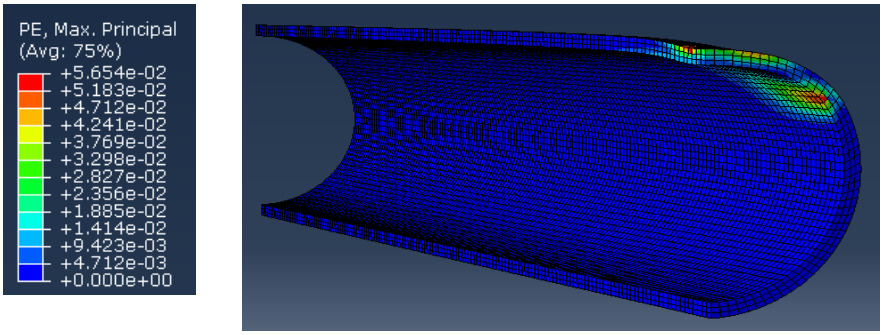

(a)

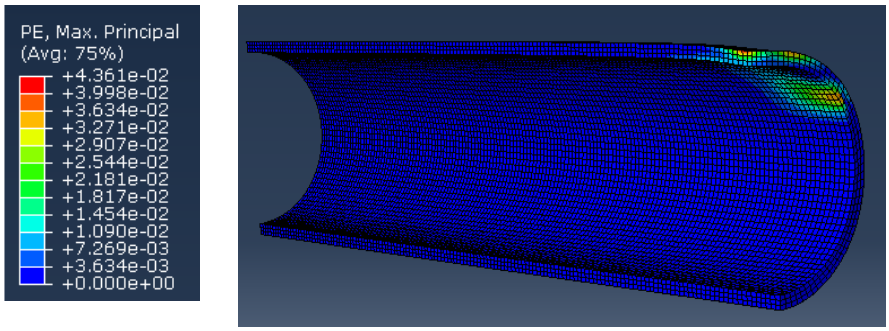

(b)

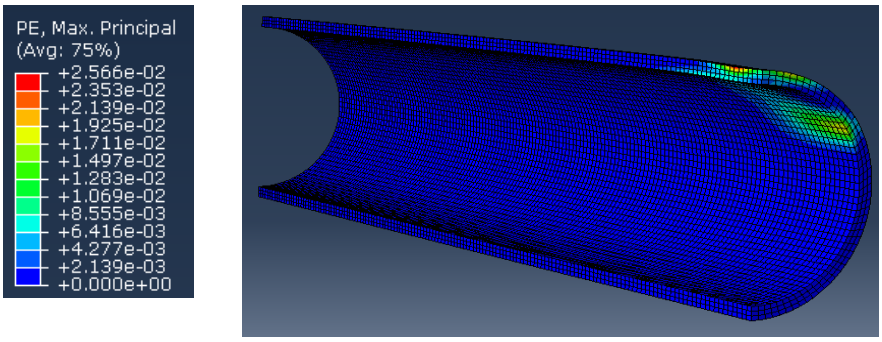

(c)

Figure 6.61: Maximum principal plastic strains along the length of the pipe section with *ECC* coating having thicknesses of (a) 31.75mm (b) 45mm (c) 63.5mm.

Figure 6.62, (a) and (b), shows the comparison of the reduction of diameter (R) in the impact zone and reduction in diameter to diameter ratios (*R/D)* for pipes with different thicknesses of concrete and *ECC* coatings. It is observed that the use of *ECC* coating significantly decreases the damage caused to the pipe due to the impact load and reduces the severity of the damage from major to minor [DNV (2010b)]. In general it is observed that with the increase in the thickness of *ECC* coating, the damage caused to the pipe decreases. It is important to note that the damage caused to the pipe is found to be similar for the case of plain concrete and *ECC* coated pipes.

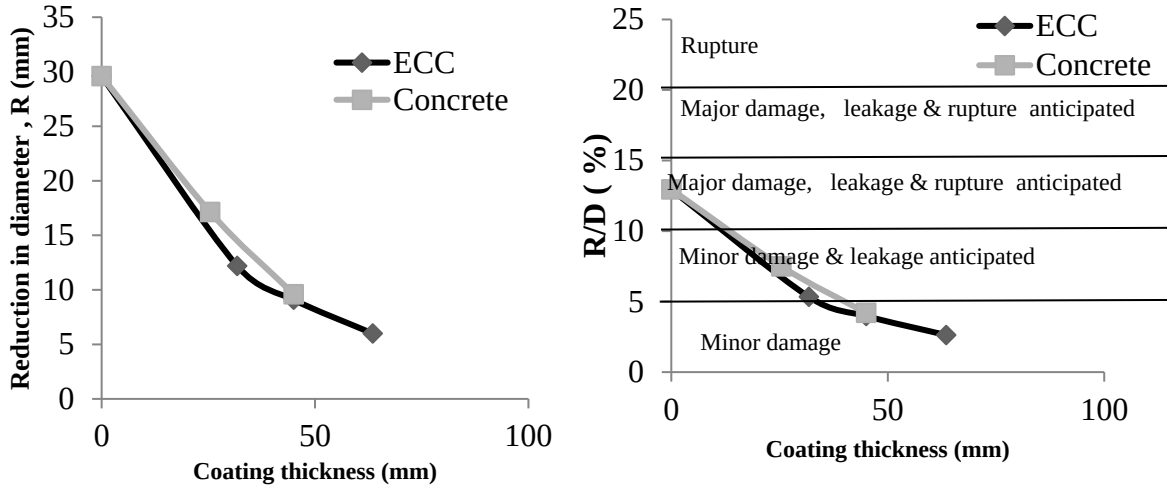

(a) (b)

Figure 6.62: (a) Reduction in diameter (R) and (b) reduction in diameter to diameter ratios (*R/D)* for pipe with different thicknesses of coatings.

6.10.2.1 Effect of bond

In the analyses described in sections 6.10.1 and 6.10.2, a perfect bond was assumed between the coatings and the pipes. In order to investigate the effect of bond on the response of *ECC* coated pipes same case studies as discussed in section 6.10.2 are considered. The following analyses are carried out with the assumption that no bond exists between the pipes and ECC coating.

- Case study EC-1: No coating
- Case study U-EC-2: Coating with a thickness of 31.75mm
- Case study U-EC-3: Coating with a thickness of 45mm

- Case study U-EC-4: Coating with a thickness of 63.5mm

Figure 6.63 to Figure 6.65 show the effect of bond (between pipe and *ECC* coating) on the reduction in the diameter along the length of the pipe for the case studies investigated. In general it is observed that the reduction in the diameter of the pipe is less for *ECC* coated pipes (compared to pipe without coating) irrespective of the bond between the pipe and the *ECC* coating. It is important to observe that the bond has significant effect on the damage sustained by the pipe due to impact as an increased reduction in the diameter is observed for the case of unbonded pipes.

Figure 6.66 shows the comparison of the reduction in diameter to diameter ratios (*R/D)* for *ECC* coated pipes (bonded and un-bonded). In general it is observed that the reduction in the diameter is less for *ECC* coated pipes (compared to pipe without coating) irrespective of the bond between the pipe and the *ECC* coating. However, it is observed that for the case of un-bonded pipes, the reduction in the diameter is larger. Based on the above it can be concluded that the bond between the pipe and the protective coating can significantly affect the level of damage sustained by the pipe due to impact.

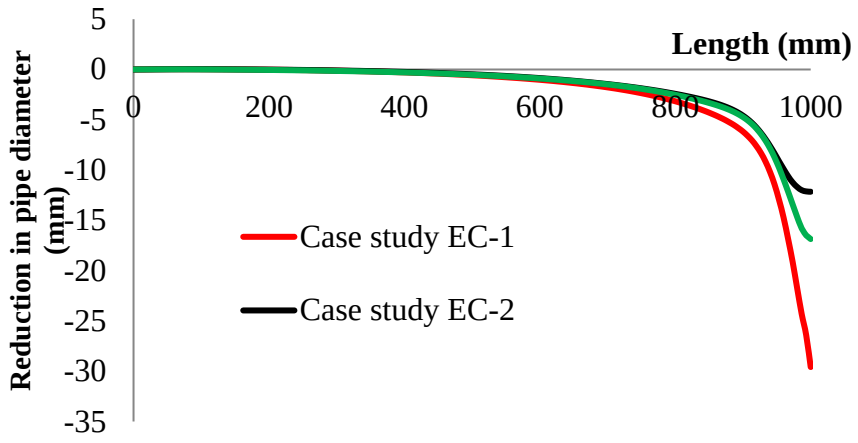

Figure 6.63: Effect of bond (between pipe and *ECC* coating) on the reduction in the diameter along the length of the pipe for case studies *EC-1*, *EC-2* and *U-EC-2*.

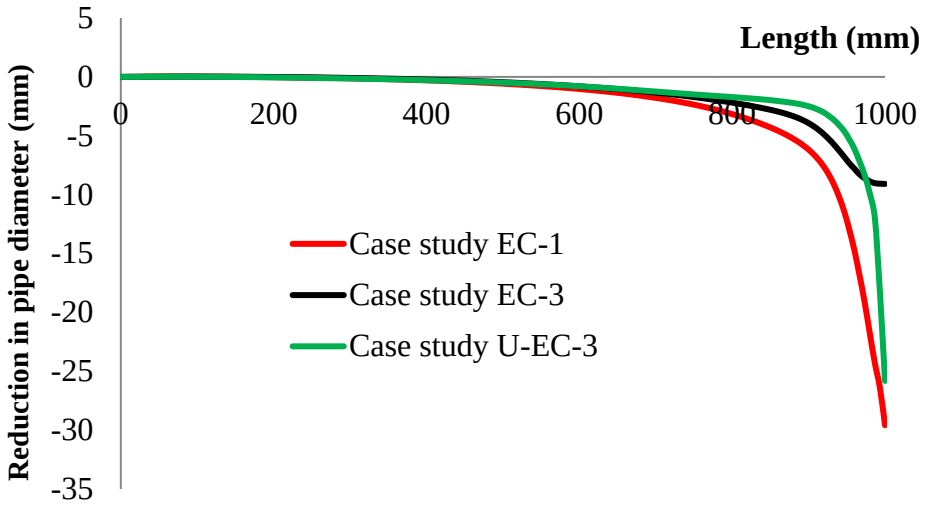

Figure 6.64: Effect of bond (between pipe and ECC coating) on the reduction in the diameter along the length of the pipe for case studies *EC-1*, *EC-3* and *U-EC-3*.

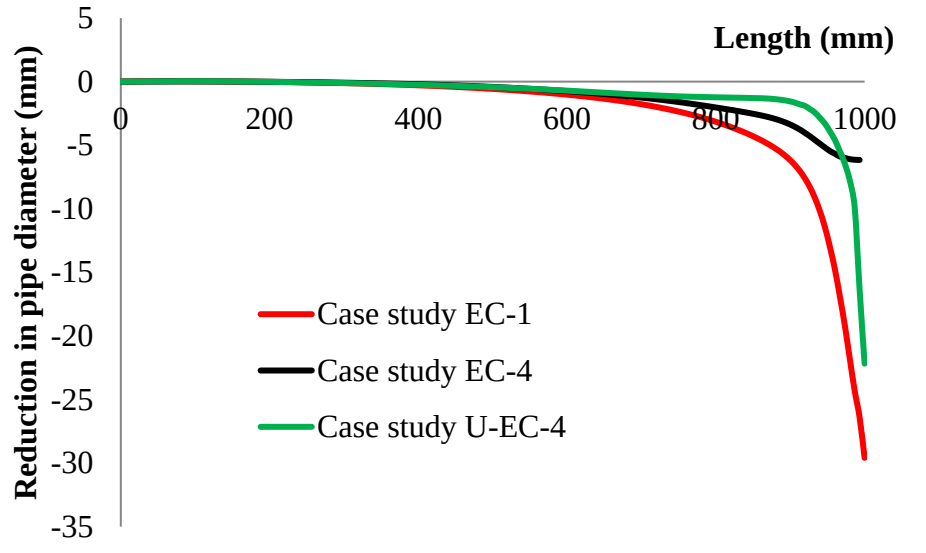

Figure 6.65: Effect of bond (between pipe and ECC coating) on the reduction in the diameter along the length of the pipe for case studies *EC-1*, *EC-4* and *U-EC-4*.

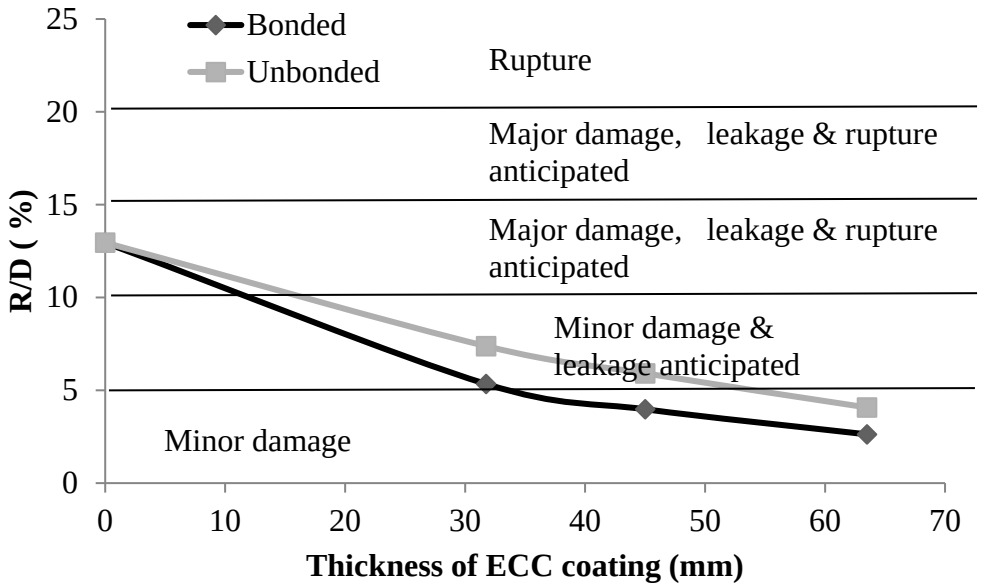

Figure 6.66: *R/D* ratios for pipe with bonded and unbonded *ECC* coating.

6.11 CONCLUSIONS

Based on the *NLFEA* conducted in this Chapter to investigate the influence of the end conditions on the *in-situ* behaviour of the subsea pipes under impact loading the following conclusions are drawn:

- Pipes with their ends being: (i) fixed but allowed to slide horizontally or (ii) free exhibit more global deformation compared to pipes with fully fixed ends (with axial restraint) with the latter however exhibiting higher levels of local damage in the impact region.

- Pipes laid on a rigid base exhibited a larger reduction in diameter of their cross-section (damage) in the impact region and less global deformation along their length compared to pipes laid on a softer soil bed. This is due to the fact that the pipes laid on a rigid base exhibit a stiffer response that result in higher values of contact force, shorter duration of impact and higher levels of damage in the impact region.

The length of 4000mm (L/D = 8.75) is observed to be sufficient to ensure that the behaviour of the pipe under impact is not influenced by the end conditions.

Based on the predictions obtained from *NLFEA* investigating the influence of the subsoil conditions on the impact behaviour of the pipes the following conclusion can be drawn:

- As the stiffness of the soil layer supporting the pipe decreases, the level of damage sustained locally in the impact region reduces whereas global deformation (exhibited along the whole length of the pipe) increases.

- When the soil layer supporting the pipe is characterised by higher values of stiffness, the level of damage sustained locally in the impact region increases whereas global deformation becomes less pronounced.

Based on the numerical predictions concerning the influence of axial loading on the impact behaviour of the pipes it is shown that:

- The development of axial loading can affect the behaviour of the subsea pipes under impact loading.

- Increasing levels of compressive axial loading (resulting in axial compressive stresses of up to 50% of f_y) will result in a significant reduction of the pipe diameter (expressing the level of damage sustained) within the impact region.

- The development of tensile axial loading (resulting in axial tensile stresses of up to 30% of f_y) results in a smaller reduction of the pipe diameter in the impact region compared to that exhibited in the case of the pipe without axial loading.

The predictions obtained from the case studies investigating the influence of the level of the (internal or external) pressure imposed onto the walls of the pipe show that:

- Increasing levels of internal (positive) pressure (resulting in the hoop stresses 15% of f_y) results in a reduction of the level of damage sustained by the pipe in the

impact region (expressed reduction in the diameter) and an increase in the global deformation along its length. However, the increase of the external (negative) pressure results in a significant decrease in the diameter of the pipe in the impact area. This level of damage can also result in the collapse of the pipe cross-section.

The case studies investigating the effect of the pipe geometry on its behaviour under impact loading reveal that:

- for a particular pipe diameter, as the thickness of the pipe walls decrease, the magnitude of the maximum contact force generated in the impact region also decreases.

- the damage sustained in the impact region of the pipe reduces as the thickness of the pipe wall increase.

The predicted behaviour of the pipe under the combined action of impact, axial load and pressure revealed that:

- this can differ significantly from the behaviour exhibited under purely impact loading. In fact it is demonstrated that certain combinations of the above actions can have a detrimental effect on the response of the pipe (resulting in higher levels of damage). It is important to note that the code of practice [DNV (2010a)] used by the industry does not consider the combined effect of the above parameters on the impact behaviour of the pipe. This raises question concerning the ability of this method to provide safe design solutions capable of safeguarding a certain level of resilience.

The analysis of the predictions obtained from the case studies investigating numerically the effect of (concrete or ECC) coating on the impact behaviour of the pipe leads to the following conclusions:

- It is observed that the use of concrete or *ECC* coating can significantly reduce the level of damage caused to the pipe due to impact loading. More specifically the use

of the subject coatings resulted in a reduction of the level sustained from major (exhibited for the pipe without coating) to minor [DNV (2010a)].

- Increasing the thickness of the concrete or *ECC* coating results in a decrease in the level of damage sustained by the pipe (expressed as a reduction of the pipe diameter) both locally (at the impact region) and globally (along the whole length).

- The coatings made from concrete or *ECC* significantly reduces the magnitude of the plastic strains in the pipe (steel) irrespective of its thickness.

- The bond between the pipe and the protective coating can significantly affect the level of damage sustained by the pipe due to impact. When ignoring the bond at interface of the *ECC* layer and steel a small increase in damage was observed.

CHAPTER 7

CONCLUSIONS AND RECOMMENDATIONS FOR FUTURE WORK

7.1 CONCLUSIONS

Subsea steel pipes form extended networks for the transportation of oil and gas over large distances. These networks play a vital role in fulfilling the energy requirements of the society and industry. Such systems can potentially be subjected to a wide range of actions that can result in the pipes sustaining damage usually observed in the form of a permanent deformation or rupture. Accidental loads stemming from high-mass low-velocity impacts are often characterised by high loading rates and intensities. In order to ensure that subsea pipes continue to operate even after being subjected to such extreme loading conditions their behaviour should be characterised by an intended level of resilience to avoid disruptions to the supply of oil and gas.

The performance of the pipes under impact loading can be assessed (i) experimentally *via* drop-weight testing, (ii) numerically through the use of *NLFEA* and (iii) by employing simplified analytical methods. Based on the critical review of available published experimental, numerical and analytical studies investigating the response of pipes under impact loading presented in Chapter 2, the following conclusions are drawn:

- The majority of experimental studies conducted to date investigating the behaviour of pipes under impact dealt with specimens characterized by relatively small cross-sections (compared to the actual pipes used by offshore industry) and subjected to low impact energies compared to those encountered during accidental collisions of large objects (e.g. icebergs, rocks, fishing equipment etc.) onto subsea pipes. Furthermore the experimental setups employed in these tests do not account for a range of parameters associated with the subsea conditions to which the pipe may be

subjected to. Such conditions include: (i) the sea-bed on which the pipe is laid, (ii) the internal and external pressures and (iii) development of axial loads.

- A large part of the published *NLFEA* studies investigating the behaviour of pipes under impact loading were carried out using quasi-static analysis thus ignoring the effects of inertia and the wave propagation problem aspect.

- Analytical approaches provide a practical tool to assess the damage caused to the pipes due to impact loads. However these approaches are based on approximate models and therefore ignore the effect of certain parameters associated with subsea operational conditions of the pipes which can affect the validity of the predictions obtained.

Generated impact loads due to the collision of heavy objects onto subsea installations such as pipes are imposed for very short durations i.e. few milliseconds. They are generally characterised by high intensity loads which are many times higher than those observed under equivalent static loading and can result in large strain-rates in the pipes. Such elevated values of strain-rates are widely considered to affect the material properties of steel (strain-rate sensitivity) and in turn the dynamic response of the pipes under impact loading. In addition, concrete coating can be used for protecting pipelines to reduce the level of damage sustained during impact. Therefore, the critical analysis of the published experimental studies carried out on steel and concrete specimens under increasing loading rates was conducted in Chapter 3 in order to study in detail the effect of loading rate on the mechanical properties of steel and concrete. The subject investigation revealed that:

- The experimentally observed shift in steel or concrete specimens (e.g. dog-bone, reinforcing bar, cylinder or prism) behaviour from that established under equivalent static loading once certain limits of applied loading rates are surpassed is largely attributed to parameters related with the structural response. The latter response is associated with the dynamic characteristics of the structure (specimen) considered (mass, stiffness), the geometry of the specimens, the interaction with the

experimental setup and the nature of the problem at hand which is a wave propagation problem within a nonlinear medium.

- The behaviour exhibited by steel and concrete specimens under high loading rates differs from that established under equivalent static loading once certain limits of loading rate are surpassed.

- Increasing loading rates have a more significant effect on steel specimen characterised with a lower static yield strength.

- The increase in compressive strength of concrete under increasing loading rates is mainly attributed due to the development of radial confinement in high loading rate tests which cannot be considered as the material property of the concrete.

- There exists a difference of opinion regarding the dynamic tensile strength of concrete. Cotsovos & Pavlović (2008c), Cadoni *et al.* [Cadoni *et al.* (2009)]2009) consider this strength enhancement in concrete due to the inertia acting along the length of the specimen which is the structural property of concrete. However, Lu & Li (2011) consider this enhancement in the concrete tensile strength due to the material property of concrete and it is largely attributed to the micro crack inertia.

- The use of static material properties in the *FE* investigation to study the behaviour of steel and concrete specimens under increasing loading rates can provide reasonable predictions concerning their dynamic response.

The dynamic response exhibited by steel pipes under impact loading is investigated numerically via *NLFEA* in chapters 4 and 5 and, to some extent, experimentally via drop weight testing in Chapter 5. The predictions obtained from the *NLFEA* were validated using relevant test data available in the literature or acquired from the experiments carried out in Chapter 5. Based on the latter investigation the following conclusions are drawn:

- The dynamic behaviour exhibited by steel pipes under impact loads is both local and global. This can be explained when viewing this problem as a wave propagation problem within a non-linear medium. During collision, waves are generated and travel away from the impact area. As a result, a localised response is exhibited in the form of damage observed at the contact area of the pipe and the impactor. The level of this localised damage can vary from a simple dent to a localized failure exhibited in the form of large deformation or even collapse of the pipe's cross-section. Global behaviour is exhibited due to the waves propagating away from the impact region and resulting in the pipe deforming along its whole length.

- Parameters associated with the characteristics of the impacting object (speed and mass), the support conditions imposed onto the pipe specimen, the level of applied axial loading, as well as the level of internal and external pressures imposed onto the walls of the pipes can significantly affect, in some cases detrimentally, the exhibited behaviour of pipes under impact loading.

- The existing assessment methods employed in practice for predicting the level of damage sustained by pipes during impact do not accurately consider the effect of the above parameters. Therefore questions rise concerning their ability to provide accurate and safe/conservative predictions concerning the exhibited behaviour, as it was shown that the effect of the above parameters can have a detrimental effect on the integrity of subsea pipes under the combined action of axial loading and pressures (internal and external) acting on the walls of the pipe.

In Chapter 6, the validated *NLFEA* models were employed to investigate the effect of various parameters associated with the geometry of the pipes (thickness, diameter and length), the end conditions imposed onto the pipes, the properties of the supporting soil on which the pipes are laid, the internal and external pressures acting on the walls of the pipes, as well as the development of axial loading on the *in-situ* behaviour of the full scale pipes under impact loading. The *NLFEA* models employed in this chapter represents more realistically the problem at hand and provide more detailed descriptions of the behaviour of subsea pipes under impact loads compared to the majority of

experimental and numerical studies carried out to date. This chapter also assesses the ability of the concrete and *ECC* coatings with different thicknesses to absorb part of the energy transmitted during the impact, thus protecting the pipes and reducing the level of damage sustained. Based on the *NLFEA*, investigating the influence of the above mentioned parameters on the *in-situ* behaviour of the subsea pipes under impact it is found that:

- Irrespective of the end conditions used, the maximum reduction in the diameter of the pipe is exhibited in the impact region. The reduction in diameter decreases rapidly away from the impact zone. It is also observed that pipes with their ends being either vertically restrained (allowed to slide horizontally) or free exhibit a more global deformation compared to the pipe with fixed ends with the latter exhibiting however higher levels of local damage in the impact region.

- A length of 4000mm (L/D = 8.75) for the considered pipe (D = 457mm & t = 25.4mm) is sufficient to ensure that its behaviour is not influenced by the end conditions.

- As the stiffness of the subsea soil on which the pipe is laid decreases, the maximum reduction in the diameter in the impact region also decreases and this damage is exhibited over a larger span of the pipe.

- The reduction in the diameter for the pipes laid on a rigid base and on high stiffness soil considered herein is similar. Therefore it is logical to conclude that further increase in the stiffness of the subsea soil will not significantly influence the reduction in the pipe diameter in the impact region.

- The increase of the compressive axial loading results in significant reduction in the pipes diameter in the impact region compared to its counterpart without axial load. However, the increase of axial tensile load results in smaller reduction of pipe diameter in the impact region.

- The increase in the internal (positive) pressure results in smaller reduction of diameter in the impact region and leads to an increase of the global deformation along its length. However, the increase of the external (negative) pressure results in a significant decrease in the diameter of the pipe in the impact area.

- An approximately linear relationship is observed between the reduction in the pipe diameter in the impact region and the increasing impact energy (16kJ to 67kJ).

- The permanent deformation exhibited in the impact area decreases as the thickness of the pipe increases.

- A pipe subjected to combined actions of axial loading and internal and external pressures acting on its walls can significantly affect detrimentally its behaviour under impact. The recommended practice [DNV (2010a)] used in industry does not consider the combined effect of the above parameters accurately and as a result it may lead to unsafe predictions.

- The use of concrete or *ECC* coating significantly reduces the level of damage caused to the pipes due to the impact loading.

- The severity of the damage reduces to the minor category [DNV (2010b)] when using concrete or *ECC* coating compared to major category observed in the case of pipes without coating.

- The increase in the thickness of the coating made from concrete or *ECC* results in the reduction of the permanent damage caused to the pipe in the impact region and along its length.

- An approximately linear relationship is established between the reduction in the pipe diameter in the impact region and the thickness (up to three times the pipe thickness) of concrete or *ECC* coating.

- The level of bond achieved between the pipe and the protective coating can significantly affect the level of damage sustained by the pipes due to impact.

7.2 RECOMMENDATIONS FOR FUTURE WORK

While the presented work may help in understanding and assessing the short comings in the current assessments method regarding many aspects related to the dynamic behaviour of pipes when subjected to impact loading, more questions raise and need to be investigated. Here, some of potential issues are indicated:

- A detailed numerical investigation can be conducted to model the behaviour of steel specimens under high loading rates. This will allow investigating the reasons that cause the increase of strength observed in the experimental studies carried out to date on steel specimens under high rate loading.

- The validated *NLFEA* models can be further extended to study more extensively the influence of each parameter presented in Chapter 6 on the behaviour of the pipes under impact. By doing so more detailed design curves (similar to the one developed in Chapter 6) can be produced that can present the residual capacity or degree of damage sustained by pipes when subjected to certain levels of impact energy under operational conditions. This will allow the development of effective design solutions which can be used by engineers and industry for assessing more accurately the level of damage sustained by the pipe under impact.

- Pipes constructed from steel are also used for onshore transportation of gas and oil over large distances. In addition to operational loading these pipes can also be subjected to abnormal loading stemming from blast, fire and seismic activities. Thus the validated *NLFEA* models can also be extended to investigate the behaviour of pipes for the above conditions. As the material behaviour of steel is significantly influenced by temperature change, therefore the numerical study can also be carried out to investigate the effect of temperature cycles on the behaviour of steel pipes.

- The pipes constructed from high strength steel grades such as *X70* and *X80* are being used in long distance pipelines, whereas, *X90* and *X100* are currently being evaluated

[Hillenbrand *et al.* (2001)]. Therefore the numerical study can be extended to investigate the *in-situ* behaviour of such pipes under high loading rates. The predictions can be compared with the steel pipes constructed from *X65* steel grade considered in the present study.

- The subsea bed on which pipes are laid is modelled as elastic springs in the present study. Thus the *NLFEA* models can be extended to investigate the impact behaviour of the pipe laid on soil bed modelled with its non-linear properties using *3D* elements. The development of such models can result in significant increase in the computational cost. Therefore the predictions acquired from both *FE* models when considering *3D* elements with non-linear material properties and elastic springs can be compared in order to determine the level of accuracy compromised using elastic springs, which on the other hand provide a less expensive computational solution.

The above recommendations for future work would extend the scope of the *NLFEA* models and would allow a better understanding of the behaviour of pipes (both onshore and offshore) under accidental loads. It will also allow the development of more intricate *NLFEA* models capable of predicting the dynamic response of both onshore and offshore pipes when subjected to accidental loading and can form a basis for effective design solutions of steel pipes under accidental loads that can be used by engineers and the oil and gas industry.

Appendix A

IMPACT TEST RESULTS

Table A.1: Results of Impact tests; Clamped support, Mid-span impact, without internal pressure.

Author (year)	Yield stress (MPa)	Pipe Diameter (mm)	Pipe thickness (mm)	Span length (mm)	Energy (J)	Mass (kg)	Initial velocity (m/s)	Residual Displacement (mm)	Maximum contact force (kN)	Time (milliseconds)	Residual velocity (m/s)
Jones *et al.* (1992)	312.5	22	2	220	495	10	9.95	33.73	19.4	8.817	1.24
Jones *et al.* (1992)	312.5	22	2	220	675	10	11.62	44.4	20.16	9.17	0.98
Jones *et al.* (1992)	312.5	22	2	220	575	10	10.72	38.71	18.79	9.481	1.13
Jones *et al.* (1992)	312.5	22	2	220	385	10	8.78	29.72	16.47	8.79	1.36
Jones *et al.* (1992)	312.5	22	2	220	634	10	11.26	40.28	24.2	9.894	1.11
Jones *et al.* (1992)	312.5	22	2	220	294	10	7.67	22.28	15.76	8.759	1.38
Jones *et al.* (1992)	559	42	2	420	799	17.5	9.56	24.04	34.25	9.7	2.91
Jones *et al.* (1992)	559	42	2	420	1204	17.5	11.73	45.72	35.55	14.674	1.25
Jones *et al.* (1992)	559	42	2	420	1198	17.5	11.7	40.93	35.52	13.77	1.5
Jones *et al.* (1992)	559	42	2	420	1017	17.5	10.78	32.02	35.33	11.428	2.39
Jones *et al.* (1992)	559	42	2	420	863	17.5	9.93	25.84	32.19	11.348	2.81
Jones *et al.* (1992)	559	42	2	420	934	17.5	10.33	28.31	39.28	10.782	3.02
Jones *et al.* (1992)	559	42	2	420	1127	17.5	11.35	39.24	33.88	13.467	1.8

Table A.1: **Results of Impact tests; Clamped support, Mid-span impact, without internal pressure** (**Continued**).											
Author (year)	**Yield stress (MPa)**	**Pipe Diameter (mm)**	**Pipe thickness (mm)**	**Span length (mm)**	**Energy (J)**	**Mass (kg)**	**Initial velocity (m/s)**	**Residual Displacement (mm)**	**Maximum contact force (kN)**	**Time (milliseconds)**	**Residual velocity (m/s)**
Jones *et al.* (1992)	516	80	2	800	1665	33.5	9.97	42.7	-	-	-
Jones *et al.* (1992)	516	80	2	800	2158	33.5	11.35	55.7	47.16	18.313	3.25
Jones *et al.* (1992)	516	80	2	800	1537	49.5	7.88	46.79	-	-	-
Jones *et al.* (1992)	516	80	2	800	3188	49.5	11.35	84.62	-	-	-
Jones *et al.* (1992)	516	80	2	800	3188	49.5	11.35	85.41	-	-	-
Jones *et al.* (1992)	516	80	2	800	2467	49.5	9.98	64.39	51.45	27.855	2.8
Jones *et al.* (1992)	516	80	2	800	1937	49.5	8.85	56.91	46.45	24.174	2.83
Jones *et al.* (1992)	516	80	2	800	1278	49.5	7.19	40.03	35.38	23.275	1.75
Jones *et al.* (1992)	468	120	2	1200	2387	79.5	7.75	49.03	65.24	23.329	2.82
Jones *et al.* (1992)	468	120	2	1200	3880	79.5	9.88	61.98	79.54	19.325	2.3
Jones *et al.* (1992)	468	120	2	1200	5303	79.5	11.55	78.28	97	28.456	3.98
Jones *et al.* (1992)	468	120	2	1200	5312	79.5	11.56	79.31	-	-	-
Jones *et al.* (1992)	468	120	2	1200	4671	79.5	10.84	79.04	105	23.14	4.01
Jones *et al.* (1992)	468	120	2	1200	2883	98	7.67	53.3	-	-	-
Jones *et al.* (1992)	468	120	2	1200	4871	98	9.97	76.03	85	25.726	3.07
Jones *et al.* (1992)	468	120	2	1200	5768	98	10.85	90.74	-	-	-
Jones *et al.* (1992)	468	120	2	1200	1932	98	6.28	45.39	68	24.208	1.99
Jones *et al.* (1992)	470	60	2	600	589	21	7.49	22.02	32.71	13.001	2.34
Jones *et al.* (1992)	470	60	2	600	821	21	8.84	31.1	27.81	14.4	2.51
Jones *et al.* (1992)	470	60	2	600	1042	21	9.96	37.87	29.4	14.198	2.72
Jones *et al.* (1992)	470	60	2	600	1369	21	11.42	46.06	36.61	13.295	2.96
Jones *et al.* (1992)	470	60	2	600	1280	21	11.04	43.67	53.16	14.779	3.12
Jones *et al.* (1992)	470	60	2	600	946	21	9.49	36.79	-	-	-
Jones *et al.* (1992)	470	60	2	600	1143	30	8.73	44.44	27.68	17.304	2.37

Table A.1: **Results of Impact tests; Clamped support, Mid-span impact, without internal pressure** (**Continued**).											
Author (year)	**Yield stress (MPa)**	**Pipe Diameter (mm)**	**Pipe thickness (mm)**	**Span length (mm)**	**Energy (J)**	**Mass (kg)**	**Initial velocity (m/s)**	**Residual Displacement (mm)**	**Maximum contact force (kN)**	**Time (milliseconds)**	**Residual velocity (m/s)**
Jones *et al.* (1992)	470	60	2	600	1970	30	11.46	60.67	50.52	18.112	3.06
Jones *et al.* (1992)	-	120	1.925	1195	1960	100	6.26	43.2	-	-	-
Jones *et al.* (1992)	-	120	1.925	1195	5880	100	10.85	93.4	-	-	-
Jones *et al.* (1992)	-	120	1.925	1195	3920	100	8.86	70.9	-	-	-
Jones *et al.* (1992)	-	120	1.925	1195	5880	100	10.85	86.1	-	-	-
Jones *et al.* (1992)	-	120	1.925	1195	5880	100	8.86	95.7	-	-	-
Jones *et al.* (1992)	360.5	324	9.4	3194	19180	978	6.26	54.2	-	-	-
Jones *et al.* (1992)	360.5	324	9.4	3194	57540	978	10.85	103.1	-	-	-
Jones *et al.* (1992)	360.5	324	9.4	3194	95900	978	14	149.7	-	-	-
Jones *et al.* (1992)	360.5	324	9.4	3194	76720	978	12.53	131.6	-	-	-
Jones *et al.* (1992)	360.5	324	9.4	3194	38360	978	8.86	89.1	-	-	-
C S Ng & W Q Shen (2006)	772.6	57	1.6	570	1305	80	5.72	45.48	44.03	-	-
C S Ng & W Q Shen (2006)	772.6	57	1.6	570	1338	80	5.79	48.12	49.13	-	-
C S Ng & W Q Shen (2006)	772.6	57	1.6	570	1324	80	5.76	47.1	39.24	-	-
Jones & Brich (2010)	557	58	1	300	-	10.75	9.36	32	-	-	-
Jones & Brich (2010)	557	58	1	300	-	10.75	8.1	29.2	-	-	-
Jones & Brich (2010)	557	58	1	300	-	10.75	8.74	31.6	-	-	-
Jones & Brich (2010)	557	58	1	300	-	10.75	9.04	33.1	-	-	-
Chen & Shen (1998)	519.5	19	0.9	160	264	48.7	3.3	-	-	-	-
Chen & Shen (1998)	519.5	19	0.9	160	114	48.7	2.16	15.5	13.64	-	-
Chen & Shen (1998)	519.5	19	0.9	160	66	48.7	1.65	12.8	12.2	-	-
Chen & Shen (1998)	519.5	19	0.9	160	107	48.7	2.09	14.3	13.08	-	-
Chen & Shen (1998)	519.5	19	0.9	180	138	48.7	2.39	-	-	-	-
Chen & Shen (1998)	519.5	19	0.9	180	92	48.7	1.95	12.5	11.6	-	-

Table A.1: Results of Impact tests; Clamped support, Mid-span impact, without internal pressure (Continued).											
Author (year)	**Yield stress (MPa)**	**Pipe Diameter (mm)**	**Pipe thickness (mm)**	**Span length (mm)**	**Energy (J)**	**Mass (kg)**	**Initial velocity (m/s)**	**Residual Displacement (mm)**	**Maximum contact force (kN)**	**Time (milliseconds)**	**Residual velocity (m/s)**
Chen & Shen (1998)	519.5	19	0.9	200	100	48.7	2.03	15.7	11.56	-	-
Chen & Shen (1998)	519.5	19	0.9	200	94	48.7	1.97	15.2	10.8	-	-
Chen & Shen (1998)	519.5	19	0.9	200	90	48.7	1.93	14.3	10.04	-	-
Chen & Shen (1998)	519.5	19	0.9	200	168	48.7	2.63	-	-	-	-
Chen & Shen (1998)	519.5	19	0.9	200	87	48.7	1.89	13.2	-	-	-
Chen & Shen (1998)	-	19	1.2	160	183	48.7	2.74	17.3	20.68	-	-
Chen & Shen (1998)	-	19	1.2	160	165	48.7	2.61	13.7	17.32	-	-
Chen & Shen (1998)	-	19	1.2	160	159	48.7	2.56	13.1	17.08	-	-
Chen & Shen (1998)	-	19	1.2	180	161	48.7	2.57	16.4	17.2	-	-
Chen & Shen (1998)	-	19	1.2	180	151	48.7	2.49	14.1	16.68	-	-
Chen & Shen (1998)	-	19	1.2	180	128	48.7	2.29	13.3	-	-	-
Chen & Shen (1998)	-	19	1.2	180	224	48.7	3.03	-	-	-	-
Chen & Shen (1998)	-	19	1.2	200	114	48.7	2.17	13.4	13.6	-	-
Chen & Shen (1998)	-	19	1.2	200	138	48.7	2.39	14.9	14.08	-	-
Chen & Shen (1998)	-	19	1.2	200	143	48.7	2.42	16.3	14.8	-	-
Chen & Shen (1998)	-	19	1.2	200	159	48.7	2.56	17.9	15.4	-	-
Chen & Shen (1998)	515.5	19	1.6	160	241	48.7	3.15	15.4	25.28	-	-
Chen & Shen (1998)	515.5	19	1.6	160	192	48.7	2.81	14	21.52	-	-
Chen & Shen (1998)	515.5	19	1.6	160	181	48.7	2.73	13.9	20.4	-	-
Chen & Shen (1998)	515.5	19	1.6	180	163	48.7	2.59	12.5	19.68	-	-
Chen & Shen (1998)	515.5	19	1.6	180	204	48.7	2.89	14.8	23.4	-	-
Chen & Shen (1998)	515.5	19	1.6	180	195	48.7	2.83	14.3	21.8	-	-
Chen & Shen (1998)	515.5	19	1.6	180	176	48.7	2.69	14.1	20.24	-	-
Chen & Shen (1998)	515.5	19	1.6	200	166	48.7	2.61	12.6	1660	-	-

Table A.1: Results of Impact tests; Clamped support, Mid-span impact, without internal pressure (Continued).											
Author (year)	**Yield stress (MPa)**	**Pipe Diameter (mm)**	**Pipe thickness (mm)**	**Span length (mm)**	**Energy (J)**	**Mass (kg)**	**Initial velocity (m/s)**	**Residual Displacement (mm)**	**Maximum contact force (kN)**	**Time (milliseconds)**	**Residual velocity (m/s)**
Chen & Shen (1998)	515.5	19	1.6	200	168	48.7	2.63	14.5	16.76	-	-
Chen & Shen (1998)	515.5	19	1.6	200	169	48.7	2.63	14.4	17	-	-
Chen & Shen (1998)	515.5	19	1.6	200	197	48.7	2.85	15.5	-	-	-
Chen & Shen (1998)	510.1	38	1.2	320	207	48.7	2.92	15.5	23.48	-	-
Chen & Shen (1998)	510.1	38	1.2	320	321	48.7	3.63	21.6	26.12	-	-
Chen & Shen (1998)	510.1	38	1.2	320	499	48.7	4.53	31.1	28.04	-	-
Chen & Shen (1998)	510.1	38	1.2	320	751	48.7	5.56	44	-	-	-
Chen & Shen (1998)	510.1	38	1.2	320	624	48.7	5.07	38.2	28.88	-	-
Chen & Shen (1998)	510.1	38	1.2	320	521	48.7	4.63	33.2	-	-	-
Chen & Shen (1998)	510.1	38	1.2	360	633	48.7	5.09	38.9	25.6	-	-
Chen & Shen (1998)	510.1	38	1.2	360	546	48.7	4.74	33.5	25.4	-	-
Chen & Shen (1998)	510.1	38	1.2	360	355	48.7	3.82	23.9	23.4	-	-
Chen & Shen (1998)	510.1	38	1.2	360	552	48.7	4.76	33.9	-	-	-
Chen & Shen (1998)	510.1	38	1.2	360	514	48.7	4.59	32	-	-	-
Chen & Shen (1998)	510.1	38	1.2	400	601	48.7	4.97	38.1	23.36	-	-
Chen & Shen (1998)	510.1	38	1.2	400	359	48.7	3.84	27.7	19.2	-	-
Chen & Shen (1998)	510.1	38	1.2	400	529	48.7	4.67	34.6	22.68	-	-
Chen & Shen (1998)	510.1	38	1.2	400	506	48.7	4.56	31.6	-	-	-
Chen & Shen (1998)	516.7	38	1.6	320	554	48.7	4.77	19.4	-	-	-
Chen & Shen (1998)	516.7	38	1.6	320	799	48.7	5.73	32.6	-	-	-
Chen & Shen (1998)	516.7	38	1.6	320	668	48.7	5.24	26.3	-	-	-
Chen & Shen (1998)	516.7	38	1.6	320	602	48.7	4.97	22.8	-	-	-
Chen & Shen (1998)	516.7	38	1.6	360	549	48.7	4.75	21.7	-	-	-
Chen & Shen (1998)	516.7	38	1.6	360	385	48.7	3.98	15.7	-	-	-

Table A.1: Results of Impact tests; Clamped support, Mid-span impact, without internal pressure (Continued).											
Author (year)	**Yield stress (MPa)**	**Pipe Diameter (mm)**	**Pipe thickness (mm)**	**Span length (mm)**	**Energy (J)**	**Mass (kg)**	**Initial velocity (m/s)**	**Residual Displacement (mm)**	**Maximum contact force (kN)**	**Time (milliseconds)**	**Residual velocity (m/s)**
Chen & Shen (1998)	516.7	38	1.6	360	580	48.7	4.88	21.7	-	-	-
Chen & Shen (1998)	516.7	38	1.6	360	459	48.7	4.34	18.1	-	-	-
Chen & Shen (1998)	516.7	38	1.6	400	506	48.7	4.56	19.9	-	-	-
Chen & Shen (1998)	516.7	38	1.6	400	525	48.7	4.64	20.6	-	-	-
Chen & Shen (1998)	516.7	38	1.6	400	608	48.7	5	25.6	-	-	-
Chen & Shen (1998)	516.7	38	1.6	400	541	48.7	4.71	21.6	-	-	-
Chen & Shen (1998)	530.4	57	1.6	480	1128	48.7	6.81	47.5	-	-	-
Chen & Shen (1998)	530.4	57	1.6	480	1401	48.7	7.59	55.2	-	-	-
Chen & Shen (1998)	530.4	57	1.6	480	2417	48.7	9.97	81.8	-	-	-
Chen & Shen (1998)	530.4	57	1.6	480	1930	48.7	8.91	69	-	-	-
Chen & Shen (1998)	530.4	57	1.6	480	2220	48.7	9.55	75	-	-	-
Chen & Shen (1998)	530.4	57	1.6	480	2103	48.7	9.3	72.4	-	-	-
Chen & Shen (1998)	530.4	57	1.6	540	2218	48.7	9.55	78.5	-	-	-
Chen & Shen (1998)	530.4	57	1.6	540	2159	48.7	9.42	77.3	-	-	-
Chen & Shen (1998)	530.4	57	1.6	540	1778	48.7	8.55	68.7	-	-	-
Chen & Shen (1998)	530.4	57	1.6	540	2202	48.7	9.51	77.5	-	-	-
Chen & Shen (1998)	530.4	57	1.6	600	2120	48.7	9.33	80.9	-	-	-
Chen & Shen (1998)	530.4	57	1.6	600	2202	48.7	9.51	82.9	-	-	-
Chen & Shen (1998)	530.4	57	1.6	600	2223	48.7	9.56	83.4	-	-	-
Chen & Shen (1998)	530.4	57	1.6	600	2199	48.7	9.51	81.5	-	-	-
Chen & Shen (1998)	529.7	76	1.6	640	2783	48.7	10.69	71.3	-	-	-
Chen & Shen (1998)	529.7	76	1.6	640	2441	48.7	10.02	67.5	-	-	-
Chen & Shen (1998)	529.7	76	1.6	640	2663	48.7	10.46	68	-	-	-
Chen & Shen (1998)	529.7	76	1.6	640	2328	48.7	9.78	52.2	-	-	-

Table A.1: **Results of Impact tests; Clamped support, Mid-span impact, without internal pressure** (**Continued**).											
Author (year)	**Yield stress (MPa)**	**Pipe Diameter (mm)**	**Pipe thickness (mm)**	**Span length (mm)**	**Energy (J)**	**Mass (kg)**	**Initial velocity (m/s)**	**Residual Displacement (mm)**	**Maximum contact force (kN)**	**Time (milliseconds)**	**Residual velocity (m/s)**
Chen & Shen (1998)	529.7	76	1.6	720	2306	48.7	9.74	53.1	-	-	-
Chen & Shen (1998)	529.7	76	1.6	720	2424	48.7	9.98	56	-	-	-
Chen & Shen (1998)	529.7	76	1.6	720	2457	48.7	10.05	62.9	-	-	-
Chen & Shen (1998)	529.7	76	1.6	720	2059	48.7	9.2	47.7	-	-	-
Chen & Shen (1998)	529.7	76	1.6	800	2352	48.7	9.83	55	-	-	-
Chen & Shen (1998)	529.7	76	1.6	800	2376	48.7	9.88	58.8	-	-	-
Chen & Shen (1998)	529.7	76	1.6	800	2400	48.7	9.93	67.1	-	-	-

Table A.2: Results of Impact tests; Clamped support, Quarter span impact, without internal pressure.

Author (year)	**Yield stress (MPa)**	**Pipe Diameter (mm)**	**Pipe thickness (mm)**	**Span length (mm)**	**Energy (J)**	**Mass (kg)**	**Initial velocity (m/s)**	**Residual displacement (mm)**	**Maximum contact force (kN)**
Jones *et al.* (1992)	312.5	22	2	220	294	10	7.67	15.62	-
Jones *et al.* (1992)	312.5	22	2	220	370	10	8.6	22.75	-
Jones *et al.* (1992)	312.5	22	2	220	294	10	7.67	18.68	-
Jones *et al.* (1992)	312.5	22	2	220	490	10	9.9	28.41	-
Jones *et al.* (1992)	312.5	22	2	220	589	10	10.85	34.7	-
Jones *et al.* (1992)	312.5	22	2	220	547	14	8.84	29.97	-
Jones *et al.* (1992)	312.5	22	2	220	675	14	9.82	37.1	-
Jones *et al.* (1992)	312.5	22	2	220	830	14	10.89	-	-
Jones *et al.* (1992)	312.5	22	2	220	756	14	10.39	-	-

Table A.2: Results of Impact tests; Clamped support, Quarter span impact, without internal pressure (Continued).									
Author (year)	**Yield stress (MPa)**	**Pipe Diameter (mm)**	**Pipe thickness (mm)**	**Span length (mm)**	**Energy (J)**	**Mass (kg)**	**Initial velocity (m/s)**	**Residual displacement (mm)**	**Maximum contact force (kN)**
Jones *et al.* (1992)	312.5	22	2	220	717	14	10.12	42.6	-
Jones *et al.* (1992)	312.5	22	2	220	743	14	10.3	39.38	-
Jones *et al.* (1992)	312.5	22	2	220	269	14	6.2	16.97	-
Jones *et al.* (1992)	312.5	22	2	220	420	14	7.75	22.01	-
Jones *et al.* (1992)	559	42	2	420	622	21	7.7	17.02	-
Jones *et al.* (1992)	559	42	2	420	836	21	8.92	22.9	-
Jones *et al.* (1992)	559	42	2	420	1032	21	9.91	32.42	-
Jones *et al.* (1992)	559	42	2	420	1107	21	10.27	36.2	-
Jones *et al.* (1992)	559	42	2	420	1218	21	10.77	40.62	-
Jones *et al.* (1992)	559	42	2	420	1374	21	11.44	45.51	-
Jones *et al.* (1992)	559	42	2	420	926	21	9.39	29.7	-
Jones *et al.* (1992)	559	42	2	420	732	21	8.35	19.92	-
Jones *et al.* (1992)	559	42	2	420	533	21	7.13	15.84	-
Jones *et al.* (1992)	516	80	2	800	1622	53.5	7.79	44.76	-
Jones *et al.* (1992)	516	80	2	800	2067	53.5	8.79	48.1	-
Jones *et al.* (1992)	516	80	2	800	2707	53.5	10.06	63.86	-
Jones *et al.* (1992)	516	80	2	800	2343	53.5	9.36	60.8	-
Jones *et al.* (1992)	516	80	2	800	2204	53.5	9.08	53.05	-
Jones *et al.* (1992)	516	80	2	800	1817	53.5	8.24	41.74	-
Jones *et al.* (1992)	516	80	2	800	1283	53.5	6.93	32.52	-
Jones *et al.* (1992)	516	80	2	800	3386	53.5	11.25	101.94	-
Jones *et al.* (1992)	468	120	2	1200	2566	98	7.24	53.12	-
Jones *et al.* (1992)	468	120	2	1200	3782	98	8.79	73.05	-
Jones *et al.* (1992)	468	120	2	1200	3210	98	8.09	64.68	-

Table A.2: Results of Impact tests; Clamped support, Quarter span impact, without internal pressure (Continued).									
Author (year)	**Yield stress (MPa)**	**Pipe Diameter (mm)**	**Pipe thickness (mm)**	**Span length (mm)**	**Energy (J)**	**Mass (kg)**	**Initial velocity (m/s)**	**Residual displacement (mm)**	**Maximum contact force (kN)**
Jones *et al.* (1992)	468	120	2	1200	4251	98	9.31	75.61	-
Jones *et al.* (1992)	468	120	2	1200	5198	98	10.3	95.52	-
Jones *et al.* (1992)	468	120	2	1200	4768	98	9.86	87.63	-
Jones *et al.* (1992)	470	60	2	600	520	21	7.04	19.99	-
Jones *et al.* (1992)	470	60	2	600	871	21	9.11	30.32	-
Jones *et al.* (1992)	470	60	2	600	1040	21	9.95	31.73	-
Jones *et al.* (1992)	470	60	2	600	1250	21	10.91	36.91	-
Jones *et al.* (1992)	470	60	2	600	1398	21	11.54	40.08	-
Jones *et al.* (1992)	470	60	2	600	1153	30	8.77	38.72	-
Jones *et al.* (1992)	470	60	2	600	1792	30	10.93	50.31	-
Jones *et al.* (1992)	470	60	2	600	1698	30	10.64	53.3	-
Jones & Brich (2010)	557	58	1	300	-	10.75	9.34	31.1	-
Jones & Brich (2010)	557	58	1	300	-	10.75	8.08	25.9	-
Jones & Brich (2010)	557	58	1	300	-	10.75	10.43	32.1	-
Chen & Shen (1998)	519.5	19	0.9	160	125	48.7	2.27	-	13.64
Chen & Shen (1998)	519.5	19	0.9	160	106	48.7	2.09	13.5	12.84
Chen & Shen (1998)	519.5	19	0.9	160	79	48.7	1.81	10.5	12.32
Chen & Shen (1998)	519.5	19	0.9	160	69	48.7	1.68	9	12.12
Chen & Shen (1998)	519.5	19	0.9	180	85	48.7	1.87	12.2	11.96
Chen & Shen (1998)	519.5	19	0.9	180	72	48.7	1.72	10.7	11.76
Chen & Shen (1998)	519.5	19	0.9	180	67	48.7	1.66	9.8	11.8
Chen & Shen (1998)	519.5	19	0.9	200	72	48.7	1.73	11.2	11.76
Chen & Shen (1998)	519.5	19	0.9	200	67	48.7	1.66	10.3	11.48
Chen & Shen (1998)	519.5	19	0.9	200	61	48.7	1.58	10	11.12

Table A.2: Results of Impact tests; Clamped support, Quarter span impact, without internal pressure (Continued).									
Author (year)	**Yield stress (MPa)**	**Pipe Diameter (mm)**	**Pipe thickness (mm)**	**Span length (mm)**	**Energy (J)**	**Mass (kg)**	**Initial velocity (m/s)**	**Residual displacement (mm)**	**Maximum contact force (kN)**
Chen & Shen (1998)	519.5	19	0.9	200	55	48.7	1.5	8.3	10.24
Chen & Shen (1998)	-	19	1.2	160	106	48.7	2.09	9.6	18.6
Chen & Shen (1998)	-	19	1.2	160	96	48.7	1.99	9.2	16.84
Chen & Shen (1998)	-	19	1.2	180	139	48.7	2.39	14.1	18.24
Chen & Shen (1998)	-	19	1.2	180	129	48.7	2.3	11.7	18.08
Chen & Shen (1998)	-	19	1.2	180	108	48.7	2.11	10.2	17.2
Chen & Shen (1998)	-	19	1.2	180	88	48.7	1.9	9.3	15.52
Chen & Shen (1998)	-	19	1.2	200	77	48.7	1.78	7.8	13.64
Chen & Shen (1998)	-	19	1.2	200	94	48.7	1.97	10	26.04
Chen & Shen (1998)	-	19	1.2	200	83	48.7	1.85	9.4	24.43
Chen & Shen (1998)	-	19	1.2	200	159	48.7	2.56	11.9	-
Chen & Shen (1998)	515.5	19	1.6	160	120	48.7	2.22	9.5	-
Chen & Shen (1998)	515.5	19	1.6	160	119	48.7	2.22	9.3	21.88
Chen & Shen (1998)	515.5	19	1.6	180	129	48.7	2.3	10.4	-
Chen & Shen (1998)	515.5	19	1.6	180	111	48.7	2.14	9.4	-
Chen & Shen (1998)	515.5	19	1.6	180	119	48.7	2.21	9.9	-
Chen & Shen (1998)	515.5	19	1.6	180	115	48.7	2.17	9.7	20.52
Chen & Shen (1998)	515.5	19	1.6	200	139	48.7	2.39	12	-
Chen & Shen (1998)	515.5	19	1.6	200	100	48.7	2.02	9.7	-
Chen & Shen (1998)	515.5	19	1.6	200	108	48.7	2.1	9.9	18.92
Chen & Shen (1998)	515.5	19	1.6	200	211	48.7	2.95	14.7	-
Chen & Shen (1998)	510.1	38	1.2	320	501	48.7	4.54	33.7	-
Chen & Shen (1998)	510.1	38	1.2	320	406	48.7	4.08	25.5	-
Chen & Shen (1998)	510.1	38	1.2	320	325	48.7	3.66	20.5	32.28

Table A.2: Results of Impact tests; Clamped support, Quarter span impact, without internal pressure (Continued).									
Author (year)	**Yield stress (MPa)**	**Pipe Diameter (mm)**	**Pipe thickness (mm)**	**Span length (mm)**	**Energy (J)**	**Mass (kg)**	**Initial velocity (m/s)**	**Residual displacement (mm)**	**Maximum contact force (kN)**
Chen & Shen (1998)	510.1	38	1.2	360	285	48.7	3.42	19.4	-
Chen & Shen (1998)	510.1	38	1.2	360	301	48.7	3.52	20.1	29.6
Chen & Shen (1998)	510.1	38	1.2	360	238	48.7	3.13	17	-
Chen & Shen (1998)	510.1	38	1.2	400	286	48.7	3.43	20.6	24.84
Chen & Shen (1998)	510.1	38	1.2	400	320	48.7	3.63	21.8	-
Chen & Shen (1998)	510.1	38	1.2	400	238	48.7	3.13	17	-
Chen & Shen (1998)	516.7	38	1.6	320	440	48.7	4.25	16.2	-
Chen & Shen (1998)	516.7	38	1.6	320	430	48.7	4.21	15.2	40.28
Chen & Shen (1998)	516.7	38	1.6	320	436	48.7	4.23	15.3	-
Chen & Shen (1998)	516.7	38	1.6	320	512	48.7	4.59	18.8	-
Chen & Shen (1998)	516.7	38	1.6	360	441	48.7	4.26	17	-
Chen & Shen (1998)	516.7	38	1.6	360	420	48.7	4.15	15.9	37.76
Chen & Shen (1998)	516.7	38	1.6	360	411	48.7	4.11	15.8	-
Chen & Shen (1998)	516.7	38	1.6	360	319	48.7	3.62	12.8	-
Chen & Shen (1998)	516.7	38	1.6	400	369	48.7	3.89	14.8	-
Chen & Shen (1998)	516.7	38	1.6	400	396	48.7	4.03	15.2	-
Chen & Shen (1998)	516.7	38	1.6	400	417	48.7	4.14	16.6	-
Chen & Shen (1998)	516.7	38	1.6	400	407	48.7	4.09	13.4	35.28
Chen & Shen (1998)	530.4	57	1.6	480	1701	48.7	8.36	66.5	-
Chen & Shen (1998)	530.4	57	1.6	480	1448	48.7	7.72	54.1	-
Chen & Shen (1998)	530.4	57	1.6	480	1254	48.7	7.18	50.1	-

Table A.3: Results of Impact tests; Clamped support, Mid-span impact, with internal pressure.

Author (year)	Yield stress (MPa)	Pipe Diameter (mm)	Pipe thickness (mm)	Span length (mm)	Energy (J)	Mass (kg)	Initial velocity (m/s)	Internal pressure (bar)	Residual displacement (mm)	Maximum contact force (kN)
Chen & Shen (1998)	519.5	19	0.9	200	144	48.7	2.43	86.2	-	-
Chen & Shen (1998)	519.5	19	0.9	200	123	31.9	2.78	86.2	-	-
Chen & Shen (1998)	519.5	19	0.9	200	49	25.2	1.97	86.2	7.6	-
Chen & Shen (1998)	519.5	19	0.9	200	74	25.2	2.42	86.2	11.4	-
Chen & Shen (1998)	519.5	19	0.9	200	49	25.2	1.97	124	7.2	-
Chen & Shen (1998)	519.5	19	0.9	200	62	25.2	2.21	124	9.2	-
Chen & Shen (1998)	519.5	19	0.9	200	66	25.2	2.29	124	9.7	-
Chen & Shen (1998)	519.5	19	0.9	200	69	25.2	2.35	124	10.2	-
Chen & Shen (1998)	519.5	19	0.9	200	65	25.2	2.27	193	9.4	-
Chen & Shen (1998)	519.5	19	0.9	200	68	25.2	2.32	193	9.9	-
Chen & Shen (1998)	516.7	38	1.6	200	215	25.2	4.13	193	9.4	-
Chen & Shen (1998)	516.7	38	1.6	200	289	25.2	4.78	193	11.9	-
Chen & Shen (1998)	516.7	38	1.6	200	427	32.2	5.15	193	18	-
Chen & Shen (1998)	516.7	38	1.6	200	397	32.2	4.97	193	15	-
Chen & Shen (1998)	516.7	38	1.6	200	491	32.2	5.52	193	20	-
Chen & Shen (1998)	516.7	38	1.6	200	457	32.2	5.33	155	19.9	-
Chen & Shen (1998)	516.7	38	1.6	200	444	32.2	5.26	155	17.9	-
Chen & Shen (1998)	516.7	38	1.6	200	438	32.2	5.22	155	17.9	-
Chen & Shen (1998)	516.7	38	1.6	200	434	32.2	5.19	155	17.4	-
Chen & Shen (1998)	516.7	38	1.6	200	433	32.2	5.19	155	17.1	-
Chen & Shen (1998)	516.7	38	1.6	200	457	32.2	5.33	86.2	19	-
Chen & Shen (1998)	516.7	38	1.6	200	443	32.2	5.25	86.2	18.3	-
Chen & Shen (1998)	516.7	38	1.6	200	438	32.2	5.22	86.2	17.3	-

Table A.3: Results of Impact tests; Clamped support, Mid-span impact, with internal pressure.										
Author (year)	**Yield stress (MPa)**	**Pipe Diameter (mm)**	**Pipe thickness (mm)**	**Span length (mm)**	**Energy (J)**	**Mass (kg)**	**Initial velocity (m/s)**	**Internal pressure (bar)**	**Residual displacement (mm)**	**Maximum contact force (kN)**
Chen & Shen (1998)	516.7	38	1.6	200	453	32.2	5.3	86.2	18.5	-
Chen & Shen (1998)	516.7	38	1.6	200	443	32.2	5.25	86.2	17.4	-
C S Ng & W Q Shen (2006)	772.6	57	1.6	570	1278	80	5.66	63	42.13	44.35
C S Ng & W Q Shen (2006)	772.6	57	1.6	570	1244	80	5.59	63	34.95	45.94
C S Ng & W Q Shen (2006)	772.6	57	1.6	570	1150	80	5.37	95	36.64	44.67
C S Ng & W Q Shen (2006)	772.6	57	1.6	570	1217	80	5.52	95	35.64	46.58
C S Ng & W Q Shen (2006)	772.6	57	1.6	570	-	80	-	95	48.04	35.73
C S Ng & W Q Shen (2006)	772.6	57	1.6	570	1190	80	5.46	95	37.55	45.94
C S Ng & W Q Shen (2006)	772.6	57	1.6	570	1213	80	5.52	125	38.56	45.3
C S Ng & W Q Shen (2006)	772.6	57	1.6	570	1185	80	5.45	125	41.25	43.07
C S Ng & W Q Shen (2006)	772.6	57	1.6	570	1146	80	5.36	125	41.18	41.48
C S Ng & W Q Shen (2006)	772.6	57	1.6	570	-	80	-	125	35.88	42.11
C S Ng & W Q Shen (2006)	772.6	57	1.6	570	1007	80	5.03	125	24.65	46.9
C S Ng & W Q Shen (2006)	772.6	57	1.6	570	1052	80	5.14	125	26.63	46.26
Jones & Brich (2010)	557	58	1	300	-	10.75	9.34	100	36.8	-
Jones & Brich (2010)	557	58	1	300	-	10.75	8.1	100	26.1	-
Jones & Brich (2010)	557	58	1	300	-	10.75	8.74	100	29.5	-
Jones & Brich (2010)	557	58	1	300	-	10.75	8.43	100	28	-
Jones & Brich (2010)	557	58	1	300	-	10.75	8.1	150	25.4	-
Jones & Brich (2010)	557	58	1	300	-	10.75	8.74	150	30.4	-
Jones & Brich (2010)	557	58	1	300	-	10.75	8.43	150	27.3	-
Jones & Brich (2010)	557	58	1	300	-	10.75	7.75	150	21.5	-

Table A.4: Results of Impact tests; Clamped support, Quarter span impact, with internal pressure.

Author (year)	Yield stress (MPa)	Pipe Diameter (mm)	Pipe thickness (mm)	Span length (mm)	Energy (J)	Mass (kg)	Initial velocity (m/s)	Internal pressure (bar)	Residual displacement (mm)
Jones & Brich (2010)	557	58	1	300	352	10.75	8.1	100	29.9
Jones & Brich (2010)	557	58	1	300	584	10.75	10.43	100	31.5
Jones & Brich (2010)	557	58	1	300	468	10.75	9.34	150	30.7
Jones & Brich (2010)	557	58	1	300	584	10.75	10.43	150	51
Jones & Brich (2010)	557	58	1	300	352	10.75	8.1	150	29.1

Table A.5: Results of Impact tests; Clamped support, Near to support impact, without internal pressure.

Author (year)	Yield stress (MPa)	Pipe Diameter (mm)	Pipe thickness (mm)	Span length (mm)	Energy (J)	Mass (kg)	Initial velocity (m/s)	Residual displacement (mm)	Maximum contact force (kN)
Jones *et al.* (1992)	312.5	22	2	220	253	6.5	8.83	7.53	-
Jones *et al.* (1992)	312.5	22	2	220	126	6.5	6.22	5.26	-
Jones *et al.* (1992)	312.5	22	2	220	325	6.5	10	9.99	-
Jones *et al.* (1992)	312.5	22	2	220	166	6.5	7.15	6.6	-
Jones *et al.* (1992)	312.5	22	2	220	453	6.5	11.81	14.05	-
Jones *et al.* (1992)	312.5	22	2	220	61	6.5	4.32	3.29	-
Jones *et al.* (1992)	312.5	22	2	220	372	6.5	10.7	12.68	-
Jones *et al.* (1992)	312.5	22	2	220	223	6.5	8.28	8.26	-
Jones *et al.* (1992)	559	42	2	420	282	14	6.35	7.33	-
Jones *et al.* (1992)	559	42	2	420	206	14	5.42	7.74	-
Jones *et al.* (1992)	559	42	2	420	243	14	5.89	5.84	-
Jones *et al.* (1992)	559	42	2	420	326	14	6.83	7.9	-

Table A.5: Results of Impact tests; Clamped support, Near to support impact, without internal pressure (Continued).									
Author (year)	**Yield stress (MPa)**	**Pipe Diameter (mm)**	**Pipe thickness (mm)**	**Span length (mm)**	**Energy (J)**	**Mass (kg)**	**Initial velocity (m/s)**	**Residual displacement (mm)**	**Maximum contact force (kN)**
Jones *et al.* (1992)	559	42	2	420	388	14	7.45	10.89	-
Jones *et al.* (1992)	559	42	2	420	131	14	4.32	3.86	-
Jones *et al.* (1992)	559	42	2	420	167	14	4.88	4.88	-
Jones *et al.* (1992)	559	42	2	420	970	14	11.77	-	-
Jones *et al.* (1992)	516	80	2	800	589	20.5	7.58	17.71	-
Jones *et al.* (1992)	516	80	2	800	694	20.5	8.23	19.42	-
Jones *et al.* (1992)	516	80	2	800	507	20.5	7.04	12.99	-
Jones *et al.* (1992)	516	80	2	800	403	20.5	6.27	12.51	-
Jones *et al.* (1992)	516	80	2	800	305	20.5	5.46	8.67	-
Jones *et al.* (1992)	516	80	2	800	210	20.5	4.52	6.21	-
Jones *et al.* (1992)	468	120	2	1200	2871	98	7.66	-	-
Jones *et al.* (1992)	468	120	2	1200	1874	98	6.19	31.84	-
Jones *et al.* (1992)	468	120	2	1200	955	98	4.41	17.04	-
Jones *et al.* (1992)	468	120	2	1200	921	21	9.36	23.89	-
Jones *et al.* (1992)	468	120	2	1200	635	21	7.78	13.96	-
Jones *et al.* (1992)	468	120	2	1200	208	21	4.45	6.55	-
Jones *et al.* (1992)	468	120	2	1200	402	21	6.19	12.65	-
Jones *et al.* (1992)	470	60	2	600	609	21	7.62	13.95	-
Jones *et al.* (1992)	470	60	2	600	397	21	6.15	12.14	-
Jones *et al.* (1992)	470	60	2	600	311	21	5.44	10.71	-
Jones *et al.* (1992)	470	60	2	600	253	6.5	8.83	5.57	-
Jones *et al.* (1992)	470	60	2	600	350	6.5	10.38	8.79	-
Jones *et al.* (1992)	470	60	2	600	432	6.5	10.53	12.22	-
Jones *et al.* (1992)	470	60	2	600	166	6.5	7.16	4.48	-

Table A.5: Results of Impact tests; Clamped support, Near to support impact, without internal pressure (Continued).									
Author (year)	**Yield stress (MPa)**	**Pipe Diameter (mm)**	**Pipe thickness (mm)**	**Span length (mm)**	**Energy (J)**	**Mass (kg)**	**Initial velocity (m/s)**	**Residual displacement (mm)**	**Maximum contact force (kN)**
Jones *et al.* (1992)	470	60	2	600	203	6.5	7.9	6.72	-
Jones *et al.* (1992)	470	60	2	600	125	6.5	6.21	3.83	-
Chen & Shen (1998)	519.5	19	0.9	160	30	23	1.63	5.2	13.32
Chen & Shen (1998)	519.5	19	0.9	160	28	23	1.57	4.8	13.32
Chen & Shen (1998)	519.5	19	0.9	160	126	23	3.31	-	-
Chen & Shen (1998)	519.5	19	0.9	160	41	23	1.89	5.3	13.32
Chen & Shen (1998)	519.5	19	0.9	180	60	46.7	1.6	7.8	-
Chen & Shen (1998)	519.5	19	0.9	180	46	46.7	1.4	6.9	-
Chen & Shen (1998)	519.5	19	0.9	180	34	35.5	1.39	5.2	-
Chen & Shen (1998)	519.5	19	0.9	180	34	35.5	1.39	5.1	-
Chen & Shen (1998)	519.5	19	0.9	180	30	29.5	1.44	4.7	-
Chen & Shen (1998)	519.5	19	0.9	180	29	29.5	1.41	4	12.52
Chen & Shen (1998)	519.5	19	0.9	180	72	23	2.5	9.5	-
Chen & Shen (1998)	519.5	19	0.9	200	24	23	1.46	4.9	-
Chen & Shen (1998)	519.5	19	0.9	200	62	23	2.32	8.6	-
Chen & Shen (1998)	519.5	19	0.9	200	28	23	1.57	5.4	11.12
Chen & Shen (1998)	-	19	1.2	160	60	23	2.28	5	20.48
Chen & Shen (1998)	-	19	1.2	160	127	23	3.33	9.5	-
Chen & Shen (1998)	-	19	1.2	160	42	23	1.9	3.4	-
Chen & Shen (1998)	-	19	1.2	180	60	23	2.29	4.7	-
Chen & Shen (1998)	-	19	1.2	180	55	23	2.2	4.6	20.36
Chen & Shen (1998)	-	19	1.2	180	51	23	2.11	3.9	-
Chen & Shen (1998)	-	19	1.2	180	80	23	2.64	6.4	-
Chen & Shen (1998)	-	19	1.2	200	49	23	2.06	4.7	-

Table A.5: Results of Impact tests; Clamped support, Near to support impact, without internal pressure (Continued).									
Author (year)	**Yield stress (MPa)**	**Pipe Diameter (mm)**	**Pipe thickness (mm)**	**Span length (mm)**	**Energy (J)**	**Mass (kg)**	**Initial velocity (m/s)**	**Residual displacement (mm)**	**Maximum contact force (kN)**
Chen & Shen (1998)	-	19	1.2	200	51	23	2.11	5	-
Chen & Shen (1998)	-	19	1.2	200	56	23	2.21	5.4	18.52
Chen & Shen (1998)	-	19	1.2	200	53	23	2.15	5.3	-
Chen & Shen (1998)	515.5	19	1.6	160	85	23	2.71	5	-
Chen & Shen (1998)	515.5	19	1.6	160	81	23	2.65	4.7	-
Chen & Shen (1998)	515.5	19	1.6	160	79	23	2.61	4.6	-
Chen & Shen (1998)	515.5	19	1.6	180	87	23	2.76	6.1	-
Chen & Shen (1998)	515.5	19	1.6	180	82	23	2.67	5.8	-
Chen & Shen (1998)	515.5	19	1.6	180	81	23	2.65	5.2	-
Chen & Shen (1998)	515.5	19	1.6	180	98	23	2.92	8.9	-
Chen & Shen (1998)	515.5	19	1.6	200	78	23	2.6	4.3	-
Chen & Shen (1998)	515.5	19	1.6	200	79	23	2.63	5	-
Chen & Shen (1998)	515.5	19	1.6	200	83	23	2.69	5.6	-
Chen & Shen (1998)	515.5	19	1.6	200	53	23	2.15	4.1	-
Chen & Shen (1998)	510.1	38	1.2	320	106	23	3.03	8.4	-
Chen & Shen (1998)	510.1	38	1.2	320	103	23	2.99	7.2	-
Chen & Shen (1998)	510.1	38	1.2	320	175	23	3.9	11	-
Chen & Shen (1998)	510.1	38	1.2	360	110	23	3.1	8.8	-
Chen & Shen (1998)	510.1	38	1.2	360	104	23	3.01	8.1	-
Chen & Shen (1998)	510.1	38	1.2	360	107	23	3.05	8.6	-
Chen & Shen (1998)	510.1	38	1.2	360	98	23	2.92	7.5	-
Chen & Shen (1998)	510.1	38	1.2	400	82	23	2.66	7.4	-
Chen & Shen (1998)	510.1	38	1.2	400	89	23	2.78	7.6	-
Chen & Shen (1998)	510.1	38	1.2	400	107	23	3.04	8.4	-

Table A.5: Results of Impact tests; Clamped support, Near to support impact, without internal pressure (Continued).									
Author (year)	**Yield stress (MPa)**	**Pipe Diameter (mm)**	**Pipe thickness (mm)**	**Span length (mm)**	**Energy (J)**	**Mass (kg)**	**Initial velocity (m/s)**	**Residual displacement (mm)**	**Maximum contact force (kN)**
Chen & Shen (1998)	510.1	38	1.2	400	90	23	2.8	8.1	-
Chen & Shen (1998)	510.1	38	1.2	400	216	23	4.33	13.4	-
Chen & Shen (1998)	516.7	38	1.6	320	141	23	3.5	6.3	-
Chen & Shen (1998)	516.7	38	1.6	320	132	23	3.39	6.1	-
Chen & Shen (1998)	516.7	38	1.6	320	197	23	4.14	8.3	-
Chen & Shen (1998)	516.7	38	1.6	320	84	23	2.71	5.3	-
Chen & Shen (1998)	516.7	38	1.6	360	130	23	3.36	6.2	13.32
Chen & Shen (1998)	516.7	38	1.6	360	122	23	3.26	6.1	13.32
Chen & Shen (1998)	516.7	38	1.6	360	242	23	4.59	9.8	13.32
Chen & Shen (1998)	516.7	38	1.6	360	81	23	2.66	5.1	13.32
Chen & Shen (1998)	516.7	38	1.6	400	113	23	3.13	5.9	-
Chen & Shen (1998)	516.7	38	1.6	400	233	23	4.5	9.6	-
Chen & Shen (1998)	516.7	38	1.6	400	114	23	3.15	6.1	-
Chen & Shen (1998)	516.7	38	1.6	400	81	23	2.65	5.1	-

Table A.6: Results of Impact tests; Clamped ends and sand foundation, Mid span impact, without internal pressure.

Author (year)	Yield stress (MPa)	Pipe Diameter (mm)	Pipe thickness (mm)	Span length (mm)	Energy (J)	Mass (kg)	Initial velocity (m/s)	Residual displacement (mm)	Maximum contact force (kN)
C S Ng & W Q Shen (2006)	772.6	57	1.6	570	2369	80	7.7	138.35	37.06
C S Ng & W Q Shen (2006)	772.6	57	1.6	570	1748	80	6.62	76.26	33.21
C S Ng & W Q Shen (2006)	772.6	57	1.6	570	1108	80	5.27	38.37	34.17
C S Ng & W Q Shen (2006)	772.6	57	1.6	570	1331	80	5.77	55.93	33.21
C S Ng & W Q Shen (2006)	772.6	57	1.6	570	1182	80	5.44	46.39	39.6
C S Ng & W Q Shen (2006)	772.6	57	1.6	570	1211	80	5.51	45.55	38
C S Ng & W Q Shen (2006)	772.6	57	1.6	570	1243	80	5.58	50.25	48.54

Table A.7: Results of Impact tests; Clamped ends and sand foundation, Mid span impact, with internal pressure.

Author (year)	Yield stress (MPa)	Pipe Diameter (mm)	Pipe thickness (mm)	Span length (mm)	Energy (J)	Mass (kg)	Initial velocity (m/s)	Internal pressure (bar)	Residual displacement (mm)	Maximum contact force (kN)
C S Ng & W Q Shen (2006)	772.6	57	1.6	570	1178	80	5.43	63	43.7	43.43
C S Ng & W Q Shen (2006)	772.6	57	1.6	570	1022	80	5.06	63	27.56	40.88
C S Ng & W Q Shen (2006)	772.6	57	1.6	570	1099	80	5.25	63	34.8	46.95
C S Ng & W Q Shen (2006)	772.6	57	1.6	570	1055	80	5.14	63	29.98	41.52
C S Ng & W Q Shen (2006)	772.6	57	1.6	570	1076	80	5.19	63	29.2	40.24
C S Ng & W Q Shen (2006)	772.6	57	1.6	570	1061	80	5.15	95	38.15	40.24
C S Ng & W Q Shen (2006)	772.6	57	1.6	570	978	80	4.95	95	26.29	45.35
C S Ng & W Q Shen (2006)	772.6	57	1.6	570	1012	80	5.03	95	29.63	46.95
C S Ng & W Q Shen (2006)	772.6	57	1.6	570	999	80	5	95	37.56	38

Table A.7: Results of Impact tests; Clamped ends and sand foundation, Mid span impact, with internal pressure (Continued).										
Author (year)	**Yield stress (MPa)**	**Pipe Diameter (mm)**	**Pipe thickness (mm)**	**Span length (mm)**	**Energy (J)**	**Mass (kg)**	**Initial velocity (m/s)**	**Internal pressure (bar)**	**Residual displacement (mm)**	**Maximum contact force (kN)**
C S Ng & W Q Shen (2006)	772.6	57	1.6	570	991	80	4.98	95	33.93	42.79
C S Ng & W Q Shen (2006)	772.6	57	1.6	570	1025	80	5.07	125	27.38	41.2
C S Ng & W Q Shen (2006)	772.6	57	1.6	570	1101	80	5.25	125	33.37	44.39
C S Ng & W Q Shen (2006)	772.6	57	1.6	570	1043	80	5.11	125	40.16	41.84
C S Ng & W Q Shen (2006)	772.6	57	1.6	570	1023	80	5.06	125	34.6	40.24

Table A.8: Results of Impact tests; Clamped ends and Kaolin foundation, Mid span impact, without internal pressure.

Author (year)	**Yield stress (MPa)**	**Pipe Diameter (mm)**	**Pipe thickness (mm)**	**Span length (mm)**	**Energy (J)**	**Mass (kg)**	**Initial velocity (m/s)**	**Residual displacement (mm)**	**Maximum contact force (kN)**
C S Ng & W Q Shen (2006)	772.6	57	1.6	570	984	80	4.96	50.77	35.45
C S Ng & W Q Shen (2006)	772.6	57	1.6	570	-	80	-	45.73	32.89
C S Ng & W Q Shen (2006)	772.6	57	1.6	570	1249	80	5.59	48.7	42.16

Table A.9: Results of Impact tests; Clamped ends and Kaolin foundation, Mid span impact, with internal pressure.

Author (year)	**Yield stress (MPa)**	**Pipe Diameter (mm)**	**Pipe thickness (mm)**	**Span length (mm)**	**Energy (J)**	**Mass (kg)**	**Initial velocity (m/s)**	**Residual displacement (mm)**	**Maximum contact force (kN)**	**Internal pressure (bar)**
C S Ng & W Q Shen (2006)	772.6	57	1.6	570	1263	80	5.62	30.37	40.56	125
C S Ng & W Q Shen (2006)	772.6	57	1.6	570	1048	80	5.12	33.23	38.32	63

Table A.9: Results of Impact tests; Clamped ends and Kaolin foundation, Mid span impact, with internal pressure (Continued).										
Author (year)	**Yield stress (MPa)**	**Pipe Diameter (mm)**	**Pipe thickness (mm)**	**Span length (mm)**	**Energy (J)**	**Mass (kg)**	**Initial velocity (m/s)**	**Residual displacement (mm)**	**Maximum contact force (kN)**	**Internal pressure (bar)**
C S Ng & W Q Shen (2006)	772.6	57	1.6	570	1063	80	5.16	29.76	39.6	63
C S Ng & W Q Shen (2006)	772.6	57	1.6	570	1104	80	5.26	34.8	38.64	63
C S Ng & W Q Shen (2006)	772.6	57	1.6	570	1133	80	5.33	32.46	40.88	63
C S Ng & W Q Shen (2006)	772.6	57	1.6	570	1169	80	5.41	44.25	38.96	63
C S Ng & W Q Shen (2006)	772.6	57	1.6	570	1049	80	5.12	30.54	39.28	95
C S Ng & W Q Shen (2006)	772.6	57	1.6	570	1084	80	5.21	27.65	41.2	95
C S Ng & W Q Shen (2006)	772.6	57	1.6	570	1137	80	5.34	34.91	40.88	95
C S Ng & W Q Shen (2006)	772.6	57	1.6	570	-	80	-	26.76	44.39	95
C S Ng & W Q Shen (2006)	772.6	57	1.6	570	1111	80	5.28	30.97	40.24	125
C S Ng & W Q Shen (2006)	772.6	57	1.6	570	1171	80	5.42	44.82	-	125
C S Ng & W Q Shen (2006)	772.6	57	1.6	570	1140	80	5.34	32.52	42.16	125

Appendix B

BEHAVIOUR OF STEEL UNDER HIGH RATE LOADING

Part A: Dog bone specimens

Table B.1: Behaviour of mild steel under high rate loading [Singh et al. (2013)].

$\dot{\epsilon}$ (s^{-1})	Engineering stress				True stress			
	F_y (MPa)	F_u (MPa)	$(DIF)_{Fy}$	$(DIF)_{Fu}$	F_y (MPa)	F_u (MPa)	$(DIF)_{Fy}$	$(DIF)_{Fu}$
0.001	361	483	-	-	363	596	-	-
5	424	486	1.17	1.00	426	602	1.17	1.01
25	472	525	1.30	1.08	474	656	1.30	1.10
250	688	574	1.90	1.18	691	702	1.90	1.17
500	815	570	2.25	1.18	820	704	2.25	1.18
750	891	573	2.46	1.18	897	695	2.47	1.16

Table B.2: Behaviour of *ENCD* steel under high rate loading [Huh *et al.* (2009)].

$\dot{\epsilon}$ (s^{-1})	Engineering stress				True stress			
	F_y (MPa)	F_u (MPa)	$(DIF)_{Fy}$	$(DIF)_{Fu}$	F_y (MPa)	F_u (MPa)	$(DIF)_{Fy}$	$(DIF)_{Fu}$
0.003	154	293.25	-	-	153.48	397.67	-	-
0.1	206.751	308.107	1.34	1.05	206.97	397.67	1.34	1.00
0.5	225.738	322.785	1.46	1.10	227.9	418.6	1.48	1.05
1	259.5	331.22	1.68	1.12	253.48	432.55	1.65	1.03
2	276.37	339.662	1.79	1.15	274.4	437.2	1.78	1.01
5	295.36	348.101	1.91	1.18	304.65	446.51	1.98	1.02
10	322.78	362.87	2.09	1.23	320.93	460.46	2.09	1.031
20	341.77	377.64	2.21	1.28	344.18	462.8	2.24	1.00
50	360.76	388.2	2.34	1.32	367.44	490.7	2.39	1.06
100	383.96	415.6	2.49	1.41	409.302	493.023	2.66	1.00
200	413.502	434.6	2.68	1.48	441.86	513.95	2.87	1.04

Table B.3: Behaviour of *SPCC* steel under high rate loading [Huh *et al.* (2009)].

$\dot{\epsilon}$ (s^{-1})	Engineering stress				True stress			
	F_y (MPa)	F_u (MPa)	$(DIF)_{Fy}$	$(DIF)_{Fu}$	F_y (MPa)	F_u (MPa)	$(DIF)_{Fy}$	$(DIF)_{Fu}$
0.003	220.262	358.81	-	-	222.48	469.38	-	-
0.1	291.1	371.16	1.31	1.03	301.16	472.1	1.35	1.00
0.5	334.2	385.9	1.51	1.07	336.43	482.9	1.51	1.02

Table B.3: Behaviour of *SPCC* steel under high rate loading [Huh et al. (2009)] (Continued).								
$\dot{\epsilon}$ (s^{-1})	Engineering stress				True stress			
	F_y (MPa)	F_u (MPa)	$(DIF)_{Fy}$	$(DIF)_{Fu}$	F_y (MPa)	F_u (MPa)	$(DIF)_{Fy}$	$(DIF)_{Fu}$
1	349.36	385.96	1.58	1.07	385.27	485.65	1.73	1.03
2	356.92	396.18	1.61	1.10	401.55	496.5	1.80	1.05
5	377.22	403.54	1.70	1.12	406.99	504.65	1.82	1.07
10	407.63	411.01	1.84	1.14	412.40	518.21	1.85	1.10
20	415.74	425.35	1.88	1.18	423.56	520.93	1.90	1.10
50	435.4	436.5	1.97	1.21	496.512	534.49	2.23	1.13
100	438.37	449.17	1.98	1.25	533.48	534.49	2.39	1.13
200	551.925	466.73	2.50	1.30	607.75	534.49	2.73	1.13

Table B.4: Behaviour of *SPRC390E-BH* steel under high rate loading [Huh *et al.* (2009)].

$\dot{\epsilon}$ (s^{-1})	Engineering stress				True stress			
	F_y (MPa)	F_u (MPa)	$(DIF)_{Fy}$	$(DIF)_{Fu}$	F_y (MPa)	F_u (MPa)	$(DIF)_{Fy}$	$(DIF)_{Fu}$
0.003	216.74	399.11	-	-	222.62	502.70	-	-
0.1	245.81	409.7	1.13	1.02	248.64	505.40	1.11	1.00
0.5	277.53	420.26	1.28	1.05	281.08	508.10	1.26	1.01
1	288.10	422.91	1.32	1.05	289.18	521.62	1.29	1.03
2	325.11	444.05	1.5	1.11	324.32	535.13	1.45	1.06
5	340.96	438.76	1.57	1.09	373.83	540.54	1.67	1.07
10	377.97	441.41	1.74	1.10	378.37	537.83	1.69	1.06
20	383.26	449.33	1.76	1.12	389.18	567.56	1.74	1.12
50	385.9	462.55	1.78	1.15	397.29	575.67	1.78	1.14
100	425.55	465.19	1.96	1.16	427.02	581.08	1.91	1.15
200	459.9	483.7	2.12	1.21	459.45	602.70	2.06	1.19

Table B.5: Behaviour of *TRIP60* steel under high rate loading [Huh et al. (2009)].

$\dot{\epsilon}$ (s^{-1})	Engineering stress				True stress			
	F_y (MPa)	F_u (MPa)	$(DIF)_{Fy}$	$(DIF)_{Fu}$	F_y (MPa)	F_u (MPa)	$(DIF)_{Fy}$	$(DIF)_{Fu}$
0.003	424.89	657.2	-	-	424.12	831.89	-	-
0.1	446.28	648.03	1.05	0.98	444.80	770.4	1.04	0.92
0.5	464.63	666.37	1.09	1.01	465.49	794.45	1.09	0.95
1	476.85	669.43	1.12	1.01	493.09	808.70	1.16	0.97
2	504.36	675.54	1.18	1.02	493.09	804.63	1.16	0.96
5	495.2	681.74	1.16	1.03	493.09	786.98	1.16	0.94
10	513.53	690.83	1.20	1.05	493.09	824.97	1.16	0.99
20	513.53	675.54	1.20	1.02	493.09	839.02	1.16	1.00
50	522.70	709.17	1.23	1.07	527.57	852.69	1.24	1.02
100	559.38	715.28	1.31	1.08	558.58	880.23	1.31	1.05
200	632.75	727.51	1.48	1.10	627.49	880.50	1.47	1.05

Table B.6: Behaviour of *CP800* steel under high rate loading [Singh *et al.* (2011)].

$\dot{\epsilon}$ (s^{-1})	Engineering stress				True stress			
	F_y (MPa)	F_u (MPa)	$(DIF)_{Fy}$	$(DIF)_{Fu}$	F_y (MPa)	F_u (MPa)	$(DIF)_{Fy}$	$(DIF)_{Fu}$
0.001	685	872	-	-	689	946	-	-
5	718	890	1.04	1.02	724	996	1.05	1.05
25	734	904	1.07	1.03	740	1015	1.07	1.07
250	828	965	1.20	1.10	839	1095	1.2	1.15
500	981	1030	1.43	1.18	988	1164	1.43	1.23
750	990	1055	1.44	1.20	1001	1196	1.45	1.26

Table B.7: Behaviour of mild steel- Grade *St 52-3N* under high rate loading [Langseth *et al.* (2011)].

$\dot{\epsilon}$ (s^{-1})	Engineering stress			
	F_y (MPa)	F_u (MPa)	$(DIF)_{Fy}$	$(DIF)_{Fu}$
0.0001	411.35	553.47	-	-
0.01	438.55	577.23	1.06	1.04
1	472.67	606.93	1.14	1.09
21.4	562.4	641.01	1.36	1.15
180	520.40	531.34	1.26	0.96
1070	678.00	639.70	1.64	1.15

Table B.8: Behaviour of mild steel- Grade *St 52-3N* under high rate loading [Langseth et al. (2011)].

$\dot{\epsilon}$ (s^{-1})	Engineering stress			
	F_y (MPa)	F_u (MPa)	$(DIF)_{Fy}$	$(DIF)_{Fu}$
0.0001	360.97	522.47	-	-
0.01	387	542.86	1.07	1.03
1	470.74	572.18	1.30	1.09
21.2	500.15	605.97	1.38	1.15
170	488.85	500.25	1.35	0.95
1095	640.47	608.42	1.77	1.16

Table B.9: Behaviour of *TRIP600* steel under high rate loading [Huh et al. (2011)].

$\dot{\epsilon}$ (s^{-1})	True stress			
	F_y (MPa)	F_u (MPa)	$(DIF)_{Fy}$	$(DIF)_{Fu}$
0.003	422.4	748.8	-	-
0.1	422.4	758.4	1	1.01
1	432	768	1.02	1.02
3	451.2	777.6	1.06	1.03
10	451.2	796.8	1.06	1.06
30	460.8	806.4	1.09	1.07
100	480	806.4	1.13	1.07
200	489.6	806.4	1.15	1.07

Table B.10: Behaviour of *TRIP800* steel under high rate loading [Huh *et al.* (2011)].

$\dot{\epsilon}$ (s^{-1})	True stress			
	F_y (MPa)	F_u (MPa)	$(DIF)_{Fy}$	$(DIF)_{Fu}$
0.003	492.91	951.28	-	-
0.1	500.00	972.93	1.01	1.02
1	504.07	974.61	1.02	1.02
3	514.57	984.99	1.04	1.03
10	544.15	995.43	1.10	1.04
30	554.64	1005.98	1.12	1.05
100	584.28	1006.71	1.18	1.05
200	584.84	1026.52	1.18	1.07

Table B.11: Behaviour of *DP600* steel under high rate loading [Huh *et al.* (2011)].

$\dot{\epsilon}$ (s^{-1})	True stress			
	F_y (MPa)	F_u (MPa)	$(DIF)_{Fy}$	$(DIF)_{Fu}$
0.003	419.88	772.21	-	-
0.1	431.93	774.73	1.02	1.00
1	443.08	785.99	1.05	1.01
3	463.02	796.30	1.10	1.03
10	473.44	816.19	1.12	1.05
30	502.68	817.08	1.19	1.05
100	522.63	836.97	1.24	1.08
200	532.71	847.00	1.26	1.09

Table B.12: Behaviour of *DP800* steel under high rate loading [Huh *et al.* (2011)].

$\dot{\epsilon}$ (s^{-1})	True stress			
	F_y (MPa)	F_u (MPa)	$(DIF)_{Fy}$	$(DIF)_{Fu}$
0.003	556.8	864	-	-
0.1	566.4	864	1.01	1
1	576	873.6	1.03	1.01
3	585.6	883.2	1.05	1.02
10	595.2	902.4	1.06	1.04
30	633.6	921.6	1.13	1.06
100	643.2	940.8	1.15	1.08
200	662.4	950.4	1.18	1.1

Table B.13: Behaviour of *TWIP* steel under high rate loading [Shanqing Xu *et al.* (2013)].

$\dot{\epsilon}$ **(s^{-1})**	**True stress**	
	F_y **(MPa)**	$(DIF)_{Fy}$
0.001	242.12	-
0.001	263.84	-
0.001	237.76	-
0.01	252.16	1.01
0.01	245.33	0.98
1	282.55	1.13
1	281.05	1.13
100	312.85	1.26
100	338.99	1.36
200	308.17	1.24
200	308.69	1.24
400	381.92	1.54
400	453.51	1.82

Table B.14: Behaviour of *TRIP800* steel under high rate loading [Sun *et al.* (2013)].

$\dot{\epsilon}$ **(s^{-1})**	**Engineering stress**	
	F_y **(MPa)**	$(DIF)_{Fy}$
0.001	502.83	-
0.001	502.83	-
1700	777.42	1.54
2650	894.63	1.77

Table B.15: Behaviour of *DP800* steel under high rate loading [Oztruk *et al.* (2013)].

$\dot{\epsilon}$ **(s^{-1})**	**True stress**	
	F_y **(MPa)**	$(DIF)_{Fy}$
0.0044	556.02	-
0.009	581.23	1.04
0.043	583.21	1.04
0.085	620.3	1.11
0.17	681.71	1.22

Table B.16: Behaviour of *TRIP800* steel under high rate loading [Oztruk *et al.* (2013)].

$\dot{\epsilon}$ **(s^{-1})**	**True stress**	
	F_y **(MPa)**	$(DIF)_{Fy}$
0.003	556.02	-
0.01	522.63	0.93
0.045	545.57	0.98
0.085	542.08	0.97
0.17	561.71	1.01

Table B.17: Behaviour of *HSLA340* steel under high rate loading [Oztruk *et al.* (2013)].

$\dot{\epsilon}$ **(s^{-1})**	**True stress**	
	F_y **(MPa)**	$(DIF)_{Fy}$
0.0015	399.69	-
0.009	404.02	1.01
0.042	380.86	0.95
0.084	387.18	0.96
0.169	399.83	1.00

Table B.18: Behaviour of mild steel under high rate loading [Ogundare *et al.* (2013)].

$\dot{\epsilon}$ **(s^{-1})**	**True stress**	
	F_y **(MPa)**	$(DIF)_{Fy}$
0.185	594	1.20
0.37	590.5	1.19
0.74	579.75	1.17
1.11	494.64	1.00

Table B.19: Behaviour of *Aermet 100* steel under high rate loading [Brad *et al.* (2007)].

$\dot{\epsilon}$ **(s^{-1})**	**Engineering stress**	
	F_y **(MPa)**	$(DIF)_{Fy}$
0.004	1848.02	-
0.054	1854.1	1.00
1	1948.33	1.05
257.292	1939.21	1.04

Table B.20: Behaviour of *4340M* steel under high rate loading [Brad *et al.* (2007)].

$\dot{\epsilon}$ **(s^{-1})**	**Engineering stress**	
	F_y **(MPa)**	$(DIF)_{Fy}$
0.001	1231	-
0.004	1243.16	1.00
0.004	1206.69	0.98
0.057	1243	1.00
0.057	1267.48	1.02
3.96	1288.75	1.04
3.96	1322.19	1.07
300	1346.5	1.09
300	1373.86	1.11

Table B.21: Behaviour of *9420M* steel under high rate loading [Brad *et al.* (2007)].

$\dot{\epsilon}$ **(s^{-1})**	**Engineering stress**	
	F_y **(MPa)**	$(DIF)_{Fy}$
0.004	1337.39	-
0.057	1334.35	0.99
3.92	1401.22	1.047
282.89	1465.05	1.09

Table B.22: Behaviour of *ES-1C* steel under high rate loading [Brad *et al.* (2007)].

$\dot{\epsilon}$ **(s^{-1})**	**Engineering stress**	
	F_y **(MPa)**	$(DIF)_{Fy}$
0.001	1428.57	-
0.0043	1413.37	0.98
0.054	1416.41	0.99
4.1	1431.61	1.00
4.1	1446.81	1.01
281.5	1516.72	1.06
281.5	1541.03	1.07

Part B: Reinforcing bars

Table B.23: Engineering stresses of the steel reinforcing bars under high rate loading [Malvar & Crawford (1998)].

$\dot{\epsilon}$ (s^{-1})	Engineering stress		$\dot{\epsilon}$ (s^{-1})	Engineering stress	
	F_y (MPa)	$(DIF)_{Fy}$		F_y (MPa)	$(DIF)_{Fy}$
0.001	654	0.99	0.000058	339	1.02
0.01	654	1	0.00021	339	1.02
0.1	654	1.02	0.00033	339	1.05
1	654	1.08	0.0008	339	1.1
0.001	570	1.04	0.0036	339	1.13
0.01	570	1.06	0.013	339	1.26
0.1	570	1.11	0.018	339	1.3
1	570	1.17	0.024	339	1.33
0.1	401	1.15	0.13	339	1.21
1	401	1.23	0.00001	329	1
0.001	359	1.06	0.00016	329	1.06
0.01	359	1.13	0.00025	329	1.06
0.1	359	1.21	0.00037	329	1.07
1	359	1.28	0.0025	329	1.12
0.005	325	1.14	0.004	329	1.17
0.01	316	1.1	0.005	329	1.2

Table B.23: Engineering stresses of the steel reinforcing bars under high rate loading [Malvar & Crawford (1998)] (Continued).					
$\dot{\epsilon}$ **(s^{-1})**	**Engineering stress**		$\dot{\epsilon}$ **(s^{-1})**	**Engineering stress**	
	F_y **(MPa)**	$(DIF)_{Fy}$		F_y **(MPa)**	$(DIF)_{Fy}$
0.1	316	1.18	0.014	329	1.2
1	316	1.2	0.011	329	1.21
0.00001	248	1	0.009	329	1.22
0.001	248	1.137	0.011	329	1.22
0.007	193	1.14	0.012	329	1.24
0.5	193	1.5	0.019	329	1.24
100	193	2.36	0.019	329	1.28
0.00001	339	1.01	0.027	329	1.27
0.000015	339	1.01	0.028	329	1.31
0.065	329	1.32	0.51	412	1.37
0.057	329	1.36	0.5	412	1.4
0.00093	295	1.04	1.09	412	1.38
0.0018	295	1.11	0.99	412	1.39
0.025	295	1.24	0.88	412	1.4
0.04	295	1.28	1.07	412	1.42
0.08	295	1.31	1.64	412	1.43
0.08	295	1.35	1.91	412	1.41
0.14	295	1.39	1.7	412	1.39
0.085	295	1.49	1	378	1.03
0.525	295	1.41	2	378	1
0.54	295	1.36	5.5	378	1.13
0.05	562	1.15	8.8	378	1.16
0.12	562	1.16	10.48	378	1.21
0.19	562	1.22	7.5	378	1.22
0.35	562	1.25	5.8	378	1.25

Table B.23: Engineering stresses of the steel reinforcing bars under high rate loading [Malvar & Crawford (1998)] (Continued).					
$\dot{\epsilon}$ **(s^{-1})**	**Engineering stress**		$\dot{\epsilon}$ **(s^{-1})**	**Engineering stress**	
	F_y **(MPa)**	$(DIF)_{Fy}$		F_y **(MPa)**	$(DIF)_{Fy}$
0.39	562	1.25	4	378	1.24
0.5	562	1.26	3	378	1.26
0.83	562	1.28	11	378	1.33
0.00092	412	1.08	7.68	378	1.35
0.00092	412	1.1	13.5	378	1.4
0.007	412	1.15	13.5	378	1.45
0.0067	412	1.15	15.71	378	1.46
0.031	412	1.21	13.8	378	1.49
0.042	412	1.23	0.00085	600	1.06
0.084	412	1.28	0.00086	600	1.03
0.131	412	1.24	0.0055	600	1.07
0.138	412	1.27	0.031	600	1.06
0.52	412	1.31	0.031	600	1.08
0.03	600	1.09	0.5	59	1.36
0.086	600	1.11	0.51	59	1.4
0.096	600	1.13	1.03	59	1.38
0.14	600	1.11	1.05	59	1.39
0.54	600	1.13	1	59	1.41
0.43	600	1.14	0.94	59	1.42
0.61	600	1.15	1.67	59	1.43
0.94	600	1.17	1.93	59	1.41
0.94	600	1.2	1.85	59	1.4
1.63	600	1.17	0.0002	483	1
1.96	600	1.18	230	483	1.8
1.81	600	1.21	0.00021	483	1

Table B.23: Engineering stresses of the steel reinforcing bars under high rate loading [Malvar & Crawford (1998)] (Continued).					
$\dot{\epsilon}$ **(s^{-1})**	**Engineering stress**		$\dot{\epsilon}$ **(s^{-1})**	**Engineering stress**	
	F_y **(MPa)**	$(DIF)_{Fy}$		F_y **(MPa)**	$(DIF)_{Fy}$
1.84	600	1.21	230	483	2
0.05	562	1.15	225	483	2.17
0.121	562	1.16	0.00013	355	1.04
0.2	562	1.22	0.00014	355	1.01
0.33	562	1.25	0.022	355	1.2
0.4	562	1.24	0.02	355	1.23
0.47	562	1.26	0.055	355	1.24
0.93	562	1.3	0.027	355	1.26
0.00088	409	1.09	0.05	355	1.26
0.00086	59	1.1	0.11	355	1.31
0.0072	59	1.16	0.11	355	1.34
0.03	59	1.21	0.18	355	1.36
0.04	59	1.23	0.27	355	1.36
0.13	59	1.24	0.28	355	1.34
0.13	59	1.27	0.42	355	1.41
0.08	59	1.28	0.68	355	1.41
0.48	59	1.32	0.72	355	1.45
0.000094	323	1.16	0.004	329	1.16
0.000144	323	1.15	0.0004	329	1.21
0.00145	323	1.13	0.016	329	1.2
0.02	323	1.3	0.0105	329	1.2
0.055	323	1.22	0.01	329	1.2
0.031	323	1.42	0.011	329	1.22
0.07	323	1.37	0.02	329	1.23
0.09	323	1.4	0.02	329	1.24

Table B.23: Engineering stresses of the steel reinforcing bars under high rate loading [Malvar & Crawford (1998)] (Continued).

$\dot{\epsilon}$ (s^{-1})	Engineering stress		$\dot{\epsilon}$ (s^{-1})	Engineering stress	
	F_y (MPa)	$(DIF)_{Fy}$		F_y (MPa)	$(DIF)_{Fy}$
0.2	323	1.5	0.02	329	1.28
0.13	323	1.5	0.03	329	1.28
0.13	323	1.53	0.025	329	1.32
0.43	323	1.58	0.062	329	1.35
0.43	323	1.61	0.073	329	1.33
0.61	323	1.59	0.055	329	1.32
0.75	323	1.58	0.0009	295	1.03
0.75	323	1.6	0.0018	295	1.1
0.00022	339	1.03	0.025	295	1.23
0.00033	339	1.06	0.038	295	1.27
0.00084	339	1.1	0.081	295	1.3
0.0035	339	1.14	0.083	295	1.35
0.13	339	1.21	0.15	295	1.38
0.013	339	1.26	0.53	295	1.36
0.019	339	1.3	0.5	295	1.41
0.024	339	1.332	0.094	295	1.48
0.0001	329	1	0.00086	600	1.03
0.00016	329	1.06	0.00086	600	1.05
0.00024	329	1.06	0.006	600	1.08
0.00036	329	1.06	0.031	600	1.06
0.0027	329	1.11	0.036	600	1.08
0.031	600	1.09	0.48	408	1.37
0.01	600	1.1	0.53	408	1.39
0.1	600	1.1	0.93	408	1.41
0.1	600	1.1	0.93	408	1.4

Table B.23: Engineering stresses of the steel reinforcing bars under high rate loading [Malvar & Crawford (1998)] (Continued).					
$\dot{\epsilon}$ **(s^{-1})**	**Engineering stress**		$\dot{\epsilon}$ **(s^{-1})**	**Engineering stress**	
	F_y **(MPa)**	$(DIF)_{Fy}$		F_y **(MPa)**	$(DIF)_{Fy}$
0.15	600	1.12	1.05	408	1.39
1	600	1.16	1.01	408	1.39
0.96	600	1.18	1	408	1.38
1	600	1.21	1.8	408	1.39
1.7	600	1.17	1.78	408	1.41
1.5	600	1.19	1.5	408	1.44
1.63	600	1.2	1	378	1.02
1.66	600	1.22	2	378	1
1.8	600	1.22	4.89	378	1.13
0.05	562	1.15	2.87	378	1.26
0.11	562	1.15	4.1	378	1.25
0.21	562	1.21	5.9	378	1.25
0.36	562	1.24	6.9	378	1.23
0.42	562	1.24	10.3	378	1.21
0.48	562	1.25	11.06	378	1.34
0.82	562	1.28	8.24	378	1.35
0.0009	408	1.08	12.12	378	1.4
0.00095	408	1.09	0.0002	483	1
0.007	408	1.15	224	483	1.8
0.03	408	1.2	0.02	378	1.06
0.04	408	1.22	0.04	378	1.05
0.13	408	1.25	2.77	378	1.6
0.13	408	1.27	0.0022	458	1.05
0.07	408	1.27	0.0026	458	1.03
0.46	408	1.31	0.0026	458	1.06

Table B.23: Engineering stresses of the steel reinforcing bars under high rate loading [Malvar & Crawford (1998)] (Continued).					
$\dot{\epsilon}$ **(s^{-1})**	**Engineering stress**		$\dot{\epsilon}$ **(s^{-1})**	**Engineering stress**	
	F_y **(MPa)**	$(DIF)_{Fy}$		F_y **(MPa)**	$(DIF)_{Fy}$
0.053	458	1.1	1.55	710	1.1
0.043	458	1.14	0.026	661	1.06
0.049	458	1.14	0.042	661	1.06
0.0556	458	1.14	0.1	661	1.06
3.301	458	1.34	0.2	661	1.08
2.95	458	1.36	0.17	661	1.09
2.69	458	1.57	0.165	661	1.1
0.0023	458	1.01	0.27	661	1.12
0.0055	458	1.12	0.28	661	1.13
0.0059	458	1.18	0.29	661	1.13
2.71	458	1.32	0.38	661	1.14
3.28	458	1.58	0.045	661	1.09
0.0038	458	0.99	0.045	661	1.08
0.005	458	1.02	0.04	661	1.08
0.12	458	1.01	0.045	661	1.07
0.11	458	1.11	0.05	661	1.07
0.1	458	1.11	0.004	600	1.02
3.9	458	1.66	0.004	600	1.04
5.22	458	1.75	0.005	600	1.07
5.58	458	1.88	0.07	600	1.2
0.0463	458	1	4.24	600	1.26
1.62	458	1.24	3.48	600	1.15
0.03	710	1.01	0.1	600	1.13
0.032	710	1.02	0.1	600	1.09
0.465	710	1.05	0.084	600	1.09

Table B.23: Engineering stresses of the steel reinforcing bars under high rate loading [Malvar & Crawford (1998)] (Continued).					
$\dot{\epsilon}$ **(s^{-1})**	**Engineering stress**		$\dot{\epsilon}$ **(s^{-1})**	**Engineering stress**	
	F_y **(MPa)**	$(DIF)_{Fy}$		F_y **(MPa)**	$(DIF)_{Fy}$
0.885	710	1.06	0.057	600	1.09
1.01	710	1.08	0.057	600	1.07
1.63	710	1.08	0.064	600	1.06
1.63	710	1.09	0.0756	600	1.06
0.069	600	1.05	100	529.8	1.24
0.057	600	1.04	520.14	578.76	1.35
0.051	600	1.03	0.005	450.202	1
0.045	600	1.03	0.1	456.611	1.01
0.084	600	1	10	500.375	1.11
0.11	600	1.03	100	553.052	1.22
0.005	310.501	1	520.14	590.371	1.31
0.1	335.27	1.07	0.005	549.9	1.22
10	385.69	1.24	0.1	574.66	1
100	411.71	1.32	10	603.521	1.04
520.14	447.43	1.44	100	679.38	1.18
0.005	323.86	1	520.14	796.58	1.38
0.1	351.87	1.08	0.0001	586	-
10	392.3	1.21	500	728	1.24
100	421.68	1.30	0.0001	593	-
520.14	465.69	1.43	250	677	1.14
0.005	350.429	1	500	717	1.20
0.1	385.128	1.09	1000	725	1.22
10	425.602	1.21	0.0001	555	-
100	479.906	1.36	500	677	1.21981982
520.14	515.55	1.47	0.001	545	

Table B.23: Engineering stresses of the steel reinforcing bars under high rate loading [Malvar & Crawford (1998)] (Continued).					
$\dot{\epsilon}$ **(s^{-1})**	**Engineering stress**		$\dot{\epsilon}$ **(s^{-1})**	**Engineering stress**	
	F_y **(MPa)**	$(DIF)_{Fy}$		F_y **(MPa)**	$(DIF)_{Fy}$
0.005	410.298	1	250	747	1.37
0.1	436.647	1.06	500	741	1.35
10	472.169	1.15	1000	805	1.47
100	489.858	1.19	0.001	520	-
520.14	538.82	1.31	250	666	1.28
0.005	426.95	1	500	672	1.29
0.1	443.262	1.03	1000	721	1.38
10	500.387	1.17	-	-	-

Table B.24: Steel reinforcing bars under high rate loading [Malvar & Crawford (1998)].

$\dot{\epsilon}$ **(s^{-1})**	**Engineering stress**		$\dot{\epsilon}$ **(s^{-1})**	**Engineering stress**	
	F_y **(MPa)**	$(DIF)_{Fu}$		F_y **(MPa)**	$(DIF)_{Fu}$
0.00086	600	1	0.91	600	1.08
0.00086	600	1.02	1.12	600	1.06
0.007	600	1.03	1.72	600	1.06
0.006	600	1.01	1.76	600	1.07
0.031	600	1.01	1.81	600	1.09
0.1	600	1.04	0.0008	408	1.08
0.14	600	1.05	0.0008	408	1.09
0.5	600	1.03	0.005	408	1.1
0.64	600	1.04	0.007	408	1.1
0.6	600	1.07	0.034	408	1.14

Table B.24: Steel reinforcing bars under high rate loading [Malvar & Crawford (1998)] (Continued).					
$\dot{\epsilon}$ (s^{-1})	Engineering stress		$\dot{\epsilon}$ (s^{-1})	Engineering stress	
	F_y (MPa)	$(DIF)_{Fu}$		F_y (MPa)	$(DIF)_{Fu}$
1.03	600	1.09	0.072	408	1.05
0.11	408	1.01	0.46	408	1.15
0.5	408	1.01	1	408	1.17
0.93	408	1.03	1.71	408	1.19
0.86	408	1.05	1.42	408	1.21

REFERENCES

ABAQUS 2013. 6.13-1, User's Manual, ABAQUS. Inc.

Abbas, A., Pullen, A. & Cotsovos, D. (2010). Structural response of RC wide beams under low-rate and impact loading. *Magazine of Concrete Research,* 62**,** 723-740.

Abdou, M. & Abuseda, H. (2014). New heavy aggregate for offshore petroleum pipeline concrete coating Central West Sinai, Egypt. *Egyptian Journal of Petroleum,* 23**,** 389-395.

ABS 2001. Guide for building and classing - subsea pipeline systems and risers.

API 1999. Operation, and Maintenance of Offshore Hydrocarbon Pipelines (Limit State Design) API Recommended Practice 1111. American Petroleum Institute, Washington, DC.

API 2004. Specification for Line Pipe. American Petroleum Institute.

Army TM 5-855-1 Air Force AFPAM 32-1147(I), N. N. P.-., DSWA DAHSCWEMAN-97 1998. Technical Manual – Design and Analysis of Hardened Structures to Conventional Weapons Effects. The Departments of the Army, Air Force, and Navy, and the Defense Special Weapons Agency, Army TM 5-855-1 Air Force AFPAM 32-1147(I), Navy NAVFAC P-1080, DSWA DAHSCWEMAN-97, August 1998.

ASME 2003. *Gas transmission and distribution piping systems*, American Society of Mechanical Engineers.

Bai, Q. & Bai, Y. 2014. *Subsea pipeline design, analysis, and installation*, Gulf Professional Publishing.

Birtel, V. & Mark, P. Parameterised finite element modelling of RC beam shear failure. Proceedings of the 19th Annual International ABAQUS Users' Conference. Boston:[sn], 2006. 95-108.

Bischoff, P. & Perry, S. (1991). Compressive behaviour of concrete at high strain rates. *Materials and structures,* 24**,** 425-450.

Bischoff, P. H. & Perry, S. H. (1995). Impact behavior of plain concrete loaded in uniaxial compression. *Journal of engineering mechanics*.

Boyce, B. L., Crenshaw, T. B. & Dilmore, M. F. (2007). The Strain-Rate Sensitivity of High-Strength High-Toughness Steels.

Brooker, D. C. (2004). A numerical study on the lateral indentation of continuously supported tubes. *Journal of Constructional Steel Research,* 60**,** 1177-1192.

Brown, D. (2009). Tracker video analysis and modeling tool. *Open source, physics,* 4.

Cadoni, E., Dotta, M., Forni, D. & Tesio, N. (2013). High strain rate behaviour in tension of steel B500A reinforcing bar. *Materials and Structures***,** 1-11.

Cadoni, E., Fenu, L. & Forni, D. (2012). Strain rate behaviour in tension of austenitic stainless steel used for reinforcing bars. *Construction and Building Materials,* 35**,** 399-407.

Cadoni, E., Solomos, G. & Albertini, C. (2009). Mechanical characterisation of concrete in tension and compression at high strain rate using a modified Hopkinson bar. *Magazine of Concrete Research,* 61**,** 221-230.

CEB-FIP, M. C. (1990). Comite euro-international du beton. *Bulletin d'information*.

Changjiang. 2015. Available: http://www.jstpipes.com/product_show.asp?ID=476 [Accessed 01/07/2015 2015].

Chen, K. & Shen, W. Q. (1998). Further experimental study on the failure of fully clamped steel pipes. *International journal of impact engineering*, 21**,** 177-202.

Cotsovos, D. 2004. *Numerical modelling of structural concrete under dynamic (earthquake and impact) loading.* Imperial College London (University of London).

Cotsovos, D. & Pavlović, M. (2008a). Numerical investigation of concrete subjected to compressive impact loading. Part 1: A fundamental explanation for the apparent strength gain at high loading rates. *Computers & structures*, 86**,** 145-163.

Cotsovos, D. & Pavlović, M. (2008b). Numerical investigation of concrete subjected to compressive impact loading. Part 2: Parametric investigation of factors affecting behaviour at high loading rates. *Computers & structures*, 86**,** 164-180.

Cotsovos, D. & Pavlović, M. (2008c). Numerical investigation of concrete subjected to high rates of uniaxial tensile loading. *International Journal of Impact Engineering*, 35**,** 319-335.

DANS, D. D. C. D. F., DES CONDUITES, A. H. P. A. & DE LA RUGOSITE, P. (2001). FRICTION FACTOR IN HIGH PRESSURE NATURAL GAS PIPELINES FROM ROUGHNESS MEASUREMENTS.

DNV (2006). Recommended Practice DNV-RP-F105 Free spanning pipelines. *Veritas, Det Norske*.

DNV 2010a. Interference between trawl gear and pipelines. DNV: Det Norske Veritas, Oslo.

DNV 2010b. Risk Assessment of Pipelines Protection. Det Norske Veritas.

DNV 2012. DNV-OS-F101:"Submarine Pipeline Systems". *Det Norske Veritas.*

Engineering, A. 2015. Available: http://www.algram.net/case_studies_i-speed.html.

Eurocode-EC2 2004. *Eurocode 2: Design of Concrete Structures: Part 1-1: General Rules and Rules for Buildings*, British Standards Institution.

EXOVA. 2016. Available: http://www.exova.com/ [Accessed 01/02/2016 2016].

Gbenga Sueiman, A. K. S., Oussama Takieddine 2015. Subsae pipeines design challenges.

Grote, D., Park, S. & Zhou, M. (2001). Dynamic behavior of concrete at high strain rates and pressures: I. experimental characterization. *International journal of impact engineering,* 25**,** 869-886.

Hillenbrand, H., Gräf, M. & Kalwa, C. (2001). Development and production of high strength pipeline steels. *Niobium Science & Technology. TMS***,** 543-569.

Huh, H., Kang, W. J. & Han, S. S. (2002). A tension split Hopkinson bar for investigating the dynamic behavior of sheet metals. *Experimental Mechanics,* 42**,** 8-17.

Huh, H., Kim, S.-B., Song, J.-H. & Lim, J.-H. (2008). Dynamic tensile characteristics of TRIP-type and DP-type steel sheets for an auto-body. *International Journal of Mechanical Sciences,* 50**,** 918-931.

Huh, H., Lim, J. & Park, S. (2009). High speed tensile test of steel sheets for the stress-strain curve at the intermediate strain rate. *International Journal of Automotive Technology,* 10**,** 195-204.

Ishikawa, N. & Hoshikawa, T. (1994). Impact absorption energy of steel pipe beam. *Nuclear engineering and design,* 150**,** 303-308.

Jankowiak, T. & Lodygowski, T. (2005). Identification of parameters of concrete damage plasticity constitutive model. *Foundations of civil and environmental engineering,* 6**,** 53-69.

Jones, N. & Birch, R. (2010). Low-velocity impact of pressurised pipelines. *International Journal of Impact Engineering,* 37**,** 207-219.

Jones, N., Birch, S., Birch, R., Zhu, L. & Brown, M. (1992). An experimental study on the lateral impact of fully clamped mild steel pipes. *Proceedings of the Institution of Mechanical Engineers, Part E: Journal of Process Mechanical Engineering,* 206**,** 111-127.

Jones, N. & Shen, W. (1992). A theoretical study of the lateral impact of fully clamped pipelines. *Proceedings of the Institution of Mechanical Engineers, Part E: Journal of Process Mechanical Engineering,* 206**,** 129-146.

Karamanos, S. A. & Andreadakis, K. P. (2006). Denting of internally pressurized tubes under lateral loads. *International journal of mechanical sciences,* 48**,** 1080-1094.

Katayama, M., Itoh, M., Tamura, S., Beppu, M. & Ohno, T. (2007). Numerical analysis method for the RC and geological structures subjected to extreme loading by energetic materials. *International journal of impact engineering,* 34**,** 1546-1561.

Kesner, K. & Billington, S. L. (2004). Tension, compression and cyclic testing of engineered cementitious composite materials.

Kmiecik, P. & Kamiński, M. (2011). Modelling of reinforced concrete structures and composite structures with concrete strength degradation taken into consideration. *Archives of civil and mechanical engineering,* 11**,** 623-636.

Kotsovos, M. D. 2015. *Finite-Element Modelling of Structural Concrete: Short-Term Static and Dynamic Loading Conditions,* CRC Press.

Kotsovos, M. D. & Pavlović, M. 1995. *Structural concrete: finite-element analysis for limit-state design*, Thomas Telford.

Langseth, M., Lindholm, U., Larsen, P. & Lian, B. (1991). Strain-Rate Sensitivity of Mild Steel Grade St52-3N. *Journal of Engineering Mechanics,* 117**,** 719-732.

Lee, L.-H. 2007. *ON THE DESIGN OF SLIP-ON BUCKLE ARRESTORS FOR OFFSHORE PIPELINES.* Doctor of Philosophy, The University of Texas at Austin.

Li, Q., Lu, Y. & Meng, H. (2009). Further investigation on the dynamic compressive strength enhancement of concrete-like materials based on split Hopkinson pressure bar tests. Part II: numerical simulations. *International journal of impact engineering,* 36**,** 1335-1345.

Li, Q. & Meng, H. (2003). About the dynamic strength enhancement of concrete-like materials in a split Hopkinson pressure bar test. *International Journal of solids and structures,* 40**,** 343-360.

lincoln. 2015. Available: http://www.lincolncontinentalltd.com/pipelinecoating.htm [Accessed 23/09/2015 2015].

Lu, Y. & Li, Q. (2011). About the dynamic uniaxial tensile strength of concrete-like materials. *International journal of impact engineering,* 38**,** 171-180.

MAE. 2016. Available: http://www.mae.ncsu.edu/silverberg/statics%20and%20dynamics%20web/Table%202.doc [Accessed 01/02/2016 2016].

Malvar, L. & Crawford, J. Dynamic increase factors for steel reinforcing bars [C]. 28th DDESB Seminar. Orlando, USA, 1998a.

Malvar, L. J. & Crawford, J. E. 1998b. Dynamic increase factors for concrete. DTIC Document.

Ng, C. & Shen, W. (2006). Effect of lateral impact loads on failure of pressurized pipelines supported by foundation. *Proceedings of the Institution of Mechanical Engineers, Part E: Journal of Process Mechanical Engineering,* 220**,** 193-206.

NTNU. 2015. Available: https://www.ntnu.edu/simlab/testing/hpm [Accessed 06/07/2015 2015].

Ogundare, O., Momoh, I., Akinribide, O., Daniyan, A., Adetunji, A. & Olusunle, S. (2013). Effect of strain rates on mild steel under tensile loading. *Int J Sci Technol,* 2.

OPTI. 2015. Available: http://fp.optics.arizona.edu/optomech/references/OPTI_222/OPTI_222_W4.pdf [Accessed 06/07/2015 2015].

Othman, R., Guégan, P., Challita, G., Pasco, F. & LeBreton, D. (2009). A modified servo-hydraulic machine for testing at intermediate strain rates. *International Journal of Impact Engineering,* 36**,** 460-467.

Ozturk, F., Polat, A., Toros, S. & Picu, R. (2013). Strain Hardening and Strain Rate Sensitivity Behaviors of Advanced High Strength Steels. *Journal of Iron and Steel Research, International,* 20**,** 68-74.

Palmer, A., Touhey, M., Holder, S., Anderson, M. & Booth, S. (2006). Full-scale impact tests on pipelines. *International journal of impact engineering,* 32**,** 1267-1283.

Polymers, B. S. W. 2010. Protective Steel Pipe Coating with Ductile Engineered Cementitious Composites (ECC).

Siciliano, F., Stalheim, D. G. & Gray, J. M. 2008. Modern high strength steels for oil and gas transmission pipelines. 7th International Pipeline Conference, 2008. American Society of Mechanical Engineers, 187-195.

Singh, N., Cadoni, E., Singha, M. & Gupta, N. (2011). Dynamic tensile behavior of multi phase high yield strength steel. *Materials & Design,* 32**,** 5091-5098.

Singh, N., Cadoni, E., Singha, M. & Gupta, N. (2013). Dynamic Tensile and Compressive Behaviors of Mild Steel at Wide Range of Strain Rates. *Journal of Engineering Mechanics,* 139**,** 1197-1206.

Singh, N., Cadoni, E., Singha, M. & Gupta, N. (2014). Quasi-static and dynamic tensile behavior of CP800 steel. *Mechanics of Advanced Materials and Structures,* 21**,** 531-537.

STATOIL 1996. Design guidelines for trawl loads on pipelines. STATOIL, NORWAY.

Steven, C. 2000. Chapra. Numerical methods for engineers [M]. Boston: McGraw-Hill.

Sun, X., Soulami, A., Choi, K. S., Guzman, O. & Chen, W. (2012). Effects of sample geometry and loading rate on tensile ductility of TRIP800 steel. *Materials Science and Engineering: A,* 541**,** 1-7.

Tedesco, J. & Ross, C. (1998). Strain-rate-dependent constitutive equations for concrete. *Journal of pressure vessel technology,* 120**,** 398-405.

Tenaris. 2015. Available: http://www.tenaris.com/en/Products/OffshoreLinePipe/Risers.aspx [Accessed 27/07/2015 2015].

TOTAL. 2016. 2016. Available: http://www.total.co.uk/ [Accessed 01/02/2016.

Wierzbicki, T. & Suh, M. (1988). Indentation of tubes under combined loading. *International Journal of Mechanical Sciences,* 30**,** 229-248.

Xu, S., Ruan, D., Beynon, J. H. & Rong, Y. (2013). Dynamic tensile behaviour of TWIP steel under intermediate strain rate loading. *Materials Science and Engineering: A,* 573**,** 132-140.

Zeinoddini, M., Arabzadeh, H., Ezzati, M. & Parke, G. (2013). Response of submarine pipelines to impacts from dropped objects: Bed flexibility effects. *International Journal of Impact Engineering,* 62**,** 129-141.

Zeinoddini, M., Parke, G. & Harding, J. (2002). Axially pre-loaded steel tubes subjected to lateral impacts: an experimental study. *International Journal of Impact Engineering,* 27**,** 669-690.

Zhang, M., Wu, H., Li, Q. & Huang, F. (2009). Further investigation on the dynamic compressive strength enhancement of concrete-like materials based on split Hopkinson pressure bar tests. Part I: Experiments. *International journal of impact engineering,* 36**,** 1327-1334.

Zhou, X. & Hao, H. (2008a). Mesoscale modelling of concrete tensile failure mechanism at high strain rates. *Computers & Structures,* 86**,** 2013-2026.

Zhou, X. & Hao, H. (2008b). Modelling of compressive behaviour of concrete-like materials at high strain rate. *International Journal of Solids and Structures,* 45**,** 4648-4661.